THE ROLE OF INTERPLAY BETWEEN METABOLISM AND CHROMOSOMES IN TUMORIGENESIS

EDITED BY: Jiayi Wang, Lutao Du, Xuyun Zhao, Ming Yang, Bishuang Cai and Yuanyuan Lu

PUBLISHED IN: Frontiers in Cell and Developmental Biology and Frontiers in Genetics

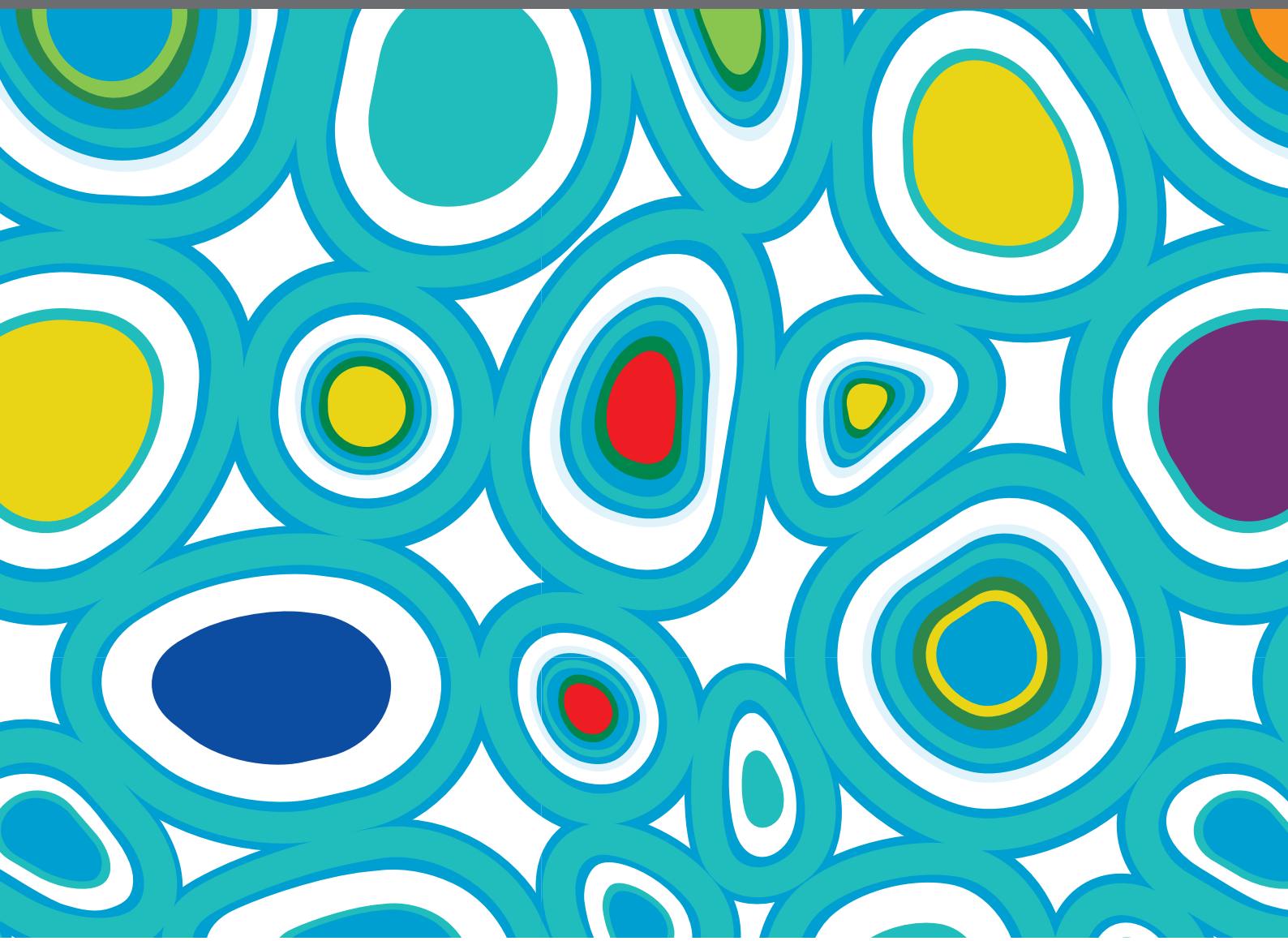

frontiers Research Topics

frontiers

ISSN 1664-8714
ISBN 978-2-83250-024-8
DOI 10.3389/978-2-83250-024-8

About Frontiers

Frontiers is more than just an open-access publisher of scholarly articles: it is a pioneering approach to the world of academia, radically improving the way scholarly research is managed. The grand vision of Frontiers is a world where all people have an equal opportunity to seek, share and generate knowledge. Frontiers provides immediate and permanent online open access to all its publications, but this alone is not enough to realize our grand goals.

Frontiers Journal Series

The Frontiers Journal Series is a multi-tier and interdisciplinary set of open-access, online journals, promising a paradigm shift from the current review, selection and dissemination processes in academic publishing. All Frontiers journals are driven by researchers for researchers; therefore, they constitute a service to the scholarly community. At the same time, the Frontiers Journal Series operates on a revolutionary invention, the tiered publishing system, initially addressing specific communities of scholars, and gradually climbing up to broader public understanding, thus serving the interests of the lay society, too.

Dedication to Quality

Each Frontiers article is a landmark of the highest quality, thanks to genuinely collaborative interactions between authors and review editors, who include some of the world's best academicians. Research must be certified by peers before entering a stream of knowledge that may eventually reach the public - and shape society; therefore, Frontiers only applies the most rigorous and unbiased reviews.
Frontiers revolutionizes research publishing by freely delivering the most outstanding research, evaluated with no bias from both the academic and social point of view. By applying the most advanced information technologies, Frontiers is catapulting scholarly publishing into a new generation.

What are Frontiers Research Topics?

Frontiers Research Topics are very popular trademarks of the Frontiers Journals Series: they are collections of at least ten articles, all centered on a particular subject. With their unique mix of varied contributions from Original Research to Review Articles, Frontiers Research Topics unify the most influential researchers, the latest key findings and historical advances in a hot research area! Find out more on how to host your own Frontiers Research Topic or contribute to one as an author by contacting the Frontiers Editorial Office: frontiersin.org/about/contact

THE ROLE OF INTERPLAY BETWEEN METABOLISM AND CHROMOSOMES IN TUMORIGENESIS

Topic Editors:
Jiayi Wang, Shanghai Jiao Tong University, China
Lutao Du, The Second Hospital of Shandong University, China
Xuyun Zhao, Shanghai Jiao Tong University, China
Ming Yang, Shandong University, China
Bishuang Cai, Icahn School of Medicine at Mount Sinai, United States
Yuanyuan Lu, Fourth Military Medical University, China

Citation: Wang, J., Du, L., Zhao, X., Yang, M., Cai, B., Lu, Y., eds. (2022). The Role of Interplay between Metabolism and Chromosomes in Tumorigenesis. Lausanne: Frontiers Media SA. doi: 10.3389/978-2-83250-024-8

Table of Contents

frontiers | Frontiers in Cell and Developmental Biology

TYPE Editorial
PUBLISHED 10 August 2022
DOI 10.3389/fcell.2022.981075

OPEN ACCESS

EDITED AND REVIEWED BY
Michael E. Symonds,
University of Nottingham,
United Kingdom

*CORRESPONDENCE
Lutao Du,
lutaodu@sdu.edu.cn
Yuanyuan Lu,
luyuan11@fmmu.edu.cn
Jiayi Wang,
karajan2@163.com

SPECIALTY SECTION
This article was submitted to Epigenomics and Epigenetics, a section of the journal Frontiers in Cell and Developmental Biology

RECEIVED 29 June 2022
ACCEPTED 07 July 2022
PUBLISHED 10 August 2022

CITATION
Du L, Lu Y and Wang J (2022), Editorial: The role of interplay between metabolism and chromosomes in tumorigenesis.
Front. Cell Dev. Biol. 10:981075.
doi: 10.3389/fcell.2022.981075

Editorial: The role of interplay between metabolism and chromosomes in tumorigenesis

Lutao Du[1,2]*, Yuanyuan Lu[3]* and Jiayi Wang[4,5]*

[1]Department of Clinical Laboratory, The Second Hospital of Shandong University, Jinan, Shandong, China, [2]Shandong Provincial Clinical Medicine Research Center for Clinical Laboratory, Jinan, Shandong, China, [3]State Key Laboratory of Cancer Biology, National Clinical Research Center for Digestive Diseases, Xijing Hospital of Digestive Diseases, Fourth Military Medical University, Xi'an, China, [4]Department of Laboratory Medicine, Shanghai Chest Hospital, Shanghai Jiao Tong University, Shanghai, China, [5]Shanghai Institute of Thoracic Oncology, Shanghai Chest Hospital, Shanghai Jiao Tong University, Shanghai, China

KEYWORDS

non-coding RNA, post-translational modification, epigenetic regulation, glycolysis, m6A modification, cancer, ceRNA

Editorial on the Research Topic
The role of interplay between metabolism and chromosomes intumorigenesis

Introduction

Tumor is one of the biggest threats to human health. Genetic and epigenetic modifications in chromosome contribute to altered gene expression in tumor formation and development (Lee and Kim, 2022). In addition, altered metabolism such as activated glycolysis pathway is an essential feature of tumor to provide energy and structural resources for tumor cell proliferation (Altman et al., 2016). Previous studies have preliminarily confirmed the relationship between chromosome and metabolism, and the role of them in jointly promoting the development of tumor. For example, metabolites produced in tumor cells can affect enzyme activity of epigenetic modification to regulate gene expression (Miranda-Goncalves et al., 2018); some metabolites directly modify chromatin as substrates, resulting in chromatin structural abnormalities and modifications (Dai et al., 2020). In addition, genetic mutations associated with chromatin instability can lead to changes in enzyme activity resulting in the production of tumor-promoting metabolites (Kim and Yeom, 2018). Accumulation of harmful metabolites can trigger further mutations in chromosomes (Janke et al., 2015; Pavlova and Thompson, 2016; Pavlova et al., 2022). In our Research Topic, we further refined the relationship between chromosomes and metabolism from the following aspects, and clarified their cancer-promoting roles.

Metabolic regulation of non-coding RNA

Non-coding RNA originates from chromosomes, and exerts cis-regulatory effects at the chromosomal level (Quinn and Chang, 2016). N^6-methyladenosine (m^6A) is the most abundant internal modification of RNA in eukaryotic cells, and has gained increasing attention in recent years. m^6A can affect RNA function by affecting RNA processing, nuclear export and RNA translation to decay (Huang et al., 2020). In addition, m^6A affects RNA stability and thus affect cell function. For example, in dendritic cell, CCR7 chemokine receptor upregulates long non-coding RNA Dpf3 via removing m^6A modification to prevent RNA degradation. Dpf3 directly binds to and suppressed HIF-1α-dependent glycolysis (Liu et al., 2019). In our Research Topic, Liu et al. and Liang et al. reported that m^6A modifications of long non-coding RNA DUXAP8 and LINC00106 both upregulate their stability, and then increase the migration, invasion, and metastasis characteristics of tumor cells and make tumor cells acquire chemotherapy-resistant properties. In addition, Liu et al. found that a glycolysis promoting gene SLC2A1 is closely associated with multiple m^6A-related genes. These data suggested the close relationship between metabolism and pan-m^6A modification system.

Competing endogenous RNAs (ceRNAs) are transcripts that can regulate each other at post-transcription level by competing for shared miRNAs (Qi et al., 2015). ceRNA network is an important way for non-coding RNAs to exert their functions (Tay et al., 2014). For example, HMGB1 mRNA has been found to promote the expression of RICTOR mRNA as the ceRNA through competitively binding with the miR-200 family, especially miR-429, then promotes glutamine metabolism and impedes immunotherapy by PD-L1+ exosomes activity (Wei et al., 2021). In our Research Topic, we also provide evidences that ceRNAs regulate tumor-related metabolism. The above mentioned long non-coding RNA DUXAP8, LINC00106 can both absorb microRNA to enhance the malignant phenotype of HCC cells. In addition, Lai et al. reported that LINC01572 and Wang et al. reported that LUCAT1 both act as ceRNAs to promote glycolysis in tumor cells. The above-mentioned glycolysis promoting gene SLC2A1 is also bio-informatic analyzed to be associated with ceRNA regulatory network. Li et al. reported that MTFR1 is a promoter of tumor progression and glycolysis by activating the AMPK/mTOR signalling pathway in LUAD. The MTFR1 negative regulator is miR-29c-3p, but the upstream ceRNA is not reported. We also published a review written by Xu et al. reported the role of non-coding RNA in cerebrospinal fluid. This review elucidates the brain tumorigenic mechanisms of non-coding RNAs in cerebrospinal fluid (mainly through m^6A modification and ceRNA regulation), and concludes the research results of various non-coding RNAs as diagnostic, prognostic markers and therapeutic agents.

Altogether, the above articles describe that the m6A modification of non-coding RNAs to upregulate its stability, or through the downstream ceRNA network to activate glycolytic metabolism to play a tumor-promoting role.

Metabolic regulation of anticancer agent

Epigenetic regulated proteins such as histone modification readers and writers have many inhibitors/stimulators that regulate tumor metabolism by affecting epigenetics (Wimalasena et al., 2020). In our Research Topic, Qi et al. reported that Paris Saponin II inhibits human head and neck squamous cell carcinoma cell proliferation and metastasis by inhibiting the expression NOS3 and the nitric oxide metabolic pathway.

Metabolic regulation by post-translational modification

There are numerous examples of post-translational modifications regulating metabolism, such as protein phosphorylation, O-Glycosylation, methylation and crotonylation. A recent study reported that UCP1 is an important thermogenic protein in brown adipose tissue, and there are two key succinylation sites on UCP1 that are critical for UCP1 stability and activity. Loss of UCP1 succinylation results in impaired mitochondria respiration, defective mitophagy, and metabolic inflexibility (Wang et al., 2019). In our Research Topic, Wang et al. reported that ataxia-telangiectasia mutated deficiency firstly augments the phosphorylation of Mad1 Ser214, and promotes its heterodimerization with Mad2. Subsequently, Mad2 is phosphorylated at Ser195. This Mad2 phosphorylation decreases DNA damage repair capacity and is related to the radiotherapy resistance.

Epigenetic regulation by glycolysis

Glycolysis also has important effects on epigenetics. For example, a large amount of lactic acid is produced through glycolysis, and then protein lactylation occurs (Zhang et al., 2019). H3K18 lactylation elevates the expression of METTL3, which in turn leads to the activation of JAK/STAT signaling pathway, and further promotes cancer (Xiong et al., 2022). In our Research Topic, Shen et al. reported that in the hypoxic HCC microenvironment induced by glycolysis, ubiquitin E3 ligase ring finger protein RNF146 is transcriptionally activated by HIF-1α and HIF-2α. RNF146 promotes PTEN ubiquitination and degradation and stimulates AKT/mTOR pathway, thereby promotes HCC cell proliferation.

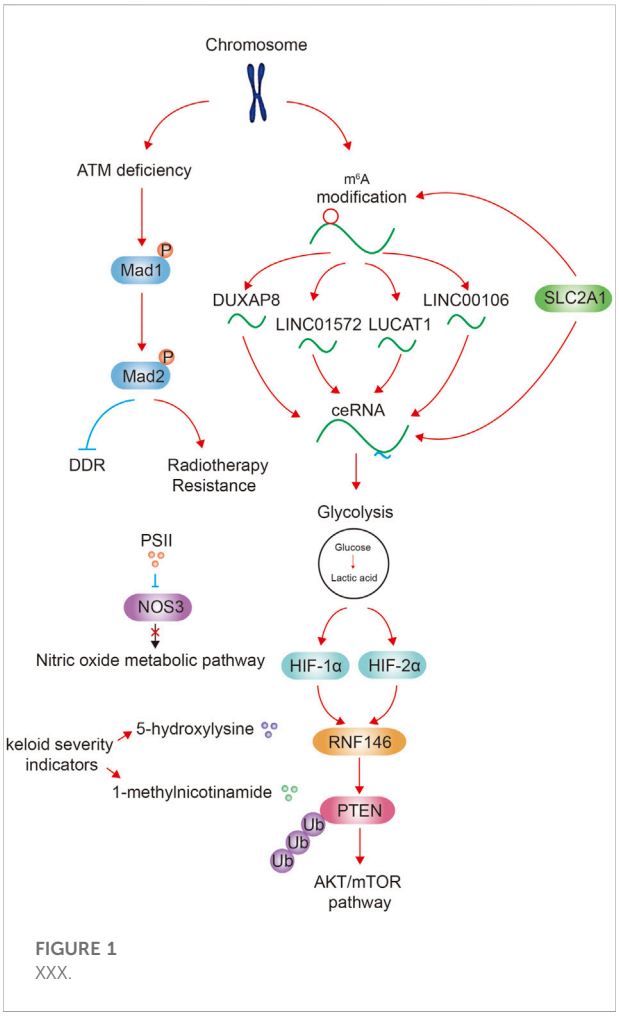

FIGURE 1
XXX.

Epigenetic modification-related metabolic markers

Markers simultaneously associated with epigenetics and metabolism are helpful for the treatment and evaluating prognosis of tumors. Existing markers include *TET2*, *IDH1/2*, *DNMT3A* recurrent mutations and so on (Nebbioso et al., 2018). Via metabolomic and transcriptomic analysis, Shan et al. found that 5-hydroxylysine and 1-methylnicotinamide are most likely to be keloid severity indicators.

In our Research Topic, a review written by Huo et al. details the relationship between epigenetic modification and metabolism in tumors. Firstly, epigenetic modifications such as deoxyribonucleic acid and ribonucleic acid methylation, non-coding ribonucleic acids and histone modifications regulate the metabolic remodeling of tumors, including glucose and lipid metabolism. In the contrary, intermediates produced by metabolism often participate in epigenetic regulation by serving as substrates or cofactors for epigenome-modifying enzymes. Therefore, the authors suggested that the metabolism-epigenome axis must be considered while approaching cancer biomarker studies.

Collectively, our Research Topic elaborated the influence of chromosomal substances such as non-coding RNA and its m^{6}A modification, as well as post-translational modification of proteins on tumor glycolysis and other metabolism, and analyzed the influence of glycolysis on ubiquitination modification. Some epigenetic modified-related metabolic markers were found. Therefore, the close relationship between chromosome and metabolism is very important for the occurrence and development of tumors. In future research and clinical treatment, we need to explore the relationship between chromosome and metabolism in more detail.

Author contributions

LD, YL, and JW read the relevant literature and wrote the editorial. YL modified the grammar.

Conflict of interest

The authors declare that the research was conducted in the absence of any commercial or financial relationships that could be construed as a potential conflict of interest.

Publisher's note

References

Altman, B. J., Stine, Z. E., and Dang, C. V. (2016). From krebs to clinic: Glutamine metabolism to cancer therapy. *Nat. Rev. Cancer* 16, 749. doi:10.1038/nrc.2016.114

Dai, Z., Ramesh, V., and Locasale, J. W. (2020). The evolving metabolic landscape of chromatin biology and epigenetics. *Nat. Rev. Genet.* 21, 737–753. doi:10.1038/s41576-020-0270-8

Huang, H., Weng, H., and Chen, J. (2020). m(6 A modification in coding and non-coding RNAs: Roles and therapeutic implications in cancer. *Cancer Cell* 37, 270–288. doi:10.1016/j.ccell.2020.02.004

Janke, R., Dodson, A. E., and Rine, J. (2015). Metabolism and epigenetics. *Annu. Rev. Cell Dev. Biol.* 31, 473–496. doi:10.1146/annurev-cellbio-100814-125544

Kim, J. A., and Yeom, Y. I. (2018). Metabolic signaling to epigenetic alterations in cancer. *Biomol. Ther.* 26, 69–80. doi:10.4062/biomolther.2017.185

Lee, J. E., and Kim, M. Y. (2022). Cancer epigenetics: Past, present and future. *Semin. Cancer Biol.* 83, 4–14. doi:10.1016/j.semcancer.2021.03.025

Liu, J., Zhang, X., Chen, K., Cheng, Y., Liu, S., Xia, M., et al. (2019). CCR7 chemokine receptor-inducible lnc-dpf3 restrains dendritic cell migration by inhibiting HIF-1α-Mediated glycolysis. *Immunity* 50, 600–615. doi:10.1016/j.immuni.2019.01.021

Miranda-Goncalves, V., Lameirinhas, A., Henrique, R., and Jeronimo, C. (2018). Metabolism and epigenetic Interplay in cancer: Regulation and putative therapeutic targets. *Front. Genet.* 9, 427. doi:10.3389/fgene.2018.00427

Nebbioso, A., Tambaro, F. P., Dell'Aversana, C., and Altucci, L. (2018). Cancer epigenetics: Moving forward. *PLoS Genet.* 14, e1007362. doi:10.1371/journal.pgen.1007362

Pavlova, N. N., and Thompson, C. B. (2016). The emerging hallmarks of cancer metabolism. *Cell Metab.* 23, 27–47. doi:10.1016/j.cmet.2015.12.006

Pavlova, N. N., Zhu, J., and Thompson, C. B. (2022). The hallmarks of cancer metabolism: Still emerging. *Cell Metab.* 34, 355–377. doi:10.1016/j.cmet.2022.01.007

Qi, X., Zhang, D. H., Wu, N., Xiao, J. H., Wang, X., Ma, W., et al. (2015). ceRNA in cancer: possible functions and clinical implications. *J. Med. Genet.* 52, 710–718. doi:10.1136/jmedgenet-2015-103334

Quinn, J. J., and Chang, H. Y. (2016). Unique features of long non-coding RNA biogenesis and function. *Nat. Rev. Genet.* 17, 47–62. doi:10.1038/nrg.2015.10

Tay, Y., Rinn, J., and Pandolfi, P. P. (2014). The multilayered complexity of ceRNA crosstalk and competition. *Nature* 505, 344–352. doi:10.1038/nature12986

Wang, G., Meyer, J. G., Cai, W., Softic, S., Li, M. E., Verdin, E., et al. (2019). Regulation of UCP1 and mitochondrial metabolism in Brown adipose tissue by reversible succinylation. *Mol. Cell* 74, 844–857. doi:10.1016/j.molcel.2019.03.021

Wei, Y., Tang, X., Ren, Y., Yang, Y., Song, F., Fu, J., et al. (2021). An RNA-RNA crosstalk network involving HMGB1 and RICTOR facilitates hepatocellular carcinoma tumorigenesis by promoting glutamine metabolism and impedes immunotherapy by PD-L1+ exosomes activity. *Signal Transduct. Target. Ther.* 6, 421. doi:10.1038/s41392-021-00801-2

Wimalasena, V. K., Wang, T., Sigua, L. H., Durbin, A. D., and Qi, J. (2020). Using chemical epigenetics to target cancer. *Mol. Cell* 78, 1086–1095. doi:10.1016/j.molcel.2020.04.023

Xiong, J., He, J., Zhu, J., Pan, J., Liao, W., Ye, H., et al. (2022). Lactylation-driven METTL3-mediated RNA m(6)A modification promotes immunosuppression of tumor-infiltrating myeloid cells. *Mol. Cell* 82, 1660–1677 e10. doi:10.1016/j.molcel.2022.02.033

Zhang, D., Tang, Z., Huang, H., Zhou, G., Cui, C., Weng, Y., et al. (2019). Metabolic regulation of gene expression by histone lactylation. *Nature* 574, 575–580. doi:10.1038/s41586-019-1678-1

frontiers in Cell and Developmental Biology

REVIEW
published: 07 October 2021
doi: 10.3389/fcell.2021.737670

Evolving Landscape of Long Non-coding RNAs in Cerebrospinal Fluid: A Key Role From Diagnosis to Therapy in Brain Tumors

Kanghong Xu[1†], Xinquan Jiang[1†], Abakundana Nsenga Ariston Gabriel[2], Xiaomeng Li[3], Yunshan Wang[2] and Shuo Xu[4,5]*

[1] School of Public Health, Shandong First Medical University and Shandong Academy of Medical Sciences, Taian, China, [2] Department of Clinical Laboratory, The Second Hospital of Shandong University, Jinan, China, [3] Department of Hematology, Jining First People's Hospital, Jining, China, [4] Department of Neurosurgery, Qilu Hospital of Shandong University and Institute of Brain and Brain-Inspired Science, Shandong University, Jinan, China, [5] Key Laboratory of Brain Function Remodeling, Qilu Hospital of Shandong University, Jinan, China

OPEN ACCESS

Edited by:
Yuanyuan Lu,
Fourth Military Medical University, China

Reviewed by:
Pei Wang,
Second Military Medical University, China
Lifang Ma,
Shanghai Jiao Tong University, China
Xiaomin Niu,
Shanghai Jiao Tong University, China
Qingqiong Luo,
Shanghai Jiao Tong University, China

***Correspondence:**
Shuo Xu
xushuo@sdu.edu.cn

[†]These authors have contributed equally to this work

Specialty section:
This article was submitted to Epigenomics and Epigenetics, a section of the journal Frontiers in Cell and Developmental Biology

Received: *07 July 2021*
Accepted: *31 August 2021*
Published: *07 October 2021*

Citation:
Xu K, Jiang X, Ariston Gabriel AN, Li X, Wang Y and Xu S (2021) Evolving Landscape of Long Non-coding RNAs in Cerebrospinal Fluid: A Key Role From Diagnosis to Therapy in Brain Tumors. Front. Cell Dev. Biol. 9:737670. doi: 10.3389/fcell.2021.737670

Long non-coding RNAs (lncRNAs) are a type of non-coding RNAs that act as molecular fingerprints and modulators of many pathophysiological processes, particularly in cancer. Specifically, lncRNAs can be involved in the pathogenesis and progression of brain tumors, affecting stemness/differentiation, replication, invasion, survival, DNA damage response, and chromatin dynamics. Furthermore, the aberrations in the expressions of these transcripts can promote treatment resistance, leading to tumor recurrence. The development of next-generation sequencing technologies and the creation of lncRNA-specific microarrays have boosted the study of lncRNA etiology. Cerebrospinal fluid (CSF) directly mirrors the biological fluid of biochemical processes in the brain. It can be enriched for small molecules, peptides, or proteins released by the neurons of the central nervous system (CNS) or immune cells. Therefore, strategies that identify and target CSF lncRNAs may be attractive as early diagnostic and therapeutic options. In this review, we have reviewed the studies on CSF lncRNAs in the context of brain tumor pathogenesis and progression and discuss their potential as biomarkers and therapeutic targets.

Keywords: lncRNA, CSF, brain tumor, biomarker, treatment, diagnostic

BACKGROUND

Brain tumors refer to the primary intracranial tumors as well as the metastatic tumors in the brain with a primary lesion. They account for 1.8% of newly diagnosed cancers and 2.3% of cancer-related deaths worldwide (Gerlinger et al., 2012; Xie et al., 2014; Hodges et al., 2017; Siegel et al., 2017). Patients often suffer from symptoms due to increased intracranial pressure (headache,

Abbreviations: lncRNA, Long non-coding RNA; CSF, Cerebrospinal fluid; CT, Computed tomography; MRI, Magnetic resonance imaging; PET, Positron emission tomography; GBM, Glioblastoma; BBB, Blood-brain barrier; CNS, Central nervous system; miRNA, microRNA; EMT, Epithelial-to-mesenchymal transition; IDH, Isocitrate dehydrogenase, HGG: High-grade glioma; EGFR, Epidermal growth factor receptor; TERT, Telomerase reverse transcriptase; ATRX, A-thalassemiamental retardation syndrome X; GSC, Glioma stem cell; LGG, Low-grade glioma; LPS, Lipopolysaccharide; MMP, Matrix metalloproteinase; TMZ, Temozolomide; PCNSL, primary CNS lymphoma; DLBCL, Diffuse large B-cell lymphoma; ZEB1, Zinc finger E-box binding homeobox 1; UTR Untranslated regions; siRNA, Small interfering RNA; ASO, Antisense oligonucleotide; ncRNA, non-coding RNA; WHO, World health organization.

nausea, and vomiting) and neurological dysfunction (seizures, hemiplegia, aphasia, and cognitive deficits) (Cahill et al., 2012; Hadidchi et al., 2019). The natural disease progression in these patients is characterized by a progressive neurological loss and a rapid decline in the quality of the patients' lives.

While considerable advancements in fundamental scientific research and clinical practice have shed light on the brain tumor pathophysiology in the past decades, challenges remain in precise and early diagnosis (Sawaya et al., 1998; Wang and Bettegowda, 2017; Nevel et al., 2018). For instance, computed tomography (CT) (Lebanony et al., 2009) and magnetic resonance imaging (MRI) are reliable in determining the spatial and structural characteristics for brain tumors; however, these non-invasive approaches can hardly determine the pathological classification and malignant degree of tumors (Cao et al., 2017; Huang et al., 2019); Surgical biopsy can overcome these limitations by extracting brain tissue samples, while it is much more invasive, expensive, and risky. Added to the difficulties associated with accessing the nature of brain tumors, there are currently limited therapeutic options available nowadays, including (Galldiks et al., 2017; Laudicella et al., 2021) resection surgeries, chemotherapy, radiotherapy, and electric field therapy (Uddin et al., 2020; López Vázquez et al., 2021). Unfortunately, total removal of the target lesion cannot always be achieved while minimizing the risk of any postoperative functional decline attributable to the surgical procedure itself (Martinez-Rios et al., 2016; Duffau, 2017). Certain brain malignancies are also prone to drive tumor progression and resist chemo- and radiotherapy. Therefore, the outcome of patients with brain tumors is still miserable. The 5- and 10-year survival rates for central nervous system (CNS) tumors are about 36% and 31%, respectively. For the patients with newly diagnosed glioblastoma, the most malignant form of brain tumor, the median survival duration does not exceed 2 years (Martinez-Rios et al., 2016; Duffau, 2017; Jeon et al., 2021; Rankin-Turner et al., 2021; Reddy et al., 2021).

In this scenario, it is essential to develop new methodologies to determine the diagnostic and prognostic parameters for various brain tumors and guide the individualized therapy (Horbinski et al., 2019; Kristensen et al., 2019). Non-coding RNAs (ncRNAs), especially long non-coding RNAs (lncRNAs), have emerged as a novel family of master regulators, because they are widely involved in the development and progression of various CNS disorders, including brain tumors (Kang et al., 2011; Hawrylycz et al., 2012; Chen and Qin, 2015; Hanan et al., 2017). Also, ncRNA-based tumor liquid biopsy has been demonstrated recently at the preclinical level, which detects tumor-specific ncRNA in a less invasive manner from certain body fluids, including serum, urine, and cerebrospinal fluid (CSF). Compared to serum and urine, brain tumor associated ncRNAs are much enriched in the CSF. Therefore, CSF has been considered a promising candidate for brain liquid biopsy. In fact, dysregulation of CSF lncRNAs has been demonstrated in multiple tumors and non-tumor nervous system disorders, including Alzheimer's disease (Zhuang et al., 2020), cerebral vasospasm secondary to subarachnoid haemorrhage (Pan et al., 2020), and cerebral ischemia-reperfusion injury (Zhang Y. et al., 2020). In this review, we focus on the regulatory mechanism of CSF lncRNAs in the pathophysiology of brain tumors and discuss its potential application as diagnostic markers and therapeutic targets.

FUNCTIONS AND CHARACTERISTICS OF CEREBROSPINAL FLUID

The main limitation of blood biopsy for brain tumors is the low serum levels of tumor specific biomarkers, mainly caused by the brain blood barrier (BBB), which is formed by brain microvascular endothelial cells sealed by tight junctions (Banks, 2019). The BBB maintains the independent circulation of CSF and microenvironment homeostasis for the brain tissue (Sweeney et al., 2019). However, the BBB also brings significant challenges to diagnosis and treat brain tumors (Jeon et al., 2021; Pottoo et al., 2021). For instance, most tumor-specific antigens are confined within this barrier, and their systematic detection can be problematic. In addition, the poor BBB penetration naturally hinders the delivery of therapeutic drugs (such as chemotherapeutic drugs, targeted therapeutic drugs, and monoclonal antibodies) into the brain (Seo et al., 2020; Zhang et al., 2021). Although researchers have been developing strategies to modulate BBB permeability, most approaches are difficult to apply in the clinical setting (Sprowls et al., 2019; Pandit et al., 2020). Under these circumstances, CSF biopsy and CSF-based therapeutics have been gradually recognized as an alternative approach to overcome these obstacles.

The CSF is an ultrafiltrate of plasma surrounding the brain and spinal cord (Parnetti et al., 2019). The majority of CSF is produced by the choroid plexus, circulates through the ventricles, the cisterns, and the subarachnoid space to be absorbed into the blood by the arachnoid villi (Johanson et al., 2008). The CSF provides biological and mechanical support to the brain, transports nutrients, signaling molecules, and debris, and regulates brain immunity (Orešković, 2015; Tumani et al., 2017; Attier-Zmudka et al., 2019). Therefore, homeostasis in the production, circulation, and absorption of the CSF is critical for brain function (Proulx, 2021). Analogously, abnormal CSF mirrors the dysregulation of brain in various neurological diseases (**Figure 1**), mainly because CSF is more closely associated with small molecules, peptides, or proteins released from the brain tissues (Johanson et al., 2008; Sakka et al., 2011). Since CSF directly mirrors the biochemical processes in the brain, CSF components are widely used to identify pathogen invasion or diagnosis of neurological diseases (**Figure 1**). Lundborg et al. (2010) reported that glial cell line-derived neurotrophic factor (GDNF) was increased in the CSF of patients with long-term pain but decreased in the blood. Tumor-specific biomarkers are also enriched in the CSF. For instance, the levels of miR-10b and miR-21 are found significantly increased in the CSF of patients with glioblastoma and brain metastasis of breast and lung cancer, compared with tumors in remission and a variety of non-neoplastic conditions (Teplyuk et al., 2012). Similarly, significantly higher CSF levels of miR-21, miR-19b, and miR-92a were identified in primary CNS lymphoma (PCNSL) (Zajdel et al., 2019). Recently, it was reported that immune cell profiling

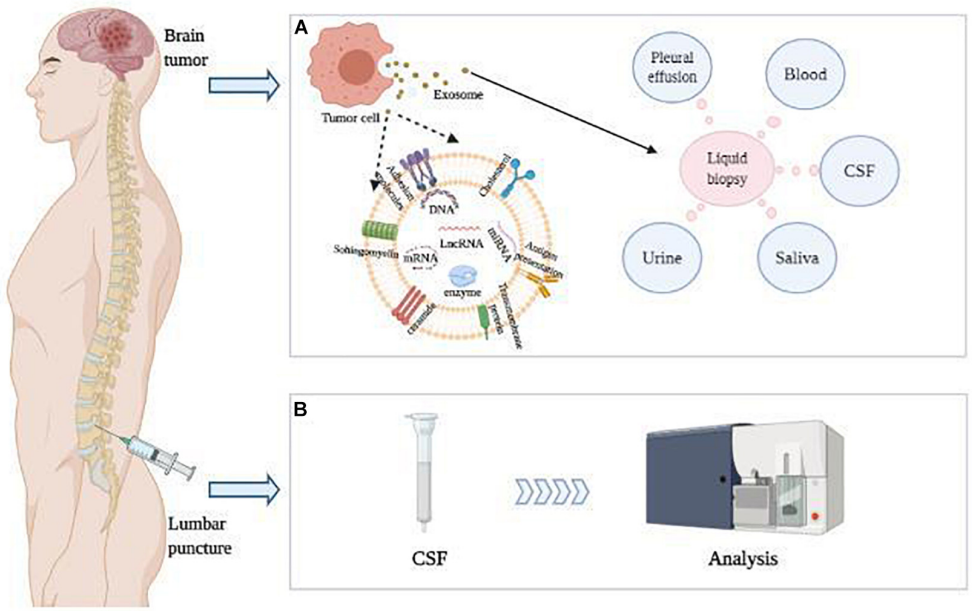

FIGURE 1 | LncRNA in CSF were detected as diagnostic and prognostic indicators of brain tumors. **(A)** Brain tumor cells release exosomes containing nucleic acids, which can be further detected in various body fluids. **(B)** CSF was obtained by lumbar puncture, and CSF lncRNAs packaged in exosomes were detected as diagnostic and prognostic indicators of brain tumors.

of the CSF enabled the characterization of the brain metastasis microenvironment (Rubio-Perez et al., 2021).

LONG NON-CODING RNA IN THE CEREBROSPINAL FLUID

LncRNAs, of which length $\geq$ 200 bp, exhibit a wide range of regulatory activities based on their subcellular localization, including gene transcriptional regulation and mRNA splicing in the nucleus, as well as mRNA stability and protein function modulation in the cytoplasm (**Figure 2**; Ramanathan et al., 2019; Yao et al., 2019). Dysregulation of lncRNAs has been demonstrated to contribute to cancer development and progression *via* abnormal epigenetic alterations in oncogene regulation pathways., including abnormal DNA methylation or histone changes at their gene promoters. More specifically, emerging data suggest that lncRNAs comprise a network of epigenetic modulators by creating platforms for chromatin-remodeling complexes and transcription factors capable of modulating the transcriptional state of lncRNA-controlled genomic loci (Romani et al., 2018; Chen et al., 2021).

Like the other ncRNAs, lncRNAs are selectively packaged, secreted, and transferred between cells by exosomes, which are small bilipid layer enclosed extracellular nano-vesicles with various physiological and pathophysiological functions (Sullivan et al., 2017; Raposo and Stahl, 2019). With exosomes as vectors, lncRNAs are able to cross the BBB and readily accessible in CSF, making it an ideal diagnostic and therapeutic candidate for multiple diseases in the CNS, such as neurodegenerative disorders, stroke, multiple sclerosis, and brain tumors (Cheng et al., 2020; Rastogi et al., 2021). For instance, lncRNAs MALAT1 and SNHG4 are downregulated in the CSF samples of patients with Alzheimer's disease and acute cerebral infarction, respectively (Zhang S. et al., 2020; Zhuang et al., 2020). lncRNA HIF1-AS3 transcriptomic downregulation in human choroid plexus tissue and abnormal PAI-1 level in CSF were observed in patients with progressive multiple sclerosis (Rodríguez-Lorenzo et al., 2020). Intriguingly, Pan et al. (2020) established a CSF lncRNA-based signature (ZFAS1, MALAT1, LINC00261, and LINC01619) to predictive cerebral vasospasm in patients with subarachnoid hemorrhage.

Abundant evidence has revealed that CSF lncRNAs were also extensively expressed in different brain tumors and involved in tumorigenesis, tumor progression, invasion, angiogenesis, and metastasis. In 2017, Ma et al. (2017) firstly observed that lncRNA HOTAIR derived from glioma cells promotes angiogenesis by regulating the endothelial VEGF expression. Similar to Ma's observation, Bian et al. (2019) found that exosomal lncRNA-ATB triggered astrocytes to facilitate the glioma invasion. Moreover, Zhang et al. demonstrated that that lncRNA SBF2-AS1 was upregulated in chemotherapy-resistant glioblastoma (GBM), and overexpression of SBF2-AS1 led to the promotion of chemotherapy resistance, which was regulated by transcription factor ZEB1. ZEB1 directly binds to the SBF2-AS1 promoter region to regulate SBF2-AS1 level and affected temozolomide (TMZ) resistance in GBM cells (Zhang Z. et al., 2019). Recently, Li D. et al. (2021) demonstrated that the expression of CSF lncRNA-CCRR was evidently up-regulated in breast cancer metastasis patients, especially in patients with

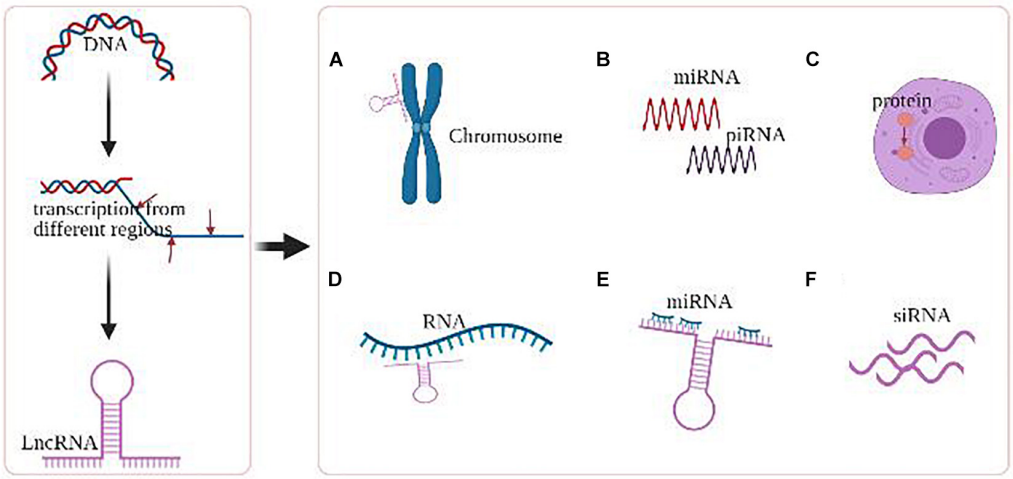

FIGURE 2 | Major epigenetic regulations of lncRNA. **(A)** LncRNAs mediate chromosomal remodeling. **(B)** LncRNAs act as small RNA (miRNA, piRNA) precursor. **(C)** LncRNAs alter cellular localization of proteins. **(D)** LncRNAs involve in the transcriptional regulation of genes. **(E)** LncRNAs act as miRNA sponge. **(F)** LncRNAs produce endogenous siRNAs with the involvement of the dicer enzyme.

brain metastasis, which provides a direct piece of evidence to demonstrate the dysregulation of CSF lncRNA in brain cancers. On the other hand, Wang M. et al. (2020) found that exosomal LGALS9 in glioblastoma CSF suppressed dendritic cell antigen presentation and cytotoxic T-cell immunity, while blocking the secretion of exosomal LGALS9 could regain sustained tumor antigen-presenting activity of dendritic cells and long-lasting antitumor immunity. Together, CSF lncRNAs have exhibited the significance as promising biomarkers and potential targets for various brain tumors.

LONG NON-CODING RNAS IMPLICATIONS IN VARIOUS BRAIN TUMORS

Glioma

As the most prevalent form of primary brain tumors, glioma develops from neural glial cells, mainly star-shaped astrocytes. Based on the classical WHO tumor classification, glioma can be subgrouped into Grade 1–4 (Louis et al., 2016). Despite highly variable histological and genetic characteristics, glioma is notorious for its rapid proliferation, extensive invasion, genetic heterogeneity, and therapeutic resistance. Even given the multiple discipline therapeutics, patients with glioma suffer from the dismal outcomes. Emerging evidence suggests that lncRNAs play a vital role in mediating glioma initiation and progression. Here, we highlighted the current research focusing on *the* implications of lncRNA on glioblastoma and LGG, respectively (**Figure 3**).

Glioblastoma

Glioblastoma (GBM, WHO Grade 4) is the most devastating type of primary brain cancer, accounting for more than half of all primary CNS tumors (Ostrom et al., 2019). In 2016, WHO classified glioblastoma into IDH (isocitrate dehydrogenase) wild-type, IDH mutant, and NOS groups (Louis et al., 2016). In the recently updated WHO classification, glioblastoma is further defined as IDH wild-type adult-type diffuse gliomas (Grade 4), with the iconic molecular profiling including TERT promoter mutation, gain of chromosome 7 and loss of chromosome 10, and EGFR amplification (Louis et al., 2021). Glioblastoma diffusely and rapidly grows to infiltrate the white matter tract and eloquent cortex, making it extremely difficult to achieve early diagnosis and maximal safety resection. Despite the optimal therapeutic approaches combined with surgical resection, targeted radiotherapy, high-dose chemotherapy as well as novel electric field treatment, the median overall survival (OS) of glioblastoma is still less than 21 months, and the 5-year survival rate is between 1–19% (Alexander and Cloughesy, 2017).

In 2019, Yang et al. (2019) reported that glioma stem cell (GSC)-derived lncRNA MALAT1 was transferred to surrounding microglia through exosomal secretion, thereby regulating the inflammatory response through the miR-1295p/HMGB1 axis to affect the secretion of IL-6, IL-8, and TNF-α. This study indicated that exosomal lncRNA played a significant role in maintaining immunosuppressive microenvironment for glioma survival and invasiveness (Yang et al., 2019). Han et al. (2016) demonstrated that lncRNA MALAT1 also mediated anti-glioma effect by suppressing the activation of extracellular regulated protein kinases/mitogen-activated protein kinase (ERK/MAPK) signaling pathway and expression of matrix metalloproteinase 2 (MMP2). Similarly, lncRNA SNHG12, a sponge of miR-129-5p, endows the glioblastoma cells with TMZ resistance by upregulating MAPK1 and activating the MAPK/ERK pathway. Clinically, SNHG12 overexpression was associated with the poor survival of patients treated with TMZ (Lu et al., 2020). Moreover, Tian et al. (2019) found that patients with glioblastoma having high expression of LncRNA AGAP2-AS1 had shorter overall

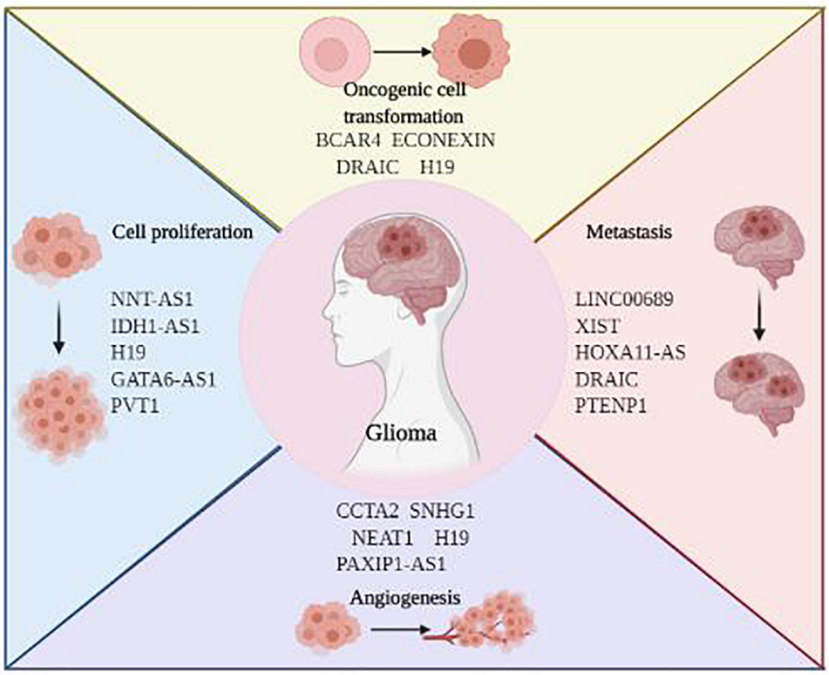

FIGURE 3 | The roles of LncRNAs in glioma development and progression.

survival time than those with low expression of AGAP2-AS1. The loss-of-function studies showed that downregulation of AGAP2-AS1 depressed cell proliferation, migration, and invasion, and promoted cell apoptosis in glioblastoma. Therefore, AGAP2-AS1 might serve as an oncogenic lncRNA and prognostic biomarker in glioblastoma (Tian et al., 2019). Han et al. (2020) reported that MIR22HG was a critical inducer of the Wnt/β-catenin signaling pathway for glioblastoma, and a specific small-molecule inhibitor, AC1L6JTK, could cause the inhibition of tumor growth *in vivo*. Interestingly, MIR22HG was also enlisted in an immune-related lncRNA signature associated with glioblastoma prognosis, indicating its pathophysiological complexity in this malignancy (Li X. et al., 2021). Together, abundant evidence has revealed that lncRNAs play critical roles in multiple aspects of glioblastoma biology.

Low Grade Glioma

In the recently updated WHO classification, the term "anaplastic" was not routinely included; therefore, familiar names like "anaplastic astrocytoma" and "anaplastic oligodendroglioma" were abandoned. Under this circumstance, LGG is now designated as WHO grade 2 astrocytoma and oligodendroglioma, accounting for approximately 5–10% of all CNS tumors (Ostrom et al., 2016). The classical low grade astrocytoma is IDH-mutant, with alternations of ATRX, TP53, and CDKN2A/B. Chromosome 1p19q codeletion is the gold standard characteristics to distinguish oligodendroglioma apart from astrocytoma, along with the alternations of TERT promoter, CIC, FUBP1, and NOTCH1 (Louis et al., 2021). Compared to glioblastoma, LGG has highly variable clinical behavior (Brat et al., 2015). Patients with certain subtype of low grade glioma can survival for decades, while some others progress to secondary glioblastoma within months (Gusyatiner and Hegi, 2018). To improve the diagnostic accuracy and optimize treatment selection, numerous attempts have been made, from the classical histologic characterization to novel molecular profiling, including lncRNA. Nevertheless, considerable controversies remain nowadays. Meanwhile, maximum safety resection might not always be feasible due to the diffuse invasion nature of LGG, and radiotherapy and chemotherapy are alternatively recommended (Franz et al., 2013, 2014).

Growing evidence demonstrates the regulatory role of lncRNA in LGG biology. For example, PR-lncRNA refers to the lncRNAs regulated by P53. *In vitro* experiments of glioma tissues and cell lines revealed that PR-lncRNA expression was negatively correlated with SOX1, SOX2, and SOX9 stem cell factors. Knockdown of SOX abolished the role of PR-lncRNA silencing in glioma cell activity, indicating that the expression and function of PR-lncRNA were significantly altered in LGG formation (Torres-Bayona et al., 2018). LncRNA H19 can enhance tumorigenesis by directly inducing the c-Myc oncogene (Barsyte-Lovejoy et al., 2006). The expression level of H19 was positively correlated with glioma malignancy (Xiao et al., 2020), and H19 could affect the immune infiltration level of glioma through changes in copy number (Yao et al., 2015). As a sponge for miR-675, H19 can regulate the proliferation and migration of glioma cells by producing miR-675 to inhibit the expression of CDK6 (Shi et al., 2014; Li et al., 2016). Moreover, lncRNA LINC00174 is extensively associated with a variety of cancers, including

glioblastoma and LGG. In particular, LINC00174 facilitates glycolysis and tumor growth by regulating the miR-152-3p/SLC2A1 axis and regulates the miR-138-5p/SOX9 axis to promote chemotherapeutic resistance to temozolomide in glioma (Shi et al., 2019; Li B. et al., 2020). Therefore, lncRNAs have the potential for diagnostic and prognostic biomarkers in patients with LGG.

Pituitary Adenoma

Pituitary adenomas are mostly located in the anterior lobe of the pituitary gland, which are usually slow-growing and benign. The symptoms of pituitary adenoma may include headache, optic nerve compression, and endocrine changes, including menopause, gigantism, acromegaly, and Cushing's disease (Bronstein et al., 2011; Holmes, 2016). In 2018, Zhu et al. (2018) suggested that osteoclast differentiation in bone-invasive pituitary adenomas was directly induced by TNFα, which was further regulated by lncRNA SNHG24. Wu et al. (2018) reported that lncRNA H19 inhibited the phosphorylation of 4E-BP1 by preventing the binding of 4E-BP1 to Raptor. In contrast, the overexpression of H19 significantly inhibited the growth of pituitary tumor cells through cell membrane transport. Zhang et al. further demonstrated that the prognosis of patients with prolactinoma was closely related to the expression level of exosomal H19. In addition, the use of cabergoline could enhance the expression of H19 to exert a synergistic therapeutic effect with exosomal H19, which implies the potential of exosomal H19 in the diagnosis and treatment of pituitary tumors (Zhang Y. et al., 2019). Recently, Mao et al. (2020) reported that lncRNA SNHG6 induced the epithelial-mesenchymal transition (EMT) in pituitary adenomas by inhibiting miR-944. Simultaneously, SNHG6/miR-944/RAB11A axis regulated pituitary adenoma proliferation and invasive behavior (Mao et al., 2020).

Meningioma

Meningiomas are the most common benign intracranial tumors arising from the arachnoid cells in the meninges, accounting for 38.3% of all CNS tumors and 54.5% of non-malignant CNS tumors (Louis et al., 2016; Ostrom et al., 2020). The overall survival for patients with benign meningiomas is good, whereas the 5-year survival rate for patients with atypical or malignant meningiomas (WHO grade 2 and 3) is less than 60% (Rohringer et al., 1989). Chromosomal abnormalities at 14q32 are commonly implicated in meningioma pathogenesis and progression (Simon et al., 1995; Weber et al., 1997; Martínez-Glez et al., 2010). MEG3, an imprinted gene located at 14q32, can encode non-coding RNAs with antiproliferative functions (Ghafouri-Fard and Taheri, 2019). Ding et al. (2020) confirmed that lncRNA MEG3 mediated the invasive behavior of meningioma cells through the miR-29c/AKAP12 axis. The upregulation in miR-29c levels can eliminate the adverse effects caused by MEG3 expression on the cell cycle, migration, invasion, and proliferation of meningioma cells (Ding et al., 2020). Zhang et al. (2010) also demonstrated that MEG3 mRNA was highly expressed in normal arachnoid cells but was lost in human meningioma cells, and there was a strong association between the loss of MEG3 expression and tumor grade. Additional evidence has shown that MEG3 could induce the expression of P53, which is a tumor suppressor gene in humans; that is, MEG3 overexpression could reduce the proliferation and metastasis of gastric cancer cells (Wei and Wang, 2017). Alternatively, lncRNA SNHG1 is also associated with meningioma progression. Zhao et al. (2019) reported that SNHG1 was overexpressed in meningioma cell lines, of which deficiency restrained cell growth and accelerated apoptosis. Further mechanism experiments demonstrated that SNHG1/miR-556-5p/TCF12 feedback loop promotes proliferation and inhibits apoptosis in meningiomas through the Wnt signaling pathway (Zhang Y. et al., 2020).

Medulloblastoma

Medulloblastoma is the most common pediatric malignant brain tumor in clinical practice and accounts for 9.2% of pediatric brain tumors (Louis et al., 2007; Millard and De Braganca, 2016; Ostrom et al., 2017). It usually occurs in the lower cerebellar hilum and then metastasizes through CSF circulation (Dufour et al., 2012; Amirjamshidi, 2017). Therefore, CSF cytology has long been one of the routine tests for medulloblastoma. New WHO CNS tumor classification has altered the subgroups of medulloblastomas to mirror new knowledge of their clinical and biological heterogeneity, including 4 principal molecular groups: WNT-activated, sonic hedgehog (SHH)-activated, group 3, and group 4 (Pietsch et al., 2014). SHH is the most common in infants and adults, while other subtypes are common in children (Northcott et al., 2012a, 2017; Taylor et al., 2012). These classifications provide targets for personalized therapy, some of which are currently being tested clinically.

Exploring on the novel molecular biomarkers in medulloblastoma initiation and progression has drawn extensive attention (Ramaswamy and Taylor, 2017). Li B. et al. (2019) reported that lncRNA TP73-AS1 and EIF5A2 were upregulated in medulloblastoma, while miR-494-3p was downregulated. They identify that ELF5A2 is a direct target of miR-494-3p, and knockdown of TP73-AS1 inhibits the proliferation, invasion, and migration of medulloblastoma and promotes cell apoptosis. These findings suggest that lncRNA TP73-AS1 is involved in the development of medulloblastoma as a pro-oncogene (Li B. et al., 2019). Gao et al. (2018a) found that lncRNA LOXL1-AS1 promoted the proliferation and metastasis of medulloblastoma by activating the PI3K/AKT pathway, providing evidence that knockdown of LncRNA LOXL1-AS1 might be a potential therapeutic strategy against medulloblastoma. Moreover, Zhang J. et al. (2020) identified that the expression of lncRNA HOTAIR was higher in medulloblastoma tissues and cell lines than normal samples, which promoted tumor growth, migration, invasion, and EMT by negatively regulating miR-1 and miR-206.

Primary Central Nervous System Lymphoma

PCNSL refers to the aggressive non-Hodgkin lymphoma in the brain without systemic involvement (Olson et al., 2002; van der Sanden et al., 2002). The most common type of PCNSL is diffuse large B-cell lymphoma (DLBCL), accounting for approximately

2–3% of brain tumors (Langner-Lemercier et al., 2016; Swerdlow et al., 2016; Fox et al., 2019). PCNSL poses an extraordinary challenge to oncologists and neurosurgeons because the impermeability of the BBB hinders the delivery of common chemotherapeutic drugs to the brain (Hanjin et al., 2018). Therefore, intrathecal chemotherapy (injection of chemotherapeutic agents into the CSF via lumbar puncture and delivery of chemotherapeutic agents to the CNS via the cerebrospinal circulation) is reasonable for this malignancy (Cortelazzo et al., 2017).

Recent studies have demonstrated that lncRNAs were widely involved in the biological mechanism of DLBCL by regulating of vital downstream factors through "sponge" intracellular molecules (Huang et al., 2020). For example, lncRNA MALAT1 acts as a ceRNA sponge for miR-195 to stimulate DLBCL cell proliferation and immune escape by activating the immune checkpoint molecules PD-L1 (Wang et al., 2019). LncRNA SNHG14 can act as a ceRNA sponge for miR-5590-3p to upregulate the downstream protein zinc finger E-box binding homeobox 1 (ZEB1). Meanwhile, ZEB1 inversely promotes immune escape of DLBCL cells by transcriptionally activating SNHG14 and PD-L1 (Zhao et al., 2019). SNHG12, another member of the lncRNA SNHG family, can also promote the tumorigenesis of DLCBL by stimulating miR-195 spongiosis (Chen et al., 2020).

Brain Metastases

Brain metastases refer to the malignant tumors metastasizing to the brain, which are the most common intracranial tumors in adults. Brain metastases may occur up to 10 times more frequently than primary brain tumors (Schouten et al., 2002; Barnholtz-Sloan et al., 2004; Tominaga et al., 2015). Primarily, brain metastases are located in the cerebral hemispheres (80%); the rest were found in the cerebellum and brainstem (Eichler and Loeffler, 2007; Suh et al., 2020). Common cancers causing brain metastases include lung cancer, melanoma, breast cancer, and renal cell carcinoma (Xie et al., 2014). Primary lung cancer is the most common cancer source for brain metastases (Gould, 2018). However, the mechanism underlying the metastatic procedure remains poorly understood. In the cases with multiple metastases, surgery alone usually cannot achieve local control (Mahajan et al., 2017; Churilla et al., 2019). Although whole-brain radiation therapy is acceptable, it is associated with significant cognitive decline (Chang et al., 2009). Similarly, the efficiency of systemic chemotherapy is quite limited, mainly because of the drug resistance and poor penetration through the BBB.

Shen et al. (2015) reported that lncRNA MALAT1 promoted brain metastasis by inducing epithelial-mesenchymal transition in lung cancer, while silencing MALAT1 inhibited highly invasive metastasis cancer cell migration and metastasis by inducing EMT. Furthermore, lncRNA lnc-BM is believed a prognostic indicator for intracranial metastasis patients with breast cancer. Elevated lnc-BM expression promotes STAT3-dependent ICAM1 and CCL2, which mediates communication between breast cancer cells and microenvironment immune cells (Wang et al., 2017). Although the differences in lncRNA expression profiles between primary and metastatic cancer are still controversial, this points to the possibility of distinguishing certain types of metastatic brain tumor with CSF biopsy (Tahira et al., 2011). For instance, Li and colleagues observed the upregulation of lncRNA-CCRR in CSF of metastatic brain tumor from breast cancer.

THE POTENTIAL OF CEREBROSPINAL FLUID LONG NON-CODING RNAS IN THE DIAGNOSIS AND TREATMENT OF BRAIN TUMORS

Cerebrospinal Fluid Long Non-coding RNAs as Brain Tumors Diagnostic and Prognostic Biomarkers

Clinical diagnosis of brain tumors depends on the evaluation of symptoms and signs, neuroimaging (such as CT, MRI, and PET-CT), and pathological examination of tissues as the gold standard (Di Lullo and Kriegstein, 2017). In this era of precision medicine, non-invasive neuroimaging can hardly provide the necessary molecular profiling of brain tumors or prognostic information. On the other hand, serial samples of brain tumors are difficult to obtain, and, therefore, tracking tumor progression is complex. Moreover, surgical biopsy of the brain tissue is challenging because of the tumor location and hemorrhagic risk. Alternatively, brain tumor biomarkers acquired from the body fluid, including circulating tumor cells, cell-free DNA, and exosomal ncRNAs, have drawn extensive attention to overcome these limitations (Mattox et al., 2019; Le Rhun et al., 2020).

A cancer biomarker can be a substance naturally produced by a tumor or the body's unique reaction to the presence of diseases (Ariston Gabriel et al., 2020; Simonato et al., 2021). Regarding brain tumors, the presence of BBB hinders the transport of nucleic acids and proteins and dramatically decreases the concentration of tumor biomarkers in the peripheral blood of patients (Antonetti et al., 2021). In contrast, CSF is more closely associated with brain tissue than serum and can be enriched for tumor specific biomarkers (Killer, 2013; Parnetti et al., 2019; Gaetani et al., 2020). LncRNAs in the CSF, therefore, are supposed to be potential candidates as sensitive and accurate early diagnostic and prognostic tools for various brain tumors (Latowska et al., 2020).

An increasing number of studies have evidenced the key roles of lncRNAs in regulating cell proliferation, apoptosis, GSC self-renewal, differentiation, and response to hypoxic stress of different brain tumors. A previous study by Jing et al. (2016) examined the expression of lncRNA CRNDE in 164 gliomas and neighboring non-tumor tissues. Overexpression of CRNDE was correlated with a higher WHO grade, recurrence, and tumor volume expansion in tumor tissues; therefore, elevated expression of this lncRNA may be considered a new prognostic marker in glioma. Similarly, lncRNA HOTAIR has been widely discussed regarding glioma biology. For instance, Suppressing HOTAIR expression inhibits glioma cell proliferation, migration, and invasion, which involves the PI3K/AKT signaling pathway (Ke et al., 2015). Therefore, this lncRNA could be considered a novel prognostic and diagnostic biomarker for glioblastoma (Tan

et al., 2018). Furthermore, the expression of lncRNA miR210HG was substantially upregulated in tumor tissue than adjacent normal tissue. Patients with glioma exhibited substantially higher serum miR210HG level than healthy controls, indicating this lncRNA is a potential diagnostic biomarker for glioma (Min et al., 2016). Considering the complicated biological effects and interactions of lncRNAs, the multiple-lncRNA signatures could be better diagnostic and prognostic indicators rather than single lncRNAs. Zhang et al. (2012) suggested that several lncRNAs could be used to distinguish between the stage and type of glioma. This study indicated that approximately 129 lncRNAs were differentially expressed between gliomas and normal brain tissue, demonstrating the capacity of lncRNAs in tumor stratification. Serial studies focused on medulloblastoma have also shown that a variety of lncRNAs, including CCAT1, CRNDE, Linc-NeD125, and PVT1, were associated with tumor progression (Northcott et al., 2012b; Song et al., 2016; Laneve et al., 2017; Gao et al., 2018b). Among these lncRNAs, Linc-NeD125 was overexpressed in medulloblastoma tissues compared to normal brain tissues; further studies showed that its ectopic expression promoted cell proliferation, migration, and invasion of medulloblastoma cells *in vitro* (Laneve et al., 2017). Interestingly, in a recent report from Li and colleagues, tissue expression and CSF expressions of lncRNA CCRR were both evidently upregulated in breast cancer patients with brain metastases. However, the upregulation of serum lncRNA level was not documented, indicating that CSF lncRNAs might be better biomarkers for intracranial tumors (Li D. et al., 2021). Together, the facts mentioned above indicate that CSF lncRNAs have great potential in diagnosing and predicting brain tumors and provide new approaches for the individualized treatment of patients. More information on lncRNAs as biomarkers for brain tumors is summarized in **Table 1**.

TABLE 1 | Prognostic and diagnostic LncRNA biomarkers for brain tumors.

Type of cancer	lncRNAs	Function	References
Glioma	miR210HG	Diagnosis biomarker	Min et al., 2016
	FAM225B	Prognosis biomarker	Li J. et al., 2020
	TP73-AS1	Prognosis biomarker	Mazor et al., 2019
	HOTAIR	Prognosis and diagnosis biomarker	Tan et al., 2018
	HOXA6as	Diagnosis biomarker	Kraus et al., 2015
	EGOT	Diagnosis biomarker	Wu et al., 2017
	GAS5	Diagnosis biomarker	Liu et al., 2018
	FTH1P3	Diagnosis biomarker	Zhang et al., 2018a
	ELF3-AS1	Prognostic biomarker	Mei et al., 2020
Pituitary adenoma	C5orf66-AS1	Diagnosis biomarker	Yu et al., 2017
	H19	Diagnosis biomarker	Zhang Y. et al., 2019
	CCAT2	Diagnosis biomarker	Fu et al., 2018
	RPSAP52	Diagnosis biomarker	D'Angelo et al., 2019
	MEG8	Diagnosis biomarker	Zhu et al., 2021
Medulloblastoma	TP73-AS1	Diagnosis biomarker	Li B. et al., 2019
	LOXL1-AS1	Prognostic biomarker	Gao et al., 2018a; Chen et al., 2019
	lnc-HLX-2-7	Diagnosis biomarker	Katsushima et al., 2021
Meningioma	LINC00702	Diagnosis biomarker	Li T. et al., 2019
	MEG3	Diagnosis biomarker	Ding et al., 2020

Although CSF lncRNAs is difficult to be used as a routine screening nowadays, it has exhibited several advantages. First, serial CSF lncRNAs can be acquired by lumber puncture, to monitor the progression in a micro-invasive and dynamic way. Second, CSF lncRNAs are directly secreted and confined within the CNS to eliminate the systemic factors, which helps us to understand the biology and pathophysiology of brain tumors. Third, multiple lncRNA microarray would further improve diagnostic accuracy such as sensitivity and specificity. Fourth, the lowest MRI resolution ranges in the order of millimeters, whereas the dimensions of the tumor cell are in micrometers. Such disparity in scale may lead to delay in diagnosis, which can be compromised by CSF lncRNA biopsy. Finally, lncRNA can be combined with the current neuroimage, rather than replace it. For instance, Wu et al. (2021) observed that lncRNA CASC19 promoted glioma progression by modulating the miR-454-3p/RAB5A axis, which was associated with unfavorable MRI features. Similarly, lncRNA SAMMSON overexpression help distinguishing patients with glioblastoma from diffuse neurosarcoidosis, which shares quite similar radiological features (Xie et al., 2019).

Cerebrospinal Fluid Long Non-coding RNA as Brain Tumor Therapeutic Agents

Although conventional strategies for brain tumor treatment have been shown to be promising, it remains a considerable challenge to improve the outcomes of patients. For instance, even given the multidiscipline approaches combined with surgical resection, targeted radiotherapy, high-dose chemotherapy, and novel electric field treatment, the median overall survival for glioblastoma is still less than 21 months (Tan et al., 2020). One of the major obstacles is the poor penetration of BBB. Many attempts have been made to deliver drugs efficiently through BBB (Allhenn et al., 2012), including the intrathecal administration (drug injection to the lumbar arachnoid space) and intraventricular administration (drug injection or infusion into the lateral ventricles of the brain, Calias et al., 2014). Kim et al. (2016) evaluated the efficiency of different anti-miR delivery strategies, including intratumoral, intrathecal, and intraventricular routes, in an orthotopic model of GBM. Intraventricular injection of anti-Let-7 resulted in a significant reduction in target gene expression in the whole tumor, indicating a promising approach for ncRNA therapy in brain tumors (Kim et al., 2016). More recently, Donovan et al. (2020) demonstrated that administration of chimeric antigen receptor T (CAR-T) cells into the CSF could be a highly effective therapy for multiple metastatic mouse models of medulloblastoma and PFA ependymoma. Yang et al. (2019) also reported that intrathecal injection of umbilical cord blood mesenchymal stem cells could improve the pain through lncRNA H19/microRNA-29a-3p/FOS axis. These studies suggest that CSF delivery is practical and promising approach to fight against brain tumors. Specifically, intrathecal and intraventricular administration of lncRNAs packaged by exosomes can be evaluated as novel

TABLE 2 | LncRNAs involved in the treatment of brain tumor.

Type of cancer	lncRNAs	Function	References
Glioma	MIR22HG	Inhibits glioblastoma progression through suppression of Wnt/β-catenin signaling	Han et al., 2019
	HOX	Inhibits the occurrence and progression of glioma	Yang et al., 2018
	TP73-AS1	Therapeutic target	Mazor et al., 2019
	MALAT1	Knockdown reverses chemoresistance to temozolomide via promoting microRNA-101	Cai et al., 2018
	TUSC7	Inhibits temozolomide resistance by targeting miR-10a	Shang et al., 2018
Pituitary adenoma	H19	Inhibits the growth of pituitary adenoma	Zhang Y. et al., 2019
	SNHG24	Induce osteoclast Differentiation of bone-invasive pituitary Adenomas by regulating TNFα	Zhu et al., 2018
	SNHG6	Induces EMT of pituitary adenoma via suppressing miR-944	Mao et al., 2020
	LINC01116	Boost the progression of pituitary adenoma cells via regulating miR-744-5p/HOXB8 pathway	Huang et al., 2021
	LINC00473	Overexpress in IPA and can promote PA cell proliferation	Li J. et al., 2021
	C5orf66-AS1	Plays an anticancer role and significantly Inhibits cell activity and invasiveness	Yu et al., 2017
	MEG3	As a tumor suppressor	Chunharojrith et al., 2015
Medulloblastoma	CCAT1	Promotion of cell proliferation and metastasis	Gao et al., 2018b
	NKX2-2AS	Suppression of cell proliferation Migration and invasion	Zhang et al., 2018b
	linc-NeD125	Ectopic expression of linc-NeD125 in invasive MB cells attenuated their proliferation, migration, and invasion	Laneve et al., 2017
	SPRY4-IT1	Promotion of cell proliferation and migration and invasion	Zhang et al., 2018b

therapeutics for various brain tumors. For instance, Lai et al. (2014) created a sensitive extracellular vesicle system with high stability and BBB permeability.

Generally, lncRNAs participate in the multiple aspects of tumor biology, such as proliferation, invasion, angiogenesis, treatment resistance, stemness maintenance, and immune suppression. Many ongoing studies, therefore, are designed to identify the lncRNAs with potential anti-tumor characteristics, as summarized in **Table 2**. For instance, TMZ-based chemotherapy is the fundamental treatment for patients with glioma, especially for malignant glioma. Several lncRNAs have been found to be involved in chemoresistance to TMZ in glioma cells, including lncRNA HOTAIR, H19, and MALAT1 (Jiang et al., 2016; Zhang L. et al., 2020). Recently, Lv et al. (2020) demonstrated that high expression of lncRNA DLEU1 predicted a poor prognosis. Furthermore, silencing lncRNA DLEU1 suppressed TMZ-activated autophagy and promoted the sensitivity of glioma cells to TMZ by triggering apoptosis (Lv et al., 2020). Considering the complicated epigenetic effects and interactions of lncRNAs, single lncRNA can be involved in different tumor biological functions. LncRNA LINC00174 is extensively associated with a variety of cancers, including glioblastoma and LGGs. In particular, LINC00174 facilitates glycolysis and tumor growth by regulating the miR-152-3p/SLC2A1 axis and regulates the miR-138-5p/SOX9 axis to promote chemotherapeutic resistance to temozolomide in glioma (Shi et al., 2019; Li B. et al., 2020). It also acts as an oncogene in glioblastoma via promoting proliferative phenotype (Wang Z. et al., 2020). Besides glioma, lncRNAs can be therapeutic targets in other brain cancers. For instance, knockdown of oncogenic lncRNA CRNDE inhibited tumor development in medulloblastoma cell lines, significantly decreased cell proliferation, and increased apoptosis (Song et al., 2016). Similarly, Xing et al. (2018) indicated that lncRNA LINC00460 promoted MMP-9 expression through targeting miR-539, acting as an oncogenic RNA in the meningioma malignancy and accelerating the proliferation and metastasis of meningioma. In conclusion, these studies suggest CSF lncRNAs have shown great potential as a therapeutic target, although further effort is needed before the clinical application.

CONCLUSION AND PROSPECTS

Brain tumors directly threaten the cognition, behavior, and neurologic functions of human beings. While considerable advancements in fundamental scientific research and clinical practice have shed light on brain tumor pathophysiology in the past decades, challenges remain in precise and early diagnosis. LncRNAs exert critical regulatory efforts in the development and progression of different brain tumors, including glioma, meningioma, pituitary adenoma, medulloblastoma, PCNSL, and brain metastasis. Compared to the other ncRNAs, such as miRNAs and circRNAs, the regulatory mechanisms of lncRNAs seems to be more complicated. For instance, miRNAs are small ncRNAs consisting of approximately 21–25 nucleotides, which act as regulators of gene expression by complementary binding of the 3′ untranslated regions (UTR) of targeted mRNAs, thus reducing the mRNA stability or modulating gene translation. On the contrary, lncRNA might exert epigenetic functions in a more comprehensive and complex manner (as shown in **Figure 2**), including transcriptional regulation of genes, acting as small RNA precursors and miRNA sponges, protein localization alternation, and production of endogenous siRNAs. Also, the interactions between these ncRNAs have been described, which construct a regulatory network of brain cancer. CSF biopsy represents a novel approach to monitor the pathophysiology of brain tumors in an efficient, mini-invasive, and continuous manner. Moreover, intrathecal or intraventricular administration has been demonstrated to deliver multiple drugs and therapeutic agents efficiently through

BBB. As we reviewed, CSF lncRNAs provide great promises for clinical applications, including the diagnosis and treatment of brain tumors.

Though promising, several challenges remain to be addressed. First, the trace amount of lncRNAs in the CSF brings considerable difficulties to detection and diagnosis. Nowadays, high-throughput RNA-seq technology develops rapidly, making it possible to simultaneously detect multiple tumor-specific lncRNAs to balance the sensitivity and accuracy of early diagnostics. In fact, numerous bioinformatics-based lncRNA signatures have been established with diagnostic and predictive potential. Second, the bioactivity of certain lncRNA needs to be fully elucidated due to its epigenetic effort before the clinical application. Third, directly targeting CSF lncRNAs is challenging, or even useless, because these lncRNAs are dominantly released to the CSF by tumor cells as biomarkers. To exert maximal therapeutics effort, intrathecal or intraventricular administration of therapeutic agents, such as small interfering RNA (siRNA), antisense oligonucleotide (ASO), small molecule inhibitors, or even exosome-sealed ncRNAs, should be considered to reduce the expression of tissue lncRNAs or inhibit their functions within the tumor microenvironment. Finally, CSF lncRNAs cannot be the only answer for the diagnostics and treatment of brain tumors. Synergy between lncRNAs and other oncogenic regulators has been primarily documented (Parasramka et al., 2017; Wu et al., 2020). With progressively better understanding of lncRNA regulatory mechanisms, we believe CSF lncRNAs combined with others wild become increasingly valuable agents in diagnosing and treating various brain tumors.

AUTHOR CONTRIBUTIONS

KX and SX conceived the structure of the manuscript and revised the manuscript. KX, XJ, and AAG designed and drafted the manuscript. XJ, YW, XL, and SX discussed and revised the manuscript. All authors read and approved the final manuscript.

FUNDING

This paper was funded by the National Natural Science Foundation of China (81502164), the Taishan Scholarship Young Expert Program (tsqn201909174), and the Department of Science and Technology of Shandong Province (2016GSF201055).

ACKNOWLEDGMENTS

The figures were created with BioRender.com, and we appreciate it.

REFERENCES

Alexander, B. M., and Cloughesy, T. F. (2017). Adult glioblastoma. *J. Clin. Oncol.* 35, 2402–2409. doi: 10.1200/JCO.2017.73.0119

Allhenn, D., Boushehri, M. A., and Lamprecht, A. (2012). Drug delivery strategies for the treatment of malignant gliomas. *Int. J. Pharm.* 436, 299–310. doi: 10.1016/j.ijpharm.2012.06.025

Amirjamshidi, A. (2017). A case of early extraneural medulloblastoma metastases in a young adult. *Asian J. Neurosurg.* 12:349. doi: 10.4103/1793-5482.175647

Antonetti, D. A., Silva, P. S., and Stitt, A. W. (2021). Current understanding of the molecular and cellular pathology of diabetic retinopathy. *Nat. Rev. Endocrinol.* 17, 195–206. doi: 10.1038/s41574-020-00451-4

Ariston Gabriel, A. N., Wang, F., Jiao, Q., Yvette, U., Yang, X., Al-Ameri, S. A., et al. (2020). The involvement of exosomes in the diagnosis and treatment of pancreatic cancer. *Mol. Cancer* 19:132. doi: 10.1186/s12943-020-01245-y

Attier-Zmudka, J., Sérot, J. M., Valluy, J., Saffarini, M., Macaret, A. S., Diouf, M., et al. (2019). Decreased cerebrospinal fluid flow is associated with cognitive deficit in elderly patients. *Front. Aging Neurosci.* 11:87. doi: 10.3389/fnagi.2019.00087

Banks, W. A. (2019). The blood-brain barrier as an endocrine tissue. *Nat. Rev. Endocrinol.* 15, 444–455. doi: 10.1038/s41574-019-0213-7

Barnholtz-Sloan, J. S., Sloan, A. E., Davis, F. G., Vigneau, F. D., Lai, P., and Sawaya, R. E. (2004). Incidence proportions of brain metastases in patients diagnosed (1973 to 2001) in the Metropolitan Detroit Cancer Surveillance System. *J. Clin. Oncol.* 22, 2865–2872. doi: 10.1200/JCO.2004.12.149

Barsyte-Lovejoy, D., Lau, S. K., Boutros, P. C., Khosravi, F., Jurisica, I., Andrulis, I. L., et al. (2006). The c-Myc oncogene directly induces the H19 noncoding RNA by allele-specific binding to potentiate tumorigenesis. *Cancer Res.* 66, 5330–5337. doi: 10.1158/0008-5472.CAN-06-0037

Bian, E. B., Chen, E. F., Xu, Y. D., Yang, Z. H., Tang, F., Ma, C. C., et al. (2019). Exosomal lncRNA-ATB activates astrocytes that promote glioma cell invasion. *Int. J. Oncol.* 54, 713–721. doi: 10.3892/ijo.2018.4644

Brat, D. J., Verhaak, R. G., Aldape, K. D., Yung, W. K., Salama, S. R., Cooper, L. A., et al. (2015). Comprehensive, integrative genomic analysis of diffuse lower-grade gliomas. *N. Engl. J. Med.* 372, 2481–2498. doi: 10.1056/NEJMoa1402121

Bronstein, M. D., Paraiba, D. B., and Jallad, R. S. (2011). Management of pituitary tumors in pregnancy. *Nat. Rev. Endocrinol.* 7, 301–310. doi: 10.1038/nrendo.2011.38

Cahill, J., Lobiondo-Wood, G., Bergstrom, N., and Armstrong, T. (2012). Brain tumor symptoms as antecedents to uncertainty: an integrative review. *J. Nurs. Scholarsh.* 44, 145–155. doi: 10.1111/j.1547-5069.2012.01445.x

Cai, T., Liu, Y., and Xiao, J. (2018). Long noncoding RNA MALAT1 knockdown reverses chemoresistance to temozolomide via promoting microRNA-101 in glioblastoma. *Cancer Med.* 7, 1404–1415. doi: 10.1002/cam4.1384

Calias, P., Banks, W. A., Begley, D., Scarpa, M., and Dickson, P. (2014). Intrathecal delivery of protein therapeutics to the brain: a critical reassessment. *Pharmacol. Ther.* 144, 114–122. doi: 10.1016/j.pharmthera.2014.05.009

Cao, Y., Tseng, C. L., Balter, J. M., Teng, F., Parmar, H. A., and Sahgal, A. (2017). MR-guided radiation therapy: transformative technology and its role in the central nervous system. *Neuro Oncol.* 19, ii16–ii29. doi: 10.1093/neuonc/nox006

Chang, E. L., Wefel, J. S., Hess, K. R., Allen, P. K., Lang, F. F., Kornguth, D. G., et al. (2009). Neurocognition in patients with brain metastases treated with radiosurgery or radiosurgery plus whole-brain irradiation: a randomised controlled trial. *Lancet Oncol.* 10, 1037–1044. doi: 10.1016/S1470-2045(09)70263-3

Chen, L. Y., Zhang, X. M., Han, B. Q., and Dai, H. B. (2020). Long noncoding RNA SNHG12 indicates the prognosis and accelerates tumorigenesis of diffuse large B-Cell lymphoma through sponging microR-195. *Onco Targets Ther.* 13, 5563–5574. doi: 10.2147/OTT.S249429

Chen, S., Li, W., and Guo, A. (2019). LOXL1-AS1 predicts poor prognosis and promotes cell proliferation, migration, and invasion in osteosarcoma. *Biosci. Rep.* 39:BSR20190447. doi: 10.1042/BSR20190447

Chen, W., and Qin, C. (2015). General hallmarks of microRNAs in brain evolution and development. *RNA Biol.* 12, 701–708. doi: 10.1080/15476286.2015.1048954

Chen, X., Guo, G., Lu, Y., Wang, S., Zhang, Y., and Huang, Q. (2021). Mechanisms and functions of long non-coding RNAs in glioma (Review). *Oncol. Rep.* 45:9. doi: 10.3892/or.2021.7960

Cheng, J., Meng, J., Zhu, L., and Peng, Y. (2020). Exosomal noncoding RNAs in Glioma: biological functions and potential clinical applications. *Mol. Cancer* 19:66. doi: 10.1186/s12943-020-01189-3

Chunharojrith, P., Nakayama, Y., Jiang, X., Kery, R. E., Ma, J., De La Hoz Ulloa, C. S., et al. (2015). Tumor suppression by MEG3 lncRNA in a human pituitary tumor derived cell line. *Mol. Cell. Endocrinol.* 416, 27–35. doi: 10.1016/j.mce.2015.08.018

Churilla, T. M., Chowdhury, I. H., Handorf, E., Collette, L., Collette, S., Dong, Y., et al. (2019). Comparison of local control of brain metastases with stereotactic radiosurgery vs surgical resection: a secondary analysis of a randomized clinical trial. *JAMA Oncol.* 5, 243–247. doi: 10.1001/jamaoncol.2018.4610

Cortelazzo, S., Ferreri, A., Hoelzer, D., and Ponzoni, M. (2017). Lymphoblastic lymphoma. *Crit. Rev. Oncol. Hematol.* 113, 304–317. doi: 10.1016/j.critrevonc.2017.03.020

D'Angelo, D., Mussnich, P., Sepe, R., Raia, M., Del Vecchio, L., Cappabianca, P., et al. (2019). RPSAP52 lncRNA is overexpressed in pituitary tumors and promotes cell proliferation by acting as miRNA sponge for HMGA proteins. *J. Mol. Med. (Berl.)* 97, 1019–1032. doi: 10.1007/s00109-019-01789-7

Di Lullo, E., and Kriegstein, A. R. (2017). The use of brain organoids to investigate neural development and disease. *Nat. Rev. Neurosci.* 18, 573–584. doi: 10.1038/nrn.2017.107

Ding, C., Yi, X., Xu, J., Huang, Z., Bu, X., Wang, D., et al. (2020). Long non-coding RNA MEG3 modifies cell-cycle, migration, invasion, and proliferation through AKAP12 by sponging miR-29c in meningioma cells. *Front. Oncol.* 10:537763. doi: 10.3389/fonc.2020.537763

Donovan, L. K., Delaidelli, A., Joseph, S. K., Bielamowicz, K., Fousek, K., Holgado, B. L., et al. (2020). Locoregional delivery of CAR T cells to the cerebrospinal fluid for treatment of metastatic medulloblastoma and ependymoma. *Nat. Med.* 26, 720–731. doi: 10.1038/s41591-020-0827-2

Duffau, H. (2017). A two-level model of interindividual anatomo-functional variability of the brain and its implications for neurosurgery. *Cortex* 86, 303–313. doi: 10.1016/j.cortex.2015.12.009

Dufour, C., Beaugrand, A., Pizer, B., Micheli, J., Aubelle, M. S., Fourcade, A., et al. (2012). Metastatic medulloblastoma in childhood: chang's classification revisited. *Int. J. Surg. Oncol.* 2012:245385. doi: 10.1155/2012/245385

Eichler, A. F., and Loeffler, J. S. (2007). Multidisciplinary management of brain metastases. *Oncologist* 12, 884–898. doi: 10.1634/theoncologist.12-7-884

Fox, C. P., Phillips, E. H., Smith, J., Linton, K., Gallop-Evans, E., Hemmaway, C., et al. (2019). Guidelines for the diagnosis and management of primary central nervous system diffuse large B-cell lymphoma. *Br. J. Haematol.* 184, 348–363. doi: 10.1111/bjh.15661

Franz, D. N., Belousova, E., Sparagana, S., Bebin, E. M., Frost, M., Kuperman, R., et al. (2014). Everolimus for subependymal giant cell astrocytoma in patients with tuberous sclerosis complex: 2-year open-label extension of the randomised EXIST-1 study. *Lancet Oncol.* 15, 1513–1520. doi: 10.1016/S1470-2045(14)70489-9

Franz, D. N., Belousova, E., Sparagana, S., Bebin, E. M., Frost, M., Kuperman, R., et al. (2013). Efficacy and safety of everolimus for subependymal giant cell astrocytomas associated with tuberous sclerosis complex (EXIST-1): a multicentre, randomised, placebo-controlled phase 3 trial. *Lancet* 381, 125–132. doi: 10.1016/S0140-6736(12)61134-9

Fu, D., Zhang, Y., and Cui, H. (2018). Long noncoding RNA CCAT2 is activated by E2F1 and exerts oncogenic properties by interacting with PTTG1 in pituitary adenomas. *Am. J. Cancer Res.* 8, 245–255.

Gaetani, L., Paolini Paoletti, F., Bellomo, G., Mancini, A., Simoni, S., Di Filippo, M., et al. (2020). CSF and blood biomarkers in neuroinflammatory and neurodegenerative diseases: implications for treatment. *Trends Pharmacol. Sci.* 41, 1023–1037. doi: 10.1016/j.tips.2020.09.011

Galldiks, N., Albert, N. L., Sommerauer, M., Grosu, A. L., Ganswindt, U., Law, I., et al. (2017). PET imaging in patients with meningioma-report of the RANO/PET Group. *Neuro Oncol.* 19, 1576–1587. doi: 10.1093/neuonc/nox112

Gao, R., Zhang, R., Zhang, C., Liang, Y., and Tang, W. (2018a). LncRNA LOXL1-AS1 promotes the proliferation and metastasis of medulloblastoma by activating the PI3K/AKT pathway. *Anal. Cell. Pathol. (Amst.)* 2018:9275685. doi: 10.1155/2018/9275685

Gao, R., Zhang, R., Zhang, C., Zhao, L., and Zhang, Y. (2018b). Long noncoding RNA CCAT1 promotes cell proliferation and metastasis in human medulloblastoma via MAPK pathway. *Tumori* 104, 43–50. doi: 10.5301/tj.5000662

Gerlinger, M., Rowan, A. J., Horswell, S., Math, M., Larkin, J., Endesfelder, D., et al. (2012). Intratumor heterogeneity and branched evolution revealed by multiregion sequencing. *N. Engl. J. Med.* 366, 883–892. doi: 10.1056/NEJMoa1113205

Ghafouri-Fard, S., and Taheri, M. (2019). Maternally expressed gene 3 (MEG3): a tumor suppressor long non coding RNA. *Biomed. Pharmacother.* 118:109129. doi: 10.1016/j.biopha.2019.109129

Gould, J. (2018). Breaking down the epidemiology of brain cancer. *Nature* 561, S40–S41. doi: 10.1038/d41586-018-06704-7

Gusyatiner, O., and Hegi, M. E. (2018). Glioma epigenetics: from subclassification to novel treatment options. *Semin. Cancer Biol.* 51, 50–58. doi: 10.1016/j.semcancer.2017.11.010

Hadidchi, S., Surento, W., Lerner, A., Liu, C. J., Gibbs, W. N., Kim, P. E., et al. (2019). Headache and Brain Tumor. *Neuroimaging Clin. N. Am.* 29, 291–300. doi: 10.1016/j.nic.2019.01.008

Han, M., Wang, S., Fritah, S., Wang, X., Zhou, W., Yang, N., et al. (2019). Interfering with long non-coding RNA MIR22HG processing inhibits glioblastoma progression through suppression of Wnt/β-catenin signalling. *Brain* 143, 512–530. doi: 10.1093/brain/awz406

Han, M., Wang, S., Fritah, S., Wang, X., Zhou, W., Yang, N., et al. (2020). Interfering with long non-coding RNA MIR22HG processing inhibits glioblastoma progression through suppression of Wnt/β-catenin signalling. *Brain* 143, 512–530.

Han, Y., Wu, Z., Wu, T., Huang, Y., Cheng, Z., Li, X., et al. (2016). Tumor-suppressive function of long noncoding RNA MALAT1 in glioma cells by downregulation of MMP2 and inactivation of ERK/MAPK signaling. *Cell Death Dis.* 7:e2123. doi: 10.1038/cddis.2015.407

Hanan, M., Soreq, H., and Kadener, S. (2017). CircRNAs in the brain. *RNA Biol.* 14, 1028–1034. doi: 10.1080/15476286.2016.1255398

Hanjin, C., Tao, L., Pengfei, L., Ali, Y., Huajun, Z., Jiekun, L., et al. (2018). Altered long noncoding RNA and messenger RNA expression in experimental intracerebral hemorrhage - a preliminary study. *Cell. Physiol. Biochem.* 45, 1284–1301. doi: 10.1159/000487464

Hawrylycz, M. J., Lein, E. S., Guillozet-Bongaarts, A. L., Shen, E. H., Ng, L., Miller, J. A., et al. (2012). An anatomically comprehensive atlas of the adult human brain transcriptome. *Nature* 489, 391–399. doi: 10.1038/nature11405

Hodges, T. R., Ott, M., Xiu, J., Gatalica, Z., Swensen, J., Zhou, S., et al. (2017). Mutational burden, immune checkpoint expression, and mismatch repair in glioma: implications for immune checkpoint immunotherapy. *Neuro Oncol.* 19, 1047–1057. doi: 10.1093/neuonc/nox026

Holmes, D. (2016). Pituitary gland: sex difference in comorbidity burden associated with nonfunctioning pituitary adenomas. *Nat. Rev. Endocrinol.* 12:374. doi: 10.1038/nrendo.2016.82

Horbinski, C., Ligon, K. L., Brastianos, P., Huse, J. T., Venere, M., Chang, S., et al. (2019). The medical necessity of advanced molecular testing in the diagnosis and treatment of brain tumor patients. *Neuro Oncol.* 21, 1498–1508. doi: 10.1093/neuonc/noz119

Huang, R. Y., Bi, W. L., Griffith, B., Kaufmann, T. J., La Fougère, C., Schmidt, N. O., et al. (2019). Imaging and diagnostic advances for intracranial meningiomas. *Neuro Oncol.* 21, i44–i61. doi: 10.1093/neuonc/noy143

Huang, T., Cai, M., Chen, C., Ling, C., Zhang, B., Zheng, W., et al. (2021). LINC01116 boosts the progression of pituitary adenoma via regulating miR-744-5p/HOXB8 pathway. *Mol. Cell. Endocrinol.* 536:111350. doi: 10.1016/j.mce.2021.111350

Huang, X., Qian, W., and Ye, X. (2020). Long noncoding RNAs in diffuse large B-cell lymphoma: current advances and perspectives. *Onco Targets Ther.* 13, 4295–4303. doi: 10.2147/OTT.S253330

Jeon, M. T., Kim, K. S., Kim, E. S., Lee, S., Kim, J., Hoe, H. S., et al. (2021). Emerging pathogenic role of peripheral blood factors following BBB disruption in neurodegenerative disease. *Ageing Res. Rev.* 68:101333. doi: 10.1016/j.arr.2021.101333

Jiang, P., Wang, P., Sun, X., Yuan, Z., Zhan, R., Ma, X., et al. (2016). Knockdown of long noncoding RNA H19 sensitizes human glioma cells to temozolomide therapy. *Onco Targets Ther.* 9, 3501–3509. doi: 10.2147/OTT.S96278

Jing, S. Y., Lu, Y. Y., Yang, J. K., Deng, W. Y., Zhou, Q., and Jiao, B. H. (2016). Expression of long non-coding RNA CRNDE in glioma and its correlation

with tumor progression and patient survival. *Eur. Rev. Med. Pharmacol. Sci.* 20, 3992–3996.

Johanson, C. E., Duncan, J. A. III, Klinge, P. M., Brinker, T., Stopa, E. G., and Silverberg, G. D. (2008). Multiplicity of cerebrospinal fluid functions: new challenges in health and disease. *Cerebrospinal Fluid Res.* 5:10. doi: 10.1186/1743-8454-5-10

Kang, H. J., Kawasawa, Y. I., Cheng, F., Zhu, Y., Xu, X., Li, M., et al. (2011). Spatio-temporal transcriptome of the human brain. *Nature* 478, 483–489. doi: 10.1038/nature10523

Katsushima, K., Lee, B., Kunhiraman, H., Zhong, C., Murad, R., Yin, J., et al. (2021). The long noncoding RNA lnc-HLX-2-7 is oncogenic in Group 3 medulloblastomas. *Neuro Oncol.* 23, 572–585. doi: 10.1093/neuonc/noaa235

Ke, J., Yao, Y. L., Zheng, J., Wang, P., Liu, Y. H., Ma, J., et al. (2015). Knockdown of long non-coding RNA HOTAIR inhibits malignant biological behaviors of human glioma cells via modulation of miR-326. *Oncotarget* 6, 21934–21949. doi: 10.18632/oncotarget.4290

Killer, H. E. (2013). Production and circulation of cerebrospinal fluid with respect to the subarachnoid space of the optic nerve. *J. Glaucoma* 22(Suppl. 5), S8–S10. doi: 10.1097/IJG.0b013e318293498b

Kim, D. G., Kim, K. H., Seo, Y. J., Yang, H., Marcusson, E. G., Son, E., et al. (2016). Anti-miR delivery strategies to bypass the blood-brain barrier in glioblastoma therapy. *Oncotarget* 7, 29400–29411. doi: 10.18632/oncotarget.8837

Kraus, T. F., Greiner, A., Guibourt, V., Lisec, K., and Kretzschmar, H. A. (2015). Identification of stably expressed lncRNAs as valid endogenous controls for profiling of human glioma. *J. Cancer* 6, 111–119. doi: 10.7150/jca.10867

Kristensen, B. W., Priesterbach-Ackley, L. P., Petersen, J. K., and Wesseling, P. (2019). Molecular pathology of tumors of the central nervous system. *Ann. Oncol.* 30, 1265–1278. doi: 10.1093/annonc/mdz164

Lai, C. P., Mardini, O., Ericsson, M., Prabhakar, S., Maguire, C., Chen, J. W., et al. (2014). Dynamic biodistribution of extracellular vesicles in vivo using a multimodal imaging reporter. *ACS Nano* 8, 483–494. doi: 10.1021/nn404945r

Laneve, P., Po, A., Favia, A., Legnini, I., Alfano, V., Rea, J., et al. (2017). The long noncoding RNA linc-NeD125 controls the expression of medulloblastoma driver genes by microRNA sponge activity. *Oncotarget* 8, 31003–31015. doi: 10.18632/oncotarget.16049

Langner-Lemercier, S., Houillier, C., Soussain, C., Ghesquières, H., Chinot, O., Taillandier, L., et al. (2016). Primary CNS lymphoma at first relapse/progression: characteristics, management, and outcome of 256 patients from the French LOC network. *Neuro Oncol.* 18, 1297–1303. doi: 10.1093/neuonc/now033

Latowska, J., Grabowska, A., Zarębska, Ż, Kuczyński, K., Kuczyńska, B., and Rolle, K. (2020). Non-coding RNAs in brain tumors, the contribution of lncRNAs, circRNAs, and snoRNAs to cancer development-their diagnostic and therapeutic potential. *Int. J. Mol. Sci.* 21:7001. doi: 10.3390/ijms21197001

Laudicella, R., Quartuccio, N., Argiroffi, G., Alongi, P., Baratto, L., Califaretti, E., et al. (2021). Unconventional non-amino acidic PET radiotracers for molecular imaging in gliomas. *Eur. J. Nucl. Med. Mol. Imaging* doi: 10.1007/s00259-021-05352-w

Le Rhun, E., Seoane, J., Salzet, M., Soffietti, R., and Weller, M. (2020). Liquid biopsies for diagnosing and monitoring primary tumors of the central nervous system. *Cancer Lett.* 480, 24–28. doi: 10.1016/j.canlet.2020.03.021

Lebanony, D., Benjamin, H., Gilad, S., Ezagouri, M., Dov, A., Ashkenazi, K., et al. (2009). Diagnostic assay based on hsa-miR-205 expression distinguishes squamous from nonsquamous non-small-cell lung carcinoma. *J. Clin. Oncol.* 27, 2030–2037. doi: 10.1200/JCO.2008.19.4134

Li, B., Shen, M., Yao, H., Chen, X., and Xiao, Z. (2019). Long noncoding RNA TP73-AS1 modulates medulloblastoma progression in vitro and in vivo by sponging miR-494-3p and targeting EIF5A2. *Onco Targets Ther.* 12, 9873–9885. doi: 10.2147/OTT.S228305

Li, B., Zhao, H., Song, J., Wang, F., and Chen, M. (2020). LINC00174 down-regulation decreases chemoresistance to temozolomide in human glioma cells by regulating miR-138-5p/SOX9 axis. *Hum. Cell* 33, 159–174. doi: 10.1007/s13577-019-00281-1

Li, D., Li, L., Chen, X., Zhou, C., Hao, B., and Cao, Y. (2021). Dysregulation of lncRNA-CCRR contributes to brain metastasis of breast cancer by intercellular coupling via regulating connexin 43 expression. *J. Cell. Mol. Med.* 25, 4826–4834. doi: 10.1111/jcmm.16455

Li, J., Qian, Y., Zhang, C., Wang, W., Qiao, Y., Song, H., et al. (2021). LncRNA LINC00473 is involved in the progression of invasive pituitary adenoma by upregulating KMT5A via ceRNA-mediated miR-502-3p evasion. *Cell Death Dis.* 12:580. doi: 10.1038/s41419-021-03861-y

Li, J., Zhang, Q., Ge, P., Zeng, C., Lin, F., Wang, W., et al. (2020). FAM225B Is a Prognostic lncRNA for Patients with Recurrent Glioblastoma. *Dis. Markers* 2020:8888085. doi: 10.1155/2020/8888085

Li, T., Ren, J., Ma, J., Wu, J., Zhang, R., Yuan, H., et al. (2019). LINC00702/miR-4652-3p/ZEB1 axis promotes the progression of malignant meningioma through activating Wnt/β-catenin pathway. *Biomed. Pharmacother.* 113:108718. doi: 10.1016/j.biopha.2019.108718

Li, W., Jiang, P., Sun, X., Xu, S., Ma, X., and Zhan, R. (2016). Suppressing H19 modulates tumorigenicity and stemness in U251 and U87MG glioma cells. *Cell. Mol. Neurobiol.* 36, 1219–1227. doi: 10.1007/s10571-015-0320-5

Li, X., Sun, L., Wang, X., Wang, N., Xu, K., Jiang, X., et al. (2021). A five immune-related lncRNA signature as a prognostic target for glioblastoma. *Front. Mol. Biosci.* 8:632837. doi: 10.3389/fmolb.2021.632837

Liu, Q., Yu, W., Zhu, S., Cheng, K., Xu, H., Lv, Y., et al. (2018). Long noncoding RNA GAS5 regulates the proliferation, migration, and invasion of glioma cells by negatively regulating miR-18a-5p. *J. Cell. Physiol.* 234, 757–768. doi: 10.1002/jcp.26889

López Vázquez, M., Du, W., Kanaya, N., Kitamura, Y., and Shah, K. (2021). Next-Generation immunotherapies for brain metastatic cancers. *Trends Cancer* 7, 809–822. doi: 10.1016/j.trecan.2021.02.003

Louis, D. N., Ohgaki, H., Wiestler, O. D., Cavenee, W. K., Burger, P. C., Jouvet, A., et al. (2007). The 2007 WHO classification of tumours of the central nervous system. *Acta Neuropathol.* 114, 97–109. doi: 10.1007/s00401-007-0243-4

Louis, D. N., Perry, A., Reifenberger, G., Von Deimling, A., Figarella-Branger, D., Cavenee, W. K., et al. (2016). The 2016 world health organization classification of tumors of the central nervous system: a summary. *Acta Neuropathol.* 131, 803–820. doi: 10.1007/s00401-016-1545-1

Louis, D. N., Perry, A., Wesseling, P., Brat, D. J., Cree, I. A., Figarella-Branger, D., et al. (2021). The 2021 WHO classification of tumors of the central nervous system: a summary. *Neuro Oncol.* 23, 1231–1251. doi: 10.1093/neuonc/noab106

Lu, C., Wei, Y., Wang, X., Zhang, Z., Yin, J., Li, W., et al. (2020). DNA-methylation-mediated activating of lncRNA SNHG12 promotes temozolomide resistance in glioblastoma. *Mol. Cancer* 19:28. doi: 10.1186/s12943-020-1137-5

Lundborg, C., Hahn-Zoric, M., Biber, B., and Hansson, E. (2010). Glial cell line-derived neurotrophic factor is increased in cerebrospinal fluid but decreased in blood during long-term pain. *J. Neuroimmunol.* 220, 108–113. doi: 10.1016/j.jneuroim.2010.01.007

Lv, Q. L., Wang, L. C., Li, D. C., Lin, Q. X., Shen, X. L., Liu, H. Y., et al. (2020). Knockdown lncRNA DLEU1 inhibits gliomas progression and promotes temozolomide chemosensitivity by regulating autophagy. *Front. Pharmacol.* 11:560543. doi: 10.3389/fphar.2020.560543

Ma, X., Li, Z., Li, T., Zhu, L., Li, Z., and Tian, N. (2017). Long non-coding RNA HOTAIR enhances angiogenesis by induction of VEGFA expression in glioma cells and transmission to endothelial cells via glioma cell derived-extracellular vesicles. *Am. J. Transl. Res.* 9, 5012–5021.

Mahajan, A., Ahmed, S., Mcaleer, M. F., Weinberg, J. S., Li, J., Brown, P., et al. (2017). Post-operative stereotactic radiosurgery versus observation for completely resected brain metastases: a single-centre, randomised, controlled, phase 3 trial. *Lancet Oncol.* 18, 1040–1048. doi: 10.1016/S1470-2045(17)30414-X

Mao, D., Jie, Y., and Lv, Y. (2020). LncRNA SNHG6 induces epithelial-mesenchymal transition of pituitary adenoma via suppressing MiR-944. *Cancer Biother. Radiopharm.* doi: 10.1089/cbr.2020.3587

Martínez-Glez, V., Alvarez, L., Franco-Hernández, C., Torres-Martin, M., De Campos, J. M., Isla, A., et al. (2010). Genomic deletions at 1p and 14q are associated with an abnormal cDNA microarray gene expression pattern in meningiomas but not in schwannomas. *Cancer Genet. Cytogenet.* 196, 1–6. doi: 10.1016/j.cancergencyto.2009.08.003

Martinez-Rios, C., Mcandrews, M. P., Logan, W., Krings, T., Lee, D., and Widjaja, E. (2016). MRI in the evaluation of localization-related epilepsy. *J. Magn. Reson. Imaging* 44, 12–22. doi: 10.1002/jmri.25269

Mattox, A. K., Yan, H., and Bettegowda, C. (2019). The potential of cerebrospinal fluid-based liquid biopsy approaches in CNS tumors. *Neuro Oncol.* 21, 1509–1518. doi: 10.1093/neuonc/noz156

Mazor, G., Levin, L., Picard, D., Ahmadov, U., Carén, H., Borkhardt, A., et al. (2019). The lncRNA TP73-AS1 is linked to aggressiveness in glioblastoma and promotes temozolomide resistance in glioblastoma cancer stem cells. *Cell Death Dis.* 10:246. doi: 10.1038/s41419-019-1477-5

Mei, J.-C., Yan, G., and Mei, S.-Q. (2020). Diagnostic and prognostic potentials of long noncoding RNA ELF3-AS1 in glioma patients. *Dis. Markers* 2020:8871746. doi: 10.1155/2020/8871746

Millard, N. E., and De Braganca, K. C. (2016). Medulloblastoma. *J. Child Neurol.* 31, 1341–1353. doi: 10.1177/0883073815600866

Min, W., Dai, D., Wang, J., Zhang, D., Zhang, Y., Han, G., et al. (2016). Long noncoding RNA miR210HG as a potential biomarker for the diagnosis of glioma. *PLoS One* 11:e0160451. doi: 10.1371/journal.pone.0160451

Nevel, K. S., Wilcox, J. A., Robell, L. J., and Umemura, Y. (2018). The utility of liquid biopsy in central nervous system malignancies. *Curr. Oncol. Rep.* 20:60. doi: 10.1007/s11912-018-0706-x

Northcott, P. A., Buchhalter, I., Morrissy, A. S., Hovestadt, V., Weischenfeldt, J., Ehrenberger, T., et al. (2017). The whole-genome landscape of medulloblastoma subtypes. *Nature* 547, 311–317. doi: 10.1038/nature22973

Northcott, P. A., Jones, D. T., Kool, M., Robinson, G. W., Gilbertson, R. J., Cho, Y. J., et al. (2012a). Medulloblastomics: the end of the beginning. *Nat. Rev. Cancer* 12, 818–834. doi: 10.1038/nrc3410

Northcott, P. A., Shih, D. J., Peacock, J., Garzia, L., Morrissy, A. S., Zichner, T., et al. (2012b). Subgroup-specific structural variation across 1,000 medulloblastoma genomes. *Nature* 488, 49–56.

Olson, J. E., Janney, C. A., Rao, R. D., Cerhan, J. R., Kurtin, P. J., Schiff, D., et al. (2002). The continuing increase in the incidence of primary central nervous system non-Hodgkin lymphoma: a surveillance, epidemiology, and end results analysis. *Cancer* 95, 1504–1510. doi: 10.1002/cncr.10851

Orešković, D. (2015). The controversy on choroid plexus function in cerebrospinal fluid production in humans: how long different views could be neglected? *Croat. Med. J.* 56, 306–310. doi: 10.3325/cmj.2015.56.306

Ostrom, Q. T., Cioffi, G., Gittleman, H., Patil, N., Waite, K., Kruchko, C., et al. (2019). CBTRUS statistical report: primary brain and other central nervous system tumors diagnosed in the United States in 2012-2016. *Neuro Oncol.* 21, v1–v100. doi: 10.1093/neuonc/noz150

Ostrom, Q. T., Gittleman, H., Liao, P., Vecchione-Koval, T., Wolinsky, Y., Kruchko, C., et al. (2017). CBTRUS Statistical Report: primary brain and other central nervous system tumors diagnosed in the United States in 2010-2014. *Neuro Oncol.* 19, v1–v88. doi: 10.1093/neuonc/nox158

Ostrom, Q. T., Gittleman, H., Xu, J., Kromer, C., Wolinsky, Y., Kruchko, C., et al. (2016). CBTRUS statistical report: primary brain and other central nervous system tumors diagnosed in the United States in 2009-2013. *Neuro Oncol.* 18, v1–v75. doi: 10.1093/neuonc/now207

Ostrom, Q. T., Patil, N., Cioffi, G., Waite, K., Kruchko, C., and Barnholtz-Sloan, J. S. (2020). CBTRUS statistical report: primary brain and other central nervous system tumors diagnosed in the United States in 2013-2017. *Neuro Oncol.* 22, iv1–iv96. doi: 10.1093/neuonc/noaa200

Pan, C. Y., Tian, M., Zhang, L. L., Tian, D., Wang, L. Y., Sun, Y. J., et al. (2020). lncRNA signature for predicting cerebral vasospasm in patients with SAH: implications for precision neurosurgery. *Mol. Ther. Nucleic Acids* 21, 983–990. doi: 10.1016/j.omtn.2020.07.028

Pandit, R., Chen, L., and Götz, J. (2020). The blood-brain barrier: physiology and strategies for drug delivery. *Adv. Drug Deliv. Rev.* 165-166, 1–14. doi: 10.1016/j.addr.2019.11.009

Parasramka, M., Yan, I. K., Wang, X., Nguyen, P., Matsuda, A., Maji, S., et al. (2017). BAP1 dependent expression of long non-coding RNA NEAT-1 contributes to sensitivity to gemcitabine in cholangiocarcinoma. *Mol. Cancer* 16:22. doi: 10.1186/s12943-017-0587-x

Parnetti, L., Gaetani, L., Eusebi, P., Paciotti, S., Hansson, O., El-Agnaf, O., et al. (2019). CSF and blood biomarkers for Parkinson's disease. *Lancet Neurol.* 18, 573–586. doi: 10.1016/S1474-4422(19)30024-9

Pietsch, T., Wohlers, I., Goschzik, T., Dreschmann, V., Denkhaus, D., Dörner, E., et al. (2014). Supratentorial ependymomas of childhood carry C11orf95-RELA fusions leading to pathological activation of the NF-κB signaling pathway. *Acta Neuropathol.* 127, 609–611. doi: 10.1007/s00401-014-1264-4

Pottoo, F. H., Javed, M. N., Rahman, J. U., Abu-Izneid, T., and Khan, F. A. (2021). Targeted delivery of miRNA based therapeuticals in the clinical management of Glioblastoma Multiforme. *Semin. Cancer Biol.* 69, 391–398. doi: 10.1016/j.semcancer.2020.04.001

Proulx, S. T. (2021). Cerebrospinal fluid outflow: a review of the historical and contemporary evidence for arachnoid villi, perineural routes, and dural lymphatics. *Cell. Mol. Life Sci.* 78, 2429–2457. doi: 10.1007/s00018-020-03706-5

Ramanathan, M., Porter, D. F., and Khavari, P. A. (2019). Methods to study RNA-protein interactions. *Nat. Methods* 16, 225–234. doi: 10.1038/s41592-019-0330-1

Ramaswamy, V., and Taylor, M. D. (2017). Medulloblastoma: from myth to molecular. *J. Clin. Oncol.* 35, 2355–2363. doi: 10.1200/JCO.2017.72.7842

Rankin-Turner, S., Vader, P., O'driscoll, L., Giebel, B., Heaney, L. M., and Davies, O. G. (2021). A call for the standardised reporting of factors affecting the exogenous loading of extracellular vesicles with therapeutic cargos. *Adv. Drug Deliv. Rev.* 173, 479–491. doi: 10.1016/j.addr.2021.04.012

Raposo, G., and Stahl, P. D. (2019). Extracellular vesicles: a new communication paradigm? *Nat. Rev. Mol. Cell Biol.* 20, 509–510. doi: 10.1038/s41580-019-0158-7

Rastogi, S., Sharma, V., Bharti, P. S., Rani, K., Modi, G. P., Nikolajeff, F., et al. (2021). The evolving landscape of exosomes in neurodegenerative diseases: exosomes characteristics and a promising role in early diagnosis. *Int. J. Mol. Sci.* 22:440. doi: 10.3390/ijms22010440

Reddy, S., Tatiparti, K., Sau, S., and Iyer, A. K. (2021). Recent advances in nano delivery systems for blood-brain barrier (BBB) penetration and targeting of brain tumors. *Drug Discov. Today* 26, 1944–1952. doi: 10.1016/j.drudis.2021.04.008

Rodríguez-Lorenzo, S., Ferreira Francisco, D. M., Vos, R., Van Het Hof, B., Rijnsburger, M., Schroten, H., et al. (2020). Altered secretory and neuroprotective function of the choroid plexus in progressive multiple sclerosis. *Acta Neuropathol. Commun.* 8:35. doi: 10.1186/s40478-020-00903-y

Rohringer, M., Sutherland, G. R., Louw, D. F., and Sima, A. A. (1989). Incidence and clinicopathological features of meningioma. *J. Neurosurg.* 71, 665–672. doi: 10.3171/jns.1989.71.5.0665

Romani, M., Pistillo, M. P., and Banelli, B. (2018). Epigenetic targeting of glioblastoma. *Front. Oncol.* 8:448. doi: 10.3389/fonc.2018.00448

Rubio-Perez, C., Planas-Rigol, E., Trincado, J. L., Bonfill-Teixidor, E., Arias, A., Marchese, D., et al. (2021). Immune cell profiling of the cerebrospinal fluid enables the characterization of the brain metastasis microenvironment. *Nat. Commun.* 12:1503. doi: 10.1038/s41467-021-21789-x

Sakka, L., Coll, G., and Chazal, J. (2011). Anatomy and physiology of cerebrospinal fluid. *Eur. Ann. Otorhinolaryngol. Head Neck Dis.* 128, 309–316. doi: 10.1016/j.anorl.2011.03.002

Sawaya, R., Hammoud, M., Schoppa, D., Hess, K. R., Wu, S. Z., Shi, W. M., et al. (1998). Neurosurgical outcomes in a modern series of 400 craniotomies for treatment of parenchymal tumors. *Neurosurgery* 42, 1044–1055; discussion 1055-1046. doi: 10.1097/00006123-199805000-00054

Schouten, L. J., Rutten, J., Huveneers, H. A., and Twijnstra, A. (2002). Incidence of brain metastases in a cohort of patients with carcinoma of the breast, colon, kidney, and lung and melanoma. *Cancer* 94, 2698–2705. doi: 10.1002/cncr.10541

Seo, S., Kim, H., Sung, J. H., Choi, N., Lee, K., and Kim, H. N. (2020). Microphysiological systems for recapitulating physiology and function of blood-brain barrier. *Biomaterials* 232:119732. doi: 10.1016/j.biomaterials.2019.119732

Shang, C., Tang, W., Pan, C., Hu, X., and Hong, Y. (2018). Long non-coding RNA TUSC7 inhibits temozolomide resistance by targeting miR-10a in glioblastoma. *Cancer Chemother. Pharmacol.* 81, 671–678. doi: 10.1007/s00280-018-3522-y

Shen, L., Chen, L., Wang, Y., Jiang, X., Xia, H., and Zhuang, Z. (2015). Long noncoding RNA MALAT1 promotes brain metastasis by inducing epithelial-mesenchymal transition in lung cancer. *J. Neurooncol.* 121, 101–108. doi: 10.1007/s11060-014-1613-0

Shi, J., Zhang, Y., Qin, B., Wang, Y., and Zhu, X. (2019). Long non-coding RNA LINC00174 promotes glycolysis and tumor progression by regulating miR-152-3p/SLC2A1 axis in glioma. *J. Exp. Clin. Cancer Res.* 38:395. doi: 10.1186/s13046-019-1390-x

Shi, Y., Wang, Y., Luan, W., Wang, P., Tao, T., Zhang, J., et al. (2014). Long non-coding RNA H19 promotes glioma cell invasion by deriving miR-675. *PLoS One* 9:e86295. doi: 10.1371/journal.pone.0086295

Siegel, R. L., Miller, K. D., and Jemal, A. (2017). Cancer statistics, 2017. *CA Cancer J. Clin.* 67, 7–30. doi: 10.3322/caac.21387

Simon, M., Von Deimling, A., Larson, J. J., Wellenreuther, R., Kaskel, P., Waha, A., et al. (1995). Allelic losses on chromosomes 14, 10, and 1 in atypical and malignant meningiomas: a genetic model of meningioma progression. *Cancer Res.* 55, 4696–4701.

Simonato, M., Agoston, D. V., Brooks-Kayal, A., Dulla, C., Fureman, B., Henshall, D. C., et al. (2021). Identification of clinically relevant biomarkers of epileptogenesis - a strategic roadmap. *Nat. Rev. Neurol.* 17, 231–242. doi: 10.1038/s41582-021-00461-4

Song, H., Han, L., Gao, Q., and Sun, Y. (2016). Long non-coding RNA CRNDE promotes tumor growth in medulloblastoma. *Eur. Rev. Med. Pharmacol. Sci.* 20, 2588–2597.

Sprowls, S. A., Arsiwala, T. A., Bumgarner, J. R., Shah, N., Lateef, S. S., Kielkowski, B. N., et al. (2019). Improving CNS delivery to brain metastases by blood-tumor barrier disruption. *Trends Cancer* 5, 495–505. doi: 10.1016/j.trecan.2019.06.003

Suh, J. H., Kotecha, R., Chao, S. T., Ahluwalia, M. S., Sahgal, A., and Chang, E. L. (2020). Current approaches to the management of brain metastases. *Nat. Rev. Clin. Oncol.* 17, 279–299. doi: 10.1038/s41571-019-0320-3

Sullivan, R., Maresh, G., Zhang, X., Salomon, C., Hooper, J., Margolin, D., et al. (2017). The emerging roles of extracellular vesicles as communication vehicles within the tumor microenvironment and beyond. *Front. Endocrinol. (Lausanne)* 8:194. doi: 10.3389/fendo.2017.00194

Sweeney, M. D., Zhao, Z., Montagne, A., Nelson, A. R., and Zlokovic, B. V. (2019). Blood-Brain barrier: from physiology to disease and back. *Physiol. Rev.* 99, 21–78. doi: 10.1152/physrev.00050.2017

Swerdlow, S. H., Campo, E., Pileri, S. A., Harris, N. L., Stein, H., Siebert, R., et al. (2016). The 2016 revision of the World Health Organization classification of lymphoid neoplasms. *Blood* 127, 2375–2390. doi: 10.1182/blood-2016-01-643569

Tahira, A. C., Kubrusly, M. S., Faria, M. F., Dazzani, B., Fonseca, R. S., Maracaja-Coutinho, V., et al. (2011). Long noncoding intronic RNAs are differentially expressed in primary and metastatic pancreatic cancer. *Mol. Cancer* 10:141. doi: 10.1186/1476-4598-10-141

Tan, A. C., Ashley, D. M., López, G. Y., Malinzak, M., Friedman, H. S., and Khasraw, M. (2020). Management of glioblastoma: state of the art and future directions. *CA Cancer J. Clin.* 70, 299–312. doi: 10.3322/caac.21613

Tan, S. K., Pastori, C., Penas, C., Komotar, R. J., Ivan, M. E., Wahlestedt, C., et al. (2018). Serum long noncoding RNA HOTAIR as a novel diagnostic and prognostic biomarker in glioblastoma multiforme. *Mol. Cancer* 17:74. doi: 10.1186/s12943-018-0822-0

Taylor, M. D., Northcott, P. A., Korshunov, A., Remke, M., Cho, Y. J., Clifford, S. C., et al. (2012). Molecular subgroups of medulloblastoma: the current consensus. *Acta Neuropathol.* 123, 465–472. doi: 10.1007/s00401-011-0922-z

Teplyuk, N. M., Mollenhauer, B., Gabriely, G., Giese, A., Kim, E., Smolsky, M., et al. (2012). MicroRNAs in cerebrospinal fluid identify glioblastoma and metastatic brain cancers and reflect disease activity. *Neuro Oncol.* 14, 689–700. doi: 10.1093/neuonc/nos074

Tian, Y., Zheng, Y., and Dong, X. (2019). AGAP2-AS1 serves as an oncogenic lncRNA and prognostic biomarker in glioblastoma multiforme. *J. Cell. Biochem.* 120, 9056–9062. doi: 10.1002/jcb.28180

Tominaga, N., Kosaka, N., Ono, M., Katsuda, T., Yoshioka, Y., Tamura, K., et al. (2015). Brain metastatic cancer cells release microRNA-181c-containing extracellular vesicles capable of destructing blood-brain barrier. *Nat. Commun.* 6:6716. doi: 10.1038/ncomms7716

Torres-Bayona, S., Aldaz, P., Auzmendi-Iriarte, J., Saenz-Antoñanzas, A., Garcia, I., Arrazola, M., et al. (2018). PR-LncRNA signature regulates glioma cell activity through expression of SOX factors. *Sci. Rep.* 8:12746. doi: 10.1038/s41598-018-30836-5

Tumani, H., Huss, A., and Bachhuber, F. (2017). The cerebrospinal fluid and barriers - anatomic and physiologic considerations. *Handb. Clin. Neurol.* 146, 21–32. doi: 10.1016/B978-0-12-804279-3.00002-2

Uddin, M. S., Mamun, A. A., Alghamdi, B. S., Tewari, D., Jeandet, P., Sarwar, M. S., et al. (2020). Epigenetics of glioblastoma multiforme: from molecular mechanisms to therapeutic approaches. *Semin. Cancer Biol.* doi: 10.1016/j.semcancer.2020.12.015

van der Sanden, G. A., Schouten, L. J., Van Dijck, J. A., Van Andel, J. P., Van Der Maazen, R. W., and Coebergh, J. W. (2002). Primary central nervous system lymphomas: incidence and survival in the Southern and Eastern Netherlands. *Cancer* 94, 1548–1556. doi: 10.1002/cncr.10357

Wang, J., and Bettegowda, C. (2017). Applications of DNA-Based liquid biopsy for central nervous system neoplasms. *J. Mol. Diagn.* 19, 24–34. doi: 10.1016/j.jmoldx.2016.08.007

Wang, M., Cai, Y., Peng, Y., Xu, B., Hui, W., and Jiang, Y. (2020). Exosomal LGALS9 in the cerebrospinal fluid of glioblastoma patients suppressed dendritic cell antigen presentation and cytotoxic T-cell immunity. *Cell Death Dis.* 11:896. doi: 10.1038/s41419-020-03042-3

Wang, Q. M., Lian, G. Y., Song, Y., Huang, Y. F., and Gong, Y. (2019). LncRNA MALAT1 promotes tumorigenesis and immune escape of diffuse large B cell lymphoma by sponging miR-195. *Life Sci.* 231:116335. doi: 10.1016/j.lfs.2019.03.040

Wang, S., Liang, K., Hu, Q., Li, P., Song, J., Yang, Y., et al. (2017). JAK2-binding long noncoding RNA promotes breast cancer brain metastasis. *J. Clin. Invest.* 127, 4498–4515. doi: 10.1172/JCI91553

Wang, Z., Wang, Q., Bao, Z., Guo, L., Chen, H., Lv, T., et al. (2020). LINC00174 is a favorable prognostic biomarker in glioblastoma via promoting proliferative phenotype. *Cancer Biomark* 28, 421–427. doi: 10.3233/CBM-191026

Weber, R. G., Boström, J., Wolter, M., Baudis, M., Collins, V. P., Reifenberger, G., et al. (1997). Analysis of genomic alterations in benign, atypical, and anaplastic meningiomas: toward a genetic model of meningioma progression. *Proc. Natl. Acad. Sci. U.S.A.* 94, 14719–14724. doi: 10.1073/pnas.94.26.14719

Wei, G. H., and Wang, X. (2017). lncRNA MEG3 inhibit proliferation and metastasis of gastric cancer via p53 signaling pathway. *Eur. Rev. Med. Pharmacol. Sci.* 21, 3850–3856.

Wu, J., Ma, C., Tang, X., Shi, Y., Liu, Z., Chai, X., et al. (2020). The regulation and interaction of PVT1 and miR181a-5p contributes to the repression of SP1 expression by the combination of XJD decoction and cisplatin in human lung cancer cells. *Biomed. Pharmacother.* 121:109632. doi: 10.1016/j.biopha.2019.109632

Wu, Y. J., Yang, Q. S., Chen, H., Wang, J. T., Wang, W. B., and Zhou, L. (2021). Long non-coding RNA CASC19 promotes glioma progression by modulating the miR-454-3p/RAB5A axis and is associated with unfavorable MRI features. *Oncol. Rep.* 45, 728–737. doi: 10.3892/or.2020.7876

Wu, Y., Liang, S., Xu, B., Zhang, R., Zhu, M., Zhou, W., et al. (2017). Long noncoding RNA eosinophil granule ontogeny transcript inhibits cell proliferation and migration and promotes cell apoptosis in human glioma. *Exp. Ther. Med.* 14, 3817–3823. doi: 10.3892/etm.2017.4949

Wu, Z. R., Yan, L., Liu, Y. T., Cao, L., Guo, Y. H., Zhang, Y., et al. (2018). Inhibition of mTORC1 by lncRNA H19 via disrupting 4E-BP1/Raptor interaction in pituitary tumours. *Nat. Commun.* 9:4624. doi: 10.1038/s41467-018-06853-3

Xiao, Y., Zhu, Z., Li, J., Yao, J., Jiang, H., Ran, R., et al. (2020). Expression and prognostic value of long non-coding RNA H19 in glioma via integrated bioinformatics analyses. *Aging (Albany NY)* 12, 3407–3430. doi: 10.18632/aging.102819

Xie, J., Wang, X., Liu, S., Chen, C., Jiang, F., Mao, K., et al. (2019). LncRNA SAMMSON overexpression distinguished glioblastoma patients from patients with diffuse neurosarcoidosis. *Neuroreport* 30, 817–821. doi: 10.1097/WNR.0000000000001278

Xie, T., Cho, Y. B., Wang, K., Huang, D., Hong, H. K., Choi, Y. L., et al. (2014). Patterns of somatic alterations between matched primary and metastatic colorectal tumors characterized by whole-genome sequencing. *Genomics* 104, 234–241. doi: 10.1016/j.ygeno.2014.07.012

Xing, H., Wang, S., Li, Q., Ma, Y., and Sun, P. (2018). Long noncoding RNA LINC00460 targets miR-539/MMP-9 to promote meningioma progression and metastasis. *Biomed. Pharmacother.* 105, 677–682. doi: 10.1016/j.biopha.2018.06.005

Yang, B., Wei, Z. Y., Wang, B. Q., Yang, H. C., Wang, J. Y., and Bu, X. Y. (2018). Down-regulation of the long noncoding RNA-HOX transcript antisense intergenic RNA inhibits the occurrence and progression of glioma. *J. Cell. Biochem.* 119, 2278–2287. doi: 10.1002/jcb.26390

Yang, J., Sun, G., Hu, Y., Yang, J., Shi, Y., Liu, H., et al. (2019). Extracellular vesicle lncRNA metastasis-associated lung adenocarcinoma transcript 1 released from

glioma stem cells modulates the inflammatory response of microglia after lipopolysaccharide stimulation through regulating miR-129-5p/High mobility group Box-1 Protein Axis. *Front. Immunol.* 10:3161. doi: 10.3389/fimmu.2019.03161

Yao, R. W., Wang, Y., and Chen, L. L. (2019). Cellular functions of long noncoding RNAs. *Nat. Cell Biol.* 21, 542–551. doi: 10.1038/s41556-019-0311-8

Yao, Y., Ma, J., Xue, Y., Wang, P., Li, Z., Liu, J., et al. (2015). Knockdown of long non-coding RNA XIST exerts tumor-suppressive functions in human glioblastoma stem cells by up-regulating miR-152. *Cancer Lett.* 359, 75–86. doi: 10.1016/j.canlet.2014.12.051

Yu, G., Li, C., Xie, W., Wang, Z., Gao, H., Cao, L., et al. (2017). Long non-coding RNA C5orf66-AS1 is downregulated in pituitary null cell adenomas and is associated with their invasiveness. *Oncol. Rep.* 38, 1140–1148. doi: 10.3892/or.2017.5739

Zajdel, M., Rymkiewicz, G., Sromek, M., Cieslikowska, M., Swoboda, P., Kulinczak, M., et al. (2019). Tumor and cerebrospinal fluid microRNAs in primary central nervous system lymphomas. *Cancers (Basel)* 11:1647. doi: 10.3390/cancers11111647

Zhang, J., Li, N., Fu, J., and Zhou, W. (2020). Long noncoding RNA HOTAIR promotes medulloblastoma growth, migration and invasion by sponging miR-1/miR-206 and targeting YY1. *Biomed. Pharmacother.* 124:109887. doi: 10.1016/j.biopha.2020.109887

Zhang, L., He, A., Chen, B., Bi, J., Chen, J., Guo, D., et al. (2020). A HOTAIR regulatory element modulates glioma cell sensitivity to temozolomide through long-range regulation of multiple target genes. *Genome Res.* 30, 155–163. doi: 10.1101/gr.251058.119

Zhang, S., Sun, W. C., Liang, Z. D., Yin, X. R., Ji, Z. R., Chen, X. H., et al. (2020). LncRNA SNHG4 attenuates inflammatory responses by sponging miR-449c-5p and up-regulating STAT6 in microglial during cerebral ischemia-reperfusion injury. *Drug Des. Devel. Ther.* 14, 3683–3695. doi: 10.2147/DDDT.S245445

Zhang, X., Gejman, R., Mahta, A., Zhong, Y., Rice, K. A., Zhou, Y., et al. (2010). Maternally expressed gene 3, an imprinted noncoding RNA gene, is associated with meningioma pathogenesis and progression. *Cancer Res.* 70, 2350–2358. doi: 10.1158/0008-5472.CAN-09-3885

Zhang, X., Sun, S., Pu, J. K. S., Tsang, A. C. O., Lee, D., Man, V. O. Y., et al. (2012). Long non-coding RNA expression profiles predict clinical phenotypes in glioma. *Neurobiol. Dis.* 48, 1–8. doi: 10.1016/j.nbd.2012.06.004

Zhang, X., Zhou, J., Gu, Z., Zhang, H., Gong, Q., and Luo, K. (2021). Advances in nanomedicines for diagnosis of central nervous system disorders. *Biomaterials* 269:120492. doi: 10.1016/j.biomaterials.2020.120492

Zhang, Y., Li, Y., Wang, J., and Lei, P. (2018a). Long non-coding RNA ferritin heavy polypeptide 1 pseudogene 3 controls glioma cell proliferation and apoptosis via regulation of the microRNA-224-5p/tumor protein D52 axis. *Mol. Med. Rep.* 18, 4239–4246. doi: 10.3892/mmr.2018.9491

Zhang, Y., Liu, Y. T., Tang, H., Xie, W. Q., Yao, H., Gu, W. T., et al. (2019). Exosome-transmitted lncRNA H19 inhibits the growth of pituitary adenoma. *J. Clin. Endocrinol. Metab.* 104, 6345–6356. doi: 10.1210/jc.2019-00536

Zhang, Y., Wang, T., Wang, S., Xiong, Y., Zhang, R., Zhang, X., et al. (2018b). Nkx2-2as suppression contributes to the pathogenesis of sonic hedgehog medulloblastoma. *Cancer Res.* 78, 962–973. doi: 10.1158/0008-5472.CAN-17-1631

Zhang, Y., Yu, R., Li, Q., Li, Y., Xuan, T., Cao, S., et al. (2020). SNHG1/miR-556-5p/TCF12 feedback loop enhances the tumorigenesis of meningioma through Wnt signaling pathway. *J. Cell. Biochem.* 121, 1880–1889. doi: 10.1002/jcb.29423

Zhang, Z., Yin, J., Lu, C., Wei, Y., Zeng, A., and You, Y. (2019). Exosomal transfer of long non-coding RNA SBF2-AS1 enhances chemoresistance to temozolomide in glioblastoma. *J. Exp. Clin. Cancer Res.* 38:166. doi: 10.1186/s13046-019-1139-6

Zhao, L., Liu, Y., Zhang, J., Liu, Y., and Qi, Q. (2019). LncRNA SNHG14/miR-5590-3p/ZEB1 positive feedback loop promoted diffuse large B cell lymphoma progression and immune evasion through regulating PD-1/PD-L1 checkpoint. *Cell Death Dis.* 10:731. doi: 10.1038/s41419-019-1886-5

Zhu, H. B., Li, B., Guo, J., Miao, Y. Z., Shen, Y. T., Zhang, Y. Z., et al. (2021). LncRNA MEG8 promotes TNF-α expression by sponging miR-454-3p in bone-invasive pituitary adenomas. *Aging (Albany NY)* 13, 14342–14354. doi: 10.18632/aging.203048

Zhu, H., Guo, J., Shen, Y., Dong, W., Gao, H., Miao, Y., et al. (2018). Functions and mechanisms of tumor necrosis factor-α and noncoding RNAs in bone-invasive pituitary adenomas. *Clin. Cancer Res.* 24, 5757–5766. doi: 10.1158/1078-0432.CCR-18-0472

Zhuang, J., Cai, P., Chen, Z., Yang, Q., Chen, X., Wang, X., et al. (2020). Long noncoding RNA MALAT1 and its target microRNA-125b are potential biomarkers for Alzheimer's disease management via interactions with FOXQ1, PTGS2 and CDK5. *Am. J. Transl. Res.* 12, 5940–5954.

Conflict of Interest: The authors declare that the research was conducted in the absence of any commercial or financial relationships that could be construed as a potential conflict of interest.

Publisher's Note: All claims expressed in this article are solely those of the authors and do not necessarily represent those of their affiliated organizations, or those of the publisher, the editors and the reviewers. Any product that may be evaluated in this article, or claim that may be made by its manufacturer, is not guaranteed or endorsed by the publisher.

frontiers in Cell and Developmental Biology

ORIGINAL RESEARCH
published: 11 November 2021
doi: 10.3389/fcell.2021.781867

M^{6}A-Mediated Upregulation of LINC00106 Promotes Stemness and Metastasis Properties of Hepatocellular Carcinoma via Sponging Let7f

Wenjin Liang[1,2†], *Yan Wang*[1†], *Qinyu Zhang*[1], *Min Gao*[1], *Haizhou Zhou*[1] *and Zhenran Wang*[1*]

[1]General Surgery, Affiliated Hospital of Guilin Medical University, Guilin, China, [2]Hubei Key Laboratory of Medical Technology on Transplantation, Transplant Center of Wuhan University, Zhongnan Hospital of Wuhan University, Institute of Hepatobiliary Diseases of Wuhan University, Wuhan, China

OPEN ACCESS

Edited by:
Ming Yang,
Shandong University, China

Reviewed by:
Xiaobo Li,
Harbin Medical University, China
Yukuan Feng,
Mudanjiang Medical University, China
Yunshan Wangg,
Shandong University, China

***Correspondence:**
Zhenran Wang
w07ll07@163.com

[†]These authors have contributed equally to this work

Specialty section:
This article was submitted to Epigenomics and Epigenetics, a section of the journal Frontiers in Cell and Developmental Biology

Received: 23 September 2021
Accepted: 26 October 2021
Published: 11 November 2021

Citation:
Liang W, Wang Y, Zhang Q, Gao M, Zhou H and Wang Z (2021) M^{6}A-Mediated Upregulation of LINC00106 Promotes Stemness and Metastasis Properties of Hepatocellular Carcinoma via Sponging Let7f. Front. Cell Dev. Biol. 9:781867. doi: 10.3389/fcell.2021.781867

Background: Hepatocellular carcinoma (HCC) cells exhibit the stemness property, which makes the patient with HCC prone to tumor recurrence and metastasis. Despite the prominent regulatory role of long non-coding RNAs (lncRNAs) in tumor stemness, the roles and molecular mechanisms of LINC00106 in HCC are poorly understood.

Methods: LINC00106, let7f and periostin expression levels in tissue specimens and cell lines were assessed through qRT-PCR and immunohistochemistry (IHC). Various *in vivo* and *in vitro* assays, namely sphere/colony formation, proportion of side population cells (SP%), invasion, migration, western blot, and murine xenograft model were employed for assessing the stemness and metastatic properties of HCC cells. Luciferase reporter assays, RNA-seq, RNA pull-down, RNA immunoprecipitation (RIP) were conducted to clarificate the target gene and analyze the underlying mechanisms.

Results: LINC00106 was prominently upregulated in tissues and cell lines of HCC. Patients having a high LINC00106 level exhibited a poor outcome. Under *in vivo* and *in vitro* conditions, the stemness and metastatic properties of HCC cells were augmented by LINC00106. Additionally, LINC00106 was found to sponge let7f to upregulate periostin, which lead to the activation of periostin-associated PI3K-AKT signaling pathway. Moreover, m^{6}A methylation was found to cause LINC00106 upregulation while maintaining LINC00106 RNA transcript stability.

Conclusion: m^{6}A methylation triggers the upregulation of LINC00106, which promotes the stemness and metastasis properties in HCC cells by sponging let7f, thereby resulting in periostin activation. The findings indicate the potential of LINC00106 as a diagnostic marker and therapeutic target for HCC.

Keywords: Hepatocellular carcinoma, LINC00106, Let7f, stemness, metastasis, periostin

INTRODUCTION

Hepatocellular carcinoma (HCC) is the fourth most common and lethal malignancy globally (Kelley and Greten, 2021). Several studies have confirmed the presence of a distinct tumor cell subpopulation with stemness property, known as the cancer stem cell (CSC) population, in HCC (Ling et al., 2019; Ma et al., 2020). The CSC population possesses the stemness property, which can make the patients prone to tumor invasion and metastasis (Chen et al., 2021), accounting for the extremely poor prognosis of most patients at the time of HCC diagnosis (Faltas, 2012). Therefore, the specific reprogramming mechanisms of CSCs in HCC must be studied to develop an optimal treatment strategy for improving the prognosis of patients with HCC.

Long non-coding (lnc) RNAs represent non-protein-coding RNAs with a length exceeding 200 nucleotides. These RNAs are involved in the acquisition of all carcinoma hallmarks, such as inherent proliferation and survival capabilities through metabolic enhancement and linkage to the carcinoma micro-environment (Statello et al., 2020). Additionally, in several carcinomas, lncRNAs have been proven to critically regulate the stemness and metastatic properties (Zheng et al., 2019; Shu et al., 2021). Mechanical research has demonstrated that the lncRNAs inhibit the miRNA-mediated inhibition of downstream target gene expression by acting as miRNA sponging molecules (cytosolic lncRNAs) (Zuo et al., 2020), which otherwise functionally support the regulatory protein recruitment to corresponding target chromosomal zones (Yuan et al., 2017). As a newly identified molecule of lncRNA, the effects of LINC00106 on carcinoma progression remain mostly unclarified.

In this study, we demonstrated that LINC00106 was significantly upregulated both in HCC tissue and cell lines. Patients with a high level of LINC00106 had a poor prognosis. LINC00106 could enhance the stemness and metastasis properties *in vitro* and *in vivo* in HCC cells. Moreover, LINC00106 could sponge let7f, which caused periostin upregulation and the activation of downstream signaling molecules such as p-AKT and p-PI3K. Moreover, m^{6}A methylation was found to cause LINC00106 upregulation while maintaining LINC00106 RNA transcript stability. The results of this study emphasize that LINC00106 can facilitate metastasis in HCC through let7f sponging and periostin upregulation. This study indicated a potential role of LINC00106 as a novel diagnostic and treatment target for HCC.

MATERIALS AND METHODS

Patient Samples

This study was approved by the Ethics Committee of the Affiliated Hospital of Guilin Medical University, and all patients signed an informed consent formulated under the Declaration of Helsinki principles. A total of 171 patients with HCC, aged between 30 and 70 years, who underwent hepatectomy from 2014 to 2020 were enrolled. The clinical and pathological data included sex, age, tumor diameter, tumor differentiation, and clinical TNM staging. All the enrolled patients were followed up.

Cell Lines and Cell Culture

HCC cell lines (MHCC-97H, SNU-449, Huh7, Hep3B, BEL-7405, and HCC-LM3) and normal liver cells (THLE-2) were purchased from the Cell Bank of Chinese Academy of Sciences (shanghai, China). DMEM (Thermo Fisher Scientific, South America) was used as a culture medium for Huh7, HCC-LM3, Hep3B, and MHCC-97H cells, whereas RPMI-1640 from the same company was used for BEL-7405, SNU-449 and THLE-2 culture. These media contained 10% FBS from the same company. Cells were cultured in a 37°C incubator under 5% CO_2/95% atmosphere. Unless otherwise stated, all the chemicals and relevant reagents were purchased from Sigma-Aldrich (Saint Louis, MO, United States).

Vector Constructs, Lentivirus Production, and Cell Transduction

LINC00106-shRNA plus negative control, LINC00106-overexpressing vector pcDNA3.1 (+) plus corresponding control, and the mimics and inhibitor of let7f plus their negative controls were obtained from GenePharma (Shanghai, China). Mettl3 and IGF2BP1 Short interfering (si) RNA sequences were synthesized directly at GenePharma (Shanghai, China), whereas human periostin sequences (full-length) were cloned into the pcDNA3.1 vector in the presence or absence of a Flag- or HA-tag sequence (Invitrogen, Shanghai, China). Cellular transfection of shRNA and pcDNA3.1 was performed using Lipofectamine 3000 (Invitrogen, Shanghai, China), and after 48 h, the cells were collected for experimental use. For delivery of shRNAs, infection with lentiviruses generated from pLKO.1 vector-based transfection of 293T cells was performed. The lentivirus-infected cells delivering scrambled shRNA were adopted as negative control. **Supplementary Table S1** provides the sequences of the shRNA, siRNA, and mimics.

Detection of HCC Stem Cell Characteristics

After seeding HCC cells into the ultralow attachment microplates at a density of 3,000 cells per well, the cells were cultured for 10 days in DMEM/F12 medium (Invitrogen, Shanghai, China) containing insulin (4 mg/ml; Sigma, Shanghai, China), EGF (20 ng/ml; Sigma, Shanghai, China), bFGF (20 ng/ml; Sigma, Shanghai, China), and B27 (1:50, GIBCO, Shanghai, China). This procedure was followed by the acquisition of primary spheres, trypsin-based dissociation of cells, and replating, which resulted in the generation of secondary spheres through the same procedure. Finally, the sphere number was counted using a microscope (Zeiss, Germany), and the proportion of side population cells was counted by flow cytometry (Merck Millipore). Results are presented as means ± SD of triplicate wells for each experiment.

RNA Immunoprecipitation

We used the Magna RIP RNA-Binding Protein Immunoprecipitation Kit (Millipore, United States) according

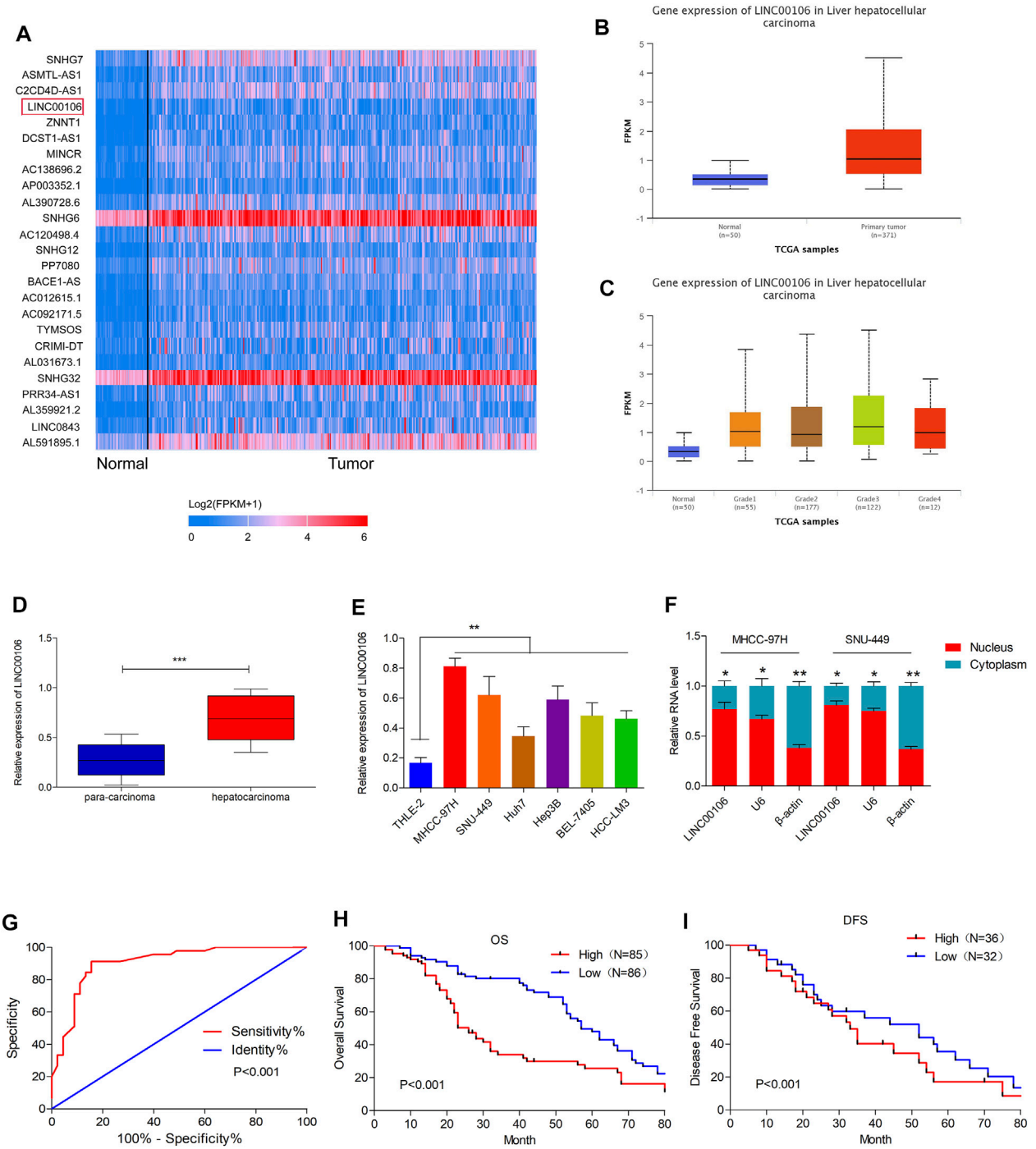

FIGURE 1 | LINC00106 is up-expressed in HCC and is positively associated with poor prognosis in HCC patients. **(A)**, The heatmap of the differentially expressed LncRNAs. Between adjacent normal liver tissues (50 cases) and HCC tissues (371 cases) across TCGA database. **(B,C)**, Comparison of LINC00106 expression between 371 HCC tissues and 50 adjacent normal liver tissues based on TCGA dataset. **(D)**, Expression of LINC00106 between 171 pairs of HCC tumor tissues and adjacent normal liver tissues. **(E)**, Relative expression of LINC00106 in HCC cell lines and THLE-2 cells. **(F)**, The expression of LINC00106 in the nucleus and the cytoplasm in HCC cell lines. **(G)**, The receiver operator characteristic (ROC) analysis determining the diagnostic value of LINC00106 expression level in differentiating between normal and malignant hepatic tissues. **(H,I)**. Kaplan-Meier analyses for the correlation between the LINC00106 level and HCC prognosis in 171 patients **(H)**. Overall survival; **(I)**. Disease free survival) (*$p < 0.05$, **$p < 0.01$).

to the manufacturer's instructions to perform RIP experiments. Briefly, cell extracts were immunoprecipitated with sepharose beads conjugated antibodies against AGO2, IGF2BP1, or IgG at 4°C for 6 h. 0.1% 10 SDS/Proteinase K (0.5 mg/ml, 30 min at 55°C) was used to remove proteins from the complex. Then, Western blot and qRT-PCR were used respectively to detect the immunoprecipitated proteins and RNAs. For MeRIP-qPCR assay, m^{6}A-modified RNA was eluted twice with 6.7 mM N6-methyladenosine 5′-monophosphate sodium salt at 4°C for 1 h. Subsequently, qRT-PCR analysis was performed to determine the m^{6}A enrichment on LNC00106 using the following primer sequences (**Supplementary Table S1**).

RNA Pull-Down Assay

Pierce™ Magnetic RNA-Protein Pull-Down Kit (Thermo Fisher Scientific, 20164) was used according to the manufacturer's instructions. Briefly, LINC00106 was labeled for attachment to streptavidin magnetic beads, which can capture protein complex combined with labeled LINC00106. LINC00106 and let7f were detected by qRT-PCR and AGO2 was assessed by western blot.

Immunohistochemistry (IHC), Western blot analysis, Quantitative real time polymerase chain reaction (qRT-PCR), Plate cloning experiment, Experiments of cell invasion and migration, *in vivo* tumor growth assay and nude murine xenograft model, Dual luciferase reporter assay, RNA-seq analysis. Details are provided in the **Supplementary Material** (Additional file 2).

Statistical Analysis

Statistical analyses were performed using GraphPad Prism 5 (GraphPad Software, Inc., San Diego, CA, United States) and SPSS v.18.0 (SPSS Inc., Chicago, IL, United States). All data are presented as mean ± SD. Pairwise comparisons were performed based on the two-tailed Student's t-test. One-way ANOVA was performed to compare differences between at least three groups. The relationships between the expression of LINC00106 and the clinicopathologic features were assessed using the chi-square test. The Kaplan-Meier method was used to plot survival curves, which were compared using the log-rank test. A p value of <0.05 was considered statistically significant.

RESULTS

LINC00106 is Upregulated in HCC and is Positively Correlated With Poor Prognosis in Patients With HCC

Initially, upregulated lncRNAs were screened in the HCC tissues (371 cases) and non-cancerous hepatic tissues (50 cases) through the TCGA database (**Figure 1A**). In HCC tissues, we observed a considerably high expression of LINC00106, whose level was positively associated with the tumor differentiation grade of HCC (**Figures 1B,C**). To confirm these results, we selected HCC and paracarcinoma tissues (82 pairs) for LINC00106 level measurement through qRT-PCR. The result demonstrated a high expression of LINC00106 in HCC tissues (**Figure 1D**).

TABLE 1 | Correlations between LINC00106 expression and clinicopathological parameters in 171 hepatocellular carcinoma patients.

Variables	LINC00106 expression		Total	*p* Value
	Low (54)	High (117)		
Age (y)				
<60	20 (26%)	56 (74%)	76	0.188
≥60	34 (45%)	61 (55%)	95	
Gender				
Male	31 (34%)	61 (56%)	92	0.524
Female	23 (29%)	56 (71%)	79	
Tumor diameter (cm)				
<5	12 (13%)	79 (87%)	91	**0.001**
≥5	42 (52%)	38 (48%)	80	
AFP (ng/ml)				
<20	21 (33%)	42 (67%)	63	0.708
≥20	33 (32%)	75 (68%)	108	
Tumor differentiation				
Well	13 (27%)	36 (73%)	49	0.585
Moderate	19 (37%)	32 (63%)	51	
Poor	22 (31%)	49 (69%)	71	
TNM stage				
I–II	19 (22%)	68 (88%)	87	**0.005**
III–IV	35 (41%)	49 (59%)	84	
Alcohol history				
No	28 (22%)	72 (88%)	100	0.235
Yes	26 (41%)	45 (59%)	71	

Bold values represents Significant p value.

Additionally, LINC00106 was found to be significantly upregulated in HCC cell lines (MHCC-97H, SNU-449, Huh7, Hep3B, BEL-7405, and HCC-LM3) compared with that in the non-cancerous hepatic THLE-2 cell (**Figure 1E**). We also found that, in HCC cell lines, the expression of LINC00106 in the nucleus is higher than that in the cytoplasm (**Figure 1F**).

Furthermore, we explored the correlation between upregulated LINC00106 and the clinicopathological characteristics of patients with HCC. The receiver operator characteristic (ROC) analysis demonstrated that upregulated LINC00106 had a remarkable diagnostic value in discriminating between HCC and adjacent healthy tissues (AUC = 0.905, $p < 0.001$) (**Figure 1G**). Furthermore, the Kaplan–Meier survival analysis indicated that the patients with a high LINC00106 level exhibited a poor prognosis both in overall survival (**Figure 1H**) and disease-free survival (**Figure 1I**). In addition, the upregulated LINC00106 was positively correlated with tumor diameter ($p < 0.05$) and TNM stage ($p < 0.05$; **Table 1**). These results suggested that LINC00106 may have an oncogenic role in HCC.

LINC00106 Promotes HCC Cell Stemness and Metastasis Properties *in vitro*

To explore whether LINC00106 can promote the stemness and metastasis properties of HCC tumors, we selected two HCC cell lines (MHCC-97H and SNU-449) with a high expression level of LINC00106 and a HCC cell line (Huh7) with a relatively low expression level of LINC00106. We downregulated the expression of LINC00106 in MHCC-97H and SNU-449 cell lines and upregulated its expression in the Huh7 cell line. By using the

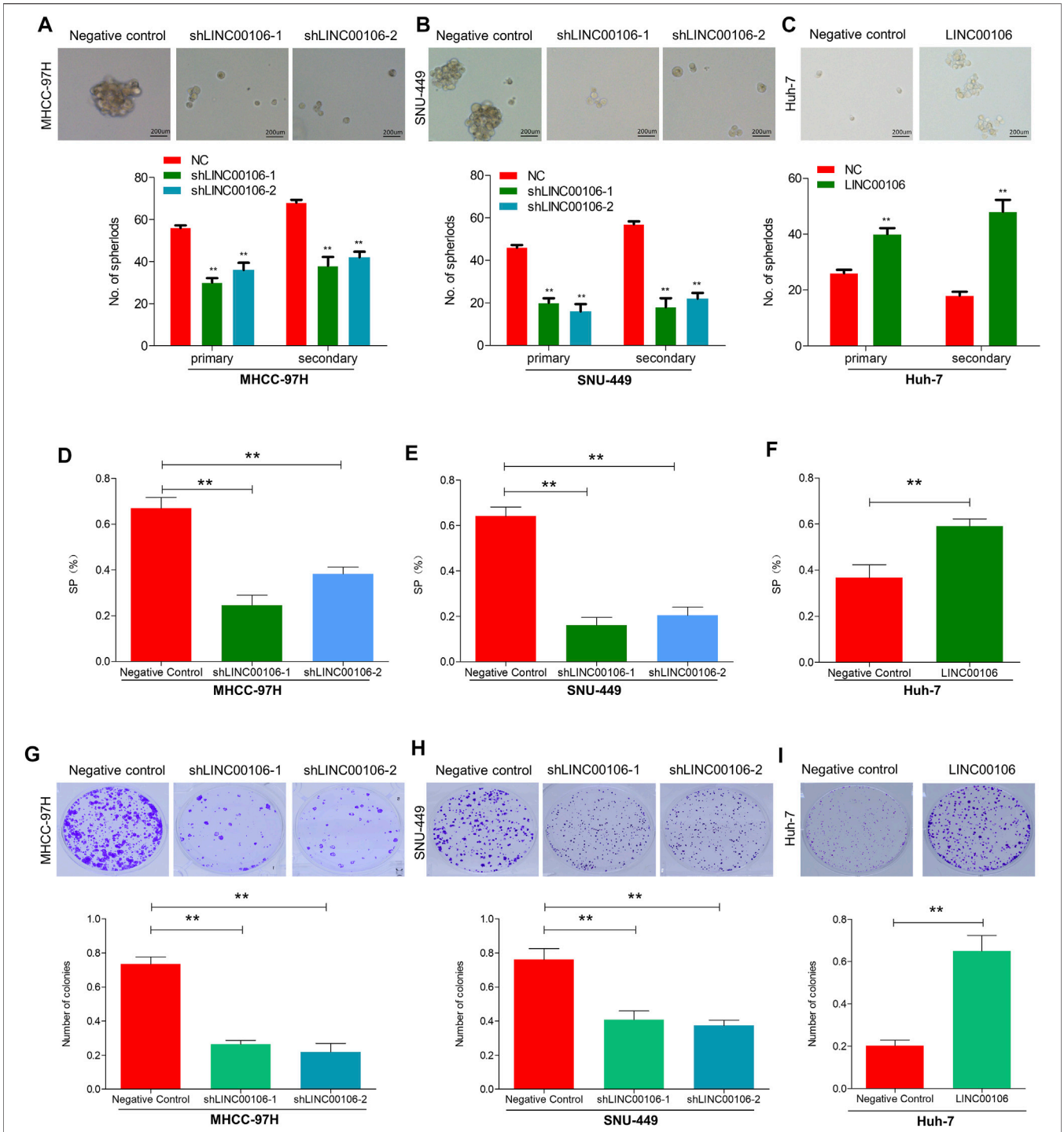

FIGURE 2 | LINC00106 promotes HCC cell stemness and metastasis properties *in vitro*. **(A–C)**, Representative images of sphere formation induced by the transfection of shLINC00106 into MHCC-97H and SNU-449 cells or the transfection of a LINC00106 overexpression plasmid into Huh7 cells. **(D–F)**, SP% was detected by the above HCC cells. **(G–I)**, The plate cloning experiment was detected by the above HCC cells (**$p < 0.01$).

spheroid formation assays and side population cell screening experiment, we attempted to verify that LINC00106 regulates the characteristics of tumor stem cells of HCC cells. The sphere (primary and secondary) formation capabilities were weakened by abnormal LINC00106 suppression in MHCC-97H and SNU-449 cells compared with that in the control cells (**Figures 2A,B**). By contrast, in Huh7 cells, the sphere (primary and secondary) formation capabilities were enhanced due to LINC00106

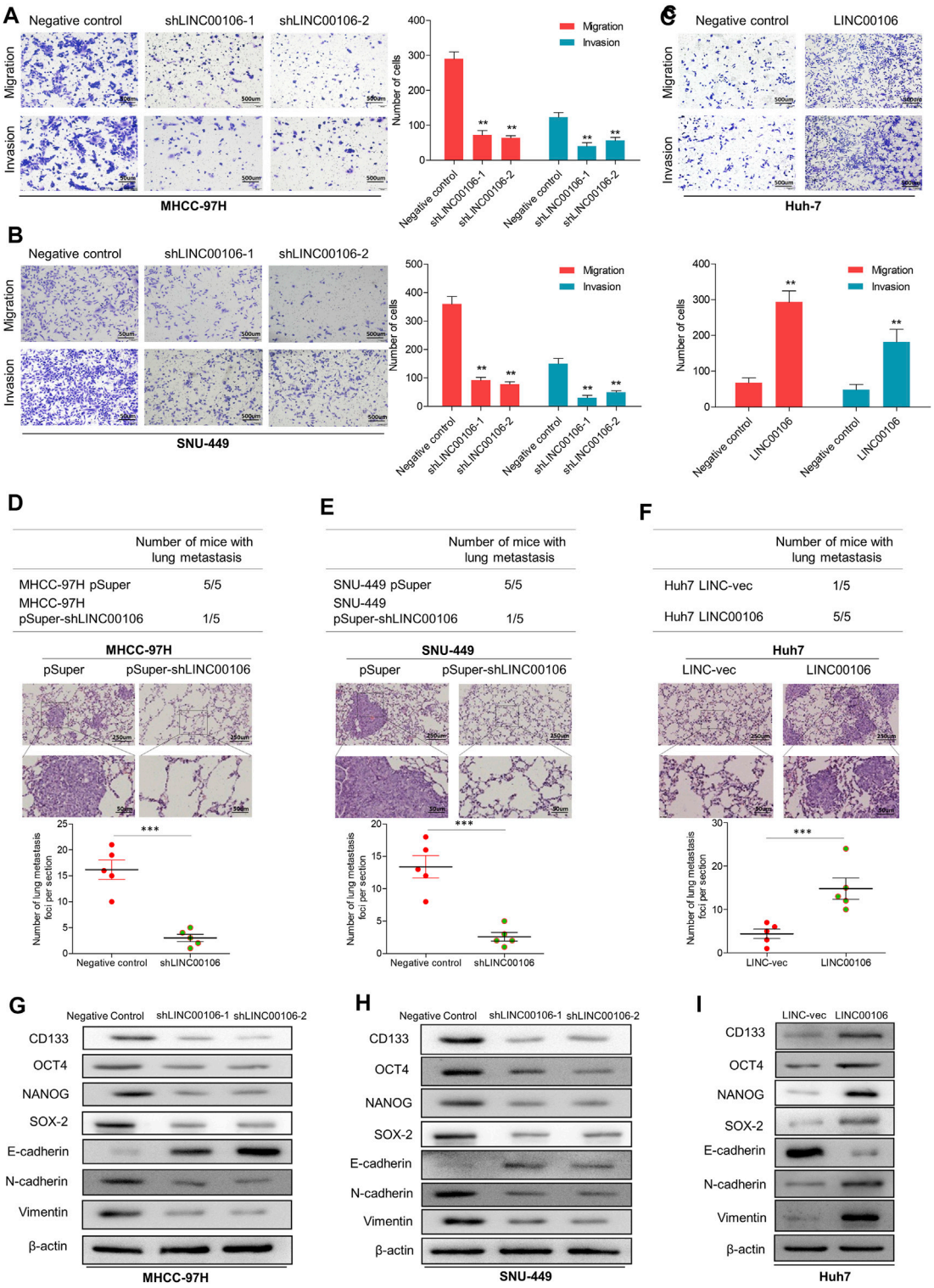

FIGURE 3 | LINC00106 promotes HCC cell stemness and metastasis properties *in vitro* and *in vivo*. **(A–C)**, Representative images of invasion and migration assays induced by the transfection of shLINC00106 into MHCC-97H and SNU-449 cells or the transfection of a LINC00106 overexpression plasmid into Huh7 cells. **(D–F)**, the foci number of lung metastases were detected by the above HCC cells. **(G–I)**: the expression levels of stemness and metastasis properties related proteins were detected in the above three groups of subcutaneous tumour (*$p < 0.05$, **$p < 0.01$).

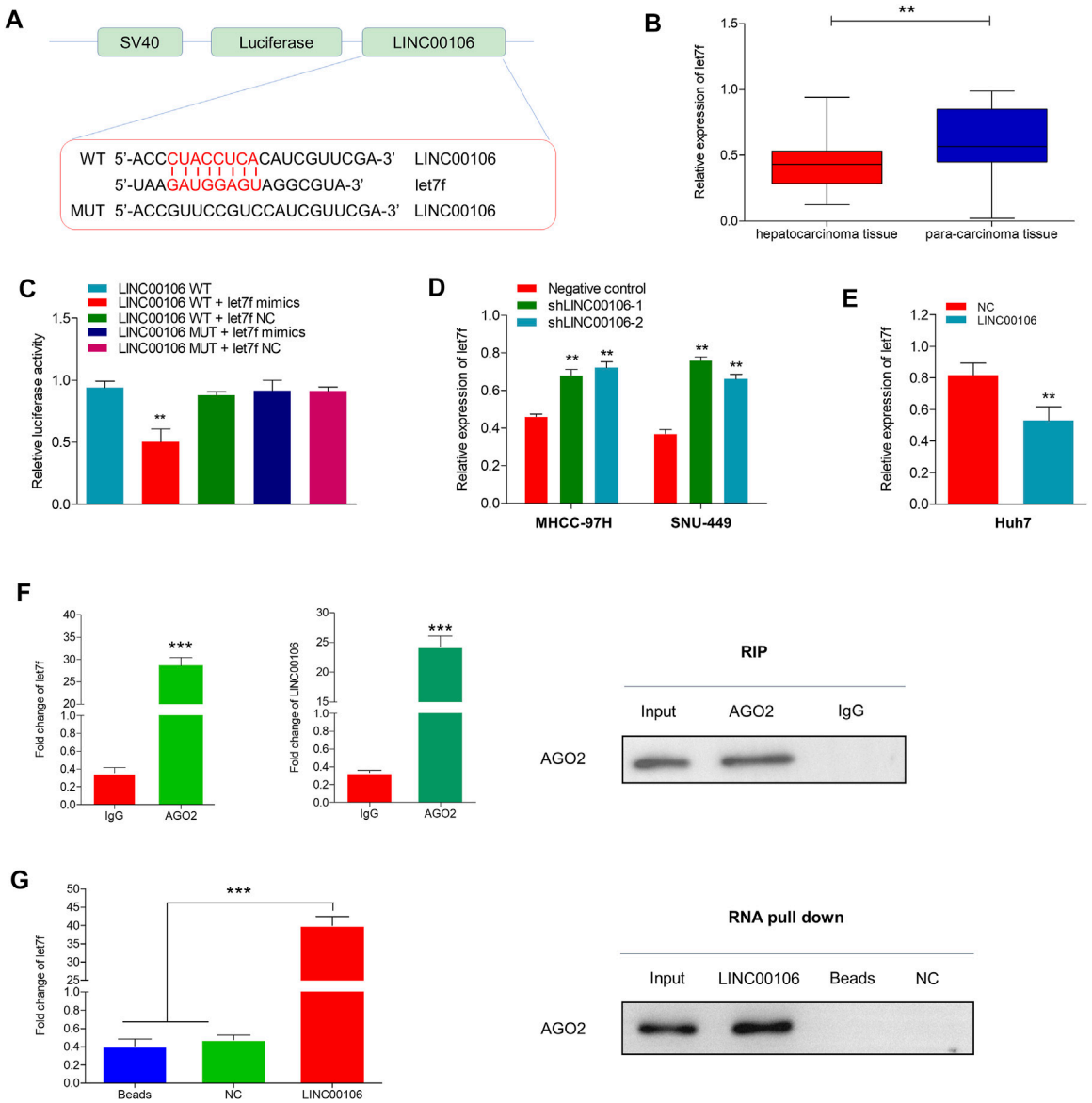

FIGURE 4 | LINC00106 sponges and downregulates let7f in HCC cells. **(A)**, Conjectured binding sites between LINC00106 and let7f by LncBase. **(B)**, Comparison of let7f expression level between 171 pairs of HCC tissues and adjacent normal liver tissues. **(C)**, The relative luciferase activities in 293T cells following the indicated transfection. **(D,E)**, Expression of let7f after LINC00106 manipulation. **(F)**, RIP assay for the relative enrichment of LINC00106 and let7f in anti-IgG or anti-AGO2 specific immuneprecipitates. **(G)**, RNA pull-down assay was used to detect the interaction between LINC00106, let7f and AGO2 (**$p < 0.01$, ***$p < 0.001$).

overexpression (**Figure 2C**). The cell ratio indicated that the ectopic suppression of LINC00106 reduced SP% in the MHCC-97H and SNU-449 cells compared with that in the control cells (**Figures 2D,E**), whereas LINC00106 overexpression enhanced SP% of Huh7 cells (**Figure 2F**).

Additionally, we verified through plate cloning experiments that the ectopic suppression of LINC00106 can attenuate the colon formation ability of MHCC-97H and SNU-449 cells compared with that of the control cells (**Figures 2G,H**), whereas LINC00106 overexpression enhanced the colon formation ability of the Huh7 cells (**Figure 2I**). According to the transwell chamber invasion and migration experiments, the invasion and migration abilities of MHCC-97H and SNU-449 cells clearly decreased after downregulation of LINC00106 (**Figures 3A,B**), whereas those in Huh7 cells were enhanced after LINC00106 was upregulated (**Figure 3C**). These results suggested that LINC00106 has an oncogenic role in promoting stemness and metastasis properties in HCC cells.

LINC00106 Promotes the Metastasis Properties of HCC Cells *in vivo*

To verify the effect of LINC00106 on the metastasis properties of HCC cells *in vivo*, LINC00106 was downregulated in MHCC-97H

and SNU-449 cells and upregulated in Huh7 cells; these cells were injected via subcutaneous inoculation of cells into nude mice. The mice were sacrificed through cervical dislocation after 60 days. The tumor growth decreased significantly after LINC00106 downregulation (**Supplementary Figures S2A,B,D,E**). While the tumor growth increased significantly after LINC00106 upregulation (**Supplementary Figures S2C,F**). Besides, the above cells were also injected into the tail vein of nude mice. Then, the pulmonary metastatic foci were recorded. The number of foci of lung metastases decreased significantly after LINC00106 downregulation (**Figures 3D,E**). Conversely, the number of foci of lung metastases increased significantly after LINC00106 upregulation (**Figure 3F**). Furthermore, we collected subcutaneous tumor from different groups of nude mice and determined the expression levels of proteins related to stemness and metastasis. According to western blot results shown in **Figures 3G,H**, after LINC00106 was silenced, the markers related to stemness and metastasis, such as CD133, NANOG, N-cadherin, SOX-2, OCT4, and vimentin, exhibited a prominent downregulation. By contrast, LINC00106 overexpression promoted significant upregulation of stemness- and metastasis-associated markers (**Figure 3I**). These results confirmed that LINC00106 promotes the metastasis properties of HCC cells *in vivo*.

LINC00106 can Sponge and Decrease the Expression of MiR-let7f in HCC Cells Through CeRNA Mechanism

lncRNAs can serve as molecular sponges for microRNAs (miRNAs), which can thus prevent miRNA-mediated suppression of downstream target gene expression through the competitive endogenous RNA (ceRNA) mechanism. By using the bioinformatics database LncBase Predicted v.2, we found that LINC00106 and miR-let7f (let7f) sequences may have the potential binding relationship (**Figure 4A**). Additionally, we found that let7f was significantly and lowly expressed in HCC tissues (**Figure 4B**). The dual luciferase reporter gene assay indicated that the relative luciferase activity was weakened in the wild-type LINC00106–let7f mimic-co-transfected HCC cells, whereas it was normal in the mutant type (MUT) LINC00106–let7f mimic-co-transfected cells (**Figure 4C**). Additionally, the let7f level was markedly elevated in HCC cells with LINC00106 knockdown (MHCC-97H and SNU-449) (**Figure 4D**), whereas in Huh7 cells overexpressing LINC00106, a decline in the let7f level was observed (**Figure 4E**). Thus, presumably, LINC00106 negatively regulated let7f and further inhibited RISC-mediated downstream mRNA silencing. We further performed RIP and RNA pull-down assays to confirm this hypothesis. The RIP assay results (**Figure 4F**) indicated a significantly higher degree of enrichment of LINC00106 and let7f in the Ago2 precipitate than in the IgG control group. The foregoing finding was further verified through a subsequent RNA pull-down assay (**Figure 4G**). Overall, these data indicated that supported by the ceRNA mechanism, LINC00106 could act as a sponging molecule for let7f.

Periostin is a Target of Let7f, Which can Mediate the LINC00106-Induced Stemness and Metastasis Properties in HCC Cells

To determine the role of the LINC00106/let7f axis in HCC, a RNA-seq analysis was performed to profile the gene expressions of let7f mimic–transfected MHCC-97H cells and negative control (**Figure 5A**). Pathway analysis based on the Kyoto Encyclopedia of Genes and Genomes (KEGG) indicated that the periostin-associated PI3K-AKT axis was most prominently enriched following transfection with let7f mimics (**Figure 5B**). Meanwhile, based on aforementioned results, we found a markedly decreased periostin level following let7f transfection. Additionally, the analysis using TargetScanHuman 7.2 indicated that let7f and periostin sequences share a potential binding relationship (**Figure 5C**). The dual luciferase reporter gene assay demonstrated that the relative luciferase activity was weakened in the wild-type periostin–let7f mimic-co-transfected HCC cells, whereas the activity was normal in the MUT periostin–let7f mimic-co-transfected cells (**Figure 5D**). The mRNA levels of periostin and let7f were found to be negatively correlated (**Figure 5E**). Moreover, transfection with the let7f mimic was found to lower the expression of periostin at protein levels (**Figure 5F**), however, transfection with the let7f inhibitor provided an opposite result (**Figure 5G**). Also, we found that periostin was high expressed in HCC tissues, which is the same as Ki67 (**Supplementary Figures S2G,H**).

To verify the role of periostin in the regulation of stemness and metastasis properties through let7f in HCC cells, we restored periostin expression in let7f mimics-transfected cells. Periostin overexpression in HCC cells could alleviate the inhibitory effects of let7f mimic on stemness markers (CD133, OCT4, NANOG, and SOX-2) (**Figure 5H**). Additionally, periostin overexpression could blunt the generation of spheres induced by let7f mimics and suppression of metastatic properties (**Figures 5I,J**). These data indicated that periostin is a target of let7f, which can mediate the LINC00106-induced stemness and metastasis properties in HCC cells.

Let7f/Periostin/PI3K Signaling Pathway Mediates LINC00106-Induced HCC Stemness and Metastasis Properties

To explore the potential role of let7f/periostin/PI3K pathway in HCC carcinogenesis regulated by LINC00106, we further co-transfected the cells with sh-LINC00106 and let7f inhibitor or induced periostin overexpression. Co-transfection with sh-LINC00106 and let7f inhibitor or periostin overexpression could significantly reverse the inhibition of periostin expression (**Figures 6A,E**; **Supplementary Figures S1A,E**) to reverse the LINC00106 knockdown-induced decline in stemness-related markers, such as CD133, NANOG, SOX-2, and OCT4 (**Figures 6D,H**; **Supplementary Figures S1D,H**). The sphere formation and invasion and migration assays further verified the role of periostin overexpression or let7f inhibitor in reversing the LINC00106 knockdown-induced decline in stemness and metastatic properties (**Figures 6B,C,F,G**; **Supplementary**

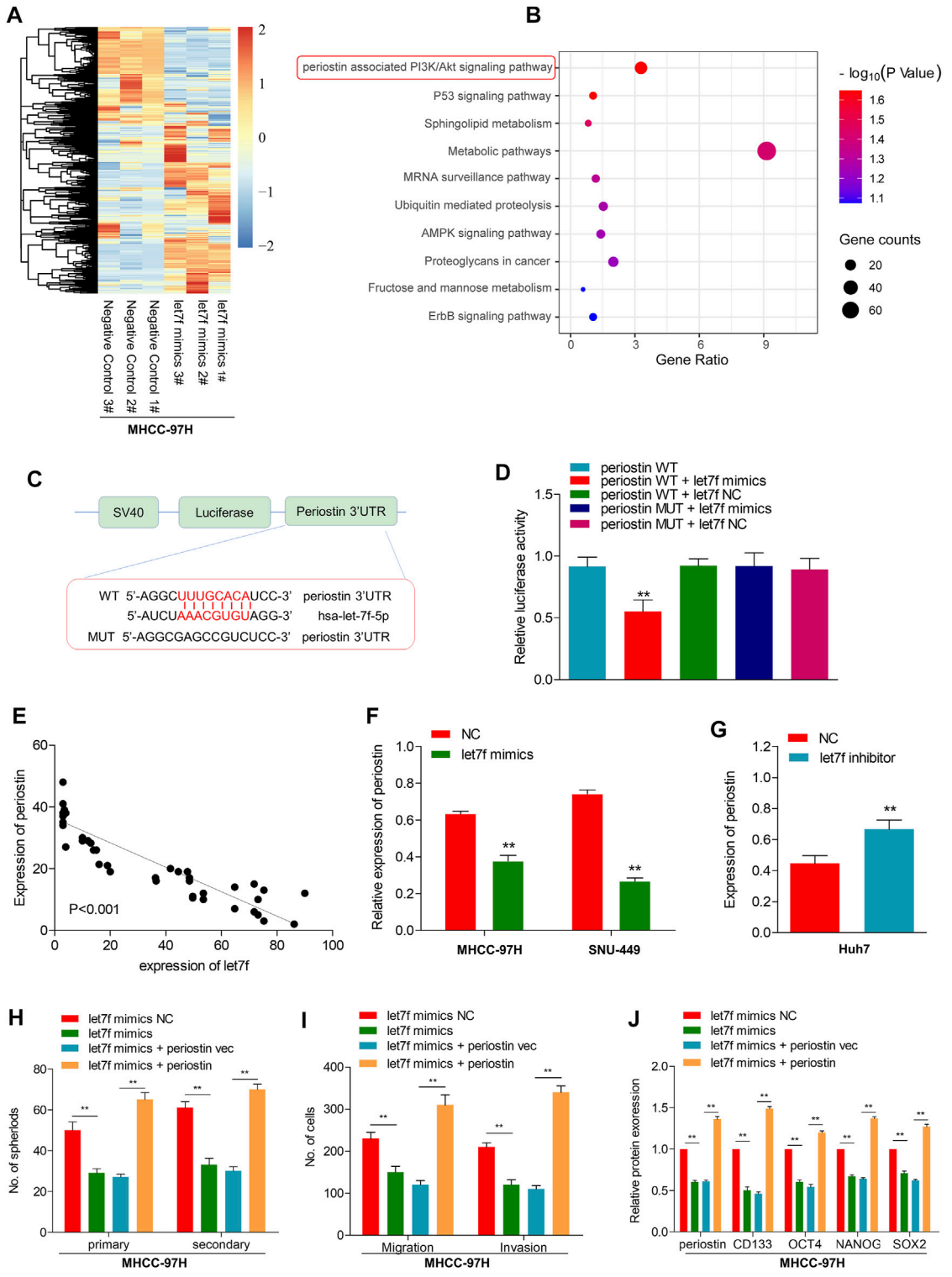

FIGURE 5 | let7f targets to periostin in HCC to regulate the LINC00106-induced stemness and metastasis properties in HCC cells. **(A)**, Heatmap summarizing the differentially expressed genes in let7f overexpressed MHCC-97H cells. **(B)**, KEGG analysis for enriched pathways in let7f overexpressed MHCC-97h cells. **(C)**, The potential binding between let7f and periostin sequences predicted by TargetScan. **(D)**, The relative luciferase activities in 293T cells co-transfected with let7f mimics or miR-NC and luciferase reporter vectors periostin-WT or periostin-Mut. **(E)**, Regression curve with respect to expression of let7f and periostin. **(F,G)**, Expression of periostin protein after knockdown or overexpression of let7f. **(H–J)**. Sphere formation capacities **(H)**, invasion and migration assays **(I)** and expression of stemness biomarkers **(J)** in MHCC-97H cells co-transfected with let7f mimics or let7f mimics NC and periostin or periostin-vec (**$p < 0.01$).

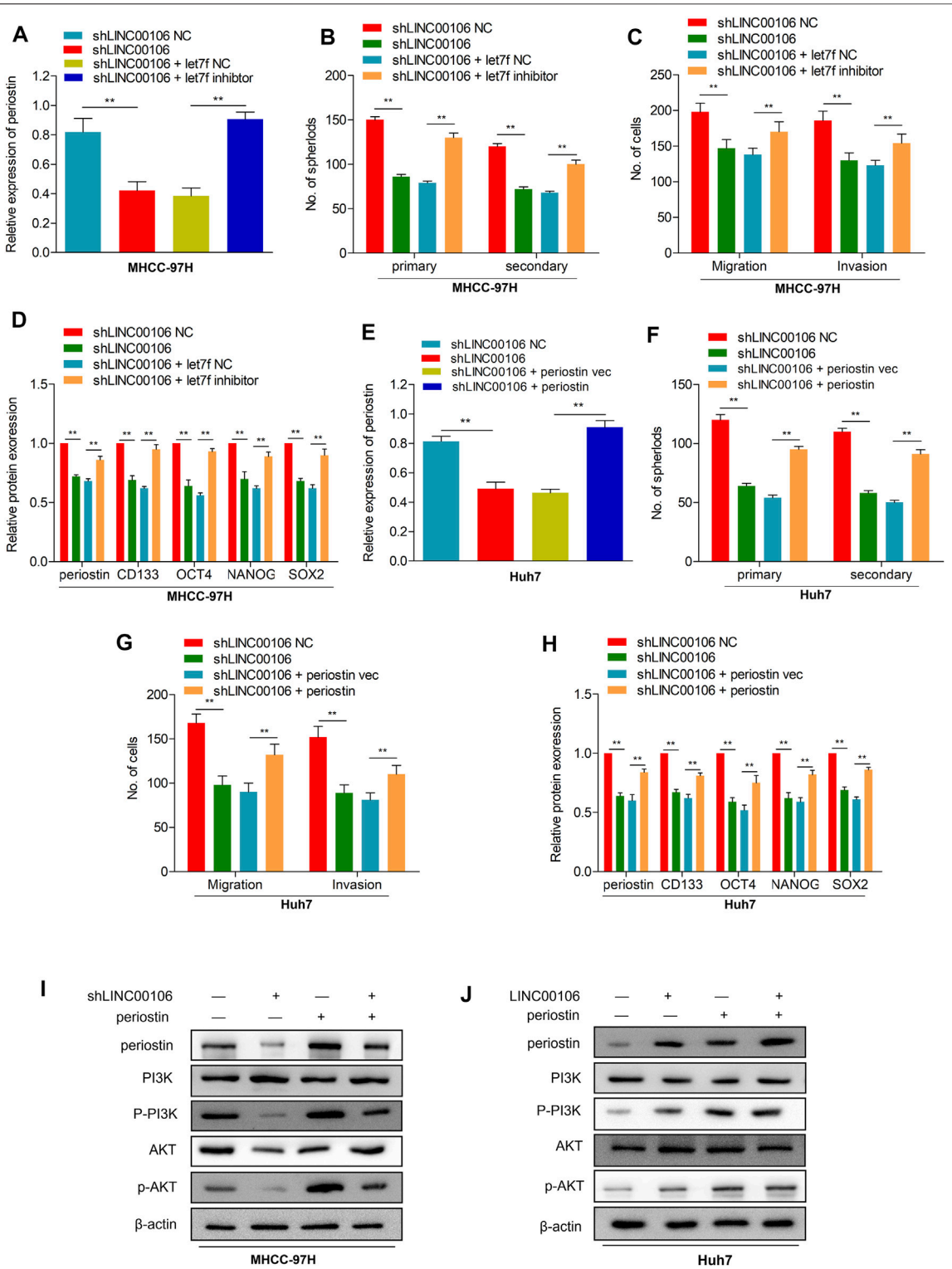

FIGURE 6 | let7f/Periostin/PI3K signaling pathway mediates LINC00106 promoted HCC stemness and metastasis properties. **(A–D)**, Expression of periostin **(A)**, Sphere formation capacities **(B)**, invasion and migration assays **(C)** and expression of stemness biomarkers **(D)** in MHCC-97H cells co-transfected with let7f inhibitors or let7f inhibitors NC and sh-LINC00106 or sh-LINC00106 NC; **(E–H)**. Expression of periostin **(E)**, Sphere formation capacities **(F)**, invasion and migration assays **(G)** and expression of stemness biomarkers **(H)** in Huh7 cells co-transfected with periostin NC or periostin-vec and sh-LINC00106 or sh-LINC00106 NC; **(I,J)**. Expression of periostin, total and phosphorylated PI3K/AKT3 following co-transfected with periostin-vec and sh-LINC00106 or LINC00106 mimics in HCC cell lines (**$p < 0.01$).

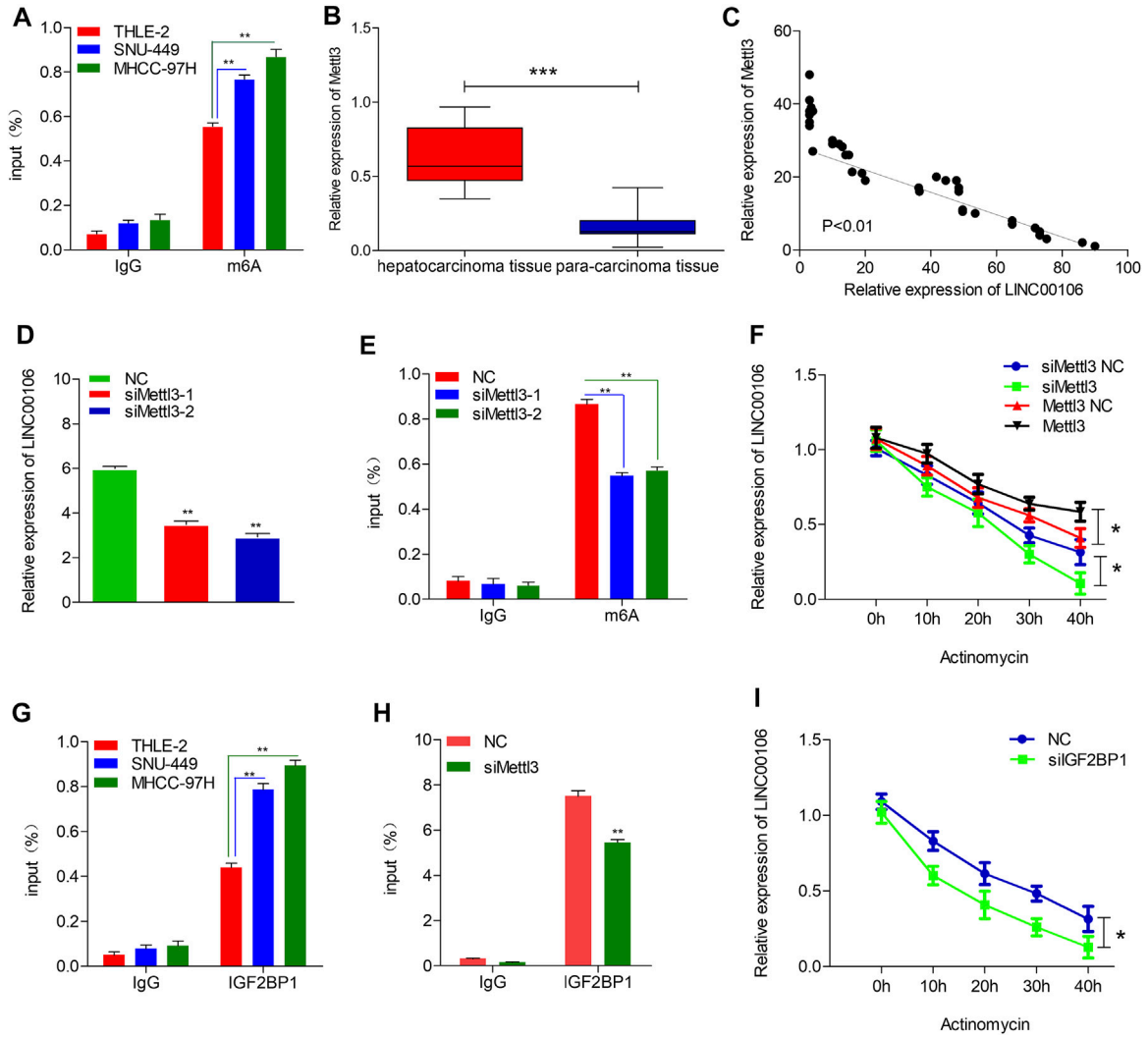

FIGURE 7 | Mettl3-induced m^{6}A modification is involved in the upregulation of LINC00106. **(A)**, RIP-qPCR showing the stronger enrichment of m^{6}A in SNU-449 and MHCC-97H cells than that in THLE-2 cell. **(B)**, Mettl3 expression was assessed in the HCC tissues and adjacent normal liver tissues. **(C)**, LINC00106 expression was positively correlated with Mettl3 expression in an analysis of HCC tissues. **(D)**, qRT-PCR of LINC00106 after Mettl3 inhibition in SNU-449 cells. **(E)**, RIP-qPCR showing the enrichment of m^{6}A in SNU-449 after Mettl3 depletion. **(F)**, The expression of LINC00106 after treatment with 2.5 μM actinomycin D for indicated times, with depletion or overexpression of Mettl3 in SNU-449 cells. **(G)**, RIP-qPCR showing the stronger enrichment of IGF2BP1 in SNU-449 and MHCC-97H cells than that in THLE-2 cell. **(H)**, RIP-qPCR showing the enrichment of IGF2BP1 in SNU-449 with Mettl3 knockdown. **(I)**, The expression of LINC00106 after treatment with 2.5 μM actinomycin D for indicated times, with IGF2BP1 knockdown in SNU-449 cells (*$p < 0.05$, **$p < 0.01$).

Figures S1B,C,F,G). Furthermore, the AKT and PI3K phosphorylation was remarkably inhibited by the knockdown of LINC00106 (**Figure 6I**), whereas it was enhanced by LINC00106 overexpression (**Figure 6J**). The foregoing findings implied that the let7f/periostin/PI3K axis mediates LINC00106-induced stemness and metastasis properties in HCC cells.

Mettl3-Mediated M^{6}A Modification Participates in LINC00106 Upregulation

To explore the mechanism leading to ectopic expression of LINC00106, we used RMVar (http://rmvar.renlab.org) prediction to reveal that numerous m^{6}A sites were distributed in LINC00106 with high confidence. Hence, we further clarified whether m^{6}A modification could upregulate the expression of LINC00106. By using the m^{6}A RNA IP (RIP) assay along with qRT-PCR, we found that m^{6}A was more significantly enriched in MHCC-97H and SNU-449 cells than in normal THLE-2 cell (**Figure 7A**). Methyltransferase like 3 (Mettl3) is a well-known m^{6}A methyltransferase ("writer") in mammalian cells. To verify the results, the expression of Mettl3 and its association with LINC00106 were assessed based on the TCGA database and HCC tissues expression detection. The results indicated that the Mettl3 level in HCC tissues was prominently elevated (**Figure 7B**), and

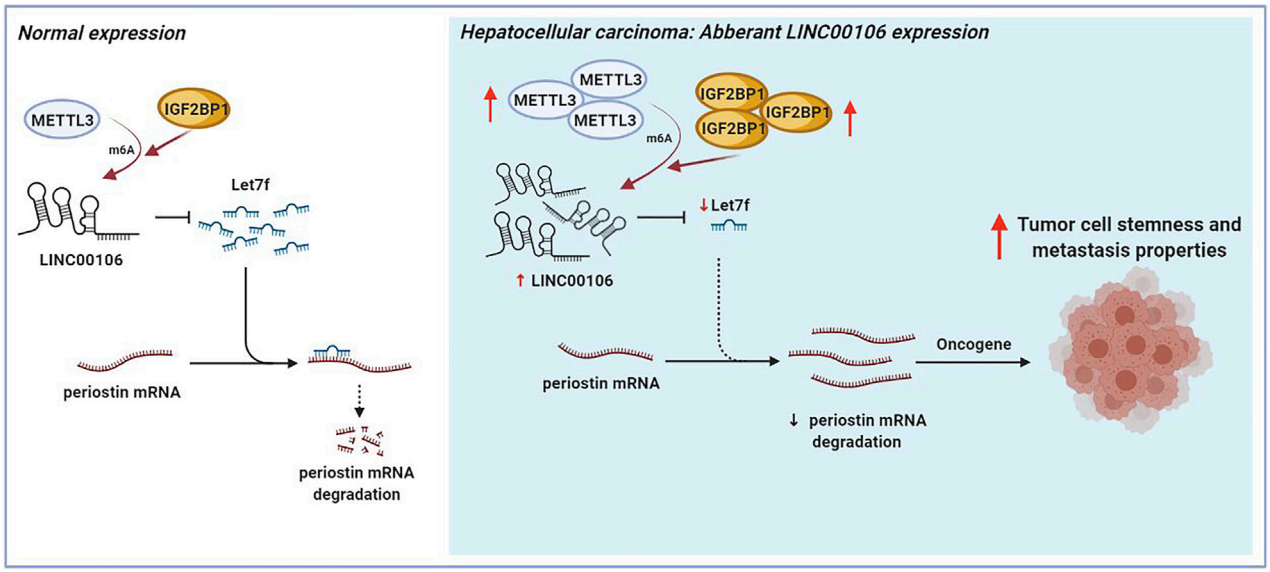

FIGURE 8 | The schematic figure shows that m^{6}A-mediated upregulation of LINC00106 promotes hepatocellular carcinoma stemness and metastasis properties via sponging let7f.

Mettl3 and LINC00106 expressions were positively correlated ($R = 0.53$, $p < 0.01$; **Figure 7C**). Moreover, silencing of Mettl3 lead to a significant reduction in LINC00106 expression (**Figure 7D**). RIP assays revealed that m^{6}A modification of LINC00106 expression was reduced upon Mettl3 silencing (**Figure 7E**). Furthermore, Mettl3 could regulate the stability of LINC00106 in HCC cells. Following the blockage of RNA *de novo* synthesis by actinomycin D treatment of cells, the stability of LINC00106 was decreased with the depletion of Mettl3. By contrast, the stability of LINC00106 was increased with the overexpression of Mettl3 (**Figure 7F**). The findings revealed that in HCC cells, Mettl3 could specifically maintain the stability of LINC00106 by facilitating m^{6}A modification.

The mechanism underlying the Mettl3-mediated LINC00106 stability in HCC cells was explored in detail in this study. The specific function of the insulin-like growth factor 2 mRNA-binding protein 1 (IGF2BP1; an m^{6}A "reader") in governing the stability of m^{6}A-modified lncRNAs in carcinomas has already been reported (Jonas et al., 2020). Using RMVar, the probable readers of LINC00106 m^{6}A loci were estimated, in which the binding sites of IGF2BP1 on LINC00106 with high confidence were found. RIP and qRT-PCR assays confirmed a direct interaction between IGF2BP1 and LINC00106 in HCC cells (**Figure 7G**). Additionally, upon inhibiting Mettl3, the IGF2BP1–LINC00106 interplay was disrupted (**Figure 7H**). We further used actinomycin D to treat cells and discovered a prominently lowered LINC00106 level following depletion of IGF2BP1 (**Figure 7I**). The results suggested that IGF2BP1 made LINC00106 more stable by binding to it, thereby displaying m^{6}A dependence. **Figure 8** illustrates the mechanism concerning the regulation of stemness and metastatic properties in HCC cells by m^{6}A-induced LINC00106.

DISCUSSION

Recurrence and metastasis in HCC caused by the stemness and metastasis properties of HCC cells not only seriously affects the survival and prognosis of patients but also enhances the requirements and challenges for diagnosis and treatment programmes (Kelley and Greten, 2021). Moreover, the underlying mechanism through which HCC cells acquire stemness and metastasis properties remains poorly understood to date.

Numerous studies have proved that the gain and loss of function of selected lncRNAs can affect the cellular processes, development, and diseases (Atianand et al., 2016; Andersen et al., 2019). One of the greatest discoveries during the postgenomic age has been the discovery of a broad, novel spectrum of human genomic regulators known as lncRNAs, whose expression patterns are exquisitely specific to the cell type in healthy and diseased states (Huo et al., 2017; Sarropoulos et al., 2019; Rinn and Chang, 2020). Several lncRNAs from human HCCs, which have been demonstrated to facilitate or suppress metastasis in carcinomas by using sequestering EMT-associated miRNAs as decoying molecules (Wong et al., 2018) or using self-renewal simulation of hepatoma stem cells (Wang et al., 2015; Wu et al., 2019). To date, none of the studies have reported the expression of LINC00106 in HCC. In the present study, LINC00106 was found to be remarkably upregulated in HCC, and patients with a high LINC00106 level displayed a poor prognosis. When the LINC00106 levels were decreased, the stemness and metastasis properties of HCC cells were suppressed *in vitro* and *in vivo*, and the stemness and EMT markers were significantly downregulated in HCC cells. Our results suggest that LINC00106 can play an oncogenic role and confer the stemness and metastasis properties to HCC cells.

Based on the aforementioned findings, we further explored the underlying molecular mechanism by which LINC00106 modulated the stemness and metastasis properties in HCC cells. Numerous studies have shown that the molecular sponges acting as miRNAs are the main regulators of lncRNAs (He et al., 2020; Statello et al., 2020). Considering the abundances of LNC00106 in the nucleus and cytoplasm, we speculate that the ceRNA mechanism may also be involved in the carcinogenic effect of LNC00106 in HCC. In order to confirm the above hypothesis, purported let7f binding sites for LINC00106 were revealed through the bioinformatics analysis, and the luciferase reporter, RIP, and RNA pull-down assays were further performed. Our results inferred that LINC00106 is capable of sponging and declining the expression of let7f through ceRNA mechanism in HCC. Additionally, the LINC00106/let7f axis could further regulate the periostin mRNA level. Periostin, as a stromal factor for healthy stem cell micro-environment, plays a crucial role during metastatic colonization for the maintenance and expansion regulation of CSCs to promote tumor metastasis (Wang and Ouyang, 2012; Zhou et al., 2015). We found that periostin overexpression in HCC cells could increase the expression of stemness markers, blunt let7f mimic-triggered sphere formation, and metastasis properties inhibition to promote HCC stemness and metastasis potential. These biological characteristics are regulated by the periostin-associated PI3K-AKT signaling pathway.

As an emerging layer of epigenetic regulation, the RNA m^{6}A can influence the fate of modified RNA molecules, which exert crucial effects on nearly all the vital bioprocesses, including cancer development (Huang et al., 2020). One critical member of the m^{6}A complex is Mettl3, which is an m^{6}A "writer". Studies have reported that METTL3 can repress SOCS2 expression in HCC through an m^{6}A-YTHDF2-dependent mechanism and contributes to HCC progression (Chen et al., 2018). In the present study, Mettl3 was found to specifically maintain LINC00106 stability by facilitating m^{6}A modification in HCC cells, so as to increase the abundances of LINC00106 in the nucleus, which can furtherly promote stemness and metastasis properties in HCC. The biological functions of the m^{6}A modification are mediated through the binding of m^{6}A to IGF2BP1 and other m^{6}A "readers". An m^{6}A-dependent stimulation of SRF expression by IGF2BP1 has been reported, which was accomplished through disruption of SRF mRNA decay directed by miRNAs, consequently resulting in improved action of SRF-dependent transcription and carcinoma cell proliferation and infiltration (Müller et al., 2018). Our findings revealed that IGF2BP1 could directly bind to LINC00106 and promote LINC00106 expression in an m^{6}A-dependent manner.

In summary, we demonstrated that LINC00106 can play an oncogenic role and promote stemness and metastasis in HCC. Moreover, LINC00106 can sponge and reduce the expression of miR-let7f in HCC through ceRNA mechanism to regulate the periostin-associated PI3K-AKT signaling pathway. Additionally, the m^{6}A modification mediated by Mettl3 resulted in abnormal LINC00106 overexpression. Our findings not only demonstrate the mechanism by which LINC00106 regulates stemness but also offer potential therapeutic targets to deal with tumor metastasis in HCC.

CONCLUSION

We demonstrated that LINC00106 can play an oncogenic role and promote stemness and metastasis properties in HCC. Mechanistically, through ceRNA mechanism, LINC00106 is capable of sponging and declining the expression of miR–let7f in HCC, so that under both *in vivo* and *in vitro* conditions, the stemness and metastatic properties of HCC cells can be augmented by the periostin-associated PI3K-AKT signaling pathway. Moreover, aberrant LINC00106 overexpression was induced by Mettl3-mediated m^{6}A modification. Thus, the findings of this study suggest that LINC00106 is a potential diagnostic marker and therapeutic target for HCC.

DATA AVAILABILITY STATEMENT

The datasets presented in this study can be found in online repositories. The names of the repository/repositories and accession number(s) can be found in the article/ **Supplementary Material**.

ETHICS STATEMENT

The studies involving human participants were reviewed and approved by the Ethics Committee of the Affiliated Hospital of Guilin Medical University. The patients/participants provided their written informed consent to participate in this study. The animal study was reviewed and approved by Animal Ethics Committee of Guangxi Medical University.

AUTHOR CONTRIBUTIONS

ZW and WL conceived and designed the experiments. WL and YW performed the experiments. WL, YW, QZ, MG, HZ analyzed the data. ZW supervised the whole experimental work and revised the manuscript. WL wrote the paper. All authors read and approved the final manuscript.

FUNDING

This research was supported in part by the National Natural Science Foundation of China (No. 81860436) and Guangxi postdoctoral special fund of China (No. 2021M693805).

ACKNOWLEDGMENTS

We wish to particularly acknowledge the patients enrolled in this study for their participation, and the Department of Pathology and Physiopathology, Guilin Medical University, for its collaboration in providing the human samples and the clinical information used in this project with appropriate ethics approval, and the Animal Experiment Center of Guangxi Medical University for providing the animal experiment platform. We also acknowledge Professor Bo Tang and Hongliang Dai for their guidance on this research.

SUPPLEMENTARY MATERIAL

The Supplementary Material for this article can be found online at: https://www.frontiersin.org/articles/10.3389/fcell.2021.781867/full#supplementary-material

REFERENCES

Andersen, R. E., Hong, S. J., Lim, J. J., Cui, M., Harpur, B. A., Hwang, E., et al. (2019). The Long Noncoding RNA Pnky Is a Trans-acting Regulator of Cortical Development *In Vivo*. *Dev. Cel* 49 (4), 632–642. doi:10.1016/j.devcel.2019.04.032

Atianand, M. K., Hu, W., Satpathy, A. T., Shen, Y., Ricci, E. P., Alvarez-Dominguez, J. R., et al. (2016). A Long Noncoding RNA lincRNA-EPS Acts as a Transcriptional Brake to Restrain Inflammation. *Cell* 165 (7), 1672–1685. doi:10.1016/j.cell.2016.05.075

Chen, G., Wang, Y., Zhao, X., Xie, X.-z., Zhao, J.-g., Deng, T., et al. (2021). A Positive Feedback Loop between Periostin and TGFβ1 Induces and Maintains the Stemness of Hepatocellular Carcinoma Cells via AP-2α Activation. *J. Exp. Clin. Cancer Res.* 40 (1). doi:10.1186/s13046-021-02011-8

Chen, M., Wei, L., Law, C., Tsang, F. H., Shen, J., Cheng, C. L., et al. (2018). RNA N6-Methyladenosine Methyltransferase-like 3 Promotes Liver Cancer Progression through YTHDF2-dependent Posttranscriptional Silencing of SOCS2. *Hepatology* 67 (6), 2254–2270. doi:10.1002/hep.29683

Faltas, B. (2012). Cornering Metastases: Therapeutic Targeting of Circulating Tumor Cells and Stem Cells. *Front. Oncol.* 2. doi:10.3389/fonc.2012.00068

He, H., Wang, Y., Ye, P., Yi, D., Cheng, Y., Tang, H., et al. (2020). Long Noncoding RNA ZFPM2-AS1 Acts as a miRNA Sponge and Promotes Cell Invasion through Regulation of miR-139/GDF10 in Hepatocellular Carcinoma. *J. Exp. Clin. Cancer Res.* 39 (1). doi:10.1186/s13046-020-01664-1

Huang, H., Weng, H., and Chen, J. (2020). M6A Modification in Coding and Non-coding RNAs: Roles and Therapeutic Implications in Cancer. *Cancer Cell* 37 (3), 270–288. doi:10.1016/j.ccell.2020.02.004

Huo, X., Han, S., Wu, G., Latchoumanin, O., Zhou, G., Hebbard, L., et al. (2017). Dysregulated Long Noncoding RNAs (lncRNAs) in Hepatocellular Carcinoma: Implications for Tumorigenesis, Disease Progression, and Liver Cancer Stem Cells. *Mol. Cancer* 16 (1). doi:10.1186/s12943-017-0734-4

Jonas, K., Calin, G. A., and Pichler, M. (2020). RNA-binding Proteins as Important Regulators of Long Non-coding RNAs in Cancer. *Ijms* 21 (8), 2969. doi:10.3390/ijms21082969

Kelley, R. K., and Greten, T. F. (2021). Hepatocellular Carcinoma - Origins and Outcomes. *N. Engl. J. Med.* 385 (3), 280–282. doi:10.1056/nejmcibr2106594

Ling, S., Shan, Q., Zhan, Q., Ye, Q., Liu, P., Xu, S., et al. (2019). USP22 Promotes Hypoxia-Induced Hepatocellular Carcinoma Stemness by a HIF1α/USP22 Positive Feedback Loop upon TP53 Inactivation. *Gut* 69 (7), 1322–1334. doi:10.1136/gutjnl-2019-319616

Ma, X.-L., Hu, B., Tang, W.-G., Xie, S.-H., Ren, N., Guo, L., et al. (2020). CD73 Sustained Cancer-Stem-Cell Traits by Promoting SOX9 Expression and Stability in Hepatocellular Carcinoma. *J. Hematol. Oncol.* 13 (1). doi:10.1186/s13045-020-0845-z

Müller, S., Glaß, M., Singh, A. K., Haase, J., Bley, N., Fuchs, T., et al. (2018). IGF2BP1 Promotes SRF-dependent Transcription in Cancer in a m6A- and miRNA-dependent Manner. *Nucleic Acids Res.* 47 (1), 375–390. doi:10.1093/nar/gky1012

Rinn, J. L., and Chang, H. Y. (2020). Long Noncoding RNAs: Molecular Modalities to Organismal Functions. *Annu. Rev. Biochem.* 89 (1), 283–308. doi:10.1146/annurev-biochem-062917-012708

Sarropoulos, I., Marin, R., Cardoso-Moreira, M., and Kaessmann, H. (2019). Developmental Dynamics of lncRNAs across Mammalian Organs and Species. *Nature* 571 (7766), 510–514. doi:10.1038/s41586-019-1341-x

Shu, G., Su, H., Wang, Z., Lai, S., Wang, Y., Liu, X., et al. (2021). LINC00680 Enhances Hepatocellular Carcinoma Stemness Behavior and Chemoresistance by Sponging miR-568 to Upregulate AKT3. *J. Exp. Clin. Cancer Res.* 40 (1). doi:10.1186/s13046-021-01854-5

Statello, L., Guo, C.-J., Chen, L.-L., and Huarte, M. (2020). Gene Regulation by Long Non-coding RNAs and its Biological Functions. *Nat. Rev. Mol. Cel Biol* 22 (2), 96–118. doi:10.1038/s41580-020-00315-9

Wang, Y., He, L., Du, Y., Zhu, P., Huang, G., Luo, J., et al. (2015). The Long Noncoding RNA lncTCF7 Promotes Self-Renewal of Human Liver Cancer Stem Cells through Activation of Wnt Signaling. *Cell Stem Cell* 16 (4), 413–425. doi:10.1016/j.stem.2015.03.003

Wang, Z., and Ouyang, G. (2012). Periostin: A Bridge between Cancer Stem Cells and Their Metastatic Niche. *Cell Stem Cell* 10 (2), 111–112. doi:10.1016/j.stem.2012.01.002

Wong, C.-M., Tsang, F. H.-C., and Ng, I. O.-L. (2018). Non-coding RNAs in Hepatocellular Carcinoma: Molecular Functions and Pathological Implications. *Nat. Rev. Gastroenterol. Hepatol.* 15 (3), 137–151. doi:10.1038/nrgastro.2017.169

Wu, J., Zhu, P., Lu, T., Du, Y., Wang, Y., He, L., et al. (2019). The Long Non-coding RNA LncHDAC2 Drives the Self-Renewal of Liver Cancer Stem Cells via Activation of Hedgehog Signaling. *J. Hepatol.* 70 (5), 918–929. doi:10.1016/j.jhep.2018.12.015

Yuan, J.-h., Liu, X.-n., Wang, T.-t., Pan, W., Tao, Q.-f., Zhou, W.-p., et al. (2017). The MBNL3 Splicing Factor Promotes Hepatocellular Carcinoma by Increasing PXN Expression through the Alternative Splicing of lncRNA-PXN-AS1. *Nat. Cel Biol* 19 (7), 820–832. doi:10.1038/ncb3538

Zheng, A., Song, X., Zhang, L., Zhao, L., Mao, X., Wei, M., et al. (2019). Long Non-coding RNA LUCAT1/miR-5582-3p/TCF7L2 axis Regulates Breast Cancer Stemness via Wnt/β-Catenin Pathway. *J. Exp. Clin. Cancer Res.* 38 (1). doi:10.1186/s13046-019-1315-8

Zhou, W., Ke, S. Q., Huang, Z., Flavahan, W., Fang, X., Paul, J., et al. (2015). Periostin Secreted by Glioblastoma Stem Cells Recruits M2 Tumour-Associated Macrophages and Promotes Malignant Growth. *Nat. Cel Biol.* 17 (2), 170–182. doi:10.1038/ncb3090

Zuo, X., Chen, Z., Gao, W., Zhang, Y., Wang, J., Wang, J., et al. (2020). M6A-mediated Upregulation of LINC00958 Increases Lipogenesis and Acts as a Nanotherapeutic Target in Hepatocellular Carcinoma. *J. Hematol. Oncol.* 13 (1). doi:10.1186/s13045-019-0839-x

Conflict of Interest: The authors declare that the research was conducted in the absence of any commercial or financial relationships that could be construed as a potential conflict of interest.

Publisher's Note: All claims expressed in this article are solely those of the authors and do not necessarily represent those of their affiliated organizations, or those of the publisher, the editors and the reviewers. Any product that may be evaluated in this article, or claim that may be made by its manufacturer, is not guaranteed or endorsed by the publisher.

frontiers in Cell and Developmental Biology

ORIGINAL RESEARCH
published: 09 December 2021
doi: 10.3389/fcell.2021.783385

m6A Modification-Mediated *DUXAP8* Regulation of Malignant Phenotype and Chemotherapy Resistance of Hepatocellular Carcinoma Through miR-584-5p/MAPK1/ERK Pathway Axis

Zefeng Liu[1,2], Jin Lu[3], He Fang[1,2], Jiyao Sheng[1,2], Mengying Cui[1,2], Yongsheng Yang[1], Bo Tang[1,4]* and Xuewen Zhang[1,2]**

[1]Department of Hepatobiliary Pancreatic Surgery, The Second Hospital of Jilin University, Changchun, China, [2]Jilin Engineering Laboratory for Translational Medicine of Hepatobiliary and Pancreatic Diseases, Changchun, China, [3]Cancer Center, The First Hospital of Jilin University, Changchun, China, [4]Department of Health Sciences, Hiroshima Shudo University, Hiroshima, Japan

Hepatocellular carcinoma (HCC) has a poor prognosis due to its high malignancy, rapid disease progression, and the presence of chemotherapy resistance. Long-stranded non-coding RNAs (lncRNAs) affect many malignant tumors, including HCC. However, their mechanism of action in HCC remains unclear. This study aimed to clarify the role of *DUXAP8* in regulating the malignant phenotype and chemotherapy resistance in HCC. Using an *in vivo* xenograft tumor model, the regulatory functions and mechanisms of lncRNA *DUXAP8* in the progression and response of HCC to chemotherapy were explored. It was found that *DUXAP8* was significantly upregulated in a patient-derived xenograft tumor model based on sorafenib treatment, which is usually associated with a relatively poor prognosis in patients. In HCC, *DUXAP8* maintained its upregulation in the expression by increasing the stability of m6A methylation-mediated RNA. *DUXAP8* levels were positively correlated with the proliferation, migration, invasion, and chemotherapy resistance of HCC *in vivo* and *in vitro*. In the mechanistic study, it was found that *DUXAP8* competitively binds to miR-584-5p through a competing endogenous RNA (ceRNA) mechanism, thus acting as a molecular sponge for miR-584-5p to regulate *MAPK1* expression, which in turn activates the *MAPK/ERK* pathway. These findings can provide ideas for finding new prognostic indicators and therapeutic targets for patients with HCC.

Keywords: DUXAP8, hepatocellular carcinoma, m6A methylation modification, chemotherapy resistance, malignant phenotype, miR-584-5p, MAPK1

OPEN ACCESS

Edited by:
Lutao Du,
Second Hospital of Shandong University, China

Reviewed by:
Ying Hu,
Harbin Institute of Technology, China
Seyed Mehdi Jafarnejad,
Queen's University Belfast, United Kingdom
Wenhui Lou,
Fudan University, China
Bei Sun,
Harbin Medical University, China

****Correspondence:***
Yongsheng Yang
yyswxt@126.com
Bo Tang
dr_sntangbo@163.com
Xuewen Zhang
zhangxw@jlu.edu.cn

Specialty section:
This article was submitted to Epigenomics and Epigenetics, a section of the journal Frontiers in Cell and Developmental Biology

Received: *26 September 2021*
Accepted: *29 November 2021*
Published: *09 December 2021*

Citation:
Liu Z, Lu J, Fang H, Sheng J, Cui M, Yang Y, Tang B and Zhang X (2021) m6A Modification-Mediated DUXAP8 *Regulation of Malignant Phenotype and Chemotherapy Resistance of Hepatocellular Carcinoma Through miR-584-5p/MAPK1/ERK Pathway Axis. Front. Cell Dev. Biol. 9:783385. doi: 10.3389/fcell.2021.783385*

INTRODUCTION

Hepatocellular carcinoma (HCC) is one of the five most common malignant tumors globally (Zhu et al., 2019). Worldwide, nearly 700,000 people die each year from HCC (Fang et al., 2018; Wu et al., 2019), and its death toll ranks second among all malignant tumor-associated deaths. HCC poses a serious health burden globally (Petrick et al., 2020; Reinders et al., 2020; Yang et al., 2020). In China, the number of deaths due to HCC is the second-highest among all malignant tumors, which come

right after lung cancer (Raoul and Edeline, 2020). Despite recent improvements in surgical techniques and chemotherapy regimens, the prognosis of HCC remains poor, and its prevalence is approaching its mortality (Jemal et al., 2011). Particularly, the occurrence of chemotherapy resistance has severely hampered the therapeutic outcome of HCC. Sorafenib, a tyrosine kinase inhibitor, is currently the first-line medication for treating unresectable HCC (Bruix et al., 2019) and can extend the survival of HCC patients by an average of 12.3 months (Kudo et al., 2018; Rimassa and Worns, 2020), but this benefit of increased survival may be lost due to the emergence of drug resistance. The etiology of HCC and the mechanisms of chemotherapy resistance are still unclear; thus, a deeper understanding of genetics and epigenetic mechanisms behind the development and progression of HCC and chemotherapy resistance is required to develop more effective therapeutic intervention strategies.

The development of whole-genome and transcriptome sequencing technologies has revealed the composition of the human genome, where less than 2% of genes are protein-coding genes and the rest are all non-coding genes (Harrow et al., 2012; Shi et al., 2016). There is increasing evidence that complex functions in living organisms may be regulated by a range of RNAs from non-coding regions of the genome. Long non-coding RNAs (LncRNAs) represent a group of RNA molecules with a transcript length exceeding 200 nucleotides and encode only short polypeptides or do not encode proteins (Zheng et al., 2015). Recent studies have indicated that lncRNAs are involved in many critical biological processes, such as X-chromosome inactivation, stem cell maintenance, transcriptional regulation, and epigenetic regulation (Zhang et al., 2018). Additionally, lncRNAs are involved in the regulation of many diseases, especially playing an essential role in the occurrence and development of malignant tumors. Some lncRNAs act as protein co-regulators directly binding to their helper proteins and regulating the expression of downstream tumor-associated genes (Chen et al., 2016; Yuan et al., 2016; Zhu et al., 2016). Another part of lncRNAs act as competitive endogenous RNAs (ceRNAs) (Yuan et al., 2014; Li et al., 2015b), and such lncRNAs achieve microRNA detachment and regulate the expression of microRNA-targeted oncogenes or tumor suppressor genes through molecular sponge effects. These studies suggested that the abnormal expression of lncRNAs plays an essential role in tumor development.

The pseudogene-derived lncRNA, Double Homeobox A Pseudogene 8 (*DUXAP8*), is located on chromosome 22q11.1 with a full length of 2,107 bp (Sun et al., 2017). Recently, *DUXAP8* has been shown to be highly expressed in various malignant tumors. It has been shown that *DUXAP8* can significantly inhibit the expression of *PLEKHO1* in gastric cancer, enhancing the proliferation and migration of tumor cells (Ma et al., 2017a). In glioma, downregulation of *DUXAP8* inhibits the proliferation of tumor cells (Zhao et al., 2019). In non-small cell lung cancer (NSCLC), *DUXAP8* promotes tumor cell proliferation and invasion through epigenetic silencing of *Egr1* and *RHOB* (Sun et al., 2017). In pancreatic cancer, *DUXAP8* promotes tumor growth through epigenetic silencing of *CDKN1A* and *KLF2* (Lian et al., 2018). While the mechanism of action of *DUXAP8* in HCC is unclear, Wang et al. (2020) reported that *DUXAP8* can be used for the diagnosis of HCC and can predict the prognosis of HCC. In this study, it was found that *DUXAP8* was highly expressed in liver cancer tissues and cells, where high expression of *DUXAP8* often predicts poor prognosis in patients. In *in vivo* and *in vitro* experiments, it was found that overexpression of *DUXAP8* promoted the malignant phenotype and chemotherapy resistance in HCC. Mechanistically, it was found that *DUXAP8* upregulated *MAPK1* through competitive binding to miR-584-5p, which activated the *MAPK/ERK* pathway and promoted the proliferation, invasive migration, stemness maintenance, and chemotherapy resistance of HCC. These results provided a deeper understanding of the driving mechanisms of lncRNAs in HCC development, progression, and resistance to chemotherapy. They revealed the importance of *DUXAP8* in HCC progression, which can help identify new prognostic indicators and therapeutic targets for HCC patients.

MATERIALS AND METHODS

Cell Lines and Cell Culture

Standard human hepatocytes THLE-3 and HCC cell lines MHCC-97H, Huh7, HCC-LM3, Bel-7405, SNU-449, SK-Hep-1, and SNU-182 were purchased from the American Type Culture Collection or the Cell Bank of the National Collection of Authenticated Cell Cultures (Shanghai, China). The conventional culture of HCC cell lines was performed (Li et al., 2015a). Cells were cultured in appropriate culture media containing 10% fetal bovine serum (FBS; Gibco) supplemented with penicillin (100 U/ml) and streptomycin (100 μg/ml). All cell lines were cultured at 37°C in an incubator using 5% CO_2/95% air and 100% humidity to minimize the chances of bacterial contamination. Cells were passaged every 1–2 days to maintain logarithmic growth.

Patients and Specimens

All studies involving human samples were reviewed and approved by the Ethics Committee of the Second Hospital of Jilin University. The study protocol conformed to the ethical standards of the Declaration of Helsinki. Written informed consent was also obtained from all patients according to the Helsinki Declaration. Liver cancer and pericarcinomatous tissues were obtained from HCC patients at the Second Hospital of Jilin University (n = 79). The examined clinicopathological features included age, sex, number of tumor nodules, etiology, serum alpha fetoprotein (AFP) level, cancer staging, tumor size, and the presence of vascular invasion. Cancer staging was based on the 6th edition of the International Union Against Cancer tumor–node–metastasis (TNM) Classification.

Chemical Reagents and Antibodies

Lipofectamine 2000 transfection reagent and total RNA extractant (TRIzol) were purchased from Invitrogen (Grand Island, NY, United States); *P-CREB* antibodies were purchased from Cell Signaling Technology (Danvers, MA, United States);

P38 and P-P38 antibodies were purchased from Abcam Corporation (Cambridge, MA, United States); and all other antibodies were purchased from Proteintech (Rosemont, IL, United States). Unless otherwise stated, all other chemical reagents were purchased from Sigma-Aldrich (St. Louis, MO, United States).

Reverse Transcription Quantitative Polymerase Chain Reaction (RT–qPCR)

Total RNA was extracted using the RNA Simple Total RNA Kit (TIANGEN, DP419), and RNA in the cytoplasm and nucleus was isolated using the Nuclear/Cytoplasmic Isolation Kit (BioVision, San Francisco, CA, United States) according to the manufacturer's instructions. Complementary DNA (cDNA) was synthesized using the RevertAid First Strand cDNA Synthesis Kit (Thermo Scientific, #K1622) and Poly(A) Polymerase Reaction Buffer (NEB, M0276s) according to the manufacturer's instructions. According to the manufacturer's instructions, real-time qRT–PCR analysis was performed using the Platinum SYBR Green qPCR SuperMix-UDG kit (Life Technologies, Gaithersburg, MD, United States). Fold changes in RNA expression were quantified using the $2^{-\Delta\Delta Ct}$ method. The primer sequences used in this study are listed in **Supplementary Table S1**.

Immunohistochemistry (IHC)

The paraffin sections of tissues were dewaxed in xylene and hydrated using graded ethanol. The heat-mediated and antigen repair citrate (0.01 M, pH 6.0) was used in performing the IHC experiment. Endogenous peroxidase activity was blocked using 3% H_2O_2 at room temperature for 15 min. Thereafter, the sections were incubated with goat serum for 1 h to block the nonspecific binding site and then incubated overnight at 4°C using the primary antibody. The sections were then re-warmed at room temperature for 30 min, rinsed three times with phosphate-buffered saline (PBS) for 5 min each, and incubated with horseradish peroxidase (HRP)-labeled secondary antibody at room temperature for 1 h. Each section was rinsed thrice again with PBS for 5 min each. Color development was conducted using the HRP DAB kit (Thermo Science, Shanghai, China). Nuclei were re-stained with hematoxylin, and sections were sealed with neutral glue. Images were obtained using an Olympus X71 inverted microscope (Olympus Corp., Tokyo, Japan).

Western Blot

Tissues or cells were homogenized and lysed using a lysis buffer. After the protein concentration was determined using the bicinchoninic acid method, β-mercaptoethanol, and bromophenol blue were added to the sample buffer for electrophoresis. Proteins were separated through 10% polyacrylamide gel electrophoresis and then transferred to polyvinylidene difluoride membranes (Bio-Rad, Shanghai, China). The membranes were incubated overnight at 4°C with primary antibodies. After incubation with secondary antibodies for 2 h at room temperature, the reaction bands were visualized using an enhanced chemiluminescence system, and the intensity of the bands was quantified using an image analysis system.

Methylated RNA Immunoprecipitation qPCR (MeRIP–qPCR)

The level of m6A in *DUXAP8* was determined using MeRIP–qPCR. The intracellular RNA was first extracted using the TRIzol reagent and then bound to protein A/G magnetic beads with anti-m6A antibody or immunoglobulins (IgG; Cell Signaling Technology) (3 μg), and mixed with 100-μg total RNA in an immunoprecipitation buffer containing RNase/protease. The m6A-modified RNA was eluted twice with 6.7-mM N6-methyladenosine 5′-monophosphate disodium salt at 4°C for 1 h. RT–qPCR analysis was subsequently performed to determine the extent of m6A enrichment on *DUXAP8*.

Luciferase Assay

The complementary DNA fragment containing wild-type or mutant *DUXAP8* fragment/*MAPK1* 3′ untranslated region (UTR) was subcloned to the downstream of luciferase in the pGL3-basic luciferase reporter gene (Promega, Beijing, China). The firefly luciferase gene containing wild-type or mutant *DUXAP8* fragment/*MAPK1* was cotransfected with an empty vector or miR-584-5p mimics, and luciferase activity was measured using the Dual-Luciferase Kit (Promega, Beijing, China) 48 h after transfection.

RNA Immunoprecipitation (RIP) Analysis

According to the manufacturer's instructions, the Magna RIPTM RNA Binding Protein Immunoprecipitation Kit (Millipore, United States) was used. Briefly, cell extracts were immunoprecipitated with antibodies against AGO2 or IgG and magnetic beads at 4°C for 6 h. The proteins in the complex were removed using 0.1% SDS/proteinase K (0.5-mg/ml, 55°C for 30 min), and immunoprecipitated proteins and RNA were detected using Western blot and RT–qPCR, respectively.

RNA Pull-Down Experiments

The Pierce Magnetic RNA-Protein Pull-Down Kit (Thermo Fisher Scientific, 20,164) was used according to the manufacturer's instructions. Briefly, cell lysates were treated with RNAase-free DNAase I and then incubated with the treated cell lysate, streptavidin-labeled magnetic beads, and a biotin-labeled *DUXAP8* probe. The magnetic beads could capture proteins/miRNAs that interact with *DUXAP8*. A Pierce™ RNA 3′ End Desthiobiotinylation Kit (Thermo, 20,163) was used for *DUXAP8* biotinylation labeling. The proteins and RNA in the captured protein-RNA complexes were analyzed using Western blot and RT–qPCR.

Establishment of a Subcutaneous Xenotransplanted Tumor Model in Mice

Four-week-old BALB/c nude mice were purchased from the Experimental Animal Center of Jilin University (Changchun,

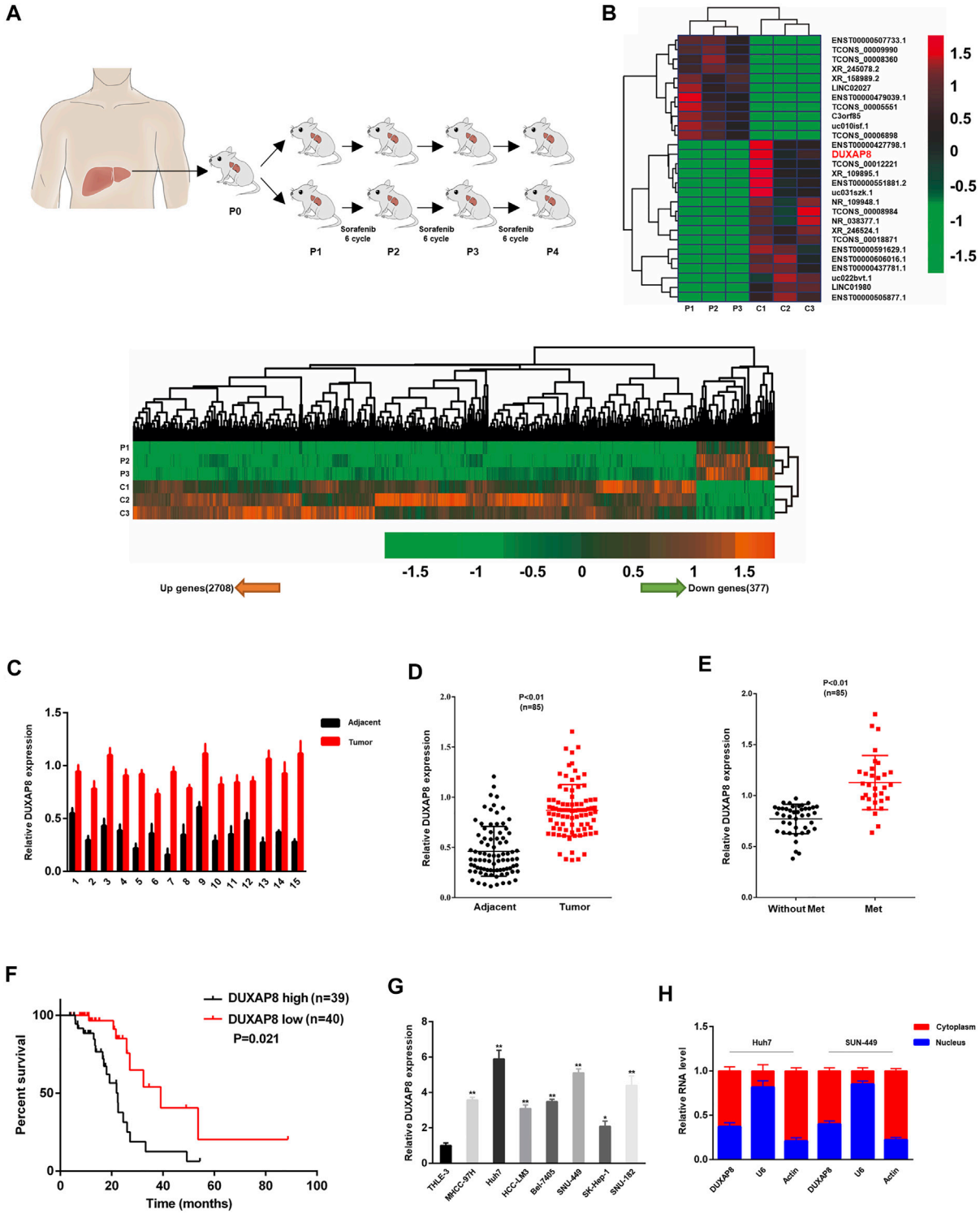

FIGURE 1 | *DUXAP8* is highly expressed in sorafenib-treated patient-derived xenograft (PDX) hepatocellular carcinoma model, and its upregulation predicts poor prognosis of HCC. **(A)** Experimental procedure of the sorafenib-treated PDX HCC model. **(B)** The heat map indicates the differential expression of lncRNAs in sorafenib-treated and control P4-PDX mice. **(C)** Comparison of *DUXAP8* expression in liver cancer tissues of 15 HCC patients with paired pericarcinomatous normal tissues. **(D)** Comparison of *DUXAP8* expression in HCC tissues of 85 HCC patients with paired pericarcinomatous normal tissues. **(E)** Relationship between *DUXAP8* expression in liver cancer tissues of 85 patients and the presence of distant metastasis. **(F)** Kaplan-Meier analysis of the correlation between *DUXAP8* expression levels and HCC prognosis in 79 patients. **(G)** Comparison of *DUXAP8* expression in HCC cell lines and THLE-3 cells. **(H)** RT–qPCR assay of the distribution of *DUXAP8* in the nucleus and cytoplasm of HCC cells. Data are expressed as mean, $^{*}p < 0.05$, $^{**}p < 0.01$.

China). All experimental animal protocols were performed according to the "Guide for the Care and Use of Laboratory Animals" issued by the National Institutes of Health. Experimental animal protocols for this study were reviewed and approved by the Animal Experiment Ethics Committee of the First Hospital of Jilin University. During modeling, 2×10^6 Huh7 cells with silenced *DUXAP8* expression or negative control Huh7 cells were injected subcutaneously into the lateral abdominal region of each mouse. The tumor volume was measured weekly and calculated as V = (length × width^2)/2. The tumors were then excised and weighed 4 weeks later.

Statistical Analysis

All values were expressed as mean ± standard deviation. Comparisons between groups were made using a t-test or one-way analysis of variance. Qualitative data were analyzed using the chi-square test. Linear regression analysis was conducted for correlations between gene expression levels. Statistical analyses were performed using GraphPad Prism v8.0 (GraphPad, Inc., United States) and Statistical Software Package for Social Sciences (v 22.0; SPSS, Inc., Chicago, IL, United States). Differences were statistically significant when $p < 0.05$.

RESULTS

High Expression of *DUXAP8* in an Animal Model of Patient-Derived Xenograft (PDX) HCC Treated With Sorafenib

Sorafenib is an oral multi-kinase inhibitor. As the standard FDA-approved targeted therapy for HCC, sorafenib exhibits a survival benefit and has dramatically improved the prognosis of HCC patients, especially in patients with advanced HCC. However, acquired or intrinsic chemotherapy resistance severely affects its overall efficacy in treating HCC (Liu et al., 2019; Wei et al., 2019; Xiang et al., 2019). To clarify the molecular mechanism of drug resistance to sorafenib in HCC, a PDX model for sorafenib treatment was first established, in which surgically resected primary HCC tissue was finely trimmed and directly transplanted into mice with immunodeficiency. Tumor-bearing mice were treated with saline (vector) or sorafenib for several generations (**Figure 1A**). Differentially expressed lncRNAs between P4-PDX treated with vector or sorafenib were identified using lncRNA sequencing analysis (**Figure 1B**). Among identified lncRNAs, the significantly upregulated *DUXAP8* (ENST00000607933.1) was selected to investigate its role in HCC and chemosensitivity further (**Supplementary Figure S1A**).

It was confirmed by RT–qPCR that *DUXAP8* expression in HCC tissues was significantly higher than that of normal tissues adjacent to cancer, and the same results were obtained after expanding the sample size (**Figures 1C,D**). Correlation analysis with clinicopathological parameters showed that high levels of *DUXAP8* correlated with the TNM stage of cancer, tumor size, microvascular invasion, and distant metastasis (**Figure 1E**; **Supplementary Table S2**), and that HCC patients with high *DUXAP8* expression tended to have a poorer prognosis (**Figure 1F**). which is consistent with the results of the GEPIA database (**Supplementary Figures S1B,C**). We found that the expression of *DUXAP8* in seven HCC cell lines (MHCC-97H, Huh7, HCC-LM3, Bel-7405, SNU-449, SK-Hep-1, SNU-182) was significantly higher than its expression in the normal hepatocyte cell line THLE-3 (**Figure 1G**), and further confirmed that *DUXAP8* was mainly localized in the cytoplasm (**Figure 1H**). In conclusion, these findings suggested that *DUXAP8* is highly expressed in HCC tissues and positively correlates with the malignancy of HCC, and may function as a chemotherapy-resistant molecule in HCC.

Overexpression of *DUXAP8* Promoted the Characteristics of Migration, Invasion, and Stemness of HCC Cells

To investigate the effect of *DUXAP8* on the biological behavior of HCC cells, shRNAs, and lentiviral vectors of *DUXAP8* mimics were transfected into *DUXAP8* high-expressing HCC cell lines (Huh7, SNU-449) and *DUXAP8* low-expressing HCC cell lines (SK-Hep-1, HCC-LM3), respectively, and the transfection efficiency was verified by RT-qPCR (**Supplementary Figures S2A,B**). To clarify whether *DUXAP8* affects the features of migration and invasion of HCC cells, Transwell assays were performed, which showed that the knockdown of *DUXAP8* significantly decreased the migratory and invasive ability of Huh7 and SNU-449 cells. In contrast, overexpression promoted the migration and invasion of SK-Hep-1 and HCC-LM3 cells (**Figures 1A,C,E**; **Supplementary Figure S2C**). Epithelial–mesenchymal transition (EMT) is closely related to the migration and invasion of tumor cells, and it was found through Western blot that when *DUXAP8* was knocked down, the epithelial marker E-cadherin increased and the mesenchymal marker N-cadherin and vimentin decreased in HCC cell lines (**Figures 2B,D**); when *DUXAP8* was overexpressed, it produced the opposite effect (**Figure 2F**; **Supplementary Figure S2D**), indicating that *DUXAP8* positively regulated EMT process in HCC cells. Altogether, *DUXAP8* overexpression promoted the migration and invasion of HCC cells.

Next, the effect of *DUXAP8* on the stem cell characteristics of HCC cells was investigated. The spheroid-forming ability was reduced when *DUXAP8* was knocked down in Huh7 and SNU-449 cells (**Figures 2G,I**). In contrast, *DUXAP8* overexpression significantly improved the spheroid-forming ability of SK-Hep-1 and HCC-LM3 cells (**Figure 2K**; **Supplementary Figure S2E**). The potential regulatory effects of *DUXAP8* on the expression of the cancer stem cell marker, *CD133*, and stem cell-related genes, including *OCT4*, *NANOG*, and *Sox2* were then investigated. It can be seen that *DUXAP8* knockdown significantly suppressed the

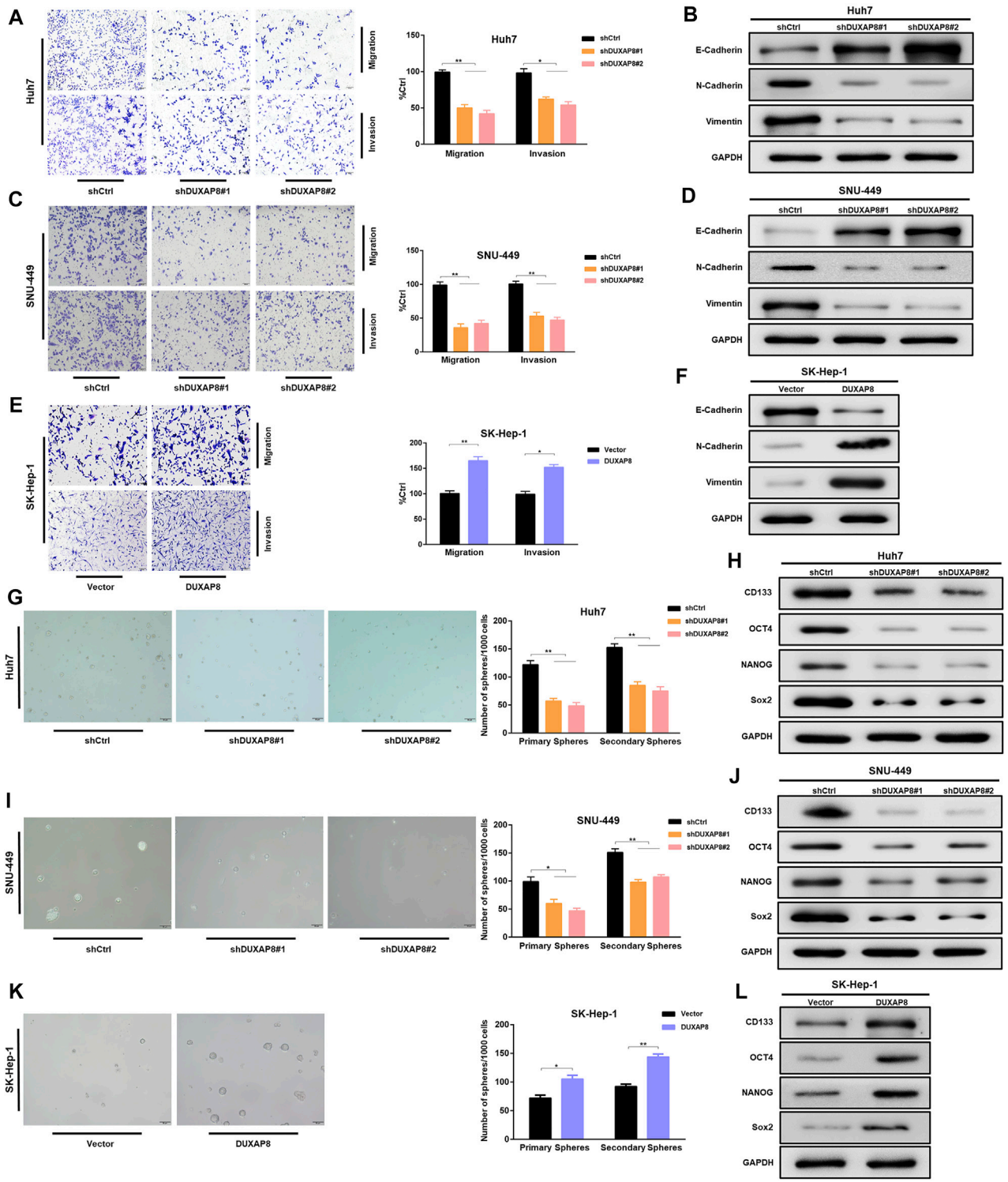

FIGURE 2 | *DUXAP8* can regulate the characteristics of migration, invasion, and stemness of HCC cells. **(A,C,E)** DUXAP8 or shDUXAP8 and the control cells were subjected to Transwell migration and Matrigel invasion assays. **(B,D,F)** Western blot detects the expression of epithelial–mesenchymal transformation markers in *DUXAP8*-downregulated Huh7 and SNU-449 cells and *DUXAP8*-overexpressed SK-Hep-1 cells. **(G,I,K)** Statistical analysis of the primary and secondary spheroid-forming ability of *DUXAP8*-downregulated Huh7 and SNU-449 cells and *DUXAP8*-overexpressed SK-Hep-1 cells, with representative images showing secondary spheroid formation in these cells. **(H,J,L)** Western blot detects the expression levels of stemness-related genes in *DUXAP8*-downregulated Huh7 and SNU-449 cells and *DUXAP8*-overexpressed SK-Hep-1 cells. Data are expressed as mean, $^{*}p < 0.05$, $^{**}p < 0.01$.

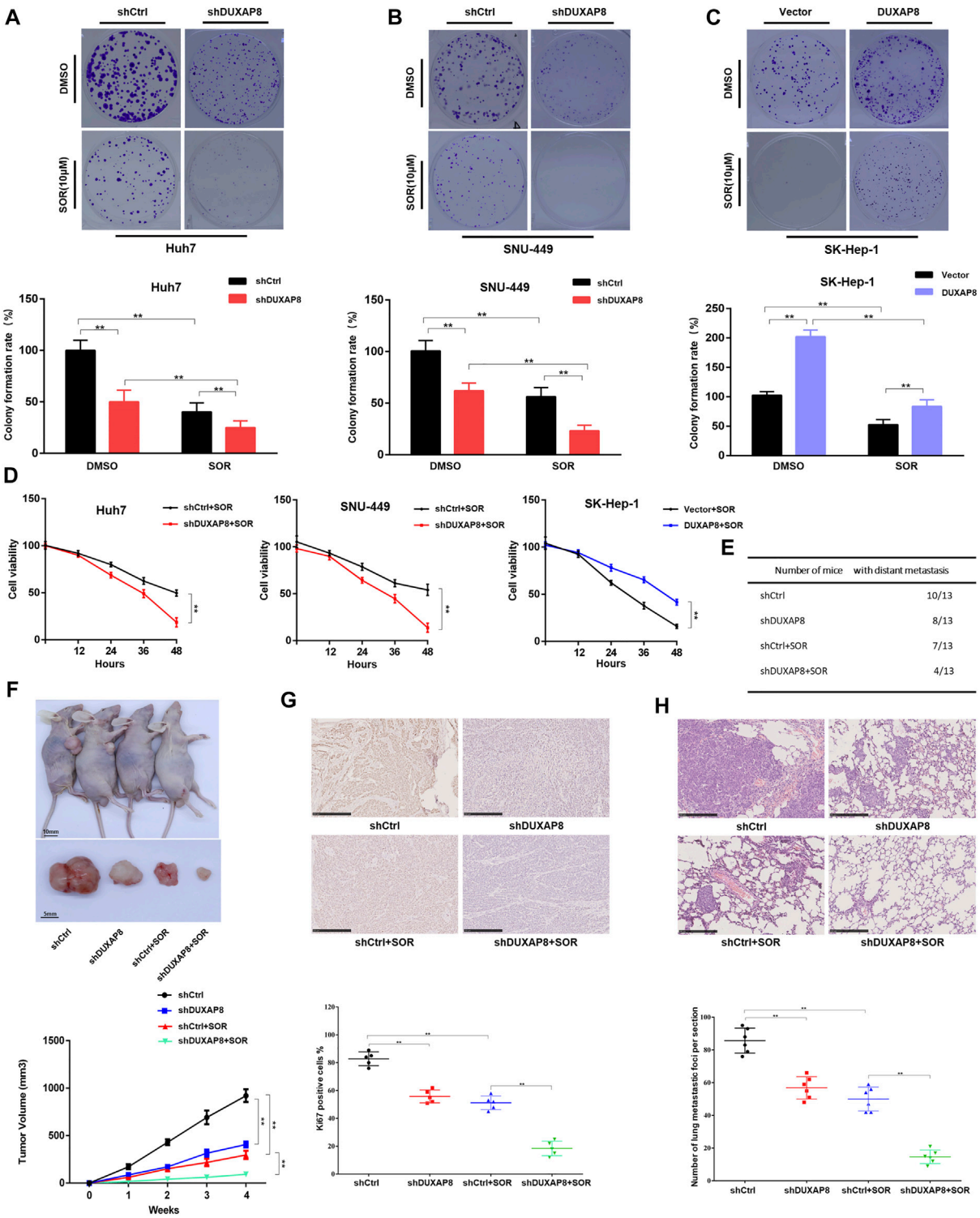

FIGURE 3 | *DUXAP8* promotes the chemotherapy resistance of HCC to sorafenib *in vivo* and *in vitro*. **(A,B)** Colony formation of cells transfected with *shDUXAP8* after sorafenib treatment. **(C)** Colony formation of cells transfected with *DUXAP8*-overexpressing plasmid after sorafenib treatment. **(D)** Cell viability of Huh7/SNU-449 cells transfected with *shDUXAP8* and SK-Hep-1 cells transfected with *DUXAP8*-overexpressed plasmid under the effect of sorafenib wasanalyzedusingCCK8. **(E)** Summary table of pulmonary metastases. **(F)** Typical images of xenograft tumors formed by liver cancer cells transfected with shCtrl or *shDUXAP8* in sorafenib-treated nude mice. Tumor growth curves of HCC cells transfected with shCtrl or *shDUXAP8* in sorafenib-treated nude mice. **(G)** *Ki67* expression in xenograft tumors formed by shCtrl- or *shDUXAP8*-transfected HCC cells in sorafenib-treated nude mice **(H)** Number of metastatic foci per section in the lungs of nude mice treated with sorafenib after caudal vein injection of HCC cells transfected with shCtrl or *shDUXAP8*. Data are expressed as mean, $^{**}p < 0.01$.

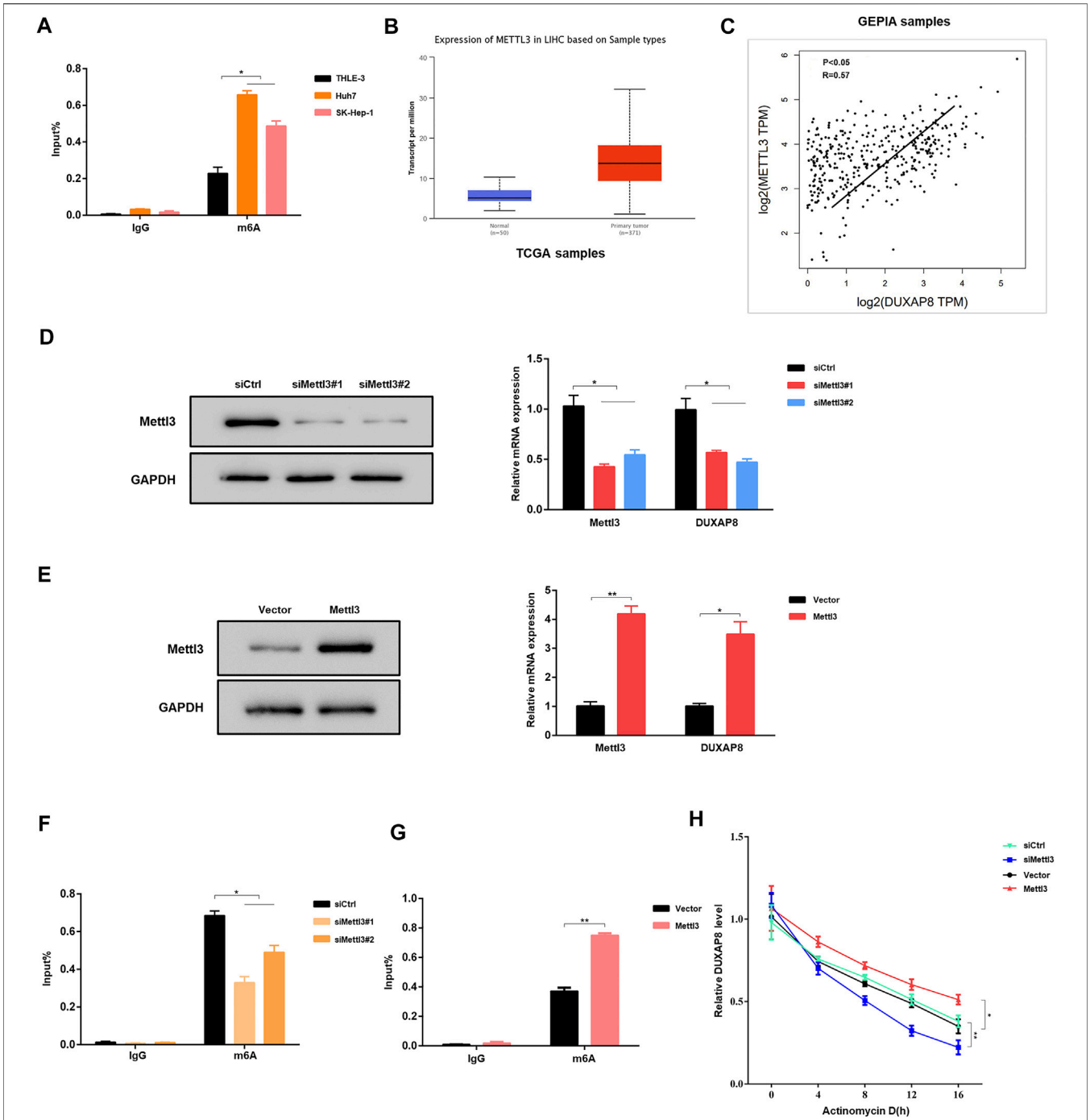

FIGURE 4 | Mettl3-mediated m6A modifications are involved in the upregulation of *DUXAP8*. **(A)** MeRIP–qPCR results showed that the m6A enrichment of *DUXAP8* was higher in Huh7 and SK-Hep-1 cells than in THLE-3 cells. **(B)** The expression of methyltransferase 3 (Mettl3) in HCC was analyzed using the TCGA database. **(C)** The results of TCGA database showed that the expression level of *Mettl3* was positively correlated with *DUXAP8*. **(D,E)** Effect of Mettl3 knockdown and overexpression on *DUXAP8* expression. **(F,G)** Effect of *Mettl3* knockdown and overexpression on the degree of m6A enrichment of *DUXAP8*. **(H)** Effect of Mettl3 knockdown and overexpression on *DUXAP8* stability in the presence of dactinomycin. Data are expressed as mean, $^{*}p < 0.05$, $^{**}p < 0.01$.

expression of *CD133, OCT4, NANOG*, and *Sox2* (**Figures 2H,J**, **Supplementary Figure S2G**), while the expression of *CD133, OCT4, NANOG*, and *Sox2* was promoted when *DUXAP8* was overexpressed (**Figure 2L**, **Supplementary Figures S2F,H**). Thus, *DUXAP8* overexpression promoted the stem cell features of HCC cells.

Overexpression of *DUXAP8* Promoted the Proliferation of HCC Cells and Reduced the Chemosensitivity of HCC Cells to Sorafenib

It was further investigated whether *DUXAP8* affected the chemosensitivity of HCC cells to sorafenib. It was observed that the knockdown of *DUXAP8* inhibited the proliferation ability of HCC cells and enhanced the chemosensitivity of HCC cells to sorafenib, while its overexpression promoted the proliferation of HCC cells and decreased the chemosensitivity of HCC cells to sorafenib (**Figures 3A–D**, **Supplementary Figure S3A–C**), indicating that *DUXAP8* mediated the development of chemotherapy resistance to sorafenib in HCC cells. Furthermore, consistent with the above *in vitro* findings, in *in vivo* experiments, knockdown of *DUXAP8* decreased the size and Ki67-positive rate of transplanted tumors in saline (NS) and sorafenib-treated nude mice (**Figures 3F,G**). Additionally, in the pulmonary metastasis model, it was found that knockdown of *DUXAP8* significantly inhibited the ability of pulmonary metastasis of HCC cells, as evidenced by the reduction in the number of mice with metastatic lung tumors and the decrease in the number of lung tumors in mice treated with NS or sorafenib (**Figures 3E,H**, **Supplementary Figure S3D**). In summary, these results suggested that overexpression of *DUXAP8* promoted the proliferation of HCC cells and reduced the chemosensitivity of HCC cells against sorafenib.

Mettl3-Mediated m6A Modifications Involved in the Upregulation of *DUXAP8*

Subsequently, the mechanism of *DUXAP8* upregulation in HCC cells was investigated. N6-methyladenosine (m6A) is the most common internal post-transcriptional modification in eukaryotic RNA (Wei et al., 1975; Schwartz et al., 2013), affecting RNA transcription, processing, translation, and metabolism. As a novel RNA epigenetic modification, the m6A modification plays an essential role in gene expression, including mRNA metabolism and other fundamental life processes and in the development of malignant tumors. RMBase (http://rna.sysu.edu.cn/rmbase/index.php) was used to find that *DUXAP8* has many m6A-binding sites. Therefore, it was hypothesized that the upregulation of *DUXAP8* in HCC might be associated with its m6A modification. The experimental results of MeRIP–qPCR verified the hypothesis that HCC cell lines (Huh7, SK-Hep-1) had a significantly higher level of m6A enrichment of *DUXAP8* than that of the normal hepatocyte line (THLE-3) (**Figure 4A**). Methyltransferase 3 (Mettl3) is a methyltransferase in m6A modification, which plays a vital role in mediating the m6A modification process in mammalian cells. By searching the Cancer Genome Atlas (TCGA) database, it was found that the expression level of Mettl3 was significantly higher in liver cancer tissues than in the corresponding pericarcinomatous tissues (**Figure 4B**), and there was a significant positive correlation between the expression levels of Mettl3 and *DUXAP8* (**Figure 4C**). When Mettl3 was silenced, it was observed that the expression level of *DUXAP8* also showed a significant decrease (**Figure 4D**); when Mettl3was overexpressed, the expression level of *DUXAP8* also indicated a corresponding increase (**Figure 4E**). It was also found that the m6A enrichment of *DUXAP8* in HCC cells decreased also when Mettl3 was silenced (**Figure 4F**), while the m6A enrichment of *DUXAP8* in HCC cells was correspondingly increased when Mettl3 was overexpressed (**Figure 4G**). The silencing of Mettl3 in the presence of dactinomycin, a drug that inhibits RNA synthesis, decreased the stability of *DUXAP8*, while Mettl3 overexpression produced the opposite result (**Figure 4H**). Altogether, as a methyltransferase in m6A modification, Mettl3 is essential to increase *DUXAP8* expression in HCC cells.

The Effect of *DUXAP8* on the Malignant Phenotype and Chemosensitivity of HCC Through Competitive Binding to miR-584-5p

Cytoplasmic lncRNAs are often assumed to be competitive endogenous RNAs that can competitively bind to microRNAs, thereby producing an "isolation" effect on these microRNAs, reducing their regulatory effect on target genes (Tay et al., 2014). Considering the localization of *DUXAP8* in the nucleus and cytoplasm (**Figure 1H**), it was hypothesized that *DUXAP8* also exerts oncogenic effects in HCC through the ceRNA mechanism. To test this hypothesis, RNA sequencing analysis of *DUXAP8*-knockdown HCC cells was conducted to screen out significantly upregulated microRNAs, and the bioinformatics database, Encyclopedia of RNA Interactomes (previously known as starBase v2.0) was used, to predict the microRNAs that can target and bind to *DUXAP8*. In this study, two microRNAs were intersected, and three microRNAs (miR-584-5p, miR-409-3p, miR-374b-5p) were screened. miR-584-5p was selected, which exhibited the largest fold change, for subsequent experimental validation (**Figure 5A**, **Supplementary Figure S4A**). MiR-584-5p has been shown to be involved in regulating multiple malignant tumors (Xiang et al., 2015; Zhang et al., 2020), and it was found that in HCC tissues, *DUXAP8* showed a significant negative correlation with miR-584-5p expression (**Figure 5B**). Additionally, the overexpression of miR-584-5p could significantly reduce the luciferase activity of *DUXAP8* WT, but it had no effect on the luciferase activity of *DUXAP8* MUT (**Figure 5C**). The expression of miR-584-5p was significantly increased in HCC cells after the knockdown of *DUXAP8*, but miR-584-5p expression was significantly reduced when *DUXAP8* was overexpressed (**Figure 5D**). In the RIP, it was found that *DUXAP8* and miR-584-5p were highly enriched in AGO2 precipitation (**Figure 5E**). In the results of RNA pull-down assay, it was found that miR-584-5p and AGO2 were highly enriched in the biotin-labeled *DUXAP8* group (**Figure 5F**). The above experimental results suggested that *DUXAP8* acted as a molecular sponge for miR-584-5p in HCC through the ceRNA mechanism.

Next, it was investigated whether *DUXAP8* affects the malignant phenotype of HCC by competitively binding to miR-584-5p. When *DUXAP8* was knocked down, it significantly reduced the migration and invasion ability of Huh7 and SNU-449 cells while decreasing their spheroid-forming ability, and inhibited the expression of *CD133, OCT4,*

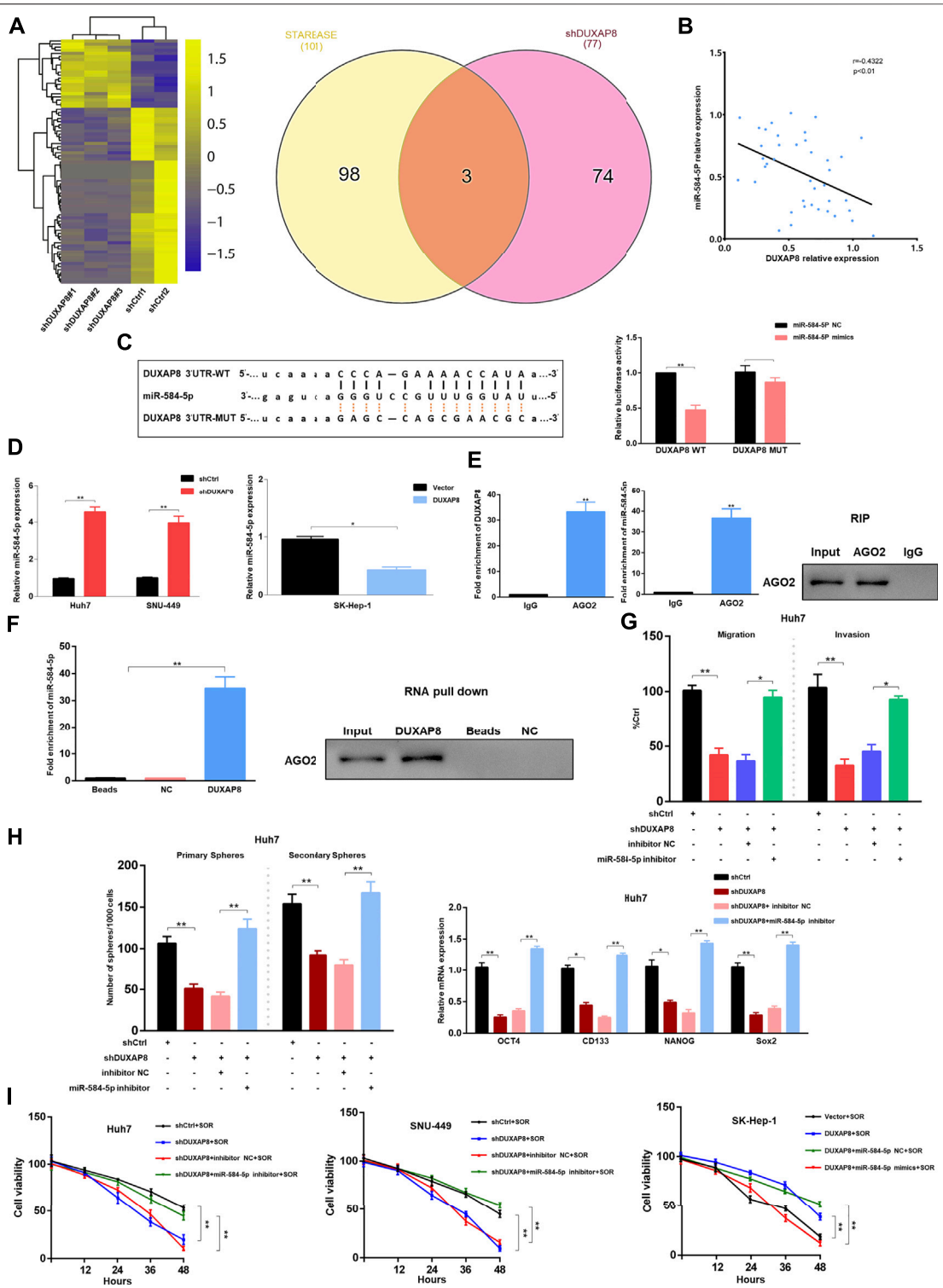

FIGURE 5 | In HCC, *DUXAP8* acts as a molecular sponge for miR-584-5p, which downregulates miR-584-5p and affects the malignant phenotype and chemosensitivity of HCC. **(A)** The heat map demonstrating the differentially expressed microRNAs in HCC after *DUXAP8* downregulation, and Wayne plot showing the differentially expressed microRNAs after the intersection of RNA sequencing results with the bioinformatics database. **(B)** Correlation analysis between the expression of *DUXAP8* and miR-584-5p. **(C)** Dual-luciferase reporter assay detecting the relative activity of luciferase in transfected HCC cells. **(D)** Effect of *DUXAP8* downregulation and overexpression on miR-584-5p expression in HCC cells. **(E)** RIP assay detecting the relative enrichment of *DUXAP8* and miR-584-5p in anti-IgG or anti-AGO2 specific immunoprecipitates. **(F)** RNA pull-down assay was used to detect the interrelationship between *DUXAP8*, miR-584-5p, and AGO2. **(G,H)** Effects of *DUXAP8* and miR-584-5p downregulation on the migration, invasion, primary and secondary spheroid-forming ability, and stemness-related gene expression levels in Huh7 cells. **(I)** The viability of HCC cells with downregulated *DUXAP8* and miR-584-5p under the effect of sorafenib. Data are expressed as mean, $^{*}p < 0.05$, $^{**}p < 0.01$.

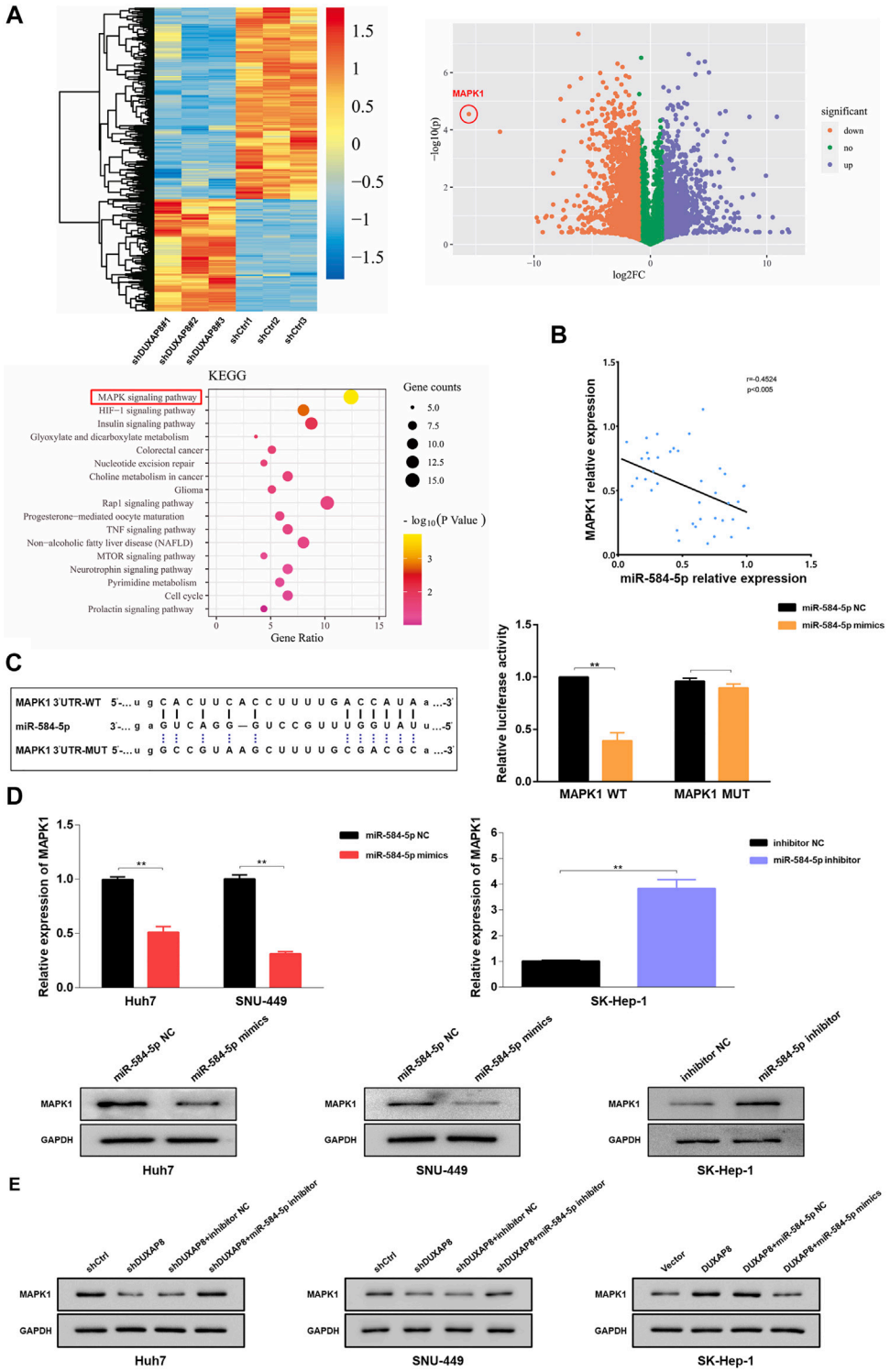

FIGURE 6 | miR-584-5p targets *MAPK1* in HCC. **(A)** The heat map and volcano plot demonstrating the differentially expressed genes in HCC after *DUXAP8* downregulation, and Kyoto Encyclopedia of Genes and Genomes analysis of the main associated pathways. **(B)** The result of the correlation analysis showing that miR-584-5p was negatively correlated with MAPK1 expression. **(C)** Dual-luciferase reporter assay detecting the relative activity of luciferase in transfected HCC cells. **(D)** Effect of miR-584-5p downregulation and overexpression on *MAPK1* expression in HCC cells. **(E)** Effect of down-regulation or overexpression of *DUXAP8* and miR-584-5p on *MAPK1* expression in HCC during co-transfection. Data are expressed as mean, $^{**}p < 0.01$.

NANOG, and *Sox2*, although such inhibitory effects of *DUXAP8* could be reversed using the knockdown of miR-584-5p (**Figures 5G,H**, **Supplementary Figure S4B–D**). When *DUXAP8* was overexpressed, it promoted the migration, invasion, and spheroid-forming ability of SK-Hep-1 cells and the expression of *CD133, OCT4, NANOG*, and *Sox2*. And this promotion effect could also be reversed through the overexpression of miR-584-5p (**Supplementary Figure S4E–G**).

As shown in **Figure 5I**, the knockdown of *DUXAP8* enhanced the chemosensitivity of HCC cells to sorafenib, while *DUXAP8* overexpression decreased the chemosensitivity of HCC cells to sorafenib, both results could be reversed by the knockdown and overexpression of miR-584-5p, respectively. In conclusion, *DUXAP8* could competitively bind to miR-584-5p through the ceRNA mechanism, thus affecting the malignant phenotype and chemosensitivity of HCC.

miR-584-5p Affects the *MAPK/ERK* Pathway by Targeting *MAPK1*, a Protein Involved in *DUXAP8* Regulation of the Malignant Phenotype and Chemosensitivity in HCC

To investigate the mechanism by which *DUXAP8* affects the malignant phenotype and chemotherapy resistance of HCC, RNA sequencing analysis of *DUXAP8*-knockdown HCC cells was performed. The results showed significant differences in the number of genes regulated by *DUXAP8* expression, and the *MAPK/ERK* pathway was the predominantly relevant signaling pathway (**Figure 6A**). *MAPK1* (mitogen-activated protein kinase 1, *ERK2*) is an essential biomarker of the *MAPK/ERK* pathway and can serve as a binding site for numerous biochemical signals (Jung et al., 2016; Wu et al., 2016). It has been shown that the activation of the *MAPK/ERK* pathway is closely associated with the invasion and migration, proliferation, drug resistance, and glycolysis in HCC (Liet al., 2020a; Li et al., 2020b; He et al., 2020). Therefore, it was hypothesized that miR-584-5p regulates the malignant phenotype and chemosensitivity of HCC by targeting *MAPK1* and affecting the *MAPK/ERK* pathway. it was that *MAPK1* negatively correlated with miR-584-5p expression in HCC tissues (**Figure 6B**), and the overexpression of miR-584-5p could significantly reduce the luciferase activity of *MAPK1* WT, but had no effect on the luciferase activity of *MAPK1* MUT (**Figure 6C**). Overexpression of miR-584-5p significantly reduced the expression of *MAPK1* of Huh7 and SNU- 449, whereas its knockdown produced the opposite result in SK-Hep-1 (**Figure 6D**). We also found that the knockdown of *DUXAP8* significantly reduced *MAPK1* expression in Huh7 and SNU-449 cells, however, this effect could be reversed by the downregulation of miR-584-5p. In contrast, overexpression of *DUXAP8* increased the expression of *MAPK1* in SK-Hep-1 cells, while overexpression of miR-584-5p reversed this effect (**Figure 6E**). The above experimental results showed that miR-584-5p could directly target *MAPK1* in HCC cells.

When miR-584-5p was overexpressed, it significantly reduced the migration and invasion ability of Huh7 and SNU-449 cells while reducing their spheroid-forming ability and also inhibited the expression of *CD133*, *OCT4*, *NANOG*, and *Sox2*, although this inhibitory effect could be reversed by *MAPK1* overexpression (**Supplementary Figure S5**). When miR-584-5p was knocked down, it promoted the migration, invasion, and spheroid-forming ability of SK-Hep-1 cells and the expression of *CD133*, *OCT4*, *NANOG*, and *Sox2*, and this effect could also be reversed by the knockdown of *MAPK1*. The overexpression of miR-584-5p enhanced the chemosensitivity of HCC cells to sorafenib, while its knockdown decreased the chemosensitivity of HCC cells to sorafenib, and both results could also be reversed through the overexpression and knockdown of *MAPK1*, respectively (**Supplementary Figure S5**).

Correlation analyses show that the expression of *DUXAP8* was positively correlated with *MAPK1* in HCC tissues (**Figure 7A**). Western blot results showed that the knockdown of *DUXAP8* downregulated the phosphorylation level of *ERK/CREB*, while the overexpression of *MAPK1* abolished the inhibitory effect of *DUXAP8* knockdown on the phosphorylation level of above proteins. However, there was no effect on the phosphorylation level of *JNK/p-38* (**Figure 7D**). This suggested that *DUXAP8* exerts its biological function by activating the *MAPK/ERK* pathway. To verify this conclusion, a rescue experiment was performed. When *DUXAP8* was knocked down, it significantly reduced the migration, invasion, and spheroid-forming ability of Huh7 and SNU-449 cells and the expression of *CD133, OCT4, NANOG*, and *Sox2*, but this inhibitory effect could be reversed by the overexpression of *MAPK1* (**Figures 7B,C**, **Supplementary Figure S6**). When *DUXAP8* was overexpressed, it promoted the migration, invasion and spheroid-forming ability of SK-Hep-1 cells and the expression of *CD133, OCT4, NANOG*, and *Sox2*, and this effect could also be reversed by the knockdown of *MAPK1* (**Supplementary Figure S6**). The knockdown of *DUXAP8* enhanced the chemosensitivity of HCC cells to sorafenib, while its overexpression reduced the chemosensitivity of HCC cells to sorafenib, and both results could be reversed by the overexpression and knockdown of *MAPK1*, respectively (**Supplementary Figure S6**).

In summary, *DUXAP8* competitively bound to miR-584-5P through the ceRNA mechanism (**Figure 8**), thus targeting *MAPK1* and activating the *MAPK/ERK* pathway to regulate the malignant phenotype and chemotherapy resistance of HCC.

DISCUSSION

The mechanisms of drug resistance in HCC are quite complex, involving the increased expression of drug efflux transporters (a type of protein that recognizes and pumps anticancer drugs out of tumor cells), intracellular redistribution of drugs, inactivation of the apoptosis signaling pathway, and activation of tumor stem cells (Butler et al., 2013; Salehan and Morse, 2013; Llovet et al., 2015). However, to date, the exact mechanism of drug resistance in HCC remains to be investigated.

In this study, the role of *DUXAP8* in promoting malignant phenotype and chemotherapy resistance in HCC was revealed, and it was confirmed for the first time that Mettl3-mediated m6A modifications were involved in the upregulation of *DUXAP8*. In

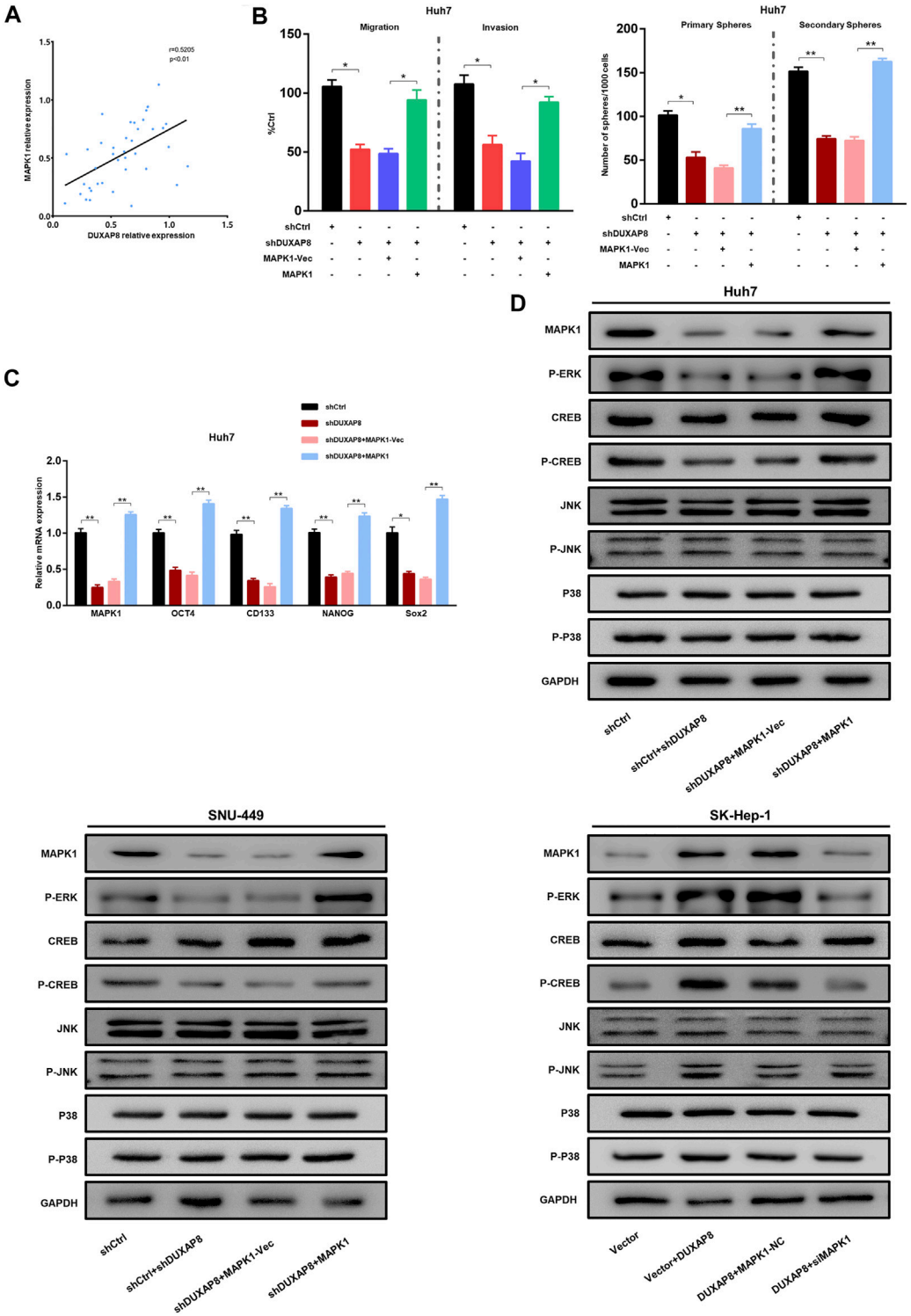

FIGURE 7 | The *DUXAP8*/miR-584-5p/*MAPK1* axis regulates the malignant phenotype of HCC. **(A)** The result of the correlation analysis showing that *DUXAP8* was positively correlated with the expression of *MAPK1*. **(B)** Effects of *DUXAP8* downregulation and *MAPK1* overexpression on the migration, invasion, and primary and secondary spheroid-forming ability of Huh7 cells. **(C)** Effects of *DUXAP8* downregulation and *MAPK1* overexpression on the expression levels of stemness-related genes in Huh7 cells. **(D)** Effects of *DUXAP8* downregulation and *MAPK1* overexpression on *ERK/CREB/JNK/P38* and their phosphorylation levels in HCC cell lines. Data are expressed as mean, $^{*}p < 0.05$, $^{**}p < 0.01$.

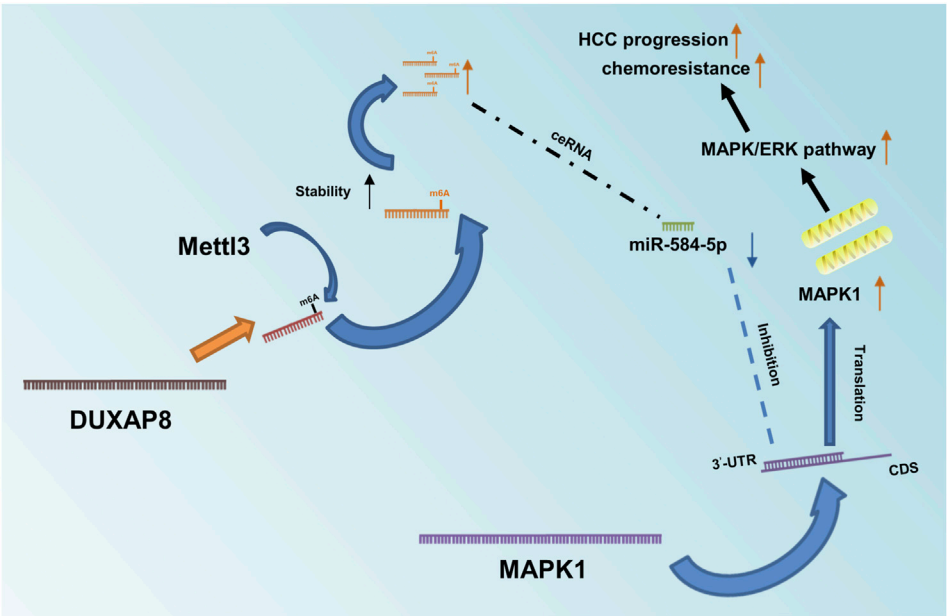

FIGURE 8 | Diagram of *DUXAP8*'s role in HCC and its mechanism. Mettl3-mediated m6A methylation modification stabilizes and upregulates *DUXAP8*, which competitively binds to miR-584-5p through a ceRNA mechanism, thereby targeting *MAPK1* and activating the *MAPK/ERK* pathway to regulate the malignant phenotype and chemotherapy resistance of HCC.

summary, it was found that *DUXAP8* exhibited high expression in sorafenib-treated PDX models and was positively correlated with the TNM cancer stage, tumor size, microvascular invasion, and distant metastasis. The results of *in vivo* and *in vitro* experiments showed that *DUXAP8* is positively correlated with the proliferation, migration, invasion, and sorafenib resistance of HCC. *DUXAP8* upregulates *MAPK1* through competitively binding to miR-584-5p, which activates the *MAPK/ERK* pathway to perform its biological functions.

There is increasing evidence supporting that lncRNAs play an essential role in the occurrence and development of malignant tumors (Yuan et al., 2014; Li et al., 2015b; Chen et al., 2016; Yuan et al., 2016; Zhu et al., 2016). Until now, *DUXAP8* is highly expressed in various malignant tumors. *DUXAP8* can significantly inhibit the expression of *PLEKHO1* in gastric cancer, which enhances the proliferation and migration of tumor cells (Ma et al., 2017a). In glioma, the downregulation of *DUXAP8* inhibits the proliferation of tumor cells (Zhao et al., 2019). In non-small cell lung cancer (NSCLC), *DUXAP8* promotes tumor cell proliferation and invasion through epigenetically silencing *Egr1* and *RHOB* (Sun et al., 2017). In pancreatic carcinoma, *DUXAP8* promotes tumor growth through epigenetically silencing *CDKN1A* and *KLF2* (Lian et al., 2018). This study found significantly elevated expression of *DUXAP8* in HCC compared to that of the adjacent normal liver tissue, and this result is consistent with that in previous reports.

As a novel epigenetic RNA modification, m6A is closely related to the phenotype and mechanism of malignant tumors and plays an essential role in the self-renewal of tumor stem cells and the metabolism, recurrence and metastasis of various malignant tumors. The dynamic regulatory proteins modified by m6A include methyltransferases (Writers), demethylases (Erasers), and reading genes (Readers) (Zhao et al., 2017). The methyltransferases are multicomponent compounds consisting of *METTL3, METTL14, WTAP, KIAA1429, RBM15*, and *ZC3H13* (Knuckles et al., 2018). Recent studies (Jo et al., 2013; Bansal et al., 2014; Ma et al., 2017b; Cui et al., 2017; Visvanathan et al., 2018) have shown that m6A-related proteins are involved in the development and progression of different types of malignant tumors, such as acute myeloid leukemia, cholangiocarcinoma, glioblastoma, and hepatocellular carcinoma (HCC). In this study, it was demonstrated for the first time that *DUXAP8* is overexpressed in HCC because Mettl3-mediated m6A modification confers its stability.

Existing studies have demonstrated that lncRNAs are involved in the regulation of many diseases and play an essential role in the occurrence and development of malignant tumors. Some lncRNAs act as protein co-regulators by directly binding to helper proteins and regulating the expression of downstream tumor-associated genes (Chen et al., 2016; Yuan et al., 2016; Zhu et al., 2016). Another part of lncRNAs functions as competitive endogenous RNAs (ceRNAs) (Yuan et al., 2014; Li et al., 2015b). Such lncRNAs isolate microRNAs and regulate the expression of microRNA-targeted oncogenes or tumor suppressor genes through molecular sponge effects. Argonaute 2 (AGO2) is a core component of the microRNA (miRNA)-induced silencing complex (RISC), linking miRNAs and their mRNA target sites(Meister et al., 2004). And the mechanisms through which lncRNAs regulate the biological functions of malignant tumors largely depend on their subcellular localization (Statello et al., 2021). Considering that

DUXAP8 is mainly localized in the cytoplasm, while RNA sequencing analysis and bioinformatics analysis also indicate that *DUXAP8* has a putative binding site for miR-584-5p, it was therefore suspected that *DUXAP8* also affects HCC progression through a ceRNA mechanism. The luciferase reporter assay, RIP and RNA pull-down experiments confirmed this speculation. Meanwhile, the expression of miR-584-5p was correspondingly reversed when the expression of *DUXAP8* was changed. These data suggested that *DUXAP8* acts as a molecular sponge, which binds to miR-584-5p to perform its biological function. miR-584-5p was further investigated and it was found that miR-584-5p significantly inhibited the features of migration, invasion, and stemness of HCC and correspondingly enhanced its chemosensitivity to sorafenib. RNA sequencing analysis revealed that the downregulation of *DUXAP8* had a significant effect on the *MAPK/ERK* pathway, accompanied by the downregulation of *MAPK1*. Previous studies have reported that *MAPK/ERK* pathway is closely related to the invasion and migration, proliferation, drug resistance, and glycolysis in HCC (Li et al., 2020a; Li et al., 2020b; He et al., 2020). Additionally, *MAPK1* is an essential biomarker of the *MAPK/ERK* pathway and can serve as a binding site for numerous biochemical signals (Jung et al., 2016; Wu et al., 2016). Therefore, it was suggested that miR-584-5p might play an oncogenic role in HCC by targeting the downregulation of *MAPK1*, and subsequent findings supported this hypothesis. Through luciferase reporter assay, expression correlation analysis and cell function up-and downregulation assays in HCC, it was demonstrated that miR-584-5p could indeed directly affect the expression level of *MAPK1* in HCC cells. Meanwhile, the knockdown and overexpression of *MAPK1* could effectively reverse the effects of miR-584-5p knockdown and overexpression on the malignant phenotype and chemosensitivity of HCC cells to sorafenib. Then, it was further shown that the knockdown of *DUXAP8* inhibited the phosphorylation level of *ERK/CREB*, while the overexpression of *MAPK1* reduced the inhibitory effect of *DUXAP8* knockdown on the phosphorylation level of *ERK/CREB*. It was also suggested that *DUXAP8* exerts its biological function by activating the *MAPK/ERK* pathway.

In conclusion, this study revealed the role and potential mechanism of *DUXAP8* in promoting the malignant phenotype of HCC and chemoresistance. Mechanistically, *DUXAP8* endogenously competes for the binding of miR-584-5p through the ceRNA mechanism, reducing its inhibitory effect -on *MAPK1* and thus activating the *MAPK/ERK* pathway to promote the proliferation, invasive migration, stemness maintenance, and chemoresistance in HCC. These results have deepened the understanding of the driving mechanisms of lncRNAs in the development, progression, and chemotherapy resistance of HCC and provided greater insight into the importance of *DUXAP8* in HCC progression, which may help provide ideas for finding new prognostic indicators and therapeutic targets for HCC patients.

DATA AVAILABILITY STATEMENT

The datasets presented in this study can be found in online repositories. The names of the repository/repositories and accession number(s) can be found below: https://doi.org/10.6084/m9.figshare.17049722.v1, https://doi.org/10.6084/m9.figshare.17049716.v1, https://doi.org/10.6084/m9.figshare.17049686.v1.

ETHICS STATEMENT

The studies involving human participants were reviewed and approved by Ethics Committee of the Second Hospital of Jilin University. The patients/participants provided their written informed consent to participate in this study. The animal study was reviewed and approved by Animal Experiment Ethics Committee of the First Hospital of Jilin University.

AUTHOR CONTRIBUTIONS

ZL, YY, BT, and XZ developed the original hypothesis and supervised the experimental design. ZL, JL, and HF performed *in vitro* and *in vivo* experiments. ZL, JS, and MC analyzed the data. ZL, BT, and XZ wrote and revise the manuscript. All authors read and approved the final.

FUNDING

The work was funded by the project of Hepatobiliary and Pancreatic Disease Translational Medicine Platform Construction (2017F009), This work was supported by grants from Medical and Health Talents Project of Jilin Province (2019SCZT003), Health special project of Jilin Province (2020sczt017), Sponsored by National Science Foundation of The First Hospital of Jilin University (JDYY92018041).

ACKNOWLEDGMENTS

We thank Enago—https://www.enago.cn/fanyi/tougaoji-fanyi.htm for their assistance in manuscript translation and editing.

SUPPLEMENTARY MATERIAL

The Supplementary Material for this article can be found online at: https://www.frontiersin.org/articles/10.3389/fcell.2021.783385/full#supplementary-material

REFERENCES

Bansal, H., Yihua, Q., Iyer, S. P., Ganapathy, S., Proia, D., Penalva, L. O., et al. (2014). WTAP Is a Novel Oncogenic Protein in Acute Myeloid Leukemia. *Leukemia* 28, 1171–1174. doi:10.1038/leu.2014.16

Bruix, J., da Fonseca, L. G., and Reig, M. (2019). Insights into the success and Failure of Systemic Therapy for Hepatocellular Carcinoma. *Nat. Rev. Gastroenterol. Hepatol.* 16, 617–630. doi:10.1038/s41575-019-0179-x

Butler, E. B., Zhao, Y., Muñoz-Pinedo, C., Lu, J., and Tan, M. (2013). Stalling the Engine of Resistance: Targeting Cancer Metabolism to Overcome Therapeutic Resistance. *Cancer Res.* 73, 2709–2717. doi:10.1158/0008-5472.CAN-12-3009

Chen, Z.-z., Huang, L., Wu, Y.-h., Zhai, W.-j., Zhu, P.-p., and Gao, Y.-f. (2016). LncSox4 Promotes the Self-Renewal of Liver Tumour-Initiating Cells through Stat3-Mediated Sox4 Expression. *Nat. Commun.* 7, 12598. doi:10.1038/ncomms12598

Cui, Q., Shi, H., Ye, P., Li, L., Qu, Q., Sun, G., et al. (2017). m 6 A RNA Methylation Regulates the Self-Renewal and Tumorigenesis of Glioblastoma Stem Cells. *Cel Rep.* 18, 2622–2634. doi:10.1016/j.celrep.2017.02.059

Fang, K.-C., Kao, W.-Y., Su, C.-W., Chen, P.-C., Lee, P.-C., Huang, Y.-H., et al. (2018). The Prognosis of Single Large Hepatocellular Carcinoma Was Distinct from Barcelona Clinic Liver Cancer Stage A or B: The Role of Albumin-Bilirubin Grade. *Liver Cancer* 7, 335–358. doi:10.1159/000487407

Harrow, J., Frankish, A., Gonzalez, J. M., Tapanari, E., Diekhans, M., Kokocinski, F., et al. (2012). GENCODE: the Reference Human Genome Annotation for the ENCODE Project. *Genome Res.* 22, 1760–1774. doi:10.1101/gr.135350.111

He, H., Chen, T., Mo, H., Chen, S., Liu, Q., and Guo, C. (2020). Hypoxia-inducible Long Noncoding RNA NPSR1-AS1 Promotes the Proliferation and Glycolysis of Hepatocellular Carcinoma Cells by Regulating the MAPK/ERK Pathway. *Biochem. Biophysical Res. Commun.* 533, 886–892. doi:10.1016/j.bbrc.2020.09.076

Jemal, A., Bray, F., Center, M. M., Ferlay, J., Ward, E., and Forman, D. (2011). Global Cancer Statistics. *CA: A Cancer J. Clinicians* 61, 69–90. doi:10.3322/caac.20107

Jo, H.-J., Shim, H.-E., Han, M.-E., Kim, H.-J., Kim, K.-S., Baek, S., et al. (2013). WTAP Regulates Migration and Invasion of Cholangiocarcinoma Cells. *J. Gastroenterol.* 48, 1271–1282. doi:10.1007/s00535-013-0748-7

Jung, Y.-C., Han, S., Hua, L., Ahn, Y.-H., Cho, H., Lee, C.-J., et al. (2016). Kazinol-E Is a Specific Inhibitor of ERK that Suppresses the Enrichment of a Breast Cancer Stem-like Cell Population. *Biochem. Biophysical Res. Commun.* 470, 294–299. doi:10.1016/j.bbrc.2016.01.066

Knuckles, P., Lence, T., Haussmann, I. U., Jacob, D., Kreim, N., Carl, S. H., et al. (2018). Zc3h13/Flacc Is Required for Adenosine Methylation by Bridging the mRNA-Binding Factor Rbm15/Spenito to the m6A Machinery Component Wtap/Fl(2)d. *Genes Dev.* 32, 415–429. doi:10.1101/gad.309146.117

Kudo, M., Finn, R. S., Qin, S., Han, K.-H., Ikeda, K., Piscaglia, F., et al. (2018). Lenvatinib versus Sorafenib in First-Line Treatment of Patients with Unresectable Hepatocellular Carcinoma: a Randomised Phase 3 Non-inferiority Trial. *The Lancet* 391, 1163–1173. doi:10.1016/S0140-6736(18)30207-1

Li, L., Tang, J., Zhang, B., Yang, W., LiuGao, M., Wang, R., et al. (2015a). Epigenetic Modification of MiR-429 Promotes Liver Tumour-Initiating Cell Properties by Targeting Rb Binding Protein 4. *Gut* 64, 156–167. doi:10.1136/gutjnl-2013-305715

Li, Q.-T., Feng, Y.-M., Ke, Z.-H., Qiu, M.-J., He, X.-X., Wang, M.-M., et al. (2020b). KCNN4 Promotes Invasion and Metastasis through the MAPK/ERK Pathway in Hepatocellular Carcinoma. *J. Investig. Med.* 68, 68–74. doi:10.1136/jim-2019-001073

Li, Q., Ren, B., Gui, Q., Zhao, J., Wu, M., Shen, M., et al. (2020a). Blocking MAPK/ERK Pathway Sensitizes Hepatocellular Carcinoma Cells to Temozolomide via Downregulating MGMT Expression. *Ann. Transl Med.* 8, 1305. doi:10.21037/atm-20-5478

Li, T., Xie, J., Shen, C., Cheng, D., Shi, Y., Wu, Z., et al. (2015b). Amplification of Long Noncoding RNA ZFAS1 Promotes Metastasis in Hepatocellular Carcinoma. *Cancer Res.* 75, 3181–3191. doi:10.1158/0008-5472.CAN-14-3721

Lian, Y., Yang, J., Lian, Y., Xiao, C., Hu, X., and Xu, H. (2018). DUXAP8, a Pseudogene Derived lncRNA, Promotes Growth of Pancreatic Carcinoma Cells by Epigenetically Silencing CDKN1A and KLF2. *Cancer Commun.* 38, 64. doi:10.1186/s40880-018-0333-9

Liu, H., Wang, M., Liang, N., and Guan, L. (2019). PDCD2 Sensitizes HepG2 Cells to Sorafenib by Suppressing Epithelial-mesenchymal T-ransition. *Mol. Med. Rep.* 19, 2173–2179. doi:10.3892/mmr.2019.9860

Llovet, J. M., Villanueva, A., Lachenmayer, A., and Finn, R. S. (2015). Advances in Targeted Therapies for Hepatocellular Carcinoma in the Genomic Era. *Nat. Rev. Clin. Oncol.* 12, 408–424. doi:10.1038/nrclinonc.2015.103

Ma, H.-w., Xie, M., Sun, M., Chen, T.-y., Jin, R.-r., Ma, T.-s., et al. (2017a). The Pseudogene Derived Long Noncoding RNA DUXAP8 Promotes Gastric Cancer Cell Proliferation and Migration via Epigenetically Silencing PLEKHO1 Expression. *Oncotarget* 8, 52211–52224. doi:10.18632/oncotarget.11075

Ma, J. z., Yang, F., Zhou, C. c., Liu, F., Yuan, J. h., Wang, F., et al. (2017b). METTL14 Suppresses the Metastatic Potential of Hepatocellular Carcinoma by Modulating N 6 -methyladenosine-dependent Primary MicroRNA Processing. *Hepatology* 65, 529–543. doi:10.1002/hep.28885

Meister, G., Landthaler, M., Patkaniowska, A., Dorsett, Y., Teng, G., and Tuschl, T. (2004). Human Argonaute2 Mediates RNA Cleavage Targeted by miRNAs and siRNAs. *Mol. Cel* 15, 185–197. doi:10.1016/j.molcel.2004.07.007

Petrick, J. L., Florio, A. A., Znaor, A., Ruggieri, D., Laversanne, M., Alvarez, C. S., et al. (2020). International Trends in Hepatocellular Carcinoma Incidence, 1978-2012. *Int. J. Cancer* 147, 317–330. doi:10.1002/ijc.32723

Raoul, J.-L., and Edeline, J. (2020). Systemic Treatment of Hepatocellular Carcinoma: Standard of Care in China and Elsewhere. *Lancet Oncol.* 21, 479–481. doi:10.1016/S1470-2045(20)30082-6

Reinders, M. T. M., van Meer, S., Burgmans, M. C., de Jong, K. P., Klümpen, H.-J., de Man, R. A., et al. (2020). Trends in Incidence, Diagnosis, Treatment and Survival of Hepatocellular Carcinoma in a Low-Incidence Country: Data from the Netherlands in the Period 2009-2016. *Eur. J. Cancer* 137, 214–223. doi:10.1016/j.ejca.2020.07.008

Rimassa, L., and Wörns, M. A. (2020). Navigating the New Landscape of Second-line Treatment in Advanced Hepatocellular Carcinoma. *Liver Int.* 40, 1800–1811. doi:10.1111/liv.14533

Salehan, M. R., and Morse, H. R. (2013). DNA Damage Repair and Tolerance: a Role in Chemotherapeutic Drug Resistance. *Br. J. Biomed. Sci.* 70, 31–40. doi:10.1080/09674845.2013.11669927

Schwartz, S., Agarwala, S. D., Mumbach, M. R., Jovanovic, M., Mertins, P., Shishkin, A., et al. (2013). High-resolution Mapping Reveals a Conserved, Widespread, Dynamic mRNA Methylation Program in Yeast Meiosis. *Cell* 155, 1409–1421. doi:10.1016/j.cell.2013.10.047

Shi, X., Nie, F., Wang, Z., and Sun, M. (2016). Pseudogene-expressed RNAs: a New Frontier in Cancers. *Tumor Biol.* 37, 1471–1478. doi:10.1007/s13277-015-4482-z

Statello, L., Guo, C.-J., Chen, L.-L., and Huarte, M. (2021). Gene Regulation by Long Non-coding RNAs and its Biological Functions. *Nat. Rev. Mol. Cel Biol.* 22, 96–118. doi:10.1038/s41580-020-00315-9

Sun, M., Nie, F.-q., Zang, C., Wang, Y., Hou, J., Wei, C., et al. (2017). The Pseudogene DUXAP8 Promotes Non-small-cell Lung Cancer Cell Proliferation and Invasion by Epigenetically Silencing EGR1 and RHOB. *Mol. Ther.* 25, 739–751. doi:10.1016/j.ymthe.2016.12.018

Tay, Y., Rinn, J., and Pandolfi, P. P. (2014). The Multilayered Complexity of ceRNA Crosstalk and Competition. *Nature* 505, 344–352. doi:10.1038/nature12986

Visvanathan, A., Patil, V., Arora, A., Hegde, A. S., Arivazhagan, A., Santosh, V., et al. (2018). Essential Role of METTL3-Mediated m6A Modification in Glioma Stem-like Cells Maintenance and Radioresistance. *Oncogene* 37, 522–533. doi:10.1038/onc.2017.351

Wang, X.-K., Liao, X.-W., Huang, R., Huang, J.-L., Chen, Z.-J., Zhou, X., et al. (2020). Clinical Significance of Long Non-coding RNA DUXAP8 and its Protein Coding Genes in Hepatocellular Carcinoma. *J. Cancer* 11, 6140–6156. doi:10.7150/jca.47902

Wei, C.-M., Gershowitz, A., and Moss, B. (1975). Methylated Nucleotides Block 5′ Terminus of HeLa Cell Messenger RNA. *Cell* 4, 379–386. doi:10.1016/0092-8674(75)90158-0

Wei, L., Wang, X., Lv, L., Liu, J., Xing, H., Song, Y., et al. (2019). The Emerging Role of microRNAs and Long Noncoding RNAs in Drug Resistance of Hepatocellular Carcinoma. *Mol. Cancer* 18, 147. doi:10.1186/s12943-019-1086-z

Wu, L., Cao, K., Ni, Z., Wang, S., Li, W., Liu, X., et al. (2019). Rhein Reverses Doxorubicin Resistance in SMMC-7721 Liver Cancer Cells by Inhibiting Energy Metabolism and Inducing Mitochondrial Permeability Transition Pore Opening. *Biofactors* 45, 85–96. doi:10.1002/biof.1462

Wu, L. K., Liu, Y. C., Ma, G., Shi, L. L., and He, X. M. (2016). High Levels of Glucose Promote the Activation of Hepatic Stellate Cells via the P38-Mitogen-Activated Protein Kinase Signal Pathway. *Genet. Mol. Res.* 15. doi:10.4238/gmr.15038419

Xiang, Q.-F., Zhan, M.-X., Li, Y., Liang, H., Hu, C., Huang, Y.-M., et al. (2019). Activation of MET Promotes Resistance to Sorafenib in Hepatocellular Carcinoma Cells via the AKT/ERK1/2-EGR1 Pathway. *Artif. Cell Nanomedicine, Biotechnol.* 47, 83–89. doi:10.1080/21691401.2018.1543195

Xiang, X., Mei, H., Qu, H., Zhao, X., Li, D., Song, H., et al. (2015). miRNA-584-5p Exerts Tumor Suppressive Functions in Human Neuroblastoma through Repressing Transcription of Matrix Metalloproteinase 14. *Biochim. Biophys. Acta (Bba) - Mol. Basis Dis.* 1852, 1743–1754. doi:10.1016/j.bbadis.2015.06.002

Yang, M., Parikh, N. D., Liu, H., Wu, E., Rao, H., Feng, B., et al. (2020). Incidence and Risk Factors of Hepatocellular Carcinoma in Patients with Hepatitis C in China and the United States. *Sci. Rep.* 10, 20922. doi:10.1038/s41598-020-77515-y

Yuan, J.-h., Yang, F., Wang, F., Ma, J.-z., Guo, Y.-j., Tao, Q.-f., et al. (2014). A Long Noncoding RNA Activated by TGF-β Promotes the Invasion-Metastasis Cascade in Hepatocellular Carcinoma. *Cancer Cell* 25, 666–681. doi:10.1016/j.ccr.2014.03.010

Yuan, S.-x., Wang, J., Yang, F., Tao, Q.-f., Zhang, J., Wang, L.-l., et al. (2016). Long Noncoding RNADANCRincreases Stemness Features of Hepatocellular Carcinoma by Derepression ofCTNNB1. *Hepatology* 63, 499–511. doi:10.1002/hep.27893

Zhang, M., Weng, W., Zhang, Q., Wu, Y., Ni, S., Tan, C., et al. (2018). The lncRNA NEAT1 Activates Wnt/β-Catenin Signaling and Promotes Colorectal Cancer Progression via Interacting with DDX5. *J. Hematol. Oncol.* 11, 113. doi:10.1186/s13045-018-0656-7

Zhang, Y., Wang, H., Li, C., Gao, L., Zheng, Y., Chang, W., et al. (2020). CircSMYD4 Regulates Proliferation, Migration and Apoptosis of Hepatocellular Carcinoma Cells by Sponging miR-584-5p. *Cancer Cel Int.* 20, 556. doi:10.1186/s12935-020-01648-3

Zhao, B. S., Roundtree, I. A., and He, C. (2017). Post-transcriptional Gene Regulation by mRNA Modifications. *Nat. Rev. Mol. Cel Biol.* 18, 31–42. doi:10.1038/nrm.2016.132

Zhao, X., Hao, S., Wang, M., Xing, D., and Wang, C. (2019). Knockdown of pseudogene DUXAP8 Expression in Glioma Suppresses Tumor Cell Proliferation. *Oncol. Lett.* 17, 3511–3516. doi:10.3892/ol.2019.9994

Zheng, L., Li, X., Gu, Y., Lv, X., and Xi, T. (2015). The 3′UTR of the Pseudogene CYP4Z2P Promotes Tumor Angiogenesis in Breast Cancer by Acting as a ceRNA for CYP4Z1. *Breast Cancer Res. Treat.* 150, 105–118. doi:10.1007/s10549-015-3298-2

Zhu, P., Wang, Y., Huang, G., Ye, B., Liu, B., Wu, J., et al. (2016). Lnc-β-Catm Elicits EZH2-dependent β-catenin Stabilization and Sustains Liver CSC Self-Renewal. *Nat. Struct. Mol. Biol.* 23, 631–639. doi:10.1038/nsmb.3235

Zhu, Y.-J., Zheng, B., Luo, G.-J., Ma, X.-K., Lu, X.-Y., Lin, X.-M., et al. (2019). Circular RNAs Negatively Regulate Cancer Stem Cells by Physically Binding FMRP against CCAR1 Complex in Hepatocellular Carcinoma. *Theranostics* 9, 3526–3540. doi:10.7150/thno.32796

Conflict of Interest: The authors declare that the research was conducted in the absence of any commercial or financial relationships that could be construed as a potential conflict of interest.

Publisher's Note: All claims expressed in this article are solely those of the authors and do not necessarily represent those of their affiliated organizations, or those of the publisher, the editors and the reviewers. Any product that may be evaluated in this article, or claim that may be made by its manufacturer, is not guaranteed or endorsed by the publisher.

frontiers in Cell and Developmental Biology

ORIGINAL RESEARCH
published: 14 December 2021
doi: 10.3389/fcell.2021.783088

Long Non-Coding RNA LINC01572 Promotes Hepatocellular Carcinoma Progression *via* Sponging miR-195-5p to Enhance PFKFB4-Mediated Glycolysis and PI3K/AKT Activation

Shihui Lai[1,2†], *Zhipeng Quan*[1,2†], *Yuesong Hao*[1,2†], *Jun Liu*[1,2], *Zhiqian Wang*[1,2], *Luo Dai*[1,2], *Hongliang Dai*[1,2*], *Songqing He*[1,2*] *and Bo Tang*[1,2*]

[1]*Department of Hepatobiliary Surgery, The First Affiliated Hospital of Guangxi Medical University, Nanning, China,* [2]*Key Laboratory of Basic and Clinical Application Research for Hepatobiliary Diseases of Guangxi, Nanning, China*

Background: Accumulating evidence indicates that type 2 diabetes mellitus (T2DM) is a risk factor for hepatocellular carcinoma (HCC), and T2DM-associated HCC represents a common type of HCC cases. We herein identify an lncRNA LINC01572 that was aberrantly upregulated in T2DM-related HCC *via* high-throughput screening. Based on this, the study was undertaken to identify the functional role and mechanism of LINC01572 in HCC progression.

Methods: RT-qPCR was used to detect the expressions of LINC01572 in HCC tissues and cell lines. Gain- or loss-of-function assays were applied to evaluate the *in vitro* and *in vivo* functional significance of LINC01572 in the HCC cell proliferation, migration, and invasion using corresponding experiments. Bioinformatics, RIP, RNA pull-down, and luciferase reporter assays were performed to explore the regulatory relationship of the LINC01572/miR-195-5p/PFKFB4 signaling axis.

Result: In this study, we profiled lncRNAs in HCC tissues and corresponding adjacent tissues from HCC patients with T2DM by RNA sequencing. Our data showed that LINC01572 was aberrantly upregulated in HCC tissues as compared with control, especially in those with concurrent T2DM. The high level of LINC01572 was correlated with advanced tumor stage, increased blood HbA1c level, and shortened survival time. The overexpression of LINC01572 significantly promoted HCC cell proliferation, migration, invasion, and epithelial-to-mesenchymal transition (EMT), while the knockdown of LINC01572 had the opposite effects on HCC cells. A mechanistic study revealed that LINC01572-regulated HCC progression *via* sponging miR-195-5p to increase the level of PFKFB4 and subsequent enhancement of glycolysis and activation of PI3K-AKT signaling.

Conclusion: LINC01572 acts as ceRNA of miR-195-5p to restrict its inhibition of PFKFB4, thereby enhancing glycolysis and activates PI3K/AKT signaling to trigger HCC malignancy.

Keywords: T2DM-related HCC, LINC01572, MiR-195-5p, PFKFB4, glycolysis

OPEN ACCESS

Edited by:
Lutao Du,
Second Hospital of Shandong University, China

Reviewed by:
Hui Feng,
University of North Carolina at Chapel Hill, United States
Xiaobo Li,
Harbin Medical University, China

***Correspondence:**
Hongliang Dai
jy2006hldai@sohu.com
Songqing He
Dr_hesongqing@163.com
Bo Tang
dr_sntangbo@163.com

[†]These authors have contributed equally to this work and share first authorship

Specialty section:
This article was submitted to Epigenomics and Epigenetics, a section of the journal Frontiers in Cell and Developmental Biology

Received: *25 September 2021*
Accepted: *11 November 2021*
Published: *14 December 2021*

Citation:
Lai S, Quan Z, Hao Y, Liu J, Wang Z, Dai L, Dai H, He S and Tang B (2021) Long Non-Coding RNA LINC01572 Promotes Hepatocellular Carcinoma Progression via Sponging miR-195-5p to Enhance PFKFB4-Mediated Glycolysis and PI3K/AKT Activation. Front. Cell Dev. Biol. 9:783088. doi: 10.3389/fcell.2021.783088

INTRODUCTION

Hepatocellular carcinoma (HCC) is the most common type in primary liver cancer and has extremely poor prognosis in spite of continuous progress of treatment strategies due to a high recurrence rate and difficult recognition in early stages. As such, HCC has ranked the second leading cause of cancer-related deaths globally (Sun et al., 2020; Ge et al., 2021). Hepatitis B virus (HBV) and hepatitis C virus (HCV) infection remain the leading causes of HCC incidence. Notably, accumulating evidence in recent years shows that type 2 diabetes mellitus (T2DM) is also closely associated with the increased risk of various malignancies, including HCC (Wild, 2011; Singh et al., 2018). Due to increased prevalence of unhealthy lifestyles, the incidence of T2DM has increased at an alarming rate, and at present, up to 9% of the world population is afflicted by this condition. This figure is projected to rise to 12% in 2025 if it continues like this (Jin and Liu, 2021), which would potentially contribute to the increased incidence of HCC. Based on this, further understanding the pathogenesis of T2DM-related HCC would help develop new diagnostic markers and therapeutic targets so as to clinically improve the therapeutic efficiency and prognosis.

Long non-coding RNAs (lncRNAs) is open reading frame (ORF)–free RNA molecules with a length >200 nucleotides. Although initially, this class of molecules was considered non-sense components for the organism, recent years have seen the critical role of lncRNAs in a variety of human diseases, including HCC, which implies that lncRNAs might become potentially efficient HCC diagnostic and therapeutic biomarkers (Chen et al.,

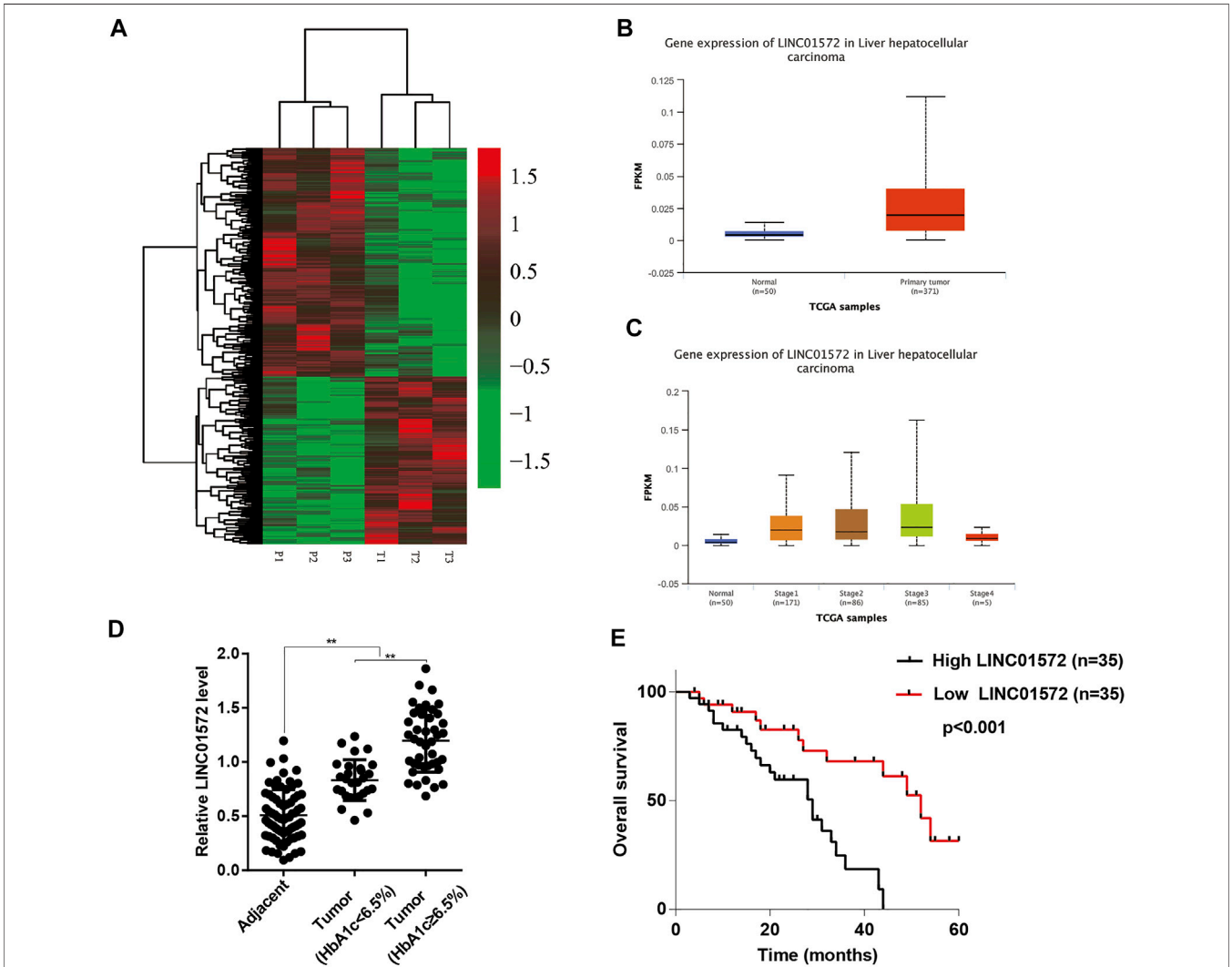

FIGURE 1 | LINC01572 is highly expressed in HCC and is associated with poor prognosis. **(A)** Heatmap of the differential expression of LncRNA in cancer tissues and corresponding adjacent tissues from HCC patients with concurrent T2DM. **(B)** Comparison of LINC01572 expression in HCC (n = 371) and normal liver (n = 50) tissues based on TCGA dataset. **(C)** Analysis of LINC01572 expression in HCC samples at different stages based on TCGA dataset. **(D)** RT-qPCR analysis of LINC01572 expression in HCC tissues and adjacent normal tissues, in which HCC samples were subgrouped based on blood HbA1c level. **(E)** Kaplan–Meier analysis of survival time based on the LINC01572 expression in 70 HCC patients. $^{**}p < 0.01$.

TABLE 1 | Relationship between LINC01572 and clinicopathological parameters in 70 HCC patients.

Variable	All cases	LINC01572 expression		*p*
		Low (*n* = 35)	High (*n* = 35)	
Age (years)				
< 50	28	11	17	—
≥ 50	42	24	18	0.1432
Gender				
Male	48	23	25	—
Female	22	12	10	0.6066
Tumor nodule number				
Solitary	30	17	13	—
Multiple (≥ 2)	40	18	22	0.3340
HBV infection				
Positive	44	21	23	—
Negative	26	14	12	0.6208
Tumor size (cm)				
< 5	46	22	24	—
≥ 5	24	13	11	0.6146
TNM stage				
I-II	31	22	9	—
III-IV	39	13	26	0.0018
Serum AFP (μg/L)				
≤ 200	43	24	19	—
> 200	27	11	16	0.2196
HbA1c (%)				
< 6.5	28	20	8	—
≥ 6.5	42	15	27	0.0147

2018; Zhao et al., 2019; Teng et al., 2020). Searching and identification of valuable HCC-related lncRNAs have emerged as a promising HCC research perspective (Hu et al., 2021; Mohan et al., 2021).

Long intergenic non-coding RNA 01572 (LINC01572) is a newly identified lncRNA molecule, with extremely limited information available regarding its role in cancer progression, although it has been revealed to be differentially expressed in lung squamous cancer (Chen et al., 2017) and regulate cisplatin resistance in gastric cancer (Song et al., 2020). Whether LINC01572 regulates HCC, fate is completely unclear. In the present study, we found that LINC01572 was upregulated in HCC tissues, those from patients complicated with T2DM in particular. On the basis of this, we then further analyzed its biological significance in HCC progression and also explored the possible molecular mechanism, in an attempt to provide a potentially effective diagnostic and therapeutic target for HCC, especially those complicated by T2DM.

MATERIALS AND METHODS

Chemicals and Antibodies

TRIzol reagents were obtained from Invitrogen (Grand Island, NY, United States). Antibodies against E-cadherin, N-cadherin, vimentin, and β-catenin were purchased from Cell Signaling Technology (Danvers, MA, United States), and those against β-actin and PFKFB4 were purchased from Abcam (Cambridge, MA, United States). All other chemicals were purchased from Sigma-Aldrich unless otherwise stated (St. Louis, MO, United States).

Patient Samples and Cell Lines

Seventy pairs of HCC tumor and corresponding adjacent normal tissues were collected from HCC patients at The First Affiliated Hospital of Guangxi Medical University. These tissues were placed in liquid nitrogen immediately after surgical resection and then transferred to −80°C for later use. All enrolled patients have provided written informed consent, and the study was reviewed and approved by the Ethics Committee of Guangxi Medical University.

Human HCC cell lines SK-hep1, SNU-449, SMMC-7721, HCC-LM3, Huh7, and MHCC-97H were purchased from ATCC (American Type Culture Collection) or the Institute of Biochemistry and Cell Biology (Chinese Academy of Sciences, Shanghai, China). SK-hep1, SNU-449, and SMMC-7721 were cultured in the RPMI-1640 medium containing 10% fetal bovine serum (FBS, Gibco), 1% penicillin, and streptomycin. Other cells were cultured in DMEM containing 10% fetal bovine serum (Gibco), 1% penicillin, and streptomycin. All the cells were subcultured in a 37°C incubator with 5% CO_2.

Plasmid Construction and Cell Transfection

HCC cells were inoculated into six-well plates and used for *in vitro* transfection when the cell density reached 70~80% using Lipofectamine 3000 (Thermo Fisher Scientific). The cells were transfected with pcDNA3.1 (+) vectors expressing LINC01572, LINC01572 short hairpin RNA (shRNA), or PFKFB4, miR-195-5p mimics, and PFKFB4 small interference RNA (siRNA) and their corresponding controls (GenePharma, Shanghai, China) for 48 h. shLINC01572 was transfected into hepatocellular carcinoma cell SNU-449 using lentivirus in mouse xenograft.

Reverse Transcription Quantitative Polymerase Chain Reaction (RT-qPCR)

An RNA Simple Total RNA Kit (TIANGEN, DP419) was used to extract total RNA from tissues and cultured cells according to the manufacturer's instructions. The extracted mRNA and miRNA were then reversely transcribed into cDNA using a RevertAid First-Strand cDNA Synthesis Kit (Thermo Scientific, #K1622) and miRcute Plus miRNA First-Strand cDNA Kit (TIANGEN, Beijing, China), respectively. Subsequently, iTaq Universal SYBR® Green Supermix (Bio-RAD, United States) and miRcute Plus miRNA qPCR Kit (SYBR, TIANGEN, Beijing, China) were used for RT-qPCR amplification. The RNA level was quantified using the $2^{-\Delta\Delta Ct}$ method.

Western Blotting

Total protein was extracted from cell lysate and quantified by using the BCA method. Subsequently, an equal amount of protein was subjected to polyacrylamide gel electrophoresis (SDS-PAGE). Separated protein was then transferred to the polyvinylidene difluoride (PVDF) membrane. The membrane was blocked with 5% non-fat milk for 1 h at room temperature and then

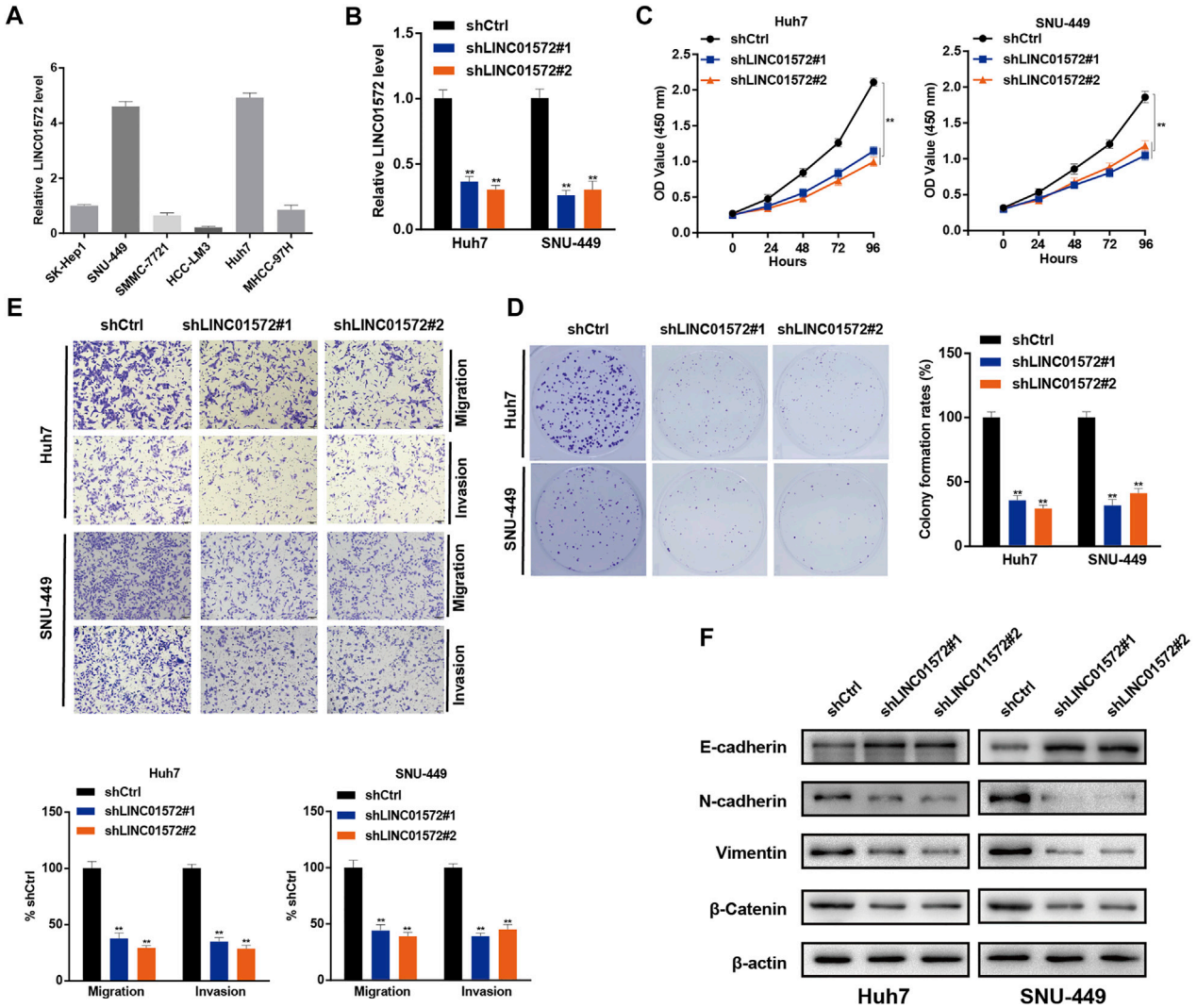

FIGURE 2 | LINC01572 silencing inhibited proliferation, migration, and invasion of HCC cells. **(A)** RT-qPCR analysis of LINC01572 expression in six HCC cell lines. **(B)** RT-qPCR analysis of the suppressive effect of specific shRNA on the LINC01572 level. **(C,D)** Effect of LINC01572 knockdown on Huh7 and SNU-449 cell proliferation. **(E,F)** Effect of LINC01572 knockdown on Huh7 and SNU-449 cell migration, invasion, and EMT marker expression. All data are shown as mean ± standard deviation (n = 3). $^{**}p < 0.01$.

incubated with primary antibodies and horseradish peroxide (HRP)–labeled secondary antibodies. Bound antibodies were detected using enhanced chemiluminescence (ECL).

Cell Counting Kit-8 (CCK-8)

The cells were seeded into 96-well plates and cultured at 37°C for 0~96 h. Subsequently, 10 μL CCK-8 reaction reagent (Dojindo, Japan) was then added to each well, and after 2 h of incubation at 37°C, the absorbance value was detected at a wavelength of 450 nm.

Colony Formation Assay

The cells were seeded in 6-well plates and allowed to grow for 10~14 days at 37°C. At the end of the growth, cell colonies were fixed with 70% methanol and stained by crystal violet solution (Solarbio) for 30 min. The clones containing more than 50 cells were counted for analysis.

Transwell Assay

Transwell assay was conducted to evaluate the migration and invasion of HCC cells. In the invasion assay, the chamber bottom was pre-coated with Matrigel, whereas in the migration assay, no Matrigel was applied. The cells suspended in a serum-free medium were seeded onto transwell inserts. After 24~48 h, the migrated and invasive cells were fixed with paraformaldehyde and stained with crystal violet for visualization.

Luciferase Activity Assay

The wild-type and mutant-type luciferase plasmids for LINC01572 or PFKFB4 were constructed using PmiRGLO

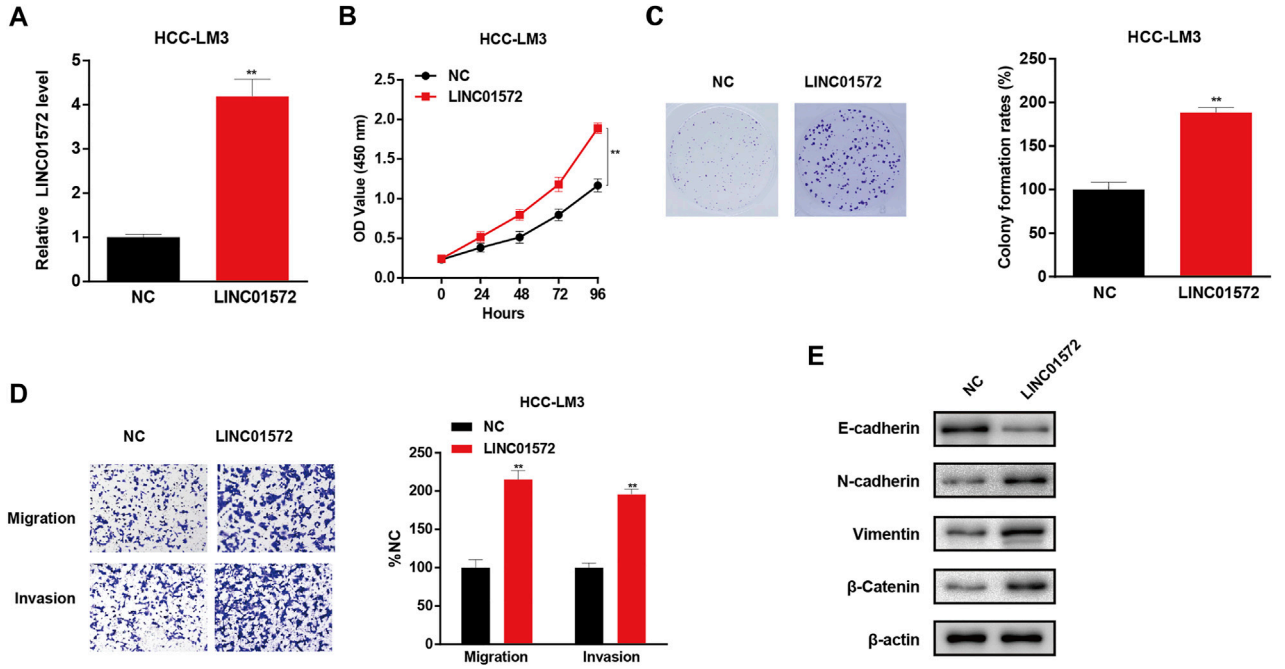

FIGURE 3 | LINC01572 overexpression promoted the proliferation, migration, and invasion of HCC cells. **(A)** RT-qPCR analysis of LINC01572 level in LINC01572 overexpressed HCC-LM3 cells. **(B,C)** Effect of LINC01572 overexpression on HCC cell proliferation. **(D,E)** Effect of LINC01572 overexpression on HCC cell migration, invasion, and EMT marker expression. All data are shown as mean ± standard deviation (n = 3). $^{**}p < 0.01$.

dual-luciferase reporters. The constructed plasmid was co-transfected into SNU-449 and HCC-LM3 cells with miR-195-5p mimics or NC mimics. A dual-luciferase reporter assay system (Promega, Madison, United States) was used to determine the luciferase activity.

RNA Immunoprecipitation (RIP) Assay

RIP assay was performed using a Magna RIP™ RNA-Binding Protein Immunoprecipitation Kit (Millipore, United States) according to the manufacturer's instructions. The cell extracts were used for immunoprecipitation of RNA with beads conjugated with antibodies against AGO2. The proteins in the complex were removed by 0.1% SDS/protease K (0.5 mg/ml) at 55°C for 30 min. Immunoprecipitated LINC01572 and miR-195-5p were detected by RT-qPCR.

RNA Pull-Down

LINC01572 was labeled using a Pierce™ RNA 3 End Desthiobiotinylation Kit (Thermo, 20163) for the attachment to streptavidin magnetic beads. The RNA pull-down assay was performed using a Thermo Scientific Pierce Magnetic RNA-Protein pull-down Kit (Thermo, 20164), followed by the AGO2 analysis by Western blot, and miR-195-5p by RT-qPCR.

Statistical Analysis

Data were expressed as mean ± standard deviation (SD) for at least three independent experiments, and GraphPad Prism 8.0 (GraphPad Software Inc., San Diego, CA, United States) was used for plotting and statistical analysis. Student's t test and one-way analysis of variance (ANOVA) were performed for comparison between groups. Pearson's correlation analysis was used for identifying the correlation between gene expressions. $p < 0.05$ was considered statistically significant.

RESULT

LINC01572 Was Highly Expressed in Hepatocellular Carcinoma and Associated With Poor Prognosis

To identify that the lncRNAs were potentially involved in T2DM-related HCC progression, transcriptome sequencing was performed on three pairs of tumor and adjacent tissue samples from T2DM–HCC patients. The results showed that LINC01572 lied in the forefront among the differentially expressed lncRNAs (**Figure 1A**). In line with this, TCGA dataset showed that LINC01572 is upregulated in HCC samples as compared with adjacent non-cancerous tissues (**Figure 1B**), and further, its expression was correlated with the advanced HCC stage (**Figure 1C**). In addition, the RT-qPCR assay revealed that LINC01572 was further elevated in high-blood HbA1c subgroup (**Figure 1D**). Moreover, LINC01572 expression was significantly correlated with advanced tumor stage and HbA1c level (**Table 1**). In particular, the Kaplan–Meier survival analysis data indicated that the higher level of LINC01572 was associated with shorter survival time in HCC ($p < 0.001$) (**Figure 1E**). These

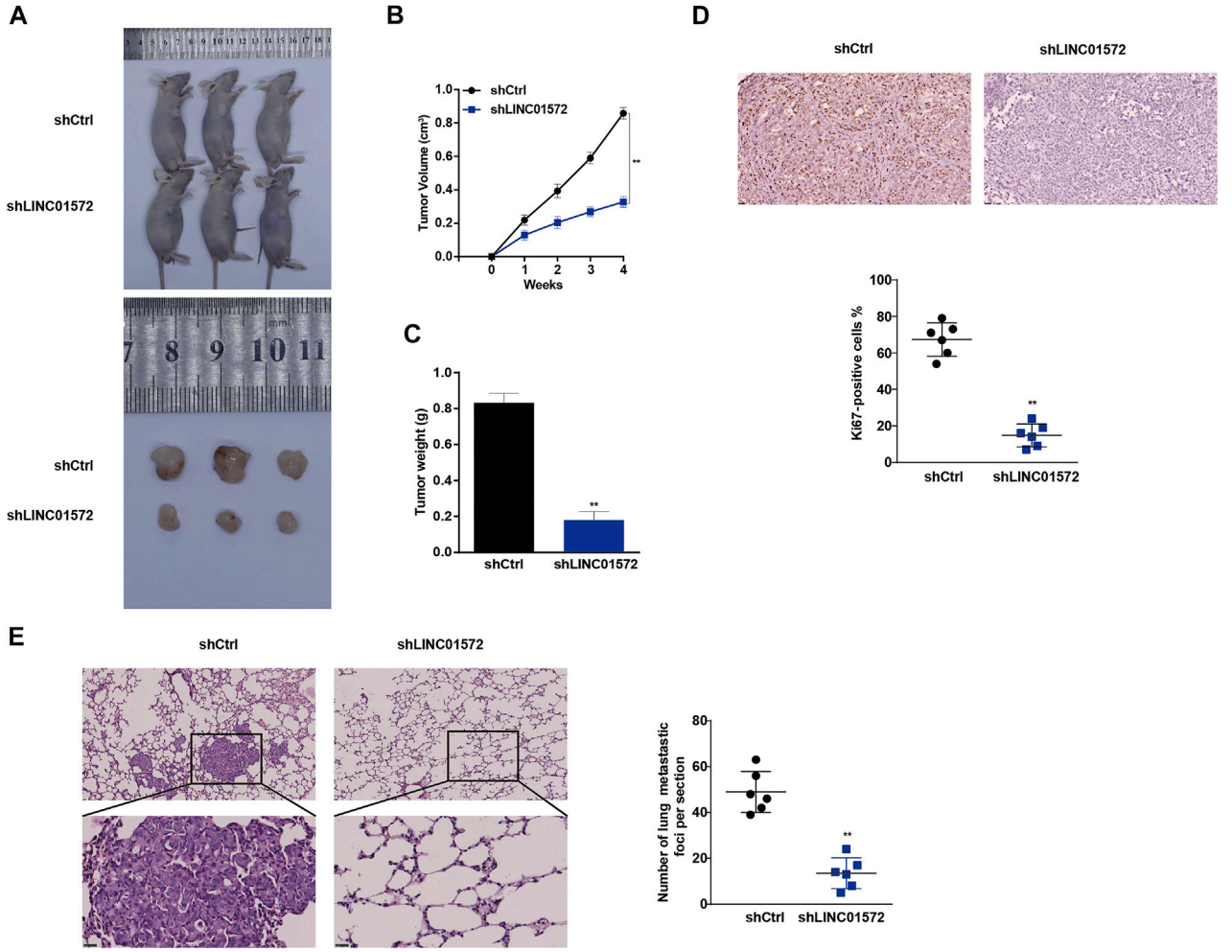

FIGURE 4 | Silencing of LINC01572 inhibits the HCC cell growth and distant metastasis *in vivo*. **(A)** Representative image of tumors following injection of SNU-449-shLINC01572 or control cells **(B,C)** Xenograft tumor volume and weight in nude mice subcutaneously injected with SNU-449-shLINC01572 or control cells. **(D)** Ki67-positive cell numbers in the sections of xenograft tumors from nude mice injected with SNU-449-shLINC01572 or control cells. **(E)** Number of lung metastatic nodules following tail vein injection of SNU-449-shLINC01572 or control cells. All data are shown as mean ± standard deviation (n = 3). $^{**}p < 0.01$.

data suggest that LINC01572 might play a key role in T2DM-related HCC progression.

LINC01572 Affected Proliferation, Migration, and Invasion of Hepatocellular Carcinoma Cells

In order to identify the role of LINC01572 in HCC, Huh7 and SNU-449 cells were selected for loss-of-function assays and overexpression of LINC01572 in HCC-LM3 cells, according to the basal level of LINC01572 in HCC cell lines (**Figure 2A**). RT-qPCR showed that the LINC01572 level was significantly repressed upon shLINC01572 transfection and enhanced by LINC01572 overexpression (**Figures 2B**, **3A**). Subsequently, cck-8 and colony formation assays showed that downregulation of LINC01572 remarkably decreased the growth rate of Huh7 and SNU-449 cells (**Figures 2C,D**), while overexpression significantly promoted the growth of HCC-LM3 cells (**Figures 3B,C**). Transwell assays revealed that migration and invasion were significantly prevented by shLINC01572 transfection in Huh7 and SNU-449 cells (**Figure 2E**) and enhanced in LINC01572 overexpressed HCC-LM3 cells (**Figure 3D**). Furthermore, the enhanced E-cadherin and decreased N-cadherin, vimentin, and β-catenin were also found with LINC01572 knockdown, whereas overexpression of LINC01572 in HCC-LM3 cells produced an opposite result (**Figures 2F**, **3E**). The aforementioned results demonstrated that LINC01572 stimulates the proliferation, migration, and invasion of HCC cells *in vitro*.

Silencing of LINC01572 Inhibits Hepatocellular Carcinoma Cell Growth and Distant Metastasis *In Vivo*

In order to identify the role of LINC01572 *in vivo* in HCC progression, a mice xenograft model was established. As

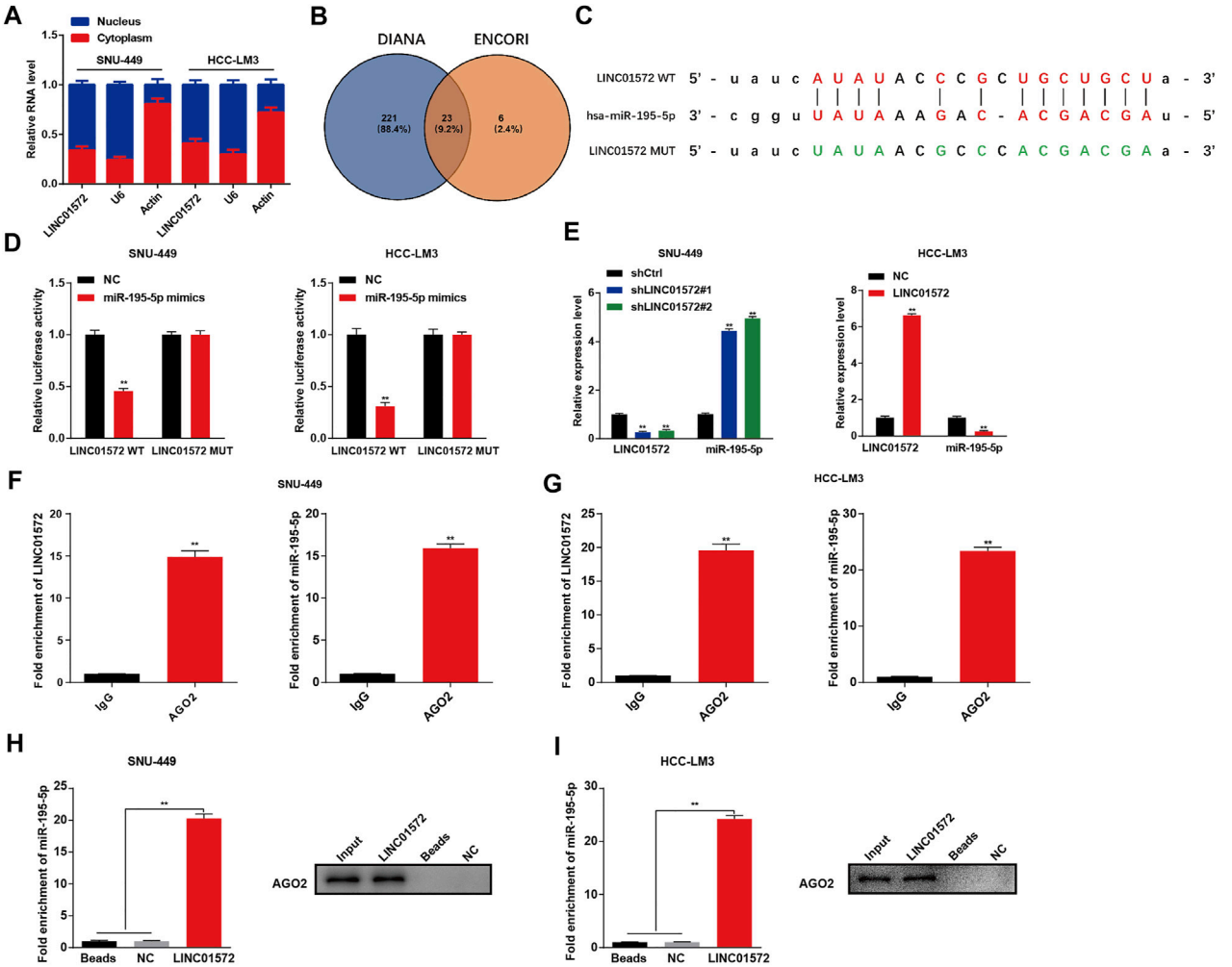

FIGURE 5 | LINC01572 sponges and downregulates miR-195-5p in HCC cells. **(A)** Distribution of LINC01572 in nucleus and cytoplasm fraction was detected by RT-qPCR assay **(B)** DIANA Tool and ENCORI were used to predict the downstream target gene of LINC01572, and the intersection was obtained. **(C)** ENCORI was used to predict the binding sites of LINC01572 and miR-195-5p. **(D)** Target relationship of LINC01572 and miR-195-5p was verified by dual-luciferase assay **(E)** Relative expression of miR-195-5p after LINC01572 knockdown and overexpression. **(F,G)** RIP assay was used to detected the relative enrichment of LINC01572 and miR-195-5p in anti-IgG–specific or anti-AGO2–specific immunoprecipitates. **(H,I)** RNA pull-down assay showing the interaction between LINC01572 and miR-195-5p. All data are shown as mean ± standard deviation ($n = 3$). $^{**}p < 0.01$.

shown in **Figures 4A–C**, tumor volume and weight were significantly lower in the shLINC01572 group. Furthermore, it was observed that Ki67-positive cells in xenograft tumors were also reduced (**Figure 4D**). In addition, in the lung metastasis model, we observed that the number of lung metastatic nodules in the shLINC01572 group was significantly lower than that in the control group (**Figure 4E**). These results suggest that silencing LINC01572 restrains HCC growth and metastasis *in vivo*.

LINC01572 Upregulates PFKFB4 Expression to Increase Glycolysis and Activate PI3K/AKT by Sponging miR-195-5p

To understand the mechanism underlying LINC01572-mediated HCC malignant behavior, the subcellular location of LINC01572 was analyzed using the nuclear/cytosol fraction assay. It was found that a considerable proportion of LINC01572 was distributed in the cytoplasm of HCC cells (**Figure 5A**). We thus reckoned that LINC01572 might exert its biological function in HCC *via* a ceRNA mechanism. Using DIANA Tools and ENCORI, we obtained 23 miRNAs that could potentially bind to LINC01572 (**Figure 5B**). Among others, it has been reported that miRNA-195-5p acts as a suppressor in HCC (Xu et al., 2015). Therefore, miRNA-195-5p was selected for the subsequent study subsequently. The potential biding between LINC01572 and miR-195-5p was predicted by ENCORI (**Figure 5C**). Next, the binding between LINC01572 and miR-195-5p was confirmed by the dual-luciferase assay (**Figure 5D**). RT-qPCR data revealed that LINC01572 negatively modulated the expression of miR-195-5p (**Figure 5E**). The RIP assay showed

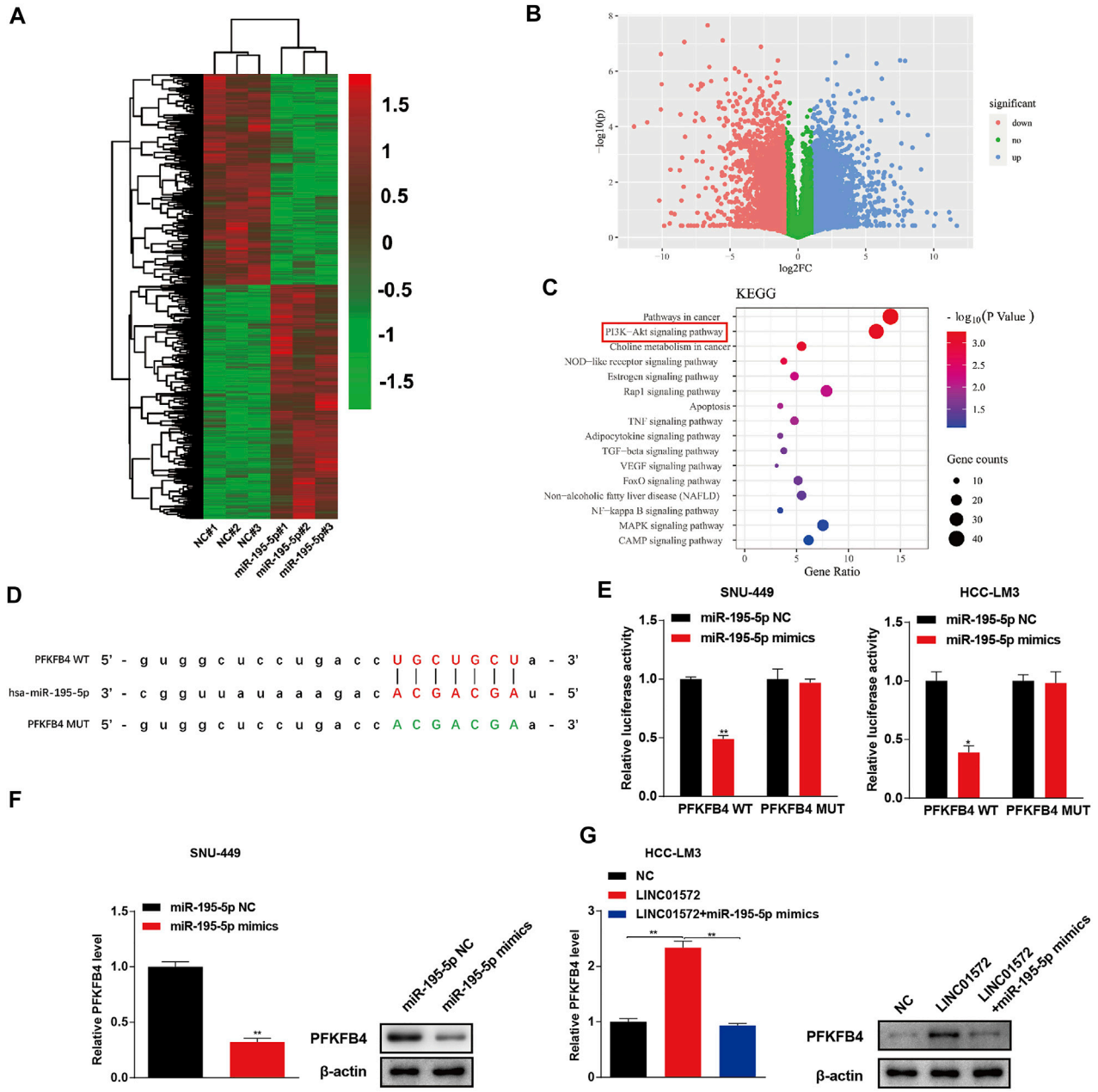

FIGURE 6 | miR-195-5p targets to PFKFB4 in HCC. **(A)** Heatmap of the differentially expressed genes after miR-195-5p overexpressed in SNU-449 cells **(B)** Volcano plot showing the significantly expressed genes. **(C)** KEGG analysis was used to screen the enriched pathways after miR-195-5p overexpressed. **(D)** Binding sites of miR-195-5p and PFKFB4 was predicted by using the ENCORI. **(E)** The target relationship of miR-195-5p and PFKFB4 were verified by dual-luciferase assay. **(F)** Influence of miR-195-5p mimics on the PFKFB4 level in SNU-449 cells. **(G)** Influence of miR-195-5p on LINC01572-induced upregulation of PFKFB4. All data are shown as mean ± standard deviation (n = 3). $^{*}p < 0.05$, $^{**}p < 0.01$.

a significantly increased enrichment of LINC01572 and miR-195-5p in the AGO2 precipitate compared with the IgG control (**Figures 5F,G**). In line with this, the RNA pull-down assay showed a significantly increased binding of AGO2 and miR-195-5p to LINC01572 (**Figures 5H,I**).

In order to determine the molecular mechanism underlying LINC01572/miR-195-5p–triggered HCC malignant behaviors, microarray analysis was performed to identify the potential targets on SNU-449 cells transfected with miR-195-5p mimics and negative control (**Figure 6A**). As a result, it was found that PFKFB4 was significantly downregulated following miR-195-5p mimics transfection (**Figure 6B**). The KEGG analysis further showed that PI3K-AKT signaling was potentially involved in the miR-195-5p effect (**Figure 6C**). The ENCORI prediction algorithm also showed that PFKFB4 was a potential target of miR-195-5p (**Figure 6D**). The dual-luciferase reporter activity

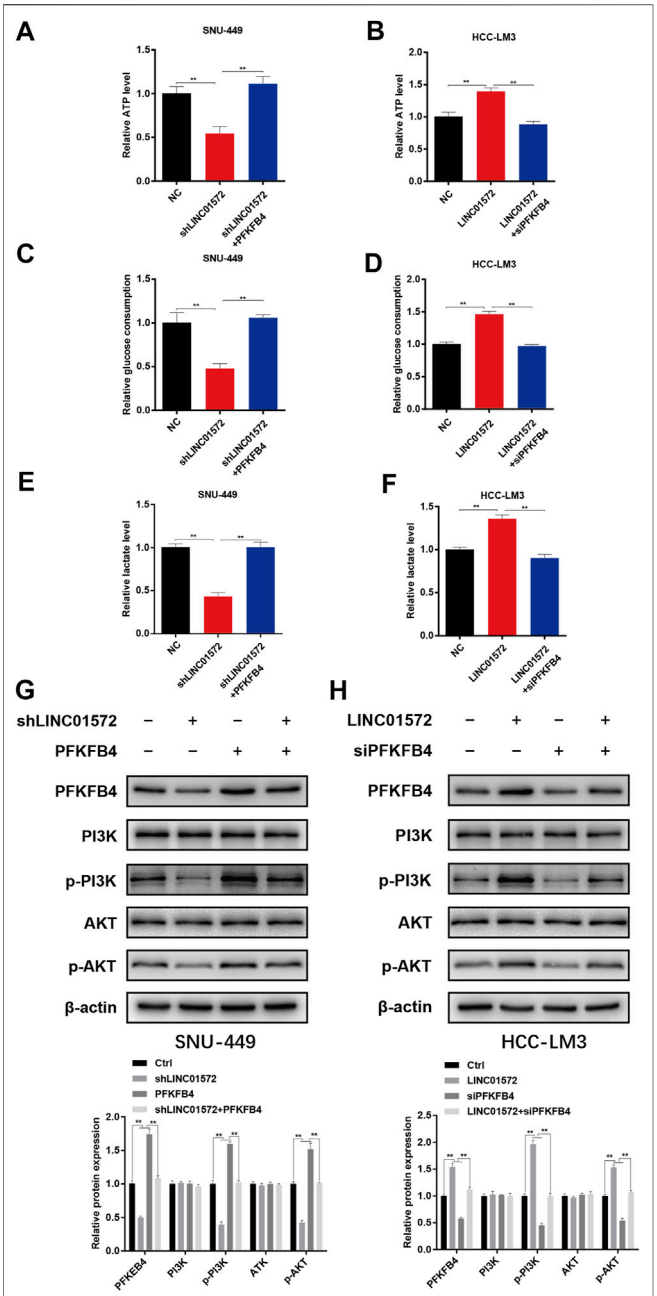

FIGURE 7 | LINC01572 increases glycolysis and activates PI3K/AKT signaling by regulating the PFKFB4 expression. **(A,B)** ATP production, **(C,D)** glucose consumption, and **(E,F)** lactate production following transfection of indicated constructs. **(G,H)** Effect of PFKFB4 overexpression or silencing on PI3K/AKT signaling, following LINC01572 silencing or overexpression, respectively. All data are shown as mean ± standard deviation (n = 3). $^{**}p < 0.01$.

assay showed that miR-195-5p significantly decreased luciferase activity in cells co-transfected with PFKFB4-WT but not PFKFB4-MUT (**Figure 6E**). Furthermore, miR-195-5p mimics significantly decreased the expression of PFKFB4 and prevented LINC01572-mediated upregulation of PFKFB4 (**Figures 6F,G**).

PFKFB4 is a key glycolysis regulator which activates the rate-limiting enzyme phosphofructokinase-1 (PFK-1) in glycolysis *via* its product fructose-2,6-biphosphate and has been proposed recently as a potential oncogene in HCC (Shen et al., 2021). Considering the significance of glycolysis in HCC malignancy (Hu L. et al., 2019; Feng et al., 2020; Gu et al., 2020), we reckoned that LINC01572 might have a glycolysis-promoting potential *via* increase in the PFKFB4 level. In line with this notion, we found that LINC01572 knockdown significantly inhibited the glycolytic process, which was effectively reversed by PFKFB4 overexpression (**Figures 7A,C,E**), whereas LINC01572 overexpression promoted HCC glycolysis, and PFKFB4 silencing remarkably blunted this effect (**Figures 7B,D,F,H**).

PI3K-AKT signaling has documented an important HCC-promoting pathway (Liao et al., 2019; Zhao et al., 2021), and a recent study has shown that transcriptional enhancement of the PFKFB4 expression promotes glioma malignancy progression by activating PI3K/AKT signaling (Zhang et al., 2021). We thus analyzed whether PI3K-AKT signaling was modulated by LINC01572 *via* PFKFB4. As expected, our results showed that LINC01572 positively affected the phosphorylation of PI3K/AKT in a PFKFB4-dependent manner (**Figures 7G,H**). Collectively, these data indicate that LINC01572 enhances PFKFB4 expression to enhance the glycolysis process and activate PI3K-AKT signaling in HCC *via* competitive sponging of miR-195-5p.

Upregulation of PFKFB4 Inhibits shLINC01572-Mediated Malignant Behaviors in Hepatocellular Carcinoma

Next, the functional significance of PFKFB4 in LINC01572-mediated HCC malignancy was explored *via* a series of rescue experiments. It was shown that the PFKFB4 level was significantly inhibited by shLINC01572 transfection and restored by PFKFB4 overexpression (**Figure 8A**). CCK-8 and colony formation demonstrated that shLINC01572-mediated HCC cell proliferation inhibition was significantly blunted by PFKFB4 overexpression (**Figures 8B,C**). shLINC01572-mediated HCC cell migration and invasion reduction were also restored by PFKFB4 overexpression (**Figure 8D**). In addition, PFKFB4 overexpression effectively reversed the MET process by shLINC01572 transfection in HCC cells (**Figure 8E**).

DISCUSSION

HCC develops primarily due to chronic hepatitis caused by HBV and HCV infection and resultant liver cirrhosis and fibrosis, causing approximately one million deaths each year worldwide (Lombardi et al., 2018). Increasing evidence shows that concurrent T2DM strongly predisposes to the occurrence of HCC (Dyal et al., 2016; Gerbes et al., 2018; Tan et al., 2019). More attention should be paid to HCC patients accompanied by T2DM as past decades have seen a noticeable increase in T2DM and T2DM-related HCC (Shi et al., 2021). This study aimed at identifying potential lncRNA molecules critically involved in T2DM-related HCC. This study demonstrated that LINC01572

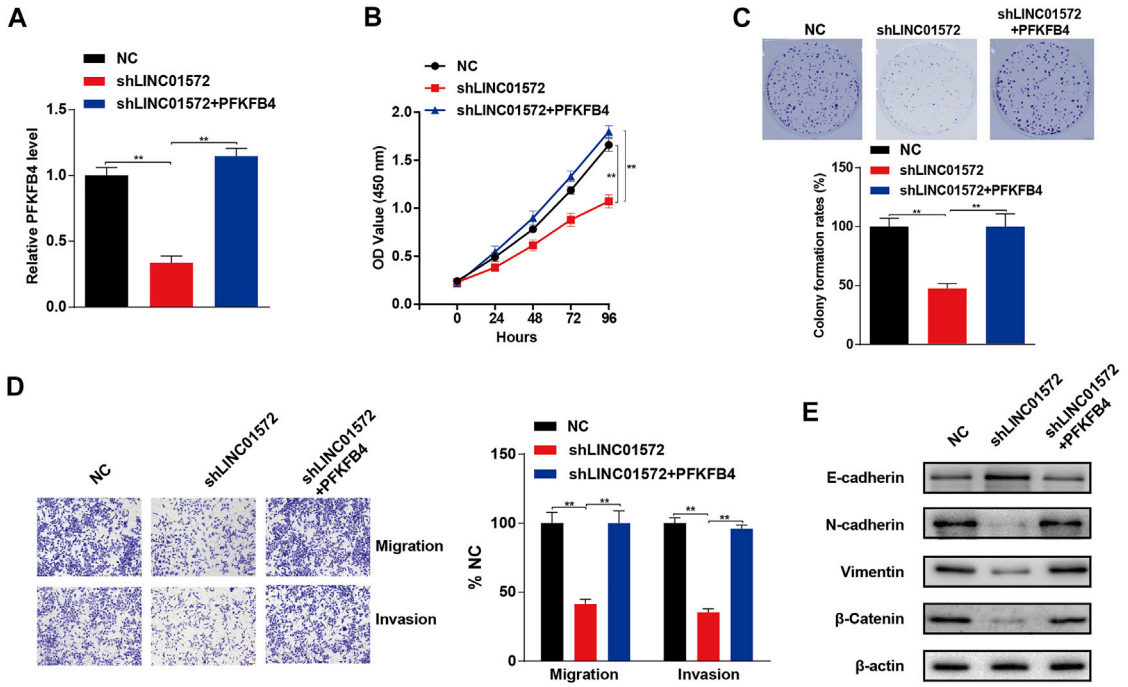

FIGURE 8 | PFKFB4 reverses LINC01572 provoked inhibition of proliferation, invasion, and migration in HCC cells. **(A)** RT-qPCR was used to detect the PFKFB4 level. **(B,C)** cck-8 and colony formation assays assessing the proliferation ability following LINC01572 silencing in the presence or absence of PFKFB4 overexpression. **(D,E)** Effect of LINC01572 silencing on HCC cell migration, invasion, and EMT marker expression in the presence or absence of PFKFB4 overexpression. All data are shown as mean ± standard deviation (n = 3). $^{**}p < 0.01$.

was aberrantly upregulated in HCC tissues, especially those from patients complicated by T2DM. A mechanistic study revealed that LINC01572 promoted HCC malignancy *via* sponging miR-195-5p to enhance PFKFB4-mediated glycolysis and PI3K/AKT signaling activation.

LncRNA has been proven to be critically associated with the occurrence, progression, and metastasis of cancers (Hu Y.-p. et al., 2019; Huang et al., 2021). LINC01572 is a newly recognized lncRNA molecule, and functionally, only one study reported that it mediated cisplatin resistance in gastric cancer cells (Song et al., 2020). However, its role in HCC is still unknown. In this study, we profiled lncRNAs in HCC tissues and corresponding adjacent tissues from HCC patients with T2DM by RNA sequencing. Our data showed that LINC01572 was aberrantly upregulated in HCC tissues as compared with the control, especially in those with concurrent T2DM. The high level of LINC01572 was correlated with the advanced T stage, increased blood HbA1c level, and shortened survival time. The overexpression of LINC01572 significantly promoted HCC cell proliferation, migration, invasion, and epithelial-to-mesenchymal transition (EMT), while the knockdown of LINC01572 had the opposite effects on HCC cells. Furthermore, silencing LINC01572 significantly restricted the growth and metastasis of HCC *in vivo*. Collectively, these results suggest that LINC01572 is carcinogenic and plays a role in the progression of HCC, particularly T2DM-related HCC.

We subsequently performed mechanistic experiments to further understand how LINC01572 modulates HCC progression. LncRNAs might adopt different mechanisms to regulate gene expression, depending on their subcellular location. Generally, lncRNAs located in the nucleus interact with RNA-binding proteins to control gene expression at transcriptional level (Zhang et al., 2020), whereas cytoplasmic lncRNAs might interact with miRNA as a competitive endogenous RNA (ceRNA), controlling gene expression at the post-transcriptional level (Han et al., 2020). A previous study showed that LINC01572 enhanced HCC cell proliferation and migration by inducing the transcription of downstream target genes as an eRNA(Lee et al., 2021). In this study, we found that LINC01572 was not only distributed in the nucleus but also in the cytoplasm of HCC cells, implying that ceRNA mechanism might be alternatively involved in LINC01572-mediated HCC malignancy.

Using ENCORI, we predicted that LINC01572 had a possible interaction with miRNA-195-5p. This predication was further confirmed by a series of data in our study, including those from the double-luciferase assay, RIP assay, RNA pull-down experiments, and modulating relationship between LINC01572 and miRNA-195-5p as revealed by RT-qPCR. These results indicate that LINC01572 might exert its oncogenic role in HCC *via* target binding to miRNA-195-5p, which seems to be plausible as miRNA-195-5p has documented to be a tumor suppressor in HCC (Xu et al., 2015).

Subsequently, using high-throughput screening and various confirmatory experiments, we presented evidence showing that 6-

phosphofructo-2-kinase/fructose-2, 6-bisphosphatase 4 (PFKFB4) is a critical target molecule to mediate LINC01572/miR-195-5p effects in HCC. In actual fact, the carcinogenic role of PFKFB4 has been documented in a variety of malignant tumors, including in HCC (Cai et al., 2021; Shen et al., 2021; Wang et al., 2021). Considering that in cancers, PFKFB4 is critically involved in enhanced aerobic glycolysis, a phenomenon termed the Warburg effect (Chen et al., 2021; Zhou et al., 2021), and we reckoned LINC01572 might exert its oncogenic effect *via* PFKFB4-enhanced glycolysis. This postulation was corroborated in our study as the influence of LINC01572 on both glycolysis and HCC malignant behaviors was dependent on the PFKFB4 level. In addition to mediating the Warburg effect, our KEGG enrichment analysis revealed that the PI3K/AKT pathway significantly affected the signaling transduction process by miR-195-5p. In line with this, our data showed that PI3K/AKT signaling was under control of LINC01572. More importantly, this process was PFKFB4-dependent, indicating that PFKFB4-mediated PI3K/AKT signaling activation represents another paralleled mechanism to enhanced glycolysis mediating the LINC01572 effect in HCC. Consistently, it has been documented that PFKFB4 exerts its oncogenic effect on glioma *via* increased activation of PI3K/AKT signaling (Zhang et al., 2021). Collectively, our results support that PFKFB4 relays the LINC01572 effect in HCC *via* enhanced glycolysis and paralleled hyperactivated PI3K/AKT signaling.

Taken together, we herein provide evidence demonstrating that lncRNA LINC01572 plays a pivotal role in promoting HCC cell malignancy *via* a ceRNA mechanism involving miR-195-5p and the glycolytic rate–limiting enzyme PFKFB4. This finding suggests a potential target for diagnosis, treatment, and prognosis of HCC, especially those complicated by T2DM.

DATA AVAILABILITY STATEMENT

The original contributions presented in the study are publicly available. This data can be found here: https://doi.org/10.6084/m9.figshare.16968199.v1, and https://doi.org/10.6084/m9.figshare.16968247.v1.

ETHICS STATEMENT

The studies involving human participants were reviewed and approved by the Ethics Committee of Guangxi Medical University. The patients/participants provided their written informed consent to participate in this study. The animal study was reviewed and approved by the Ethics Committee of Guangxi Medical University.

AUTHOR CONTRIBUTIONS

SL, BT, SH, and HD developed the original hypothesis and supervised the experiment; SL, ZQ, and YH performed *in vitro* and *in vivo* experiments; JL and ZW participated in the clinical specimen detection; SL and LD analyzed data and performed the statistical analysis; and SL, BT, and HD wrote and revised the manuscript. All authors read and approved the final manuscript.

FUNDING

This research was supported in part by the National Natural Science Foundation of China (Nos. 81871938 and 82173118), the Guangxi Natural Science Foundation for Key Program of Research and Development (GuiKe AB21075003), and the Guangxi Natural Science Foundation for Guangdong-Guangxi United Program (2021GXNSFDA075014).

SUPPLEMENTARY MATERIAL

The Supplementary Material for this article can be found online at: https://www.frontiersin.org/articles/10.3389/fcell.2021.783088/full#supplementary-material

REFERENCES

Cai, Y.-C., Yang, H., Shan, H.-B., Su, H.-F., Jiang, W.-Q., and Shi, Y.-X. (2021). PFKFB4 Overexpression Facilitates Proliferation by Promoting the G1/S Transition and Is Associated with a Poor Prognosis in Triple-Negative Breast Cancer. *Dis. Markers* 2021, 8824589. doi:10.1155/2021/8824589

Chen, J., Huang, X., Wang, W., Xie, H., Li, J., Hu, Z., et al. (2018). LncRNA CDKN2BAS Predicts Poor Prognosis in Patients with Hepatocellular Carcinoma and Promotes Metastasis via the miR-153-5p/ARHGAP18 Signaling axis. *Aging* 10 (11), 3371–3381. doi:10.18632/aging.101645

Chen, W.-J., Tang, R.-X., He, R.-Q., Li, D.-Y., Liang, L., Zeng, J.-H., et al. (2017). Clinical Roles of the Aberrantly Expressed lncRNAs in Lung Squamous Cell Carcinoma: a Study Based on RNA-Sequencing and Microarray Data Mining. *Oncotarget* 8 (37), 61282–61304. doi:10.18632/oncotarget.18058

Chen, Y., Song, S., Zhang, L., and Zhang, Y. (2021). Circular RNA Hsa_circ_0091579 Facilitates the Warburg Effect and Malignancy of Hepatocellular Carcinoma Cells via the miR-624/H3F3B axis. *Clin. Transl Oncol.* 23, 2280–2292. doi:10.1007/s12094-021-02627-4

Dyal, H. K., Aguilar, M., Bartos, G., Holt, E. W., Bhuket, T., Liu, B., et al. (2016). Diabetes Mellitus Increases Risk of Hepatocellular Carcinoma in Chronic Hepatitis C Virus Patients: A Systematic Review. *Dig. Dis. Sci.* 61 (2), 636–645. doi:10.1007/s10620-015-3983-3

Feng, J., Dai, W., Mao, Y., Wu, L., Li, J., Chen, K., et al. (2020). Simvastatin Re-sensitizes Hepatocellular Carcinoma Cells to Sorafenib by Inhibiting HIF-1α/ppar-Γ/pkm2-Mediated Glycolysis. *J. Exp. Clin. Cancer Res.* 39 (1), 24. doi:10.1186/s13046-020-1528-x

Ge, Y., Gu, P., Wang, W., Cao, L., Zhang, L., Li, J., et al. (2021). Benzo[a]pyrene Stimulates miR-650 Expression to Promote the Pathogenesis of Fatty Liver Disease and Hepatocellular Carcinoma via SOCS3/JAK/STAT3 Cascades. *J. Mol. Cel. Biol.* 13, 556. doi:10.1093/jmcb/mjab052

Gerbes, A., Zoulim, F., and Tilg, H. (2018). Correction: Gut Roundtable Meeting Paper: Selected Recent Advances in Hepatocellular Carcinoma. *Gut* 67 (3), 594. doi:10.1136/gutjnl-2017-315068corr1

Gu, Y., Ji, F., Liu, N., Zhao, Y., Wei, X., Hu, S., et al. (2020). Loss of miR-192-5p Initiates a Hyperglycolysis and Stemness Positive Feedback in Hepatocellular Carcinoma. *J. Exp. Clin. Cancer Res.* 39 (1), 268. doi:10.1186/s13046-020-01785-7

Han, T.-S., Hur, K., Cho, H.-S., and Ban, H. S. (2020). Epigenetic Associations between lncRNA/circRNA and miRNA in Hepatocellular Carcinoma. *Cancers* 12 (9), 2622. doi:10.3390/cancers12092622

Hu, L., Zeng, Z., Xia, Q., Liu, Z., Feng, X., Chen, J., et al. (2019a). Metformin Attenuates Hepatoma Cell Proliferation by Decreasing Glycolytic Flux through the HIF-1α/PFKFB3/PFK1 Pathway. *Life Sci.* 239, 116966. doi:10.1016/j.lfs.2019.116966

Hu, Y.-p., Jin, Y.-p., Wu, X.-s., Yang, Y., Li, Y.-s., Li, H.-f., et al. (2019b). LncRNA-HGBC Stabilized by HuR Promotes Gallbladder Cancer Progression by Regulating miR-502-3p/SET/AKT axis. *Mol. Cancer* 18 (1), 167. doi:10.1186/s12943-019-1097-9

Hu, X., Zhu, H., Shen, Y., Zhang, X., He, X., and Xu, X. (2021). The Role of Non-coding RNAs in the Sorafenib Resistance of Hepatocellular Carcinoma. *Front. Oncol.* 11, 696705. doi:10.3389/fonc.2021.696705

Huang, X., Pan, L., Zuo, Z., Li, M., Zeng, L., Li, R., et al. (2021). LINC00842 Inactivates Transcription Co-regulator PGC-1α to Promote Pancreatic Cancer Malignancy through Metabolic Remodelling. *Nat. Commun.* 12 (1), 3830. doi:10.1038/s41467-021-23904-4

Jin, Z.-L., and Liu, W. (2021). Progress in Treatment of Type 2 Diabetes by Bariatric Surgery. *World J. Diabetes* 12 (8), 1187–1199. doi:10.4239/wjd.v12.i8.1187

Lee, Y.-E., Lee, J., Lee, Y. S., Jang, J. J., Woo, H., Choi, H. I., et al. (2021). Identification and Functional Characterization of Two Noncoding RNAs Transcribed from Putative Active Enhancers in Hepatocellular Carcinoma. *Mol.Cells* 44 (9), 658–669. doi:10.14348/molcells.2021.0173

Liao, J., Jin, H., Li, S., Xu, L., Peng, Z., Wei, G., et al. (2019). Apatinib Potentiates Irradiation Effect via Suppressing PI3K/AKT Signaling Pathway in Hepatocellular Carcinoma. *J. Exp. Clin. Cancer Res.* 38 (1), 454. doi:10.1186/s13046-019-1419-1

Lombardi, A., Grimaldi, A., Zappavigna, S., Misso, G., and Caraglia, M. (2017). Hepatocarcinoma: Genetic and Epigenetic Features. *Minerva Gastroenterol.* 64 (1), 14–27. doi:10.23736/s1121-421x.17.02408-4

Mohan, C. D., Rangappa, S., Nayak, S. C., Sethi, G., and Rangappa, K. S. (2021). Paradoxical Functions of Long Noncoding RNAs in Modulating STAT3 Signaling Pathway in Hepatocellular Carcinoma. *Biochim. Biophys. Acta (Bba) - Rev. Cancer* 1876 (1), 188574. doi:10.1016/j.bbcan.2021.188574

Shen, C., Ding, L., Mo, H., Liu, R., Xu, Q., and Tu, K. (2021). Long Noncoding RNA FIRRE Contributes to the Proliferation and Glycolysis of Hepatocellular Carcinoma Cells by Enhancing PFKFB4 Expression. *J. Cancer* 12 (13), 4099–4108. doi:10.7150/jca.58097

Shi, T., Kobara, H., Oura, K., and Masaki, T. (2021). Mechanisms Underlying Hepatocellular Carcinoma Progression in Patients with Type 2 Diabetes. *J. Hepatocell Carcinoma* 8, 45–55. doi:10.2147/jhc.S274933

Singh, M. K., Das, B. K., Choudhary, S., Gupta, D., and Patil, U. K. (2018). Diabetes and Hepatocellular Carcinoma: A Pathophysiological Link and Pharmacological Management. *Biomed. Pharmacother.* 106, 991–1002. doi:10.1016/j.biopha.2018.06.095

Song, Z., Jia, N., Li, W., and Zhang, X.-Y. (2020). LINC01572 Regulates Cisplatin Resistance in Gastric Cancer Cells by Mediating miR-497-5p. *Onco Targets Ther.* 13, 10877–10887. doi:10.2147/ott.S267915

Sun, C., Huang, S., Hou, Y., Li, Z., Xia, D., Zhang, L., et al. (2020). Long Noncoding RNA AC092171.4 Promotes Hepatocellular Carcinoma Progression by Sponging microRNA-1271 and Upregulating GRB2. *Aging* 12 (14), 14141–14156. doi:10.18632/aging.103419

Tan, Y., Wei, S., Zhang, W., Yang, J., Yang, J., and Yan, L. (2019). Type 2 Diabetes Mellitus Increases the Risk of Hepatocellular Carcinoma in Subjects with Chronic Hepatitis B Virus Infection: a Meta-Analysis and Systematic Review. *Cancer Manag. Res.* 11, 705–713. doi:10.2147/cmar.S188238

Teng, F., Zhang, J.-X., Chang, Q.-M., Wu, X.-B., Tang, W.-G., Wang, J.-F., et al. (2020). Correction to: LncRNA MYLK-AS1 Facilitates Tumor Progression and Angiogenesis by Targeting miR-424-5p/E2F7 axis and Activating VEGFR-2 Signaling Pathway in Hepatocellular Carcinoma. *J. Exp. Clin. Cancer Res.* 39 (1), 277. doi:10.1186/s13046-020-01780-y

Wang, F., Wu, X., Li, Y., Cao, X., Zhang, C., and Gao, Y. (2021). PFKFB4 as a Promising Biomarker to Predict a Poor Prognosis in Patients with Gastric Cancer. *Oncol. Lett.* 21 (4), 296. doi:10.3892/ol.2021.12557

Wild, S. H. (2011). Diabetes, Treatments for Diabetes and Their Effect on Cancer Incidence and Mortality: Attempts to Disentangle the Web of Associations. *Diabetologia* 54 (7), 1589–1592. doi:10.1007/s00125-011-2169-6

Xu, H., Hu, Y.-W., Zhao, J.-Y., Hu, X.-M., Li, S.-F., Wang, Y.-C., et al. (2015). MicroRNA-195-5p Acts as an Anti-oncogene by Targeting PHF19 in Hepatocellular Carcinoma. *Oncol. Rep.* 34 (1), 175–182. doi:10.3892/or.2015.3957

Zhang, L., Liu, Z., Dong, Y., and Kong, L. (2021). E2F2 Drives Glioma Progression via PI3K/AKT in a PFKFB4-dependent Manner. *Life Sci.* 276, 119412. doi:10.1016/j.lfs.2021.119412

Zhang, X.-Z., Liu, H., and Chen, S.-R. (2020). Mechanisms of Long Non-coding RNAs in Cancers and Their Dynamic Regulations. *Cancers* 12 (5), 1245. doi:10.3390/cancers12051245

Zhao, L., Hu, K., Cao, J., Wang, P., Li, J., Zeng, K., et al. (2019). lncRNA Miat Functions as a ceRNA to Upregulate Sirt1 by Sponging miR-22-3p in HCC Cellular Senescence. *Aging* 11 (17), 7098–7122. doi:10.18632/aging.102240

Zhao, T., Guo, B.-J., Xiao, C.-L., Chen, J.-J., Lü, C., Fang, F.-F., et al. (2021). Aerobic Exercise Suppresses Hepatocellular Carcinoma by Downregulating Dynamin-Related Protein 1 through PI3K/AKT Pathway. *J. Integr. Med.* 19 (5), 418–427. doi:10.1016/j.joim.2021.08.003

Zhou, Y., Lin, F., Wan, T., Chen, A., Wang, H., Jiang, B., et al. (2021). ZEB1 Enhances Warburg Effect to Facilitate Tumorigenesis and Metastasis of HCC by Transcriptionally Activating PFKM. *Theranostics* 11 (12), 5926–5938. doi:10.7150/thno.56490

Conflict of Interest: The authors declare that the research was conducted in the absence of any commercial or financial relationships that could be construed as a potential conflict of interest.

Publisher's Note: All claims expressed in this article are solely those of the authors and do not necessarily represent those of their affiliated organizations, or those of the publisher, the editors, and the reviewers. Any product that may be evaluated in this article, or claim that may be made by its manufacturer, is not guaranteed or endorsed by the publisher.

frontiers in Cell and Developmental Biology

REVIEW
published: 24 December 2021
doi: 10.3389/fcell.2021.793428

Interplay Among Metabolism, Epigenetic Modifications, and Gene Expression in Cancer

Miaomiao Huo[1†], *Jingyao Zhang*[1†], *Wei Huang*[1,2*] *and Yan Wang*[1,2*]

[1]*Key Laboratory of Cancer and Microbiome, State Key Laboratory of Molecular Oncology, National Cancer Center/National Clinical Research Center for Cancer/Cancer Hospital, Chinese Academy of Medical Sciences and Peking Union Medical College, Beijing, China,* [2]*Beijing Key Laboratory of Cancer Invasion and Metastasis Research, Department of Biochemistry and Molecular Biology, School of Basic Medical Sciences, Capital Medical University, Beijing, China*

OPEN ACCESS

Edited by:
Lutao Du,
Second Hospital of Shandong University, China

Reviewed by:
Marco Sciacovelli,
University of Cambridge, United Kingdom
Jian Zhang,
Fourth Military Medical University, China
Lei Chen,
Eastern Hepatobiliary Surgery Hospital, China

***Correspondence:**
Wei Huang
weihuang@ccmu.edu.cn
Yan Wang
yanwang@cicams.ac.cn

†*These authors have contributed equally to this work and share first authorship*

Specialty section:
This article was submitted to Epigenomics and Epigenetics, a section of the journal Frontiers in Cell and Developmental Biology

Received: *12 October 2021*
Accepted: *01 December 2021*
Published: *24 December 2021*

Citation:
Huo M, Zhang J, Huang W and Wang Y (2021) Interplay Among Metabolism, Epigenetic Modifications, and Gene Expression in Cancer. Front. Cell Dev. Biol. 9:793428. doi: 10.3389/fcell.2021.793428

Epigenetic modifications and metabolism are two fundamental biological processes. During tumorigenesis and cancer development both epigenetic and metabolic alterations occur and are often intertwined together. Epigenetic modifications contribute to metabolic reprogramming by modifying the transcriptional regulation of metabolic enzymes, which is crucial for glucose metabolism, lipid metabolism, and amino acid metabolism. Metabolites provide substrates for epigenetic modifications, including histone modification (methylation, acetylation, and phosphorylation), DNA and RNA methylation and non-coding RNAs. Simultaneously, some metabolites can also serve as substrates for nonhistone post-translational modifications that have an impact on the development of tumors. And metabolic enzymes also regulate epigenetic modifications independent of their metabolites. In addition, metabolites produced by gut microbiota influence host metabolism. Understanding the crosstalk among metabolism, epigenetic modifications, and gene expression in cancer may help researchers explore the mechanisms of carcinogenesis and progression to metastasis, thereby provide strategies for the prevention and therapy of cancer. In this review, we summarize the progress in the understanding of the interactions between cancer metabolism and epigenetics.

Keywords: epigenetic modifications, metabolic reprogramming, metabolic enzymes, gut microbiota, clinical trails

INTRODUCTION

Cancer is a disease with high morbidity and mortality and is a serious threat to human health (Bray et al., 2021). Genome instability and mutations contribute to the extraordinary diversity of cancer, and tumors acquire multiple hallmarks during their multistep development, including the reprogramming of energy metabolism (Hanahan and Weinberg, 2011; Sung et al., 2021). Over the past few decades, researchers have found that the metabolic characteristics of tumor cells are significantly different from those of normal cells. Tumor cells have high nutrient and energy requirements, based on their characteristics of sustaining proliferative signaling, evading growth suppressors, and deregulating cellular energetics (Hanahan and Weinberg, 2011). The metabolic reprogramming of tumor cells enables them to obtain essential nutrients from a nutrition-deficient environment to maintain continuous cell growth and proliferation (Pavlova and Thompson, 2016). On one hand, the activation of oncogenes and the deficiency of tumor suppressor genes promote the metabolic reprogramming of tumors, to achieve stronger nutrient-utilization ability and provide material and

energy for biosynthesis. At the same time, a lack of nutrition in solid tumors also requires malignant tumor cells to possess metabolic flexibility to maintain growth and survival (Boroughs and DeBerardinis, 2015). Altered metabolic profiles mainly occur with respect to the uptake and metabolism of glucose and amino acids and the synthesis of lipids. For example, the Warburg effect, observed in cancer, suggests that even under sufficient oxygen conditions, malignant tumor cells are active in anaerobic glycolysis, which yields lactic acid, instead of oxidative phosphorylation like that in normal differentiated cells, characterized by a high glucose uptake rate and active glycolysis; moreover, a high level of the metabolite lactic acid correlates with poor tumor prognosis (Warburg, 1956; Som et al., 1980; Vander Heiden et al., 2009). Although aerobic glycolysis is an inefficient way to generate adenosine 5′-triphosphate (ATP), it meets the nutrient needs for cancer cell proliferation via the incorporation of metabolized nutrients into biomass. This reveals a link between cellular metabolism and cell growth control (Vander Heiden et al., 2009). As a highly versatile nutrient, glutamine is also important for tumor cell growth. Cancer cells take up glutamine via glutamine transporter (ASCT2), also known as solute carrier family 1 member 5 (SLC1A5) (Wang et al., 2015). Further, cancer cells are addicted to glutamine through oncogene-dependent pathways involving c-MYC, AKT (Serine/Threonine Kinase 1), and p53 (Tumor Protein P53) (Wettersten et al., 2017). Likewise, as a principal growth-supporting substrate, glutamine provides nitrogen for the biosynthesis of purine and pyrimidine nucleotides, glucosamine-6-phosphate, and nonessential amino acids (Pavlova and Thompson, 2016). Additionally, a process known as glutaminolysis can divert abundant glutamine to replenish the tricarboxylic acid (TCA) cycle (Wong et al., 2017). Lifestyle-related factors, especially diet and nutrition, have a profound effect on human health. Moreover, the gut microbiota plays an important role in this by further metabolizing nutrients from the diet and producing a variety of chromatin-modifying compounds, ultimately regulating histone methylation and acetylation by modulating the intracellular pools of metabolites (Dai et al., 2020).

Heritable changes in gene expression that do not include changes to the DNA sequence itself are termed epigenetic changes. Epigenetics mainly are manifested as DNA methylation, histone post-translational modifications (PTMs), such as acetylation, methylation, phosphorylation, ubiquitination, glycosylation, lactylation, succinylation, and other acyl modifications, including O-linked N-acetylglucosamine modification (O-GlcNAcylation) (Esteller, 2008; Tan et al., 2011; Suva et al., 2013; Huang et al., 2014; Tessarz and Kouzarides, 2014; Dai et al., 2020), as well as RNA methylation, including N6-methyladenosine (m^6A) and 5-methylcytosine (m^5C) (Han et al., 2020). Epigenetic plasticity in the process of tumorigenesis and development facilitates the acquisition of hallmark characteristics of cancer (Esteller, 2008; Hanahan and Weinberg, 2011). Many metabolic intermediates serve as epigenetic modification substrates or cofactors, and the various epigenetic processes are primarily governed by the concentrations of the involved reactants (Simithy et al., 2017; Wagner et al., 2017; Thakur and Chen, 2019).

Epigenetic modificatios and metabolism are two fundamental biological processes. Epigenetic alterations and metabolic reprogramming in cancer are highly interrelated. Oncogene-driven metabolic reprogramming alters the epigenetic landscape by regulating DNA and histone modification-related enzyme activity. However, the expression of metabolic genes is regulated by epigenetic mechanisms, thus, altering the metabolome. Therefore, the crosstalk between epigenetics and metabolism plays a crucial role in carcinogenesis and cancer progression through the proliferation, metastasis, and heterogeneity of cancer cells.

EPIGENETIC MODIFICATIONS

Increasing evidence suggests that cancer is a metabolic disease. Epigenetic regulation plays a crucial role in metabolic regulation and tumorigenesis (Li et al., 2018; Bates, 2020). To maintain homeostasis and ensure cell survival, cells must dynamically respond to changes in the environment and reprogram their metabolic state. Similarly, the harmonization of gene expression is required to ensure normal cell function. Epigenetic modifications provide an ideal mechanism for the regulation of gene expression and metabolic reprogramming. Specifically, changes in histone modification are fast and reversible and rely on metabolic intermediates as cofactors for modification. Therefore, it is of great significance to understand the relationship among the metabolic environment, epigenetic modifications, and the expression of genes that play a role in many diseases, particularly cancer (Li et al., 2018).

Deoxyribonucleic Acid and Ribonucleic Acid Methylation

Many studies have shown that DNA and RNA methylation plays an important role in regulating cancer metabolism (Saghafinia et al., 2018; Uddin et al., 2021). Abnormal methylation in the promoter region of tumor suppressor genes is key to tumorigenesis and cancer development (Nishiyama and Nakanishi, 2021). Zinc finger DHHC-Type containing 1 (*ZDHHC1*), a recently discovered tumor suppressor gene, is silenced in a variety of cancers through abnormal hypermethylation to inhibit glucose metabolism and the pentose phosphate pathway (Le et al., 2020). The transcription factor brother of the regulator of imprinted sites (BORIS) regulates the methylation of pyruvate kinase M1/2 (*PKM*) exons and the alternative splicing of *PKM* mRNA to mediate the Warburg effect and promote breast cancer (Singh et al., 2017). In colon cancer, hypermethylation of the derlin3 (*DERL3*) promoter region promotes high expression of solute carrier family 2 member 1 (*SLC2A1*) to enhance the Warburg effect (Lopez-Serra et al., 2014). Methyltransferase 3, N6-adenosine-methyltransferase complex catalytic subunit 3 (METTL3) attaches m6A-IGF2BP2/3 to stabilize the expression of hexokinase 2 (HK2), resulting in the expression of phosphorylated glucose hexokinases, and *SLC2A1*, resulting in the expression of glucose transporter (GLUT1), in colon cancer to activate the glycolytic pathway (Shen et al., 2020) (**Figure 1**).

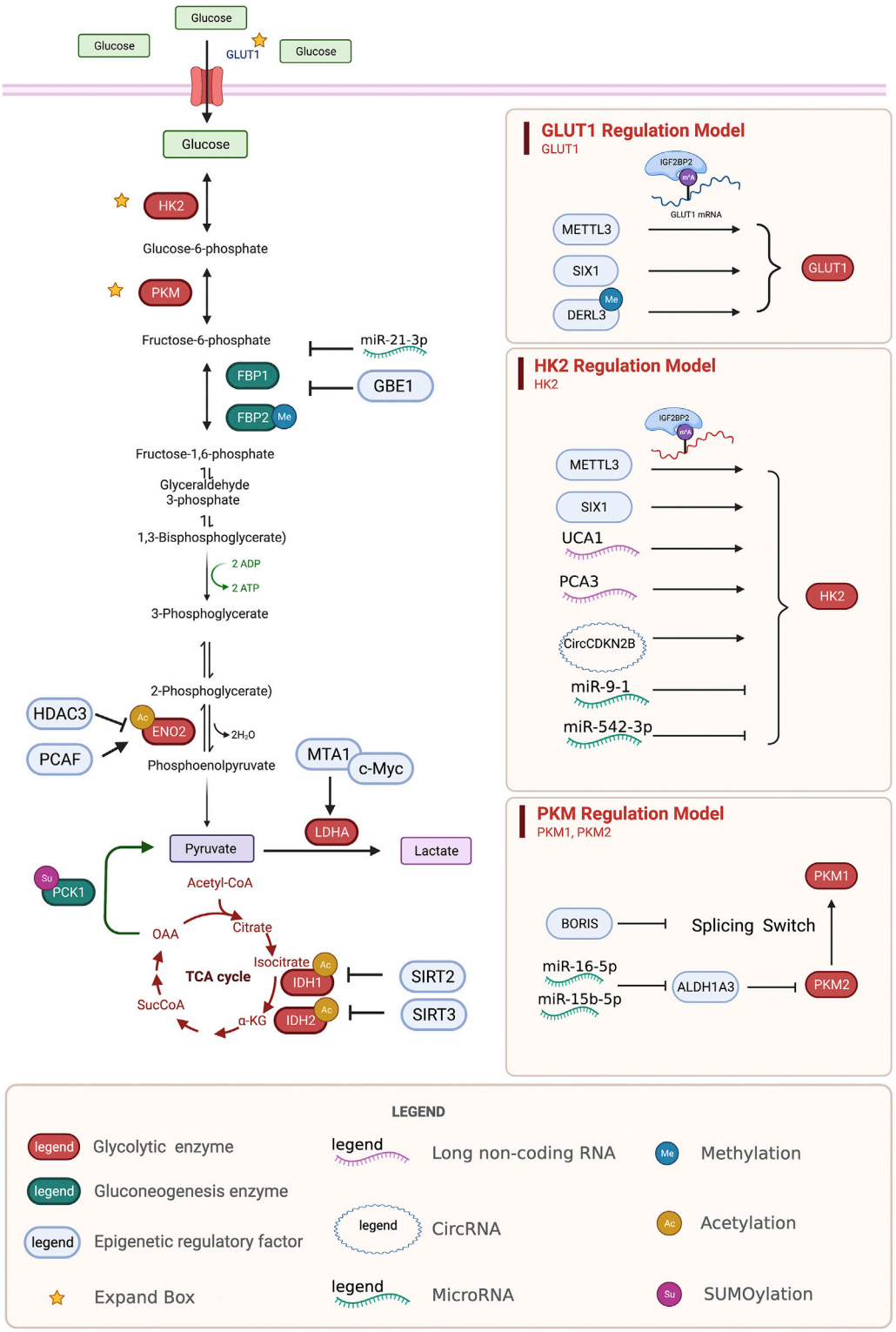

FIGURE 1 | Regulation of glycolysis and gluconeogenesis enzymes by epigenetic modifications. Epigenetic regulatory enzymes, lncRNA, and circRNA regulate the epigenetic regulation of the key proteins, GLUT1, HK2, PKM, ENO2, LDHA, IDH, and the key enzymes FBP and PCK in the process of gluconeogenesis. GLUT1, glucose transporter type 1; HK2, hexokinase 2; PKM, pyruvate kinase M1/2; ENO2, enolase 2; LDHA, lactate dehydrogenase A; IDH, isocitrate dehydrogenase (NADP (+)); FBP, fructose-bisphosphatase; PCK, phosphoenolpyruvate carboxykinase.

The reduced transcription of fructose bisphosphates 1 (*FBP1*), a rate-limiting enzyme in gluconeogenesis, mediates disruptions to gluconeogenesis and increased glycolytic activity, causing tumor progression and poor prognosis (Hirata et al., 2016). Under hypoxic conditions, HIF1a promotes the methylation of *FBP1* by upregulating the expression of glycogen-branching enzyme 1 (GBE1) in lung adenocarcinoma (Li L. et al., 2020). The promoter region of fructose-bisphosphatase 2 (*FBP2*) in gastric cancer is densely methylated to promote glucose metabolism (Li et al., 2013) (**Figure 1**).

Peroxisome proliferator activated receptor alpha (PPARα), a nuclear receptor that regulates lipid homeostasis, inhibits DNA methyltransferase 1 (DNMT1)-mediated cyclin dependent kinase inhibitor 1A (CDKN1A) and PRMT6-mediated cyclin dependent kinase inhibitor 1b (CDKN1B) to promote colon cancer (Luo et al., 2019). YTH n6-methyladenosine RNA binding protein 2 (YTHDF2) is downstream of epidermal growth factor receptor/src proto-oncogene, non-receptor tyrosine kinase/extracellular signal-regulated kinase (EGFR/SRC/ERK) and plays an important role in the proliferation and invasion of glioma cells. Studies have shown that YTHDF2 mediates the downregulation of liver X receptor-alpha (*LXRA*) mRNA through m6A to influence glioblastoma (GBM) cholesterol homeostasis (Fang et al., 2021). Argininosuccinate synthase 1 (ASS1) in cisplatin-resistant bladder cancer cells is hypermethylated, resulting in greatly downregulated expression, suppressing the apoptotic effects of cisplatin (Yeon et al., 2018).

Non-Coding Ribonucleic Acids

Recent studies have shown that non-coding RNAs regulate the metabolic remodeling of tumors, including sugar metabolism, lipid metabolism, cholesterol metabolism, and amino acid metabolism (Xu et al., 2021c; Sellitto et al., 2021). However, the mechanism by which long non-coding RNAs regulate tumor metabolism is still unclear. Many studies have explored the relationship between metabolism and non-coding RNAs. Urothelial cancer associated 1 (UCA1) has been shown to increase the activation of HK2 by inhibiting miR203 and to regulate glucose metabolism by increasing glucose uptake and lactic acid production, promoting the proliferation and metastasis of esophageal cancer (Liu H.-E. et al., 2020). CircCDKN2B-AS1, the cyclic structure of the long non-coding RNA CDKN2B-AS1, can combine with IMP U3 small nucleolar ribonucleoprotein 3 (IMP3) to stabilize the transcription of *HK2* and promote aerobic glycolysis and the malignant phenotype in cervical cancer (Zhang Y. et al., 2020). Prostate cancer associated 3 (*PCA3*) targets miR-132–3P and weakens its interaction with SREBP1, leading to lipid metabolism disorders caused by antimony exposure in prostate cancer (Guo et al., 2021) (**Figure 1**).

HIF1α upregulates the transcription of genes encoding glucose transporters and glycolytic enzymes to regulate tumor glucose metabolism. In recent years, several studies have shown that long non-coding RNAs (lncRNAs) play key roles in regulating the HIF1α pathway (Tan Y. T. et al., 2021). LncRNA-p21 is a hypoxia-reactive lncRNA that can bind HIF1α to inhibit the ubiquitination of HIF1α and then promote glycolysis under hypoxic conditions, contributing to the Warburg effect (Yang et al., 2014). HIFAL (the anti-sense lncRNA of HIF1α) recruits PHD3 to PKM2 to promote the hydroxylation of its proline residues, and the PKM2/PHD3 complex is then guided by heterogeneous nuclear ribonucleoprotein F (hnRNPF) into the nucleus to enhance the transcriptional activation of HIF1α and promote glycolysis (Zheng et al., 2021). Meanwhile, HIF-1α-stabilizing long noncoding RNA (HISLA) inhibits the interaction between prolyl hydroxylase domain-containing protein 2 (PHD2) and HIF1α to prevent the degradation of HIF1α and promote glycolysis, hindering breast cell apoptosis (Chen et al., 2019). Many genes involved in glucose metabolism are transcriptionally activated by HIF1α (Semenza, 2003) (**Figure 2**).

Recent research on microRNAs has led to increasing evidence on the pivotal role of miRNAs in all stages of tumor development. MiR-9-1 targets HK2 to inhibit glycolysis, reduce the formation of lactic acid, and promote metabolic reprogramming in nasopharyngeal carcinoma cells (Xu Q. L. et al., 2021). Meanwhile, miR-542–3p elevates HK2 to induce glycolysis in GBM (Kim et al., 2021). miRNA-1185-2-3p inhibits Golgi phosphoprotein 3 (GOLPH3L) and affects central carbon metabolism regulated by GOLPH3L (Xu et al., 2021b). MiR-16–5p and 15b-5p coregulate ALDH1A3, which can inhibit the ubiquitination of PKM2 and regulate glycolysis to exert anti-cancer effects (Huang X. et al., 2021). In ovarian cancer, miR-424–5p inhibits mitochondrial elongation factor 2 (MIEF2), which regulates mitochondrial fission, inhibits glucose metabolism from oxidative phosphorylation to glycolysis, and inhibits tumor growth (Zhao et al., 2020). LIX1-like protein (LIX1L) promotes miR-21–3p, inhibits FBP1, reduces lactic acid production, and affects sugar metabolism to inhibit tumor growth (Zou et al., 2021) (**Figure 1**). MiR-15a-5p inhibits acetate uptake and acyl-CoA synthetase short chain family member 2 (ACSS2) and H4 acetylation in the nucleus under hypoxia, inhibiting fatty acid synthesis in lung cancer cells and further suppressing malignancy in lung cancer (Ni et al., 2020).

Histone Modifications

Various PTMs act on histones. Most histone modification sites are at the N-terminal end of the nucleosome tail of H3 and H4 histones. Common histone modifications include methylation, acetylation, ubiquitination, SUMOylation, and phosphorylation (Ahringer and Gasser, 2018). However, in recent years, new histone modifications have been discovered, including crotonylation, GlcNAcylation, and citrullination (Blakey and Litt, 2015; Zhang M. et al., 2020).

Different histone modifications are associated with different chromatin states—specifically, the methylation of H3K4 activates transcription, trimethylation at H3K27 is associated with transcription inhibition, acetylation of the histone tail generally promotes transcription, and deacetylation of histones inhibits transcription (Carter and Zhao, 2021). Epigenetic changes control the expression of many metabolic genes, which are important in cancer metabolism (Sun et al., 2021). Increasing evidence shows that histone methylation and metabolic variations in cancer cells are highly correlated

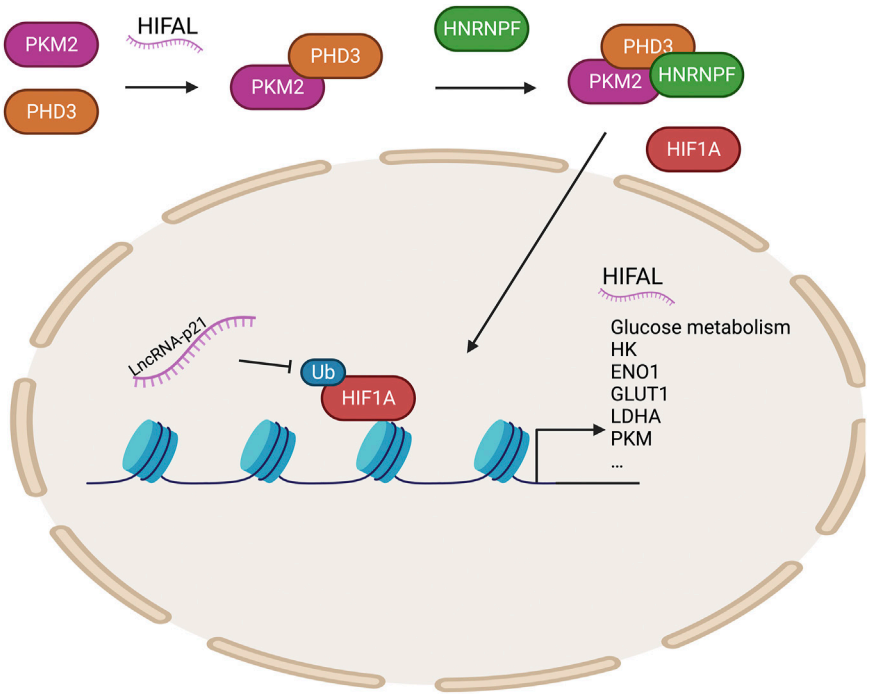

FIGURE 2 | Epigenetic regulation of HIF1A regulates glycolytic enzymes. HIFAL recruits PHD3 to PKM2, and the PKM2/PHD3 complex is then guided by HNRNPF into the nucleus to enhance the transcriptional activation of HIF1α to promote the expression of genes related to glucose metabolism. LncRNA-P21 protects HIF1A stability. PHD3, prolyl hydroxylase domain-containing protein 3; HNRNPF, heterogeneous nuclear ribonucleoprotein F; HIFAL, anti-sense lncRNA of HIF1A; PKM2, pyruvate kinase M2.

(Rausch et al., 2021). Enhancer of zeste 2 polycomb repressive complex 2 subunit (EZH2), a key epigenetic enhancer, suppresses gene transcription by promoting H3K27me3 (Zhang T. et al., 2020). Recently, EZH2 was shown to affect tumor cell metabolism, including carbohydrate metabolism, amino acid metabolism, and lipid metabolism. EZH2 regulates the Warburg effect to promote tumorigenesis and cancer development. EZH2-mediated histone H3 lysine 27 trimethylation mediates the downregulation of LINC00261 to promote glycolysis in pancreatic cancer (Zhai et al., 2021). EZH2 is enriched in the *WNT* promoter region and regulates H3K27me3 to suppress the transcription of *WNTs*, including *WNT-1*, *6*, *10a*, and *10b* genes, which are involved in the process of adipogenesis (Wang et al., 2010). In lung cancer, lysine methyltransferase 2D (KMT2D) is highly expressed and regulates the super enhancers H3K4me1 and H3K27ac of period circadian regulator 2 (PER2; circadian inhibitory factor), affecting the expression of *PER2* and its downstream glycolytic genes (Alam et al., 2020). As a H3K27me2 reader, PHD Finger Protein 20 Like 1(PHF20L1) plays important roles in promoting the Warburg effect via many glycolysis-related genes (GRGs) in breast cancer (Hou et al., 2020). Lysine-specific histone demethylase 1 (LSD1) also plays an important role in the metabolic regulation of hepatocellular carcinoma. LSD1 mediates the methylation of H3K4 to inhibit the expression of PPARgamma coactivator 1alpha (PGC1α), thereby, affecting mitochondrial oxidative respiration (Sakamoto et al., 2015). Meanwhile, the interaction between LSD1 and snail family transcriptional repressor 2 (SNAIL2, also known as SLUG, an important epigenetic regulator of *de novo* adipose tissue) mediates the demethylation of H3K9 and stimulates FASN expression and lipogenesis (Liu Y. et al., 2020; Manuel and Haeusler, 2020). Protein arginine methyltransferase 5 (PRMT5) regulates fat cells by promoting the expression of fatty acid synthase (*FASN*; lipid synthesis gene) by methylating sterol regulatory element binding transcription factor 1 (SREBP1) (Jia et al., 2020).

Acetylation and deacetylation can also affect the transcriptional output of metabolic genes in various working models. EZH2-deficient cells show increased H3K27 acetylation, indicating that acetylation and trimethylation of H3K27 have a repulsive effect in regulating WNT expression (Wang et al., 2010). In contrast, EZH2 can also inhibit the expression of apolipoprotein E (APOE) in adipocytes to promote lipoprotein-dependent lipid accumulation (Yiew et al., 2019). Histone deacetylase 11 (HDAC11) inhibits histone acetylation of serine/threonine kinase 11(*STK11*) promoter to inhibit its transcription, thereby, promoting the glycolysis pathway and leading to tumor stemness (Bi et al., 2021). Sirtuin 6 (SIRT6) blocks the expression of hypoxia inducible factor 1 subunit alpha (*HIF1α*) to regulate glucose homeostasis by regulating the deacetylation of H3K9 (Zhong et al., 2010). Sirtuin 4 (SIRT4) inhibits the expression of sirtuin 1 (SIRT1) by inhibiting glutamine metabolism, and SIRT1 promotes the deacetylation

of H4K16 to regulate the stemness of breast cancer cells (Du et al., 2020). Ubiquitously transcribed *TPR* gene on the X chromosome (*UTX*) is enriched in the uncoupling protein 1 (*UCP1*) and PPARG coactivator 1 Alpha (*PGC1α*) promoters and mediates the demethylation of H3K27me3, which interacts with the histone acetyltransferase (HAT) protein CREB binding protein (CBP), leading to the acetylation of H3K27 (H3K27ac). UTX mediates H3K27me3 demethylation and H3K27ac and converts the target gene from a transcriptionally repressed state to a transcriptionally activated state to positively regulate the thermogenesis of brown adipocytes (Zha et al., 2015). Under hypoxia, acetate increases the acetylation of H3K9, H3K27 and H3K56 in the promoter regions of *ACACA* and *FASN* to activate *de novo* lipid synthesis (Gao et al., 2016). E1A binding protein P300/CREB-binding protein (P300/CBP) mediates histone acetylation of H3K18 and H3K27 in hepatocellular carcinoma to regulate the expression of glycolysis-related metabolic enzymes. In addition, the p300 inhibitor B029-2 effectively blocks the metabolic reprogramming of hepatocellular carcinoma (Cai et al., 2021). Histone lactation is also an emerging epigenetic modification of histone lysine residues (Liberti and Locasale, 2020). It depends on tumor protein P53–E1A-binding protein P300 (p53–P300) to promote gene transcription and promote M2-like features in the late phase of M1 macrophage division (Zhang et al., 2019).

Although many studies have focused on the modification of histones, many reports have shown that these histone modification enzymes regulate the modification of non-histone proteins, such as the sirtuin (SIRT) family, the deacetylase histone deacetylase (HDAC) family, the protein arginine n-methyltransferase (PRMT) family (Eom and Kook, 2014; Biggar and Li, 2015; Rodríguez-Paredes and Lyko, 2019; Navas and Carnero, 2021). These proteins, by regulating metabolic enzymes, play an important role in the occurrence and development of tumors.

The SIRT family is an NAD^+-dependent type III deacetylase. Many members of this family have recently been shown to regulate tumor metabolism through acetylation (Navas and Carnero, 2021). Sirtuin 2 (SIRT2) mediates the deacetylation of isocitrate dehydrogenase (NADP (+)) 1 (IDH1), thereby, promoting IDH1 activity and the production of α-ketoglutarate (α-KG), inhibiting liver metastasis of colon cancer and improving prognosis (Wang et al., 2020). SIRT3 inhibits the acetylation of *IDH2* at K413 and promotes isocitrate dehydrogenase (NADP (+)) 2 (IDH2) activity by promoting IDH2 dimerization to inhibit glycolysis (Zou et al., 2017). Sirtuin 7 (SIRT7) in the liver increases fatty acid uptake and triglyceride synthesis and storage. SIRT7 inhibits the degradation of testicular nuclear receptor 4 (TR4) via the ddb1-and cul4-associated factor 1/damage specific DNA binding protein 1/cullin 4b (DCAF1/DDB1/CUL4B) complex (Yoshizawa et al., 2014) (**Figure 1**).

The acetylation of K394 (regulated by the deacetylase P300/CBP-associated factor (PCAF) and histone deacetylase 3 (HDAC3) of enolase 2 (ENO2), a key enzyme of glycolysis) inhibits ENO2 activity and glycolysis (Zheng et al., 2020). Gluconeogenesis is an important metabolic process in liver cell homeostasis; however, it is significantly reduced in liver cancer. The tumor suppressor Nur77 interacts with the rate-limiting enzyme PEPCK1 in gluconeogenesis to increase gluconeogenesis and inhibit the Warburg effect in hepatocellular cancer (HCC) to prevent the development of this disease. However, PEPCK1 after SUMOylation becomes unstable and the interaction weakens, inhibiting gluconeogenesis and promoting glycolysis (Bian et al., 2017). In addition, metastasis associated 1 (MTA1) interacts with the transcription factor myc proto-oncogene protein (MYC) to regulate its transcription on the lactate dehydrogenase A (LDHA; an enzyme that catalyzes the production of lactic acid from pyruvate) via its promoter (Guddeti et al., 2019) and MTA1 upregulates HIF1α under hypoxic conditions by stimulating HIFα transcription (Huang W. et al., 2021). Six homeobox 1 (SIX1) is a key transcription factor that regulates glycolysis-related enzymes (GLUT1 and HK2). SIX1 increases the level of O-GlcNAcylation, and its O-GlcNAcylation enhances the stability of SIX1, coordinates glucose metabolism, and promotes the proliferation of HCC (Chu et al., 2020) (**Figure 1**).

EPIGENETIC REGULATION BY METABOLITES AND METABOLIC ENZYMES

Metabolism is an umbrella term for a variety of different orderly chemical reactions that occur in organisms to maintain life and serve cellular demands, including energy generation and protein biosynthesis, thereby, maintaining biological structure and functions and responding to the environment. Metabolism can be regarded as a process of continuous material and energy exchange. Intermediates produced by metabolism often participate in epigenetic regulation by serving as substrates or cofactors for epigenome-modifying enzymes. During environmental disturbances, cellular metabolism transmits regulatory signals to the genome via epigenetic modifications (Reid et al., 2017; Cavalli and Heard, 2019) (**Table 1**).

Metabolites Serve as Substrates for Epigenetic Modifications

As a carrier of epigenetic information, chromatin plays an important role in regulating gene silencing and activation and permits stable inheritance through reversible DNA and histone modification to maintain the biological functions of proteins (Allis and Jenuwein, 2016). In chromatin, DNA and histones are the substrates that are mainly modified. The most widely studied of all modifications are methylation-demethylation, acetylation-deacetylation, phosphorylation, ubiquitination, and ADP-ribosylation. As discussed earlier, changes in the metabolite pool caused by cancer metabolic reprogramming also affect the state of epigenetic modifications. Consequently, metabolic alterations in cancer have an effect on malignant phenotypes of cancer cells by manipulating epigenetic modifications (**Figure3**).

Glucose Metabolism

Glycolysis involves the breakdown of glucose or glycogen into pyruvate and nicotinamide adenine dinucleotide (NADH),

accompanied by the production of a small amount of ATP. Under anoxic conditions, pyruvate can accept hydrogen from triose phosphate and gets reduced to lactate under the catalytic action of lactate dehydrogenase. Under aerobic conditions, pyruvate can be further oxidized and decomposed to form acetyl-CoA and enter the TCA cycle. Intermediates and metabolites, such as acetyl-CoA, α-KG, succinate, fumarate and citrate, produced from glucose metabolism, have diverse effects on epigenetic modifications.

Acetyl-CoA

Acetyl-CoA is a core metabolite and a substrate for further metabolism and acetylation. A variety of metabolic processes in cells participate in the formation of the acetyl-CoA pool. Glucose metabolism intermediates, such as acetate, citrate, and pyruvate, under the catalytic action of acetyl-CoA synthetase short-chain family member (ACSS), ATP citrate lyase (ACLY), and the pyruvate dehydrogenase complex (PDC), respectively, produce acetyl-CoA. In addition to glucose metabolism, the metabolism of amino acids and fatty acids also generate acetyl-CoA (Zaidi et al., 2012; Nagaraj et al., 2017; Sivanand et al., 2018). Acetylation occurs widely in histones and some non-histone proteins and plays a regulatory role in tumorigenesis and development.

Histone acetylation is regulated by the intracellular acetyl-CoA concentration. Acetyl-CoA serves as an acetyl group donor in acetylation reactions. This process is catalyzed by HATs (Lee et al., 2014). Histone acetylation is determined by the ratio of acetyl-CoA/coenzyme A and is generally deregulated in cancer. In human gliomas and prostate tumors, Histone acetylation marks are significantly regulated by pAkt (Ser473) levels, which modulates the metabolic enzyme ATP-citrate lyase, a key determinant of acetyl-CoA metabolism (Lee et al., 2014). Tumor cell surface GRP78 of activated α2-macroglobulin signals regulate tumor cell proliferation by inducing and activating ACLY and ACSS1 expression to generate acetyl-CoA (Gopal and Pizzo, 2017). Acetyl-CoA also serves as nonhistone acetylation modification substrate to produce effects on the development of tumors. PHD finger-like domain-containing protein 5A (PHF5A) is acetylated at lysine 29 by p300 to promote cancer cell capacity for stress resistance and consequently, contributes to colon carcinogenesis. PHF5A K29 hyperacetylation induces the alternative splicing of *KDM3A* mRNA, which enhances its stability and promotes its expression (Wang H.-Y. et al., 2019; Wang Z. et al., 2019). Under low oxygen states or hypoxia, lysine acetyltransferase and CBP rely on acetate-dependent acetyl CoA synthetase 2 (ACSS2) to acetylate HIF-2, which contributes to cancer cell proliferation, migration, and invasion (Chen et al., 2015).

Nicotinamide Adenine Dinucleotide (NAD^+)

The metabolite NAD^+ serves as a catalytic cofactor for sirtuins, class III HDACs, and is essential for the deacetylation of lysine residues of sirtuins. NAD^+ homeostasis is related to many diseases, including neurodegeneration, diabetes, and cancer. The ratio of NAD^+/NADH regulates sirtuins activity, which is found to be higher in cancer cells than in noncancerous cells (Houtkooper et al., 2012; Moreira et al., 2016; Katsyuba et al., 2020). Under genotoxic stress or nutrient restriction conditions, upregulation of the NAD^+ biosynthetic enzyme NAMPT protects cells against death via the deacetylation activity of SIRT3 and SIRT4 (Yang et al., 2007). In cancer, NAD^+ is intended to reprogram metabolism to enable tumor progression, development, and survival (Hanahan and Weinberg, 2011). As an NAD^+-consuming enzyme, SIRT1 acts as a tumor promoter and is upregulated in several human cancers. In HCC, the inhibition of NAD^+ metabolism causes DNA damage in the early stages of tumorigenesis because of the inactivation of NAD^+-consuming enzymes such as SIRT1. Genomic stability can be improved by NAD^+ supplementation to prevent tumorigenesis (Tummala et al., 2014). Apart from deacetylase activity, sirtuins have multiple NAD^+-dependent catalytic functions, such as desuccinylase, demalonylase, demyristoylase, depalmitoylase, and/or mono-ADP-ribosyltransferase activities. In ovarian cancers, nicotinamide mononucleotide adenylyl transferase 2 (NMNAT2), which mediates the synthesis of NAD^+ is highly upregulated. Knockdown of NMNAT2 significantly decreases NAD^+ in cytoplasm but increases NAD^+ in the nucleus and consequently supports the catalytic activity of the mono (ADP-ribosyl) transferase (MART) PARP-16, resulting in ribosome mono-ADP-ribosylation (MARylation). There is a significant positive correlation between NMNAT-2 and MARylation levels in the samples of ovarian cancer patients, and a high level of MARylation will lead to poor prognosis with respect to progression free survival (Challa et al., 2021). In addition, mitochondrial dysfunction also affects the level of acetylation. Mitochondrial dysfunction causes a decreased NAD^+/NADH ratio and increased reactive oxygen species (ROS), resulting in senescence (Wiley and Campisi, 2016). STAT3 deficiency induces senescence, mitochondrial dysfunction, and a lower NAD^+/NADH ratio (Igelmann et al., 2021). The dynamic changes of NAD^+/NADH ratio also has an effect on nonhistone deacetylation of lysine residues of sirtuins. In breast cancer, NAMPT causes p53 deacetylation and SIRT1 activation by increasing the NAD^+ pool (Behrouzfar et al., 2017).

α-Ketoglutarate, Succinyl-CoA, Fumarate

Intermediates of the TCA cycle, α-KG, succinyl-CoA, fumarate, and citrate, regulate epigenetic modifications through their concentration in the metabolite pool. α-KG is a key cofactor for jumonji-domain-containing histone demethylases (JHDMs), which synergistically catalyze histone demethylation (Klose et al., 2006). In Acute Myeloid Leukemia (AML) stem cells, the α-KG level is restricted by the branched-chain amino acid transaminase 1 (BCAT1), which is overexpressed in leukemia stem cells and transfers α-amino groups from BCAAs to α-KG, resulting in α-KG instability to maintain leukemia stem-cell function (Raffel et al., 2017). The α-KG dehydrogenase complex (α-KGDC) is the hub enzyme of various metabolic pathways involved in mitochondrial function and is a modulator of α-KG (Vatrinet et al., 2017). Succinyl-CoA is a substrate for succinylation (Zhang et al., 2011). Succinylation, as a post-translational modification of proteins, can convert the side chain of cationic lysine residues into anionic ones and then affect

TABLE 1 | Regulation of epigenetic modifications by metabolites and metabolic enzymes.

Metabolites or metabolic enzymes	Epigenetic modifications	Functions in cancer	References
Metabolites			
Acetyl-CoA	DNA, RNA and Protein acetylation	Plays a regulatory role in tumorigenesis and development	Gopal and Pizzo (2017)
NAD^+	Protein dacetylation, desuccinylase, demalonylase	Enables tumor progression, development and survival	Hanahan and Weinberg (2011)
Succinyl CoA	Protein succinylation	Promotes tumor growth and progression	Li et al. (2020b)
2-hydroxyglutarate	Protein hypermethylation	Contributes to poor prognosis	Cavalli and Heard (2019)
Lactate	Protein lactylation	Contributes to tumorigenesis and indicates poor prognosis	Yu et al. (2021)
Palmitic acids	Protein palmitoylation	Participates in tumorigenesis and cell survival	Yao et al. (2019)
Farnesyl group	Protein farnesylation	Contributes to cancer cell growth	Tamanoi et al. (2001)
Geranylgeranyl group	Protein geranylgeranylation	Essential for cell proliferation and migration	Dou et al. (2015), Mi et al. (2015); Lin and Yang (2016)
β-hydroxybutyrate	Protein β-hydroxybutyrylation	Promotes tumor growth	Liu et al. (2019)
Glutamine	Produce a variety of metabolites	Replenishes the TCA cycle for biosynthesis to meet the needs of proliferation	DeBerardinis et al. (2008), Kuhn et al. (2010)
SAM	DNA, RNA and Protein methylation	Enhances subcutaneous tumor growth	Dann et al. (2015)
UDP-GlcNAc	O-GlcNAcylation	Promotes tumorigenesis	Peng et al. (2017)
Metabolic enzymes			
ACLY and ACSS1	Acetylation	Contributes to cancer cell proliferation, migration and invasion	Gopal and Pizzo (2017)
α-KGDC	Protein succinylation	Promotes tumor growth and progression	Wang et al. (2017)
SDH	Hypersuccinylation; Hypermethylation	SDH loss causes drug resistance and promotes angiogenesis	Isaacs et al. (2005); Selak et al. (2005); MacKenzie et al. (2007); Smestad et al. (2018)
FH	Hypersuccinylation; Hypermethylation	FH deficiency results in angiogenesis and EMT	Isaacs et al. (2005); Selak et al. (2005); MacKenzie et al. (2007); Cancer Genome Atlas Research et al. (2016); Sciacovelli et al. (2016)
IDH1 and IDH2	Protein hypermethylation	Contributes to poor prognosis	Figueroa et al. (2010); Lu et al. (2012)
OGT	*O-GlcNAcylation*	Promotes tumorigenesis	Slawson and Hart (2011); de Queiroz et al. (2014); Yang and Qian (2017)

the structure and function of proteins (Smestad et al., 2018). The increase of succinylation has different functions in the progression of a variety of tumors. α-KGDC binds to the promoter regions of lysine acetyltransferase 2A (*KAT2A*, also known as *GCN5*), and KAT2A also acts as a succinyltransferase and succinylates histone H3 on lysine 79, which facilitates histone succinylation and tumor cell proliferation (Wang et al., 2017). Lysine-222 succinylation is increased in gastric cancer, and LDHA lysine-222 succinylation, catalyzed by CPT1A via the stabilization of LDHA, promotes GC invasion and proliferation (Li X. et al., 2020). In pancreatic ductal adenocarcinoma, succinyl-CoA synthetase ADP-forming subunit β (SUCLA2) phosphorylation at S79 leads to dissociation from kidney-type glutaminase (GLS). Thus, the concentration of succinyl coenzyme A is increased and upregulates the succinylation of GLS at site K311. GLS K311 succinylation enhances the oligomerization, activity, and glutaminolysis to improve the concentration of nicotinamide adenine dinucleotide phosphate (NADPH) and glutathione, thereby, counteracting oxidative stress and promoting tumor growth (Tong et al., 2021).

Loss-of-function mutations in the TCA cycle enzymes fumarate hydratase (FH) and succinate dehydrogenase (SDH) have been identified as driver mutations in cancer and mediators of epigenetic reprogramming (Pollard et al., 2003). In an SDH-loss cell model, the accumulation of succinate and succinyl-CoA results in global lysine hypersuccinylation, which modulates genome-wide transcription and hinders DNA repair ability and drug resistance (Smestad et al., 2018). In paraganglioma, SDH deficiency causes succinate accumulation and establishes a hypermethylation phenotype resulting from epigenetic silencing through the inhibition of 2-OG-dependent histone and DNA demethylases. In addition to SDH, inactivating FH mutations can also lead to this phenomenon (Letouze et al., 2013). The hypermethylation phenotype caused by SDH-inactivating mutations also exists in gastrointestinal stromal tumors (Killian et al., 2013). In renal cancer, the inactivating mutations of SDH or FH deficiency results in the subsequent accumulation of succinate or fumarate, respectively, thus, the inhibition of hypoxia-inducible factor (HIF) prolyl hydroxylases (HPH), which protect the stabilization of HIF and promote angiogenesis by increasing α-KG intake can alleviate this situation (Isaacs et al., 2005; Selak et al., 2005; MacKenzie et al., 2007). Moreover, germline mutations of FH cause an aggressive and metastatic form of type 2 papillary renal-cell carcinoma, which is linked to a widespread DNA

hypermethylation pattern (Cancer Genome Atlas Research et al., 2016). Loss of FH triggers epigenetic suppression of miR-200 and epithelial-to-mesenchymal transition by inhibiting Tet-mediated demethylation (Sciacovelli et al., 2016).

2-Hydroxyglutarate

Gain-of-function isocitrate dehydrogenase (IDH) mutations produce an oncometabolite, 2-hydroxyglutarate (2-HG), specifically the D enantiomer (D-2HG), and affect clinical therapy and prognosis (Dang et al., 2010; Cancer Genome Atlas Research et al., 2015). IDH1 and IDH2 mutations result in global hypermethylation and specific hypermethylation in AML by inhibiting demethylases such as KDM4C (Figueroa et al., 2010; Lu et al., 2012). 2-HG-mediated inhibition of the H3K9 demethylase KDM4C is induced during adipocyte differentiation (Lu et al., 2012). In addition to affecting the function of methyltransferase, 2-HG might also perturb the overall architecture of the genome and contribute to cancer and prognosis by affecting methyltransferase activity (Cavalli and Heard, 2019). Interestingly, kidney tumors present an accumulation of the L enantiomer of 2HG (L-2HG), because of the low expression of L-2HG dehydrogenase (L2HGDH). Similar to the function of D-2HG, L-2HG inhibits ten-eleven translocation (TET) as well, which converts 5-methylcytosine (5mC) to 5-hydroxymethylcytosine (5hmC). L-2HG is significantly increased in tumors compared with their expression in normal kidney, and L2HGDH expression inhibits proliferation and colony formation in RCC cells (Shim et al., 2014). In response to hypoxia, L-2HG is selectively produced to increase histone methylation levels, especially histone 3 lysine 9 (H3K9me3) (Intlekofer et al., 2015).

Lactate

Lactate, a metabolic by-product of pyruvate metabolism in cancer cells, is a substrate for histone lactylation. The lactylation of histone lysine residues (Kla) driven by lactate directly stimulates gene transcription from chromatin, linking metabolism and gene regulation. The production of intracellular lactic acid is the main determinant of lactylation modification. Therefore, the balance between glycolysis and mitochondrial metabolism can regulate lactylation modification (Izzo and Wellen, 2019; Zhang et al., 2019; Liberti and Locasale, 2020). Histone lactylation is elevated in ocular melanoma and is indicative of poor prognosis. Histone lactylation also contributes to tumorigenesis by facilitating *YTHDF2* expression, which acts as an m6A reader to recognize and mediate the degradation of m6A-modified Period Circadian Regulator 1 *PER1* and *P53* mRNAs to accelerate tumorigenesis (Yu et al., 2021).

Lipid Metabolism

Lipid signal transduction, especially the phosphatidylinositol 3 kinase (PI3K) pathway, is one of the most common signal transduction systems in cancer cells. Lipophilic groups are widespread modifiers and the following five types of lipids can be covalently attached to proteins: fatty acids, isoprenoids, sterols, phospholipids, and glycosylphosphatidylinositol anchors (Resh, 2013). In addition to

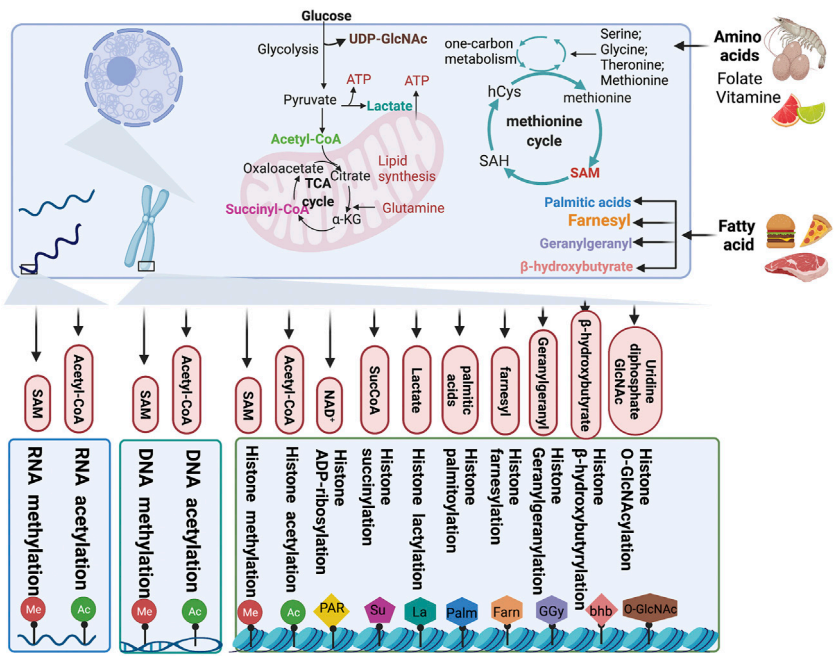

FIGURE 3 | Chromatin modification by metabolites. Metabolites produced from cellular metabolic pathways are used as substrates for DNA, RNA, and chromatin modification. Moreover, the intracellular pools of metabolites can modulate the activity of chromatin-modifying enzymes. TCA, tricarboxylic acid; αKG, α-ketoglutarate; SucCoA, succinyl-CoA; PAR, poly (ADP–ribose); GlcNAc, β-N-acetylglucosamine; SAH, S-adenosylhomocysteine; SAM, S-adenosylmethionine.

providing a substrate for rare acylation, fatty acid metabolism also produces acetyl-COA, as a substrate for energy metabolism and epigenetic modifications (Edmunds et al., 2014).

Palmitic Acid

Palmitoylation is a type of fatty acylation in which long-chain fatty acids (usually 16-carbon-long palmitic acid) are covalently modified to protein cysteine residues by thioester bonds. Palmitoylation plays a vital role in many biological processes (Zhang et al., 2018). In several human cancers, signal transducer and activator of transcription 3 (STAT3) is palmitoylated by zinc finger DHHC-Type palmitoyltransferase 19 (ZDHHC19), a palmitoyl acyltransferase, at the SRC homology 2 (SH2) domain, which promotes its dimerization and transcriptional activation. Under cytokine stimulation, the association between ZDHHC19 and STAT3 is promoted, which directly activates STAT3 by enhancing its palmitoylation with fatty acids (Niu et al., 2019). Palmitoylation mediated by the palmitoyltransferase zinc finger DHHC-Type palmitoyltransferase 3 (ZDHHC3) in the cytoplasmic domain of PD-L1 blocks its ubiquitination to stabilize PD-L1, thereby, suppressing PD-L1 degradation by lysosomes and PD-L1-mediated immune evasion in cancer (Yao et al., 2019). In addition to ZDHHC3, ZDHHC9 has been identified as a palmitoyltransferase for PD-L1 in breast cancer (Yang et al., 2019). In p53-mutant glioma, zinc finger DHHC-Type palmitoyltransferase 5 (ZDHHC5) is transcriptionally upregulated and mediates EZH2 palmitoylation, which affects methyltransferase activity of EZH2 and causing trimethylation of histone 3 at lysine 27 (H3K27me3 level) decreased, and then contributes to malignancy and tumor progression (Chen X. et al., 2017). MC1R palmitoylation mediated by the protein-acyl transferase zinc finger DHHC-Type palmitoyltransferase (ZDHHC13) activates MC1R signaling, which triggers increased pigmentation, ultraviolet-B-induced G1-like cell cycle arrest, and the control of senescence and melanomagenesis. Thus, MC1R palmitoylation protects against melanomagenesis (Chen S. et al., 2017). The c-Met β-chain is palmitoylated at the cysteine site, which enhances its stability and release from the Golgi for transport to the plasma membrane, making it a novel therapeutic target for c-Met-driven cancers (Coleman et al., 2016). Palmitoyltransferases are upregulated in GBM and induce marked palmitoylation of proteins that participate in cell survival control and cell cycle regulation in GBM (Chen et al., 2020).

Farnesyl Group

Protein farnesylation is a lipid PTM essential for the cancer-causing activity of proteins, such as gtpase Ras (Sebti, 2005). Farnesyltransferase inhibitors inhibit cancer cell growth and regulate cell cycle changes (Tamanoi et al., 2001).

Geranylgeranyl Group

GGylation is an essential modification affecting cell survival in many types of cancer. In breast cancer, the Hippo pathway mediates GGylation-dependent cell proliferation and migration (Dou et al., 2015; Mi et al., 2015; Lin and Yang, 2016). In gastric cancer, GGylation promotes proliferation, migration, and invasion of gastric cancer cells through the YAP signaling pathway. Inhibition of GGylation by the mevalonate pathway inhibitor atorvastatin and the geranylgeranyltransferase I inhibitor GGTI-298 can impair cell proliferation and migration (Wei et al., 2020).

β-Hydroxybutyrate

Acetyl CoA produced by lipolysis can not only enter the TCA cycle for oxidation but also result in the synthesis of ketone bodies in the liver. β-Hydroxybutyrate (β-HB) is a ketone body produced by fatty acid hydrolysis. Elevated β-HB levels lead to a new type of histone mar, lysine β-hydroxybutyrylation (Kbhb) (Xie et al., 2016). β-HB is an endogenous and specific inhibitor of class I HDACs (Shimazu et al., 2013). In HCT116 cells, β-HB-mediated p53 Kbhb at K120, K319, and K370 sites results in lower levels of p53 acetylation and consequently, decreased activity of p53, leading to weakened tumor-suppressive function (Liu et al., 2019). MTA2 can transcriptionally regulate BDH1-mediated histone β-HB modification through the R-loop structure in synergy with HDAC2/CHD4 and promote the proliferation of hepatoma stem cells (Zhang et al., 2021).

Amino Acid and One-Carbon Metabolism

One-carbon metabolism plays a crucial role in integrating metabolites from amino acids, glucose, and vitamins and participating in a variety of biosynthetic processes, including the biosynthesis of lipids, nucleotides, and proteins. Hyperactivation of the one-carbon metabolism pathway drives oncogenesis and forges links between cellular epigenetic status and metabolism (Locasale, 2013). Serine metabolism is also an important determinant of S-adenosylmethionine (SAM) levels. Serine is a single carbon donor of the folate cycle and is used for methionine regeneration and SAM synthesis (Locasale, 2013).

Glutamine

Glutamine is the most abundant amino acid in the intracellular metabolite pool. After entering a cell, in the mitochondria, glutamine is transformed into glutamate, the precursor of the TCA cycle intermediate α-KG. Cells rely on glutamine to replenish the TCA cycle. Anaplerosis allows cancer cells to use the TCA cycle for biosynthesis to meet the needs of proliferation, and glutamine as an indispensable nutrient therein (DeBerardinis et al., 2008; Kuhn et al., 2010).

SAM

SAM, a major methyl donor, is synthesized from the methionine cycle and serves as a substrate for methylation to maintain the epigenetic status, including histone methylation catalyzed by histone methyltransferases, DNA methylation mediated by DNA methyltransferase (DNMT), RNA methylation (Teperino et al., 2010; Varier and Timmers, 2011; Anderson et al., 2012; Locasale, 2013), and PTMs such as the methylation of lysine and arginine residues of nonhistone proteins (Chen et al., 2011; Yang and Bedford, 2013). Amino-acid transporters are often required for tumor cell import of essential amino acids. The amino acid transporters LAT1 and LAT4 are significantly upregulated in tumors to facilitate the uptake of methionine for cell proliferation and differentiation in cancer cells (Haase et al., 2007). In lung cancer, cells that highly express LAT1 show increased abundance

of SAM, improving the activity of the histone methyltransferase EZH2 and consequently, increasing H3K27me3 levels to enhance subcutaneous tumor growth (Dann et al., 2015). The levels of SAM are controlled by multiple metabolic pathways and intracellular metabolism, as well as environmental inputs, such as nutrient availability, which also elevate SAM concentrations.

Uridine Diphosphate N-Acetylglucoseamine (UDP-GlcNAc)

The hexosamine biosynthetic pathway produces nucleotide sugars that can be used as substrates for glycosylation. UDP-GlcNAc is a metabolite of the hexosamine biosynthetic pathway, which integrates glucose, amino acid, fatty acid, and nucleotide metabolism. O-GlcNAc transferase (OGT) adds O-GlcNAc groups from the donor substrate UDP-GlcNAc to proteins for O-GlcNAcylation (Yang and Qian, 2017; Li et al., 2018). The methylcytosine dioxygenases TET1, TET2, and TET3 can also become O-GlcNAcylated by OGT through protein–protein interactions (Hardiville and Hart, 2016; Yang and Qian, 2017). Previous studies have shown that O-GlcNAc glycosylation is abnormally upregulated in many tumors and plays an essential role in the proliferation of malignant cancer cells (Slawson and Hart, 2011; de Queiroz et al., 2014; Yang and Qian, 2017). Phosphoglycerate kinase 1 (PGK1) O-GlcNAcylation levels are significantly upregulated in colorectal cancer; O-GlcNAcylation activates PGK1 activity to upregulate the TCA cycle and results in lactate production. The O-GlcNAcylation of PGK1 at T255 increases colon cancer cell proliferation. Furthermore, PGK1 T255 O-GlcNAcylation contributes to tumorigenesis by promoting glycolysis and upregulating the TCA cycle (Nie et al., 2020). Yes-associated protein (YAP) is O-GlcNAcylated at serine 109 by OGT, and the O-GlcNAcylated YAP disrupts the interaction with the upstream kinase large tumor suppressor kinases (LATS) 1. Consequently, O-GlcNAcylation activates the transcriptional activity of YAP by preventing the phosphorylation mediated by LATS1. Thus, glucose-induced YAP O-GlcNAcylation and activation promote tumorigenesis (Peng et al., 2017). OGT O-GlcNAcylates SRPK2 at a nuclear localization signal and triggers SRPK2 binding to importin α, which results in the import of SRPK2 into the nucleus and the phosphorylation of serine/arginine-rich proteins, promoting the splicing of lipogenic pre-mRNAs. O-GlcNAc promotes tumor growth by enhancing the intracellular localization of SRPK2 and regulating *de novo* lipid synthesis in tumor cells at the post-transcriptional level (Tan W. et al., 2021).

Epigenetic Regulation by Gut Microbiota-Mediated Changes in the Metabolic Pool

The biochemical reaction networks of metabolism can be manipulated by several factors including diet, nutrition, gut microbiota, and chemical exposure. These environmental factors regulate chromatin methylation and acetylation by modifying the intracellular pool of metabolites. There is increasing evidence that the gut microbiome is closely related to the risk, development, and progression of cancer. Metabolites produced by gut microbiota influence host metabolism via the modulation of metabolites, including the lipopolysaccharide endotoxin, bile acids, trimethylamine N-oxide, and short-chain fatty acids (SCFAs) (Schroeder and Backhed, 2016). Microbiota-derived metabolites represent stimuli that regulate epigenetic modifying enzymes and are involved in intestinal inflammation and carcinogenesis (**Figure 4**).

Bile Acids

Bile acids are produced in the liver and metabolized by enzymes produced by intestinal bacteria. Intestinal bacteria are very important for maintaining a healthy intestinal microbiota, balancing lipid and glucose metabolism, insulin sensitivity, and natural immunity. Bile acids have a wide range of gene-mediating effects, including bile acid metabolism, glucose and lipid metabolism, energy expenditure, intestinal motility and bacterial growth, inflammation, liver regeneration, and hepatocarcinogenesis (de Aguiar Vallim et al., 2013; Wahlstrom et al., 2016). The epigenetic regulation of cofactors senses changes in bile acid metabolism, regulates PTMs of histones, and causes chromatin remodeling to regulate gene transcription and maintain the balance of bile acids. Bile acids activate Farnesoid X receptor (FXR) and change the interaction between FXR and transcriptional cofactors, resulting in altered PTMs of FXR and histones to effectively modulate the expression of target genes (Kemper, 2011). An abnormal concentration of bile acids is believed to promote colorectal cancer (Fearon and Vogelstein, 1990).

Butyrate

Butyrate is a microbiota-derived SCFA that has been confirmed to be an inhibitor of HDAC *in vitro* and *in vivo*. Exposure to butyrate causes the accumulation of acetylated histones (Candido et al., 1978; Wu S.-e. et al., 2020). In intestinal epithelia, histone H3K18 results in abundant crotonylation modification, especially in small intestine crypts and the colon; the class I histone deacetylases HDAC1, HDAC2, and HDAC3 can catalyze histone decrotonylation. As an HDAC inhibitor, gut microbiota-derived butyrate affects histone decrotonylation and is linked to gene regulation (Fellows et al., 2018). Clostridial clusters, *Anaerostipes*, and *Eubacterium* cause histone acylation modification through butyrate, thus, improving intestinal development and the immune balance (Wu J. et al., 2020). Butyrate increases histone methylation in the promoter region of *NF-κB1*, downregulating its expression (Liu et al., 2016; Yang and Yu, 2018).

Phytate

Phytate digestion and inositol phosphates produced by phytate metabolism induce HDAC activity in intestinal epithelial cells. Dietary phytate metabolism mediated by microbiota-dependent mechanisms improves recovery from intestinal damage. Moreover, microbiota-derived phytate digestion is significantly decreased in the intestinal contents of ulcerative colitis patients relative to that in inflammatory bowel disease patients. In addition, phytate-treated mice exhibit improved survival

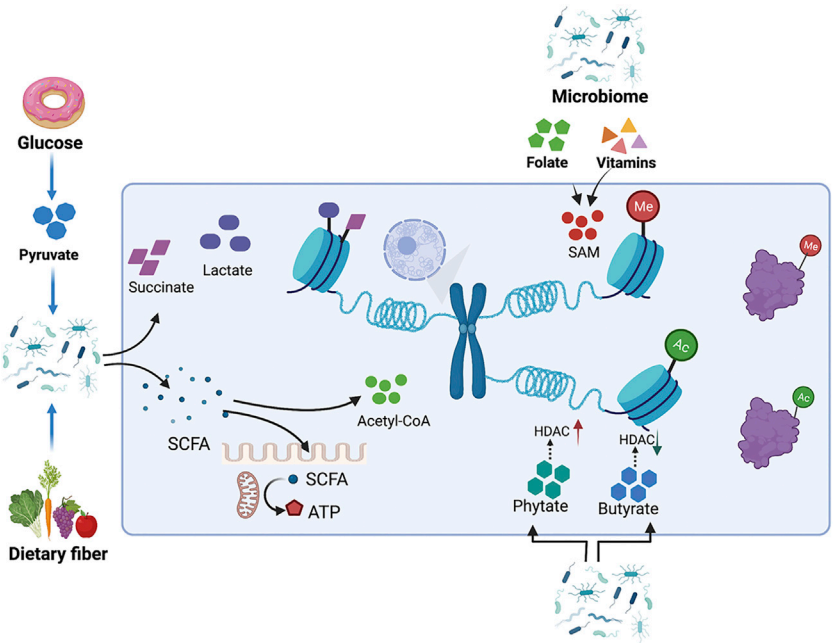

FIGURE 4 | Metabolites produced by the intestinal microbiota influence host metabolism by modulating the metabolite pool. The gut microbiome regulates histone methylation and acetylation by modulating the intracellular pools of metabolites, such as SAM and acetyl-CoA. Metabolites from the gut microbiome, like phytate and butyrate, also cause changes in histone acetylation by affecting the enzyme activity of HDAC. Pyruvate can either be catabolized into succinate, lactate, or acetyl-CoA. SCFAs can provide acyl-CoA as a donor for histone acylation, while also directly inhibiting the activity of HDACs.

compared to vehicle-treated mice with dextran sodium sulfate-induced colitis (Wu S.-e. et al., 2020).

The human gut microbiota also catabolizes the conversion of pyruvate into succinate, lactate, or acetyl-CoA to further generate energy (Oliphant and Allen-Vercoe, 2019); this process is accompanied by changes in the metabolite pool. Dietary fiber, including non-starch polysaccharides, resistant starch, and oligosaccharides, are very rich and diverse in our diet and facilitate gut microbial and consequently beneficial metabolite diversity (Riva et al., 2019). The gut microbiota break cellulose into SCFAs as a metabolic intermediate; SCFAs inhibit HDACs and serve as energy substrates. SCFAs also affect histone crotonylation and acetylation levels (Kasubuchi et al., 2015; Koh et al., 2016; Zhao et al., 2016; Fellows et al., 2018; Sabari et al., 2018). SCFAs induce epithelial anti-inflammatory IL-10 receptor alpha subunit (*IL-10RA*) mRNA and antimicrobial peptides by inhibiting HDACs (Campbell et al., 2012; Zheng et al., 2017). *Lactobacillus* and *Bifidobacterium* synthesize folate to increase DNA methylation and m6A mRNA in the intestine to ensure normal development of the intestine (Wu J. et al., 2020). In addition to folate, vitamins B2, B6, and B1 from intestinal microbiota can also lead to the synthesis of SAM as a methyl group donor to methylate DNA, RNA, and histones (Wu J. et al., 2020). Microbial metabolism also provides TCA cycle intermediates, such as α-KG, succinate, and fumarate, which serve as substitutes for epigenetic modifications (Wu J. et al., 2020). The gut microbiota also indirectly regulates the activity of epigenetically modified genes by regulating gene expression. According to a recent report, enterotoxigenic *Bacteroides fragilis* stimulation promotes PHF5A-mediated RNA alternative splicing of *KAT2A* via the downregulation of miR-149–3p, promoting intestinal inflammation and malignancy. This process depends on METTL14-mediated m6A methylation (Cao et al., 2021).

CLINICAL TRIALS

Recent studies have shown that tumor metabolism and epigenetic regulation are closely linked and important for maintaining cell growth and regulating cancer metastasis. Therefore, inhibitors of rate-limiting enzymes in key metabolic pathways used by cancer cells are actively being investigated (Erez and DeBerardinis, 2015). Inhibiting such key enzymes has potential for cancer treatment, but they would also have an effect on normal cells; therefore, inhibiting rate-limiting enzymes of metabolic pathways is often toxic (Rodríguez-Enríquez et al., 2014).

In 2017, the FDA approved the first cancer metabolism drug enasidenib, an IDH2 inhibitor, for which the main indication is relapsed and refractory AML (Mullard, 2017). IDH2 is the key rate-limiting enzyme in the TCA cycle and catalyzes the conversion of isocitrate to α-KG. Cancer cells show a functional mutation in *IDH2* (Yao et al., 2021). Enasidenib, an IDH2 inhibitor, is undergoing phase 1b/2 clinical trials in multiple countries. The current research results show that compared to that with azacitidine treatment alone, the

TABLE 2 | Clinical trials of IDH, HDAC, SAM cycle and others.

Category	Drugs	NCT number	Title	Condition	Status	Phase
IDH inhibitors	Enasidenib	NCT02677922	A Safety and Efficacy Study of Oral AG-120 Plus Subcutaneous Azacitidine and Oral AG-221 Plus Subcutaneous Azacitidine in Subjects with Newly Diagnosed Acute Myeloid Leukemia (AML)	Active, not recruiting	Leukemia, Myeloid, Acute	Phase 1/ Phase 2
	Enasidenib	NCT01915498	Phase 1/2 Study of Enasidenib (AG-221) in Adults with Advanced Hematologic Malignancies with an Isocitrate Dehydrogenase Isoform 2 (IDH2) Mutation	Active, not recruiting	Hematologic Neoplasms	Phase 1/ Phase 2
	AG881	NCT02481154	Study of Orally Administered AG-881 in Patients with Advanced Solid Tumors, Including Gliomas, with an IDH1 and/or IDH2 Mutation	Active, not recruiting	Glioma	Phase 1
HDAC inhibitors	Romidepsin	NCT00426764	A Trial of Romidepsin for Progressive or Relapsed Peripheral T-cell Lymphoma	Completed	Peripheral T-cell Lymphoma	Phase 2
	Romidepsin	NCT00106431	A Single Agent Phase II Study of Romidepsin (Depsipeptide, FK228) in the Treatment of Cutaneous T-cell Lymphoma (CTCL)	Completed	Cutaneous T-cell Lymphoma	Phase 2
	Vorinostat	NCT01266031	Phase I/II Adaptive Randomized Trial of Bevacizumab Versus Bevacizumab Plus Vorinostat in Adults with Recurrent Glioblastoma	Completed	Recurrent Glioblastoma	Phase 1/ Phase 2
SAM cycle inhibitors	Ethylornithine	NCT01483144	Trial of Eflornithine Plus Sulindac in Patients with Familial Adenomatous Polyposis (FAP)	Completed	Familial Adenomatous Polyposis	Phase 3
	Ethylornithine	NCT00033371	Celecoxib With or Without Eflornithine in Preventing Colorectal Cancer in Patients with Familial Adenomatous Polyposis	Completed	Colorectal Cancer, Familial Adenomatous Polyposis	Phase 2
	Ethylornithine	NCT01059071	Safety Study for Refractory or Relapsed Neuroblastoma with DFMO Alone and in Combination with Etoposide	Completed	Neuroblastoma	Phase 1
Others	Physical activity and dietary change	NCT00811824	Effects of Physical Activity and Dietary Change in Minority Breast Cancer Survivors	Completed	Breast Cancer	Phase 2
	Vitamin C	NCT02877277	Epigenetics, Vitamin C and Abnormal Hematopoiesis - Pilot Study	Completed	Myelodysplastic Syndrome, Acute Myeloid Leukemia	Not Applicable

overall drug response rate of enasidenib combined with azacitidine is improved, and the combination has good drug tolerance, thereby, improving the prognosis of patients with IDH2 AML (NCT02677922) (**Table 2**) (DiNardo et al., 2021). In addition, clinical studies have also shown that the drug responsiveness and tolerability are good in patients with IDH2-mutant myelodysplastic syndrome (NCT01915498) (**Table 2**) (Stein et al., 2020).

IDH mutations result in the conversion of α-KG to 2-hydroxyglutarate, which competitively inhibits α-KG-dependent enzymes as the two small molecules, 2-HG and α-KG, are similar in structure (Pirozzi and Yan, 2021). These enzymes include histone demethylases (Jumonji domain-containing protein/lysine demethylase family, JMJD/KDM family) and DNA/RNA methylation-modification-related enzymes (Tet family) (White et al., 2020; Waitkus and Yan, 2021). This causes epigenetic dysregulation and cell differentiation arrest, a key factor in tumor cell proliferation after mutations (White et al., 2020). In addition, in 2018, the mutant IDH1 inhibitor ivosidenib was used to treat relapsed or refractory AML. The IDH1 and IDH2 dual inhibitor AG-881 has also been shown to cross the blood-brain barrier. Recently, the results of a phase I clinical trial (NCT02481154) (**Table 2**) of AG-881 for low-grade gliomas demonstrated that it is safe and can shrink tumors in many non-enhanced glioma patients (Mellinghoff et al., 2021).

Histone deacetylase is a key target for tumor therapy. Therefore, many studies have explored compound inhibitors of histone deacetylase to find new anti-tumor strategies. HDAC inhibitor romidepsin (also called FK228) affects iron metabolism, mediates increased intracellular iron accumulation, decreases the expression of export-type ferroprotein, and increases reactive oxygen species (ROS) production, thereby, mediating iron death. This result has a guiding role for the combined treatment strategy using HDAC inhibitors and iron-targeted chemotherapy (Oliveira et al., 2021). The results of the second-phase clinical study show that FK228 can effectively control T-cell lymphoma, with safety and reliability (NCT00426764, NCT00106431) (**Table 2**) (Foss et al., 2014; Foss et al., 2016). The HDAC inhibitor BAS-2 inhibits HDAC6, affects the *ENO1* gene and *LDHA* related to glucose metabolism, and ultimately affects glycolysis in breast cancer (Dowling et al., 2021). Studies have shown that 1A12 can inhibit the acetylation level of histone H3, and it can also affect the glucose metabolism level in preclinical test subjects (Chan et al., 2014). HDAC inhibitors (panobinostat, vorinostat, and romidepsin) reduce glycolysis in a c-MYC-dependent manner, triggering the metabolic reprogramming of glioblastoma (Nguyen et al., 2020). Currently, the HDAC inhibitors vorinostat, romidepsin, and panobinostat have been approved by the FDA for the treatment of clinical lymphoma and multiple myeloma (Cappellacci et al., 2020). However, current research

shows that vorinostat does not work well in glioma (NCT01266031) (**Table 2**) (Puduvalli et al., 2020).

SAM is a methyl donor for DNA and histone methylation (Haws et al., 2020). Metformin has been found to affect the epigenetic metabolic regulation of tumors in recent years. It reduces SAH (a potent inhibitor of all SAM-dependent methylation reactions) and promotes the accumulation of SAM. This leads to an increase in the overall DNA methylation level of metastatic cancer cells (Cuyàs et al., 2018). One study found that ethylornithine has chemopreventative and therapeutic effects on colon cancer, reducing folate-dependent metabolites such as SAM, the thymidine pool, and other intermediate products of related pathways (Witherspoon et al., 2013). On one hand, ethylornithine has an important effect in delaying the progression of familial polyposis (NCT01483144, NCT00033371) (**Table 2**) (Burke et al., 2020), while on the other, studies have shown that it has the potential to prevent the recurrence of high-risk neuroblastoma (NCT01059071) (**Table 2**) (Saulnier Sholler et al., 2015).

In addition to drugs, lifestyle changes can affect epigenetic changes. A healthy lifestyle is associated with high levels of DNA methylation, whereas overall tissue and blood DNA hypomethylation are associated with an increased risk of cancer. The results of clinical trials (NCT00811824) (**Table 2**) show that lifestyle changes (diet and weight loss) can effectively change DNA methylation (Delgado-Cruzata et al., 2015). A high-fat diet can induce DNA methylation changes in the whole genome, which was found to involve metabolic disease-related genes and cancer-related genes (Jacobsen et al., 2012). Previous studies have shown that patients with malignant hematological tumors often lack vitamin C. Vitamin C can enhance the activity of TET protein in tumor cells, increase the level of 5hmC, decrease the level of 5mC in cells, and increase sensitivity to anticancer drugs. A clinical study in Denmark (NCT02877277) (**Table 2**) showed that vitamin C supplementation in patients with myeloma increases the 5hmC/5mC ratio of mononuclear myeloid cells, enhancing the clinical efficacy of DNMT inhibitors (Gillberg et al., 2019).

CONCLUSION AND PERSPECTIVES

In this review, we elucidated how the crosstalk between epigenetic regulation and metabolic reprogramming changes during the process of tumorigenesis and development. Metabolic reprogramming in tumors changes the epigenetic landscape of tumor cells. Metabolites can serve as substrates for epigenetic modifications, and some metabolic enzymes can also affect chromatin modification. Therefore, we suggest that the metabolism-epigenome axis must be considered while approaching cancer biomarker studies.

Additionally, the role of metabolism synergy and epigenetic modifications in the physiology and pathology of the gut microbiota and corresponding effect on the host is proposed to be valuable and have prospective applications in cancer research. On the one hand, the metabolism of the gut microbiota and the products provide substrates for epigenetic modifications, whereas on the other hand, they directly affect the activity of epigenetic modification enzymes, resulting in epigenetic modification changes. Lifestyle-related factors, such as exercise and nutrition, are very important factors that affect human health through the gut microbiota, and the emerging role of gut microbial diversity in epigenetics emphasizes the link between lifestyle choices and cancer.

Although great progress has been made in understanding the epigenetic–metabolism axis in the past few decades, the internal mechanism of this heritable change in tumorigenesis and development and its application to tumor prevention and treatment remain elusive. Therefore, the mechanisms of metabolically-regulated epigenomic landscape responses in tumorigenesis and development need to be investigated, and further potential therapeutic applications in this regard must be studied.

AUTHOR CONTRIBUTIONS

YW and WH designed the content of the review with input from all the co-authors. MH and JZ wrote the original review draft. YW and WH revised the article with feedback from all the co-authors. All authors approved this work for publication. Figures in this work were created with BioRender.com.

FUNDING

This work was supported by the National Natural Science Foundation of China (41,931,291, 42,125,707, 81,902,960), the Non-profit Central Research Institute Fund of Chinese Academy of Medical Sciences (2019PT310027), the State Key Laboratory of Molecular Oncology (SKLMO-2021–21), Cooperative Project of Beijing-Tianjin-Hebei Regional Basic Research (19JCZDJC65700(Z)).

REFERENCES

Ahringer, J., and Gasser, S. M. (2018). Repressive Chromatin in *Caenorhabditis elegans*: Establishment, Composition, and Function. *Genetics* 208 (2), 491–511. doi:10.1534/genetics.117.300386

Alam, H., Tang, M., Maitituoheti, M., Dhar, S. S., Kumar, M., Han, C. Y., et al. (2020). KMT2D Deficiency Impairs Super-enhancers to Confer a Glycolytic Vulnerability in Lung Cancer. *Cancer Cell* 37 (4), 599–617. e597. doi:10.1016/j.ccell.2020.03.005

Allis, C. D., and Jenuwein, T. (2016). The Molecular Hallmarks of Epigenetic Control. *Nat. Rev. Genet.* 17 (8), 487–500. doi:10.1038/nrg.2016.59

Anderson, O. S., Sant, K. E., and Dolinoy, D. C. (2012). Nutrition and Epigenetics: an Interplay of Dietary Methyl Donors, One-Carbon Metabolism and DNA Methylation. *J. Nutr. Biochem.* 23 (8), 853–859. doi:10.1016/j.jnutbio.2012.03.003

Bates, S. E. (2020). Epigenetic Therapies for Cancer. *N. Engl. J. Med.* 383 (7), 650–663. doi:10.1056/NEJMra1805035

Behrouzfar, K., Alaee, M., Nourbakhsh, M., Gholinejad, Z., and Golestani, A. (2017). Extracellular NAMPT/visfatin Causes P53 Deacetylation via NAD Production and SIRT1 Activation in Breast Cancer Cells. *Cell Biochem Funct* 35 (6), 327–333. doi:10.1002/cbf.3279

Bi, L., Ren, Y., Feng, M., Meng, P., Wang, Q., Chen, W., et al. (2021). HDAC11 Regulates Glycolysis through the LKB1/AMPK Signaling Pathway to Maintain Hepatocellular Carcinoma Stemness. *Cancer Res.* 81 (8), 2015–2028. doi:10.1158/0008-5472.Can-20-3044

Bian, X.-l., Chen, H.-z., Yang, P.-b., Li, Y.-p., Zhang, F.-n., Zhang, J.-y., et al. (2017). Nur77 Suppresses Hepatocellular Carcinoma via Switching Glucose Metabolism toward Gluconeogenesis through Attenuating Phosphoenolpyruvate Carboxykinase Sumoylation. *Nat. Commun.* 8, 14420. doi:10.1038/ncomms14420

Biggar, K. K., and Li, S. S.-C. (2015). Non-histone Protein Methylation as a Regulator of Cellular Signalling and Function. *Nat. Rev. Mol. Cel Biol* 16 (1), 5–17. doi:10.1038/nrm3915

Blakey, C. A., and Litt, M. D. (2015). "Histone Modifications-Models and Mechanisms," in *Epigenetic Gene Expression and Regulation*. Editors S. Huang, M. D. Litt, and C. A. Blakey (Oxford: Academic Press), 21–42. doi:10.1016/b978-0-12-799958-6.00002-0

Boroughs, L. K., and DeBerardinis, R. J. (2015). Metabolic Pathways Promoting Cancer Cell Survival and Growth. *Nat. Cel Biol* 17 (4), 351–359. doi:10.1038/ncb3124

Bray, F., Laversanne, M., Weiderpass, E., and Soerjomataram, I. (2021). The Ever-Increasing Importance of Cancer as a Leading Cause of Premature Death Worldwide. *Cancer* 127 (16), 3029–3030. doi:10.1002/cncr.33587

Burke, C. A., Dekker, E., Lynch, P., Samadder, N. J., Balaguer, F., Hüneburg, R., et al. (2020). Eflornithine Plus Sulindac for Prevention of Progression in Familial Adenomatous Polyposis. *N. Engl. J. Med.* 383 (11), 1028–1039. doi:10.1056/NEJMoa1916063

Cai, L.-Y., Chen, S.-J., Xiao, S.-H., Sun, Q.-J., Ding, C.-H., Zheng, B.-N., et al. (2021). Targeting P300/CBP Attenuates Hepatocellular Carcinoma Progression through Epigenetic Regulation of Metabolism. *Cancer Res.* 81 (4), 860–872. doi:10.1158/0008-5472.Can-20-1323

Campbell, Y., Fantacone, M. L., and Gombart, A. F. (2012). Regulation of Antimicrobial Peptide Gene Expression by Nutrients and By-Products of Microbial Metabolism. *Eur. J. Nutr.* 51 (8), 899–907. doi:10.1007/s00394-012-0415-4

Cancer Genome Atlas Research, N., Brat, D. J., Verhaak, R. G., Aldape, K. D., Yung, W. K., Salama, S. R., et al. (2015). Comprehensive, Integrative Genomic Analysis of Diffuse Lower-Grade Gliomas. *N. Engl. J. Med.* 372 (26), 2481–2498. doi:10.1056/NEJMoa1402121

Cancer Genome Atlas Research, N., Linehan, W. M., Spellman, P. T., Ricketts, C. J., Creighton, C. J., Fei, S. S., et al. (2016). Comprehensive Molecular Characterization of Papillary Renal-Cell Carcinoma. *N. Engl. J. Med.* 374 (2), 135–145. doi:10.1056/NEJMoa1505917

Candido, E., Reeves, R., and Davie, J. R. (1978). Sodium Butyrate Inhibits Histone Deacetylation in Cultured Cells. *Cell* 14 (1), 105–113. doi:10.1016/0092-8674(78)90305-7

Cao, Y., Wang, Z., Yan, Y., Ji, L., He, J., Xuan, B., et al. (2021). Enterotoxigenic Bacteroides Fragilis Promotes Intestinal Inflammation and Malignancy by Inhibiting Exosome-Packaged miR-149-3p. *Gastroenterology* 161, 1552–1566. doi:10.1053/j.gastro.2021.08.003

Cappellacci, L., Perinelli, D. R., Maggi, F., Grifantini, M., and Petrelli, R. (2020). Recent Progress in Histone Deacetylase Inhibitors as Anticancer Agents. *Curr. Med. Chem.* 27 (15), 2449–2493. doi:10.2174/0929867325666181016163110

Carter, B., and Zhao, K. (2021). The Epigenetic Basis of Cellular Heterogeneity. *Nat. Rev. Genet.* 22 (4), 235–250. doi:10.1038/s41576-020-00300-0

Cavalli, G., and Heard, E. (2019). Advances in Epigenetics Link Genetics to the Environment and Disease. *Nature* 571 (7766), 489–499. doi:10.1038/s41586-019-1411-0

Challa, S., Khulpateea, B. R., Nandu, T., Camacho, C. V., Ryu, K. W., Chen, H., et al. (2021). Ribosome ADP-Ribosylation Inhibits Translation and Maintains Proteostasis in Cancers. *Cell* 184 (17), 4531–4546. e4526. doi:10.1016/j.cell.2021.07.005

Chan, C. T., Qi, J., Smith, W., Paranol, R., Mazitschek, R., West, N., et al. (2014). Syntheses and Discovery of a Novel Class of Cinnamic Hydroxamates as Histone Deacetylase Inhibitors by Multimodality Molecular Imaging in Living Subjects. *Cancer Res.* 74 (24), 7475–7486. doi:10.1158/0008-5472.Can-14-0197

Chen, C., Nott, T. J., Jin, J., and Pawson, T. (2011). Deciphering Arginine Methylation: Tudor Tells the Tale. *Nat. Rev. Mol. Cel Biol* 12 (10), 629–642. doi:10.1038/nrm3185

Chen, F., Chen, J., Yang, L., Liu, J., Zhang, X., Zhang, Y., et al. (2019). Extracellular Vesicle-Packaged HIF-1α-Stabilizing lncRNA from Tumour-Associated Macrophages Regulates Aerobic Glycolysis of Breast Cancer Cells. *Nat. Cel Biol* 21 (4), 498–510. doi:10.1038/s41556-019-0299-0

Chen, R., Xu, M., Nagati, J. S., Hogg, R. T., Das, A., Gerard, R. D., et al. (2015). The acetate/ACSS2 Switch Regulates HIF-2 Stress Signaling in the Tumor Cell Microenvironment. *PLoS One* 10 (2), e0116515. doi:10.1371/journal.pone.0116515

Chen, S., Zhu, B., Yin, C., Liu, W., Han, C., Chen, B., et al. (2017a). Palmitoylation-dependent Activation of MC1R Prevents Melanomagenesis. *Nature* 549 (7672), 399–403. doi:10.1038/nature23887

Chen, X., Li, H., Fan, X., Zhao, C., Ye, K., Zhao, Z., et al. (2020). Protein Palmitoylation Regulates Cell Survival by Modulating XBP1 Activity in Glioblastoma Multiforme. *Mol. Ther. - Oncolytics* 17, 518–530. doi:10.1016/j.omto.2020.05.007

Chen, X., Ma, H., Wang, Z., Zhang, S., Yang, H., and Fang, Z. (2017b). EZH2 Palmitoylation Mediated by ZDHHC5 in P53-Mutant Glioma Drives Malignant Development and Progression. *Cancer Res.* 77 (18), 4998–5010. doi:10.1158/0008-5472.CAN-17-1139

Chu, Y., Jiang, M., Wu, N., Xu, B., Li, W., Liu, H., et al. (2020). O-GlcNAcylation of SIX1 Enhances its Stability and Promotes Hepatocellular Carcinoma Proliferation. *Theranostics* 10 (21), 9830–9842. doi:10.7150/thno.45161

Coleman, D. T., Gray, A. L., Kridel, S. J., and Cardelli, J. A. (2016). Palmitoylation Regulates the Intracellular Trafficking and Stability of C-Met. *Oncotarget* 7 (22), 32664–32677. doi:10.18632/oncotarget.8706

Cuyàs, E., Fernández-Arroyo, S., Verdura, S., García, R. Á.-F., Stursa, J., Werner, L., et al. (2018). Metformin Regulates Global DNA Methylation via Mitochondrial One-Carbon Metabolism. *Oncogene* 37 (7), 963–970. doi:10.1038/onc.2017.367

Dai, Z., Ramesh, V., and Locasale, J. W. (2020). The Evolving Metabolic Landscape of Chromatin Biology and Epigenetics. *Nat. Rev. Genet.* 21 (12), 737–753. doi:10.1038/s41576-020-0270-8

Dang, L., White, D. W., Gross, S., Bennett, B. D., Bittinger, M. A., Driggers, E. M., et al. (2010). Cancer-associated IDH1 Mutations Produce 2-hydroxyglutarate. *Nature* 465 (7300), 966. doi:10.1038/nature09132

Dann, S. G., Ryskin, M., Barsotti, A. M., Golas, J., Shi, C., Miranda, M., et al. (2015). Reciprocal Regulation of Amino Acid Import and Epigenetic State through Lat1 and EZH 2. *EMBO J.* 34 (13), 1773–1785. doi:10.15252/embj.201488166

de Queiroz, R. M., Carvalho, Ã. r., and Dias, W. B. (2014). O-GlcNAcylation: The Sweet Side of the Cancer. *Front. Oncol.* 4, 132. doi:10.3389/fonc.2014.00132

DeBerardinis, R. J., Lum, J. J., Hatzivassiliou, G., and Thompson, C. B. (2008). The Biology of Cancer: Metabolic Reprogramming Fuels Cell Growth and Proliferation. *Cel Metab.* 7 (1), 11–20. doi:10.1016/j.cmet.2007.10.002

Delgado-Cruzata, L., Zhang, W., McDonald, J. A., Tsai, W. Y., Valdovinos, C., Falci, L., et al. (2015). Dietary Modifications, Weight Loss, and Changes in Metabolic Markers Affect Global DNA Methylation in Hispanic, African American, and Afro-Caribbean Breast Cancer Survivors. *J. Nutr.* 145 (4), 783–790. doi:10.3945/jn.114.202853

de Aguiar Vallim, T. Q., Tarling, E. J., and Edwards, P. A. (2013). Pleiotropic Roles of Bile Acids in Metabolism. *Cel Metab.* 17 (5), 657–669. doi:10.1016/j.cmet.2013.03.013

DiNardo, C. D., Schuh, A. C., Stein, E. M., Montesinos, P., Wei, A. H., de Botton, S., et al. (2021). Enasidenib Plus Azacitidine versus Azacitidine Alone in Patients with Newly Diagnosed, Mutant-IDH2 Acute Myeloid Leukaemia (AG221-AML-005): a Single-Arm, Phase 1b and Randomised, Phase 2 Trial. *Lancet Oncol.* 22 (11), 1597–1608. doi:10.1016/s1470-2045(21)00494-0

Dou, X., Wei, J., Sun, A., Shao, G., Childress, C., Yang, W., et al. (2015). PBK/TOPK Mediates Geranylgeranylation Signaling for Breast Cancer Cell Proliferation. *Cancer Cel Int* 15, 27. doi:10.1186/s12935-015-0178-0

Dowling, C. M., Hollinshead, K. E. R., Di Grande, A., Pritchard, J., Zhang, H., Dillon, E. T., et al. (2021). Multiple Screening Approaches Reveal HDAC6 as a Novel Regulator of Glycolytic Metabolism in Triple-Negative Breast Cancer. *Sci. Adv.* 7 (3), eabc4897. doi:10.1126/sciadv.abc4897

Du, L., Liu, X., Ren, Y., Li, J., Li, P., Jiao, Q., et al. (2020). Loss of SIRT4 Promotes the Self-Renewal of Breast Cancer Stem Cells. *Theranostics* 10 (21), 9458–9476. doi:10.7150/thno.44688

Edmunds, L. R., Sharma, L., Kang, A., Lu, J., Vockley, J., Basu, S., et al. (2014). c-Myc Programs Fatty Acid Metabolism and Dictates Acetyl-CoA Abundance and Fate. *J. Biol. Chem.* 289 (36), 25382–25392. doi:10.1074/jbc.M114.580662

Eom, G. H., and Kook, H. (2014). Posttranslational Modifications of Histone Deacetylases: Implications for Cardiovascular Diseases. *Pharmacol. Ther.* 143 (2), 168–180. doi:10.1016/j.pharmthera.2014.02.012

Erez, A., and DeBerardinis, R. J. (2015). Metabolic Dysregulation in Monogenic Disorders and Cancer - Finding Method in Madness. *Nat. Rev. Cancer* 15 (7), 440–448. doi:10.1038/nrc3949

Esteller, M. (2008). Epigenetics in Cancer. *N. Engl. J. Med.* 358 (11), 1148–1159. doi:10.1056/NEJMra072067

Fang, R., Chen, X., Zhang, S., Shi, H., Ye, Y., Shi, H., et al. (2021). EGFR/SRC/ERK-stabilized YTHDF2 Promotes Cholesterol Dysregulation and Invasive Growth of Glioblastoma. *Nat. Commun.* 12 (1), 177. doi:10.1038/s41467-020-20379-7

Fearon, E. R., and Vogelstein, B. (1990). A Genetic Model for Colorectal Tumorigenesis. *Cell* 61 (5), 759–767. doi:10.1016/0092-8674(90)90186-i

Fellows, R., Denizot, J., Stellato, C., Cuomo, A., Jain, P., Stoyanova, E., et al. (2018). Microbiota Derived Short Chain Fatty Acids Promote Histone Crotonylation in the colon through Histone Deacetylases. *Nat. Commun.* 9 (1), 105. doi:10.1038/s41467-017-02651-5

Figueroa, M. E., Abdel-Wahab, O., Lu, C., Ward, P. S., Patel, J., Shih, A., et al. (2010). Leukemic IDH1 and IDH2 Mutations Result in a Hypermethylation Phenotype, Disrupt TET2 Function, and Impair Hematopoietic Differentiation. *Cancer Cell* 18 (6), 553–567. doi:10.1016/j.ccr.2010.11.015

Foss, F., Coiffier, B., Horwitz, S., Pro, B., Prince, H. M., Sokol, L., et al. (2014). Tolerability to Romidepsin in Patients with Relapsed/refractory T-Cell Lymphoma. *Biomark Res.* 2, 16. doi:10.1186/2050-7771-2-16

Foss, F., Horwitz, S., Pro, B., Prince, H. M., Sokol, L., Balser, B., et al. (2016). Romidepsin for the Treatment of Relapsed/refractory Peripheral T Cell Lymphoma: Prolonged Stable Disease Provides Clinical Benefits for Patients in the Pivotal Trial. *J. Hematol. Oncol.* 9, 22. doi:10.1186/s13045-016-0243-8

Gao, X., Lin, S.-H., Ren, F., Li, J.-T., Chen, J.-J., Yao, C.-B., et al. (2016). Acetate Functions as an Epigenetic Metabolite to Promote Lipid Synthesis under Hypoxia. *Nat. Commun.* 7, 11960. doi:10.1038/ncomms11960

Gillberg, L., Ørskov, A. D., Nasif, A., Ohtani, H., Madaj, Z., Hansen, J. W., et al. (2019). Oral Vitamin C Supplementation to Patients with Myeloid Cancer on Azacitidine Treatment: Normalization of Plasma Vitamin C Induces Epigenetic Changes. *Clin. Epigenet* 11 (1), 143. doi:10.1186/s13148-019-0739-5

Gopal, U., and Pizzo, S. V. (2017). Cell Surface GRP78 Promotes Tumor Cell Histone Acetylation through Metabolic Reprogramming: a Mechanism Which Modulates the Warburg Effect. *Oncotarget* 8 (64), 107947–107963. doi:10.18632/oncotarget.22431

Guddeti, R. K., Bali, P., Karyala, P., and Pakala, S. B. (2019). MTA1 Coregulator Regulates LDHA Expression and Function in Breast Cancer. *Biochem. Biophysical Res. Commun.* 520 (1), 54–59. doi:10.1016/j.bbrc.2019.09.078

Guo, S., Zhang, Y., Wang, S., Yang, T., Ma, B., Li, X., et al. (2021). LncRNA PCA3 Promotes Antimony-Induced Lipid Metabolic Disorder in Prostate Cancer by Targeting MIR-132-3 P/SREBP1 Signaling. *Toxicol. Lett.* 348, 50–58. doi:10.1016/j.toxlet.2021.05.006

Haase, C., Bergmann, R., Fuechtner, F., Hoepping, A., and Pietzsch, J. (2007). L-type Amino Acid Transporters LAT1 and LAT4 in Cancer: Uptake of 3-O-Methyl-6- 18F-Fluoro-L-Dopa in Human Adenocarcinoma and Squamous Cell Carcinoma *In Vitro* and *In Vivo*. *J. Nucl. Med.* 48 (12), 2063–2071. doi:10.2967/jnumed.107.043620

Han, X., Wang, M., Zhao, Y.-L., Yang, Y., and Yang, Y.-G. (2021). RNA Methylations in Human Cancers. *Semin. Cancer Biol.* 75, 97–115. doi:10.1016/j.semcancer.2020.11.007

Hanahan, D., and Weinberg, R. A. (2011). Hallmarks of Cancer: the Next Generation. *Cell* 144 (5), 646–674. doi:10.1016/j.cell.2011.02.013

Hardivillé, S., and Hart, G. W. (2016). Nutrient Regulation of Gene Expression by O-GlcNAcylation of Chromatin. *Curr. Opin. Chem. Biol.* 33, 88–94. doi:10.1016/j.cbpa.2016.06.005

Haws, S. A., Yu, D., Ye, C., Wille, C. K., Nguyen, L. C., Krautkramer, K. A., et al. (2020). Methyl-Metabolite Depletion Elicits Adaptive Responses to Support Heterochromatin Stability and Epigenetic Persistence. *Mol. Cel* 78 (2), 210–223. e218. doi:10.1016/j.molcel.2020.03.004

Hirata, H., Sugimachi, K., Komatsu, H., Ueda, M., Masuda, T., Uchi, R., et al. (2016). Decreased Expression of Fructose-1,6-Bisphosphatase Associates with Glucose Metabolism and Tumor Progression in Hepatocellular Carcinoma. *Cancer Res.* 76 (11), 3265–3276. doi:10.1158/0008-5472.Can-15-2601

Hou, Y., Liu, W., Yi, X., Yang, Y., Su, D., Huang, W., et al. (2020). PHF20L1 as a H3K27me2 Reader Coordinates with Transcriptional Repressors to Promote Breast Tumorigenesis. *Sci. Adv.* 6 (16), eaaz0356. doi:10.1126/sciadv.aaz0356

Houtkooper, R. H., Pirinen, E., and Auwerx, J. (2012). Sirtuins as Regulators of Metabolism and Healthspan. *Nat. Rev. Mol. Cel Biol* 13 (4), 225–238. doi:10.1038/nrm3293

Huang, H., Sabari, B. R., Garcia, B. A., Allis, C. D., and Zhao, Y. (2014). SnapShot: Histone Modifications. *Cell* 159 (2), 458, 2014 . e451. doi:10.1016/j.cell.2014.09.037

Huang, W., Zhang, J., Huo, M., Gao, J., Yang, T., Yin, X., et al. (2021a). CUL4B Promotes Breast Carcinogenesis by Coordinating with Transcriptional Repressor Complexes in Response to Hypoxia Signaling Pathway. *Adv. Sci.* 8 (10), 2001515. doi:10.1002/advs.202001515

Huang, X., Hou, Y., Weng, X., Pang, W., Hou, L., Liang, Y., et al. (2021b). Diethyldithiocarbamate-copper Complex (CuET) Inhibits Colorectal Cancer Progression via miR-16-5p and 15b-5p/ALDH1A3/PKM2 axis-mediated Aerobic Glycolysis Pathway. *Oncogenesis* 10 (1), 4. doi:10.1038/s41389-020-00295-7

Igelmann, S., Lessard, F., Uchenunu, O., Bouchard, J., Fernandez-Ruiz, A., Rowell, M.-C., et al. (2021). A Hydride Transfer Complex Reprograms NAD Metabolism and Bypasses Senescence. *Mol. Cel* 81 (18), 3848–3865. e3819. doi:10.1016/j.molcel.2021.08.028

Intlekofer, A. M., Dematteo, R. G., Venneti, S., Finley, L. W. S., Lu, C., Judkins, A. R., et al. (2015). Hypoxia Induces Production of L-2-Hydroxyglutarate. *Cel Metab.* 22 (2), 304–311. doi:10.1016/j.cmet.2015.06.023

Isaacs, J. S., Jung, Y. J., Mole, D. R., Lee, S., Torres-Cabala, C., Chung, Y.-L., et al. (2005). HIF Overexpression Correlates with Biallelic Loss of Fumarate Hydratase in Renal Cancer: Novel Role of Fumarate in Regulation of HIF Stability. *Cancer Cell* 8 (2), 143–153. doi:10.1016/j.ccr.2005.06.017

Izzo, L. T., and Wellen, K. E. (2019). Histone Lactylation Links Metabolism and Gene Regulation. *Nature* 574 (7779), 492–493. doi:10.1038/d41586-019-03122-1

Jacobsen, S. C., Brøns, C., Bork-Jensen, J., Ribel-Madsen, R., Yang, B., Lara, E., et al. (2012). Effects of Short-Term High-Fat Overfeeding on Genome-wide DNA Methylation in the Skeletal Muscle of Healthy Young Men. *Diabetologia* 55 (12), 3341–3349. doi:10.1007/s00125-012-2717-8

Jia, Z., Yue, F., Chen, X., Narayanan, N., Qiu, J., Syed, S. A., et al. (2020). Protein Arginine Methyltransferase PRMT5 Regulates Fatty Acid Metabolism and Lipid Droplet Biogenesis in White Adipose Tissues. *Adv. Sci.* 7 (23), 2002602. doi:10.1002/advs.202002602

Kasubuchi, M., Hasegawa, S., Hiramatsu, T., Ichimura, A., and Kimura, I. (2015). Dietary Gut Microbial Metabolites, Short-Chain Fatty Acids, and Host Metabolic Regulation. *Nutrients* 7 (4), 2839–2849. doi:10.3390/nu7042839

Katsyuba, E., Romani, M., Hofer, D., and Auwerx, J. (2020). NAD+ Homeostasis in Health and Disease. *Nat. Metab.* 2 (1), 9–31. doi:10.1038/s42255-019-0161-5

Kemper, J. K. (2011). Regulation of FXR Transcriptional Activity in Health and Disease: Emerging Roles of FXR Cofactors and post-translational Modifications. *Biochim. Biophys. Acta (Bba) - Mol. Basis Dis.* 1812 (8), 842–850. doi:10.1016/j.bbadis.2010.11.011

Killian, J. K., Kim, S. Y., Miettinen, M., Smith, C., Merino, M., Tsokos, M., et al. (2013). Succinate Dehydrogenase Mutation Underlies Global Epigenomic Divergence in Gastrointestinal Stromal Tumor. *Cancer Discov.* 3 (6), 648–657. doi:10.1158/2159-8290.CD-13-0092

Kim, J., Park, M. W., Park, Y. J., Ahn, J. W., Sim, J. M., Kim, S., et al. (2021). miR-542-3p Contributes to the HK2-Mediated High Glycolytic Phenotype in Human Glioma Cells. *Genes* 12 (5), 633. doi:10.3390/genes12050633

Klose, R. J., Kallin, E. M., and Zhang, Y. (2006). JmjC-domain-containing Proteins and Histone Demethylation. *Nat. Rev. Genet.* 7 (9), 715–727. doi:10.1038/nrg1945

Koh, A., De Vadder, F., Kovatcheva-Datchary, P., and Bäckhed, F. (2016). From Dietary Fiber to Host Physiology: Short-Chain Fatty Acids as Key Bacterial Metabolites. *Cell* 165 (6), 1332–1345. doi:10.1016/j.cell.2016.05.041

Kuhn, K. S., Muscaritoli, M., Wischmeyer, P., and Stehle, P. (2010). Glutamine as Indispensable Nutrient in Oncology: Experimental and Clinical Evidence. *Eur. J. Nutr.* 49 (4), 197–210. doi:10.1007/s00394-009-0082-2

Le, X., Mu, J., Peng, W., Tang, J., Xiang, Q., Tian, S., et al. (2020). DNA Methylation Downregulated ZDHHC1 Suppresses Tumor Growth by Altering Cellular Metabolism and Inducing Oxidative/ER Stress-Mediated Apoptosis and Pyroptosis. *Theranostics* 10 (21), 9495–9511. doi:10.7150/thno.45631

Lee, J. V., Carrer, A., Shah, S., Snyder, N. W., Wei, S., Venneti, S., et al. (2014). Akt-dependent Metabolic Reprogramming Regulates Tumor Cell Histone Acetylation. *Cel Metab.* 20 (2), 306–319. doi:10.1016/j.cmet.2014.06.004

Letouzé, E., Martinelli, C., Loriot, C., Burnichon, N., Abermil, N., Ottolenghi, C., et al. (2013). SDH Mutations Establish a Hypermethylator Phenotype in Paraganglioma. *Cancer Cell* 23 (6), 739–752. doi:10.1016/j.ccr.2013.04.018

Li, H., Wang, J., Xu, H., Xing, R., Pan, Y., Li, W., et al. (2013). Decreased Fructose-1,6-Bisphosphatase-2 Expression Promotes Glycolysis and Growth in Gastric Cancer Cells. *Mol. Cancer* 12 (1), 110. doi:10.1186/1476-4598-12-110

Li, L., Yang, L., Fan, Z., Xue, W., Shen, Z., Yuan, Y., et al. (2020a). Hypoxia-induced GBE1 Expression Promotes Tumor Progression through Metabolic Reprogramming in Lung Adenocarcinoma. *Sig Transduct Target. Ther.* 5 (1), 54. doi:10.1038/s41392-020-0152-8

Li, X., Egervari, G., Wang, Y., Berger, S. L., and Lu, Z. (2018). Regulation of Chromatin and Gene Expression by Metabolic Enzymes and Metabolites. *Nat. Rev. Mol. Cel Biol* 19 (9), 563–578. doi:10.1038/s41580-018-0029-7

Li, X., Zhang, C., Zhao, T., Su, Z., Li, M., Hu, J., et al. (2020b). Lysine-222 Succinylation Reduces Lysosomal Degradation of Lactate Dehydrogenase a and Is Increased in Gastric Cancer. *J. Exp. Clin. Cancer Res.* 39 (1), 172. doi:10.1186/s13046-020-01681-0

Liberti, M. V., and Locasale, J. W. (2020). Histone Lactylation: A New Role for Glucose Metabolism. *Trends Biochem. Sci.* 45 (3), 179–182. doi:10.1016/j.tibs.2019.12.004

Lin, Q., and Yang, W. (2016). The Hippo-YAP/TAZ Pathway Mediates Geranylgeranylation Signaling in Breast Cancer Progression. *Mol. Cell Oncol.* 3 (3), e969638. doi:10.4161/23723548.2014.969638

Liu, H.-E., Shi, H.-H., and Luo, X.-J. (2020a). Upregulated Long Noncoding RNA UCA1 Enhances Warburg Effect via miR-203/HK2 Axis in Esophagal Cancer. *J. Oncol.* 2020, 1–11. doi:10.1155/2020/8847687

Liu, K., Li, F., Sun, Q., Lin, N., Han, H., You, K., et al. (2019). p53 β-hydroxybutyrylation Attenuates P53 Activity. *Cell Death Dis* 10 (3), 243. doi:10.1038/s41419-019-1463-y

Liu, Y., Lin, H., Jiang, L., Shang, Q., Yin, L., Lin, J. D., et al. (2020b). Hepatic Slug Epigenetically Promotes Liver Lipogenesis, Fatty Liver Disease, and Type 2 Diabetes. *J. Clin. Invest.* 130 (6), 2992–3004. doi:10.1172/jci128073

Liu, Y., Upadhyaya, B., Fardin-Kia, A. R., Juenemann, R. M., and Dey, M. (2016). Dietary Resistant Starch Type 4-derived Butyrate Attenuates Nuclear Factor-Kappa-B1 through Modulation of Histone H3 Trimethylation at Lysine 27. *Food Funct.* 7 (9), 3772–3781. doi:10.1039/c6fo00856a

Locasale, J. W. (2013). Serine, glycine and One-Carbon Units: Cancer Metabolism in Full circle. *Nat. Rev. Cancer* 13 (8), 572–583. doi:10.1038/nrc3557

Lopez-Serra, P., Marcilla, M., Villanueva, A., Ramos-Fernandez, A., Palau, A., Leal, L., et al. (2014). A DERL3-Associated Defect in the Degradation of SLC2A1 Mediates the Warburg Effect. *Nat. Commun.* 5, 3608. doi:10.1038/ncomms4608

Lu, C., Ward, P. S., Kapoor, G. S., Rohle, D., Turcan, S., Abdel-Wahab, O., et al. (2012). IDH Mutation Impairs Histone Demethylation and Results in a Block to Cell Differentiation. *Nature* 483 (7390), 474–478. doi:10.1038/nature10860

Luo, Y., Xie, C., Brocker, C. N., Fan, J., Wu, X., Feng, L., et al. (2019). Intestinal PPARα Protects against Colon Carcinogenesis via Regulation of Methyltransferases DNMT1 and PRMT6. *Gastroenterology* 157 (3), 744–759. e744. doi:10.1053/j.gastro.2019.05.057

MacKenzie, E. D., Selak, M. A., Tennant, D. A., Payne, L. J., Crosby, S., Frederiksen, C. M., et al. (2007). Cell-Permeating α-Ketoglutarate Derivatives Alleviate Pseudohypoxia in Succinate Dehydrogenase-Deficient Cells. *Mol. Cel Biol* 27 (9), 3282–3289. doi:10.1128/MCB.01927-06

Manuel, C. R., and Haeusler, R. A. (2020). Insulin-stimulated Lipogenesis Gets an Epigenetic Makeover. *J. Clin. Invest.* 130 (6), 2809–2810. doi:10.1172/jci137050

Mellinghoff, I. K., Penas-Prado, M., Peters, K. B., Burris, H. A., 3rd, Maher, E. A., Janku, F., et al. (2021). Vorasidenib, a Dual Inhibitor of Mutant IDH1/2, in Recurrent or Progressive Glioma; Results of a First-In-Human Phase I Trial. *Clin. Cancer Res.* 27 (16), 4491–4499. doi:10.1158/1078-0432.Ccr-21-0611

Mi, W., Lin, Q., Childress, C., Sudol, M., Robishaw, J., Berlot, C. H., et al. (2015). Geranylgeranylation Signals to the Hippo Pathway for Breast Cancer Cell Proliferation and Migration. *Oncogene* 34 (24), 3095–3106. doi:10.1038/onc.2014.251

Moreira, J., Hamraz, M., Abolhassani, M., Bigan, E., Pérès, S., Paulevé, L., et al. (2016). The Redox Status of Cancer Cells Supports Mechanisms behind the Warburg Effect. *Metabolites* 6 (4), 33. doi:10.3390/metabo6040033

Mullard, A. (2017). FDA Approves First-In-Class Cancer Metabolism Drug. *Nat. Rev. Drug Discov.* 16 (9), 593. doi:10.1038/nrd.2017.174

Nagaraj, R., Sharpley, M. S., Chi, F., Braas, D., Zhou, Y., Kim, R., et al. (2017). Nuclear Localization of Mitochondrial TCA Cycle Enzymes as a Critical Step in Mammalian Zygotic Genome Activation. *Cell* 168 (1-2), 210–223. e211. doi:10.1016/j.cell.2016.12.026

Navas, L. E., and Carnero, A. (2021). NAD+ Metabolism, Stemness, the Immune Response, and Cancer. *Sig Transduct Target. Ther.* 6 (1), 2. doi:10.1038/s41392-020-00354-w

Nguyen, T. T. T., Zhang, Y., Shang, E., Shu, C., Torrini, C., Zhao, J., et al. (2020). HDAC Inhibitors Elicit Metabolic Reprogramming by Targeting Super-enhancers in Glioblastoma Models. *J. Clin. Invest.* 130 (7), 3699–3716. doi:10.1172/jci129049

Ni, Y., Yang, Y., Ran, J., Zhang, L., Yao, M., Liu, Z., et al. (2020). miR-15a-5p Inhibits Metastasis and Lipid Metabolism by Suppressing Histone Acetylation in Lung Cancer. *Free Radic. Biol. Med.* 161, 150–162. doi:10.1016/j.freeradbiomed.2020.10.009

Nie, H., Ju, H., Fan, J., Shi, X., Cheng, Y., Cang, X., et al. (2020). O-GlcNAcylation of PGK1 Coordinates Glycolysis and TCA Cycle to Promote Tumor Growth. *Nat. Commun.* 11 (1), 36. doi:10.1038/s41467-019-13601-8

Nishiyama, A., and Nakanishi, M. (2021). Navigating the DNA Methylation Landscape of Cancer. *Trends Genet.* 37, 1012–1027. doi:10.1016/j.tig.2021.05.002

Niu, J., Sun, Y., Chen, B., Zheng, B., Jarugumilli, G. K., Walker, S. R., et al. (2019). Fatty Acids and Cancer-Amplified ZDHHC19 Promote STAT3 Activation through S-Palmitoylation. *Nature* 573 (7772), 139–143. doi:10.1038/s41586-019-1511-x

Oliphant, K., and Allen-Vercoe, E. (2019). Macronutrient Metabolism by the Human Gut Microbiome: Major Fermentation By-Products and Their Impact on Host Health. *Microbiome* 7 (1), 91. doi:10.1186/s40168-019-0704-8

Oliveira, T., Hermann, E., Lin, D., Chowanadisai, W., Hull, E., and Montgomery, M. (2021). HDAC Inhibition Induces EMT and Alterations in Cellular Iron Homeostasis to Augment Ferroptosis Sensitivity in SW13 Cells. *Redox Biol.* 47, 102149. doi:10.1016/j.redox.2021.102149

Pavlova, N. N., and Thompson, C. B. (2016). The Emerging Hallmarks of Cancer Metabolism. *Cel Metab.* 23 (1), 27–47. doi:10.1016/j.cmet.2015.12.006

Peng, C., Zhu, Y., Zhang, W., Liao, Q., Chen, Y., Zhao, X., et al. (2017). Regulation of the Hippo-YAP Pathway by Glucose Sensor O-GlcNAcylation. *Mol. Cel* 68 (3), 591–604. e595. doi:10.1016/j.molcel.2017.10.010

Pirozzi, C. J., and Yan, H. (2021). The Implications of IDH Mutations for Cancer Development and Therapy. *Nat. Rev. Clin. Oncol.* 18, 645–661. doi:10.1038/s41571-021-00521-0

Pollard, P., Wortham, N., and Tomlinson, I. (2003). The TCA Cycle and Tumorigenesis: the Examples of Fumarate Hydratase and Succinate Dehydrogenase. *Ann. Med.* 35 (8), 634–635. doi:10.1080/07853890310018458

Puduvalli, V. K., Wu, J., Yuan, Y., Armstrong, T. S., Vera, E., Wu, J., et al. (2020). A Bayesian Adaptive Randomized Phase II Multicenter Trial of Bevacizumab with or without Vorinostat in Adults with Recurrent Glioblastoma. *Neuro Oncol.* 22 (10), 1505–1515. doi:10.1093/neuonc/noaa062

Raffel, S., Falcone, M., Kneisel, N., Hansson, J., Wang, W., Lutz, C., et al. (2017). BCAT1 Restricts αKG Levels in AML Stem Cells Leading to IDHmut-like DNA Hypermethylation. *Nature* 551 (7680), 384–388. doi:10.1038/nature24294

Rausch, C., Zhang, P., Casas-Delucchi, C. S., Daiß, J. L., Engel, C., Coster, G., et al. (2021). Cytosine Base Modifications Regulate DNA Duplex Stability and Metabolism. *Nucleic Acids Res.*, gkab509. doi:10.1093/nar/gkab509

Reid, M. A., Dai, Z., and Locasale, J. W. (2017). The Impact of Cellular Metabolism on Chromatin Dynamics and Epigenetics. *Nat. Cel Biol* 19 (11), 1298–1306. doi:10.1038/ncb3629

Resh, M. D. (2013). Covalent Lipid Modifications of Proteins. *Curr. Biol.* 23 (10), R431–R435. doi:10.1016/j.cub.2013.04.024

Riva, A., Kuzyk, O., Forsberg, E., Siuzdak, G., Pfann, C., Herbold, C., et al. (2019). A Fiber-Deprived Diet Disturbs the fine-scale Spatial Architecture of the Murine colon Microbiome. *Nat. Commun.* 10 (1), 4366. doi:10.1038/s41467-019-12413-0

Rodríguez-Enríquez, S., Gallardo-Pérez, J. C., Hernández-Reséndiz, I., Marín-Hernández, A., Pacheco-Velázquez, S. C., López-Ramírez, S. Y., et al. (2014). Canonical and New Generation Anticancer Drugs Also Target Energy Metabolism. *Arch. Toxicol.* 88 (7), 1327–1350. doi:10.1007/s00204-014-1246-2

Rodríguez-Paredes, M., and Lyko, F. (2019). The Importance of Non-histone Protein Methylation in Cancer Therapy. *Nat. Rev. Mol. Cel Biol* 20 (10), 569–570. doi:10.1038/s41580-019-0147-x

Sabari, B. R., Tang, Z., Huang, H., Yong-Gonzalez, V., Molina, H., Kong, H. E., et al. (2018). Intracellular Crotonyl-CoA Stimulates Transcription through P300-Catalyzed Histone Crotonylation. *Mol. Cel* 69 (3), 533. doi:10.1016/j.molcel.2018.01.013

Saghafinia, S., Mina, M., Riggi, N., Hanahan, D., and Ciriello, G. (2018). Pan-Cancer Landscape of Aberrant DNA Methylation across Human Tumors. *Cel Rep.* 25 (4), 1066–1080. e1068. doi:10.1016/j.celrep.2018.09.082

Sakamoto, A., Hino, S., Nagaoka, K., Anan, K., Takase, R., Matsumori, H., et al. (2015). Lysine Demethylase LSD1 Coordinates Glycolytic and Mitochondrial Metabolism in Hepatocellular Carcinoma Cells. *Cancer Res.* 75 (7), 1445–1456. doi:10.1158/0008-5472.Can-14-1560

Saulnier Sholler, G. L., Gerner, E. W., Bergendahl, G., MacArthur, R. B., VanderWerff, A., Ashikaga, T., et al. (2015). A Phase I Trial of DFMO Targeting Polyamine Addiction in Patients with Relapsed/Refractory Neuroblastoma. *PLoS One* 10 (5), e0127246. doi:10.1371/journal.pone.0127246

Schroeder, B. O., and Bäckhed, F. (2016). Signals from the Gut Microbiota to Distant Organs in Physiology and Disease. *Nat. Med.* 22 (10), 1079–1089. doi:10.1038/nm.4185

Sciacovelli, M., Gonçalves, E., Johnson, T. I., Zecchini, V. R., da Costa, A. S. H., Gaude, E., et al. (2016). Fumarate Is an Epigenetic Modifier that Elicits Epithelial-To-Mesenchymal Transition. *Nature* 537 (7621), 544–547. doi:10.1038/nature19353

Sebti, S. M. (2005). Protein Farnesylation: Implications for normal Physiology, Malignant Transformation, and Cancer Therapy. *Cancer Cell* 7 (4), 297–300. doi:10.1016/j.ccr.2005.04.005

Selak, M. A., Armour, S. M., MacKenzie, E. D., Boulahbel, H., Watson, D. G., Mansfield, K. D., et al. (2005). Succinate Links TCA Cycle Dysfunction to Oncogenesis by Inhibiting HIF-α Prolyl Hydroxylase. *Cancer Cell* 7 (1), 77–85. doi:10.1016/j.ccr.2004.11.022

Sellitto, A., Pecoraro, G., Giurato, G., Nassa, G., Rizzo, F., Saggese, P., et al. (2021). Regulation of Metabolic Reprogramming by Long Non-coding RNAs in Cancer. *Cancers* 13 (14), 3485. doi:10.3390/cancers13143485

Semenza, G. L. (2003). Targeting HIF-1 for Cancer Therapy. *Nat. Rev. Cancer* 3 (10), 721–732. doi:10.1038/nrc1187

Shen, C., Xuan, B., Yan, T., Ma, Y., Xu, P., Tian, X., et al. (2020). m6A-dependent Glycolysis Enhances Colorectal Cancer Progression. *Mol. Cancer* 19 (1), 72. doi:10.1186/s12943-020-01190-w

Shim, E.-H., Livi, C. B., Rakheja, D., Tan, J., Benson, D., Parekh, V., et al. (2014). L-2-Hydroxyglutarate: an Epigenetic Modifier and Putative Oncometabolite in Renal Cancer. *Cancer Discov.* 4 (11), 1290–1298. doi:10.1158/2159-8290.CD-13-0696

Shimazu, T., Hirschey, M. D., Newman, J., He, W., Shirakawa, K., Le Moan, N., et al. (2013). Suppression of Oxidative Stress by β-Hydroxybutyrate, an Endogenous Histone Deacetylase Inhibitor. *Science* 339 (6116), 211–214. doi:10.1126/science.1227166

Simithy, J., Sidoli, S., Yuan, Z.-F., Coradin, M., Bhanu, N. V., Marchione, D. M., et al. (2017). Characterization of Histone Acylations Links Chromatin Modifications with Metabolism. *Nat. Commun.* 8 (1), 1141. doi:10.1038/s41467-017-01384-9

Singh, S., Narayanan, S. P., Biswas, K., Gupta, A., Ahuja, N., Yadav, S., et al. (2017). Intragenic DNA Methylation and BORIS-Mediated Cancer-specific Splicing Contribute to the Warburg Effect. *Proc. Natl. Acad. Sci. USA* 114 (43), 11440–11445. doi:10.1073/pnas.1708447114

Sivanand, S., Viney, I., and Wellen, K. E. (2018). Spatiotemporal Control of Acetyl-CoA Metabolism in Chromatin Regulation. *Trends Biochem. Sci.* 43 (1), 61–74. doi:10.1016/j.tibs.2017.11.004

Slawson, C., and Hart, G. W. (2011). O-GlcNAc Signalling: Implications for Cancer Cell Biology. *Nat. Rev. Cancer* 11 (9), 678–684. doi:10.1038/nrc3114

Smestad, J., Erber, L., Chen, Y., and Maher, L. J., 3rd (2018). Chromatin Succinylation Correlates with Active Gene Expression and Is Perturbed by Defective TCA Cycle Metabolism. *iScience* 2, 63–75. doi:10.1016/j.isci.2018.03.012

Som, P., Atkins, H. L., Bandoypadhyay, D., Fowler, J. S., MacGregor, R. R., Matsui, K., et al. (1980). A Fluorinated Glucose Analog, 2-Fluoro-2-Deoxy-D-Glucose (F-18): Nontoxic Tracer for Rapid Tumor Detection. *J. Nucl. Med.* 21 (7), 670–675.

Stein, E. M., Fathi, A. T., DiNardo, C. D., Pollyea, D. A., Roboz, G. J., Collins, R., et al. (2020). Enasidenib in Patients with Mutant IDH2 Myelodysplastic Syndromes: a Phase 1 Subgroup Analysis of the Multicentre, AG221-C-001 Trial. *Lancet Haematol.* 7 (4), e309–e319. doi:10.1016/s2352-3026(19)30284-4

Sun, L., Zhang, H., and Gao, P. (2021). Metabolic Reprogramming and Epigenetic Modifications on the Path to Cancer. *Protein Cell.* doi:10.1007/s13238-021-00846-7

Sung, H., Ferlay, J., Siegel, R. L., Laversanne, M., Soerjomataram, I., Jemal, A., et al. (2021). Global Cancer Statistics 2020: GLOBOCAN Estimates of Incidence and Mortality Worldwide for 36 Cancers in 185 Countries. *CA A. Cancer J. Clin.* 71 (3), 209–249. doi:10.3322/caac.21660

Suva, M. L., Riggi, N., and Bernstein, B. E. (2013). Epigenetic Reprogramming in Cancer. *Science* 339 (6127), 1567–1570. doi:10.1126/science.1230184

Tamanoi, F., Gau, C.-L., Jiang, C., Edamatsu, H., and Kato-Stankiewicz, J. (2001). Protein Farnesylation in Mammalian Cells: Effects of Farnesyltransferase Inhibitors on Cancer Cells. *Cmls, Cel. Mol. Life Sci.* 58 (11), 1636–1649. doi:10.1007/PL00000802

Tan, M., Luo, H., Lee, S., Jin, F., Yang, J. S., Montellier, E., et al. (2011). Identification of 67 Histone marks and Histone Lysine Crotonylation as a New Type of Histone Modification. *Cell* 146 (6), 1016–1028. doi:10.1016/j.cell.2011.08.008

Tan, W., Jiang, P., Zhang, W., Hu, Z., Lin, S., Chen, L., et al. (2021a). Posttranscriptional Regulation of De Novo Lipogenesis by Glucose-Induced O-GlcNAcylation. *Mol. Cel* 81 (9), 1890–1904. doi:10.1016/j.molcel.2021.02.009

Tan, Y. T., Lin, J. F., Li, T., Li, J. J., Xu, R. H., and Ju, H. Q. (2021b). LncRNA-mediated Posttranslational Modifications and Reprogramming of Energy Metabolism in Cancer. *Cancer Commun.* 41 (2), 109–120. doi:10.1002/cac2.12108

Teperino, R., Schoonjans, K., and Auwerx, J. (2010). Histone Methyl Transferases and Demethylases; Can They Link Metabolism and Transcription? *Cel Metab.* 12 (4), 321–327. doi:10.1016/j.cmet.2010.09.004

Tessarz, P., and Kouzarides, T. (2014). Histone Core Modifications Regulating Nucleosome Structure and Dynamics. *Nat. Rev. Mol. Cel Biol* 15 (11), 703–708. doi:10.1038/nrm3890

Thakur, C., and Chen, F. (2019). Connections between Metabolism and Epigenetics in Cancers. *Semin. Cancer Biol.* 57, 52–58. doi:10.1016/j.semcancer.2019.06.006

Tong, Y., Guo, D., Lin, S.-H., Liang, J., Yang, D., Ma, C., et al. (2021). SUCLA2-coupled Regulation of GLS Succinylation and Activity Counteracts Oxidative Stress in Tumor Cells. *Mol. Cel* 81 (11), 2303–2316. e2308. doi:10.1016/j.molcel.2021.04.002

Tummala, K. S., Gomes, A. L., Yilmaz, M., Graña, O., Bakiri, L., Ruppen, I., et al. (2014). Inhibition of De Novo NAD + Synthesis by Oncogenic URI Causes Liver Tumorigenesis through DNA Damage. *Cancer Cell* 26 (6), 826–839. doi:10.1016/j.ccell.2014.10.002

Uddin, M. B., Wang, Z., and Yang, C. (2021). The m6A RNA Methylation Regulates Oncogenic Signaling Pathways Driving Cell Malignant Transformation and Carcinogenesis. *Mol. Cancer* 20 (1), 61. doi:10.1186/s12943-021-01356-0

Vander Heiden, M. G., Cantley, L. C., and Thompson, C. B. (2009). Understanding the Warburg Effect: the Metabolic Requirements of Cell Proliferation. *Science* 324 (5930), 1029–1033. doi:10.1126/science.1160809

Varier, R. A., and Timmers, H. T. M. (2011). Histone Lysine Methylation and Demethylation Pathways in Cancer. *Biochim. Biophys. Acta (Bba) - Rev. Cancer* 1815 (1), 75–89. doi:10.1016/j.bbcan.2010.10.002

Vatrinet, R., Leone, G., De Luise, M., Girolimetti, G., Vidone, M., Gasparre, G., et al. (2017). The α-ketoglutarate Dehydrogenase Complex in Cancer Metabolic Plasticity. *Cancer Metab.* 5, 3. doi:10.1186/s40170-017-0165-0

Wagner, G. R., Bhatt, D. P., O'Connell, T. M., Thompson, J. W., Dubois, L. G., Backos, D. S., et al. (2017). A Class of Reactive Acyl-CoA Species Reveals the Non-enzymatic Origins of Protein Acylation. *Cel Metab.* 25 (4), 823–837. doi:10.1016/j.cmet.2017.03.006

Wahlström, A., Sayin, S. I., Marschall, H.-U., and Bäckhed, F. (2016). Intestinal Crosstalk between Bile Acids and Microbiota and its Impact on Host Metabolism. *Cel Metab.* 24 (1), 41–50. doi:10.1016/j.cmet.2016.05.005

Waitkus, M. S., and Yan, H. (2021). Targeting Isocitrate Dehydrogenase Mutations in Cancer: Emerging Evidence and Diverging Strategies. *Clin. Cancer Res.* 27 (2), 383–388. doi:10.1158/1078-0432.Ccr-20-1827

Wang, B., Ye, Y., Yang, X., Liu, B., Wang, Z., Chen, S., et al. (2020). SIRT 2-dependent IDH 1 Deacetylation Inhibits Colorectal Cancer and Liver Metastases. *EMBO Rep.* 21 (4), e48183. doi:10.15252/embr.201948183

Wang, H.-Y., Long, Q.-Y., Tang, S.-B., Xiao, Q., Gao, C., Zhao, Q.-Y., et al. (2019a). Histone Demethylase KDM3A Is Required for Enhancer Activation of Hippo Target Genes in Colorectal Cancer. *Nucleic Acids Res.* 47 (5), 2349–2364. doi:10.1093/nar/gky1317

Wang, L., Jin, Q., Lee, J.-E., Su, I.-h., and Ge, K. (2010). Histone H3K27 Methyltransferase Ezh2 Represses Wnt Genes to Facilitate Adipogenesis. *Proc. Natl. Acad. Sci.* 107 (16), 7317–7322. doi:10.1073/pnas.1000031107

Wang, Q., Hardie, R. A., Hoy, A. J., van Geldermalsen, M., Gao, D., Fazli, L., et al. (2015). Targeting ASCT2 -mediated Glutamine Uptake Blocks Prostate Cancer Growth and Tumour Development. *J. Pathol.* 236 (3), 278–289. doi:10.1002/path.4518

Wang, Y., Guo, Y. R., Liu, K., Yin, Z., Liu, R., Xia, Y., et al. (2017). KAT2A Coupled with the α-KGDH Complex Acts as a Histone H3 Succinyltransferase. *Nature* 552 (7684), 273–277. doi:10.1038/nature25003

Wang, Z., Yang, X., Liu, C., Li, X., Zhang, B., Wang, B., et al. (2019b). Acetylation of PHF5A Modulates Stress Responses and Colorectal Carcinogenesis through Alternative Splicing-Mediated Upregulation of KDM3A. *Mol. Cel* 74 (6), 1250–1263. e1256. doi:10.1016/j.molcel.2019.04.009

Warburg, O. (1956). On the Origin of Cancer Cells. *Science* 123 (3191), 309–314. doi:10.1126/science.123.3191.309

Wei, J., Peng, K., Zhu, J., Wang, L., Han, T., Sun, A., et al. (2020). Geranylgeranylation Promotes Proliferation, Migration and Invasion of Gastric Cancer Cells through the YAP Signaling Pathway. *Am. J. Transl Res.* 12 (9), 5296–5307.

Wettersten, H. I., Aboud, O. A., Lara, P. N., Jr., and Weiss, R. H. (2017). Metabolic Reprogramming in clear Cell Renal Cell Carcinoma. *Nat. Rev. Nephrol.* 13 (7), 410–419. doi:10.1038/nrneph.2017.59

White, K., Connor, K., Clerkin, J., Murphy, B. M., Salvucci, M., O'Farrell, A. C., et al. (2020). New Hints towards a Precision Medicine Strategy for IDH Wild-type Glioblastoma. *Ann. Oncol.* 31 (12), 1679–1692. doi:10.1016/j.annonc.2020.08.2336

Wiley, C. D., and Campisi, J. (2016). From Ancient Pathways to Aging Cells-Connecting Metabolism and Cellular Senescence. *Cel Metab.* 23 (6), 1013–1021. doi:10.1016/j.cmet.2016.05.010

Witherspoon, M., Chen, Q., Kopelovich, L., Gross, S. S., and Lipkin, S. M. (2013). Unbiased Metabolite Profiling Indicates that a Diminished Thymidine Pool Is the Underlying Mechanism of colon Cancer Chemoprevention by Alpha-Difluoromethylornithine. *Cancer Discov.* 3 (9), 1072–1081. doi:10.1158/2159-8290.Cd-12-0305

Wong, C. C., Qian, Y., and Yu, J. (2017). Interplay between Epigenetics and Metabolism in Oncogenesis: Mechanisms and Therapeutic Approaches. *Oncogene* 36 (24), 3359–3374. doi:10.1038/onc.2016.485

Wu, J., Zhao, Y., Wang, X., Kong, L., Johnston, L. J., Lu, L., et al. (2020a). Dietary Nutrients Shape Gut Microbes and Intestinal Mucosa via Epigenetic Modifications. *Crit. Rev. Food Sci. Nutr.*, 1–15. doi:10.1080/10408398.2020.1828813

Wu, S.-e., Hashimoto-Hill, S., Woo, V., Eshleman, E. M., Whitt, J., Engleman, L., et al. (2020b). Microbiota-derived Metabolite Promotes HDAC3 Activity in the Gut. *Nature* 586 (7827), 108–112. doi:10.1038/s41586-020-2604-2

Xie, Z., Zhang, D., Chung, D., Tang, Z., Huang, H., Dai, L., et al. (2016). Metabolic Regulation of Gene Expression by Histone Lysine β-Hydroxybutyrylation. *Mol. Cel* 62 (2), 194–206. doi:10.1016/j.molcel.2016.03.036

Xu, Q. L., Luo, Z., Zhang, B., Qin, G. J., Zhang, R. Y., Kong, X. Y., et al. (2021a). Methylation-associated Silencing of miR-9-1 Promotes Nasopharyngeal Carcinoma Progression and Glycolysis via HK2. *Cancer Sci.* 112, 4127–4138. doi:10.1111/cas.15103

Xu, Y., Chen, W., Liang, J., Zeng, X., Ji, K., Zhou, J., et al. (2021b). The miR-1185-2-3p-Golph3l Pathway Promotes Glucose Metabolism in Breast Cancer by Stabilizing P53-Induced SERPINE1. *J. Exp. Clin. Cancer Res.* 40 (1), 47. doi:10.1186/s13046-020-01767-9

Xu, Y., Qiu, M., Shen, M., Dong, S., Ye, G., Shi, X., et al. (2021c). The Emerging Regulatory Roles of Long Non-coding RNAs Implicated in Cancer Metabolism. *Mol. Ther.* 29 (7), 2209–2218. doi:10.1016/j.ymthe.2021.03.017

Yang, F., Zhang, H., Mei, Y., and Wu, M. (2014). Reciprocal Regulation of HIF-1α and LincRNA-P21 Modulates the Warburg Effect. *Mol. Cel* 53 (1), 88–100. doi:10.1016/j.molcel.2013.11.004

Yang, H., Yang, T., Baur, J. A., Perez, E., Matsui, T., Carmona, J. J., et al. (2007). Nutrient-sensitive Mitochondrial NAD+ Levels Dictate Cell Survival. *Cell* 130 (6), 1095–1107. doi:10.1016/j.cell.2007.07.035

Yang, J., and Yu, J. (2018). The Association of Diet, Gut Microbiota and Colorectal Cancer: what We Eat May Imply what We Get. *Protein Cell* 9 (5), 474–487. doi:10.1007/s13238-018-0543-6

Yang, X., and Qian, K. (2017). Protein O-GlcNAcylation: Emerging Mechanisms and Functions. *Nat. Rev. Mol. Cel Biol* 18 (7), 452–465. doi:10.1038/nrm.2017.22

Yang, Y., and Bedford, M. T. (2013). Protein Arginine Methyltransferases and Cancer. *Nat. Rev. Cancer* 13 (1), 37–50. doi:10.1038/nrc3409

Yang, Y., Hsu, J.-M., Sun, L., Chan, L.-C., Li, C.-W., Hsu, J. L., et al. (2019). Palmitoylation Stabilizes PD-L1 to Promote Breast Tumor Growth. *Cell Res* 29 (1), 83–86. doi:10.1038/s41422-018-0124-5

Yao, H., Lan, J., Li, C., Shi, H., Brosseau, J.-P., Wang, H., et al. (2019). Inhibiting PD-L1 Palmitoylation Enhances T-Cell Immune Responses against Tumours. *Nat. Biomed. Eng.* 3 (4), 306–317. doi:10.1038/s41551-019-0375-6

Yao, K., Liu, H., Yin, J., Yuan, J., and Tao, H. (2021). Synthetic Lethality and Synergetic Effect: the Effective Strategies for Therapy of IDH-Mutated Cancers. *J. Exp. Clin. Cancer Res.* 40 (1), 263. doi:10.1186/s13046-021-02054-x

Yeon, A., You, S., Kim, M., Gupta, A., Park, M. H., Weisenberger, D. J., et al. (2018). Rewiring of Cisplatin-Resistant Bladder Cancer Cells through Epigenetic Regulation of Genes Involved in Amino Acid Metabolism. *Theranostics* 8 (16), 4520–4534. doi:10.7150/thno.25130

Yiew, N. K. H., Greenway, C., Zarzour, A., Ahmadieh, S., Goo, B., Kim, D., et al. (2019). Enhancer of Zeste Homolog 2 (EZH2) Regulates Adipocyte Lipid Metabolism Independent of Adipogenic Differentiation: Role of Apolipoprotein E. *J. Biol. Chem.* 294 (21), 8577–8591. doi:10.1074/jbc.RA118.006871

Yoshizawa, T., Karim, M. F., Sato, Y., Senokuchi, T., Miyata, K., Fukuda, T., et al. (2014). SIRT7 Controls Hepatic Lipid Metabolism by Regulating the Ubiquitin-Proteasome Pathway. *Cel Metab.* 19 (4), 712–721. doi:10.1016/j.cmet.2014.03.006

Yu, J., Chai, P., Xie, M., Ge, S., Ruan, J., Fan, X., et al. (2021). Histone Lactylation Drives Oncogenesis by Facilitating m6A Reader Protein YTHDF2 Expression in Ocular Melanoma. *Genome Biol.* 22 (1), 85. doi:10.1186/s13059-021-02308-z

Zaidi, N., Swinnen, J. V., and Smans, K. (2012). ATP-citrate Lyase: a Key Player in Cancer Metabolism. *Cancer Res.* 72 (15), 3709–3714. doi:10.1158/0008-5472.CAN-11-4112

Zha, L., Li, F., Wu, R., Artinian, L., Rehder, V., Yu, L., et al. (2015). The Histone Demethylase UTX Promotes Brown Adipocyte Thermogenic Program via Coordinated Regulation of H3K27 Demethylation and Acetylation. *J. Biol. Chem.* 290 (41), 25151–25163. doi:10.1074/jbc.M115.662650

Zhai, S., Xu, Z., Xie, J., Zhang, J., Wang, X., Peng, C., et al. (2021). Epigenetic Silencing of LncRNA LINC00261 Promotes C-Myc-Mediated Aerobic Glycolysis by Regulating miR-222-3p/HIPK2/ERK axis and Sequestering IGF2BP1. *Oncogene* 40 (2), 277–291. doi:10.1038/s41388-020-01525-3

Zhang, D., Tang, Z., Huang, H., Zhou, G., Cui, C., Weng, Y., et al. (2019). Metabolic Regulation of Gene Expression by Histone Lactylation. *Nature* 574 (7779), 575–580. doi:10.1038/s41586-019-1678-1

Zhang, H., Chang, Z., Qin, L.-n., Liang, B., Han, J.-x., Qiao, K.-l., et al. (2021). MTA2 Triggered R-Loop Trans-regulates BDH1-Mediated β-hydroxybutyrylation and Potentiates Propagation of Hepatocellular Carcinoma Stem Cells. *Sig Transduct Target. Ther.* 6 (1), 135. doi:10.1038/s41392-021-00464-z

Zhang, M., Zhao, J., Lv, Y., Wang, W., Feng, C., Zou, W., et al. (2020a). Histone Variants and Histone Modifications in Neurogenesis. *Trends Cel Biol.* 30 (11), 869–880. doi:10.1016/j.tcb.2020.09.003

Zhang, T., Gong, Y., Meng, H., Li, C., and Xue, L. (2020b). Symphony of Epigenetic and Metabolic Regulation-Interaction between the Histone Methyltransferase EZH2 and Metabolism of Tumor. *Clin. Epigenet* 12 (1), 72. doi:10.1186/s13148-020-00862-0

Zhang, X., Zhang, Y., Fang, C., Zhang, L., Yang, P., Wang, C., et al. (2018). Ultradeep Palmitoylomics Enabled by Dithiodipyridine-Functionalized Magnetic Nanoparticles. *Anal. Chem.* 90 (10), 6161–6168. doi:10.1021/acs.analchem.8b00534

Zhang, Y., Zhao, L., Yang, S., Cen, Y., Zhu, T., Wang, L., et al. (2020c). CircCDKN2B-AS1 Interacts with IMP3 to Stabilize Hexokinase 2 mRNA and Facilitate Cervical Squamous Cell Carcinoma Aerobic Glycolysis Progression. *J. Exp. Clin. Cancer Res.* 39 (1), 281. doi:10.1186/s13046-020-01793-7

Zhang, Z., Tan, M., Xie, Z., Dai, L., Chen, Y., and Zhao, Y. (2011). Identification of Lysine Succinylation as a New post-translational Modification. *Nat. Chem. Biol.* 7 (1), 58–63. doi:10.1038/nchembio.495

Zhao, D., Guan, H., Zhao, S., Mi, W., Wen, H., Li, Y., et al. (2016). YEATS2 Is a Selective Histone Crotonylation Reader. *Cel Res* 26 (5), 629–632. doi:10.1038/cr.2016.49

Zhao, S., Zhang, X., Shi, Y., Cheng, L., Song, T., Wu, B., et al. (2020). MIEF2 Over-expression Promotes Tumor Growth and Metastasis through Reprogramming of Glucose Metabolism in Ovarian Cancer. *J. Exp. Clin. Cancer Res.* 39 (1), 286. doi:10.1186/s13046-020-01802-9

Zheng, F., Chen, J., Zhang, X., Wang, Z., Chen, J., Lin, X., et al. (2021). The HIF-1α Antisense Long Non-coding RNA Drives a Positive Feedback Loop of HIF-1α Mediated Transactivation and Glycolysis. *Nat. Commun.* 12 (1), 1341. doi:10.1038/s41467-021-21535-3

Zheng, L., Kelly, C. J., Battista, K. D., Schaefer, R., Lanis, J. M., Alexeev, E. E., et al. (2017). Microbial-Derived Butyrate Promotes Epithelial Barrier Function through IL-10 Receptor-dependent Repression of Claudin-2. *J. Immunol.* 199 (8), 2976–2984. doi:10.4049/jimmunol.1700105

Zheng, Y., Wu, C., Yang, J., Zhao, Y., Jia, H., Xue, M., et al. (2020). Insulin-like Growth Factor 1-induced Enolase 2 Deacetylation by HDAC3 Promotes Metastasis of Pancreatic Cancer. *Sig Transduct Target. Ther.* 5 (1), 53. doi:10.1038/s41392-020-0146-6

Zhong, L., D'Urso, A., Toiber, D., Sebastian, C., Henry, R. E., Vadysirisack, D. D., et al. (2010). The Histone Deacetylase Sirt6 Regulates Glucose Homeostasis via Hif1α. *Cell* 140 (2), 280–293. doi:10.1016/j.cell.2009.12.041

Zou, J., Zhu, X., Xiang, D., Zhang, Y., Li, J., Su, Z., et al. (2021). LIX1-like Protein Promotes Liver Cancer Progression via miR-21-3p-Mediated Inhibition of Fructose-1,6-Bisphosphatase. *Acta Pharmaceutica Sinica B* 11 (6), 1578–1591. doi:10.1016/j.apsb.2021.02.005

Zou, X., Zhu, Y., Park, S.-H., Liu, G., O'Brien, J., Jiang, H., et al. (2017). SIRT3-Mediated Dimerization of IDH2 Directs Cancer Cell Metabolism and Tumor Growth. *Cancer Res.* 77 (15), 3990–3999. doi:10.1158/0008-5472.Can-16-2393

Conflict of Interest: The authors declare that the research was conducted in the absence of any commercial or financial relationships that could be construed as a potential conflict of interest.

Publisher's Note: All claims expressed in this article are solely those of the authors and do not necessarily represent those of their affiliated organizations, or those of the publisher, the editors and the reviewers. Any product that may be evaluated in this article, or claim that may be made by its manufacturer, is not guaranteed or endorsed by the publisher.

frontiers in Cell and Developmental Biology

ORIGINAL RESEARCH
published: 03 January 2022
doi: 10.3389/fcell.2021.803981

The Antitumoral Effect of Paris Saponin II on Head and Neck Squamous Cell Carcinomas Mediated *via* the Nitric Oxide Metabolic Pathway

Wenwen Qi[1,2], Fangyuan Zhu[2], Min Wang[3], Zhenxiao Teng[1,2], Runtong Xu[2], Yue Xi[3], Qiu Meng[2], Xinhao Wu[1,2], Hui Zhao[2], Min Ma[4], Xiaozhi Hou[2], Baowei Wang[2], Xiaoming Li[2], Chengcheng Liu[5], Xiang Zhang[6†], Fenglei Xu[2*†] and Ming Xia[1,2*†]*

[1]Department of Otolaryngology, Shandong Provincial Hospital, Cheeloo College of Medicine, Shandong University, Jinan, China, [2]Department of Otolaryngology, Shandong Provincial Hospital Affiliated to Shandong First Medical University, Jinan, China, [3]Department of Pathology, Shandong Provincial Hospital Affiliated to Shandong First Medical University, Jinan, China, [4]Cancer Center, Shandong Provincial Hospital Affiliated to Shandong First Medical University, Jinan, China, [5]Shandong Provincial Hospital Affiliated to Shandong First Medical University, Jinan, China, [6]Department of Pharmacy, Central Hospital Affiliated to Shandong First Medical University, Jinan, China

OPEN ACCESS

Edited by:
Jiayi Wang,
Shanghai Jiaotong University, China

Reviewed by:
Qinghua Cui,
Peking University, China
Ranji Cui,
Second Affiliated Hospital of Jilin University, China

***Correspondence:**
Ming Xia
xiamingsdu@sohu.com
Fenglei Xu
xufenglei@sdu.edu.cn
Xiang Zhang
2506610420@qq.com

†These authors have contributed equally to this work

Specialty section:
This article was submitted to Epigenomics and Epigenetics, a section of the journal Frontiers in Cell and Developmental Biology

Received: 28 October 2021
Accepted: 01 December 2021
Published: 03 January 2022

Citation:
Qi W, Zhu F, Wang M, Teng Z, Xu R, Xi Y, Meng Q, Wu X, Zhao H, Ma M, Hou X, Wang B, Li X, Liu C, Zhang X, Xu F and Xia M (2022) The Antitumoral Effect of Paris Saponin II on Head and Neck Squamous Cell Carcinomas Mediated via the Nitric Oxide Metabolic Pathway. Front. Cell Dev. Biol. 9:803981. doi: 10.3389/fcell.2021.803981

Paris saponin has shown great therapeutic value in cancer therapy. We used isolated Paris saponin II (PSII), an active component of Paris saponin, and demonstrated its antitumor effect on human head and neck squamous cell carcinoma cell lines. Additionally, we investigated its mechanisms of action *in vivo* by establishing a xenograft mouse model. The results showed that PSII had presented strong anticancer effects on both hypopharyngeal malignant tumor cell lines (FaDu) and laryngeal carcinoma cell lines (Tu212 and Tu686). In addition, we successfully isolated and cultured the head and neck squamous stem cells and the primary fibroblasts to perform metabonomics studies. The results showed that RPII remarkably decreased energy metabolism, and type III nitric oxide synthase 3 (NOS3) may be a target to block tumor growth. Furthermore, we found that PSII inhibited HNSCC proliferation and metastasis by inhibiting the nitric oxide metabolic pathway. Overall, these results demonstrated that PSII is a potent anticancer agent, and the metabonomics analysis is a valuable tool to investigate and establish the antitumor effects of traditional Chinese medicines.

Keywords: Paris saponin II, head and neck squamous carcinomas, type III nitric oxide synthase, nitric oxide metabolic pathway, cancer stem cells

INTRODUCTION

Head and neck squamous cell carcinoma is one of the most common cancers in the world (Schinke et al., 2021), and its 5-year overall survival (OS) rate is only 45% (HammermanHammerman et al., 2015; Johnson et al., 2020). A possible reason for the failure of the cancer treatment is associated with the existence of "cancer stem cells" (CSCs) in tumors, which numerous studies have shown to have a major impact on the recurrence and metastasis of tumors, as well as the resistance to radio/chemotherapy treatment (Chen et al., 2020; Chang et al., 2021). Another possible reason is the tumor microenvironment (TME), which may have important implications for tumor therapy (Hinshaw and Shevde, 2019). Tumorigenesis is often driven by the changes in the living environment, which is referred to as TME (Wu and Dai, 2017). In the TME, the metabolites play an important role in several

steps of tumorigenesis, including immune escape, local drug resistance, distant metastasis, and recurrence (Reina-Campos et al., 2017; García-Cañaveras et al., 2019; Li et al., 2019). In the past few decades, researchers have found a number of tumor suppressors and oncogenes, which are involved in the development of tumors, including some key metabolic enzymes, especially related to redox reactions and glycolysis (Jin et al., 2019; Ferro et al., 2020). The accumulation of protein aggregates, autophagic stress, oxidative stress, and mitochondrial dysfunction are common in many pathological processes of tumors (Lin et al., 2019). As indicated by many studies, oxidative stress can contribute to protein aggregation (Tripathi et al., 2020). Furthermore, mitochondrial dysfunction can promote DNA damage and instability by producing excessive amounts of reactive oxygen species (ROS) (Saki and Prakash, 20172017; Luo et al., 2020). Consequently, mitochondrial dysfunction is considered a metabolic hallmark of cancer cells. Metabolomics is a novel and convenient approach to explore the toxicity and features of medicine (Hsu et al., 2016; Vitale et al., 2019; Battaglia et al., 2020). Therefore, metabonomics is a promising approach to investigate the mechanisms and safety of medicine.

Paridis saponins (PSs), a natural extract of Paris polyphylla Smith var. yunnanensis used as an anticancer drug in traditional Chinese medicine (TCM) which is also an active component of Paris saponin II (PSII), has shown a strong antitumor power in various cancers, such as hepatocellular carcinoma (HCC) (Cheng et al., 2008), lung cancer (Man et al., 2015), and ovarian cancer (Xiao et al., 2009). Recent studies have reported promising roles of PS in the regulation of glycolytic and lipid metabolism (Man et al., 2017; Man et al., 2020). All these results indicate that PSII may be a valuable anti-HNSCC agent. In this study, we used a metabonomics approach to investigate the metabolic features in the HNSCC cell lines treated with PSII. The marker metabolites were used to evaluate the anticancer capacity of drugs (Sak and Everaus, 2015). After analyzing the changes in these metabolomics in PSII-treated HNSCC cell lines by a metabonomics approach, we investigated the mechanism mediating the antitumor effects of PSII intervening tumor development. In addition, a mouse model was developed to explore the inhibitory effect of PSII on HNSCC growth (Supsavhad et al., 2016; Gilardi et al., 2020). Our study demonstrated that PSII is a potent anticancer agent in the HNSCC. Additionally, it also showed that a metabonomics approach can be a valuable tool to elucidate the antitumor effects of TCM preparations.

MATERIALS AND METHODS

Materials

We purchased Paris saponin II (PSII) (purity > 99%) from Chengdu Must Bio-technology Technology Co., Ltd (Chengdu, China). The HNSCC cell lines including the hypopharyngeal cancer cell line FaDu and the laryngeal carcinoma cell lines Tu212 and Tu686 were purchased from American Type Culture Collection (ATCC; Rockville, MD, United States). Antibodies against Bcl-2, Ki67, nitric oxide synthase 3 (NOS3), CytC, Lc3b, β-actin, and Bax were purchased from Cell Signaling Technology Inc. (CST Inc., Danvers, MA, United States).

Cell Culture

Two cell lines (Tu686 and FaDu) were cultured in Dulbecco's modified Eagle medium (DMEM) which were obtained from Thermo Fisher Scientific Inc./Gibco (Waltham, MA, United States) supplemented with 10% fetal bovine serum (FBS) obtained from Haoyang Biological Manufacture Co. Ltd. (Tianjin, China), as well as penicillin/streptomycin (P/S; 100 U/ml/100 pg/ml). Tu212 cell lines were cultured in Iscove's Modified Dulbecco's Medium (IMDM) which was bought from Thermo Fisher Scientific Inc./Gibco supplemented with 10% FBS and P/S. All the cell lines were routinely cultured in a humidified cell incubator at 37°C with 5% CO_2.

Cell Viability Assay

We measured cell viability using the methyl thiazolyl tetrazolium (MTT) assay. FaDu, Tu686, and Tu212 cells were plated in 96-well plates at a cell concentration of 3×10^3 cells/well. After overnight incubation for one night, the cultured medium was changed with a new medium containing different concentrations of PSII (0, 0.025, 0.05, 0.1, 0.2, 0.4, 0.8, and 1.6 μg/ml), and then we incubated them for 24, 48, 72, and 96 h at 37°C with 5% CO_2 in a cell incubator, Afterward, 20 μl of MTT reagent (5 mg/ml) was added to each well, and the cells were incubated for 4 h at 37°C. Subsequently, the supernatants in the wells were cautiously aspirated, and 100 μl of dimethyl sulfoxide (DMSO) solution was added to each well. The 96-well plates were shaken for 10 min at room temperature and then the absorbance values were measured at 570 nm on a microplate reader (Bio-Rad Laboratories Inc., Hercules, CA, United States).

Invasion and Migration Assays

We used transwell plates (Coming Costar, Lowell, MA, United States) to assay cell invasion and migration. In the migration assay, we starved the cells in a serum-free medium (SFM) for 12 h at 37°C with 5% CO_2. We then added 700 μl of DMEM or IMDM with 20% FBS to the lower well and 500 μl of SFM, including 1×10^5 cells to the upper transwell inserts. After culturing for 48 h at 37°C with 5% CO_2, we counted the number of cells that adhered to the lower surface of the insert membrane. We performed the invasion assay in the same way, except that the transwell insert membrane was coated with Matrigel (BD Biosciences, San Jose, CA, United States).

Colony Forming Assay

We seeded the three HNSCC cell lines in six-well plates at a cell concentration of 1×10^3 cells/well, and the plates were incubated for 24 h at 37°C with 5% CO_2. After incubation for 24 h, we replaced the old medium with a new medium containing PSII and continued incubation for 10 days. Subsequently, after washing cells with phosphate-buffered saline (PBS), the cells were fixed with methyl alcohol and stained with a 1% crystal violet solution. Ultimately, after washing the cells with PBS, we observed the cells under a microscope and acquired images of various fields to count the number of colonies.

Cell Scratch Test Assay

Once cultured, the cells reached close to 100% confluence, the cell monolayer was mechanically scratched. Scratch healing was observed at 0, 12, 24, and 48 h under a microscope at ×40 magnification (white light bright field). We used ImageJ software [National Institute of Health (NIH), Bethesda, MD, United States] to calculate the migration area on the scratch, using the following formula: Scratch area rate (%) = 12, 24, and 48 h after migration scratch area/initial scratch area ×100%.

Cell Line Microsphere Culture for Stem Cell

The corresponding SFM was prepared by adding double antibody as follows: 20 ng/ml epidermal growth factor (EGF; PeproTech US, Cranbury, NJ, United States), 20 ng/ml basic fibroblast growth factor (bFGF, Thermo Fisher Scientific Inc./Gibco), and 2% B27 (Invitrogen, Carlsbad, CA, United States) were added into DMEM/F12 culture medium (Thermo Fisher Scientific Inc./Gibco). Logarithmic growth phase HNSCC cell lines (FaDu, Tu212, and Tu686) were digested with 0.25% trypsin (Thermo Fisher Scientific Inc./Gibco) and dissociated into a single cell suspension. Then the resuspended cells were inoculated into SFM at a density less than 10^4/ml for routine culture and added into an ultralow adsorption T25 or smaller glass flask, which was placed vertically in an incubator and shaken several times a day. The formation of microspheres was observed, and half of the cell suspension solution was replaced every 2–3 days, and the cells were subcultured every 6–8 days. During subculturing, microspheres were collected by centrifugation and resuspended in an accutase solution (MilliporeSigma, Burlington, MA, United States) and digested at 37°C for 5–10 min. The microspheres were pipetted up and down several times until they dispersed into single cells. After centrifugation and washing, the microspheres were counted and inoculated into SFM for subculture at a density less than 10^4/ml.

Flow Cytometry

Logarithmic growth phase tumor cells and stem cells were collected, digested, centrifuged, and resuspended in PBS. After counting, the number of cells was adjusted to 1×10^6 cells/group. Anti-CD24-fluorescein isothiocyanate (FITC) was used as negative control, and the proportion of anti-CD44-phycoerythrin (PE)/anti-CD133-allophycocyanin (APC) cells in each group was determined by flow cytometry analysis. When the anti-CD44-PE and anti-CD133-APC were both positive, it revealed the presence of stem cells.

Primary Culture of Fibroblasts From Head and Neck Tumor Tissue

We selected the pathology of patients with hypopharyngeal malignant tumor for the first time as experimental subjects which was approved by the Ethics Committee at our institution. When rapid intraoperative pathology confirmed that the pathological type was squamous cell carcinoma of the head and neck, we collected tumor tissues for study. The head and neck tumor tissues were washed three times with cold PBS mixed with double antibodies in an ultraclean workbench. Then the tissue blocks were placed in a 10-cm sterile petri dish and cut into 1- to 2-mm tissue blocks with cold PBS as described to wash away the free cells. Subsequently, using tweezers, the tissue blocks were placed on the bottom surface of a culture flask with a spacing of about 0.5 cm. The flask was inverted, and 3 ml of the medium (DMEM+20%FBS + double antibody) was added to the bottom of the flask, and the tissue blocks were incubated for 4 h. Then 3 ml of the medium was added again, and the culture flask was inverted and incubated for an additional 48 h. The growth of primary tumor–associated fibroblasts was observed under a microscope, and the migration ability of the purified cells was examined by a transwell migration assay.

Immunofluorescence for Identifying Primary Culture of Fibroblasts

Tumor-associated fibroblasts were seeded into a petri dish with a pretreated cover glass and allowed to grow. After the cells had nearly formed a monolayer, the cover glass was removed, and the cells were washed twice with PBS. Then cells were fixed for 2 h with paraformaldehyde, permeabilized with 5% Triton X-100 for 20 min, blocked with 2% BSA, and washed twice with PBS. The cells were treated with the corresponding primary antibody against FAP (CST Inc.) and SMA (Abcam, Cambridge, United Kingdom), followed by incubation with appropriate secondary antibodies. Ultimately, all fibroblasts were stained with 4',6-diamidino-2-phenylindole (DAPI).

High-Resolution Untargeted Metabolomics Analysis

We performed untargeted metabolomics analysis of the three HNSCC cell lines treated with/without PSII. The metabolites in the samples were analyzed by ultrahigh performance liquid chromatography–quadrupole time-of-flight mass spectrometry (UHPLC-Q-TOF MS). The retention time and molecular weight of the metabolites in the samples were compared with those in the local database. Also, the 25 PPM, secondary fragmentation spectrum, collision energy, and other information were matched to identify the structure of metabolites in biological samples, and the identification results were confirmed through strict manual secondary check and confirmation. The assessment level is Level 2.

Western Blot Analysis

FaDu and Tu686 cells were treated with PSII (0, 0.05, and 0.1 μg/ml) for 48 h at 37°C with 5% CO_2. Cells were collected and lysed in lysis buffer with protease inhibitors to extract proteins. We separated proteins by 12% sodium dodecyl sulfate–polyacrylamide gel electrophoresis (SDS-PAGE). Then the separated proteins were electroblotted onto a polyvinylidene difluoride (PVDF) membrane using a blotting apparatus (Bio-Rad Laboratories). After blocking the membranes with 5% non-fat milk, the membranes were incubated overnight at 4°C with the corresponding primary antibodies, followed by labeling with the appropriate secondary antibody at room temperature for 1 h. We

A

Tab.1 The physical characteristics of PSII

Item	Molecular Formula	Molecular Weight	Lot No.	Appearance	Loss on drying	Assay by HPLC
Result	$C_{51}H_{82}O_{20}$	1015.18	MUST-20062810	White Powder	≤2.0%	98.97%

B

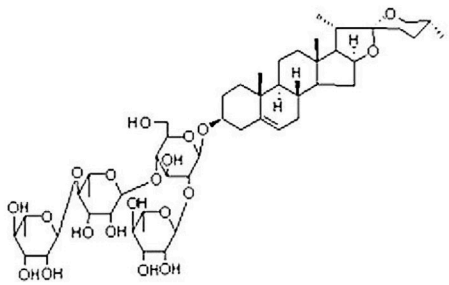

C

Tab.2 The Peak table of PSII

Peak Number	Retention Time	Area	height	Area%
1	7.064	56198	2388	0.389
2	7.617	12213	946	0.084
3	23.678	80442	3360	0.556
4	26.318	14312394	207744	98.971
Total	64.677	14461248	214439	100.000

D

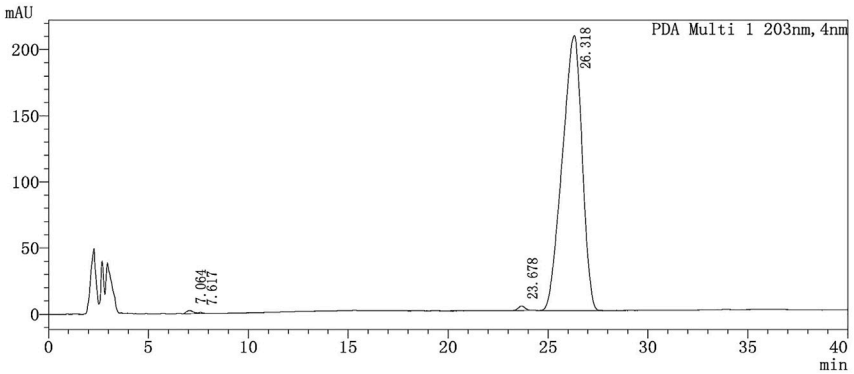

FIGURE 1 | Drug instruction. **(A)** The physical characteristics of PSII. **(B)** Structural formula of PSII. **(C)** The peak table of PSII. **(D)** The peak figure of PSII. Eluant: acetonitrile:water = 50/50, 50 min. Flow velocity: 1.0 ml/min. Chromatographic column: MinXi Teeh CG-C18 5mic 250 × 4.6 mm. Column temperature: 40°C. The sample solvent: methyl alcohol.

used β-actin as the internal control. Eventually, the immunoreacted protein bands were visualized using the Pro-lighting horseradish peroxidase (HRP) agent for Western blotting detection (Tiangen Biotech Co., Ltd., Beijing, China). The Western blot analysis of mouse xenograft tumors was performed in the same way as that for the cells.

Quantitative Real-Time Polymerase Chain Reaction (qRT-PCR) Analysis

Total RNA was isolated from FaDu and Tu686 cells using TRIzol (Invitrogen), and the quality of the isolated RNA by the absorbance at 260 and 280 nm was determined. cDNA synthesis was carried out using Rever-tAidTM M-MuLV RT (Fermentas, Hanover, MD, United States) according to the instructions, and the obtained cDNA was stored at −80°C. Polymerase chain reactions were performed in a final volume of 50 ml including 2 μl each of the forward and reverse primers, 25 μl 2*Taq Master Mix, 2 μl cDNA, and RNase-free water. After transfection, total RNA was obtained from the transfected cells with TRIzol, and cDNA was obtained by reverse transcription as described. Real-time quantitative PCR was performed to detect the mRNA level.

Transfection of Cells

The primers used were synthesized by Ding Guo Changsheng Biotechnology Co., Ltd. (Beijing, China). The NOS3-F primer sequence is GTGATGGCGAAGCGAGTGAAGG, and the NOS3-R primer sequence is CACCACGTCATACTCATC CATACACAG. The FaDu and Tu686 cells were inoculated in six-well plates, and when confluence reached about 85%, siRNA targeting NOS3 (NOS3-siRNA) was diluted with serum-free DMEM and mixed gently with Lipofectamine 2000 (Biyuntian Biological Technology Co., Shanghai, China). After mixing, the mixture was incubated for 20 min at room temperature. Afterward, FaDu and Tu686 cells were plated in culture plates to transfect for 6 h and then cultured in a complete medium for 48 h.

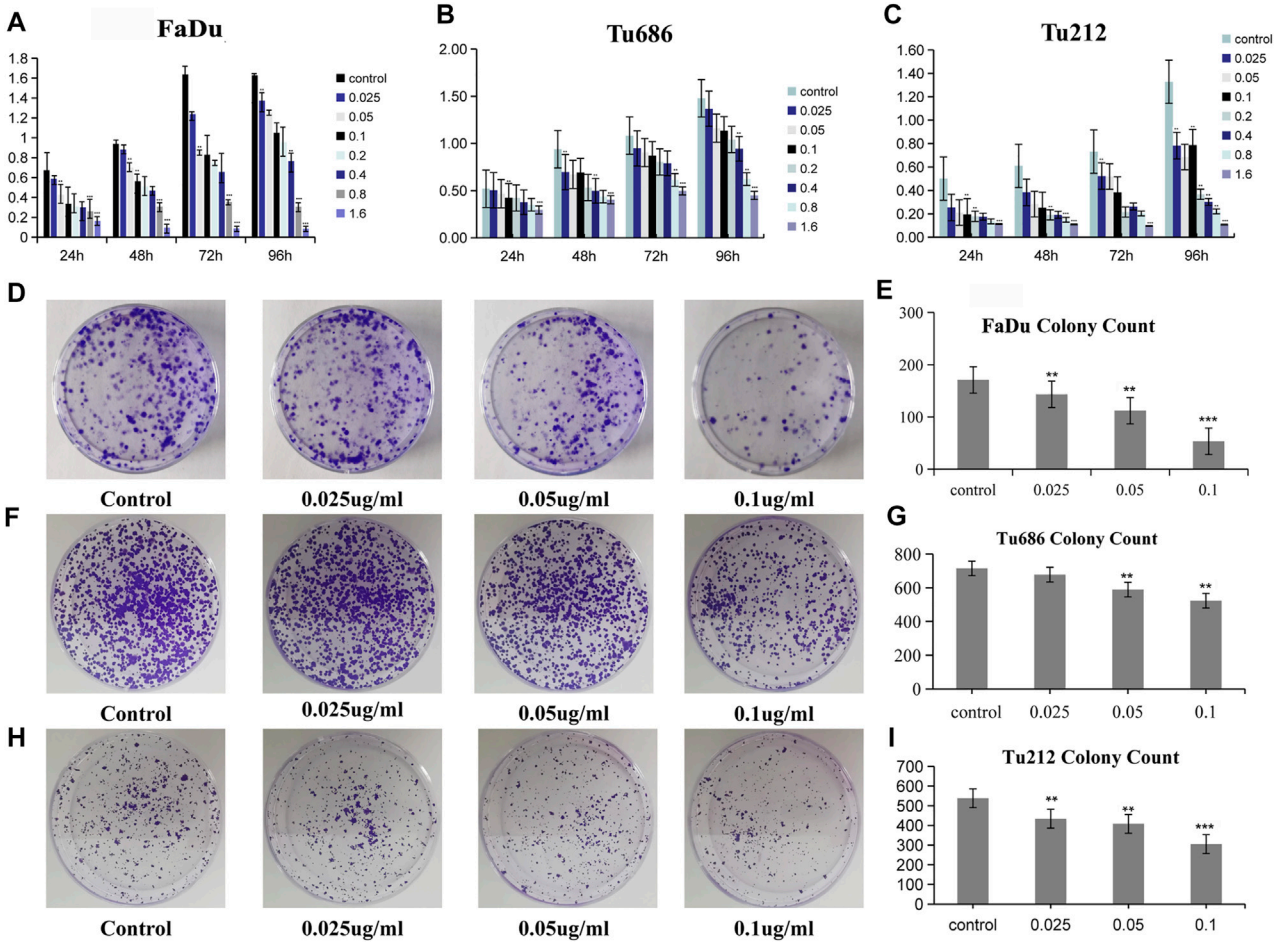

FIGURE 2 | PSII reduced the viability of HNSCC cell. **(A)** The inhibitory effect of PSII on FaDu cell viability by MTT. **(B)** The inhibitory effect of PSII on Tu686 cell viability by MTT. **(C)** The inhibitory effect of PSII on Tu212 cell viability by MTT. **(D)** FaDu cells formed colonies. **(E)** The statistical figure of FaDu cells clone formation assay. **(F)** Tu686 cells formed colonies. **(G)** The statistical figure of Tu686 clone formation assay. **(H)** Tu212 cells formed colonies. **(I)** The statistical figure of Tu212 clone formation assay. Bars, 50 μm. All the experiments were carried out three times. The bar graphs and the table show quantification of the results, and each data represent the mean ± SD of three independent experiments (*$p < 0.05$; **$p < 0.01$; ***$p < 0.001$ vs the control group).

Xenograft Tumorigenicity Assay

A total of 5×10^6 cells in 0.2 ml of PBS were injected subcutaneously into 4-week-old BALB/c nude female mice purchased from Taconic Biosciences (Rensselaer, NY, United States) After 5 days, the mice were randomly assigned to two groups, namely, the PSII group and control group. The PSII group was administered with about 100 μl of solution (5 mg/kg) by intraperitoneal injection once every 3 days. We measured the tumor growth once every 5 days according to the following equation: Volume = (width^2 × length)/2. On the 60th day, mice were anesthetized with ether and then killed. Eventually, the xenograft tumors were removed and processed for immunohistochemical (IHC) analysis.

Histopathological Examination

The spleen, lung, liver, heart, and kidney tissues of the mice were fixed in 10% formalin for the histopathological examination. After the dehydration process, we embedded the tissues in paraffin wax and cut them into 5-μm-thick sections using microtome. Then we stained the sections with hematoxylin and eosin (H&E). Ultimately, H&E-stained histopathology images were acquired using an Olympus microscope (Olympus Corporation, Tokyo, Japan).

Immunohistochemical (IHC) Analysis

First, we cut the xenografts into 5-μm-thick sections using microtome. Then the slices were labeled and placed in an oven at 60°C for 2 h. After dewaxing the paraffin sections, the endogenous peroxidases of the sections were blocked. Subsequently, the sections were boiled in 10 mM sodium citrate plus 0.05% Tween-20 (pH 6) for 10 min in a microwave oven for antigen retrieval. The tissue sections were uniformly covered with 5% BSA and sealed at 37°C for 30 min. Then the sections were incubated with the corresponding primary antibody for 12 h at 4°C in the dark. Afterward, the sections were washed three times with PBS and incubated with

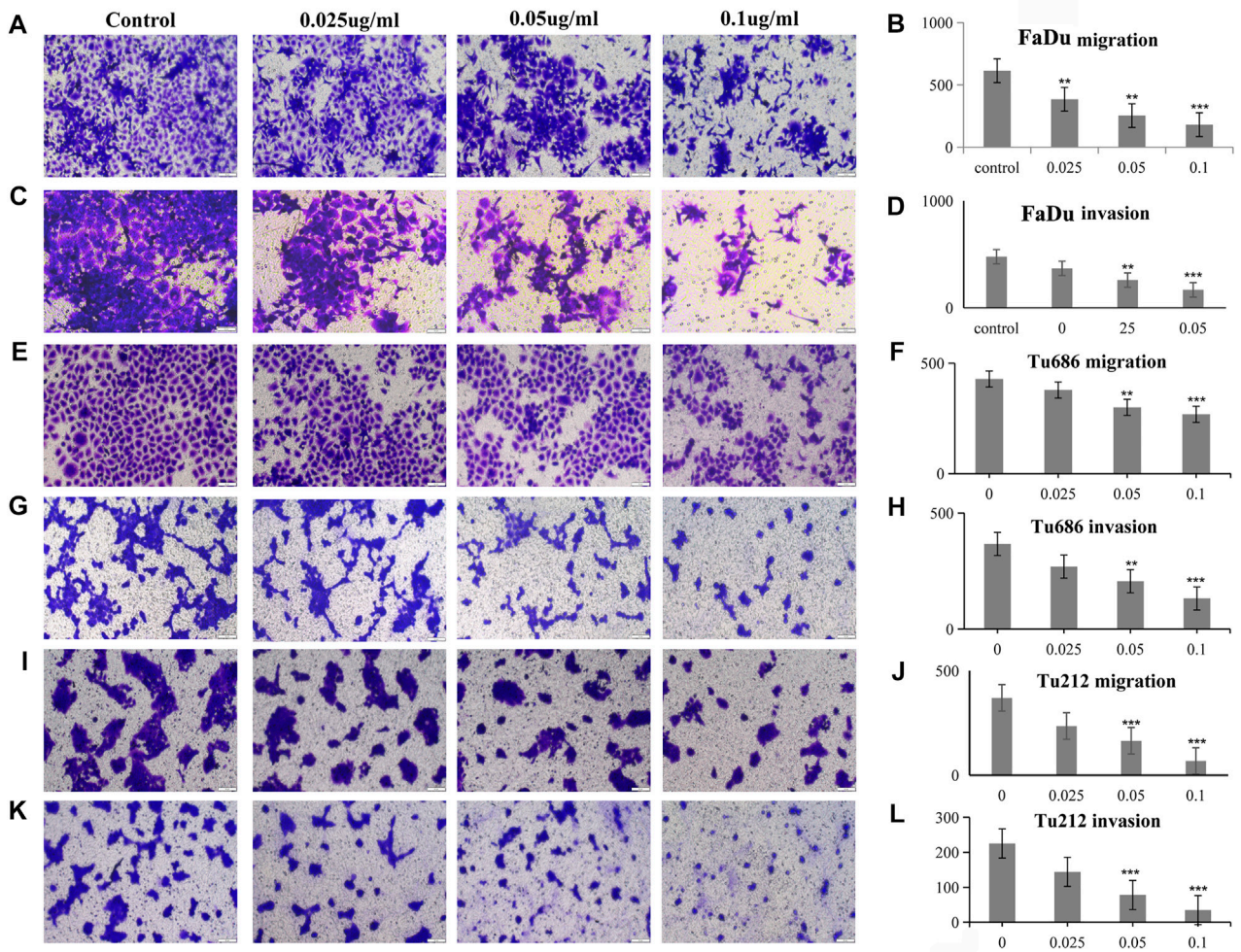

FIGURE 3 | PSII reduced the motility of human squamous cell carcinoma cell by transwell assay. **(A)** PSII inhibited FaDu cell mobility by migration. **(B)** The statistical figure of FaDu cell migration assay. **(C)** PSII inhibited FaDu cell mobility by invasion. **(D)** The statistical figure of FaDu cell invasion assay. **(E)** PSII inhibited Tu686 cell mobility by migration. **(F)** The statistical figure of Tu686 cell migration assay. **(G)** PSII inhibited Tu686 cell mobility by invasion. **(H)** The statistical figure of Tu686 cell invasion assay. **(I)** PSII inhibited Tu212 cell mobility by migration. **(J)** The statistical figure of Tu212 cell migration assay. **(K)** PSII inhibited Tu212 cell mobility by invasion. **(L)** The statistical figure of Tu212 cells invasion assay. Bars, 50 μm. All the experiments were carried out three times. The bar graphs and the table show quantification of the results, and each data represent the mean ± SD of three independent experiments (*$p < 0.05$; **$p < 0.01$; ***$p < 0.001$ vs the control group).

the appropriate secondary antibody (1:200) for 60 min at room temperature. Then the sections were stained using a diaminobenzidine (DAB) HRP Color Development Kit (Beyotime Biotechnology, Shanghai, China) according to the manufacturer's instructions. Next, the sections were stained with hematoxylin to stain the nucleus, dehydrated, and covered with neutral resin. Eventually, images of the sections were acquired on an Olympus microscope.

Statistical Analysis

SPSS (version 20.0) software (IBM Corporation, Armonk, NY, United States) was used for statistical analysis. One-way analysis of variance (ANOVA) and Student's *t*-test were performed to evaluate the significance. Every test was performed three times, and the error bars represent the standard error of the mean (SEM) in which differences with $p < 0.05$ were considered significant.

RESULTS

Preparation and Characterization of Paris Saponin II

As shown in **Figure 1A**, the molecular formula of PSII is C51H82O20, and its molecular weight is 1015.18. PSII has a white powder appearance, and its structural formula is as shown in **Figure 1B**. Chromatographic separation at a column temperature of 40°C, using a MinXi Teeh CG-C18 5 μm 250 × 4.6-mm chromatography column, with methyl alcohol as sample solvent, resulted in four peaks.

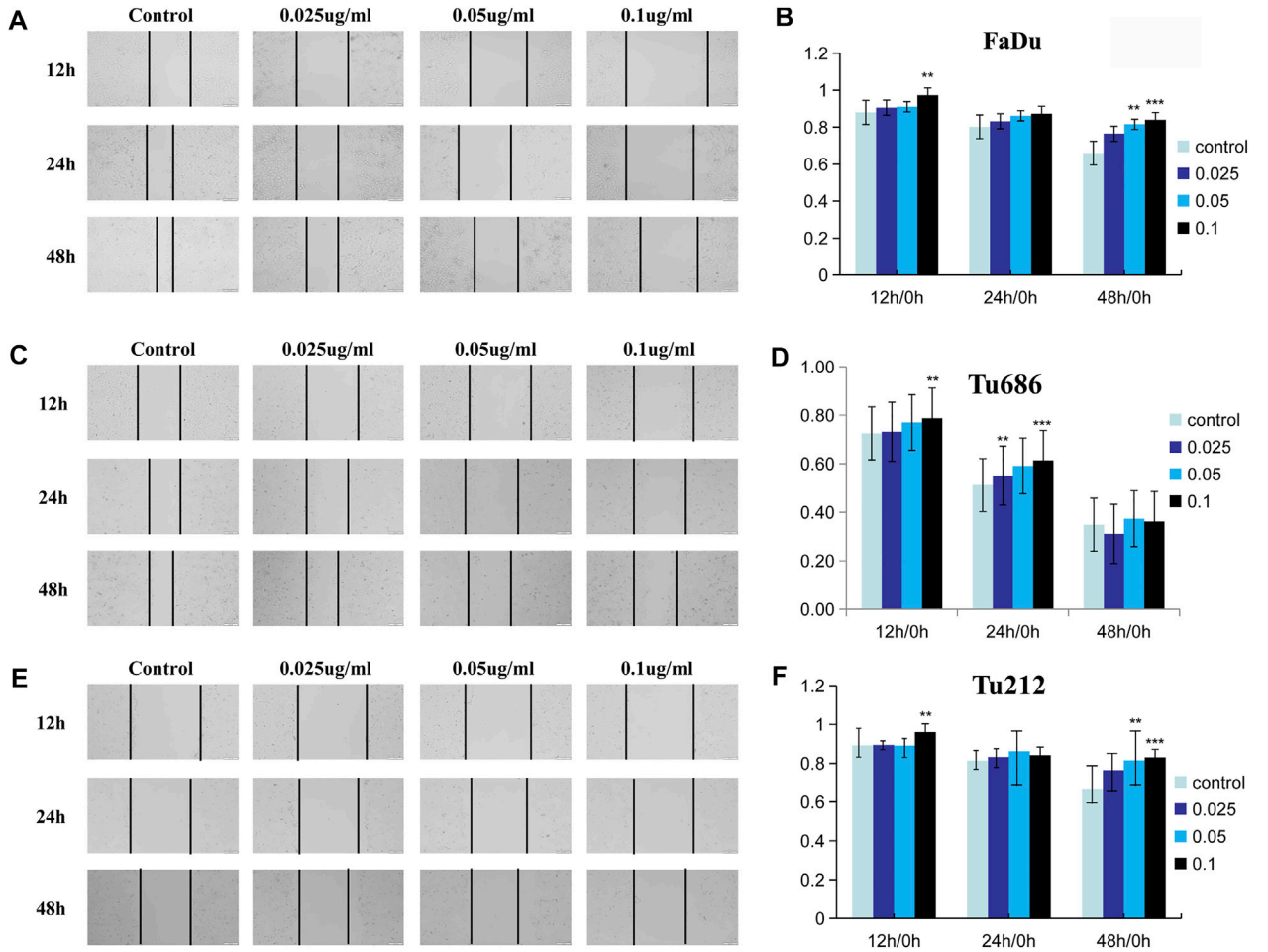

FIGURE 4 | PSII reduced the motility of human squamous cell carcinoma cell by cell scratch test. **(A)** PSII inhibited FaDu mobility by the cell scratch test in a dose- and time-dependent manner. **(B)** The statistical figure of FaDu cells scratch test. **(C)** PSII inhibited Tu686 mobility by the cell scratch test in a dose- and time-dependent manner **(D)**. The statistical figure of Tu686 cells scratch test. **(E)** PSII inhibited Tu212 mobility by the cell scratch test in a dose- and time-dependent manner **(F)**. The statistical figure of Tu212 cell scratch test. Bars, 50 μm. All the experiments were carried out three times. The bar graphs and the table show quantification of the results, and each data represent the mean ± SD of three independent experiments (*$p < 0.05$; **$p < 0.01$; ***$p < 0.001$ vs the control group).

PSII Inhibited the Proliferation of HNSCC Cell Lines

The measurement of cell proliferation by the MTT assay, as shown in **Figures 2A–C**, revealed that treatment with PSII significantly inhibited the proliferation of FaDu, Tu686, and Tu212 cells in a time- and concentration-dependent manner, especially after 48 h or at a concentration of 0.1 μg/ml PSII. In addition, the colony formation assay also indicated that PSII inhibited the proliferation of FaDu, Tu686, and Tu212 cells (**Figures 2D–I**).

PSII Reduced the Motility of HNSCC Cells

The analysis of tumor cell motility by transwell assays and cell scratch assays revealed, as shown in **Figure 3**, that the PSII extract inhibited migration and invasion in FaDu, Tu686, and Tu212 cells. In particular, the cell scratch assay results in **Figure 4** showed the inhibitory effect of PSII on these three HNSCC cell lines, and cell motility clearly decreased after treatment with 0.1 μg/ml PSII.

PSII Inhibited the Growth of HNSCC Microsphere Cells

We prepared SFM by adding 20 ng/ml bFGF, 20 ng/ml EGF, and 2% B27. After subculturing four times in this SFM, we calculated the pelletizing rate of tumor cells (≥100 μm), as shown in **Figure 5B**. Anti-CD24-FITC was used as a negative control, and the proportion of anti-CD44-PE/anti-CD133-APC cells in each group was determined by flow cytometry. The results shown in **Figures 5C,D** indicated that PSII suppressed the stemness of carcinoma cell stem microspheres.

PSII Significantly Reduced the Viability of Primary Tumor–Associated Fibroblasts

After we successfully isolated primary tumor–associated fibroblasts, we used immunofluorescence analysis to phenotypically identify these cells. We measured the

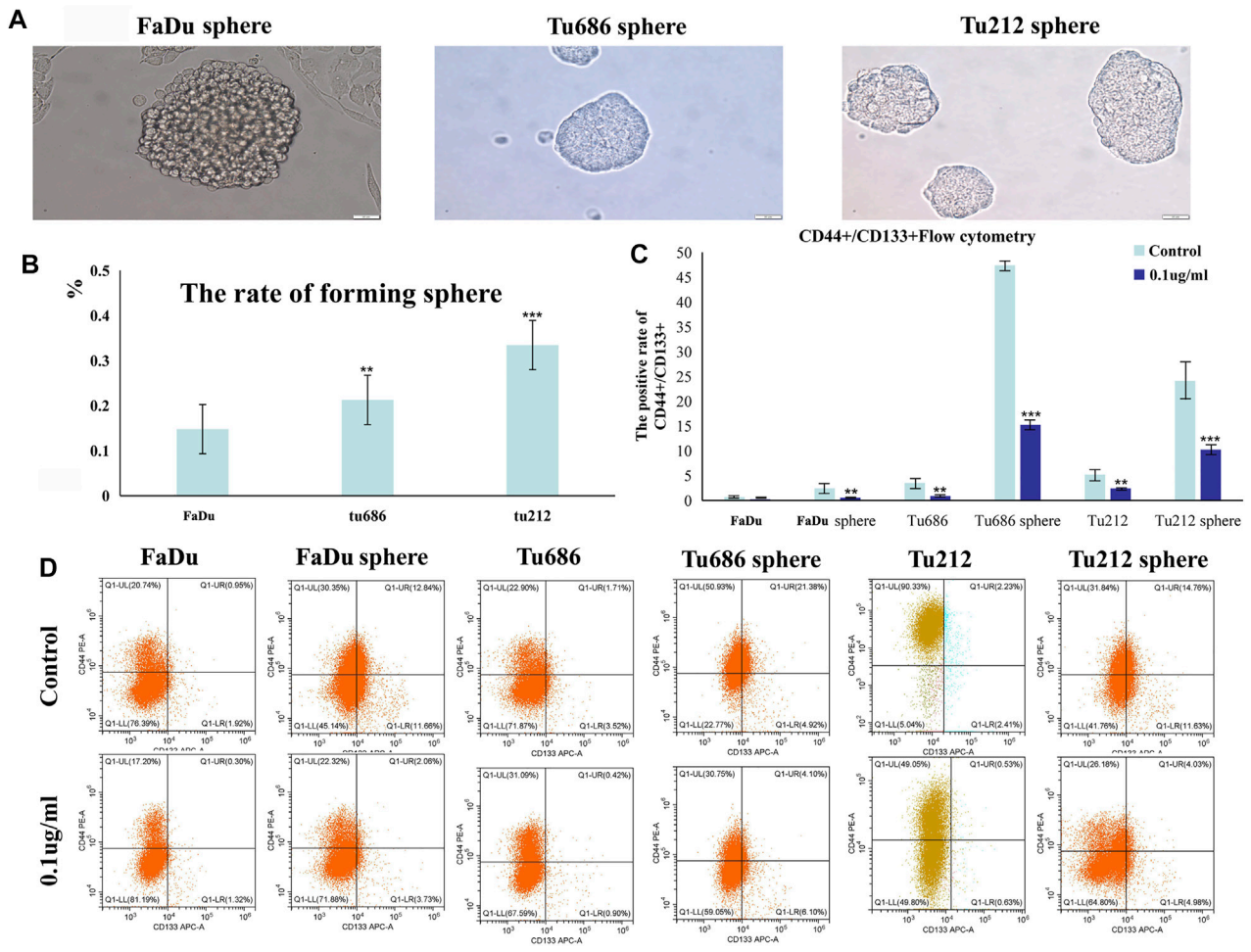

FIGURE 5 | Growth of human squamous cell carcinoma microsphere cells cultured in the serum-free medium. **(A)** Human squamous cell carcinoma spheres generated in SFM. **(B)** The statistical figure of forming sphere rate. **(C)** The positive rate of CD44+/CD133 + by flow cytometry. **(D)** Representative flow cytometry pictures of the cell stem are shown. Bars, 50 μm. All the experiments were carried out three times. The bar graphs and the table show quantification of the results, and each data represent the mean ± SD of three independent experiments (*p < 0.05; **p < 0.01; ***p < 0.001 vs the control group).

viability of the primary tumor–associated fibroblasts by the MTT assay. As shown in **Figure 6C**, treatment with PSII significantly reduced the viability of primary tumor–associated fibroblasts. In addition, the results of the migration assay shown in **Figure 6D** demonstrated the inhibitory effect of PSII on the migration ability of primary tumor–associated fibroblasts.

PSII Had an Impact on the Metabolites in HNSCC Cell Lines

Principal component analysis (PCA) performed on the peaks extracted from all experimental samples revealed, as shown in **Figures 10A,B**, that the experiments had good repeatability, as indicated by their close clustering together in positive and negative ion modes. All the metabolite tests in this study (identified with positive and negative ions) were classified and counted according to the attribution information of their chemical taxonomy. The proportions of various metabolites are shown in **Figures 10C,D**. The histograms used to visually display the identified multiple changes of significantly differentially expressed metabolites, and multiple analyses of significantly differentially expressed metabolites in positive and negative ion modes are shown in **Figures 10E,F**. The abscissa in the histogram graphs represents the differential expression multiple, red color represents the differential expression multiple greater than 1, and the green color represents the differential expression multiple less than 1. The ordinate indicates the significantly different metabolites.

NOS3 May Be a Downstream Target of PSII

Treatment of FaDu and Tu686 cells with PSII (0, 0.025, 0.05, and 0.1 ug/ml) for 48 h revealed, as shown in **Figure 7**, that the mRNA and protein expression levels of genes involved in the mitochondrial pathway (CytC), cell autophagy (Lc3b), and apoptosis (Bax, Bcl-2, and caspase-9) were all altered by

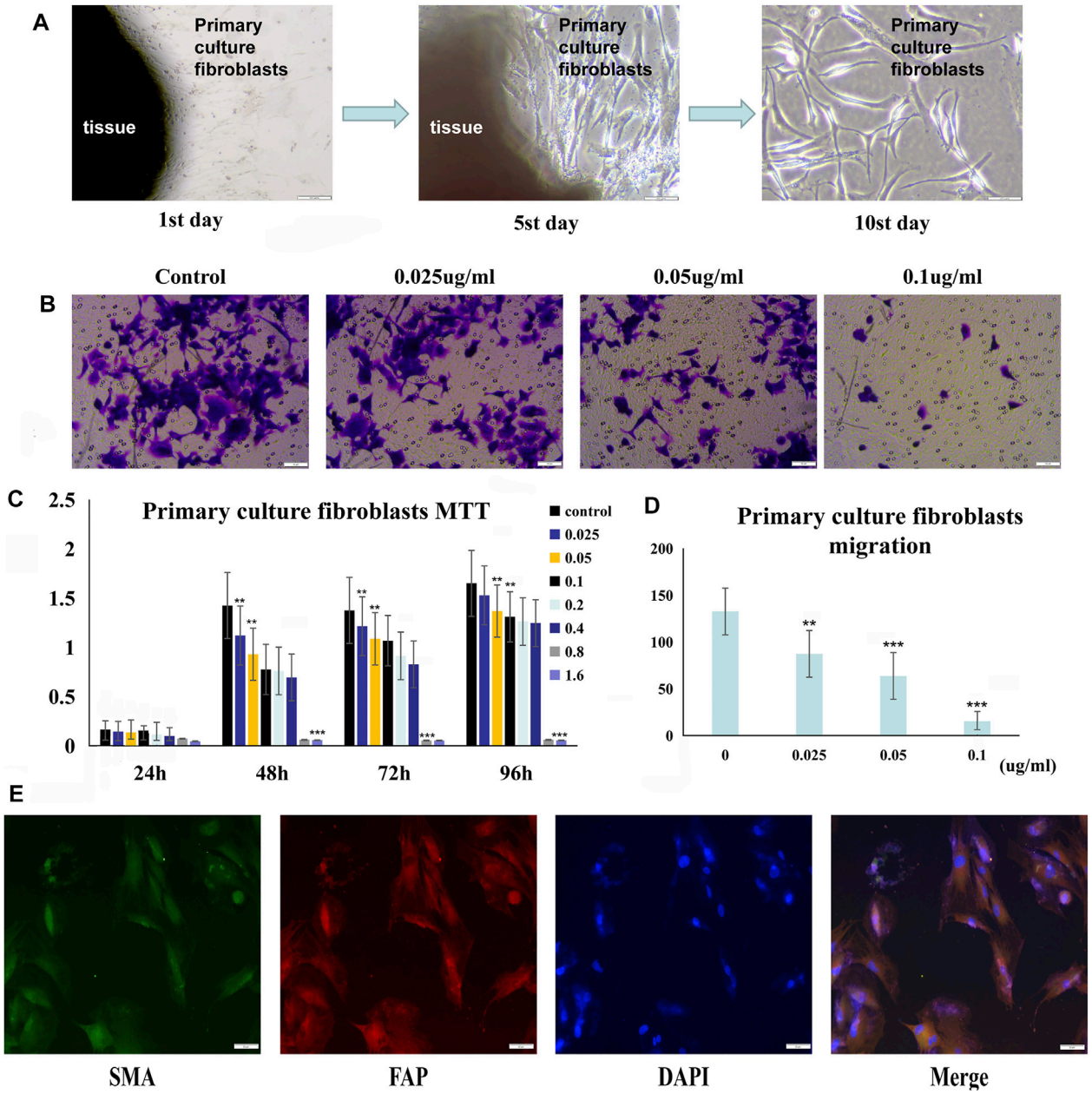

FIGURE 6 | PSII reduced the growth and motility of primary culture fibroblasts from head and neck tumor tissue. **(A)** The process of human squamous cell carcinoma primary culture fibroblasts as described in Materials and Methods. **(B)** The migration of cancer primary culture fibroblasts in a dose-dependent manner. **(C)** The MTT statistical figure of cancer primary culture fibroblasts in a dose- and time-dependent manner. **(D)** The migration statistical figure of cancer primary culture fibroblasts in a dose-dependent manner. **(E)** Immunofluorescence for identifying primary culture of fibroblasts. Cells were treated with the corresponding primary antibody against FAP, SMA, followed by incubation with appropriate secondary antibodies and all fibroblasts were stained with DAPI. Bars, 50 μm. All the experiments were carried out three times. The bar graphs and the table show quantification of the results, and each data represent the mean ± SD of three independent experiments (*$p < 0.05$; **$p < 0.01$; ***$p < 0.001$ vs the control group).

treatment with PSII. We used the Chinese Medicine Data website (http://herb.ac.cn/) to predict the target of PSII in cancer, and the result suggested many targets. Considering the metabolite results, we supposed that NOS3 may be a target. Additionally, NOS3 knockdown experiments using siRNA against NOS3 in HNSCC cells confirmed the effects of NOS3. Moreover, Western blot analysis confirmed that the protein expression levels of Bax, CytC, and Lc3b were decreased and that of Bcl-2 was increased when NOS3 expression was knocked down in FaDu and Tu686 cells (**Figures 8C,D**). These results confirmed that NOS3 is a downstream target of PSII in HNSCC.

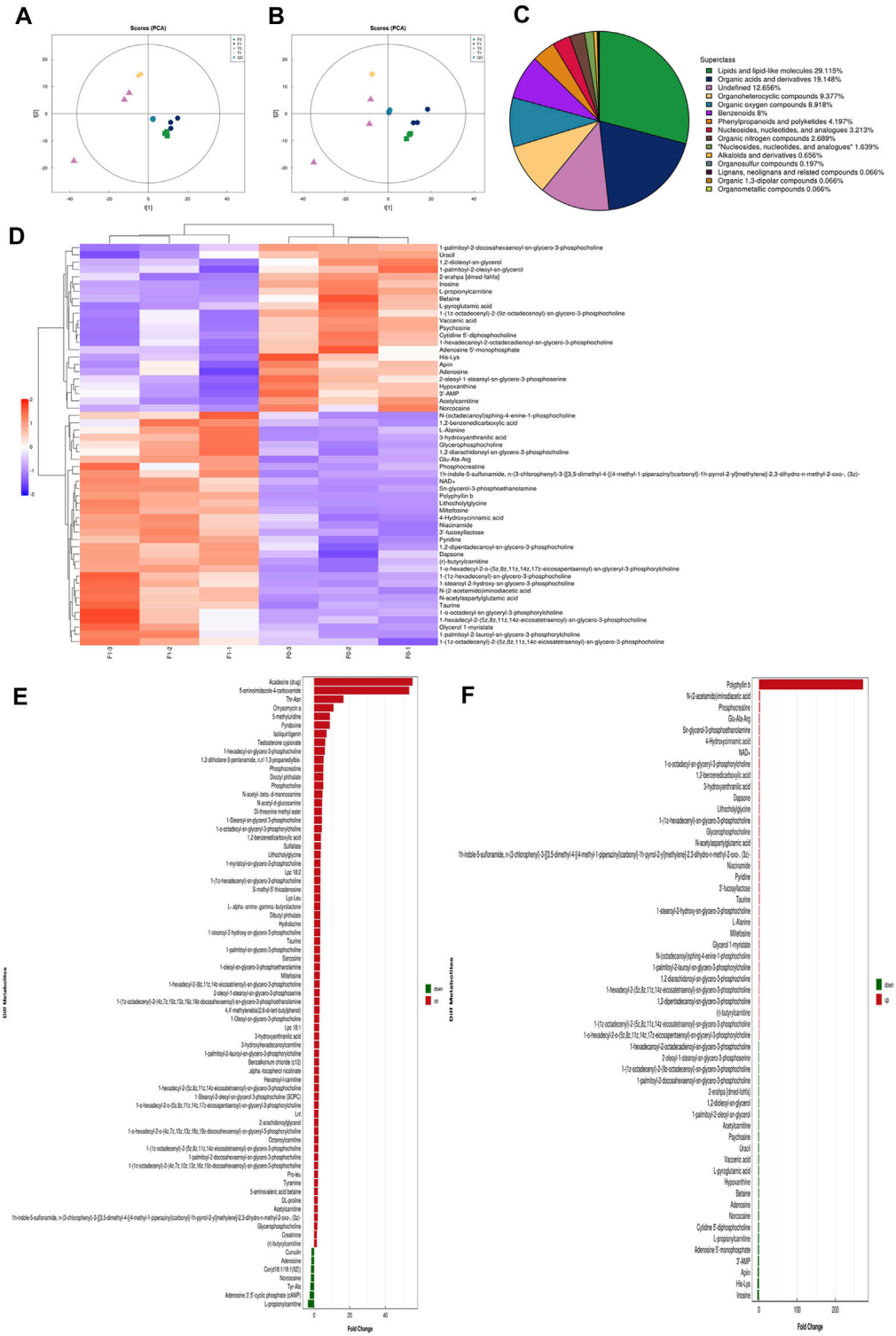

FIGURE 7 | High-resolution untargeted metabolomics analysis. **(A)** PCA analysis diagram of positive ion model population sample. **(B)** PCA analysis diagram of the total sample of anion mode. **(C)** The proportion of the number of various metabolites. **(D)** Hierarchical cluster heat map of significant differential metabolites. **(E)** Histogram of the identified multiple changes of significant differential metabolites, and multiple analyses of significant differential metabolite expression in positive ion mode. **(F)** Histogram of the identified multiple changes of significant metabolic differences and multiple analyses of metabolite expression in negative ion mode. All the experiments were carried out three times. Each data represent the mean ± SD of three independent experiments (*$p < 0.05$; **$p < 0.01$; ***$p < 0.001$ vs the control group).

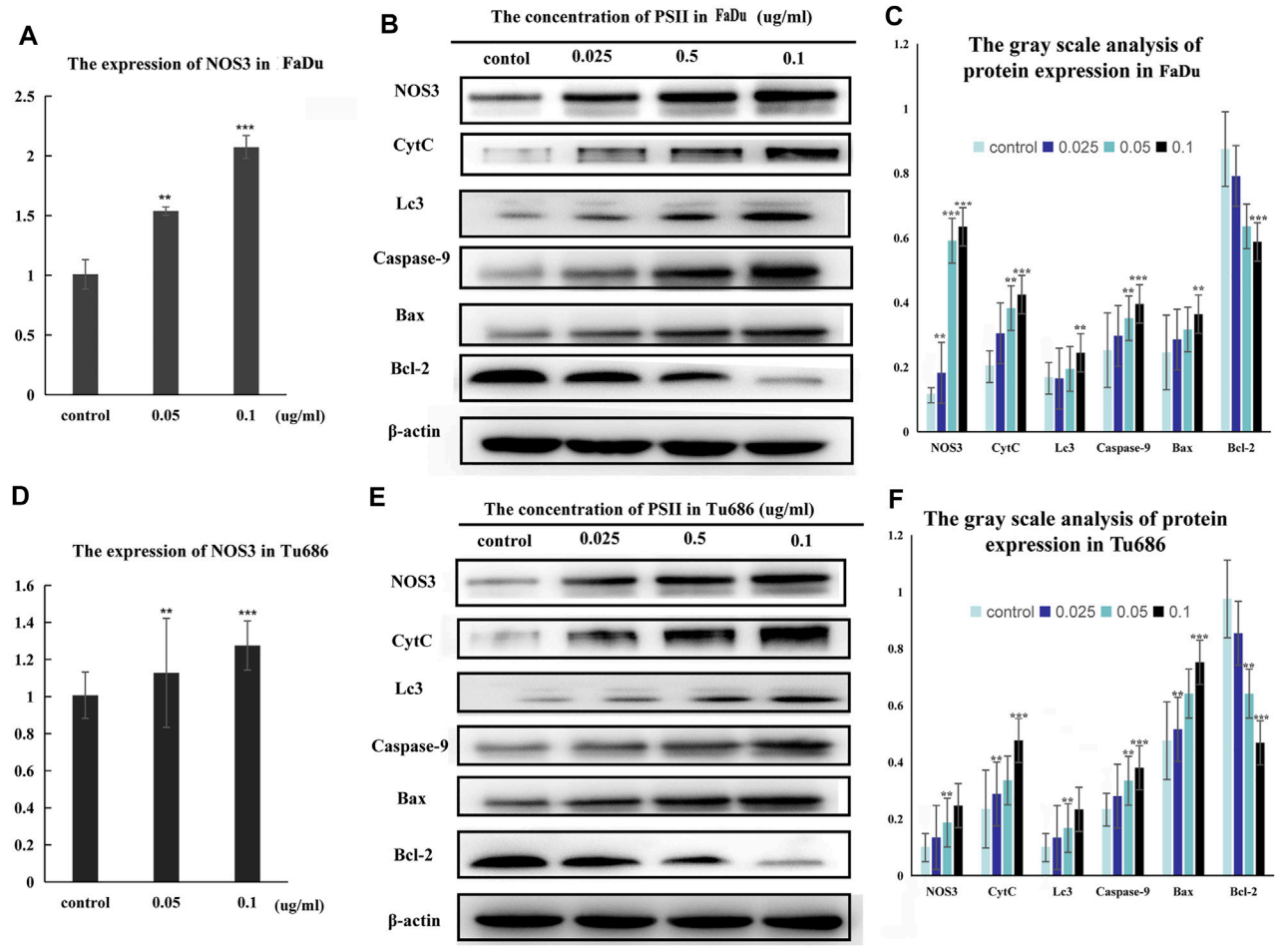

FIGURE 8 | Signal pathway inducted by PSII in HNSCC cells. **(A)** The mRNA expression of NOS3 in FaDu cells by RT-PCR assay. **(B)** PSII treatment induced apoptosis and autophagy by mitochondrial pathway (NOS3, CytC, Lc3, caspase-9, Bax, and Bcl-2) in FaDu cells. **(C)** The gray scale analysis of protein expression in FaDu cells by Western blot. **(D)** The expression of NOS3 mRNA in Tu686 cells by RT-PCR assay. **(E)** PSII treatment induced apoptosis and autophagy by mitochondrial pathway (NOS3, CytC, Lc3, caspase-9, Bax, and Bcl-2) in Tu686 cells. **(F)** The gray scale analysis of protein expression in Tu686 cells by Western blot. We used β-actin as control. All the experiments were carried out three times. Each data represent the mean ± SD of three independent experiments (*$p < 0.05$; **$p < 0.01$; ***$p < 0.001$ vs the control group).

PSII Inhibited the Growth of Subcutaneous Tumors by Regulating NOS3

We studied the inhibitory effect of PSII in an *in vivo* mouse tumor, which we developed by injecting Tu686 HNSCC cells into both sides of the flank of BALB nude mice. As shown in **Figures 9A,B**, the volume of xenograft tumor growth was significantly reduced after PSII treatment compared with the control group. On the 60th day, as shown in **Figure 9B**, the average volume of tumors in the PSII group (46.89 ± 3.99 mm^3) was smaller than that in the control groups (273.71 ± 10.07 mm^3), and there was no statistical difference in weight between the two groups. Our analysis of the protein levels of NOS3, Bcl-2, and Ki67 by IHC staining indicated, as shown in **Figure 9C**, that treatment with PSII led to decreased protein levels of Bcl-2 and Ki67 and an increased protein level of NOS3. Furthermore, the histopathological examination showed that PSII had no adverse effects on the lung, heart, spleen, liver, and kidney. Additionally, the Western blot analysis of mouse tumors showed that the inhibitory effect of PSII on the growth of subcutaneous tumors is mediated through the mitochondrial pathway, cell autophagy, and apoptosis. All the *in vivo* results indicated that PSII induced autophagy and apoptosis in HNSCC cells.

DISCUSSION

In 2018, there were more than 5,80,000 newly diagnosed cases of HNSCC. However, despite advances in therapeutic approaches, survival rates remain poor for patients with HNSCC (Jung et al., 2020; Kitamura et al., 2020). More than half of HNSCC patients suffer relapse, and most die from distant metastasis, and lymph nodes metastases play an important role (Shah et al., 2020; Wang et al., 2020). Therefore, it is important to fully understand the molecular signaling pathways that contribute to HNSCC

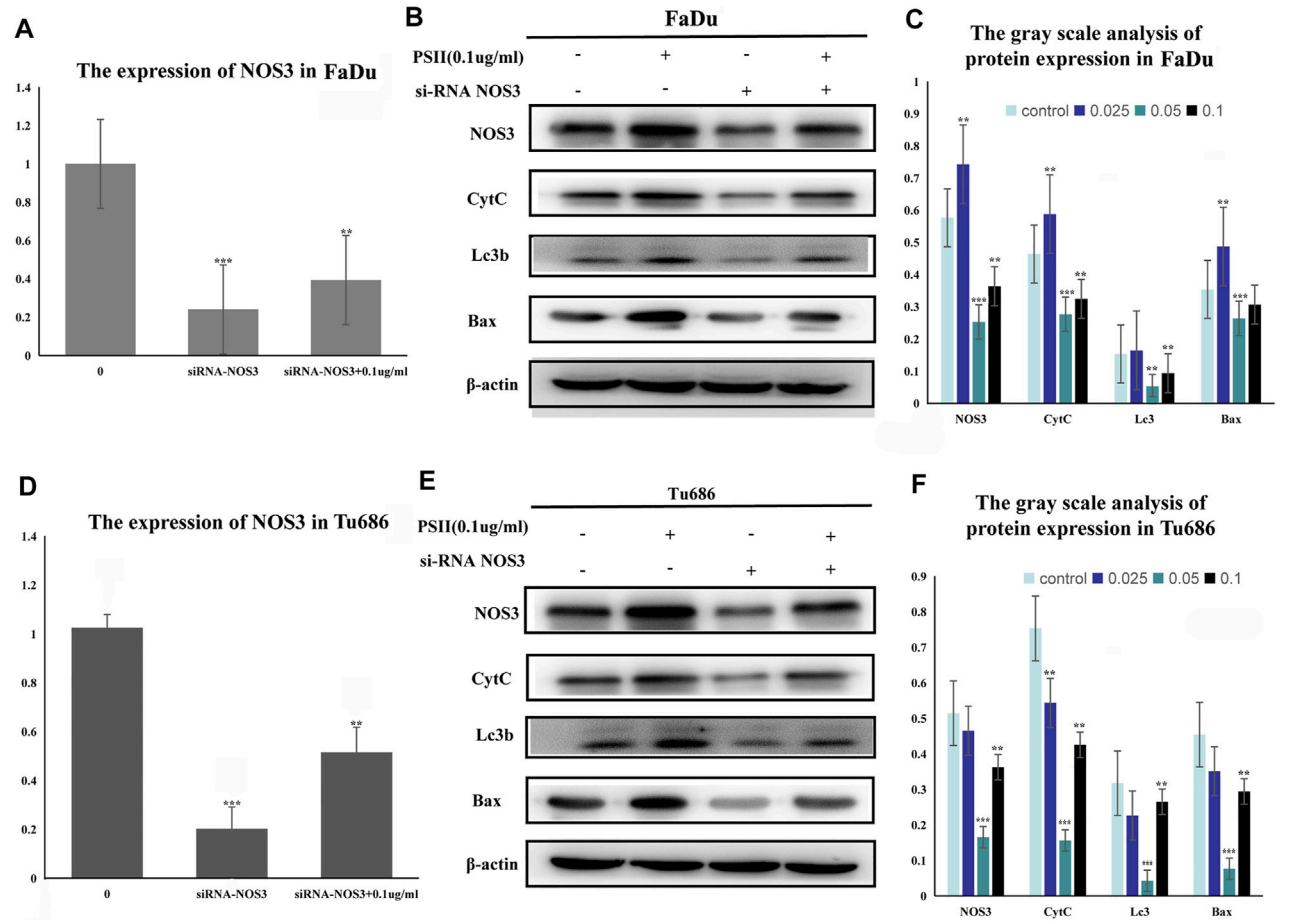

FIGURE 9 | Inhibitive effect of PSII on human squamous cell carcinoma cells by targeting NOS3. **(A)** The mRNA expression of NOS3 in FaDu cells by RT-PCR assay after transfection. **(B)** The transfection of NOS3 siRNA reversed the protein expression induced by PSII (NOS3, CytC, Lc3b, and Bax) in FaDu cells. **(C)** The gray scale analysis of protein expression in FaDu cells by Western blot. **(D)** The mRNA expression of NOS3 in Tu686 cells by RT-PCR assay after transfection. **(E)** The transfection of NOS3 siRNA reversed the protein expression induced by PSII (NOS3, CytC, Lc3b, and Bax) in Tu686 cells. **(F)** The gray scale analysis of protein expression in Tu686 cells by Western blot. We used β-actin as control. All the experiments were carried out three times. Each data represent the mean ± SD of three independent experiments (*$p < 0.05$; **$p < 0.01$; ***$p < 0.001$ vs the control group).

proliferation and metastasis in order to develop more effective therapeutic methods.

For thousands of years, Paridis saponin (PS) and its components have always been used as hemostatic regulatory, antifungal, anti-inflammatory, antimicrobial, and antibacterial medications in China (White et al., 2015; Moldogazieva et al., 2018). Recent studies have reported promising roles of PS in the regulation of glycolytic and lipid metabolism (Man et al., 2017; Man et al., 2020). In addition, the PSII extract has been approved as an antitumor agent for many years in China, but its mechanism of action is not well understood. In our research, we investigated the therapeutic effects of PSII on various HNSCC cells and showed that PSII can inhibit the viability and motility of HNSCC cell lines (**Figures 2–4**), cancer stem cells (**Figure 5**), and primary cultured fibroblasts (**Figure 6**).

Sixty years ago, researchers found that cancer cells could reprogram their metabolic capability to develop metastastic potential. Metabolism plays an increasingly important role in cancer development and has become a new research field. From the research on metabolism, researchers have found promising approaches for development of cancer therapies (Lee et al., 2012; Zuo and Wan, 2019). In order to detect the metabolites affected by PSII, we performed untargeted metabolomics analyses of three HNSCC cell lines with/without PSII. The metabolites in the samples were detected by UHPLC-Q-TOF-MS. The retention time and molecular weight of the metabolites in the samples were compared with those in the local database. From the proportion of various metabolites shown in **Figures 10C,D**, we were able to find some key differentially expressed metabolic enzymes, such as hexokinases (HKs), phosphoglycerate kinase (PGK), pyruvate kinases (PK), and lactate dehydrogenase (LDH), which have been found to be closely related to tumor aerobic glycolysis (Zhang et al., 2018; Shi et al., 2019; Yeung et al., 2019). In addition, metabolites in the PSII-treated group showed significant differences compared with those in the control group.

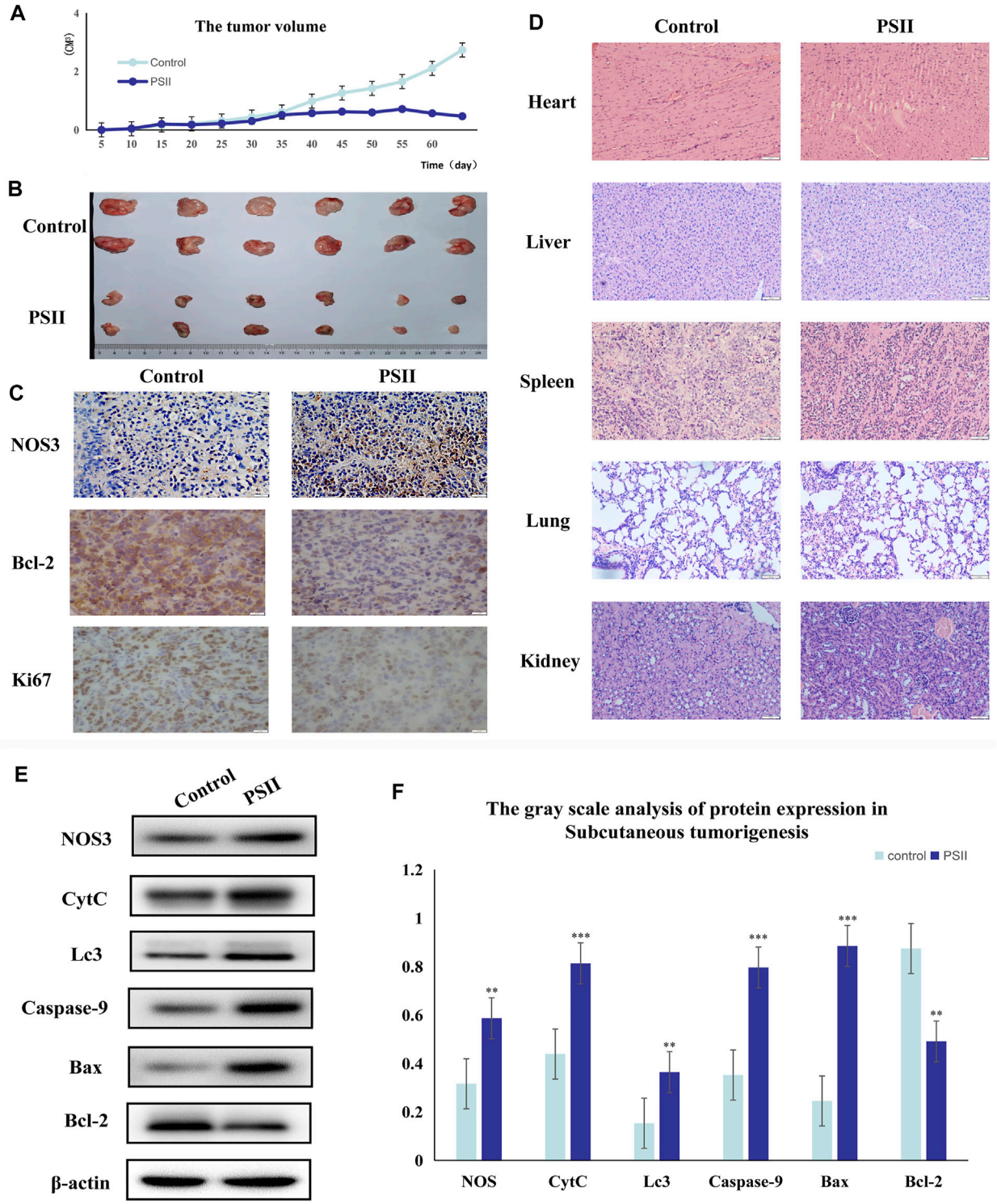

FIGURE 10 | Suppression of tumorigenesis in a xenograft model. **(A)** Growth curves of the volumes of xenograft tumors after the injection of Tu686 cells. **(B)** The representative tumor pictures. **(C)** IHC analysis of NOS3, Bcl-2, and Ki67. **(D)** Histopathological examination of the lung, heart, kidney, liver, and spleen. **(E)** The protein expression of tumorigenesis in a xenograft model by Western blot analysis. **(F)** The gray scale analysis of protein expression in Tu686 cells by Western blot. Bars, 50 μm. All the experiments were carried out three times. The bar graphs and the table show quantification of the results, and each data represent the mean ± SD of three independent experiments (*$p < 0.05$; **$p < 0.01$; ***$p < 0.001$ vs the control group).

Additionally, we predicted a downstream target of PSII in cancer using the Chinese Medicine Data Website (http://herb.ac.cn/), which is a high-throughput experiment- and reference-guided database of TCM compounds. From this website, we identified potential targets of PSII, such as AHSA1, NOS3, IKBKB, and BCL2. Cross-analysis with metabolomics results revealed that the NOS3-mediated energy metabolism pathway may be the pathway mediating the effects of PSII. Endothelial nitric oxide synthase (NOS3) is an important member of the nitric oxide synthase (NOS) enzyme family that plays an important role in nitric oxide (NO) production. The biological function of NOS enzymes and the activity of NO have been the focus of cancer research for many years. NO metabolism plays an important role in various stages of tumor development, such as in oncogene activation, inhibition of DNA repair enzymes, DNA damage, and tumor suppressor genes, as well as the regulation of apoptosis and metastasis. For many years, the dual role of NO in cancer has been recognized, and more and more studies are investigating deeper mechanisms. The inhibition of oxidative phosphorylation in tumor cells was found to lead to elevated glycolytic metabolism (Ghashghaeinia et al., 2019; Najjar et al., 2019). Compared with their differentiated offspring, stem cells rely more on glycolysis which preferentially metabolizes lactate via mitochondrial respiration (Deshmukh et al., 2016; Liang et al., 2020), indicating that the changes occurring in metabolism occur earlier than those in stemness (Shyh-Chang et al., 2013). In recent years, NOS3 has been found to play various roles in malignant tumors. For instance, NOS3 is closely related to oxidative stress, autophagy, and energy metabolism. In our project, we examined the effects of NOS3 with siRNA targeting its expression in HNSCC cells. Moreover, the Western blot analysis indicated that the expression of Bax, CytC, and Lc3b as well as partially could be reversed in FaDu and Tu686 cells (**Figures 8C,D**). These results confirmed that NOS3 was a downstream target of the PSII extract treatment in HNSCC. Also, as shown in **Figure 7**, the mRNA and proteins expression levels of genes involved in the mitochondrial pathway (CytC), cell autophagy (Lc3b), and apoptosis (Bax, Bcl-2, and caspase-9) were all changed after PSII treatment. In order to determine the curative effect of PSII *in vivo*, Tu686 HNSCC cells were subcutaneously injected into the nude mice. The volume of xenograft tumor was suppressed after PSII treatment as shown in **Figure 9**. To examine the mechanism through which PSII exerts its effects *in vivo*, we measured NOS3, Bcl-2, and Ki67 protein expression by immunohistochemical staining. In addition, the histopathological examination showed that PSII had no adverse effects on the heart, liver, spleen, lung, and kidney. These results suggested that PSII extract induced autophagy and apoptosis in HNSCC cells *in vivo* with no side effects on organs.

As mentioned earlier, the TME, which includes CSCs, fibroblasts, metabolites, and various kinds of immune cells (Reina-Campos et al., 2017; García-Cañaveras et al., 2019; Li et al., 2019), can affect many steps of tumor development, including immune escape, distant metastasis, drug resistance, and recurrence (Batlle and Clevers, 2017; Jahanafrooz et al., 2020). Redox signaling and oxidative stress are major components of the TME that could regulate various kinds of metabolites (Catalano et al., 2013; Moldogazieva et al., 2018; Bonanno et al., 2019). Mitochondria are both generators and targets of ROS, so oxidative stress plays an important role in mitochondrial dysfunction. Mitochondrial turnover is dependent on autophagy, which declines with age and is frequently dysfunctional in cancer (White et al., 2015). Autophagy is also necessary to recycle ferritin, and autophagy defects cause perturbation in iron homeostasis that increases susceptibility to oxidative stress. The crosstalk between autophagy, redox signaling, and mitochondrial dysfunction is not well understood (Lee et al., 2012).

In this work, we reported that PSII could inhibit the viability and motility of HNSCC cell lines, cancer stem cells, and primary cultured fibroblasts from the tissue through the mitochondrial pathway by targeting NOS3 as well as inducing autophagy and apoptosis through a series of changes of metabolites *in vivo* and *in vitro*. Our study indicated that PSII may be a novel strategy for HNSCC, and the metabonomics method can be a novel tool to investigate and establish the antitumor effects of TCM preparations.

DATA AVAILABILITY STATEMENT

The original contributions presented in the study are included in the article/supplementary files; further inquiries can be directed to the corresponding author.

ETHICS STATEMENT

The studies involving human participants were reviewed and approved by the Biomedical Research Ethic Committee of Shandong Provincial Hospital. The patients/participants provided their written informed consent to participate in this study. The animal study was reviewed and approved by the Ethics Committee of Cheeloo College of Medicine, Shandong University.

AUTHOR CONTRIBUTIONS

WQ drafted the important content of the manuscript and explained it, and carried out rigorous conception and design of the subject. FZ, MW, ZT, and RX carried out a detailed analysis of the data in the article. YX, QM, HZ, and XW carried out the collection of clinical samples. XH, BW, XL, and CL conducted experimental operations. In addition, XZ, FX, and MX provided the subject ideas and careful proofreading of the manuscript.

FUNDING

This work was supported by the grants from the Medical Science and Technology Innovation Center, Shandong First Medical University and Shandong Academy of Medical Sciences, the National Natural Science Foundation of China (#81770979, #82071013, #81900922, #82071035), the Key Research and Development Program Foundation of Shandong Province (2018GSF118091), Natural Science Foundation of Shandong Province (Grant No. ZR2019BH019), and the Taishan Young Expert Scholars Fund (#tsqn201812134).

REFERENCES

Batlle, E., and Clevers, H. (2017). Cancer Stem Cells Revisited. *Nat. Med.* 623 (10), 1124–1134. doi:10.1038/nm.4409

Battaglia, A. M., Chirillo, R., Sacco, I. A., Costanzo, F., and Biamonte, F. (2020). Ferroptosis and Cancer: Mitochondria Meet the "Iron Maiden" Cell Death. *Cells.* 9 (6), 1505. doi:10.3390/cells9061505

Bonanno, L., Zulato, E., Pavan, A., Attili, I., Pasello, G., Conte, P., et al. (2019). LKB1 and Tumor Metabolism: The Interplay of Immune and Angiogenic Microenvironment in Lung Cancer. *Int. J. Mol. Sci.* 1620 (8), 1874. doi:10.3390/ijms20081874

Catalano, V., Turdo, A., Di Franco, S., Dieli, F., Todaro, M., and Stassi, G. (2013). Tumor and its Microenvironment: a Synergistic Interplay. *Semin. Cancer Biol.* 23 (6 Pt B), 522–532. doi:10.1016/j.semcancer.2013.08.007

Chang, J., Li, H., Zhu, Z., Mei, P., Hu, W., Xiong, X., et al. (2021). microRNA-21-5p from M2 Macrophage-Derived Extracellular Vesicles Promotes the Differentiation and Activity of Pancreatic Cancer Stem Cells by Mediating KLF3. *Cell Biol Toxicol.* 17 (6). doi:10.1007/s10565-021-09597-x

Chen, L., Yang, Q.-C., Li, Y.-C., Yang, L.-L., Liu, J.-F., Li, H., et al. (2020). Targeting CMTM6 Suppresses Stem Cell-Like Properties and Enhances Antitumor Immunity in Head and Neck Squamous Cell Carcinoma. *Cancer Immunol. Res.* 8 (2), 179–191. doi:10.1158/2326-6066.CIR-19-0394

Cheng, Z.-X., Liu, B.-R., Qian, X.-P., Ding, Y.-T., Hu, W.-J., Sun, J., et al. (2008). Proteomic Analysis of Anti-Tumor Effects by Rhizoma Paridis Total Saponin Treatment in HepG2 Cells. *J. Ethnopharmacology.* 20120 (2), 129–137. doi:10.1016/j.jep.2008.07.030

Deshmukh, A., Deshpande, K., Arfuso, F., Newsholme, P., and Dharmarajan, A. (2016). Cancer Stem Cell Metabolism: a Potential Target for Cancer Therapy. *Mol. Cancer.* 15 (151), 69. doi:10.1186/s12943-016-0555-x

Ferro, F., Servais, S., Besson, P., Roger, S., Dumas, J.-F., and Brisson, L. (2020). Autophagy and Mitophagy in Cancer Metabolic Remodelling. *Semin. Cell Developmental Biol.* 98, 129–138. doi:10.1016/j.semcdb.2019.05.029

García-Cañaveras, J. C., Chen, L., and Rabinowitz, J. D. (2019). The Tumor Metabolic Microenvironment: Lessons From Lactate. *Cancer Res.* 79 (13), 3155–3162. doi:10.1158/0008-5472.CAN-18-3726

Ghashghaeinia, M., Köberle, M., Mrowietz, U., and Bernhardt, I. (2019). Proliferating Tumor Cells Mimick Glucose Metabolism of Mature Human Erythrocytes. *Cell Cycle.* 18 (12), 1316–1334. doi:10.1080/15384101.2019.1618125

Gilardi, M., Wang, Z., Proietto, M., Chillà, A., Calleja-Valera, J. L., Goto, Y., et al. (2020). Tipifarnib as a Precision Therapy for HRAS-Mutant Head and Neck Squamous Cell Carcinomas. *Mol. Cancer Ther.* 19 (9), 1784–1796. doi:10.1158/1535-7163.MCT-19-0958

HammermanHammerman, P. S., Hayes, D. N., and Grandis, J. R. (2015). Therapeutic Insights From Genomic Studies of Head and Neck Squamous Cell Carcinomas. *Cancer Discov.* 5 (3), 239–244. doi:10.1158/2159-8290.CD-14-1205

Hinshaw, D. C., and Shevde, L. A. (2019). The Tumor Microenvironment Innately Modulates Cancer Progression. *Cancer Res.* 1579 (18), 4557–4566. doi:10.1158/0008-5472.CAN-18-3962

Hsu, C.-C., Tseng, L.-M., and Lee, H.-C. (2016). Role of Mitochondrial Dysfunction in Cancer Progression. *Exp. Biol. Med. (Maywood).* 241 (12), 1281–1295. doi:10.1177/1535370216641787

Jahanafrooz, Z., Mosafer, J., Akbari, M., Hashemzaei, M., Mokhtarzadeh, A., and Baradaran, B. (2020). Colon Cancer Therapy by Focusing on Colon Cancer Stem Cells and Their Tumor Microenvironment. *J. Cell Physiol.* 235 (5), 4153–4166. doi:10.1002/jcp.29337

Jin, N., Bi, A., Lan, X., Xu, J., Wang, X., Liu, Y., et al. (2019). Identification of Metabolic Vulnerabilities of Receptor Tyrosine Kinases-Driven Cancer. *Nat. Commun.* 10 (1), 2701. doi:10.1038/s41467-019-10427-2

Johnson, D. E., Burtness, B., Leemans, C. R., Lui, V. W. Y., Bauman, J. E., and Grandis, J. R. (2020). Head and Neck Squamous Cell Carcinoma. *Nat. Rev. Dis. Primers.* 106 (1), 92. doi:10.1038/s41572-020-00224-3

Jung, K., Narwal, M., Min, S. Y., Keam, B., and Kang, H. (2020). Squamous Cell Carcinoma of Head and Neck: What Internists Should Know. *Korean J. Intern. Med.* 35 (5), 1031–1044. doi:10.3904/kjim.2020.078

Kitamura, N., Sento, S., Yoshizawa, Y., Sasabe, E., Kudo, Y., and Yamamoto, T. (2020). Current Trends and Future Prospects of Molecular Targeted Therapy in Head and Neck Squamous Cell Carcinoma. *Int. J. Mol. Sci.* 22 (221), 240. doi:10.3390/ijms22010240

Lee, J., Giordano, S., and Zhang, J. (2012). Autophagy, Mitochondria and Oxidative Stress: Cross-Talk and Redox Signalling. *Biochem. J.* 15441 (2), 523–540. doi:10.1042/BJ20111451

Li, X., Kumar, A., and Carmeliet, P. (2019). Metabolic Pathways Fueling the Endothelial Cell Drive. *Annu. Rev. Physiol.* 81 (81), 483–503. doi:10.1146/annurev-physiol-020518-114731

Liang, R., Arif, T., Kalmykova, S., Kasianov, A., Lin, M., Menon, V., et al. (2020). Restraining Lysosomal Activity Preserves Hematopoietic Stem Cell Quiescence and Potency. *Cell Stem Cell.* 526 (3), 359–376. e7. doi:10.1016/j.stem.2020.01.013

Lin, Y., Jiang, M., Chen, W., Zhao, T., and Wei, Y. (2019). Cancer and ER Stress: Mutual Crosstalk Between Autophagy, Oxidative Stress and Inflammatory Response. *Biomed. Pharmacother.* 118, 109249. doi:10.1016/j.biopha.2019.109249

Luo, Y., Ma, J., and Lu, W. (2020). The Significance of Mitochondrial Dysfunction in Cancer. *Int. J. Mol. Sci.* 521 (16), 5598. doi:10.3390/ijms21165598

Man, S., Li, J., Fan, W., Chai, H., Liu, Z., and Gao, W. (2015). Inhibition of Pulmonary Adenoma in Diethylnitrosamine-Induced Rats by Rhizoma Paridis Saponins. *J. Steroid Biochem. Mol. Biol.* 154, 62–67. doi:10.1016/j.jsbmb.2015.07.004

Man, S., Lv, P., Cui, J., Liu, F., Peng, L., Ma, L., et al. (2020). Paris Saponin II-Induced Paraptosis-Associated Cell Death Increased the Sensitivity of Cisplatin. *Toxicol. Appl. Pharmacol.* 406, 406115206. doi:10.1016/j.taap.2020.115206

Man, S., Qiu, P., Li, J., Zhang, L., and Gao, W. (2017). Global Metabolic Profiling for the Study of Rhizoma Paridis Saponins-Induced Hepatotoxicity in Rats. *Environ. Toxicol.* 32 (1), 99–108. doi:10.1002/tox.22215

Moldogazieva, N. T., Mokhosoev, I. M., Feldman, N. B., and Lutsenko, S. V. (2018). ROS and RNS Signalling: Adaptive Redox Switches through Oxidative/Nitrosative Protein Modifications. *Free Radic. Res.* 52 (5), 507–543. doi:10.1080/10715762.2018.1457217

Najjar, Y. G., Najjar, A. V., Sander, C., Rao, U., Karunamurthy, A., Bhatia, R., et al. (2019). Tumor Cell Oxidative Metabolism as a Barrier to PD-1 Blockade Immunotherapy in Melanoma. *JCI Insight.* 4 (45), e124989. doi:10.1172/jci.insight.124989

Reina-Campos, M., Moscat, J., and Diaz-Meco, M. (2017). Metabolism Shapes the Tumor Microenvironment. *Curr. Opin. Cell Biol.* 48, 47–53. doi:10.1016/j.ceb.2017.05.006

Sak, K., and Everaus, H. (2015). Role of Flavonoids in Future Anticancer Therapy by Eliminating the Cancer Stem Cells. *Cscr.* 10 (3), 271–282. doi:10.2174/1574888x10666141126122316

Saki, M., and Prakash, A. (20172017). DNA Damage Related Crosstalk Between the Nucleus and Mitochondria. *Free Radic. Biol. Med.* 107, 216–227. doi:10.1016/j.freeradbiomed.2016.11.050

Schinke, H., Heider, T., Herkommer, T., Simon, F., Blancke Soares, A., Kranz, G., et al. (2021). Digital Scoring of EpCAM and Slug Expression as Prognostic Markers in Head and Neck Squamous Cell Carcinomas. *Mol. Oncol.* 15 (4), 1040–1053. doi:10.1002/1878-0261.12886

Shah, P. A., Huang, C., Li, Q., Kazi, S. A., Byers, L. A., Wang, J., et al. (2020). NOTCH1 Signaling in Head and Neck Squamous Cell Carcinoma. *Cells.* 9 (12), 2677. doi:10.3390/cells9122677

Shi, T., Ma, Y., Cao, L., Zhan, S., Xu, Y., Fu, F., et al. (2019). B7-H3 Promotes Aerobic Glycolysis and Chemoresistance in Colorectal Cancer Cells by Regulating HK2. *Cell Death Dis.* 10 (4), 308. doi:10.1038/s41419-019-1549-6

Shyh-Chang, N., DaleyDaley, G. Q., and Cantley, L. C. (2013). Stem Cell Metabolism in Tissue Development and Aging. *Development.* 140 (12), 2535–2547. doi:10.1242/dev.091777

Supsavhad, W., Dirksen, W. P., Martin, C. K., and Rosol, T. J. (2016). Animal Models of Head and Neck Squamous Cell Carcinoma. *Vet. J.* 210, 7–16. doi:10.1016/j.tvjl.2015.11.006

Tripathi, D., Nam, A., Oldenburg, D. J., and Bendich, A. J. (2020). Reactive Oxygen Species, Antioxidant Agents, and DNA Damage in Developing Maize Mitochondria and Plastids. *Front. Plant Sci.* 11, 11596. doi:10.3389/fpls.2020.00596

Vitale, I., Manic, G., Coussens, L. M., Kroemer, G., and Galluzzi, L. (2019). Macrophages and Metabolism in the Tumor Microenvironment. *Cell Metab.* 30 (1), 36–50. doi:10.1016/j.cmet.2019.06.001

Wang, J., Chen, X., Tian, Y., Zhu, G., Qin, Y., Chen, X., et al. (2020). Six-Gene Signature for Predicting Survival in Patients With Head and Neck Squamous Cell Carcinoma. *Aging.* 12 (1), 767–783. doi:10.18632/aging.102655

White, E., MehnertMehnert, J. M., and ChanChan, C. S. (2015). Autophagy, Metabolism, and Cancer. *Clin. Cancer Res.* 1521 (22), 5037–5046. doi:10.1158/1078-0432.CCR-15-0490

Wu, T., and Dai, Y. (2017). Tumor Microenvironment and Therapeutic Response. *Cancer Lett.* 387 (387), 61–68. doi:10.1016/j.canlet.2016.01.043

Xiao, X., Bai, P., Bui NguyenNguyen, T. M., Xiao, J., Liu, S., Yang, G., et al. (2009). The Antitumoral Effect of Paris Saponin I Associated With the Induction of Apoptosis Through the Mitochondrial Pathway. *Mol. Cancer Ther.* 8 (5), 1179–1188. doi:10.1158/1535-7163.MCT-08-0939

Yeung, C., Gibson, A. E., IssaqIssaq, S. H., Oshima, N., Baumgart, J. T., Edessa, L. D., et al. (2019). Targeting Glycolysis Through Inhibition of Lactate Dehydrogenase Impairs Tumor Growth in Preclinical Models of Ewing Sarcoma. *Cancer Res.* 79 (19), 5060–5073. doi:10.1158/0008-5472.CAN-19-0217

Zhang, Y., Yu, G., Chu, H., Wang, X., Xiong, L., Cai, G., et al. (2018). Macrophage-Associated PGK1 Phosphorylation Promotes Aerobic Glycolysis and Tumorigenesis. *Mol. Cell.* 1971 (2), 201–215. e7. doi:10.1016/j.molcel.2018.06.023

Zuo, H., and Wan, Y. (2019). Metabolic Reprogramming in Mitochondria of Myeloid Cells. *Cells.* 9 (1), 5. doi:10.3390/cells9010005

Conflict of Interest: The authors declare that the research was conducted in the absence of any commercial or financial relationships that could be construed as a potential conflict of interest.

Publisher's Note: All claims expressed in this article are solely those of the authors and do not necessarily represent those of their affiliated organizations, or those of the publisher, the editors, and the reviewers. Any product that may be evaluated in this article, or claim that may be made by its manufacturer, is not guaranteed or endorsed by the publisher.

frontiers in Genetics

ORIGINAL RESEARCH
published: 09 February 2022
doi: 10.3389/fgene.2021.804248

Metabolomic Profiling Reveals That 5-Hydroxylysine and 1-Methylnicotinamide Are Metabolic Indicators of Keloid Severity

Mengjie Shan[1,2], *Hao Liu*[1,2], *Yan Hao*[1,2], *Kexin Song*[1], *Tian Meng*[1], *Cheng Feng*[1], *Youbin Wang*[1]* *and Yongsheng Huang*[2]*

[1]*Department of Plastic Surgery, Peking Union Medical College Hospital, Beijing, China,* [2]*Graduate School, Chinese Academy of Medical Sciences and Peking Union Medical College, Beijing, China*

OPEN ACCESS

Edited by:
Xuyun Zhao,
Shanghai Jiao Tong University, China

Reviewed by:
Richard B. Parsons,
King's College London,
United Kingdom
Wentao Zhu,
China Agricultural University, China

***Correspondence:**
Youbin Wang
wybenz@sina.com
Yongsheng Huang
yongsheng@ibms.pumc.edu.cn

Specialty section:
This article was submitted to Epigenomics and Epigenetics, a section of the journal Frontiers in Genetics

Received: *29 October 2021*
Accepted: *28 December 2021*
Published: *09 February 2022*

Citation:
Shan M, Liu H, Hao Y, Song K, Meng T, Feng C, Wang Y and Huang Y (2022) Metabolomic Profiling Reveals That 5-Hydroxylysine and 1-Methylnicotinamide Are Metabolic Indicators of Keloid Severity. Front. Genet. 12:804248. doi: 10.3389/fgene.2021.804248

Background: Keloid is a skin fibroproliferative disease with unknown pathogenesis. Metabolomics provides a new perspective for revealing biomarkers related to metabolites and their metabolic mechanisms.

Method: Metabolomics and transcriptomics were used for data analysis. Quality control of the data was performed to standardize the data. Principal component analysis (PCA), PLS-DA, OPLS-DA, univariate analysis, CIBERSORT, neural network model, and machine learning correlation analysis were used to calculate differential metabolites. The molecular mechanisms of characteristic metabolites and differentially expressed genes were identified through enrichment analysis and topological analysis.

Result: Compared with normal tissue, lipids have a tendency to decrease in keloids, while peptides have a tendency to increase in keloids. Significantly different metabolites between the two groups were identified by random forest analysis, including 1-methylnicotinamide, 4-hydroxyproline, 5-hydroxylysine, and L-prolinamide. The metabolic pathways which play important roles in the pathogenesis of keloids included arachidonic acid metabolism and D-arginine and D-ornithine metabolism. Metabolomic profiling reveals that 5-hydroxylysine and 1-methylnicotinamide are metabolic indicators of keloid severity. The high-risk early warning index for 5-hydroxylysine is 4×10^8-6.3×10^8 ($p = 0.0008$), and the high-risk predictive index for 1-methylnicotinamide is 0.95×10^7-1.6×10^7 ($p = 0.0022$).

Conclusion: This study was the first to reveal the metabolome profile and transcriptome of keloids. Differential metabolites and metabolic pathways were calculated by machine learning. Metabolomic profiling reveals that 5-hydroxylysine and 1-methylnicotinamide may be metabolic indicators of keloid severity.

Keywords: keloid, metabolomic, random forest, PLS-DA, machine learning, neural network model

1 INTRODUCTION

Keloid is a pathological fibroproliferative disease (Ogawa, 2017). Its characteristics of invasion and migration to surrounding tissues are similar to the growth pattern of benign tumors, but it does not metastasize (Andrews et al., 2016). Keloids often protrude on the original skin lesion area accompanied by pain and itching, which causes a serious burden on the patient's quality of life and even affects limb function (Berman et al., 2017). Although there are many methods for the treatment of keloids, due to the unknown pathogenesis and high recurrence rate, safe and effective treatment and prevention protocols have not been identified. Therefore, exploring the pathogenesis of keloids will help find effective biomarkers and therapeutic targets to inhibit or eliminate keloids.

The current research mostly describes the pathogenesis of keloids from the perspectives of genetic susceptibility, immunity, and inflammation (Ogawa, 2017). Metabolomics is a new high-throughput sequencing discipline after genomics, transcriptomics, and proteomics, and it is an important part of reflecting changes in the body (Rinschen et al., 2019). Metabolomics is a subdiscipline of systems biology based on cluster index analysis, using high-throughput detection and data processing as the means and aiming at information modeling and system integration (Bujak et al., 2015). The metabolome refers to all of the low–molecular weight metabolites of a certain organism or cell in a specific physiological period (Bujak et al., 2015). Researchers conduct qualitative and quantitative analyses of metabolites to explore and predict diagnosis- and prognosis-related biomarkers that reflect the disease development status of treatment targets. 5-Hydroxylysine is usually present in collagen in the form of glycosylation (Herbert et al., 2012). 1-Methylnicotinamide is an immune regulatory metabolite in human ovarian cancer (Kilgour et al., 2021). 1-Methylnicotinamide regulates thrombogenesis and inflammatory processes (Chlopicki et al., 2007). The role of these two metabolites in keloid has not been studied. Research on metabolomics based on keloids is still needed. Our research explores the mechanism of metabolites in the development of keloids from the perspective of metabolomics.

2 MATERIALS AND METHODS

2.1 Human Samples

This study was approved by the Medical Ethics Committee of Peking Union Medical College Hospital (JS-2907), China. All participants provided written informed consent.

From May 2019 to May 2021, a total of 35 patients were included in this study, including 12 cosmetic patients and 23 keloid patients. Patients were 20–47 years old (17 males, 18 females). The collected specimens were divided into two groups: 20 keloid tissues from keloid patents (group K) were used as the experimental group. Eight normal skin tissues from keloid patients (group N) and 12 healthy tissues from cosmetic patients (group C) served as the control group. Five keloid tissues and five normal skin tissues were obtained from the same patient. The modified Vancouver Scar Scale (mVSS) is used to measure the severity of keloids (Ramadan et al., 2021).

All the sequencing samples were from the chest, and the enrolled patients did not have any systemic diseases or receive other treatments to remove possible factors that interfere with the results of the experiment. Normal skin samples surrounding the keloid tissue are 2–3 mm away and need to be removed together during surgery.

2.2 Untargeted Metabolome

In our research, we studied the metabolome of samples using a liquid chromatography–mass spectrometry (LC–MS/MS) method. LC–MS data were obtained by coupling an UltiMate 3000 liquid chromatograph (Thermo Fisher Scientific, United States) and a Q Exactive Plus mass spectrometer (Thermo Fisher Scientific, United States). Detailed parameter information is described in the methods of chromatographic conditions and mass spectrometry conditions. The mass spectrometer works in the full scan mode, with a scan rate of 100–1,000 m/z, and automatically performs MS/MS fragment scans. The obtained raw data were converted into mzXML format through Proteowizard software (v3.0.8789) (Chambers et al., 2012). The XCMS package of R (v3.1.3) was used to perform peak identification, peak filtration, and peak alignment. A data matrix was obtained including the mass-to-charge ratio (m/z), retention time (retention time), and peak area (intensity). The positive ion mode obtained 4,193 precursor molecules; 7,163 precursor molecules were obtained in the negative ion mode, and the data were exported to Excel for subsequent analysis. We analyzed 548 skin metabolites confirmed using MS/MS analysis. An LTQ Orbitrap high-resolution mass spectrometry–liquid chromatography mass spectrometer (Thermo Fisher Scientific) was used for the qualitative verification of 5-hydroxylysine and 1-methylnicotinamide. 1-Methylnicotinamide was verified using N-methylnicotinamide (Beijing Soleibao Technology Co., Ltd., SM9380, China). 5-Hydroxylysine was verified using DL-5-hydroxylysine hydrochloride (Sigma–Aldrich, H0377, United States).

2.3 Skin Sample Preparation

Fresh surgical specimens were quickly frozen in liquid nitrogen and stored at −80°C. A total of 63.1–101.9 mg of each sample was accurately weighed in a 2-ml EP tube, and 1 ml tissue extract and three steel beads were added (Thermo, Waltham, United States). The sample was placed into a high-throughput tissue grinder (Xinzhi Biological Technology Co., Ltd., SCIENTZ-48, Ningbo, China) and ground for 60 s at 55 Hz. This operation was repeated twice. Ultrasound was performed at room temperature for 30 min, and the samples were placed on ice for 30 min. The samples were centrifuged at 4°C for 10 min at 12,000 rpm, and then 650 μL of the supernatant from each sample was transferred into another 2-ml centrifuge tube. The samples were concentrated and dried in vacuum (Eppendorf, 5,305, Hamburg, Germany). The samples were dissolved in 200 μL of 2-chlorobenzalanine (4 ppm) (Aladdin, 103616-89-3, Shanghai, China) 50% acetonitrile solution (stored at −20°C), and the supernatant was filtered through a 0.22-μm membrane to

obtain the prepared samples. Twenty microliters from each sample was tested and mixed into a QC sample. The sample was used for LC–MS detection.

2.4 Chromatographic Condition

Chromatographic separation was accomplished in a Thermo Ultimate 3000 system equipped with an ACQUITY UPLC® HSS T3 (150 × 2.1 mm, 1.8 μm, Waters) column maintained at 40°C. The temperature of the autosampler was 8°C. Gradient elution of analytes was performed with 0.1% formic acid in water (C) and 0.1% formic acid in acetonitrile (D) or 5 mM ammonium formate in water (A) and acetonitrile (B) at a flow rate of 0.25 ml/min. Injection of 2 μL of each sample was performed after equilibration. An increasing linear gradient of solvent B (v/v) was used as follows: 0~1 min, 2% B/D; 1~9 min, 2~50% B/D; 9~12 min, 50–98% B/D; 12~13.5 min, 98% B/D; 13.5~14 min, 98~2% B/D; and 14~20 min, 2% D-positive model (14~17 min, 2% B-negative model) (Zelena et al., 2009).

2.5 Mass Spectrometry Conditions

The ESI-MSn experiments were executed on a Thermo Q Exactive Plus mass spectrometer, with spray voltages of 3.5 kV and −2.5 kV in positive and negative modes, respectively. Sheath gas and auxiliary gas were set at 30 and 10 arbitrary units, respectively. The capillary temperature was 325°C. The analyzer scanned over a mass range of m/z 81-1,000 for full scan at a mass resolution of 70,000. Data-dependent acquisition (DDA) MS/MS experiments were performed with HCD scans. The normalized collision energy was 30 eV. Dynamic exclusion was implemented to remove some unnecessary information in MS/MS spectra (Zelena et al., 2009).

2.6 Data Preprocessing

Data quality control ensures repeatability and accuracy of metabolomics measurements. As the chromatographic system and mass spectrometer are in direct contact with samples, they are easily polluted with an increase in the number of samples to be analyzed, resulting in signal drift and system measurement error. The quality control samples were used to evaluate the signal drift of the mass spectrometry data during the acquisition process. These drifts can be further identified and corrected by precise algorithms to improve the quality of the data. The QC-RFSC algorithm of the R statTarget package (Bioconductor, version 3.13) was used to correct the signal peak of each sample feature.

2.7 Bioinformatics Analysis

These metabolites were annotated using the KEGG database (Kanehisa and Goto, 2000) (https://www.genome.jp/kegg/pathway.html), HMDB database (https://hmdb.ca/metabolites), and LIPIDMaps database (http://www.lipidmaps.org/). PLS-DA is an upgraded version of linear discriminant analysis, which is suitable for omics data where explanatory variables have a large number of collinearity problems (Gromski et al., 2015). Orthogonal partial least squares discriminant analysis is an improvement of PLS-DA. In OPLS-DA, the regression model is built between explanatory variables (metabolite data) and response variables (grouping information) that contain grouping information, and the model filters out information that is not related to grouping (Westerhuis et al., 2010). The random forest algorithm is a combination of bagging and decision trees and is used to calculate important metabolites (Hanko et al., 2021). Data normalization, principal component analysis (PCA), partial least squares discriminant analysis (PLS-DA), orthogonal partial least squares discriminant analysis (OPLS-DA), random forest (RF) analysis, and support vector machine (SVM) analysis were performed with the R package MetaboAnalystR. To make the data close to a normal distribution, the normalization function in the MetaboAnalystR package (with arguments MedianNorm, LogNorm, and AutoNorm) was adopted. We applied univariate analysis (*t*-test) to calculate the statistical significance (*p* value). The metabolites with Value Importance in Projection (VIP) > 1, p value < 0.05, and log2 (fold change) > 1 were considered to be differential metabolites. For clustering heatmaps, the data were normalized as z scores and plotted by the Pheatmap package in R language. A volcano plot was used to filter metabolites of interest based on log2 (fold change) and -log10 (*p* value), using the ggplot2 package in R language. The metabolites with a p value < 0.05 (*t*-test) were used to conduct an overrepresentation analysis (ORA) or enrichment analysis, and the resulting KEGG pathways with a p value < 0.05 (ORA) were considered statistically significantly enriched.

2.8 Hematoxylin–Eosin Staining

HE staining labels the nucleus in blue–purple and the cytoplasm in red. HE staining was used to observe the morphology of keloid tissue. First, the tissue sections were dried at room temperature for 20 min. Second, the hematoxylin dye was added for 3 min. Third, 0.5% hydrochloric acid alcohol was added for a few seconds to distinguish the samples. Fourth, eosin was added for 30 min, the slides were dehydrated with gradient alcohol, and then xylene was used to make any unstained samples transparent. Finally, the samples were observed under a stereomicroscope.

2.9 CIBERSORT

The CIBERSORT deconvolution algorithm is a machine learning method based on linear support vector regression (SVR), implemented through the R package (version 3.5.3, R Foundation for Statistical Computing, Vienna, Austria). The CIBERSORT deconvolution algorithm is used to transform the gene expression information of the transcriptome into the proportion information of immune cells, and the abundance of immune cells can be obtained through visual analysis of histograms, heatmaps, and violin maps. GSE92566 was downloaded (https://www.ncbi.nlm.nih.gov/geo/query/acc.cgi?acc = GSE92566) from GEO datasets. The threshold was set to $p < 0.05$, |log2 (fold change) |≥1. After GSE92566 was normalized, the gene expression information was converted into immune cell abundance information through the CIBERSORT algorithm of the R package (Chen et al., 2018).

2.10 Neural Network Model

The neural network model was built in MATLAB (version 9.2.0.538062, MathWorks, United States) using the BP algorithm (multilayer feedforward neural network model) for fitting. The row data are normalized to distribute between [0, 1]. After normalization, the data were randomly divided into a training set and validation set at a ratio of 3:1. The entire neural network model includes an input layer, a hidden layer, and an output layer. The hidden layer was set to 2. The tansig function was used between the input layer and the hidden layer: the digital S-shaped function was for information transmission, and the hidden layer to the output layer adopt the Purelin function (linear function) for transmission. The number of network training iterations is 9,000, and every 1,000 iterations display the primary error. The target error is 10^{-5}, and the learning rate is 0.05 based on experience. The momentum factor mc is 0.9. The model is initialized randomly. The output values of output neurons to patients and healthy controls are set to 1–15 (Esmaelpoor et al., 2020).

3 RESULTS

3.1 Morphological Characteristics of Group K and Control

The collagen fiber bundles in the dermis of keloids were thick, dense, and disorderly arranged and contained many

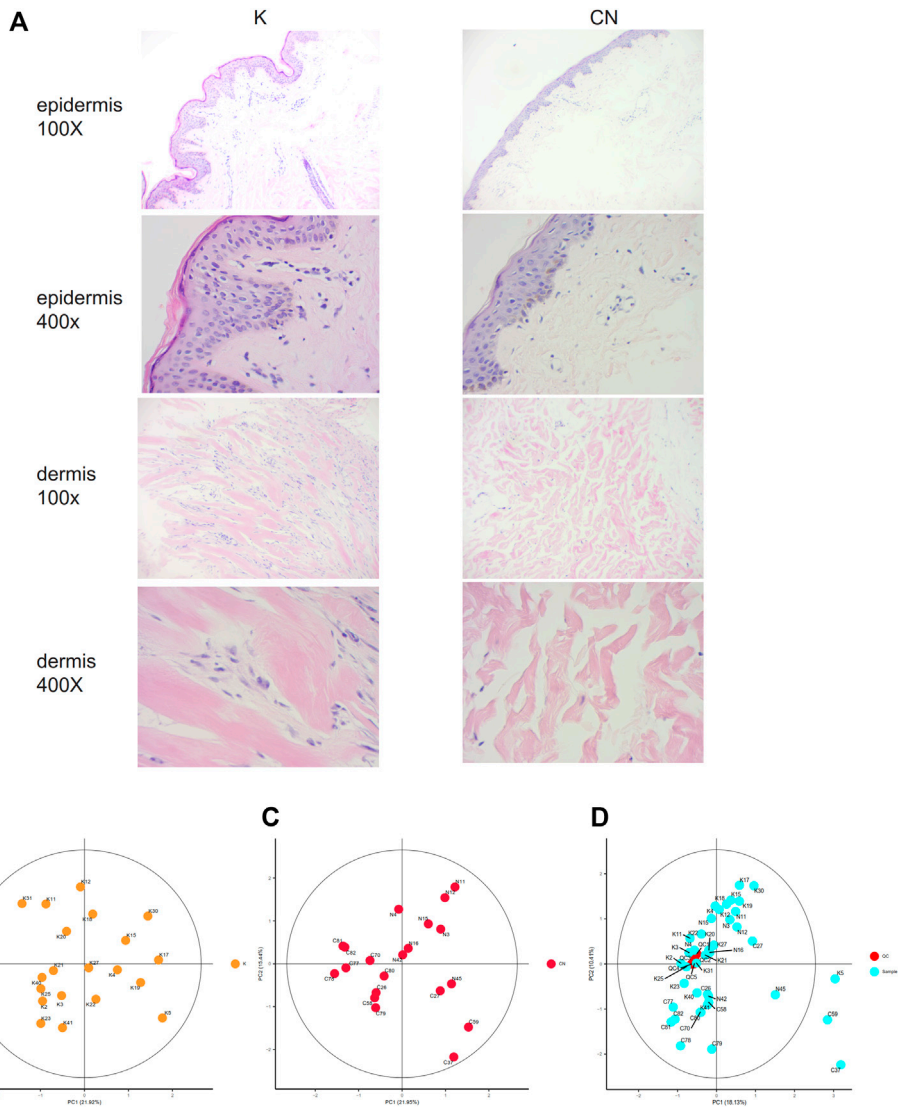

FIGURE 1 | (A) Histological images of the K group and control group, 100X. 400X. **(B)** Unsupervised principal component analysis (PCA) of keloid tissues. Each point in the figure represents a sample, and the position of the point in the figure is determined by all the metabolites in the sample. The ellipse in the figure is based on the 95% confidence interval calculated and drawn by Hotelling T2. The sample falling outside the ellipse implies that the point may be an outlier. **(C)** Unsupervised principal component analysis (PCA) of control tissues. **(D)** Calibration signal drift. QC sample points together, proving that the calibration effect is good. The red dots are QC samples after calibration, and the blue dots are test samples.

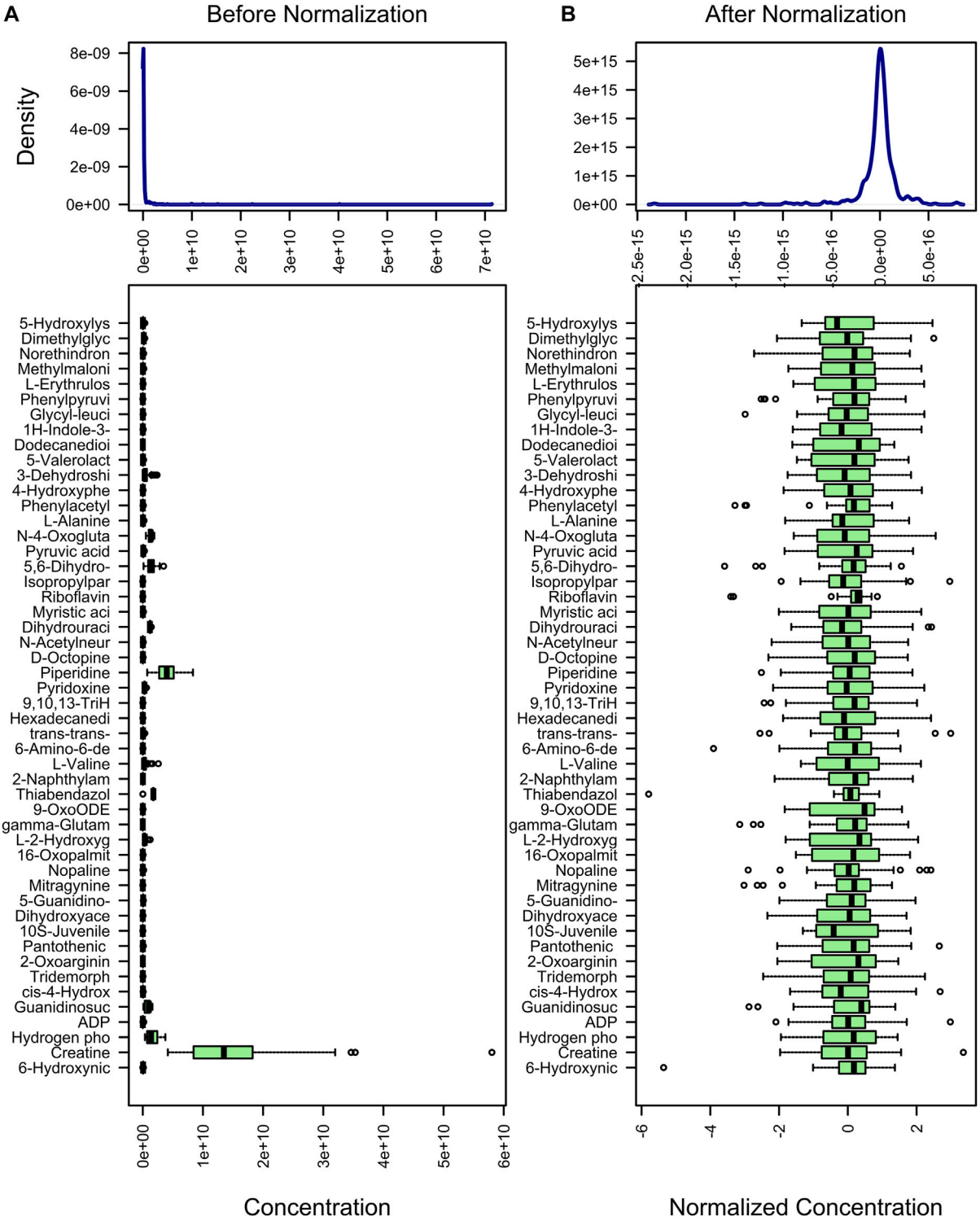

FIGURE 2 | Standardization of metabolites. The content distribution is represented by a box plot, which corresponds to outliers, minimum, lower quartile, median, upper quartile, maximum, and outliers from left to right. The picture on the left is the distribution before normalization, and the picture on the right is the distribution after normalization.

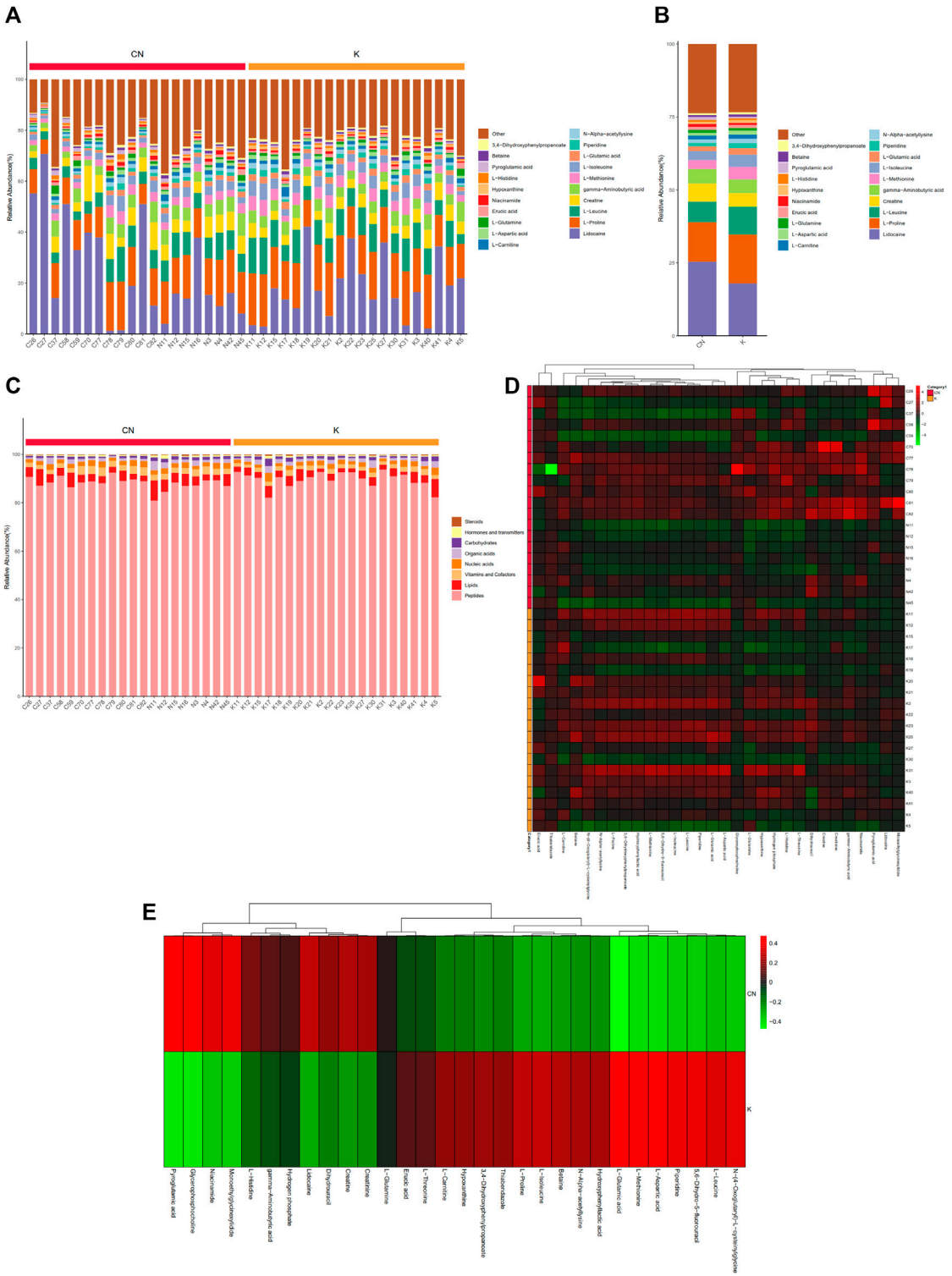

FIGURE 3 | Metabolite content statistics. **(A)** The abscissa is the sample name, sorted according to the grouping order, and different grouped samples are marked with different colors. The ordinate represents the percentage content of each metabolite, and the order of the columns corresponding to the metabolites from top to bottom is consistent with the legend. **(B) (C)** The vertical axis is the sample name information and includes grouping information. The horizontal axis is metabolites. The cluster tree at the top of the figure is the similarity clustering of the metabolite distribution in each sample, the middle heatmap is the metabolite content heatmap, and the relationship between color and metabolite content (Z score) is shown in the upper right scale ruler. **(D)** The expression of metabolites between the two groups.

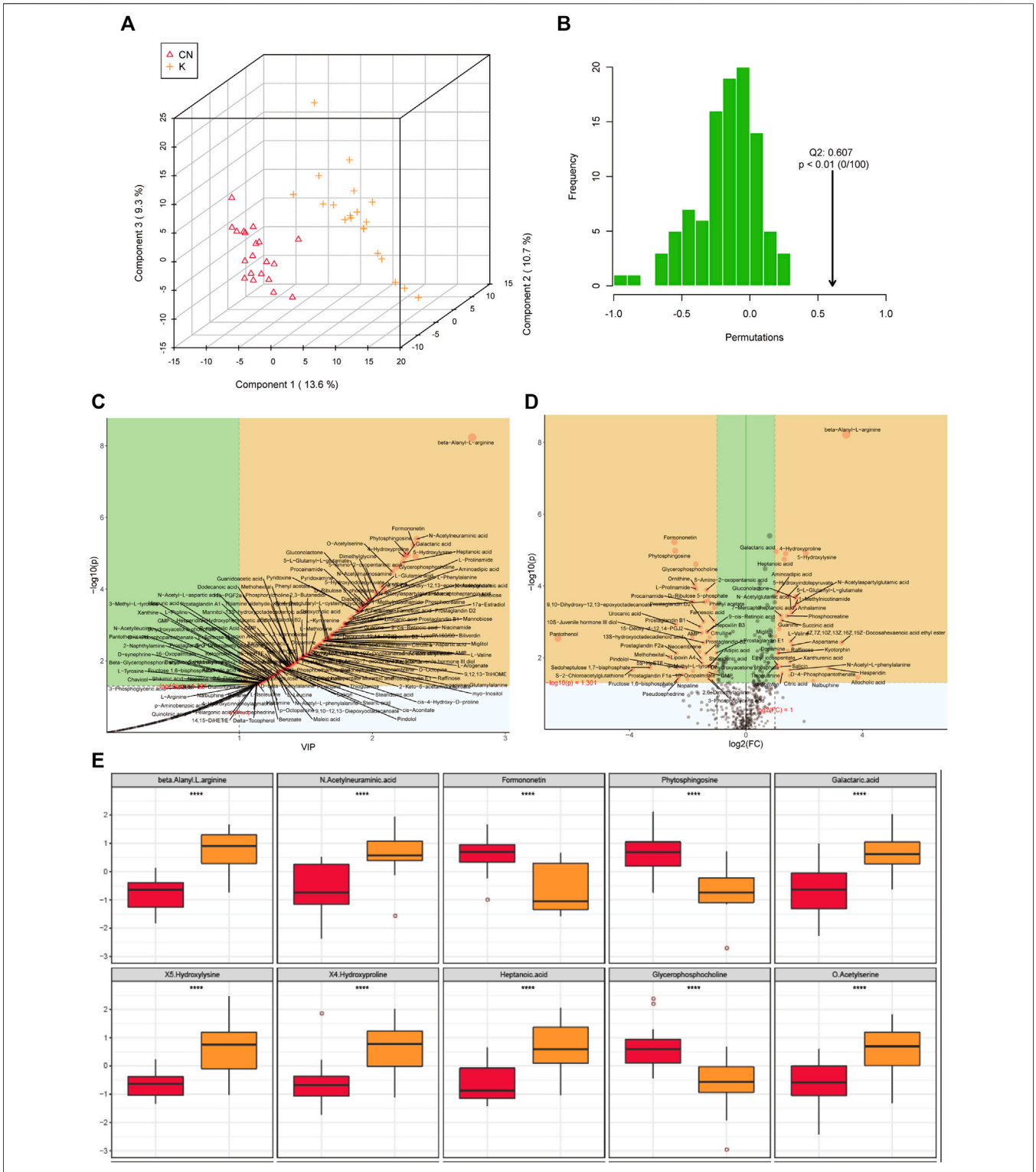

FIGURE 4 | (A) Each point corresponds to a sample, and the horizontal and vertical coordinates are the values of the two factors with the best discrimination effect. Different groups are marked with different colors, and the area marked by the ellipse is the 95% confidence area of the sample point. **(B)** The abscissa represents the distribution interval of the replacement test statistic (model prediction accuracy), the ordinate is the frequency of the test statistic in the interval during the replacement process, and the position pointed to by the arrow is the observed test statistic value. If this value is far from the random distribution, the model distinguishing effect is not random, and the model distinguishing effect is significant. **(C)** PLS-DA metabolite importance map. In the figure, each point represents a metabolite, the abscissa is VIP (value importance in projection), and the ordinate is the *p* value after FDR correction (log10 conversion). **(D)** Multiple change volcano map. Each point represents a

(*Continued*)

FIGURE 4 | metabolite, the abscissa is the multiple of change, and the ordinate is the *p* value of the *t*-test. The larger the multiple of change, the smaller the *p* value [the higher the log10(p)], and the larger the point. **(E)** Box diagram of metabolite differences. To visually display the differences in metabolites between groups, we made a box diagram of representative differential metabolites with the top ranking (top 25 with small *p* value) obtained from one-dimensional statistical analysis. *, **, *** correspond to $p < 0.05$, $p < 0.01$, $p < 0.001$.

inflammatory cells. The epidermal cells of normal skin were well differentiated and had clear layers. Collagen bundles in the dermis of healthy skin were thin and loosely arranged (**Figure 1A**). The morphology of normal skin tissue and keloid tissue was quite different. Local lipid metabolism needs further metabolome sequencing.

3.2 Quality Assessment of Data

To clarify the profiling of local lipid metabolism in keloids, we used non-targeted metabolome analysis to detect metabolites. We identified 548 metabolites by adjusting the most appropriate experimental conditions. There were 162 metabolites that were significantly different between keloids and normal skin ($p < 0.05$). Using unsupervised principal component analysis (PCA), we modeled each group of samples and then displayed the score plot (**Figures 1B,C**). This type of intragroup PCA eliminates the interference between groups, allowing us to observe the variation within the group more clearly and find possible outliners. Each point in the figure represents a sample, which is determined by all of the metabolites in the samples. There were no outliers in group K (**Figure 1B**) or the control (**Figure 1C**). The quality control (QC) samples were used to evaluate the signal drift of the entire mass spectrum data in the acquisition process, which can be further identified and corrected by accurate algorithms to improve the quality of the data. The QC samples are the samples obtained after all samples are mixed in equal amounts. During the signal data acquisition process, QC samples were inserted at the beginning, end, and middle positions to record the signal drift. There was no signal drift, and the signal strength of QC samples remained unchanged during the data acquisition process (**Figure 1D**). After the signal drift was corrected, the QC sampling points in the PCA diagram were clustered together, demonstrating that the correction effect was good.

3.3 Metabolite Standardization

The purpose of metabolite standardization is to make the mean and standard deviation of all metabolites at the same level. For analyses such as PLS-DA, OPLS-DA, and machine learning, if metabolites are not standardized, the importance of metabolites with high mean and standard deviation will tend to be higher than the importance of metabolites with low mean and standard deviation. To accurately analyze metabolites with large differences between groups, metabolite standardization is required. Before standardization, the median and upper and lower quartiles of metabolite content were uneven, and the difference was large (**Figure 2A**). However, after standardization, they were basically at the same level (**Figure 2B**). In addition, difference comparison methods such as the *t*-test and ANOVA require that the metabolite content obeys a normal distribution. Therefore, we used log transformation to make the metabolite content distribution close to the normal distribution.

3.4 Metabolite Profiles in Keloids Identified by Non-Targeted Metabolomics

To calculate the percentage of the content of each metabolite in each sample, a stacked histogram was used, as in **Figure 3A**, which can intuitively compare the differences in the composition and structure of metabolites between groups. **Figure 3A** shows the top 20 metabolites, including lidocaine, L-proline, L-leucine, creatine, gamma-aminobutyric acid, and L-methionine. The differences in metabolites between the two groups can be more intuitively realized by combining the samples between the two groups (**Supplementary Figure S1A-1B**). Creatine, L-leucine, L-proline, and lidocaine seemed to be different between the two groups (**Supplementary Figure S1B**). The remaining metabolites, more than 20, were included in other groups. We annotated all metabolites with the KEGG database br08001 to obtain the biological roles played by the metabolites, count the percentage content of each biological role, and draw a percentage content stacked column chart, as shown in **Figure 3B**. Compared with normal tissue, lipids have a tendency to decrease in keloids, while peptides have a tendency to increase in keloids (**Supplementary Figure S1**). Skin metabolites in keloids play various roles, including peptides, lipids, vitamins and cofactors, nucleic acids, organic acids, carbohydrates, hormones and transmitters, and steroids. Metabolites of concern were selected (the top 30 metabolites were selected by default), and the cluster was conducted according to the metabolite composition of the samples (**Figure 3C**). N-(4-Oxoglutaryl)-L-cysteinylglycine, L-leucine, 5,6-dihydro-5-fluorouracil, piperidine, L-aspartic acid, L-methionine, and L-glutamic acid were upregulated in group K. Pyroglutamic acid, glycerophosphocholine, niacinamide, monoethylglycinexylidide, and L-histidine were downregulated in group K (**Figure 3D**). The expression of these metabolites was reversed in the control group.

3.5 A PLS-DA Model Was Established to Analyze the Metabolites of Keloids

3.5.1 PLS-DA Looks for Factors That Can Distinguish the Grouping of Samples to the Greatest Extent

Factors can be understood as the weighted sum of all metabolites. Discriminant analysis encodes the discontinuous categorical variable to be predicted as a latent variable, and the latent variable is continuous so that regression can be established between the explanatory variable and the latent variable, which can be solved by least squares regression. As shown in

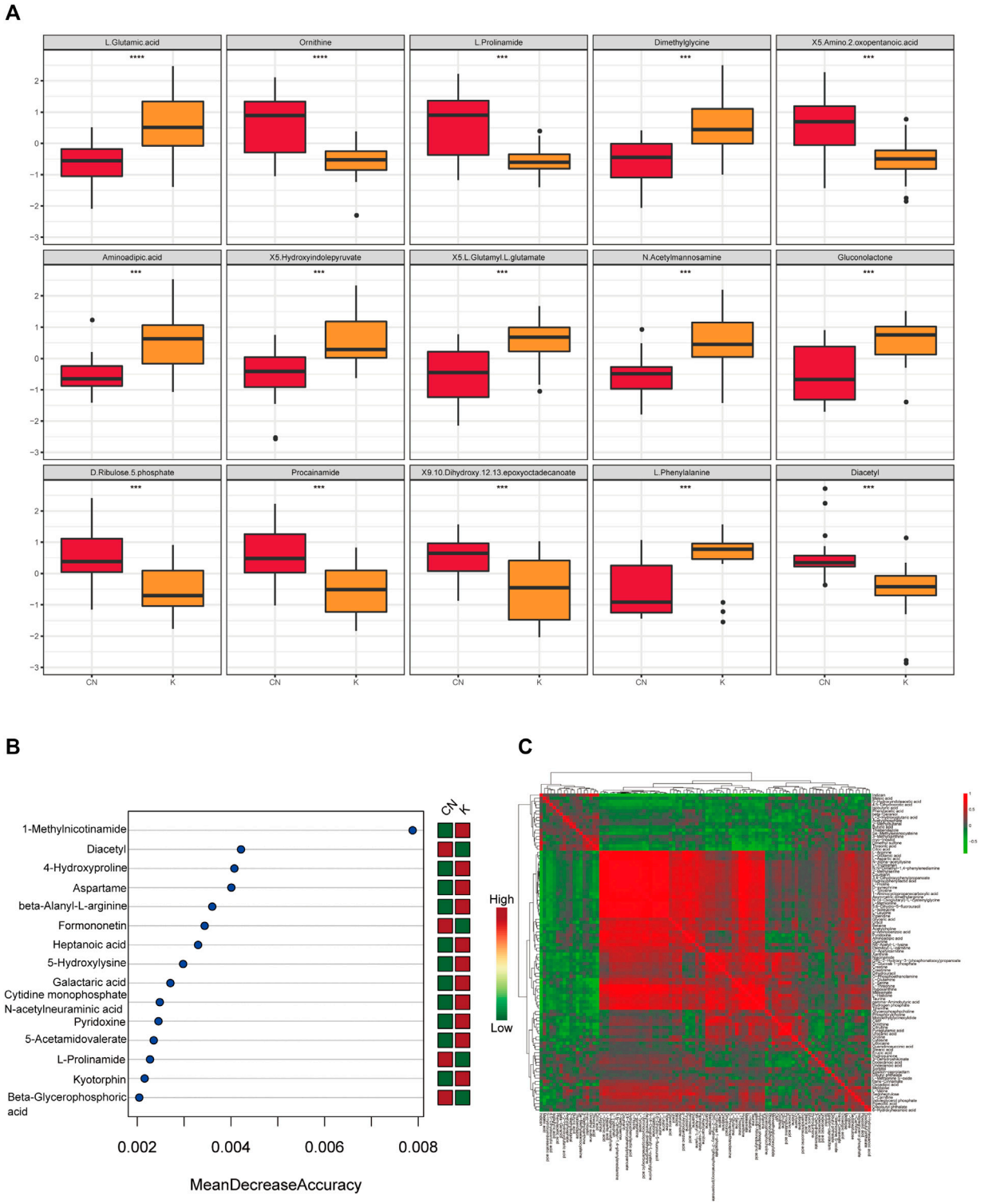

FIGURE 5 | (A) Box diagram of metabolite differences. To visually display the differences in metabolites between groups, we made a box diagram of representative differential metabolites with the top ranking (top 25 with small *p* value) obtained from one-dimensional statistical analysis. *, **, *** correspond to $p < 0.05$, $p < 0.01$, $p < 0.001$. **(B)** The 15 most important metabolites in random forests. The abscissa of the left figure is "Mean Decrease Accuracy," which measures the importance of a metabolite in a random forest; the right figure is a heatmap of the content of metabolites in two groups. **(C)** Pearson correlation heatmap. Correlation coefficient matrix of the top 100 metabolites in total content. The correlation coefficient is represented by color: red is positively correlated, and green is negatively correlated.

TABLE 1 | Random forests of metabolites.

Metabolite	Mean decrease accuracy	Mean decrease gini	t.stat	p value
1-Methylnicotinamide	0.008	0.318	–3.958	–3.958
Diacetyl	0.004	0.326	3.990	<0.001
4-Hydroxyproline	0.004	0.191	–5.028	<0.001
Aspartame	0.004	0.152	–3.153	0.004
Beta-alanyl-L-arginine	0.004	0.216	–7.585	<0.001
Formononetin	0.003	0.185	5.301	<0.001
Heptanoic acid	0.003	0.127	4.981	<0.001
5-Hydroxylysine	0.003	0.122	5.355	<0.001
Galactaric acid	0.003	0.143	–5.119	<0.001
Cytidine monophosphate N-acetylneuraminic acid	<0.001	0.029	1.104	0.28
Pyridoxine	0.002	0.124	–3.897	<0.001
5-Acetamidovalerate	0.002	0.1	–3.13	0.004
L-Prolinamide	0.002	0.109	4.51	<0.001
Kyotorphin	0.002	0.076	–2.837	0.007
Beta-glycerophosphoric acid	0.001	0.049	2.185	0.037

Figure 4A, we used the two factors with the best distinguishing effects to draw a scatter plot. The point clouds of samples in different groups are distributed in different areas, meaning that the PLS-DA model has a good discrimination effect. There were significantly different metabolites in the two groups. In OPLS-DA's permutation test, we use Q2 as the test statistic and use the permutation method to obtain the random distribution of Q2. As shown in **Figure 4B**, the actual observation Q2 indicated by the arrow is on the right side of the random distribution (the observed value is greater than the random value), meaning that Q2 is not random but significant, and the predictive ability of the model is significant, that is, there exist significantly different metabolites between the two groups (**Figure 4B**). The PLS-DA model was used to calculate the importance of metabolites (**Figure 4C**). Univariate analysis is used to measure how much metabolites differ between groups to assess how much metabolite changes will affect the organism. We measured the magnitude of this change by calculating the fold change (FC) of the metabolite change, combined with the p value, to screen some key metabolites. The change multiple of up is positive, and the multiple of down is negative. As shown in **Figure 4D**, the threshold of the p value was less than 0.05, and an absolute value of the fold change greater than 2 was defined as the yellow area. These metabolites had significant differences between groups (**Figure 4D**) and had large changes, which should be considered in further research. To visually show the difference in metabolites between groups, representative different metabolites were displayed in box diagrams (**Figure 4E**, **Figure 5A**, $p < 0.001$).

3.6 Machine Learning of Metabolite of Keloids

The random forest algorithm was used to calculate different metabolites in the two groups. The random forest algorithm is a combination of bagging and decision trees. In random forest analysis, we used "Mean Decrease Accuracy" to measure the importance of a metabolite in the random forest to distinguish groups. Changing the value of a metabolite into a random number, the degree of reduction in the accuracy of random forest prediction is "Mean Decrease Accuracy." The greater the value, the greater the importance of metabolites in the random forest. **Figure 5B** shows the 15 most important metabolites in random forests, including 1-methylnicotinamide, diacetyl, 4-hydroxyproline, beta-alanyl-L-arginine, heptanoic acid, 5-hydroxylysine, galactaric acid, cytidine monophosphate N-acetylneuraminic acid, L-prolinamide, and beta-glycerophosphoric acid (**Table 1**). **Figure 5C** shows the cluster correlation heatmap of the two groups. Correlation coefficient matrix of the top 100 metabolites in total content. The correlation coefficient is indicated by color: red represents a positive correlation, and green represents a negative correlation.

3.7 Metabolic Pathway Enrichment Analysis of Keloids

According to the metabolites with significant differences between groups ($p < 0.05$), the biological pathways that play a key role in the pathogenesis of keloids were identified, and the basic molecular mechanism was revealed. Through the KEGG enrichment analysis of metabolic pathways, whether the metabolites of interest are significantly enriched in these metabolic pathways can be assessed. **Figure 6A** shows the metabolic pathways with significant enrichment of differential metabolites, which may play a role in the occurrence and development of keloids.

Topological analysis can calculate the effect of the metabolite of interest in the metabolic pathway (measured by impact). Therefore, we combined topological analysis and enrichment analysis to determine whether a metabolic pathway plays a key role in the biological process of keloids. The metabolic pathways in the blue area in **Figure 6B** are significant metabolic pathways in the enrichment analysis, including arachidonic acid metabolism; D-arginine and D-ornithine metabolism; pantothenate and CoA biosynthesis; alanine, aspartate, and glutamate metabolism; arginine and proline metabolism; aminoacyl–tRNA biosynthesis; phenylalanine metabolism; and nicotinate and nicotinamide metabolism (**Table 2**).

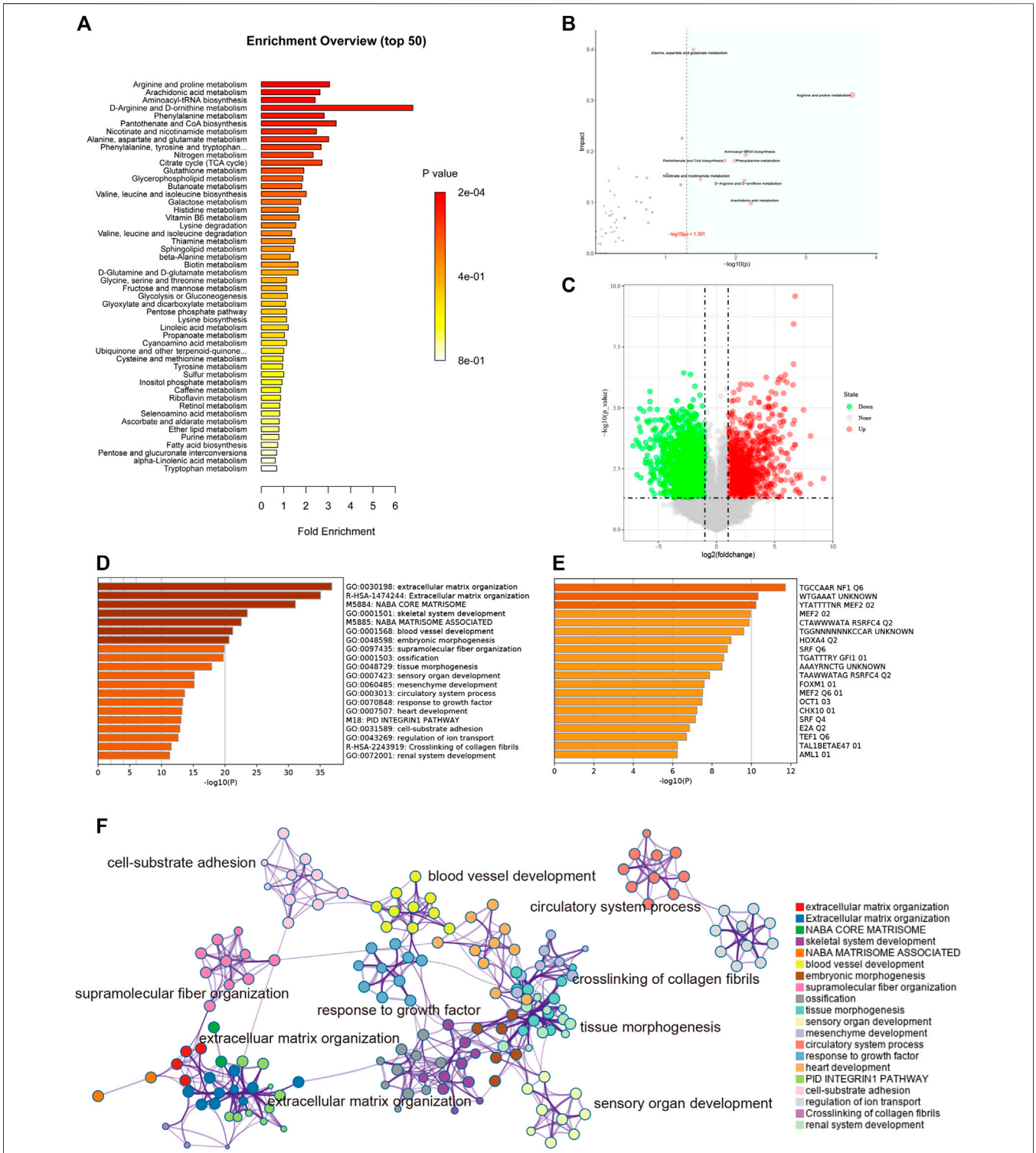

FIGURE 6 | (A) Enrichment analysis. The abscissa is the enrichment factor, which is the number of observed metabolites/theoretical metabolites in the metabolic pathway. The size of the *p* value is expressed by color: the darker the color, the smaller the *p* value. **(B)** Topological analysis. The abscissa is the *p* value, and the blue area is significant ($p < 0.05$); the ordinate is the topological analysis impact. **(C)** The volcano plot illustrates the differentially expressed genes between control and keloid tissues after analysis of the GSE92566 dataset with GEO2R. **(D)** GO enriched terms are shown, and accumulative hypergeometric *p* values and enrichment factors were calculated and used for filtering. The remaining significant terms were then hierarchically clustered into a tree based on kappa-statistical similarities among their gene memberships. Then, a kappa score of 0.3 was applied as the threshold to cast the tree into term clusters. **(E)** Transcription factor enriched terms. The darker the color, the higher the enrichment score. **(F)** Metascape analysis. We selected a subset of representative terms from this cluster and converted them into a network layout. More specifically, each term is represented by a circle node,

(*Continued*)

FIGURE 6 | where its size is proportional to the number of input genes falling into that term, and its color represents its cluster identity (i.e., nodes of the same color belong to the same cluster). Terms with a similarity score >0.3 are linked by an edge (the thickness of the edge represents the similarity score). The network was visualized with Cytoscape (v3.1.2) with a "force-directed" layout and with edges bundled for clarity. One term from each cluster is selected to have its term description labeled.

TABLE 2 | Pathway enrichment of keloid.

Description	Raw p	FDR	Impact	Fold enrichment
Arginine and proline metabolism	0.00021735	0.017388	0.31068	3.0555
Arachidonic acid metabolism	0.006079	0.15052	0.09836	2.6271
Aminoacyl-tRNA biosynthesis	0.00718	0.15052	0.19356	2.413
D-Arginine and D-ornithine metabolism	0.007526	0.15052	0.14286	6.7867
Phenylalanine metabolism	0.010442	0.16707	0.18181	2.8152
Pantothenate and CoA biosynthesis	0.014411	0.19215	0.18181	3.3514
Nicotinate and nicotinamide metabolism	0.031723	0.36255	0.14544	2.4679
Alanine, aspartate, and glutamate metabolism	0.039998	0.39998	0.4	3.0163

3.8 Gene Expression Profiles of Keloids

To better understand the pathogenesis of keloids from multiple angles, GSE92566 was used to reveal changes in gene expression profiles. The threshold was set to $p < 0.05$, |log2 (fold change) |≥1. In total, 3,370 different genes were screened, as shown in **Figure 6C**. These differentially expressed genes were enriched and related to extracellular matrix organization, NABA CORE MATRISOME, and blood vessel development (**Figure 6D**). The enrichment results of transcription factors are shown in **Figure 6E**, including NF1, MEF2, and RSRFC4. Metascape analysis (Zhou Y. et al., 2019) is shown in **Figure 6F**, including cell–substrate adhesion, blood vessel development, response to growth factor, cross-linking of collagen fibrils, and supramolecular fiber organization. The same enrichment network has its nodes colored by *p* value, as shown in **Figure 7A**. Differentially expressed genes between keloids and normal tissues were identified by protein–protein interaction (PPI) analysis with complex interactions (**Figure 7B**). The MCODE algorithm (Zhou Y. et al., 2019) was used to screen the differentially expressed genes and obtain the important genes of pathogenesis (**Figure 7C**). The CytoHubba algorithm was also used to screen the important genes during keloid formation, including POSTN, COL3A1, COL1A2, SOX9, COL5A2, COL1A1, ITGB1, COL5A1, FN1, and BGN (**Figure 7D**). The hub genes of COL1A, COL1A2, COL5A2, and COL3A1 indicate that genes related to collagen synthesis play a vital role in the pathogenesis of keloids.

3.9 Immune Microenvironment of Keloids

Keloid tissue has a high collagen content, making it difficult to be separated from immune cells in the local immune microenvironment. To better study the local immune microenvironment of keloids, the CIBERSORT algorithm was used (Xiong et al., 2018; Zhou R. et al., 2019). According to the biomarkers of gene expression profile, immune cells are typed to obtain cell abundance information (Xiong et al., 2018; Zhou R. et al., 2019). The histogram and heatmap showed that the information about the proportion of immune cells in group K and group N was uneven, and the local immune microenvironment was different (**Figures 7E,F**). The relationship between immune cells is shown in **Figure 7G**. M2 macrophage and gamma delta T-cell proportion synergistically increased (**Figure 7G**). Treg and resting dendritic cell proportion synergistically increased (**Figure 7G**). The proportion of Tregs in groups K and N was significantly different ($p = 0.032$). The proportion of Tregs, which plays an important role in immune regulation, was lower than that in normal skin tissue, which may contribute to the vigorous growth of keloid tissue (**Figure 7H**).

3.10 5-Hydroxylysine and 1-Methylnicotinamide are Related to the Severity of Keloids

Metabolites were easier to obtain in the clinic than transcriptome information, for example, using microneedle punch, tape strip, macroduct sweat collector, and suction chamber (Elpa et al., 2021). Exploring metabolites related to the pathogenesis of keloids can help doctors monitor the development of the disease at any time and provide effective biomarkers for diagnosis, treatment, and even recurrence. To explore the value of 5-hydroxylysine and 1-methylnicotinamide in clinical applications, we incorporated the metabolome sequencing data of 5-hydroxylysine and 1-methylnicotinamide into the construction of the neural network model as the input layer. The mVSS was used as a common index to measure the severity of keloids in the clinic. mVSS was the output layer. Thirty samples were used as the training set, and 10 samples were used as the validation set. The neural network model was successfully built through training. The best training performance was 0.10994 at epoch 9,000 (**Figure 8A**). The verification set was used to verify the training effect of the neural network model. The agreement between the predicted value and the actual value proved that the training effect is good (**Figures 8B,C**). The error diagram also showed that the error is acceptable (**Figure 8D**). The predicted value was consistent with the actual value, and the correlation coefficient was 0.9211 (**Figure 8E**). The successful construction of the neural network model demonstrated that the expression of 5-hydroxylysine and 1-methylnicotinamide may be predictors of the severity of keloids

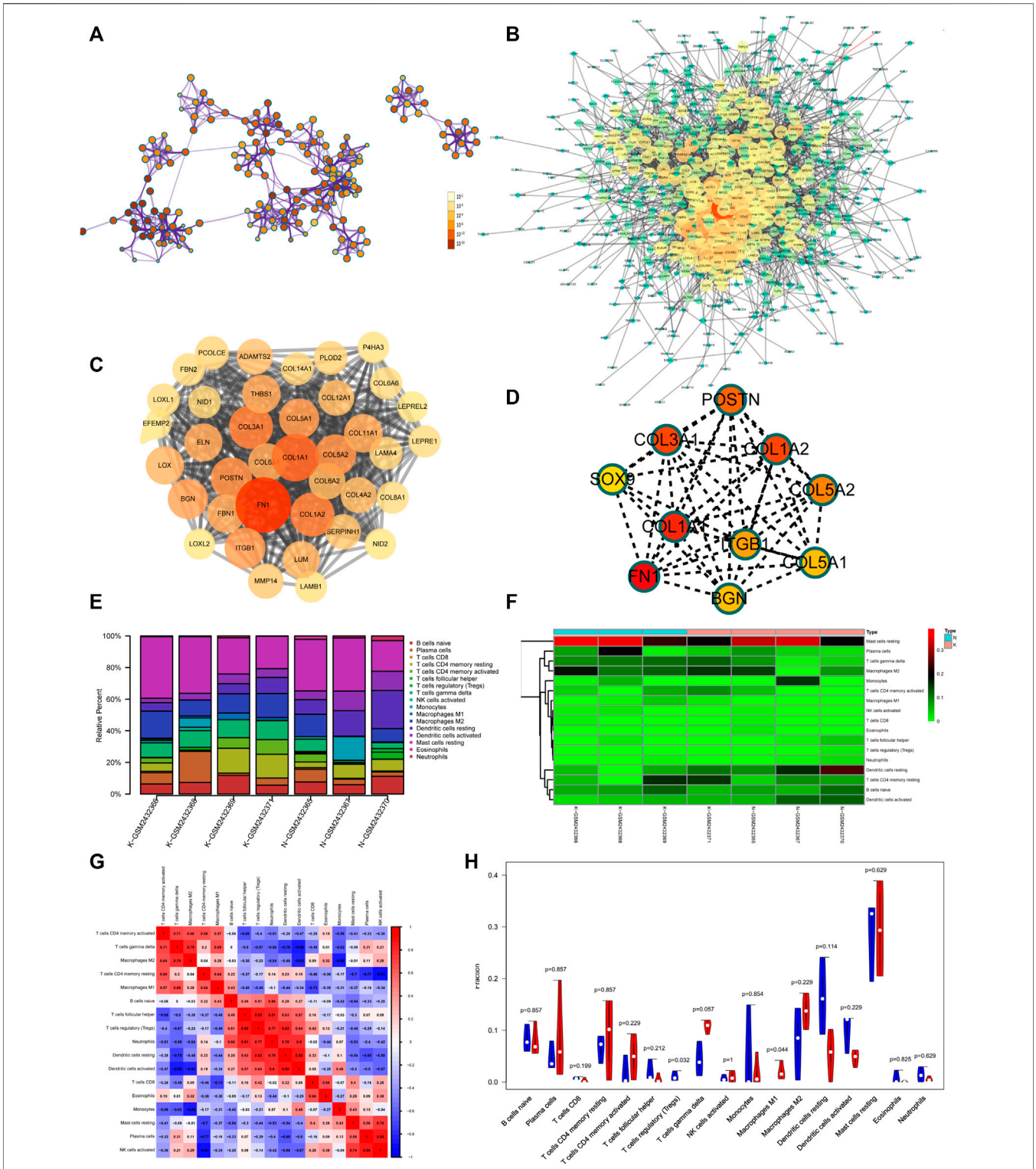

FIGURE 7 | (A) Same enrichment network has its nodes colored by *p* value, as shown in the legend. The darker the color, the more statistically significant the node is (see legend for *p* value ranges). **(B)** The protein–protein interaction (PPI) network of differentially expressed genes of GSE92566. **(C)** The MCODE algorithm was used to screen the differentially expressed genes and obtain the important genes of pathogenesis using GSE92566. **(D)** The CytoHubba algorithm was also used to screen the imported genes of GSE92566. **(E)** Fractions of immune cells between control and keloid tissue in the GEO database (GSE92566). **(F)** Heatmap of immune cells between control and keloid tissue in the GEO database (GSE92566). **(G)** A correlational heatmap of immune cells of keloids. **(H)** A violin plot of immune cells found in control and keloid tissue according to the GEO database (GSE92566); blue denotes normal tissue and red denotes keloid tissue.

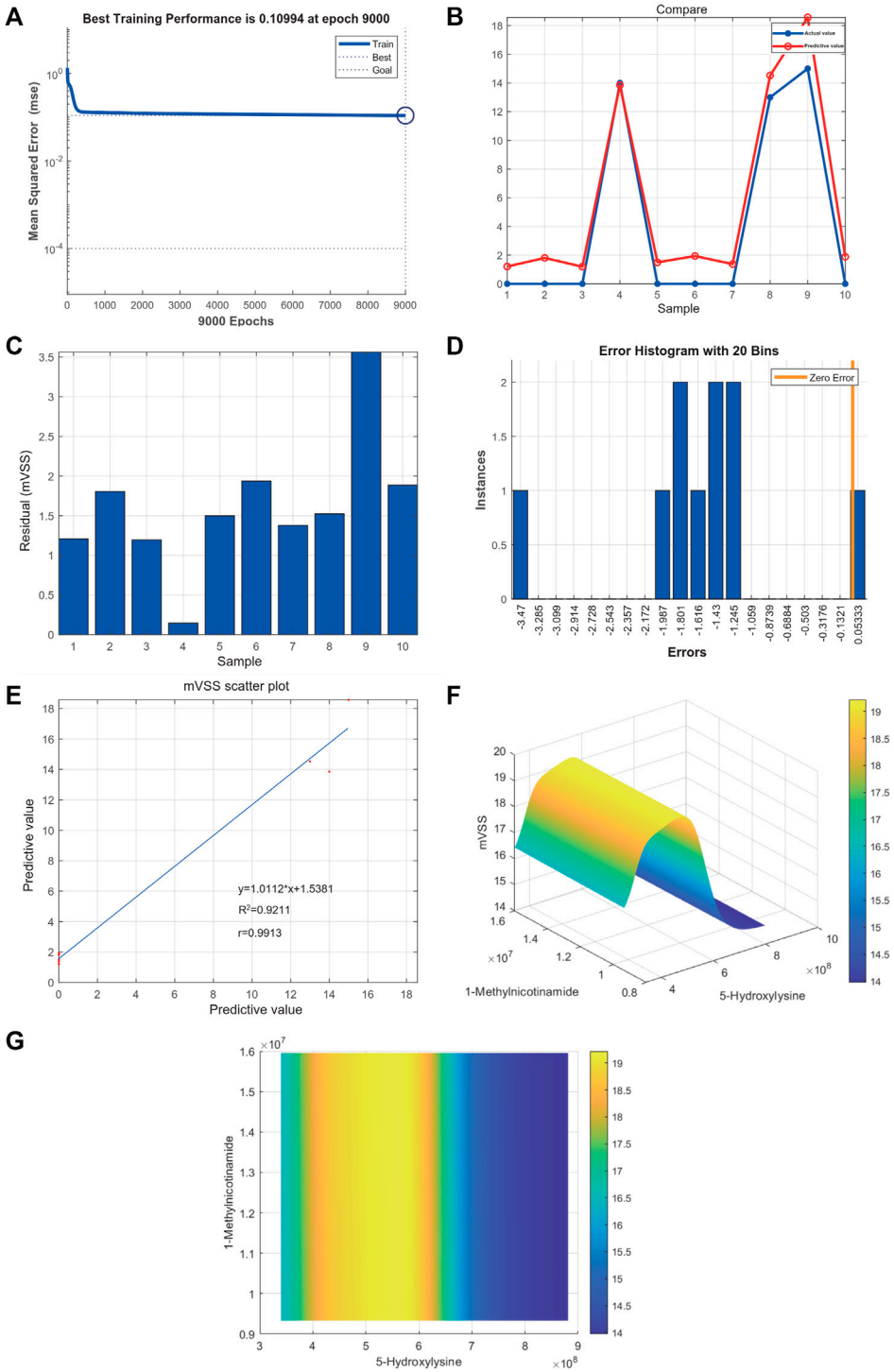

FIGURE 8 | (A) Neural network model for the prediction of keloid severity. **(A)** The best training performance was 0.10994 at epoch 9,000. **(B)** The predictive value of the data was verified against the actual value. **(C)** Absolute error diagram between the predicted value and the actual value of the data. **(D)** Error distribution map between the predicted value and the actual value of the data. **(E)** Correlation scatter plot of mVSS. y = 1.0112*x+1.5381, R^2 = 0.9211, r = 0.9913. **(F,G)** High-risk warning range of 5-hydroxylysine and 1-methylnicotinamide at the planform and three-dimensional levels.

(**Figure 8F**). The high-risk early warning index for 5-hydroxylysine was 4×10^8-6.3×10^8 (p = 0.0008), and the high-risk predictive index for 1-methylnicotinamide was 0.95×10^7-1.6×10^7 (**Figure 8G**, p = 0.0022). The receiver operator characteristic curve shows that the expression level of 5-hydroxylysine can predict keloids sensitively and specifically (AUC, 0.845; 95% CI,

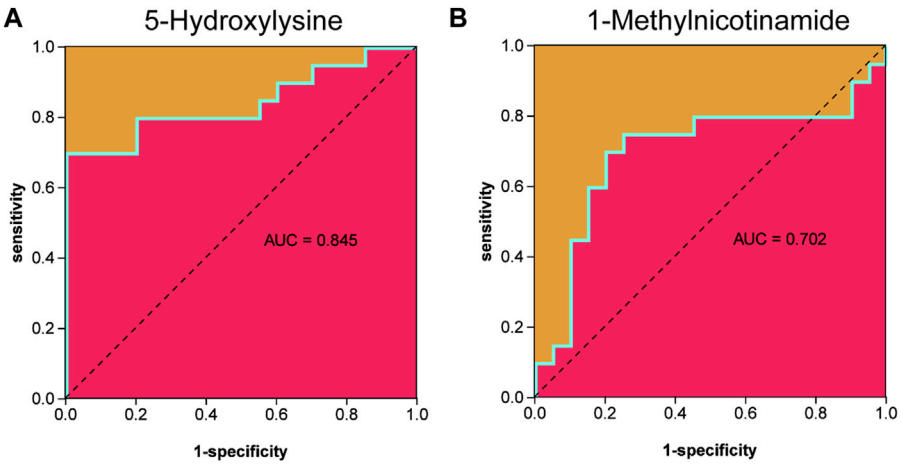

FIGURE 9 | (A) Receiver operator characteristic curve indicated that the expression level of 5-hydroxylysine could sensitively and specifically predict keloids. **(B)** The receiver operator characteristic curve indicated that the expression level of 1-methylnicotinamide could sensitively and specifically predict keloids.

0.715–0.975, **Figures 9A**, and 1-methylnicotinamide can also predict keloids (AUC, 0.702; 95% CI, 0.524–0.881, **Figure 9B**).

1-Methylnicotinamide is formed from nicotinamide N-methyltransferase (NNMT). The overexpression of NNMT is associated with the enhanced proliferation, invasion, and metastasis of various cancers (Eckert et al., 2019; Roberti et al., 2021). The expression of aldehyde oxidase 1 (AOX1) converts 1-methylnicotinamide into 1-methyl-2-pyridone-5-carboxamide (2-PYR) or 1-methyl-4-pyridone-5-carboxamide (Kilgour et al., 2021). AOX1 catalyzes the metabolism of 1-methylnicotinamide (**Supplementary Figure S2A**). The expression levels of NNMT and AOX1 could be analyzed by GSE92566. We found no significant difference in AOX1 between the two groups (**Supplementary Figure S2B**), and the expression of NNMT in group K was much higher than that of the control (**Supplementary Figure S2C**, $p = 0.0008$). The expression of NNMT at the transcription level was consistent with the metabolome sequencing data. This finding indicates that 1-methylnicotinamide may promote the vigorous proliferation and invasion of keloids. 5-Hydroxylysine is one of the raw materials of collagen biosynthesis. 5-Hydroxylysine forms due to collagen biosynthesis or posttranscriptional modification disorders (Wu et al., 2019). The formation of collagen fiber cross-links requires posttranslational modification of procollagen-lysine 2-oxoglutarate 5-dioxygenase 2 (PLOD2). Lysine hydroxylase can be divided into three different subtypes based on different functions: PLOD1, PLOD2, and PLOD3. The expression of PLOD1 (**Supplementary Figure S2D**, $p = 0.0118$) and PLOD2 (**Supplementary Figure S2E**, $p = 0.0023$) was significantly increased in group K compared to the control. The expression of PLOD3 was not significantly different between the two groups (**Supplementary Figure S2F**). The increased expression of PLOD1 and PLOD2 regulates the expression of 5-hydroxylysine in keloid tissue. These results also anastomosed with increased expression of COL3A1, COL1A2, COL1A1, COL5A2, and COL5A1 (**Figure 7D**). Qualitative verification of 1-methylnicotinamide and 5-hydroxylysine was performed using standard products (**Supplementary Figure S3**).

4 DISCUSSION

Keloid is a pathological fibroproliferative disease (Ogawa, 2017). Although an increasing number of studies on keloids have revealed the influence of genetic and environmental factors on their formation, the etiology of keloids is still unclear. Some studies have shown that metabolism is involved, from a metabolome point of view (Bujak et al., 2015). We used non-targeted LC–MS to identify and quantitatively analyze the collected skin tissue samples, and a total of 548 metabolites were identified. There were 162 metabolites that were significantly different between keloids and normal skin ($p < 0.05$). Quality control and a series of analyses were performed on the data, and several important metabolites were finally calculated through the random forest model.

Lipids are an important part of skin and have pro- and anti-inflammatory effects (Louw, 2007; Judge and Dodd, 2020). However, their role in the pathogenesis of keloids has been neglected. Lipids are mainly used as membrane components and second messengers to form biological membrane structures and stratum corneum and play a certain role in local inflammation and intracellular signal transduction (Huang and Ogawa, 2013). Compared with normal tissue, lipids have a tendency to decrease in keloids, while peptides have a tendency to increase in keloids. The decrease in lipids may be a reason for keloid formation.

Skin metabolites of keloids act as peptides, lipids, vitamins and cofactors, nucleic acids, organic acids, carbohydrates, hormones, transmitters, and steroids. The content of lipids is second only to peptides. Lipids include fats (triglycerides), lipids (phospholipids, sterols), sterols and their esters, phospholipids, and glycolipids. Keloid fibroblasts isolated and cultured *in vitro* have a reduced ability to generate PGE2 and EP2 receptors and

increase collagen synthesis (Huang and Ogawa, 2013). The expression of insulin-like growth factor I receptor in keloid fibroblasts is higher than that in normal fibroblasts, which inhibits ceramide-induced apoptosis (Ohtsuru et al., 2000). This fact may be the reason why Fas-mediated signaling molecules in keloids are not converted into ceramides. These studies have shown that lipid metabolism plays an important role in keloid formation.

1-Methylnicotinamide is the amide form of vitamin B3 and the main metabolite of nicotinamide (NA) (Przygodzki et al., 2010). The pyridine compound NA is metabolized by nicotinamide N-methyltransferase (NNMT) to form 1-methylnicotinamide. 1-Methylnicotinamide is an activator of prostacyclin production, which can regulate thrombus formation and inflammatory processes (Chlopicki et al., 2007). 1-Methylnicotinamide can improve the pathological changes in mice induced by free fatty acid binding to albumin, such as inflammation, fibrosis, and necrosis. In a study of liver injury, 1-methylnicotinamide improved liver injury by inhibiting the release of the pro-inflammatory cytokines TNF-α and IL-4 (Chlopicki et al., 2007). The expression of 1-methylnicotinamide in keloids is higher than that in normal tissue. The role of 1-methylnicotinamide in the pathogenesis of keloids has not been studied.

4-Hydroxyproline is a non-essential amino acid that is found in collagen and a few other extracellular animal proteins. Hydroxyproline is an important component of the main structural protein of collagen, which affects the stability and synthesis of collagen (Li and Wu, 2018; Tang et al., 2020). Abnormal hydroxyproline can cause defects in collagen synthesis, such as rupture of tendon connective tissue (Srivastava et al., 2016). Hydroxyproline levels reflect collagen metabolism and are significantly higher in keloid tissue. Keloid fibroblasts are similar in appearance and morphology to normal skin fibroblasts, but the hydroxyproline content and collagen production are significantly higher than those of normal skin fibroblasts (Srivastava et al., 2016).

5-Hydroxylysine is usually present in collagen in the form of glycosylation and is an important synthetic target (Herbert et al., 2012). Collagen contains a peptide sequence with a repeating triplet Gly-X-Y, where Y is usually a proline or lysine residue. During collagen synthesis, certain proline and lysine residues undergo hydroxylation and glycosylation, causing the peptide chain to fold into an alpha-helix. The collagen molecule is a triple helix structure. The formation of the triple helix requires repetition of the Gly-Xaa-Yaa sequence (Herbert et al., 2012). Gly-Pro-Hyp is the most common triplet (10.5–22%) in collagen. The preresidue at the Yaa site of the Gly-Xaa Yaa sequence is converted by prolyl-4-hydroxylase (Herbert et al., 2012), a non–heme iron enzyme that exists in the endoplasmic reticulum. The enzyme catalyzes the posttranslational and stereoselective hydroxylation of the inactive γ-carbon of the Pro residue at the Yaa position of the collagen sequence to form hydroxyproline. Most proline residues at the Yaa position of vertebrate collagen are hydroxyproline. Hydroxylysine plays an important role in stabilizing the triple helix structure of collagen. Abnormal changes or instability of the triple helix structure may cause a variety of diseases (Krane, 2008; Pálfi and Perczel, 2008; Srivastava et al., 2016). The expression of 5-hydroxylysine is higher than that in normal tissue, which may be the reason why collagen production increases and is difficult to diminish. Based on the metabolome data, we found that a single metabolite cannot accurately reflect the severity of keloids. The successful construction of the neural network model demonstrated that the expression of 5-hydroxylysine and 1-methylnicotinamide may be predictors of the severity of keloids. The high-risk early warning index for 5-hydroxylysine is 4×10^8-6.3×10^8, and the high-risk predictive index for 1-methylnicotinamide is 0.95×10^7-1.6×10^7. The results of this study may have practical clinical significance because metabolites are easier to obtain from skin tissues than transcriptomes, for example, they can be easily obtained from skin secretions. The expression level of metabolites can more conveniently reflect the development process of keloids and provide a convenient biomarker for early diagnosis, treatment, and prognosis observation.

Interestingly, when the expression of 5-hydroxylysine was the highest, the symptoms of keloids were not the most serious, which may be related to the complex mechanism of the interaction of 1-methylnicotinamide and 5-hydroxylysine and will also be an interesting research direction in the future to explore the underlying molecular reasons. Transcriptome analysis reveals the pathogenesis of keloids from the perspective of gene expression. Collagen accumulation is an important manifestation of the pathogenesis of keloids (Andrews et al., 2016). Transcriptome analysis showed that the core differentially expressed genes related to collagen synthesis play a vital role in the pathogenesis of keloids, including COL1A, COL1A2, COL5A2, and COL3A1. The analysis of the keloid immune microenvironment revealed the infiltration of immune cells around fibroblasts, which directly or indirectly affected the proliferation of fibroblasts (Zhou et al., 2021). The expression of NNMT, AOX1, PLOD1, PLOD2, and PLOD3 at the transcription level is consistent with the metabolome sequencing data (**Supplementary Figure S2**). The expression of Tregs in groups K and N was significantly different ($p = 0.032$), which may be related to the vigorous growth of keloid tissue. Tregs play a significant role in immunosuppression and self-tolerance. Tregs indirectly inhibit the production of TGF-β by reducing the number of macrophages or directly inhibit the production of TGF-β by releasing IL-10. Murao et al. (2014) found that the proportion of Tregs in keloids is relatively low, which is related to our study of inhibition. Coculture of Tregs and keloid fibroblasts can reduce the expression of type I collagen and TGF-β in keloids.

This study reveals the metabolome characteristics of keloids for the first time and calculates the metabolites with significant differences between the two groups through machine learning, and enrichment analysis further reveals the possible pathogenesis of keloids. The core genes and immune cells of keloid pathogenesis were identified by transcriptome analysis.

1-Methylnicotinamide is produced by NNMT, which is mainly expressed in tumor cells and fibroblasts. NNMT is overexpressed in various cancers and is related to proliferation, invasion, and metastasis (Eckert et al., 2019; Roberti et al., 2021). The expression of NNMT is restricted to fibroblasts and tumor cells (Kilgour et al., 2021). The overexpression of NNMT promotes metabolism in tumor-associated fibroblasts of the ovary, leading to invasion and metastasis of tumors, and is related to poor prognosis (Kilgour et al., 2021). AOX1 is expressed in fibroblasts, and AOX1 is the enzyme responsible for the degradation of 1-methylnicotinamide (Kilgour et al., 2021). There was no significant difference in AOX1 between the two groups (**Supplementary Figure S2B**), and the expression of NNMT in group K was higher than that of the control (**Supplementary Figure S2C** $p = 0.0008$), possibly indicating that the overexpression of NNMT may be a factor influencing the vigorous proliferation of keloid fibroblasts. The expression of PLOD1 and PLOD2 was abnormally increased at the transcriptional level, which affected the abnormal metabolism of 5-hydroxylysine, enhanced collagen cross-linking, and increased deposition.

The expression levels of 5-hydroxylysine and 1-methylnicotinamide can more conveniently reflect the development process of keloids and provide convenient biomarkers for early diagnosis, treatment, and prognostic observation. However, these observations still need to be clinically verified and observed on a larger scale. Although promising metabolites were determined through rigorous bioinformatics analysis and the metabolites were qualitatively verified, there was no richer experimental design and no verification of the enrichment of pathway information. We only discovered the laws of the two metabolites in the neural network model and did not conduct in-depth exploration and experimental verification of the interaction of the two metabolites, which is a limitation and will be further studied in future research.

DATA AVAILABILITY STATEMENT

The data presented in the study are deposited in the iProX repository, accession number IPX0004021000.

ETHICS STATEMENT

This study was approved by the Medical Ethics Committee of Peking Union Medical College Hospital (JS-2907), China. All participants provided written informed consent.

AUTHOR CONTRIBUTIONS

MS carried out data analysis and was the major contributor to the preparation of the manuscript. YW and YH made substantial contributions to the design of the study and revised the manuscript. HL, YH, KS, TM, and CF submitted the manuscript and did some experiments. YH revised the manuscript.

FUNDING

This study was supported by The National Natural Science Foundation of China (81871538) and Beijing Municipal Commission of Science and Technology (Z191100006619009).

ACKNOWLEDGMENTS

We thank Xiaoyan Liu for technical guidance.

SUPPLEMENTARY MATERIAL

The Supplementary Material for this article can be found online at: https://www.frontiersin.org/articles/10.3389/fgene.2021.804248/full#supplementary-material

REFERENCES

Andrews, J. P., Marttala, J., Macarak, E., Rosenbloom, J., and Uitto, J. (2016). Keloids: The Paradigm of Skin Fibrosis - Pathomechanisms and Treatment. *Matrix Biol.* 51, 37–46. doi:10.1016/j.matbio.2016.01.013

Berman, B., Maderal, A., and Raphael, B. (2017). Keloids and Hypertrophic Scars: Pathophysiology, Classification, and Treatment. *Dermatol. Surg.* 43 (Suppl. 1), S3–S18. doi:10.1097/DSS.0000000000000819

Bujak, R., Struck-Lewicka, W., Markuszewski, M. J., and Kaliszan, R. (2015). Metabolomics for Laboratory Diagnostics. *J. Pharm. Biomed. Anal.* 113, 108–120. doi:10.1016/j.jpba.2014.12.017

Chambers, M. C., Maclean, B., Burke, R., Amodei, D., Ruderman, D. L., Neumann, S., et al. (2012). A Cross-Platform Toolkit for Mass Spectrometry and Proteomics. *Nat. Biotechnol.* 30, 918–920. doi:10.1038/nbt.2377

Chen, B., Khodadoust, M. S., Liu, C. L., Newman, A. M., and Alizadeh, A. A. (2018). Profiling Tumor Infiltrating Immune Cells with CIBERSORT. *Methods Mol. Biol.* 1711, 243–259. doi:10.1007/978-1-4939-7493-1_12

Chlopicki, S., Swies, J., Mogielnicki, A., Buczko, W., Bartus, M., Lomnicka, M., et al. (2007). 1-Methylnicotinamide (MNA), a Primary Metabolite of Nicotinamide, Exerts Anti-Thrombotic Activity Mediated by a Cyclooxygenase-2/prostacyclin Pathway. *Br. J. Pharmacol.* 152, 230–239. doi:10.1038/sj.bjp.0707383

Eckert, M. A., Coscia, F., Chryplewicz, A., Chang, J. W., Hernandez, K. M., Pan, S., et al. (2019). Proteomics Reveals NNMT as a Master Metabolic Regulator of Cancer-Associated Fibroblasts. *Nature* 569, 723–728. doi:10.1038/s41586-019-1173-8

Elpa, D. P., Chiu, H.-Y., Wu, S.-P., and Urban, P. L. (2021). Skin Metabolomics. *Trends Endocrinol. Metab.* 32, 66–75. doi:10.1016/j.tem.2020.11.009

Esmaelpoor, J., Moradi, M. H., and Kadkhodamohammadi, A. (2020). A Multistage Deep Neural Network Model for Blood Pressure Estimation Using Photoplethysmogram Signals. *Comput. Biol. Med.* 120, 103719. doi:10.1016/j.compbiomed.2020.103719

Gromski, P. S., Muhamadali, H., Ellis, D. I., Xu, Y., Correa, E., Turner, M. L., et al. (2015). A Tutorial Review: Metabolomics and Partial Least Squares-Discriminant Analysis - a Marriage of Convenience or a Shotgun Wedding. *Analytica Chim. Acta* 879, 10–23. doi:10.1016/j.aca.2015.02.012

Hanko, M., Grendár, M., Snopko, P., Opšenák, R., Šutovský, J., Benčo, M., et al. (2021). Random Forest-Based Prediction of Outcome and Mortality in Patients with Traumatic Brain Injury Undergoing Primary Decompressive Craniectomy. *World Neurosurg.* 148, e450–e458. doi:10.1016/j.wneu.2021.01.002

Herbert, K. R., Williams, G. M., Cooper, G. J. S., and Brimble, M. A. (2012). Synthesis of Glycosylated 5-hydroxylysine, an Important Amino Acid Present in Collagen-Like Proteins Such as Adiponectin. *Org. Biomol. Chem.* 10, 1137–1144. doi:10.1039/c1ob06394d

Huang, C., and Ogawa, R. (2013). Roles of Lipid Metabolism in Keloid Development. *Lipids Health Dis.* 12, 60. doi:10.1186/1476-511X-12-60

Judge, A., and Dodd, M. S. (2020). Metabolism. *Essays Biochem.* 64, 607–647. doi:10.1042/EBC20190041

Kanehisa, M., and Goto, S. (2000). KEGG: Kyoto Encyclopedia of Genes and Genomes. *Nucleic Acids Res.* 28, 27–30. doi:10.1093/nar/28.1.27

Kilgour, M. K., MacPherson, S., Zacharias, L. G., Ellis, A. E., Sheldon, R. D., Liu, E. Y., et al. (2021). 1-Methylnicotinamide Is an Immune Regulatory Metabolite in Human Ovarian Cancer. *Sci. Adv.* 7 (4), eabe1174. doi:10.1126/sciadv.abe1174

Krane, S. M. (2008). The Importance of Proline Residues in the Structure, Stability and Susceptibility to Proteolytic Degradation of Collagens. *Amino Acids* 35, 703–710. doi:10.1007/s00726-008-0073-2

Kumar Srivastava, A., Khare, P., Kumar Nagar, H., Raghuwanshi, N., and Srivastava, R. (2016). Hydroxyproline: A Potential Biochemical Marker and its Role in the Pathogenesis of Different Diseases. *Curr. Protein Pept. Sci.* 17, 596–602. doi:10.2174/1389203717666151201192247

Li, P., and Wu, G. (2018). Roles of Dietary glycine, Proline, and Hydroxyproline in Collagen Synthesis and Animal Growth. *Amino Acids* 50, 29–38. doi:10.1007/s00726-017-2490-6

Louw, L. (2007). The Keloid Phenomenon: Progress toward a Solution. *Clin. Anat.* 20, 3–14. doi:10.1002/ca.20374

Murao, N., Seino, K.-i., Hayashi, T., Ikeda, M., Funayama, E., Furukawa, H., et al. (2014). Treg-Enriched CD4+ T Cells Attenuate Collagen Synthesis in Keloid Fibroblasts. *Exp. Dermatol.* 23, 266–271. doi:10.1111/exd.12368

Ogawa, R. (2017). Keloid and Hypertrophic Scars are the Result of Chronic Inflammation in the Reticular Dermis. *Int. J. Mol. Sci.* 18, 606. doi:10.3390/ijms18030606

Ohtsuru, A., Yoshimoto, H., Ishihara, H., Namba, H., and Yamashita, S. (2000). Insulin-Like Growth Factor-I (IGF-I)/IGF-I Receptor axis and Increased Invasion Activity of Fibroblasts in Keloid. *Endocr. J.* 47 (Suppl. l), S41–S44. doi:10.1507/endocrj.47.supplmarch_s41

Pálfi, V. K., and Perczel, A. (2008). How Stable Is a Collagen Triple Helix? Anab Initiostudy on Various Collagen and β-Sheet Forming Sequences. *J. Comput. Chem.* 29, 1374–1386. doi:10.1002/jcc.20896

Przygodzki, T., Kazmierczak, P., Sikora, J., and Watala, C. (2010). 1-Methylnicotinamide Effects on the Selected Markers of Endothelial Function, Inflammation and Haemostasis in Diabetic Rats. *Eur. J. Pharmacol.* 640, 157–162. doi:10.1016/j.ejphar.2010.05.014

Ramadan, H., Saber, M., Salah, M., and Samy, N. (2021). The Effectiveness of Long Pulsed Nd:YAG Laser Alone for Treatment of Keloids and Hypertrophic Scars versus its Combination with Bleomycin. *J. Cosmet. Dermatol.* 20, 3899–3906. doi:10.1111/jocd.14509

Rinschen, M. M., Ivanisevic, J., Giera, M., and Siuzdak, G. (2019). Identification of Bioactive Metabolites Using Activity Metabolomics. *Nat. Rev. Mol. Cel Biol.* 20, 353–367. doi:10.1038/s41580-019-0108-4

Roberti, A., Fernández, A. F., and Fraga, M. F. (2021). Nicotinamide N-Methyltransferase: At the Crossroads between Cellular Metabolism and Epigenetic Regulation. *Mol. Metab.* 45, 101165. doi:10.1016/j.molmet.2021.101165

Tang, M., Wang, X., Gandhi, N. S., Foley, B. L., Burrage, K., Woods, R. J., et al. (2020). Effect of Hydroxylysine-O-Glycosylation on the Structure of Type I Collagen Molecule: A Computational Study. *Glycobiology* 30, 830–843. doi:10.1093/glycob/cwaa026

Westerhuis, J. A., van Velzen, E. J. J., Hoefsloot, H. C. J., and Smilde, A. K. (2010). Multivariate Paired Data Analysis: Multilevel PLSDA versus OPLSDA. *Metabolomics* 6, 119–128. doi:10.1007/s11306-009-0185-z

Wu, Z., Hou, Y., Dai, Z., Hu, C.-A. A., and Wu, G. (2019). Metabolism, Nutrition, and Redox Signaling of Hydroxyproline. *Antioxid. Redox Signaling* 30, 674–682. doi:10.1089/ars.2017.7338

Xiong, Y., Wang, K., Zhou, H., Peng, L., You, W., and Fu, Z. (2018). Profiles of Immune Infiltration in Colorectal Cancer and Their Clinical Significant: A Gene Expression-Based Study. *Cancer Med.* 7, 4496–4508. doi:10.1002/cam4.1745

Zelena, E., Dunn, W. B., Broadhurst, D., Francis-McIntyre, S., Carroll, K. M., Begley, P., et al. (2009). Development of a Robust and Repeatable UPLC–MS Method for the Long-Term Metabolomic Study of Human Serum. *Anal. Chem.* 81, 1357–1364. doi:10.1021/ac8019366

Zhou, B., Gao, Z., Liu, W., Wu, X., and Wang, W. (2021). Important Role of Mechanical Microenvironment on Macrophage Dysfunction during Keloid Pathogenesis. *Exp. Dermatol* [Epub ahead of print]. . doi:10.1111/exd.14473

Zhou, R., Zhang, J., Zeng, D., Sun, H., Rong, X., Shi, M., et al. (2019). Immune Cell Infiltration as a Biomarker for the Diagnosis and Prognosis of Stage I-III colon Cancer. *Cancer Immunol. Immunother.* 68, 433–442. doi:10.1007/s00262-018-2289-7

Zhou, Y., Zhou, B., Pache, L., Chang, M., Khodabakhshi, A. H., Tanaseichuk, O., et al. (2019). Metascape Provides a Biologist-Oriented Resource for the Analysis of Systems-Level Datasets. *Nat. Commun.* 10, 1523. doi:10.1038/s41467-019-09234-6

Conflict of Interest: The authors declare that the research was conducted in the absence of any commercial or financial relationships that could be construed as a potential conflict of interest.

Publisher's Note: All claims expressed in this article are solely those of the authors and do not necessarily represent those of their affiliated organizations, or those of the publisher, the editors, and the reviewers. Any product that may be evaluated in this article, or claim that may be made by its manufacturer, is not guaranteed or endorsed by the publisher.

frontiers in Cell and Developmental Biology

ORIGINAL RESEARCH
published: 02 March 2022
doi: 10.3389/fcell.2022.817831

Phosphorylation of MAD2 at Ser195 Promotes Spindle Checkpoint Defects and Sensitizes Cancer Cells to Radiotherapy in ATM Deficient Cells

Yang Wang[1†], Tianyu Yu[2†], Yi Han[1], Yazhi He[1], Yiran Song[1], Leiming Guo[3], Liwei An[1], Chunying Yang[4]* and Feng Wang[1,4]**

[1]Department of Gastroenterology, Shanghai 10th People's Hospital, Tongji University School of Medicine, Shanghai, China, [2]Department of General Surgery, Pudong New Area Gongli Hospital Affiliated to Naval Military Medical University, Naval Military Medical University, Shanghai, China, [3]Department of R&D, Shanghai Creative Immune Therapeutics Co., Ltd, Shanghai, China, [4]Central Laboratory, Shanghai Putuo District People's Hospital, Tongji University School of Medicine, Shanghai, China

OPEN ACCESS

Edited by:
Jiayi Wang,
Shanghai Jiaotong University, China

Reviewed by:
Jin Hou,
Second Military Medical University, China
Xiaojun Xia,
Sun Yat-sen University Cancer Center (SYSUCC), China
Xiao Zhang,
Shanghai Jiaotong University, China

***Correspondence:**
Liwei An
anliwei@sibcb.ac.cn
Chunying Yang
yangchy930@gmail.com
Feng Wang
wolffeng2000@hotmail.com

†These authors have contributed equally to this work

Specialty section:
This article was submitted to Epigenomics and Epigenetics, a section of the journal Frontiers in Cell and Developmental Biology

Received: 18 November 2021
Accepted: 18 January 2022
Published: 02 March 2022

Citation:
Wang Y, Yu T, Han Y, He Y, Song Y, Guo L, An L, Yang C and Wang F (2022) Phosphorylation of MAD2 at Ser195 Promotes Spindle Checkpoint Defects and Sensitizes Cancer Cells to Radiotherapy in ATM Deficient Cells. Front. Cell Dev. Biol. 10:817831. doi: 10.3389/fcell.2022.817831

The spindle assembly checkpoint (SAC) is a critical monitoring device in mitosis for the maintenance of genomic stability. Specifically, the SAC complex comprises several factors, including Mad1, Mad2, and Bub1. Ataxia-telangiectasia mutated (ATM) kinase, the crucial regulator in DNA damage response (DDR), also plays a critical role in mitosis by regulating Mad1 dimerization and SAC. Here, we further demonstrated that ATM negatively regulates the phosphorylation of Mad2, another critical component of the SAC, which is also involved in DDR. Mechanistically, we found that phosphorylation of Mad2 is aberrantly increased in ATM-deficient cells. Point-mutation analysis further revealed that Serine 195 mainly mediated Mad2 phosphorylation upon ATM ablation. Functionally, the phosphorylation of Mad2 causes decreased DNA damage repair capacity and is related to the resistance to cancer cell radiotherapy. Altogether, this study unveils the key regulatory role of Mad2 phosphorylation in checkpoint defects and DNA damage repair in ATM-deficient cells.

Keywords: ATM kinase, mad2, phosphorylation, checkpoint defect, DNA damage repair

INTRODUCTION

Chromosome complementarity is naturally present in eukaryotic cells. During cell division, the gain or loss of chromosomes leads to abnormal chromosome numbers, which is termed aneuploidy and has been documented as one of the predispositions of tumorigenesis (Ganem et al., 2007; Storchova and Kuffer, 2008; Torres et al., 2010; Tang et al., 2011). To avoid abnormal chromosomes occurring, cells have evolved several checkpoints, including the DNA damage checkpoint (DDC), the DNA replication checkpoint (DRC), and the spindle assembly checkpoint (SAC), to ensure the genomic integrity of cells. SAC, also known as a mitotic checkpoint, plays a crucial role in ensuring the correct

Abbreviations: APC/C, anaphase-promoting complex or cyclosome; ATM, Ataxia-Telangiectasia Mutated kinase; CHK1, checkpoints kinases 1; CHK2, checkpoints kinases 2; DDC, DNA damage checkpoint; DRC, DNA replication checkpoint; DDR, DNA damage response; MCC, mitotic checkpoint complex; Mad2, mitotic arrest deficiency; PTM, post-translational modification; SAC, spindle assembly checkpoint; WT, wild-type.

separation of chromosomes and the stability of genetic information. The SAC prevents the anaphase-promoting complex/cyclosome (APC/C) ubiquitin ligase from recognizing and securing cyclin B, ensuring chromosomes are properly attached to spindle microtubules (Bharadwaj and Yu, 2004; Musacchio and Salmon, 2007; Santaguida and Musacchio, 2009). In the prometaphase of the cell cycle, kinetochore, without microtubule attachments, recruits evolutionarily conserved proteins such as Aurora-B, Bub1, Bub3, BubR1/Mad3, Mad1, Mad2, Cad20, and MPS1, thus activating SAC to prevent the cells from entering anaphase (Li and Nicklas, 1995; Mora-Santos et al., 2016; Overlack et al., 2017; Raaijmakers et al., 2018). Among them, Mad2, Cdc20, Mad3 (also named BubR1 in some species), and Bub3 form the mitotic checkpoint complex (MCC), which are mainly responsible for inhibiting APC/C, leading to cell cycle arrest (Yu, 2006; Musacchio and Salmon, 2007; Chao et al., 2012). Accordingly, dysregulation of these proteins, either upregulation or downregulation, results in the breakdown of SAC and eventually genomic instability (Schuyler et al., 2012).

The mitotic arrest deficiency 2 (Mad2) is a SAC protein with two natural folding states, namely open conformer (O-Mad2) and close conformer (C-Mad2) (Luo et al., 2004). The transition of O-Mad2 to C-Mad2 is a key determinant for the assembly of a core complex required for activation of SAC between Mad2 and Mad1 (Yu, 2006; Yang et al., 2008). Besides, the Mad2 transition plays an important role in the subsequent inhibition of APC/C by binding to Cad20 (Luo et al., 2002) and is suspected as a mediator determining the metaphase–anaphase transition in mitosis (Varetti et al., 2011). In eukaryotic cells, another intrinsic mechanism maintaining genome stability is DNA damage response (DDR) (Kastan, 2008). As one of the key regulators in DDR, ataxia-telangiectasia mutated (ATM) recognizes DNA damage sites and phosphorylates histone H2AX, followed by recruiting the RAD50/MRE11/NBS1 complex to the breakpoints, thus initiating the DNA damage signaling cascade and repair process (Guleria and Chandna, 2016). In addition, ATM has also been reported to regulate diverse processes *via* phosphorylating distinct substrates, including checkpoints kinases 1,2 (CHK1,2) and p53 (Squatrito et al., 2010; Serrano et al., 2013; Zhang et al., 2014).

Despite intensive studies focusing on the importance of ATM in response to DDR, growing evidence has suggested the ATM's new role in mitosis. In this regard, we previously have proven that ATM kinase is activated in mitosis in the absence of DNA damage by Aurora-B-mediated Serine 1403 phosphorylation and also participated in SAC activation partially by regulation of Bub1 activity (Yang et al., 2011; Yang et al., 2012). In addition, it has been reported that changes in Mad2 levels not only affected the function of SAC, leading to increased chromosome loss and mitotic arrest (Rossio et al., 2010; Barnhart et al., 2011), but also promoted aneuploidy and induced tumorigenesis (Sotillo et al., 2010; Schvartzman et al., 2011). Nevertheless, whether ATM and Mad2 have a regulatory interrelationship during the cell cycle remains elusive. Outstanding work has demonstrated that *in vitro* artificially produced phosphorylated Mad2 leads to its protein architectures, which in turn affects its activity *in vivo* (Kim et al., 2010). However, the regulatory mechanisms that modulate Mad2 remain unknown. In this study, we found that human Mad2 is a phosphorylatable protein naturally occurring in various cells, and its phosphorylation level is negatively regulated by ATM.

MATERIALS AND METHODS

Cell Lines and Culture

HeLa, 293FT, MCF7, and Panc-1 cells (American Type Culture Collection, Manassas, VA) were cultured in Dulbecco's modified Eagle's medium supplemented with 10% fetal bovine serum, 4 mM of L-glutamine, and 50 μg/ml of penicillin/streptomycin (all from Gibco, Carlsbad, CA). The simian virus 40-transformed human fibroblast cell lines GM9607 and GM0637 cells (National Institute of General Medical Sciences Human Mutant Cell Repository, Camden, NJ) were cultured in Roswell Park Memorial Institute 1640 medium supplemented with 10% fetal bovine serum and 50 μg/ml of penicillin/streptomycin. All cells were maintained in 5% CO_2 at 37°C.

Analysis of the Spindle-Assembly Checkpoint by Flow Cytometry

Approximately 10^6 cells were trypsinized, washed, and resuspended in 70% ethanol at −20°C. Subsequently, cells were washed by phosphate-buffered saline with neither Ca^{2+} nor Mg^{2+} (D-PBS). After blocking in the D-PBS with 1% bovine serum albumin for 30 min, cells were incubated with Alexa Fluor® 488 Mouse monoclonal to Histone H3 (phospho S10) (1:100, ab197502, Abcam) at room temperature in the dark for recognition of mitotic cells. After 3 h, cells were washed three times with D-PBS by centrifugation, stained with 50-μg/ml propidium iodide (PI; C1052, Beyotime) for 30 min at 37 °C, and finally analyzed by FACSCanto II flow cytometer (BD Biosciences, San Jose, CA, USA). The percentage of mitotic cells was quantified by Flowjo software (Tree Star).

Plasmids

The construction of Mad1-related plasmids was described in our previous study (Yang et al., 2014). Mad2 and related mutant plasmids were made using Gateway Technology. Briefly, the Mad2 complementary DNA was subcloned into pDONR221, pLVpuro-CMV-N-3Xflag (addgene#123223), and pDEST-CMV-N-EGFP (addgene#122842) vectors. DR-GFP (DR-U2OS), EJ5-GFP, and I-SceI plasmids were described in our previous study (An et al., 2018). All constructs were confirmed by DNA sequencing. The primers are shown in **Table 1**.

Reagents and Antibodies

Nocodazole and Ku55933 were ordered from Selleckchem (Texas, USA). Lambda Protein phosphatase (λPPase) was bought from Sigma-Aldrich Corporation. The anti-ATM (1:1,000, ab201022, Abcam), anti-phospho-ATM (1:1,000, ab81292, Abcam), anti-

TABLE 1 | List of primers used in this manuscript.

Primer's name	Sequences
Flag-Mad2-WT-F	5′-GGGGACAAGTTTGTACAAAAAAGCAGGCTTAATGGCGCTG CAGCTCT-3′
Flag-Mad2-WT-R	5′-GGGGACCACTTTGTACAAGAAAGCTGGGTTTCAGTCATTG ACAGGAATTTTGTAGGCC-3′
GFP-Mad2-WT-F	5′-GGGGACAAGTTTGTACAAAAAAGCAGGCTTAATGGCGCTG CAGCTCT-3′
GFP-Mad2-WT-R	5′-GGGGACCACTTTGTACAAGAAAGCTGGGTTTCAGTCATTG ACAGGAATTTTGTAGGCC-3′
Flag-Mad2-S195A-F	5′-CAAAGTAAATGCCATGGTGGCCTACAAAATTCC-3′
Flag-Mad2-S195A-R	5′-AGGCCACCATGGCATTTTACTTTGTGGATTGTAG-3′
Flag-Mad2-S195D-F	5′-CAAAGTAAATGCCATGGTGGCCTACAAAATTCC-3′
Flag-Mad2-S195D-R	5′-AGGCCACCATGGCATTTACTTTGTGGATTGTAG-3′
GFP-Mad2-S195A-F	5′-CAAAGTAAATGCCATGGTGGCCTACAAAATTCC-3′
GFP-Mad2-S195A-R	5′-AGGCCACCATGGCATTTTACTTTGTGGATTGTAG-3′
GFP-Mad2-S195D-F	5′-CAAAGTAAATGCCATGGTGGCCTACAAAATTCC-3′
GFP-Mad2-S195D-R	5′-AGGCCACCATGGCATTTACTTTGTGGATTGTAG-3′
GFP-Mad2-S120A-F	5′-CAGAGAAAAGGCACAGAAAGCTATCCAGGATGAAATC-3′
GFP-Mad2-S120A-R	5′-TAGCTTTCTGTGCCTTTTCTCTGGGTGCACTGTC-3′
GFP-Mad2-S170A-F	5′-ATGGGAAGAGGCCGGACCACAGTTTATTACCAATTC-3′
GFP-Mad2-S170A-R	5′-ACTGTGGTCCGGCCTCTTCCCATTTTTCAGGTAC-3′
GFP-Mad2-S178A-F	5′-TATTACCAATGCCGAGGAAGTCCGCCTTCGTTC-3′
GFP-Mad2-S178A-R	5′-GGACTTCCTCGGCATTGGTAATAAACTGTGGTC-3′
GFP-Mad2-S185A-F	5′-CCGCCTTCGTGCCTTTACTACTACAATCCACAAAAG-3′
GFP-Mad2-S185A-R	5′-TAGTAGTAAAAGGCACGAAGGCGGACTTCCTCAG-3′
HA-Mad1-WT-F	5′-ACTGGATCCACGATGTACCCATACGATGTTCCAGATTAC GCTATGGAAGACCTGGGGGAAAACACCA-3′
HA-Mad1-WT-R	5′-AGCTCTAGACTACGCCACGGTCTGGCGGCTGAAGAG-3′
HA-Mad1-S214A-F	5′-GAACTCCAGGCCGCACAAGAAGCAAGAGCAGACCACG AGCAGC-3′
HA-Mad1-S214A-R	5′-GCTGCTCGTGGTCTGCTCTTGCTTCTTGTGCGGCCTG GAGTTC-3′
HA-Mad1-S214E-F	5′-GAACTCCAGGCCGAGCAAGAAGCAAGAGCAGAC-3′
HA-Mad1-S214E-R	5′-GCTACTCGTGGTCTGCTCTTGCTTCTTGCTCGGCCTGGAGTTC-3′

Mad2 (1:1,000, ab70385, Abcam), anti-Mad1 (1:1,000, ab201022, Abcam), and anti-Cdc20 antibodies (1:1,000, ab183479, Abcam) were bought from Abcam (Cambridge, MA). The anti-HA (1:1,000, 3724T, Cell Signaling Technology), anti-Mad2 (1:1,000, 4636S, Cell Signaling Technology), and the HRP-conjugated secondary antibodies were purchased from Cell Signaling Technology (Danvers, MA). The anti-Flag antibody (1:1,000, F3165, Sigma) was purchased from Sigma. The anti-Mad2 antibody (1:1,000, YT2618, Immunoway) was bought from Immunoway. The anti-GFP (1:1,000, sc-9996, Santa Cruz), anti-Mad2 (1:1,000, sc-47747, Santa Cruz), anti-*p*-Thr (1:1,000, sc-5267, Santa Cruz), and anti-*p*-Ser antibodies (1:1,000, sc-81514, Santa Cruz) were bought from Santa Cruz Biotechnology. Goat anti-mouse lgG-H HRP (1:1,000, M21004L, Abmart) and goat anti-mouse lgG-L HRP (1:1,000, M21005S, Abmart) were purchased from Abmart.

Retroviral ATM and Control Short Hairpin RNA Production

Vectors carrying the human ATM short hairpin RNA (shRNA) with the target sequence of 5′-AAGCGCCTGATTCGAGATCCT-3′ or nontargeting control with the sequence of 5′-TTCTCCGAACGTGTCACGT-3′ were purchased from Genechem (Shanghai, China). The recombinant viruses of human ATM shRNA and control shRNA were transiently transfected into 293T cells with GV115 viral vector packaging system (Genechem) consisting of pHelper1.0, pHelper2.0, and GV115. After 72 h, the supernatant filled with target viruses was harvested for titer analysis and subsequently transfected into HeLa cells. Polymerase chain reaction and Western blot analysis confirmed the knockdown level.

Small Interfering RNA Transfection

Cells were transfected with ATM-specific small interfering RNA (siRNA) oligos (si-ATM: 5′-GCUAUUUACGGAGCUGAUUTT-3′) (GenePharma, China) at 50 nmol/L final concentration using INTERFERin (Polyplus-transfection, France) as the transfection reagent. A scrambled siRNA (siScr: 5′-UUCUCCGAACGUGUCACGUTT-3′) (GenePharma, China) was applied as a negative control. Cells were harvested 72 h, followed by gene expression analysis by Western blot analysis.

Western Blotting

Cells were scraped in PBS, pelleted, and lysed in NETN buffer (20-mM Tris-HCl, pH 8.0, 100-mM NaCl, 0.5% Nonidet P-40, and 1-mM ethylenediaminetetraacetic acid) supplemented with BitNuclease (Biotool) on ice for 15 min. Cell lysates were boiled after the addition of Lamelli buffer. Proteins were separated by sodium dodecyl sulfate–polyacrylamide gel electrophoresis gel and then transferred to the nitrocellulose membrane. After incubation with indicated primary and secondary antibodies, blots were filmed and detected using the Pierce chemiluminescence detection system.

Immunoprecipitation

Our previous study described immunoprecipitation (An et al., 2020). Whole-cell lysates were incubated with Flag Agarose beads or protein A/G plus agarose beads conjugated with indicated

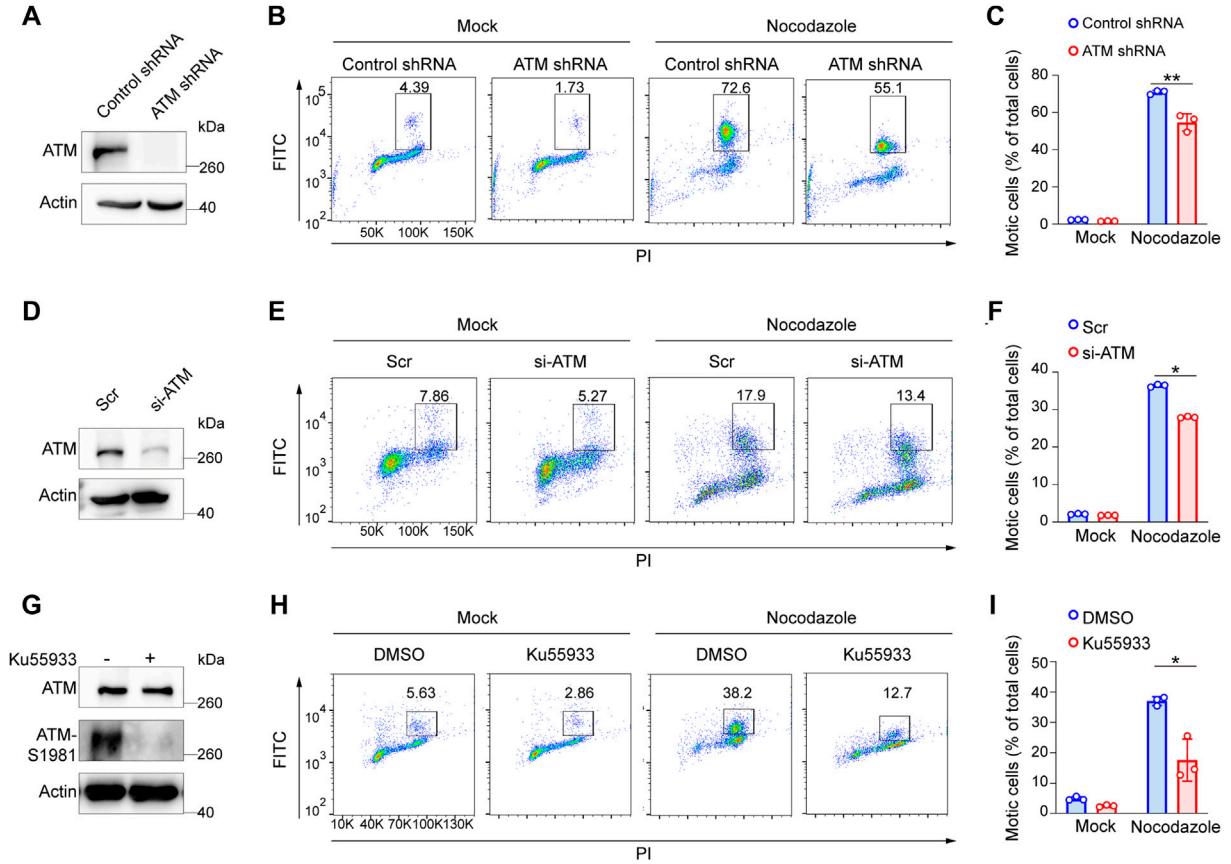

FIGURE 1 | Elimination of ATM resulted in a severe defect in SAC in absence of DNA damage. **(A)** Immunoblotting analysis of ATM level in ATM shRNA and control shRNA cells. **(B)** FACS analysis of ATM shRNA and control shRNA cells treated with nocodazole for 16 h followed by flow cytometric using anti-phospho-H3. **(C)** Mean mitotic percentages of at least triplicate samples are shown. Error bars represent variations around averages. **(D)** Immunoblotting analysis of knockdown efficiency of ATM in Panc-1 cells transfected with ATM-specific siRNA for 48 h, scrambled siRNA as a positive control. **(E)** FACS analysis of Panc-1 cells transfected with scrambled siRNA or ATM-specific siRNA treated with or without nocodazole. **(F)** Mean mitotic percentages of at least triplicate samples are shown, and error bars represent variations around averages. **(G)** Immunoblotting analysis of ATM activity in Hela cells treated with KU-55933 for 2 h. **(H)** FACS analysis of HeLa cells treated with dimethyl sulfoxide or KU-55933 and nocodazole. **(I)** Mean mitotic percentages of at least triplicate samples described in **(B)**. Error bars represent variations around averages.

antibodies overnight at 4°C, washed three times with NETN buffer. To avoid the noise of light or heavy chains, the immunoprecipitation assays, including goat anti-mouse immunoglobulin G heavy chain and goat anti-mouse immunoglobulin G light chain, were used as the secondary antibodies.

Colony Formation Assay

HeLa cells transfected with empty vector, wild-type (WT), S195A, or S195D mutant form of Mad2 (1,000 cells per well) were plated to six-well plates, irradiated with the indicated doses of X-rays, and then further cultured for 12 days. After incubation with crystal violet for 60 min at room temperature, the colonies were imaged under a stereomicroscope and counted with ImageJ.

DSB Reporter Assay

HeLa cells stably expressing the WT, S195A, or S195D mutant form of Mad2 were electroporated with the I-SceI expression construct (pCBASce) together with DR-GFP or EJ5-GFP reporter plasmid at 150 V, 975 μF using NEPA21 Super Electroporator (NEPA GENE). Cells were further recovered for 48 h after electroporation followed by flow cytometric analysis on a BD FACS CantoII Analyzer.

Statistics

Unless otherwise stated, data for the statistical analysis are obtained from at least three independent experiments. The unpaired Student's t-test was used to evaluate statistical significance. Values of $p \leq 0.05$ were considered statistically significant.

RESULTS

ATM Deficiency Causes Severe SAC Defects in the Absence of DNA Damage

ATM deficiency has been associated with chromosomal instability, thus increasing the radiosensitivity (Shiloh, 2003).

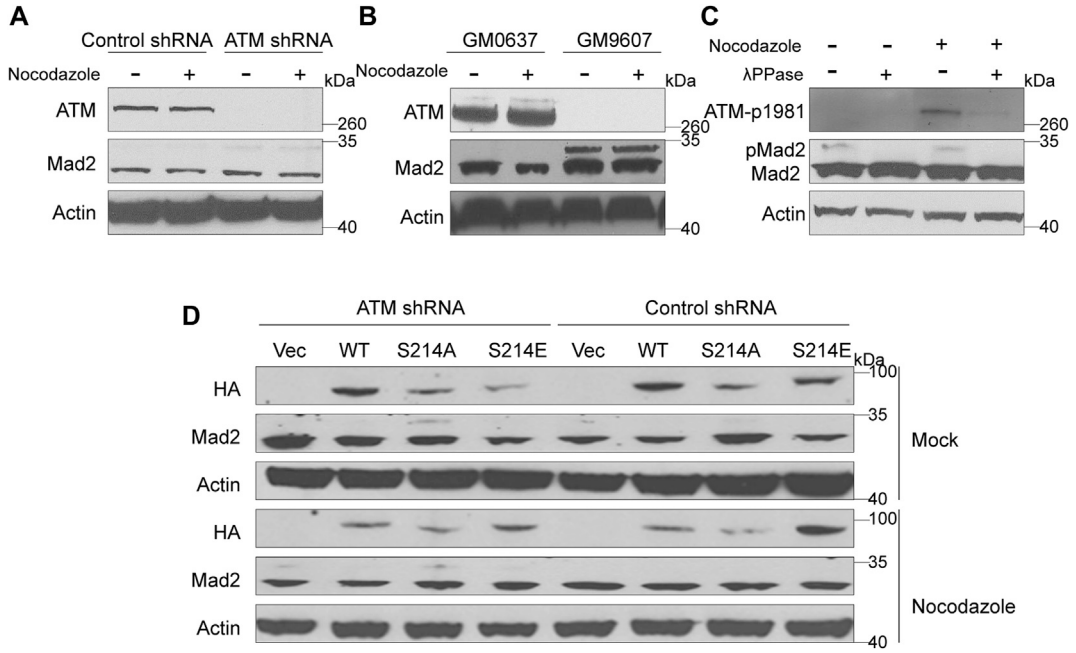

FIGURE 2 | Elimination of ATM increased phosphorylation of Mad2. **(A)** Immunoblotting analysis of control or ATM shRNA cells in absence or presence of nocodazole. **(B)** Immunoblotting analysis in simian virus 40-transformed fibroblast cell lines GM9607 and GM0637. **(C)** Immunoblotting analysis of cells treated with mock or nocodazole in presence or absence of λPPase. **(D)** Immunoblotting analysis of HeLa cells transfected with vector, WT, S214A, or S214D mutant form of Mad1 of in presence or absence of nocodazole.

To further investigate the effects of ATM for the SAC process in the absence of DNA damage, we first infected HeLa cells with lentivirus harboring control shRNA or ATM shRNA to generate stable ATM knockdown cell lines (**Figure 1A**). Then, we treated cells with nocodazole to arrect cells in the mitotic phase. Interestingly, we reproducibly observed a significant decrease in the percentage of mitotic cells in ATM-deficient cells as compared with control WT cells, revealing a severely impaired activation of SAC (**Figures 1B,C**). To confirm this discovery, we repeated this assay in Panc-1 cell lines *via* siRNA-mediated knockdown approach (**Figure 1D**) and HeLa cells *via* ATM inhibitor. Consistently, we found that depletion of ATM resulted in dramatically reduced mitotic cell population (**Figures 1E,F,H,I**). Thus, these phenomena indicated that ATMs play a crucial role in maintaining the activation of SAC.

ATM Deficiency Augments the Phosphorylation of Mad2 by Mediating Mad1 Serine 214 Phosphorylation

Mad2 is a mitotic factor downstream of the ATM during DDR, and its downregulation often impairs the function of SAC, causing shortened mitosis time (Kim et al., 2010; Yang et al., 2014). We assessed whether depletion of ATM would impact the function of Mad2. To this end, we first compared the expression level of Mad2 in GM9607 cells, a naturally ATM-deficient cell line (Yang et al., 2014), and GM0637. However, we did not observe any change in the total Mad2 protein level (**Figure 2B**). Interestingly, we found a clear Mad2 shift band that highly resembled post-translational modification (PTM) (**Figure 2B**). Authentically, this Mad2 shift band repeatedly appeared in ATM knockdown HeLa cells (**Figure 2A**), and Mad2 shift bands are inversely correlated with the ATM protein level, indicating that ATM deficiency may induce Mad2 PTM. It is worth mentioning that the emergence of the Mad2 shift band was not affected by nocodazole treatment.

ATM is a kinase that functions by regulating the phosphorylation of downstream proteins. Thus, we suspect that the shift band might be a manifestation of mad2 phosphorylation. To confirm our hypothesis, we used lambda protein phosphatase (λPPase) as a phosphorylation inhibitor on the total proteins of GM9607 cells. In addition, we also included GM0637, an ATM proficient cell line as a positive control, and examined the phosphorylation status of ATM-S1981, which is a well-known ATM protein serine site that can be autophosphorylated. Surprisingly, we found that both ATM-S1981 phosphorylation band and Mad2 shift band disappeared with λPPase treatment (**Figure 2C**), demonstrating that the shift band in **Figures 2A,B** (measured by antibody against Mad2) is phosphorylated Mad2.

Mad1 and Mad2 are two key SAC proteins. Our previous studies have proved that ATM-mediated Serine 214 phosphorylation of Mad1 promotes Mad1 homodimerization and heterodimerization with Mad2, which contributes to the activation of the SAC (Yang et al., 2014). To further investigate whether this process has an effect on Mad2 phosphorylation, we constructed three Mad1 plasmids, including HA-tagged WT, S214A (the seine to alanine mutant), which cannot be

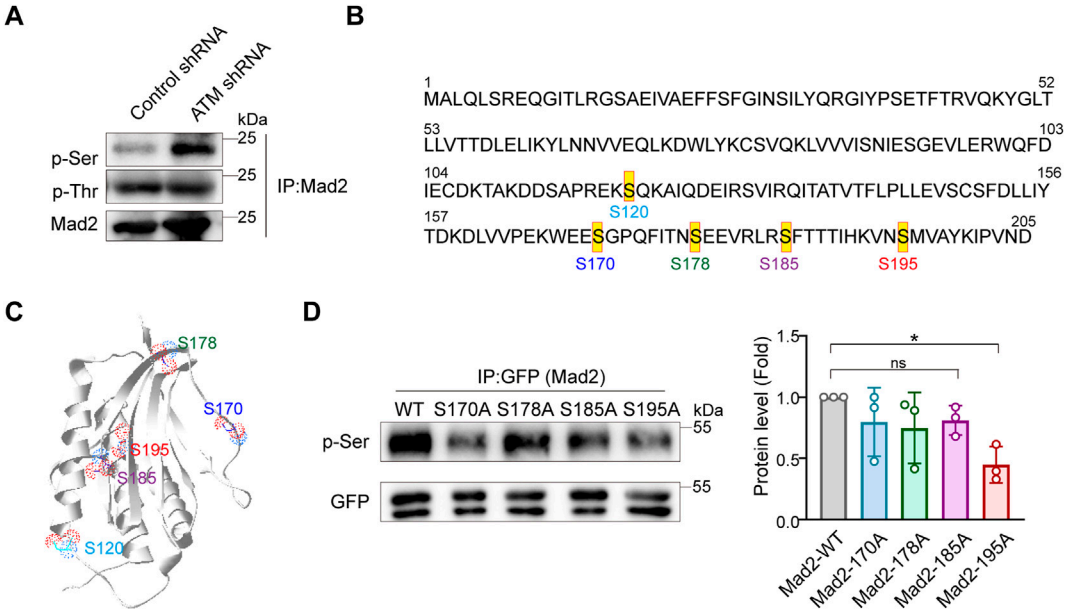

FIGURE 3 | Mad2 is mainly phosphorylated at Ser195 in ATM-loss cells. **(A)** Immunoprecipitation assay of detecting abundance of Mad2 phosphorylation in control or ATM shRNA cells. **(B)** Some phosphorylated sites in Mad2. **(C)** Structures of Mad2 S120, S170, S178, S185, and S195 are shown as ball-and-stick. **(D)** Immunoprecipitation assay of HeLa cells transfected with GFP-tagged WT, S170A, S178A, S185A, or S195A mutants of Mad2. Exogenous proteins were immunoprecipitated with anti-GFP antibody followed by immunoblotting using indicated antibodies. Statistic analyses were done by *t*-test, and *p* values are presented.

phosphorylated, and S214E (the seine to glutamic acid mutant), which is a mimic phosphorylated Mad1 (**Figure 2D**). These plasmids were transiently transferred into HeLa cells stably expressing ATM shRNA or control shRNA. We found that Mad2 phosphorylation was significantly higher in the ATM-deficient HeLa cells expressing S214A than that in other cells, indicating that Mad2 phosphorylation was negatively regulated by ATM.

Mad2 Is Mainly Phosphorylated at Ser195 Upon ATM Depletion

Phosphorylation events mainly occur at serine or tyrosine residues of proteins. Next, to identify the key residues responsible for Mad2 phosphorylation upon ATM deletion, we examined the total serine or tyrosine phosphorylation on Mad2 using individual pan phospho-Tyr or phospho-Ser antibodies. Intriguingly, we observed dramatic upregulation of serine but not tyrosine phosphorylation in ATM knockdown cells, indicating that the Mad2 shift band in this study is mainly serine-phosphorylated Mad2 (**Figure 3A**). Therefore, next, we focused on several key serine residues in Mad2, including S170, S178, S185, and S195, which have been documented to be functioning in SAC complex formation (Kim et al., 2010) (**Figures 3B,C**). To further narrow down the phosphorylated site(s), we applied the point mutation strategy and generated Aline mutant on those residues, respectively. 293FT cells were transfected with plasmids encoding GFP-tagged Mad2^{WT}, Mad2^{S170A}, Mad2^{S178A}, Mad2^{S185A}, or Mad2^{S195A}. All the GFP-tagged Mad proteins are transiently expressed. We performed immunoprecipitation using GFP antibody followed by Western blot using phospho-Ser antibodies. The results showed that S195A mutation greatly attenuated Mad2 phosphorylation (**Figure 3D**). Overall, these results demonstrated that Mad S195 is mainly phosphorylated upon ATM depletion.

S195 Phosphorylation of Mad2 Regulates the Spindle Checkpoint

We next evaluated whether S195 phosphorylation of Mad2 is essential for the SAC process in ATM-deficient cells. To this end, we utilized flow cytometry to analyze the mitotic cell population in Hela cells ectopically expressing Mad2^{WT} or Mad2^{S195A}. We found that S195A overexpression led to a much less mitotic cell population than Mad2^{WT} overexpression (**Figures 4A,B**). On the contrary, in ATM-deficient cells, overexpression of Mad2^{S195A} induced increased mitotic index than Mad2^{WT} cells after nocodazole treatment (**Figures 4A,B**). In addition to the S195A mutant, we also generated a phosphomimic mutant S195D to characterize assembly of CDC20-Mad1-Mad2 complex *via* co-immunoprecipitation assay. As shown in **Figure 4C**, Mad2^{WT} or Mad2^{S195A} can still form the complex with CDC20-Mad1. However, Flag-Mad2^{S195D} failed to bind to Cdc20 but with increased binding ability to Mad1 (**Figure 4C**). Taken together, these data suggested that S195 phosphorylation of Mad2 plays a critical role in SAC after ATM loss.

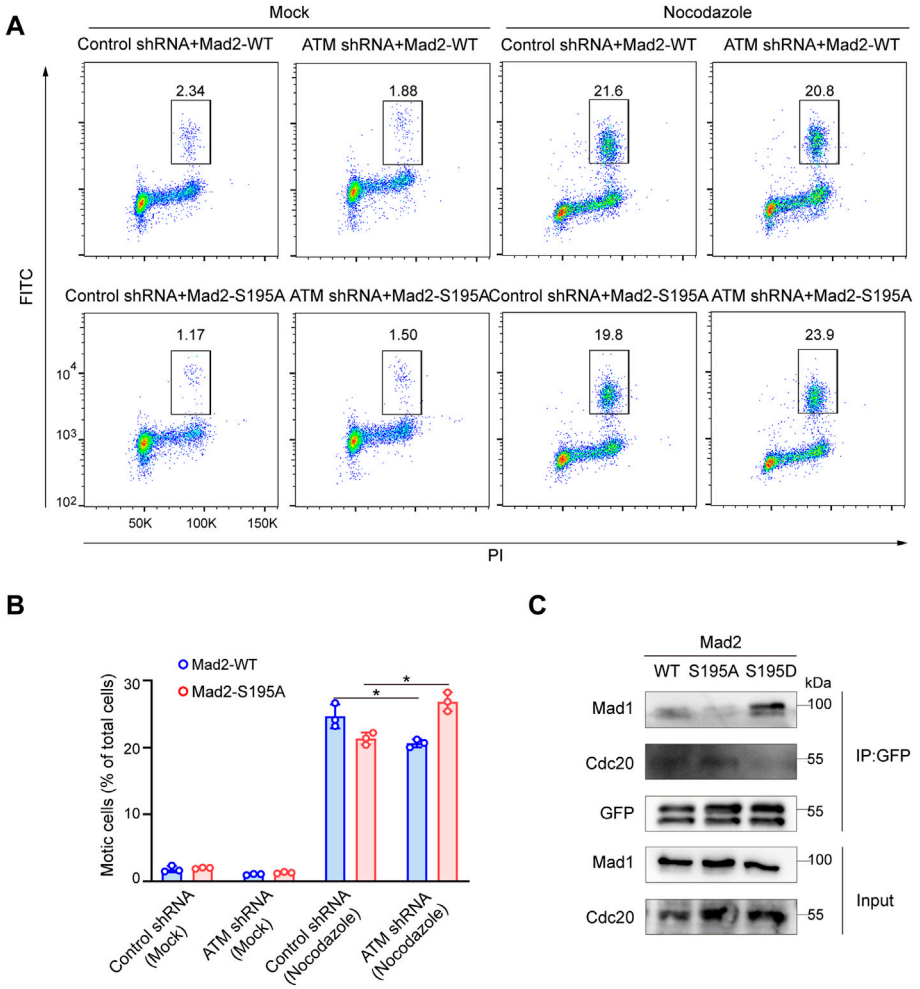

FIGURE 4 | Phosphorylation of Mad2 Serine 195 regulated Spindle Checkpoint. **(A)** FACS analysis of HeLa cells transfected with vector, WT, S195A, or S195D mutant form of Mad2 and treated with nocodazole followed by flow cytometric anti-phospho-H3 staining. **(B)** Mean mitotic percentages (at least triplicate samples) and error bars represent variations around averages. **(C)** Co-immunoprecipitation assay of Mad2 complex in 293FT cells transfected with GFP-tagged S195A or S195D mutants of Mad2.

pMad2^{S195} Impairs DNA Repair Capacity and Confers Cancer Cell Sensitivity to Radiotherapy

The cell cycle phase determines a cell's relative radiosensitivity. Cells in the G (2)-M phase are more radiosensitive compared with those in other phases (Pawlik and Keyomarsi, 2004). Mad2 phosphorylation decreased the proportion of cells in the M phase. To systemically evaluate the effect of phosphorylation of Mad2 on DNA repair and cancer cell sensitivity to radiotherapy, we first utilized a well-established DNA double-strand break (DSB) repair reporter assay to assess the ability of each mutant in promoting DNA repair (**Figures 5A,C**). We found that Mad2 phosphorylation (S195D) significantly inhibited DNA damage repair *via* both homologous recombination (HR) and nonhomologous end-joining (**Figures 5B,D**). In contrast, S195A mutant greatly stimulated the DSB repair process. Consistent with this observation, further colony formation assay revealed that expression of S195A mutant led to more colony numbers than the expression of WT and S195D, indicating that cells with Mad2-S195D increase cancer cell sensitivity to radiotherapy (**Figures 5E,F**).

DISCUSSION

Mad2 possesses typical bimodal protein with two natural folded structures, O-Mad2 and C-Mad2. Compared with the O-Mad2 architecture, the C-Mad2 architecture is more stable and has a stronger affinity with Cdc20, which inhibits the activation of APC/C. Therefore, C-Mad2 has been considered to be an activated form of Mad2. A few years ago, a splendid work showed that the activity of Mad2 can be regulated by exogenous Serine 195 phosphorylation in its C-terminal region (Kim et al., 2010). Although the phospho-mimicking Mad2^{S195D} mutant is easier to bind to high-affinity ligands such as Mad1 and

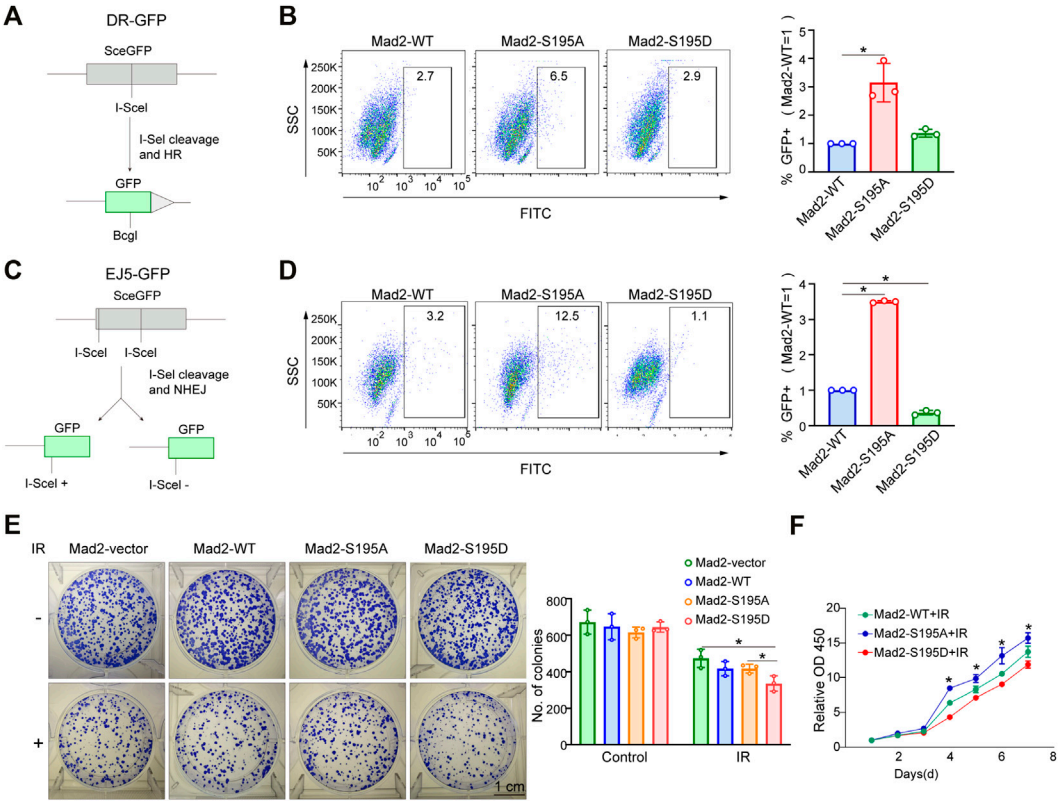

FIGURE 5 | Mad2 phosphorylation impaired DSB repair. **(A,B)** Homology-directed repair assay in control shRNA or ATM shRNA cells subjected to vector, WT, S195A, or S195D transfection. **(C,D)** Nonhomologous end-joining assay in control shRNA or ATM shRNA cells subjected to vector, WT, S195A, or S195D transfection. **(E)** Colony formation assay of control shRNA or ATM shRNA cells transfected with empty vector only, WT, S195A, or S195D with or without interventional radiology treatment. Mean ± SD, Student's t-test, n = 3, *$p < 0.05$. **(F)** CCK-8 assay analysis of cell proliferation abilities in control shRNA or ATM shRNA cells subjected to vector, WT, S195A, or S195D transfection.

MBP1, it inhibits the spontaneous formation of C-Mad2 while failing to bind to the Cdc20, a relatively low-affinity ligand. In addition, the existence of Mad2^{S195D} significantly caused severe damages to SAC complexes (Kim et al., 2010). Thus, the underlying mechanism of Mad2^{S195D}, inhibiting Mad2 function and destroying the SAC, is to differentially alter its ability of binding to Mad1 or Cdc20 by adjusting its protein structure. However, this study did not specifically investigate the existence of endogenous phosphorylation of Mad2 and is according to certain pathways.

ATM is a canonical DNA damage checkpoint protein. We recently found that ATM is also essential for maintaining genome stability in mitosis (Yang et al., 2012; Yang et al., 2014). In addition, our previous research has proved that ATM plays a critical role in SAC by phosphorylating Bub1 on Ser314, thus activating the SAC (Yang et al., 2011). Mad2 is another member of the kinetochore protein complex aside from Bub1. More interestingly, we also found that ATM affects Mad1 and Mad2 complex formation by phosphorylating Mad1 on Serine 214 (Yang et al., 2014). Therefore, we hypothesized that Mad2 may be the direct substrate of ATM kinase, as it always modulates the same pathway by phosphorylating a serious protein. In this study, although there are no phosphate-specific antibodies against Mad2 S195, we found that endogenous Mad2 phosphorylated forms highly regulated by ATM protein level are readily detected by conventional antibodies.

Mad1 is one of the evolutionarily conserved core proteins for SAC, which utilizes its Mad2 interaction motif (MIN) located at the middle region to form a complex with Mad2. During mitosis, the components of the SAC complexes are recruited to unattached kinetochores, and then, the molecular conformation of Mad2 dwelling in the complex changes from a dormant O-Mad2 to a functional C-Mad2, which is one of the key signal amplifying mechanisms for the activation of the SAC. In our previous study, we reported that the heterodimerization consisting of Mad1 and Mad2 was highly regulated by the S214 phosphorylation (S214p) site directly mediated by ATM, and the maintenance of Mad1-S214p is of great significance for preserving SAC function (Yang et al., 2014). In this study, our data indicated that the phosphorylation of Mad2 was observably promoted by S214A in the absence of ATM, whereas the plasmid of S214E and WT significantly inhibited Mad2 phosphorylation, which should occur in ATM-deficient cells. However, despite the presence of S214A, Mad2 no longer exhibited significant levels of phosphorylation in the presence of ATM (**Figure 2D**). Therefore, based on this phenotype, there

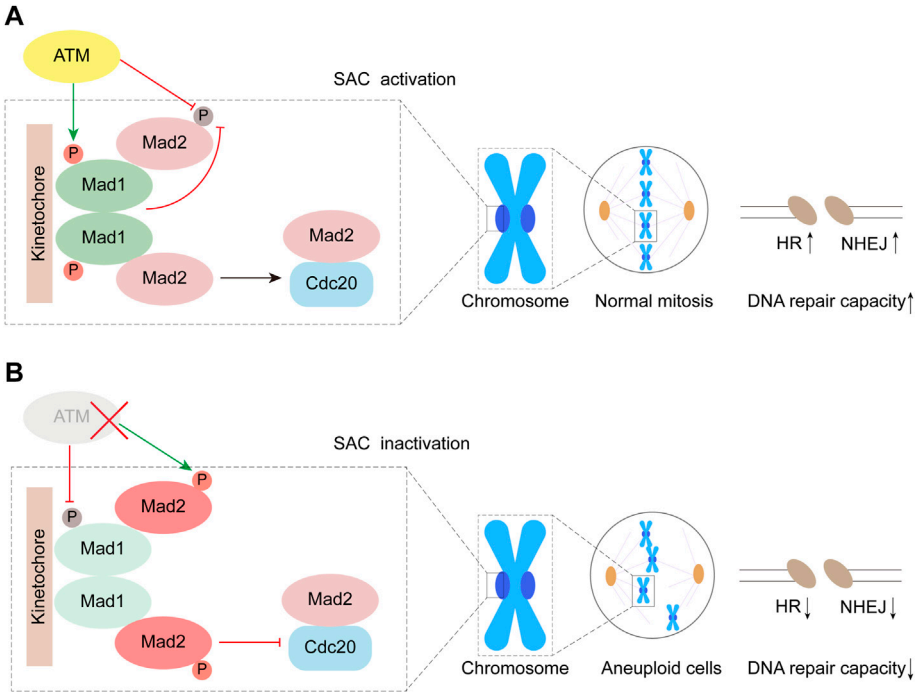

FIGURE 6 | Working model. ATM inhibits phosphorylation of Mad2 by mediating Mad1 Serine 214 phosphorylation.

may be some different pathways regulating Mad2 phosphorylation. In cells with deficient ATM, the amount of non-phosphorylated Mad2 may be directly determined by the level of S214p in Mad1, indicating that Mad1 with S214p is indispensable for ensuring Mad2 activity. When ATM is proficient in cells, ATM may inhibit Mad2 phosphorylation by urging the amount of S214p in Mad1 (**Figure 6**). Besides, it is also possible that ATM might directly act on Mad2 or regulate some involved kinases through the non-Mad1 pathway to maintain the non-phosphorylation of Mad2 (Kastan and Lim, 2000; Chen et al., 2021; Jiang et al., 2022).

Mad2 also plays a critical role in the cellular response to DNA damage (Dotiwala et al., 2010). The Mad2 expression was negatively related to the expression of γH2AX. The N-terminal domain of the Mad2 protein is important in the response to DNA damage (Fung et al., 2008). The overexpression of Mad2 promotes chemosensitivity to anticancer drugs in some tumor cells (Fung et al., 2008; Nascimento et al., 2016). However, other studies reported that Mad2 depletion causes mitotic checkpoint defects to promote mitotic exit, conferring cancer cells sensitive to anticancer drugs (Nascimento et al., 2014; Nascimento et al., 2016). In this study, we found that the Mad2 C-terminal region also exerts a role in DNA damage repair (**Figure 5**). Mad2 phosphorylation decreases M phase cells but decreases DNA repair capacity. Thus, Mad2 phosphorylation causes tumor cells to be sensitive to radiotherapy.

In general, our data demonstrate that, in addition to *in vitro*, Mad2 is a protein with a phosphorylated form also *in vivo*, and its phosphorylation level is regulated by ATM. We also consider that the phosphorylation of Mad2 may play a prominent role in DNA repair pathways. In future studies, we will pursue the kinase involved in Mad2 phosphorylation.

DATA AVAILABILITY STATEMENT

The original contributions presented in the study are included in the article/supplementary material; further inquiries can be directed to the corresponding authors.

AUTHOR CONTRIBUTIONS

YW and TY conducted the experiments, and YH performed the data analysis. YaH and YS collected the data. LG, LA, CY, and FW wrote and revised the manuscript. LA, CY, and FW designed and supervised the whole project. All authors contributed to the article and approved the submitted version. LG is employed by Shanghai Creative Immune Therapeutics Co. The remaining authors declare that the research was conducted in the absence of any commercial or financial relationships that could be construed as a potential conflict of interest.

FUNDING

This work was supported by the National Natural Science Foundation of China (nos. 81972287, 31771497) and the Natural Science Foundation of Shanghai Science and Technology Committee (no. 19ZR1447600).

REFERENCES

An, L., Dong, C., Li, J., Chen, J., Yuan, J., Huang, J., et al. (2018). RNF169 Limits 53BP1 Deposition at DSBs to Stimulate Single-Strand Annealing Repair. *Proc. Natl. Acad. Sci. USA* 115 (35), E8286–E8295. doi:10.1073/pnas.1804823115

An, L., Nie, P., Chen, M., Tang, Y., Zhang, H., Guan, J., et al. (2020). MST4 Kinase Suppresses Gastric Tumorigenesis by Limiting YAP Activation via a Non-canonical Pathway. *J. Exp. Med.* 217 (6). doi:10.1084/jem.20191817

Barnhart, E. L., Dorer, R. K., Murray, A. W., and Schuyler, S. C. (2011). Reduced Mad2 Expression Keeps Relaxed Kinetochores from Arresting Budding Yeast in Mitosis. *MBoC* 22 (14), 2448–2457. doi:10.1091/mbc.E09-01-0029

Bharadwaj, R., and Yu, H. (2004). The Spindle Checkpoint, Aneuploidy, and Cancer. *Oncogene* 23 (11), 2016–2027. doi:10.1038/sj.onc.1207374

Chao, W. C. H., Kulkarni, K., Zhang, Z., Kong, E. H., and Barford, D. (2012). Structure of the Mitotic Checkpoint Complex. *Nature* 484 (7393), 208–213. doi:10.1038/nature10896

Chen, H., Ye, Z., Xu, X., Qin, Y., Song, C., Fan, G., et al. (2021). ALDOA Inhibits Cell Cycle Arrest Induced by DNA Damage via the ATM-PLK1 Pathway in Pancreatic Cancer Cells. *Cancer Cel Int* 21 (1), 514. doi:10.1186/s12935-021-02210-5

Dotiwala, F., Harrison, J. C., Jain, S., Sugawara, N., and Haber, J. E. (2010). Mad2 Prolongs DNA Damage Checkpoint Arrest Caused by a Double-Strand Break via a Centromere-dependent Mechanism. *Curr. Biol.* 20 (4), 328–332. doi:10.1016/j.cub.2009.12.033

Fung, M. K. L., Han, H.-Y., Leung, S. C. L., Cheung, H. W., Cheung, A. L. M., Wong, Y.-C., et al. (2008). MAD2 Interacts with DNA Repair Proteins and Negatively Regulates DNA Damage Repair. *J. Mol. Biol.* 381 (1), 24–34. doi:10.1016/j.jmb.2008.05.080

Ganem, N. J., Storchova, Z., and Pellman, D. (2007). Tetraploidy, Aneuploidy and Cancer. *Curr. Opin. Genet. Dev.* 17 (2), 157–162. doi:10.1016/j.gde.2007.02.011

Guleria, A., and Chandna, S. (2016). ATM Kinase: Much More Than a DNA Damage Responsive Protein. *DNA repair* 39, 1–20. doi:10.1016/j.dnarep.2015.12.009

Jiang, J., Huang, Y., Wang, W., Sun, C., Liu, Q., Chen, Y., et al. (2022). Activation of ATM/Chk2 by Zanthoxylum Armatum DC Extract Induces DNA Damage and G1/S Phase Arrest in BRL 3A Cells. *J. ethnopharmacology* 284, 114832. doi:10.1016/j.jep.2021.114832

Kastan, M. B. (2008). DNA Damage Responses: Mechanisms and Roles in Human Disease. *Mol. Cancer Res.* 6 (4), 517–524. doi:10.1158/1541-7786.MCR-08-0020

Kastan, M. B., and Lim, D.-s. (2000). The many Substrates and Functions of ATM. *Nat. Rev. Mol. Cel Biol* 1 (3), 179–186. doi:10.1038/35043058

Kim, S., Sun, H., Ball, H. L., Wassmann, K., Luo, X., and Yu, H. (2010). Phosphorylation of the Spindle Checkpoint Protein Mad2 Regulates its Conformational Transition. *Proc. Natl. Acad. Sci.* 107 (46), 19772–19777. doi:10.1073/pnas.1009000107

Li, X., and Nicklas, R. B. (1995). Mitotic Forces Control a Cell-Cycle Checkpoint. *Nature* 373 (6515), 630–632. doi:10.1038/373630a0

Luo, X., Tang, Z., Rizo, J., and Yu, H. (2002). The Mad2 Spindle Checkpoint Protein Undergoes Similar Major Conformational Changes upon Binding to Either Mad1 or Cdc20. *Mol. Cel.* 9 (1), 59–71. doi:10.1016/s1097-2765(01)00435-x

Luo, X., Tang, Z., Xia, G., Wassmann, K., Matsumoto, T., Rizo, J., et al. (2004). The Mad2 Spindle Checkpoint Protein Has Two Distinct Natively Folded States. *Nat. Struct. Mol. Biol.* 11 (4), 338–345. doi:10.1038/nsmb748

Mora-Santos, M. d. M., Hervas-Aguilar, A., Sewart, K., Lancaster, T. C., Meadows, J. C., and Millar, J. B. A. (2016). Bub3-Bub1 Binding to Spc7/KNL1 Toggles the Spindle Checkpoint Switch by Licensing the Interaction of Bub1 with Mad1-Mad2. *Curr. Biol.* 26 (19), 2642–2650. doi:10.1016/j.cub.2016.07.040

Musacchio, A., and Salmon, E. D. (2007). The Spindle-Assembly Checkpoint in Space and Time. *Nat. Rev. Mol. Cel Biol* 8 (5), 379–393. doi:10.1038/nrm2163

Nascimento, A. V., Gattacceca, F., Singh, A., Bousbaa, H., Ferreira, D., Sarmento, B., et al. (2016). Biodistribution and Pharmacokinetics of Mad2 siRNA-Loaded EGFR-Targeted Chitosan Nanoparticles in Cisplatin Sensitive and Resistant Lung Cancer Models. *Nanomedicine* 11 (7), 767–781. doi:10.2217/nnm.16.14

Nascimento, A. V., Singh, A., Bousbaa, H., Ferreira, D., Sarmento, B., and Amiji, M. M. (2014). Mad2 Checkpoint Gene Silencing Using Epidermal Growth Factor Receptor-Targeted Chitosan Nanoparticles in Non-small Cell Lung Cancer Model. *Mol. Pharmaceutics* 11 (10), 3515–3527. doi:10.1021/mp5002894

Overlack, K., Bange, T., Weissmann, F., Faesen, A. C., Maffini, S., Primorac, I., et al. (2017). BubR1 Promotes Bub3-dependent APC/C Inhibition during Spindle Assembly Checkpoint Signaling. *Curr. Biol.* 27 (19), 2915–2927. doi:10.1016/j.cub.2017.08.033

Pawlik, T. M., and Keyomarsi, K. (2004). Role of Cell Cycle in Mediating Sensitivity to Radiotherapy. *Int. J. Radiat. Oncology*Biology*Physics* 59 (4), 928–942. doi:10.1016/j.ijrobp.2004.03.005

Raaijmakers, J. A., van Heesbeen, R. G. H. P., Blomen, V. A., Janssen, L. M. E., van Diemen, F., Brummelkamp, T. R., et al. (2018). BUB1 Is Essential for the Viability of Human Cells in Which the Spindle Assembly Checkpoint Is Compromised. *Cel Rep.* 22 (6), 1424–1438. doi:10.1016/j.celrep.2018.01.034

Rossio, V., Galati, E., Ferrari, M., Pellicioli, A., Sutani, T., Shirahige, K., et al. (2010). The RSC Chromatin-Remodeling Complex Influences Mitotic Exit and Adaptation to the Spindle Assembly Checkpoint by Controlling the Cdc14 Phosphatase. *J. Cel. Biol.* 191 (5), 981–997. doi:10.1083/jcb.201007025

Santaguida, S., and Musacchio, A. (2009). The Life and Miracles of Kinetochores. *Embo J.* 28 (17), 2511–2531. doi:10.1038/emboj.2009.173

Schuyler, S. C., Wu, Y.-F., and Kuan, V. J.-W. (2012). The Mad1-Mad2 Balancing Act - a Damaged Spindle Checkpoint in Chromosome Instability and Cancer. *J. Cel. Sci.* 125 (Pt 18), 4197–4206. doi:10.1242/jcs.107037

Schvartzman, J.-M., Duijf, P. H. G., Sotillo, R., Coker, C., and Benezra, R. (2011). Mad2 Is a Critical Mediator of the Chromosome Instability Observed upon Rb and P53 Pathway Inhibition. *Cancer cell* 19 (6), 701–714. doi:10.1016/j.ccr.2011.04.017

Serrano, M. A., Li, Z., Dangeti, M., Musich, P. R., Patrick, S., Roginskaya, M., et al. (2013). DNA-PK, ATM and ATR Collaboratively Regulate P53-RPA Interaction to Facilitate Homologous Recombination DNA Repair. *Oncogene* 32 (19), 2452–2462. doi:10.1038/onc.2012.257

Shiloh, Y. (2003). ATM and Related Protein Kinases: Safeguarding Genome Integrity. *Nat. Rev. Cancer* 3 (3), 155–168. doi:10.1038/nrc1011

Sotillo, R., Schvartzman, J.-M., Socci, N. D., and Benezra, R. (2010). Mad2-induced Chromosome Instability Leads to Lung Tumour Relapse after Oncogene Withdrawal. *Nature* 464 (7287), 436–440. doi:10.1038/nature08803

Squatrito, M., Brennan, C. W., Helmy, K., Huse, J. T., Petrini, J. H., and Holland, E. C. (2010). Loss of ATM/Chk2/p53 Pathway Components Accelerates Tumor Development and Contributes to Radiation Resistance in Gliomas. *Cancer cell* 18 (6), 619–629. doi:10.1016/j.ccr.2010.10.034

Storchova, Z., and Kuffer, C. (2008). The Consequences of Tetraploidy and Aneuploidy. *J. Cel. Sci.* 121 (Pt 23), 3859–3866. doi:10.1242/jcs.039537

Tang, Y.-C., Williams, B. R., Siegel, J. J., and Amon, A. (2011). Identification of Aneuploidy-Selective Antiproliferation Compounds. *Cell* 144 (4), 499–512. doi:10.1016/j.cell.2011.01.017

Torres, E. M., Williams, B. R., Tang, Y. C., and Amon, A. (2010). Thoughts on Aneuploidy. *Cold Spring Harbor symposia quantitative Biol.* 75, 445–451. doi:10.1101/sqb.2010.75.025

Varetti, G., Guida, C., Santaguida, S., Chiroli, E., and Musacchio, A. (2011). Homeostatic Control of Mitotic Arrest. *Mol. Cel.* 44 (5), 710–720. doi:10.1016/j.molcel.2011.11.014

Yang, C., Hao, J., Kong, D., Cui, X., Zhang, W., Wang, H., et al. (2014). ATM-mediated Mad1 Serine 214 Phosphorylation Regulates Mad1 Dimerization and the Spindle Assembly Checkpoint. *Carcin* 35 (9), 2007–2013. doi:10.1093/carcin/bgu087

Yang, C., Tang, X., Guo, X., Niikura, Y., Kitagawa, K., Cui, K., et al. (2011). Aurora-B Mediated ATM Serine 1403 Phosphorylation Is Required for Mitotic ATM Activation and the Spindle Checkpoint. *Mol. Cel.* 44 (4), 597–608. doi:10.1016/j.molcel.2011.09.016

Yang, C., Wang, H., Xu, Y., Brinkman, K. L., Ishiyama, H., Wong, S. T. C., et al. (2012). The Kinetochore Protein Bub1 Participates in the DNA Damage Response. *DNA repair* 11 (2), 185–191. doi:10.1016/j.dnarep.2011.10.018

Yang, M., Li, B., Liu, C.-J., Tomchick, D. R., Machius, M., Rizo, J., et al. (2008). Insights into Mad2 Regulation in the Spindle Checkpoint Revealed by the crystal Structure of the Symmetric Mad2 Dimer. *Plos Biol.* 6 (3), e50. doi:10.1371/journal.pbio.0060050

Yu, H. (2006). Structural Activation of Mad2 in the Mitotic Spindle Checkpoint: the Two-State Mad2 Model versus the Mad2 Template Model. *J. Cel. Biol.* 173 (2), 153–157. doi:10.1083/jcb.200601172

Zhang, P., Wei, Y., Wang, L., Debeb, B. G., Yuan, Y., Zhang, J., et al. (2014). ATM-mediated Stabilization of ZEB1 Promotes DNA Damage Response and Radioresistance through CHK1. *Nat. Cel Biol* 16 (9), 864–875. doi:10.1038/ncb3013

Conflict of Interest: LG is employed by Shanghai Creative Immune Therapeutics Co.

The remaining authors declare that the research was conducted in the absence of any commercial or financial relationships that could be construed as a potential conflict of interest.

Publisher's Note: All claims expressed in this article are solely those of the authors and do not necessarily represent those of their affiliated organizations or those of the publisher, the editors, and the reviewers. Any product that may be evaluated in this article, or claim that may be made by its manufacturer, is not guaranteed or endorsed by the publisher.

frontiers in Cell and Developmental Biology

ORIGINAL RESEARCH
published: 24 March 2022
doi: 10.3389/fcell.2022.853596

SLC2A1 is a Diagnostic Biomarker Involved in Immune Infiltration of Colorectal Cancer and Associated With m6A Modification and ceRNA

Xu-Sheng Liu[1], Jian-Wei Yang[2], Jing Zeng[3], Xue-Qin Chen[4], Yan Gao[1], Xue-Yan Kui[1], Xiao-Yu Liu[1], Yu Zhang[1], Yao-Hua Zhang[1] and Zhi-Jun Pei[1,5]**

[1]Department of Nuclear Medicine and Institute of Anesthesiology and Pain, Taihe Hospital, Hubei University of Medicine, Shiyan, China, [2]Department of Nuclear Medicine, Xiangyang Central Hospital, Affiliated Hospital of Hubei University of Arts and Science, Xiangyang, China, [3]Department of Infection Control, Taihe Hospital, Hubei University of Medicine, Shiyan, China, [4]Hubei University of Medicine, Shiyan, China, [5]Hubei Clinical Research Center for Precise Diagnosis and Treatment of Liver Cancer, Taihe Hospital, Hubei University of Medicine, Shiyan, China

OPEN ACCESS

Edited by:
Jiayi Wang,
Shanghai Jiaotong University, China

Reviewed by:
Yuan Yang,
First Hospital of Lanzhou University, China
Xinming Chen,
Guangdong Medical University, China

***Correspondence:**
Xu-Sheng Liu
lxsking@taihehospital.com
Zhi-Jun Pei
pzjzml1980@taihehospital.com

Specialty section:
This article was submitted to Epigenomics and Epigenetics, a section of the journal Frontiers in Cell and Developmental Biology

Received: 12 January 2022
Accepted: 22 February 2022
Published: 24 March 2022

Citation:
Liu X-S, Yang J-W, Zeng J, Chen X-Q, Gao Y, Kui X-Y, Liu X-Y, Zhang Y, Zhang Y-H and Pei Z-J (2022) SLC2A1 is a Diagnostic Biomarker Involved in Immune Infiltration of Colorectal Cancer and Associated With m6A Modification and ceRNA. Front. Cell Dev. Biol. 10:853596. doi: 10.3389/fcell.2022.853596

Background: Overexpression of solute carrier family 2 member 1 (SLC2A1) promotes glycolysis and proliferation and migration of various tumors. However, there are few comprehensive studies on SLC2A1 in colorectal cancer (CRC).

Methods: Oncomine, The Cancer Genome Atlas (TCGA), and Gene Expression Omnibus (GEO) databases were used to analyze the expression of SLC2A1 in pan-cancer and CRC and analyzed the correlation between SLC2A1 expression and clinical characteristics of TCGA CRC samples. The expression level of SLC2A1 in CRC was certified by cell experiments and immunohistochemical staining analysis. The Genome Ontology (GO), Kyoto Encyclopedia of Genes and Genomes (KEGG), and Gene Set Enrichment Analysis (GSEA) analyses of SLC2A1 relative genes were completed by bioinformatics analysis. The correlation between SLC2A1 expression level and CRC immune infiltration cell was analyzed by Tumor IMmune Estimation Resource (TIMER), Gene Expression Profiling Interactive Analysis (GEPIA), and TCGA database. The correlation between SLC2A1 expression level and ferroptosis and m6A modification of CRC was analyzed by utilizing TCGA and GEO cohort. Finally, the possible competing endogenous RNA (ceRNA) networks involved in SLC2A1 in CRC are predicted and constructed through various databases.

Results: SLC2A1 is highly expressed not only in CRC but also in many other tumors. ROC curve indicated that SLC2A1 had high predictive accuracy for the outcomes of tumor. The SLC2A1 expression in CRC was closely correlated with tumor stage and progression free interval (PFI). GO, KEGG, and GSEA analysis indicated that SLC2A1 relative genes were involved in multiple biological functions. The analysis of TIMER, GEPIA, and TCGA database indicated that the SLC2A1 mRNA expression was mainly positively associated with neutrophils. By the analysis of the TCGA and GEO cohort, we identified that the expression of SLC2A1 is closely associated to an m6A modification

relative gene Insulin Like Growth Factor 2 MRNA Binding Protein 3 (IGF2BP3) and a ferroptosis relative gene Glutathione Peroxidase 4 (GPX4).

Conclusion: SLC2A1 can be used as a biomarker of CRC, which is associated to immune infiltration, m6A modification, ferroptosis, and ceRNA regulatory network of CRC.

Keywords: SLC2A1, colorectal cancer, immune infiltration, m6A modification, ceRNA

INTRODUCTION

Recent studies show that colorectal cancer (CRC) is the third most common cancer and the second most deadly in the world (Sung et al., 2021). Despite significant advances in major treatments such as radical resection, radiotherapy, and chemotherapy, the 5-year survival rate for patients with CRC remains low (Chen et al., 2016; Wang et al., 2021). The occurrence, development, metastasis, and recurrence of CRC after treatment involve a variety of important signal transduction pathways in the body, which is a very complex biological process (Shen et al., 2020). Therefore, in-depth investigation of the pathogenesis of CRC can provide better reference strategies for the diagnosis and treatment of tumors.

Solute carrier family 2 member 1 (SLC2A1) encodes a glucose transporter (GLUT) that is the earliest discovery of humans, GLUT1, encoded on 1p34.2 (Kasahara and Hinkle, 1977; Uldry and Thorens, 2004). Multiple projects have indicated that the overexpression of SLC2A1 is closely related to the progression and metastasis of a variety of cancers (Rudlowski et al., 2004; Pereira et al., 2013; Deng et al., 2014; Berlth et al., 2015; Avanzato et al., 2018). SLC2A1 plays an important role in both normal human metabolism and tumor cell glycolysis (Shen et al., 2020). Although it has been found that the overexpression of SLC2A1 can further the glycolysis process and cell proliferation of CRC (Shen et al., 2020; Chen et al., 2021), the biological function of SLC2A1 in CRC has not been extensively studied. Further investigation of other biological functions that SLC2A1 may be involved in CRC will provide a new basis for improving the diagnosis and treatment of CRC.

Tumor immunotherapy (Wang et al., 2014; Ning et al., 2015), N6-methyladenosine (m6A) modification (Bai et al., 2019; Yang et al., 2020), ferroptosis (Ma et al., 2018; Yang et al., 2021), and competing endogenous RNA (ceRNA) network (Zhao et al., 2021) are hot topics of cancer gene therapy, which are broadly utilized in the investigation and therapy of CRC. Nevertheless, there are few research studies on the comprehensive analysis of SLC2A1 in CRC, particularly the relation between SLC2A1 and immune therapy, m6A modification, ferroptosis, and ceRNA regulatory network of CRC.

On this project, we processed The Cancer Genome Atlas (TCGA) CRC and the Gene Expression Omnibus (GEO) CRC cohort *via* an online network. Bioinformatics analysis was carried utilizing R language, analysis tools, and online website to research the difference of SLC2A1 expression in pan-cancer, and *in vitro* experiments and immunohistochemical (IHC) staining were performed to confirm the difference of SLC2A1 mRNA and protein expression between CRC and normal samples. At present, the SLC2A1 co-expression gene networks in CRC were analyzed and the possible biological function and signal regulation pathway involved in these relative genes were investigated. Eventually, the relation between SLC2A1 and CRC tumor ferroptosis, immunofiltration, m6A modification, and ceRNA network was investigated, which provides a basis for the development of new therapeutic strategies. The schematic diagram of the research design is shown in **Figure 1**.

MATERIALS AND METHODS

Expression of SLC2A1 in CRC

Oncomine online database (www.oncomine.org) (Rhodes et al., 2004; Rhodes et al., 2007) and TCGA cohort (https://portal.gdc.cancer.gov) (Tomczak et al., 2015) were used to analyze the expression differences of SLC2A1 in varied cancers. Student's t-test was used to compare the expression difference of SLC2A1 in tumor and control samples in Oncomine database, and data with fold change >2 and P < 1E-8 were selected for display. In the TCGA cohort, the CRC cohort used included the colon adenocarcinoma (COAD) and rectum adenocarcinoma (READ) datasets. We also analyzed CRC cohort from the TCGA and GEO (www.ncbi.nlm.nih.gov/geo; GSE9348, GSE110223, and GSE110224) (Barrett et al., 2012) databases to investigate differences in SLC2A1 expression level between tumor and control samples. By analyzing the clinical datasets of TCGA CRC cohort, the relation between SLC2A1 expression and clinicopathological characteristics of patients with CRC was investigated, and the diagnostic value of SLC2A1 for CRC was evaluated by ROC curve. Eventually, we certified the difference in SLC2A1 expression between CRC and normal samples by used qRT-PCR and IHC staining. Refer to our previous work (Liu et al., 2021a) for specific steps, including specific methods of qRT-PCR and IHC staining, as detailed in the **Supplementary Material**.

SLC2A1 Gene Co-Expression Network and Enrichment Analysis in CRC

The TCGA CRC cohort was analyzed utilizing the R statistical computing language (version 3.6.3) to investigate co-expressed genes related with SLC2A1 expression. The Pearson's correlation coefficient was used for statistical analysis, and correlations were considered as significant when $|cor| > 0.3$ and $p < 0.05$. Ggplot2 software package of R language (https://ggplot2.tidyverse.org) was utilized to draw volcano and heat map for demonstration. Top 200 genes that were positively correlated with SLC2A1 expression were selected as hub genes. The Genome Ontology

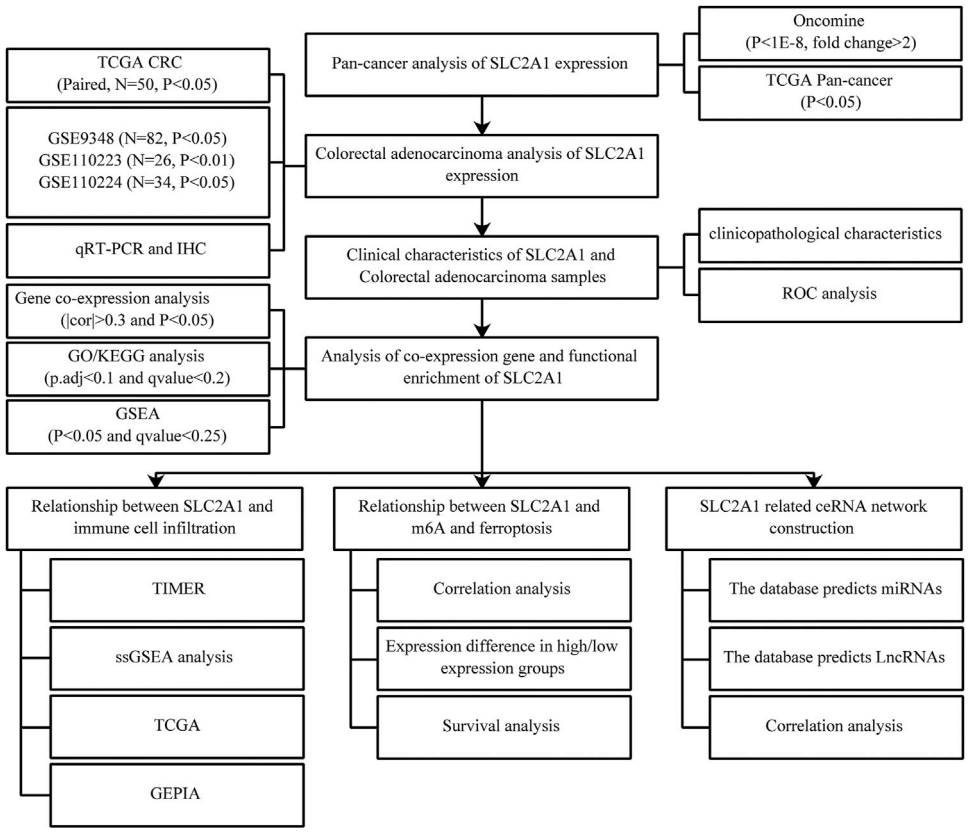

FIGURE 1 | Schematic diagram of the study design.

(GO) term and Kyoto Encyclopedia of Genes and Genomes (KEGG, http://www.genome.jp/kegg) pathway investigation of hub genes was carried by using the clusterProfiler (Yu et al., 2012) software package of R language, and the data were analyzed by using the ggplot2 software package.

Gene Set Enrichment Analysis

To study the potential function of SLC2A1 in CRC, we divided the samples in the CRC cohort into high and low groups based on the SLC2A1 median expression in CRC and carried Gene Set Enrichment Analysis (GSEA) (www.gsea-msigdb.org/gsea/index.jsp) (Subramanian et al., 2005) to research whether genes in the two groups were enriched with meaningful biological functions. The annotated gene set c2.cp.v7.2.symbols.gmt (Curated) was selected as the reference gene set. The FDR (q-value) < 0.25 and $p < 0.05$ were considered statistically significant.

Associations Between SLC2A1 and Tumor Immune Infiltrating Cells

To investigate the possible regulatory mechanism of SLC2A1 in the regulation of CRC immune cells, we utilized the TIMER database (https://cistrome.shinyapps.io/timer) to evaluate the relationship between SLC2A1 expression and immunofiltration cells in TCGA CRC samples. Immunofiltration cells include B cell, neutrophil, CD4+ T cell, CD8+ T cell, macrophage, and dendritic cell (DC). We utilized the somatic copy number alteration module of the TIMER tool to correlate genetic copy number variation (CNV) of SLC2A1 with the relative proportion of immune infiltrating cells. The GSVA (Hänzelmann et al., 2013) software package of R language was utilized to analyze the relative abundance of 24 immune cells in CRC samples with high and low SLC2A1 expression, and the specific algorithm was ssGSEA. Furthermore, we analyzed the relation between SLC2A1 and immunofiltration cell marker genes in CRC samples utilizing Tumor IMmune Estimation Resource (TIMER), Gene Expression Profiling Interactive Analysis (GEPIA), and TCGA databases. Immunofiltration marker genes refer to the previous study, in which immune markers of different immune cells are described (Liu et al., 2021b).

Associations of SLC2A1 Expression Level With m6A Modification in CRC

The association between the expression level of SLC2A1 and the m6A relative genes, including YTHDF1, WTAP, RBM15, FTO, ALKBH5, ZC3H13, YTHDF3, HNRNPC, YTHDC2, METTL14, METTL3, IGF2BP3, IGF2BP2, RBMX, RBM15B, IGF2BP1, YTHDC1, HNRNPA2B1, VIRMA, and YTHDF2 (Li et al., 2019), in GSE110224 and TCGA CRC cohort was analyzed

utilizing the R statistical computing language. In the TCGA cohort, the CRC cohort used included the COAD and READ datasets. The ratio of m6A relative genes in CRC samples with high and low SLC2A1 expression was analyzed by R statistical computing language. The Kaplan–Meier curve indicated the relation between the expression level of relative genes and the prognosis of patients with CRC. Ggplot2 software package was utilized for visual analysis of the cohort.

Associations of SLC2A1 Expression Level With Ferroptosis in CRC

The R statistical computing language was utilized to analyze the association between the expression level of SLC2A1 and ferroptosis relative genes in the GSE110224 and TCGA CRC cohort, including CDKN1A, HSPA5, EMC2, SLC7A11, NFE2L2, MT1G, HSPB1, GPX4, FANCD2, CISD1, FDFT1, SLC1A5, SAT1, TFRC, RPL8, NCOA4, LPCAT3, GLS2, DPP4, CS, CARS, ATP5MC3, ALOX15, ACSL4, and AIFM2 (Doll et al., 2019; Liu et al., 2020). In the TCGA cohort, the CRC cohort used included the COAD and READ datasets. R statistical computing language was utilized to analyze the ratio of ferroptosis relative genes in CRC samples with high and low SLC2A1 expression. The Kaplan–Meier curve indicated the relation between the expression level of relative genes and the prognosis of patients with CRC. Ggplot2 software package was used for visualizing analysis of the cohort.

Prediction and Construction of SLC2A1 ceRNA Regulatory Network in CRC

The mirDIP (www.ophid.utoronto.ca/mirDIP/) (Tokar et al., 2018), micorT CDS (www.microrna.gr/microT-CDS) (Paraskevopoulou et al., 2013), and miRNet (https://www.mirnet.ca/miRNet/home.xhtml) (Chang et al., 2020) tools were used to predict the miRNAs of target SLC2A1, and the correlation between SLC2A1 and these miRNAs was analyzed in the TCGA CRC cohort to screen negatively correlated miRNAs as target miRNAs. miRNet and starBase (www.starbase.sysu.edu.cn/starbase2/index.php) (Li et al., 2014) tools were used to predict the long non-coding RNA (lncRNAs) of target microRNA (miRNAs), and the correlation between the target miRNAs and these lncRNAs was analyzed in the TCGA CRC dataset, and the negatively correlated lncRNAs were selected as target lncRNAs. To further narrow the prediction range, the expression level of target lncRNA in CRC and its correlation with SLC2A1 were further analyzed according to the ceRNA theory. The igraph software package of R language (http://igraph.org) is used to analyze the data visually.

Statistical Methods

All statistical analysis was conducted through Xiantao platform (www.xiantao.love). Xiantao platform is a database integrating TCGA tumor microarray data, which is mainly used for gene expression analysis, correlation analysis, enrichment analysis, interactive network analysis, clinical significance analysis, and related plotting.

RESULTS

Pan-Cancer Analysis of SLC2A1 mRNA Expression Level in Different Cohort

The differences in SLC2A1 mRNA expression level between CRC and control group were analyzed by using Oncomine database and TCGA cohort. Oncomine database analysis indicated that SLC2A1 expression was higher in bladder cancer (Sanchez-Carbayo et al., 2006), breast cancer (Zhao et al., 2004; Curtis et al., 2012), CRC (Ki et al., 2007; Skrzypczak et al., 2010), esophageal cancer (Su et al., 2011), kidney cancer (Jones et al., 2005; Beroukhim et al., 2009), leukemia (Andersson et al., 2007), lung cancer (Su et al., 2007; Landi et al., 2008; Hou et al., 2010; Okayama et al., 2012; Selamat et al., 2012), ovarian cancer (Yoshihara et al., 2009), and pancreatic cancer (Pei et al., 2009) than in normal tissues. Some studies also found that the expression of SLC2A1 in breast cancer (Finak et al., 2008), esophageal cancer (Kim et al., 2010), and leukemia (Haferlach et al., 2010) was lower than that in normal samples (**Figure 2A**). **Table 1** summarizes the details of SLC2A1 expression levels in pan-cancers.

We further analyzed SLC2A1 mRNA expression level in different human cancers utilizing TCGA cohort. **Figure 2B** indicates the differences between SLC2A1 in varied tumor samples and control samples. SLC2A1 expression level in breast invasive carcinoma, cervical squamous cell carcinoma and endocervical adenocarcinoma, cholangiocarcinoma, COAD, esophageal carcinoma, glioblastoma multiforme, head and neck squamous cell carcinoma, kidney renal clear cell carcinoma, kidney renal papillary cell carcinoma, liver hepatocellular carcinoma, lung adenocarcinoma, lung squamous cell carcinoma, READ, stomach adenocarcinoma, thyroid carcinoma, and uterine corpus endometrial carcinoma was remarkably higher than that in control tissues and significantly decreased in kidney chromophobe and prostate adenocarcinoma.

Expression Levels of SLC2A1 in Patients with CRC

By analyzing CRC datasets from TCGA and GEO, we further determined the difference in SLC2A1 expression between CRC and normal samples. The results of TCGA and GEO cohort analysis demonstrated that the expression level of SLC2A1 remarkably increased in CRC compared to the control group (**Figures 2C,D**). To further confirm the precision of the analysis results, we performed the qRT-PCR and IHC staining experiments for further verification. As shown in **Figure 2F**, qRT-PCR results indicated that SLC2A1 mRNA expression remarkably increased in human CRC cell lines SW480 (2.197 ± 0.127 vs. 0.954 ± 0.058) and HCT116 (2.360 ± 0.061 vs. 0.954 ± 0.058) compared with normal human colorectal mucosa cells. The IHC staining results indicated that SLC2A1 was primarily expression in the CRC cell membrane. SLC2A1 IHC scores in tumor tissues were remarkably higher than those in paracancerous tissues (2.375 ± 0.606 vs. 0.896 ± 0.592, **Figures 2G–I**). These results point out that overexpression of SLC2A1

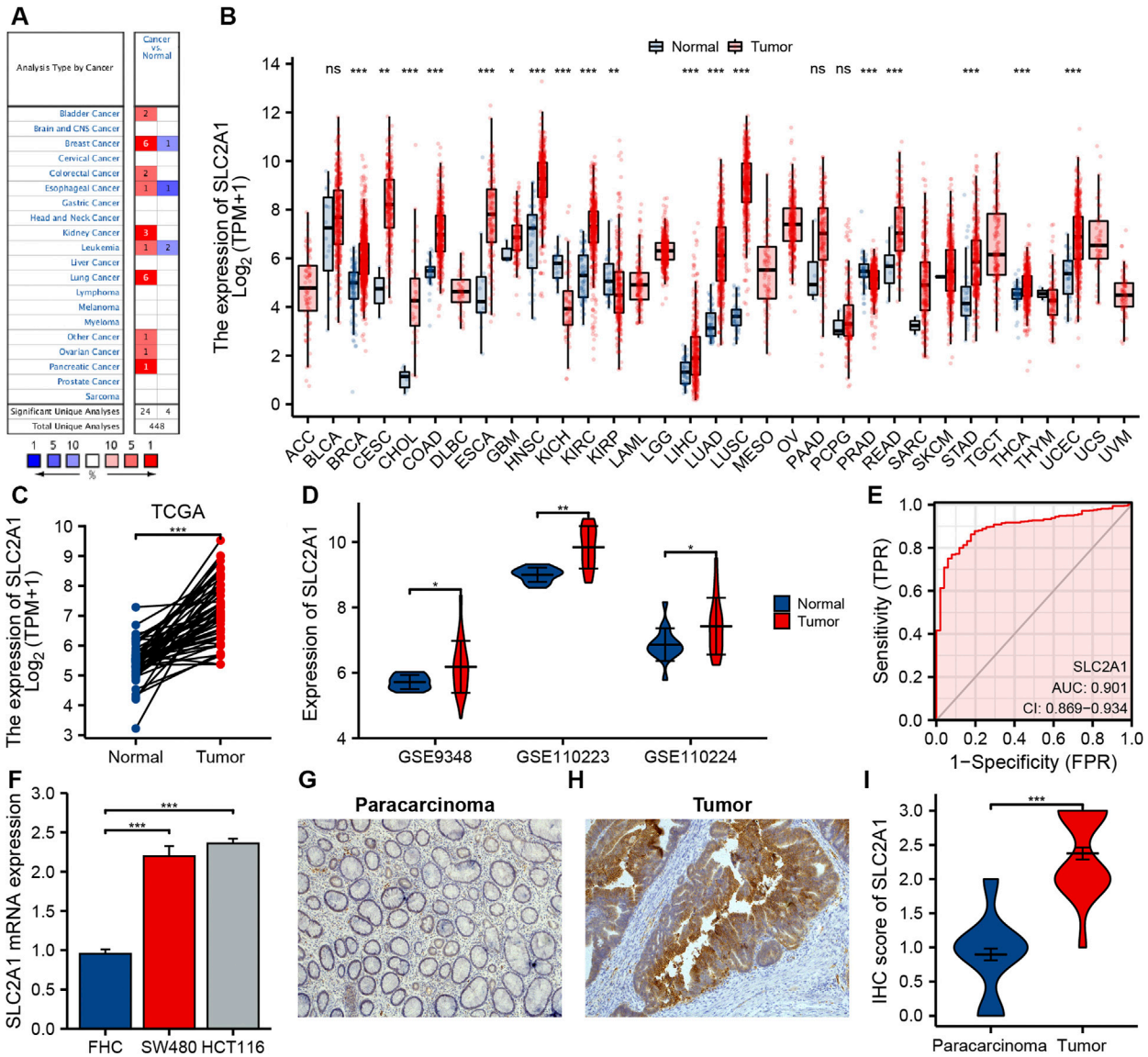

FIGURE 2 | The expression of SLC2A1 in colorectal cancer (CRC) and pan-cancer. **(A)** Oncomine database summarizes the expression of SLC2A1 in pan-cancer. **(B)** TCGA cohort summarizes the expression of SLC2A1 in pan-cancer. **(C)** Matched tumor/normal human CRC specimens showed increased expression of SLC2A1 in tumor specimens in TCGA cohort. **(D)** The GSE9348, GSE110223, and GSE110224 cohort showed an elevated expression of SLC2A1 in tumor specimens. **(E)** ROC curve analysis of SLC2A1 diagnosis. **(F)** Difference of expression of SLC2A1 in CRC cell lines and human normal colorectal mucosa cell lines. Immunohistochemistry assay was used to analyze the protein expression of SLC2A1 in paracarcinoma samples **(G)** and CRC samples **(H)**. **(I)** The mean SLC2A1 IHC score in CRC samples was remarkably higher than that of matched paracarcinoma samples. *, $p < 0.05$; **, $p < 0.01$; ***, $p < 0.001$; ****, $p < 0.0001$; ns, no significant.

may conduce to the development of CRC. To estimate the diagnostic ability of SLC2A1 in CRC, we carried the ROC curve analysis. The ROC curve indicated that SLC2A1 had high accuracy in predicting the outcomes of normal and tumor (**Figure 2E**), and the area under the ROC curve was 0.901 (95% CI: 0.869–0.934).

To confirm the significance of SLC2A1 in clinical environment, we analyzed clinical data from TCGA CRC cohort. As shown in **Figure 3**, the results showed that the SLC2A1 expression in Stage II group was lower than that in Stage III and Stage IV groups. SLC2A1 expression in N0 group was lower than that in N2 group. SLC2A1 expression in M0 group was lower than that in M1 group. During progression-free survival events, SLC2A1 expression levels in patients who died were significantly higher than those in the surviving group.

SLC2A1 Gene Co-Expression Network and Enrichment Analysis in CRC

We analyzed co-expressed genes related to SLC2A1 expression in the TCGA CRC dataset using the R statistical computing

TABLE 1 | SLC2A1 expression in cancerous versus normal tissue in ONCOMINE.

Cancer Site	Cancer Type	*p* Value	t-Test	Fold Change	Reference (PMID)
Bladder	Infiltrating Bladder Urothelial Carcinoma	1.85E-12	7.682	2.514	16432078
	Superficial Bladder Cancer	1.20E-14	10.564	3.977	16432078
Breast	Invasive Ductal Breast Carcinoma	1.03E-11	9.276	2.800	15034139
	Intraductal Cribriform Breast Adenocarcinoma	2.50E-9	11.263	2.172	TCGA Breast
	Invasive Ductal Breast Carcinoma	4.19E-27	13.974	2.557	TCGA Breast
	Invasive Breast Carcinoma	8.98E-15	8.629	2.251	TCGA Breast
	Medullary Breast Carcinoma	4.82E-10	8.059	2.728	22522925
	Mucinous Breast Carcinoma	6.44E-13	8.635	2.100	22522925
	Invasive Breast Carcinoma	4.56E-17	−11.709	−3.780	18438415
Colorectal	Colon Adenocarcinoma	1.22E-13	8.619	2.107	17640062
	Colorectal Carcinoma	1.64E-9	7.030	2.372	20957034
Esophageal	Esophageal Squamous Cell Carcinoma	6.18E-13	8.162	2.134	21385931
	Barrett's Esophagus	1.57E-10	−9.953	−3.261	21152079
Kidney	Non-Hereditary Clear Cell Renal Cell Carcinoma	9.35E-13	11.104	5.519	19470766
	Hereditary Clear Cell Renal Cell Carcinoma	7.36E-13	13.447	5.810	19470766
	Clear Cell Renal Cell Carcinoma	1.63E-12	11.171	2.912	16115910
Leukemia	B-Cell Acute Lymphoblastic Leukemia	1.54E-11	11.384	3.218	17410184
	Pro-B Acute Lymphoblastic Leukemia	4.74E-21	−11.337	−2.608	20406941
	T-Cell Acute Lymphoblastic Leukemia	4.15E-23	−12.601	−2.714	20406941
Lung	Lung Adenocarcinoma	1.12E-10	8.781	3.160	17540040
	Lung Adenocarcinoma	2.39E-23	14.833	5.153	22613842
	Squamous Cell Lung Carcinoma	1.92E-23	26.718	22.600	20421987
	Lung Adenocarcinoma	2.68E-14	10.393	4.801	20421987
	Lung Adenocarcinoma	5.86E-21	13.641	2.843	22080568
	Lung Adenocarcinoma	2.15E-16	10.850	2.086	18297132
Ovarian	Ovarian Serous Adenocarcinoma	7.49E-10	11.221	7.952	19486012
Pancreatic	Pancreatic Carcinoma	6.24E-19	14.773	8.453	19732725

language. Only the protein-coding genes were kept. The main results presented in **Figure 4A** genes were positively related with SLC2A1 expression, whereas 3,911 genes were negatively related with SLC2A1 expression ($p < 0.05$). Under the conditions of $|cor| > 0.3$ and $p < 0.05$, a total of 515 genes were obtained, including 513 positively related genes and two negatively related genes. When the threshold values were cor > 0.5 and $p < 0.05$, the three genes had the strong association: EPHA2 (cor = 0.538, p = 6.36E-50), KRT80 (cor = 0.538, p = 7.33E-50), and KRT19 (cor = 0.528, p = 9.93E-48), respectively. The results, as shown in **Figures 4B,C**, indicated that the top 50 genes are positively and negatively associated with SLC2A1 expression, respectively. The detailed description of co-expressed genes is indicated in **Supplementary Table S1**.

The GO term and KEGG pathway investigation of the first 200 co-expressed genes mainly associated with SLC2A1 expression were carried through using the clusterProfiler software package of R language. SLC2A1 co-expressed genes involved 242 biological processes, 80 cell components, 31 molecular functions, and 18 KEGG under the condition of p.adj <0.1 and q-value <0.2. The bubble graph shows the top five messages of biological processes, cell components, molecular functions, and KEGG, respectively. The GO term annotation indicated that these genes were primarily participated in epidermis development, cell–cell junction, and cadherin binding (**Figures 4D–F**). The KEGG pathway analysis indicated that these genes were chiefly participated in Shigellosis and Wnt signaling pathway (**Figure 4G**). **Supplementary Table S2** summarizes the GO term and KEGG pathway details of SLC2A1 co-expression enrichment analysis.

Gene Set Enrichment Analysis

To investigate the possible mechanism of SLC2A1 in CRC, the GSEA analysis was carried on the differential genes. A total of 194 gene sets were found, among which the top three enrichment pathways with the strongest correlation were REACTOME G ALPHA I SIGNALING EVENTS (FDR = 0.031, p = 0.001), REACTOME M PHASE (FDR = 0.031, p = 0.001), and REACTOME NEURONAL SYSTEM (FDR = 0.031, p = 0.001). At the same time, we also found that the different genes were involved in WP LNCRNA INVOLVEMENT IN CANONICAL WNT SIGNALING AND COLORECTAL CANCER (FDR = 0.200, p = 0.013), PID HIF1 TFPATHWAY (FDR = 0.232, p = 0.017), and REACTOME GLYCOLYSIS (FDR = 0.244, p = 0.019), respectively (**Figure 5**). Detailed enrichment analysis information is indicated in **Supplementary Table S3**.

Associations Between SLC2A1 and Tumor Immune Infiltrating Cells

The association between SLC2A1 expression level and CRC samples immunofiltration cells was analyzed by TIMER database. The results indicated that the expression level of SLC2A1 was positively associated with the infiltrating level of CD4+ T cell (r = 0.101, p = 4.31E-2), neutrophil (r = 0.181, p = 2.69E-4), and DC (r = 0.124, p = 1.32E-2) and negatively

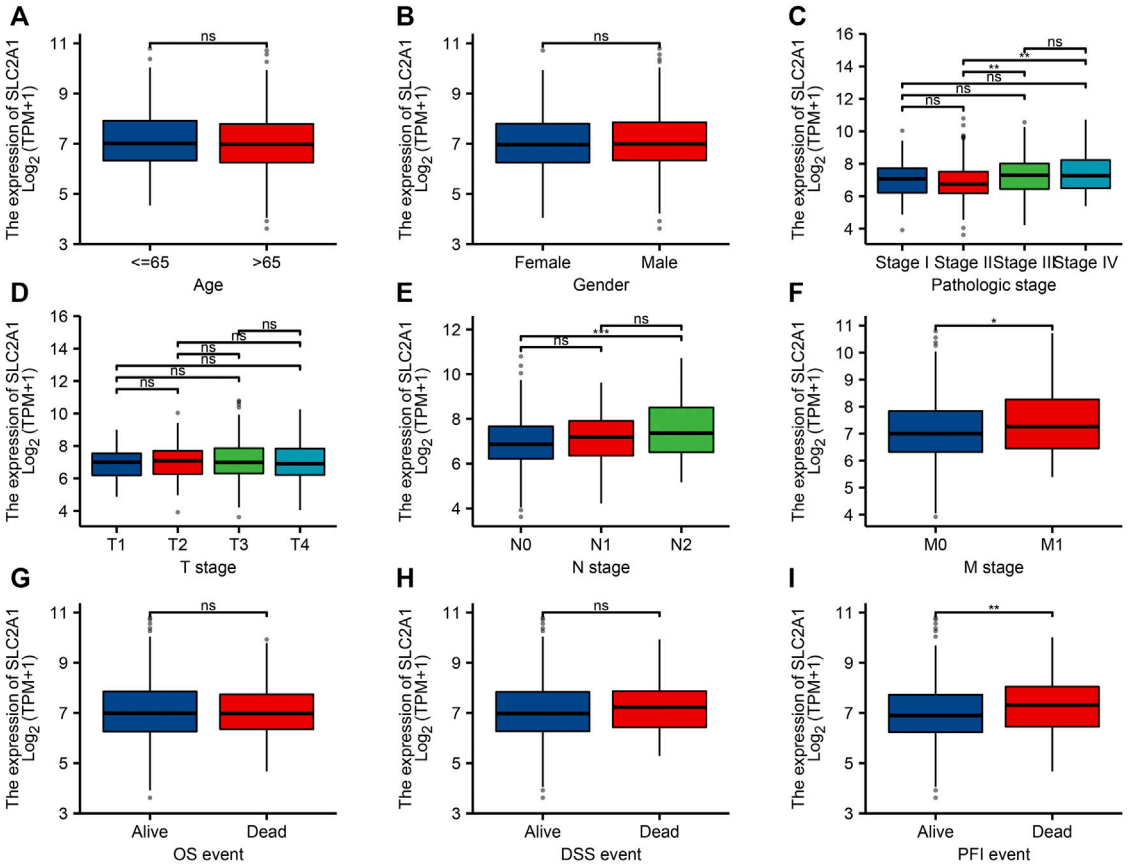

FIGURE 3 | Relationship between SLC2A1 mRNA expression and clinicopathological parameters in patients with colorectal cancer (CRC). The SLC2A1 mRNA expression level was expressed by utilizing ggplot2 software package of R language for the patient characteristics of **(A)** age, **(B)** gender, **(C)** pathologic stage, **(D)** T stage, **(E)** N stage, **(F)** M stage, **(G)** OS event, **(H)** DSS event, and **(I)** PFI event. *, $p < 0.05$; **, $p < 0.01$; ***, $p < 0.001$; ****, $p < 0.0001$; ns, no significant.

associated with the infiltrating level of B cell (r = –0.151, p = 2.41E-3) (**Figure 6A**). In addition, SLC2A1 CNV was found to be significantly correlated with the infiltration levels of B cell, neutrophil, CD8+ T cell, and DC in COAD cohort (**Figure 6B**).

The infiltration abundance of immune cells between the high and low SLC2A1 expression group was analyzed by ssGSEA algorithm, and the results showed that there were differences in the expressions of various immune cells between the two groups (**Figure 6C**), including DC (p = 0.012), eosinophils (p = 0.001), immature DC (iDC; p = 0.032), neutrophils (p = 0.001), natural killer (NK) CD56 bright cells ($p < 0.001$), NK cells (p = 0.002), plasmacytoid DC (pDC; p = 0.005), T helper cells (p = 0.003), and Th2 cells (p = 0.035), respectively.

To further evaluate the association between SLC2A1 and CRC samples immunofiltration cells, we analyzed the TIMER, GEPIA database, and TCGA CRC cohort to investigate the relationship between SLC2A1 and immunofiltration cells marker genes in various immunofiltration cells. As shown in **Table 2**, all investigations showed that SLC2A1 expression was correlated with neutrophil immune marker genes, including FCGR3A (r = 0.12, p = 4.6E-2), CD55 (r = 0.26, p = 1.1E-5) and ITGAM (r = 0.13, p = 2.6E-2). The scatter plots showed the correlation between SLC2A1 expression level and neutrophil immune marker genes, respectively (**Figure 6D**).

Associations of SLC2A1 Expression Level With m6A Modification in CRC

The modification of m6A has a remarkable effect in the make progress of CRC. We analyzed GSE110224 and TCGA CRC cohort to explore the association between expression level of SLC2A1 and 20 m6A relative genes in CRC. As shown in **Figure 7A**, analysis indicated that, in the GSE110224 and TCGA CRC cohort, the SLC2A1 expression was remarkably positively associated with IGF2BP3 and YTHDF1 ($p < 0.05$). Furthermore, in the TCGA CRC cohort, SLC2A1 expression level was remarkably positively associated with ALKBH5, FTO, IGF2BP1, IGF2BP2, METTL3, and RBM15B ($p < 0.05$) but negatively associated with METTL14, RBM15, and YTHDC2 ($p < 0.05$).

As shown in **Figures 7B,C**, the scatter plot indicated the relationship between SLC2A1 and m6A relative genes. Furthermore, TCGA CRC samples were divided into high expression group and low expression group according to the SLC2A1 expression level. As shown in **Figure 7D**, we attempt to

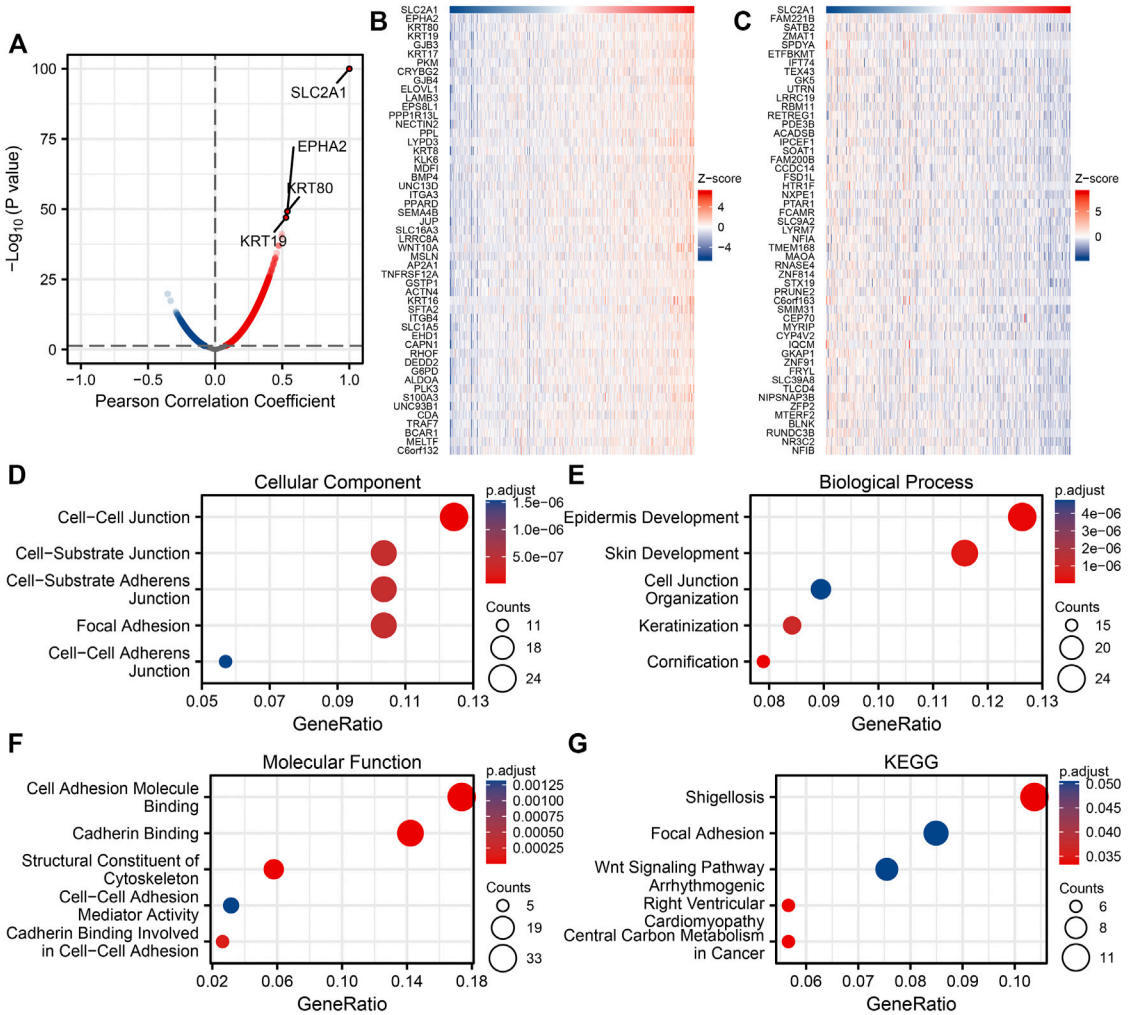

FIGURE 4 | Enrichment analysis of SLC2A1 gene co-expression network in colorectal cancer (CRC). **(A)** Volcano map indicated co-expression genes correlated with expression level of SLC2A1 in TCGA CRC cohort. **(B, C)** Heat maps indicated the top 50 co-expression genes positively and negatively associated with expression level of SLC2A1 in the TCGA CRC cohort. **(D–F)** Enrichment analysis of gene ontology (GO) terms for SLC2A1 co-expression genes. **(G)** Enrichment analysis of Kyoto Encyclopedia of Genes and Genomes (KEGG) terms for terms for SLC2A1 co-expression genes.

analyze the differential expression level of m6A relative gene between the high SLC2A1 expression group and low SLC2A1 expression group to confirm whether there is a difference in m6A modification between the two groups in CRC. The analyses indicated that, compared with the low expression group, the expression of ALKBH5, IGF2BP1, IGF2BP3, RBM15B, VIRMA, YTHDF1, and ZC3H13 increased in the SLC2A1 high expression group, whereas the expression of METTL4 decreased ($p < 0.05$). As shown in **Figure 7E**, the analysis indicated the key genes (IGF2BP3 and YTHDF1) that have expression correlation and differential expression relationship with SLC2A1. The Kaplan–Meier curves indicated that high IGF2BP3 expression was remarkably related with poor prognosis of CRC ($p < 0.05$, **Figure 7F**), whereas YTHDF1 was not related with poor prognosis of patients with CRC. These analyses point out that SLC2A1 may be strongly associated to the m6A modification of CRC, particularly through the regulating of IGF2BP3, and eventually impact the development and prognosis of CRC.

Associations of SLC2A1 Expression Level With Ferroptosis in CRC

We analyzed GSE110224 and TCGA CRC cohort to study the association between SLC2A1 and 25 ferroptosis relative genes in CRC in terms of expression level. The correlation results showed that in GSE110224 and TCGA, the expression of SLC2A1 was significantly correlated with FDFT1, GPX4, RPL8, and SLC1A5 ($p < 0.05$, **Figure 8A**). In addition, in the TCGA CRC cohort, SLC2A1 expression was positively correlated with AIFM2, ATP5MC3, CARS1, CDKN1A, CS, HSPA5, HSPB1, LPCAT3, MT1G, and TFRC ($p < 0.05$). In GSE110224 cohort, SLC2A1 expression was greatly negatively correlated with MT1G ($p < 0.05$).

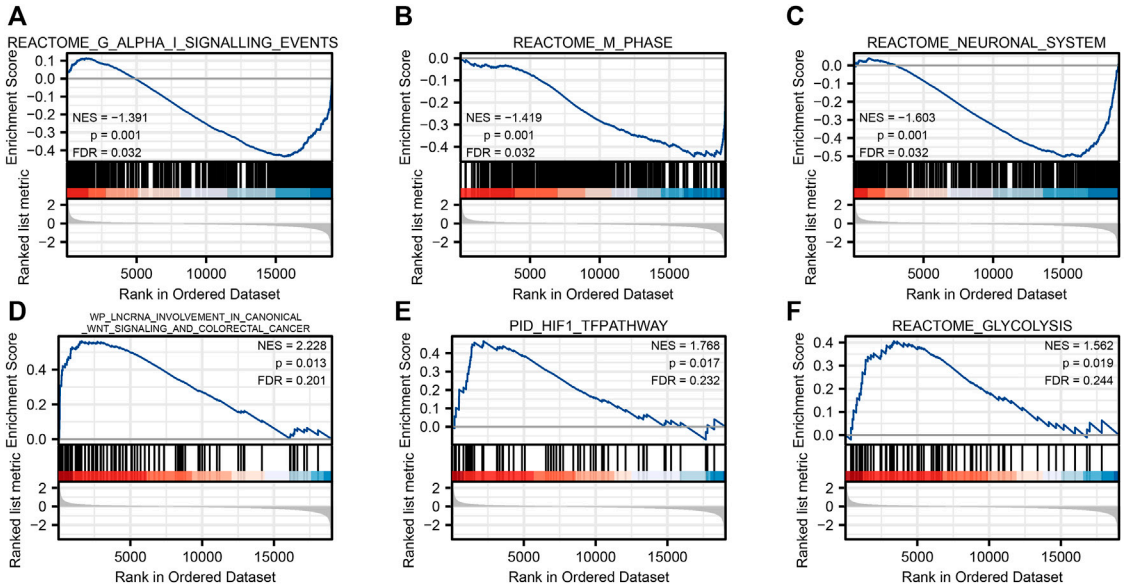

FIGURE 5 | Gene set enrichment analysis. Reactome G alpha I signaling events **(A)**, reactome m phase **(B)**, reactome neuronal system **(C)**, WP lncrna involvement in canonical Wnt signaling and colorectal cancer **(D)**, PID HIF1 TFPATHWAY **(E)**, and reactome glycolysis **(F)**.

The scatter graph demonstrated the correlation between SLC2A1 and ferroptosis of relevant genes (**Figure 8B**). In addition, according to the expression level of SLC2A1, TCGA CRC samples were set to high expression group and low expression group according to the SLC2A1 expression level. To analyze the differential expression levels of ferroptosis relative genes between the two groups in CRC (**Figure 8C**). The analyses indicated that, compared with the low expression group, the expressions of AIFM2, ALOX15, CDKN1A, DPP4, GPX4, HSPA5, LPCAT3, RPL8, SLC1A5, and TFRC increased in SLC2A1 high expression group, whereas the expression of CISD1 decreased ($p < 0.05$). As shown in **Figure 8D**, the analysis indicated the key genes (GPX4, RPL8, and SLC1A5) that have expression correlation and differential expression relationship with SLC2A1. The Kaplan–Meier curves indicated that high GPX4 expression was significantly correlated with poor prognosis in CRC ($p < 0.05$), whereas RPL8 and SLC1A5 expression were not (**Figure 8E**). These results point out that SLC2A1 may be significantly correlated to ferroptosis of CRC, especially through the regulation of GPX4, and eventually affect the development of CRC.

Prediction and Construction of SLC2A1 ceRNA Regulatory Network in CRC

Studies have shown that the regulatory mechanism of ceRNA plays a key role in CRC, so we attempted to predict and screen the ceRNA regulatory network of SLC2A1 in CRC. We predicted 47, 110, and 89 miRNAs targeting SLC2A1 using mirDIP, micorT CDS, and miRNet tools, respectively. Venn diagrams show the results predicted by the mirDIP, micorT CDS, and miRNet tools. As shown in **Figures 5**, **9A**, miRNAs were predicted by the three tools, including hsa-miR-148a-3p, hsa-miR-148b-3p, hsa-miR-328-3p, hsa-miR-132-3p, and hsa-miR-330-5p. Furthermore, we analyzed the association between these miRNAs and SLC2A1 expression levels and found that only hsa-miR-148a-3p ($r = -0.130$, $p = 0.002$) was negatively correlated with SLC2A1 expression levels in CRC (**Figure 9C**).

We further predicted that the lncRNAs might bind to hsa-miR-148a-3p using miRNet and starBase tools, and the predicted results were the same as previous studies (Liu et al., 2021a). Venn diagrams show the results predicted by the miRNet and starBase tools. A total of 14 lncRNAs were predicted by both tools, including KIF9-AS1, HCG18, HOTAIRM1, HOXA11-AS, LINC00174, NUTM2A-AS1, H19, KCNQ1OT1, HOTAIR, DHRS4-AS1, OIP5-AS1, LINC00667, A1BG-AS1, and XIST (**Figure 9B**). Further analysis of the correlation between these lncRNAs and hsa-miR-148a-3p expression levels revealed that AKIF9-AS1 ($r = -0.240$, $p < 0.001$), DHRS4-AS1 ($r = -0.120$, $p = 0.002$), H19 ($r = -0.250$, $p < 0.001$), HCG18 ($r = -0.200$, $p < 0.001$), HOTAIR ($r = -0.200$, $p < 0.001$), KIF9-AS1 ($r = -0.140$, $p < 0.001$), NUTM2A-AS1 ($r = -0.280$, $p < 0.001$), and OIP5-AS1 ($r = -0.200$, $p < 0.001$) were negatively correlated with hsa-miR-148a-3p expression levels in CRC (**Figure 9C**). The network diagram shows the relationship of the predicted ceRNA network (**Figure 9D**).

To further narrow the prediction range, we analyzed the expression of target lncRNA and its correlation with SLC2A1 expression in the CRC cohort. The results showed that only H19 was upregulated in CRC ($p < 0.001$), and there was a significant positive correlation with SLC2A1 expression ($r = 0.280$, $p < 0.001$, **Figure 9E**). Therefore, we predict that the H19-hsa-miR-148a-3p-SLC2A1 ceRNA network may play a significant role in the development of CRC. The network diagram shows the relationship of the final ceRNA network (**Figure 9F**).

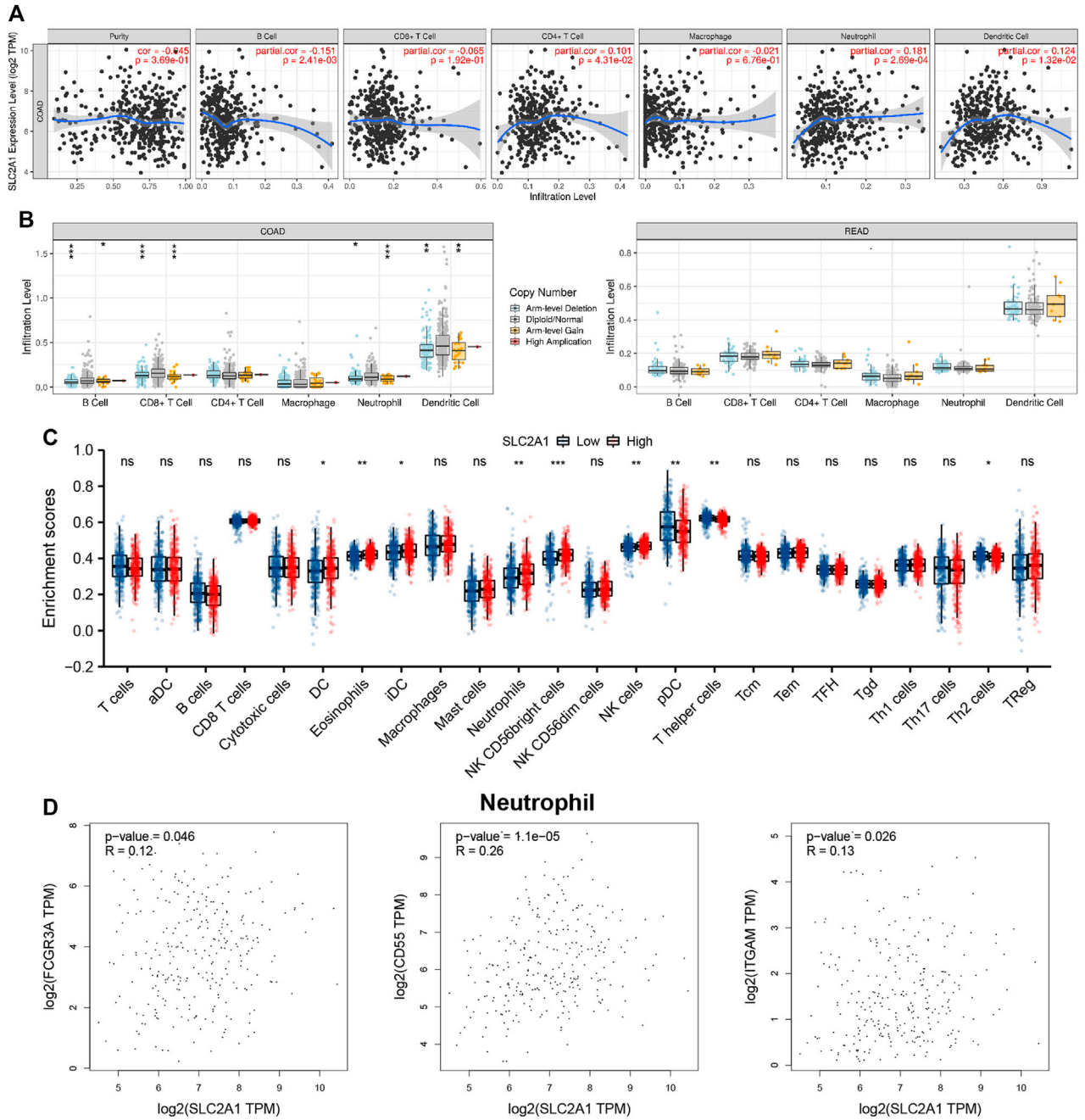

FIGURE 6 | Associations between SLC2A1 and Tumor Immune Infiltrating Cells. **(A)** Association between the expression level of SLC2A1 and immunofiltration cells in colorectal cancer (CRC). **(B)** SLC2A1 CNV affects the infiltrating levels of B cell, CD4+ T cell, macrophages, neutrophils, and dendritic cell in CRC. **(C)** Changes of 24 immune cell subtypes between high and low SLC2A1 expression groups in CRC tumor samples. **(D)** SLC2A1 expression correlated with neutrophils in CRC. *, $p < 0.05$; **, $p < 0.01$; ***, $p < 0.001$; ****, $p < 0.0001$; ns, no significant.

DISCUSSION

Glucose is one of the basic metabolites needed by animal and plant cells and the main energy source for tumor cell proliferation (Wang et al., 2020). Previous studies have confirmed that the GLUT1 protein encoded by SLC2A1 gene is mainly localized in the cell membrane. The expression level of GLUT1 in tumor cells is significantly higher than that in normal tissue cells, thus promoting the proliferation of tumor cells by enhancing the ability of glycolysis of tumor cells (Kasahara and Hinkle, 1977; Ancey et al., 2018). Studies have shown that the overexpression of SLC2A1 in cervical cancer (Rudlowski et al., 2004), gastric cancer (Berlth et al., 2015), esophageal cancer (Kato et al., 2002), and oral cancer (Pereira et al., 2013) can advance the proliferation of

TABLE 2 | Correlation analysis between SLC2A1 and immune cell marker gene in TIMER, GEPIA, and TCGA database.

Description	Gene markers	TIMER		GEPIA		TCGA	
		Purity		Tumor		Tumor	
		rho	*p*	rho	*p*	rho	*p*
B cell	CD19	0.063	2.06E-01	0.046	4.40E-01	–0.015	7.08E-01
	MS4A1	0.011	8.21E-01	–0.001	9.90E-01	–0.076	5.40E-02
	CD79A	0.049	3.21E-01	0.014	8.20E-01	0.003	9.30E-01
CD8 + T Cell	CD8A	0.030	5.43E-01	0.076	2.10E-01	0.003	9.31E-01
	CD8B	0.037	4.54E-01	0.051	4.00E-01	0.054	1.66E-01
	IL2RA	0.065	1.92E-01	0.110	8.00E-02	0.031	4.28E-01
Tfh	CXCR3	0.117	**1.81E-02**	0.130	**2.90E-02**	0.155	**7.62E-05**
	CXCR5	0.053	2.88E-01	–0.048	4.30E-01	0.033	3.98E-01
	ICOS	0.011	8.24E-01	0.079	1.90E-01	–0.042	2.89E-01
Th1	IL12RB1	–0.020	6.94E-01	0.015	8.10E-01	0.001	9.76E-01
	CCR1	0.126	**1.08E-02**	0.140	**2.20E-02**	0.076	5.34E-02
	CCR5	–0.017	7.25E-01	0.038	5.30E-01	–0.055	1.59E-01
Th2	CCR4	0.050	3.14E-01	0.049	4.20E-01	–0.009	8.28E-01
	CCR8	0.070	1.58E-01	0.090	1.40E-01	0.031	4.36E-01
	HAVCR1	0.060	2.29E-01	0.027	6.60E-01	0.074	6.13E-02
Th17	IL21R	0.108	**2.91E-02**	0.110	6.70E-02	0.019	6.35E-01
	IL23R	–0.044	3.79E-01	–0.085	1.60E-01	–0.152	**1.06E-04**
	CCR6	0.053	2.88E-01	0.095	1.20E-01	0.008	8.39E-01
Treg	FOXP3	0.059	2.36E-01	0.032	6.00E-01	0.043	2.71E-01
	NT5E	–0.009	8.54E-01	0.001	9.90E-01	–0.055	1.63E-01
	IL7R	0.082	1.00E-01	0.130	**3.70E-02**	0.000	9.96E-01
T cell exhaustion	PDCD1	0.085	8.57E-02	0.120	5.40E-02	0.111	**4.58E-03**
	CTLA4	–0.008	8.66E-01	0.053	3.80E-01	–0.027	4.88E-01
	LAG3	0.058	2.45E-01	0.082	1.70E-01	0.047	2.37E-01
M1 Macrophage	NOS2	0.072	1.47E-01	0.150	**1.50E-02**	0.068	8.61E-02
	IRF5	0.067	1.78E-01	0.098	1.10E-01	0.085	**2.98E-02**
	PTGS2	0.110	**2.73E-02**	0.170	**5.90E-03**	0.073	6.41E-02
M2 Macrophage	CD163	0.099	**4.58E-02**	0.110	6.80E-02	0.079	**4.50E-02**
	MRC1	0.122	**1.35E-02**	0.150	**1.30E-02**	0.065	1.01E-01
	CD209	0.060	2.29E-01	0.100	9.90E-02	0.042	2.84E-01
TAM	CCL2	0.024	6.25E-01	0.073	2.30E-01	0.034	3.92E-01
	CD86	0.033	5.03E-01	0.110	5.70E-02	0.023	5.67E-01
	CD68	0.208	**2.34E-05**	0.230	**1.30E-04**	–0.043	2.71E-01
Monocyte	CD14	0.131	**8.12E-03**	0.140	**2.00E-02**	0.152	**1.11E-04**
	CD33	0.040	4.20E-01	0.074	2.20E-01	0.056	1.55E-01
	ITGAX	0.164	**9.22E-04**	0.190	**1.30E-03**	0.094	**1.71E-02**
Natural killer cell	B3GAT1	0.085	8.86E-02	0.060	3.20E-01	0.031	4.34E-01
	KIR3DL1	0.091	6.79E-02	0.068	2.60E-01	–0.005	9.03E-01
	CD7	0.082	9.76E-02	0.120	**4.40E-02**	0.100	**1.07E-02**
Neutrophil	FCGR3A	0.069	1.68E-01	0.120	**4.60E-02**	0.047	2.37E-01
	CD55	0.167	**7.14E-04**	0.260	**1.10E-05**	0.118	**2.57E-03**
	ITGAM	0.119	**1.67E-02**	0.130	**2.60E-02**	0.096	**1.47E-02**
Dendritic cell	CD1C	–0.012	8.03E-01	–0.017	7.80E-01	0.000	9.97E-01
	THBD	0.134	**7.01E-03**	0.110	7.30E-02	0.125	**1.41E-03**
	NRP1	0.088	7.79E-02	0.150	**1.30E-02**	0.025	5.25E-01

Bold values indicate p < *0.05.*

cancer cells. These analyses point out that SLC2A1 may be a possible target for cancer targeted therapy. Nevertheless, there are few research studies on the synthesis study of SLC2A1 in CRC.

In this project, we predicted the high expression of SLC2A1 in a variety of cancers by analyzing Oncomine database and TCGA cohort. Analysis showed that SLC2A1 was highly expressed in nine types of tumors in the Oncomine database, and analysis of the TCGA cohort showed that SLC2A1 was highly expressed in 15 types of tumors, which was consistent with the results of previous studies (Kato et al., 2002; Rudlowski et al., 2004; van Laarhoven et al., 2006; Pereira et al., 2013; Berlth et al., 2015; Avanzato et al., 2018). Through analysis of GEO and TCGA CRC cohort, it was found that the expression level of SLC2A1 in CRC samples was significantly higher than that in normal samples. The mRNA and protein levels of SLC2A1 in CRC samples were remarkably higher than those in the normal control group through *in vitro* experiment and IHC staining, and the analysis results are the same as the above studies. We also analyzed the ability of SLC2A1 expression to predict CRC by drawing ROC curves and found that SLC2A1 has high accuracy in predicting the outcomes of normal and tumor. At the same time, the SLC2A1 expression level was found to be

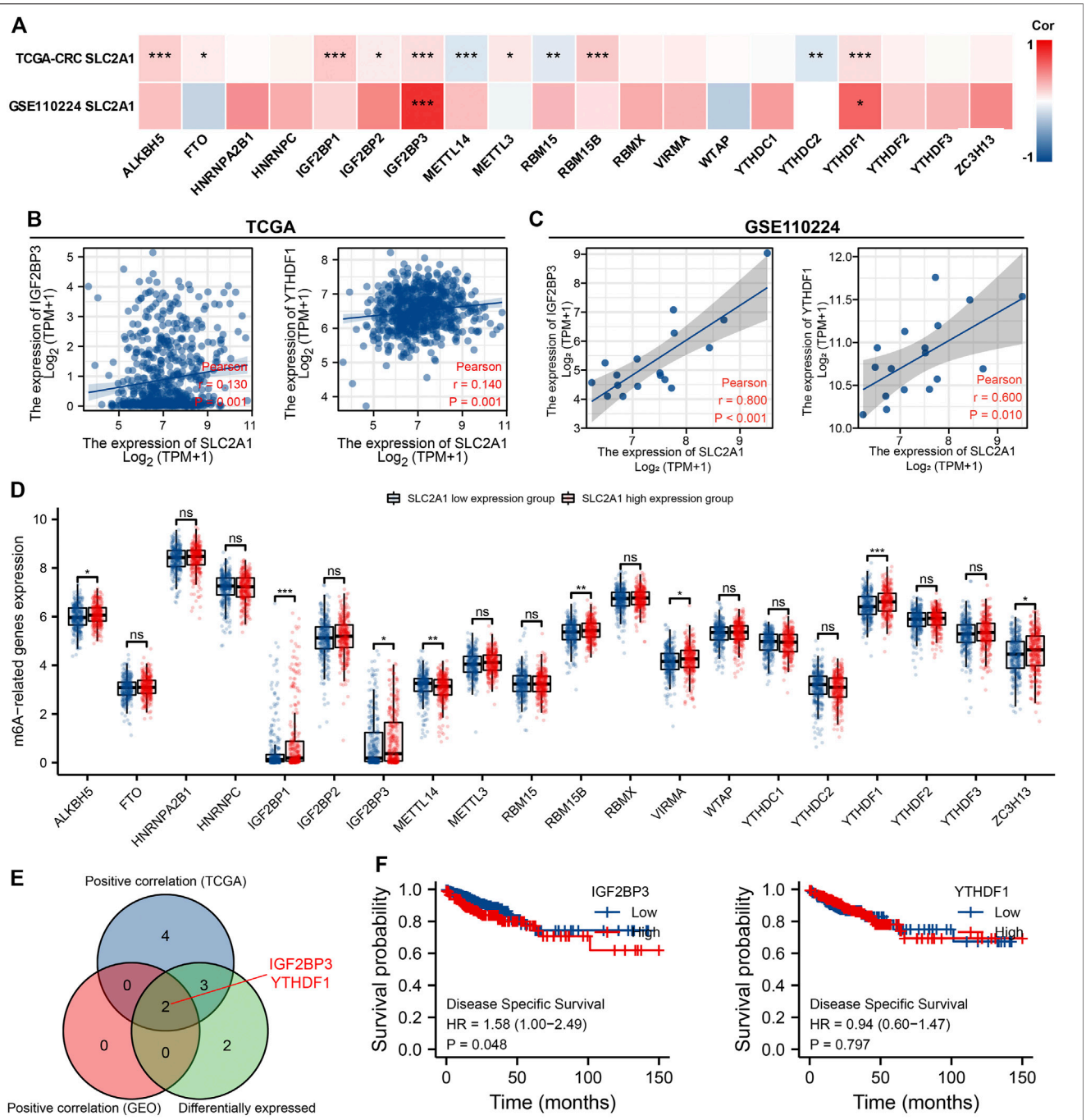

FIGURE 7 | Associations of SLC2A1 expression with m6A relative genes in colorectal cancer (CRC). **(A)** GSE110224 and TCGA CRC cohort analyzed the association between the SLC2A1 and the 20 m6A relative genes expression in CRC. **(B)** TCGA CRC cohort was analyzed and a scatter plot was drawn to display the association between SLC2A1 and the expression of m6A relative genes, including IGF2BP3 and YTHDF1. **(C)** GSE110224 cohort was analyzed, and a scatter plot was drawn to display the association between SLC2A1 and the expression of m6A relative genes, including IGF2BP3 and YTHDF1. **(D)** The differential expression of 20 m6A relative genes between high and low SLC2A1 expression groups in CRC tumor samples. **(E)** Venn diagram indicated both expression association and differential expression of genes, including IGF2BP3 and YTHDF1. **(F)** The Kaplan–Meier curve of IGF2BP3 and YTHDF1. *, $p < 0.05$; **, $p < 0.01$; ***, $p < 0.001$; ****, $p < 0.0001$; ns, no significant.

associated to CRC tumors stage and progression free interval (PFI). Finally, SLC2A1 may serve as a possible diagnostic and therapeutic marker for CRC.

Presently, research studies on the role of SLC2A1 in tumors primarily focus on glucose transport and glycolysis, although there are few studies on other biological functions that may be

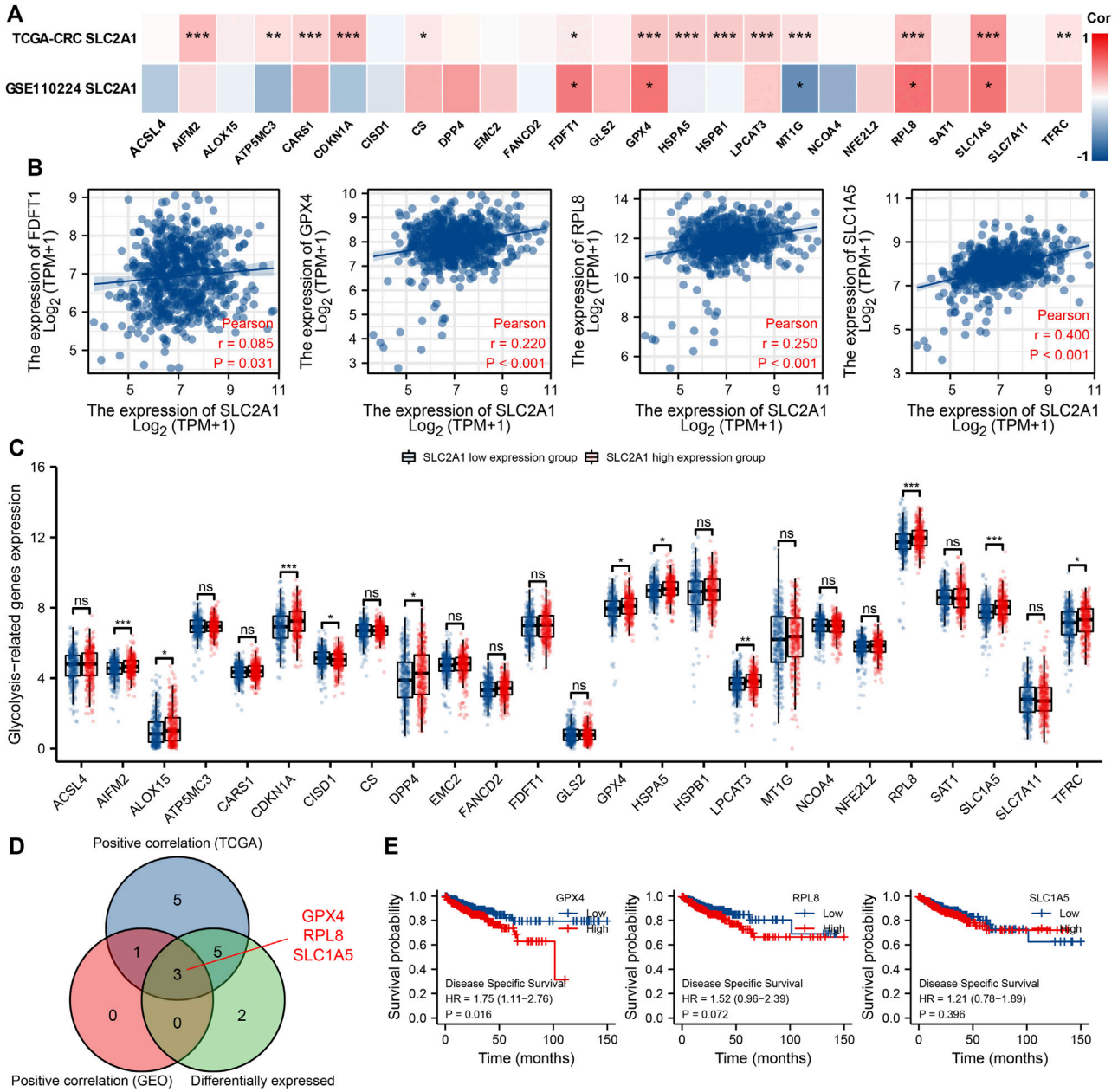

FIGURE 8 | Associations of SLC2A1 expression with ferroptosis relative genes in colorectal cancer (CRC). **(A)** GSE110224 and TCGA CRC cohort analyzed the association between the SLC2A1 and the 25 ferroptosis relative genes expression in CRC. **(B)** TCGA CRC cohort was analyzed and a scatter plot was drawn to display the correlation between SLC2A1 and the expression of ferroptosis relative genes, including FDFT1, GPX4, RPL8, and SLC1A5. **(C)** The differential expression of 25 ferroptosis relative genes between high and low SLC2A1 expression groups in CRC tumor samples. **(D)** Venn diagram indicated both expression association and differential expression of genes, including GPX4, RPL8, and SLC1A5. **(E)** Kaplan–Meier curve of GPX4, RPL8, and SLC1A5. *, $p < 0.05$; **, $p < 0.01$; ***, $p < 0.001$; ****, $p < 0.0001$; ns, no significant.

involved in SLC2A1. In this study, the R statistical computing language was utilized to analyze the SLC2A1 co-expression genes in CRC, and it was discovered that the expression of EPHA2, KRT80, and KRT19 in CRC had the remarkable association with SLC2A1. Martini et al. (2019) suggested that EPHA2 was highly expressed in CRC and its expression level was closely related to PFI, suggesting that EPHA2 could be a potential therapeutic target for metastatic CRC. Li et al. (2018) pointed out that KRT80 is an independent prognostic biomarker for CRC and promotes CRC migration and invasion by activating the AKT pathway and interacting with PRKDC. Alsharif et al. (2021) suggested that KRT19 was highly expressed in breast cancer and could stabilize the E-cadherin complex on the cell membrane, maintain cell–cell adhesion, and provide growth and survival advantages for tumor

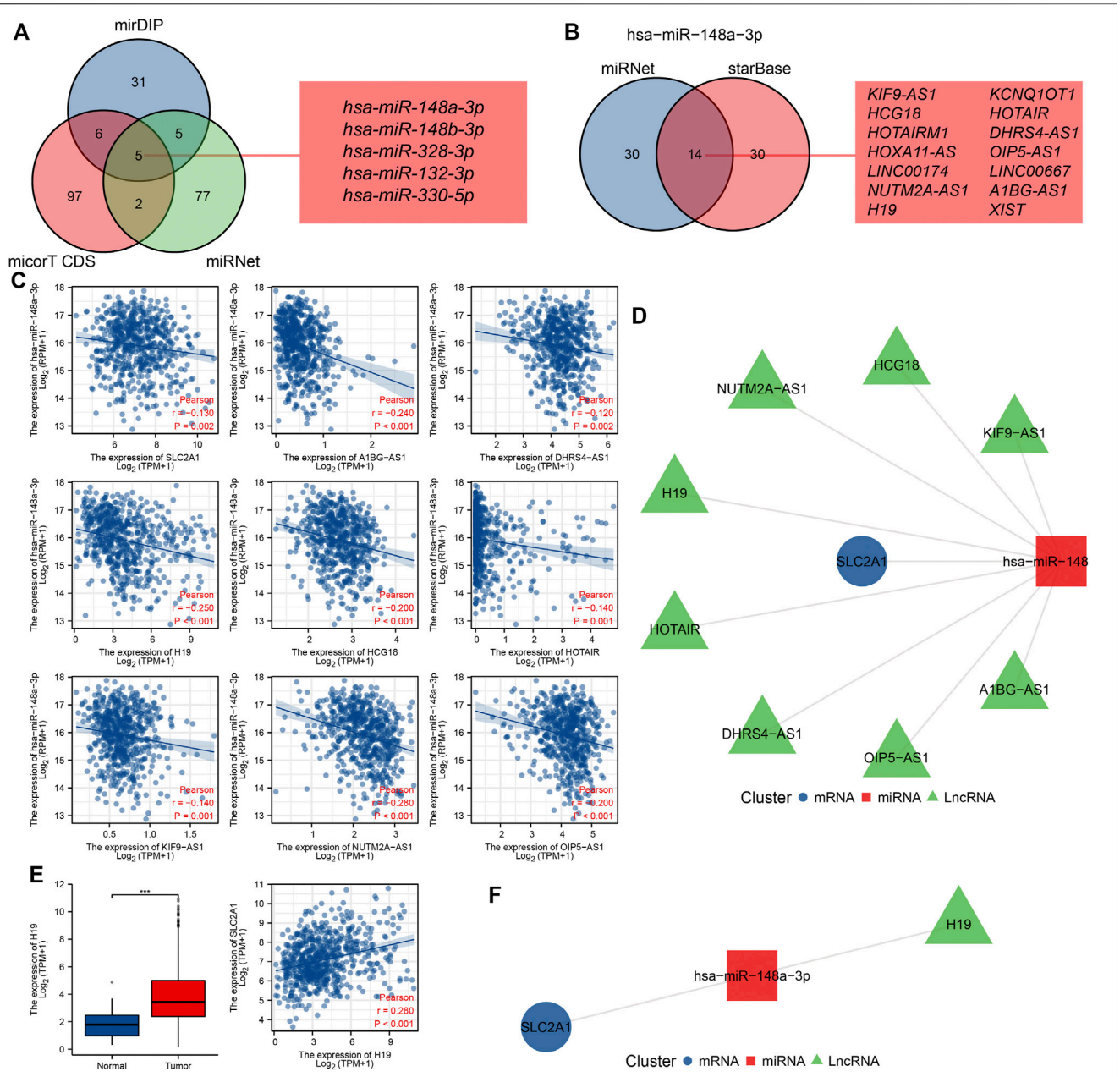

FIGURE 9 | Prediction and construction of SLC2A1 ceRNA network in colorectal cancer (CRC). **(A)** The Venn database displays miRNA of targeted SLC2A1 predicted by the mirDIP, micorT CDS, and miRNet tools. **(B)** The Venn database displays lncRNA of targeted hsa-miR-148a-3p predicted by the miRNet and starBase tools. **(C)** Scatter plots show results with expressional correlations, including SLC2A1 and hsa-miR-148a-3p, hsa-miR-148a-3p and AKIF9-AS1, hsa-miR-148a-3p and DHRS4-AS1, hsa-miR-148a-3p and H19, hsa-miR-148a-3p and HCG18, hsa-miR-148a-3p and HOTAIR, hsa-miR-148a-3p and KIF9-AS1, hsa-miR-148a-3p and NUTM2A-AS1, and hsa-miR-148a-3p and OIP5-AS1. **(D)** The network diagram shows the relationship of the predicted ceRNA network. **(E)** Only H19 was highly expressed in CRC and positively associated with SLC2A1 expression. **(F)** The network diagram shows the relationship of the final ceRNA network.

cells. The GO term and KEGG pathway analysis of top 200 co-expressed genes positively associated with SLC2A1 expression indicated that these genes were mainly correlated to epidermis development, cell–cell junction, and cadherin binding. The KEGG enrichment analysis indicated that these genes were mainly related to Shigellosis and Wnt signaling pathway. GSEA indicated that the differential genes grouped according to SLC2A1 expression were primarily participated in REACTOME G ALPHA I SIGNALING EVENTS, REACTOME M PHASE, REACTOME NEURONAL SYSTEM, WP LNCRNA INVOLVEMENT IN CANONICAL WNT SIGNALING AND COLORECTAL CANCER, PID HIF1 TFPATHWAY, and REACTOME GLYCOLYSIS pathways. According to previous research studies, we found that the

progression and metastasis of CRC are significantly correlated to the latter three pathways (Peng et al., 2020; Shen et al., 2021).

By the analysis of TIMER database, it was discovered that the expression level of SLC2A1 in CRC was negatively associated with the expression levels of B cell but positively associated with the expression levels of CD4+ T cell, neutrophil, and DC. Moreover, SLC2A1 CNV was remarkably associated with B cell, CD8+ T cell, neutrophil, and DC. These analyses point out that SLC2A1 maybe participated in the immune respond to CRC tumor microenvironment, particularly to B cell, neutrophil, and DC. The ratio of 24 tumor immune cells in CRC was detected by ssGSEA algorithm. We certified nine types of immune cells: DC, eosinophils, iDC, neutrophils, NK CD56 bright cells, NK cells, pDC, T helper cells, and Th2 cells, whose expression ratios showed considerable difference between the high and low SLC2A1 expression groups. Furthermore, through the analysis of three databases, we suggested that the expression level of SLC2A1 was remarkably positively associated with the gene markers of neutrophil, suggesting that SLC2A1 may influence the immunofiltration of SLC2A1 by affecting the expression of neutrophil. Neutrophil is an important immune cell in human body. Ning et al. (2015) found that excessive neutrophils can increase the expression of interleukin (IL)-1β and then induce the IL-17 response of CRC cells and support the occurrence of CRC. Wang et al. (2014) suggested that depletion of neutrophils or blocking of IL-1β activity significantly reduced mucosal damage and the formation of CRC tumors. We speculated that the overexpression of SLC2A1 promoted the infiltration of neutrophil in CRC and ultimately played an important role in promoting tumor proliferation. We pointed out that the high expression of SLC2A1 may enhance an anti-tumor immune response, stating that SLC2A1 plays a critical role in the immune regulation of CRC. Nevertheless, more prospective studies are needed to certify our speculation more accurately, including the relationship between SLC2A1 and neutrophil.

The modification of m6A is the prevalent common RNA modifications, which can affect tumor progression and metastasis by affecting the expression of several cancer-relative genes (Shen et al., 2020; Chen et al., 2021). On the project, we discovered that the SLC2A1 was remarkably positively associated with IGF2BP3 and YTHDF1. We also discovered that, in the group with high SLC2A1 expression, the expression levels of ALKBH5, IGF2BP1, IGF2BP3, RBM15B, VIRMA, YTHDF1, and ZC3H13 significantly increased. Yang et al. (2020) found that downregulation of IGF2BP3 could affect the expression of CCND1 and VEGF and thus inhibit DNA replication and angiogenesis in the S phase of tumor cell cycle. Bai et al. (2019) found that YTHDF1 was overexpressed in CRC, and knockdown of YTHDF1 expression could significantly inhibit the tumorigenicity of CRC cells *in vitro* and the growth of xenograft tumors in mice *in vivo*. Therefore, we speculate that SLC2A1 may interact with IGF2BP3 and YTHDF1 in CRC and ultimately affect the occurrence and development of CRC. Eventually, the Kaplan–Meier survival analysis of patients with CRC indicated that high IGF2BP3 expression correlated with significantly worse patient survival. We suggest that the promoting effect of SLC2A1 on CRC may be associated to m6A modification, and SLC2A1 can impact the CRC methylation level through its correlation with IGF2BP3 and finally impact the development and prognosis of CRC.

To grow, cancer cells show a higher need for iron than normal cells. This dependence on iron can make cancer cells more susceptible to iron-mediated necrosis, known as iron death (Ma et al., 2018). In this project, we discovered that the expression level of SLC2A1 was remarkably positively associated with ferroptosis relative genes, including FDFT1, GPX4, RPL8, and SLC1A5. We also found that, in the group with high SLC2A1 expression, the expression levels of AIFM2, ALOX15, CDKN1A, DPP4, GPX4, HSPA5, LPCAT3, RPL8, SLC1A5, and TFRC significantly increased. Eventually, the Kaplan–Meier survival analysis of patients with CRC indicated that high GPX4 expression correlated with significantly worse patient survival. Yang et al. (2021) found that cell ferroptosis may be inhibited in CRC cells through KIF20A/NUAK1/PP1β/GPX4 pathway, which may be the basis of oxaliplatin resistance. Therefore, we speculate that, in CRC, SLC2A1 may interact with GPX4 and finally affect the development of CRC. We suggest that the promoting effect of SLC2A1 on CRC may be associated to the mechanism of ferroptosis of tumor cells. SLC2A1 can achieve the inhibition of CRC ferroptosis by promoting the expression of GPX4 and ultimately promote the development of CRC.

The ceRNA network plays an important role in the development of cancer, and the theory of its role is mainly realized through the competitive binding of lncRNA or circular RNA to miRNA, which ultimately affects mRNA expression level (Salmena et al., 2011). Zhao et al. (2021) found that lncRNA MIR17HG acted as a ceRNA to regulate the expression of HK1 through sponging miR-138-5p, leading to glycolysis of CRC cells, leading to its invasion and liver metastasis. In this project, we first predicted five potential upstream miRNAs jointly through three databases, but only one miRNA (hsa-miR-148a-3p) was negatively relationship with SLC2A1 expression in CRC. Nersisyan et al. (2021) found that the downregulation of hsa-miR-148a-3p led to the upregulation of its two target genes, ITGA5 and PRNP, ultimately promoting the progression of CRC and leading to low survival rate in patients with CRC. Then, we further predicted the upstream lncRNAs of hsa-miR-148a-3p, and obtained 14 potential upstream lncRNAs. Correlation analysis showed that only eight lncRNAs expressed in CRC were negatively correlated with hsa-miR-148a-3p expression. To further narrow the scope of the ceRNA network, we analyzed the expression of eight lncRNAs in CRC and the correlation between their expression and SLC2A1 and found that only lncRNA H19 was highly expressed in CRC and positively correlated with SLC2A1 expression level. Zhang et al. (2020) found that lncRNA H19 promoted the transfer of junction CRC by binding with hnRNPA2B1. These studies further suggested the feasibility of our analysis. lncRNA H19 sponges mediated hsa-miR-148a-3p to regulate the expression of SLC2A1, thereby promoting the glycolysis and proliferation of CRC. However, although the ceRNA network of SLC2A1 has been obtained through a large number of database analyses, more basic studies are needed to further prove our analysis.

In conclusion, our study is the first one to analyze the association between SLC2A1 expression and immune invasion, m6A modification, ferroptosis, and ceRNA regulatory network in CRC from multiple perspectives. m6A can enhance the stability of SLC2A1 mRNA by modifying SLC2A1 gene, thus promoting the glycolysis and cell proliferation of CRC. SLC2A1 expression is associated with various immune infiltration cells and may influence CRC tumor immune microenvironment by promoting neutrophil infiltration. In the correlation analysis of ferroptosis, it was found that SLC2A1 might promote the expression of GPX4 and then inhibit the ferroptosis of CRC. The construction of SLC2A1 ceRNA network suggests that lncRNA H19/hsa-miR-148a-3p/SLC2A1 ceRNA network may promote the development of CRC. SLC2A1 could be considered as a potential biomarker for the diagnosis and treatment of patients with CRC. However, most of the results in this paper are obtained by bioinformatic analysis. A series of experiments will be carried out to further validate these results in the future, clarifying that the high expression of SLC2A1 can have the role of diagnostic CRC and that interference with SLC2A1 expression can achieve the purpose of treating tumors.

DATA AVAILABILITY STATEMENT

The datasets presented in this study can be found in online repositories. The names of the repository/repositories and accession number(s) can be found in the article/**Supplementary Material**.

ETHICS STATEMENT

The studies involving human participants were reviewed and approved by Ethics Committee of Taihe Hospital Affiliated of Hubei University of Medicine. Written informed consent for participation was not required for this study in accordance with the national legislation and the institutional requirements.

AUTHOR CONTRIBUTIONS

X-SL conceived the project and wrote the manuscript. X-SL, J-WY, JZ, and X-QC participated in data analysis. X-SL, YG, X-YK, X-YL, YZ, and Y-HZ participated in discussion and language editing. Z-JP reviewed the manuscript. All authors contributed to the article and approved the submitted version.

FUNDING

This work was supported by the Hubei province's Outstanding Medical Academic Leader program, the Foundation for Innovative Research Team of Hubei Provincial Department of Education T2020025, the Hubei Provincial Department of Science and Technology Innovation Group Program (grant no. 2019CFA034), Free-exploring Foundation of Hubei University of Medicine (grant no. FDFR201903), Innovative Research Program for Graduates of Hubei University of Medicine (grant no. YC2020011), Shiyan Taihe Hospital hospital-level project (2021JJXM006), and the Key Discipline Project of Hubei University of Medicine.

SUPPLEMENTARY MATERIAL

The Supplementary Material for this article can be found online at: https://www.frontiersin.org/articles/10.3389/fcell.2022.853596/full#supplementary-material

REFERENCES

Alsharif, S., Sharma, P., Bursch, K., Milliken, R., Lam, V., Fallatah, A., et al. (2021). Keratin 19 Maintains E-Cadherin Localization at the Cell Surface and Stabilizes Cell-Cell Adhesion of MCF7 Cells. *Cell Adhes. Migrat.* 15 (1), 1–17. doi:10.1080/19336918.2020.1868694

Ancey, P. B., Contat, C., and Meylan, E. (2018). Glucose Transporters in Cancer - from Tumor Cells to the Tumor Microenvironment. *Febs J.* 285 (16), 2926–2943. doi:10.1111/febs.14577

Andersson, A., Ritz, C., Lindgren, D., Edén, P., Lassen, C., Heldrup, J., et al. (2007). Microarray-based Classification of a Consecutive Series of 121 Childhood Acute Leukemias: Prediction of Leukemic and Genetic Subtype as Well as of Minimal Residual Disease Status. *Leukemia* 21 (6), 1198–1203. doi:10.1038/sj.leu.2404688

Avanzato, D., Pupo, E., Ducano, N., Isella, C., Bertalot, G., Luise, C., et al. (2018). High USP6NL Levels in Breast Cancer Sustain Chronic AKT Phosphorylation and GLUT1 Stability Fueling Aerobic Glycolysis. *Cancer Res.* 78 (13), 3432. doi:10.1158/0008-5472.CAN-17-3018

Bai, Y., Yang, C., Wu, R., Huang, L., Song, S., Li, W., et al. (2019). YTHDF1 Regulates Tumorigenicity and Cancer Stem Cell-like Activity in Human Colorectal Carcinoma. *Front. Oncol.* 9, 332. doi:10.3389/fonc.2019.00332

Barrett, T., Wilhite, S. E., Ledoux, P., Evangelista, C., Kim, I. F., Tomashevsky, M., et al. (2012). NCBI GEO: Archive for Functional Genomics Data Sets-Update. *Nucleic Acids Res.* 41 (D1), D991–D995. doi:10.1093/nar/gks1193

Berlth, F., Mönig, S., Pinther, B., Grimminger, P., Maus, M., Schlösser, H., et al. (2015). Both GLUT-1 and GLUT-14 Are Independent Prognostic Factors in Gastric Adenocarcinoma. *Ann. Surg. Oncol.* 22 (Suppl. 3), 822–831. doi:10.1245/s10434-015-4730-x

Beroukhim, R., Brunet, J.-P., Di Napoli, A., Mertz, K. D., Seeley, A., Pires, M. M., et al. (2009). Patterns of Gene Expression and Copy-Number Alterations in Von-Hippel Lindau Disease-Associated and Sporadic Clear Cell Carcinoma of the Kidney. *Cancer Res.* 69 (11), 4674–4681. doi:10.1158/0008-5472.CAN-09-0146

Chang, L., Zhou, G., Soufan, O., and Xia, J. (2020). miRNet 2.0: Network-Based Visual Analytics for miRNA Functional Analysis and Systems Biology. *Nucleic Acids Res.* 48 (W1), W244–W251. doi:10.1093/nar/gkaa467

Chen, W., Zheng, R., Baade, P. D., Zhang, S., Zeng, H., Bray, F., et al. (2016). Cancer Statistics in China, 2015. *CA Cancer J. Clin.* 66 (2), 115–132. doi:10.3322/caac.21338

Chen, H., Gao, S., Liu, W., Wong, C.-C., Wu, J., Wu, J., et al. (2021). RNA N^6-Methyladenosine Methyltransferase $METTL_3$ Facilitates Colorectal Cancer by Activating the m^6A-GLUT1-$mTORC_1$ Axis and Is a Therapeutic Target. *Gastroenterology* 160 (4), 1284–1300. doi:10.1053/j.gastro.2020.11.013

Curtis, C., Shah, S. P., Shah, S. P., Chin, S.-F., Turashvili, G., Rueda, O. M., et al. (2012). The Genomic and Transcriptomic Architecture of 2,000 Breast Tumours Reveals Novel Subgroups. *Nature* 486 (7403), 346–352. doi:10.1038/nature10983

Deng, D., Xu, C., Sun, P., Wu, J., Yan, C., Hu, M., et al. (2014). Crystal Structure of the Human Glucose Transporter GLUT1. *Nature* 510 (7503), 121–125. doi:10.1038/nature13306

Doll, S., Freitas, F. P., Shah, R., Aldrovandi, M., Da Silva, M. C., Ingold, I., et al. (2019). FSP1 Is a Glutathione-independent Ferroptosis Suppressor. *Nature* 575 (7784), 693–698. doi:10.1038/s41586-019-1707-0

Finak, G., Bertos, N., Pepin, F., Sadekova, S., Souleimanova, M., Zhao, H., et al. (2008). Stromal Gene Expression Predicts Clinical Outcome in Breast Cancer. *Nat. Med.* 14 (5), 518–527. doi:10.1038/nm1764

Haferlach, T., Kohlmann, A., Wieczorek, L., Basso, G., Kronnie, G. T., Béné, M.-C., et al. (2010). Clinical Utility of Microarray-Based Gene Expression Profiling in the Diagnosis and Subclassification of Leukemia: Report from the International Microarray Innovations in Leukemia Study Group. *J. Clin. Oncol.* 28 (15), 2529–2537. doi:10.1200/JCO.2009.23.4732

Hänzelmann, S., Castelo, R., and Guinney, J. (2013). GSVA: Gene Set Variation Analysis for Microarray and RNA-Seq Data. *BMC Bioinform.* 14 (1), 7. doi:10.1186/1471-2105-14-7

Hou, J., Aerts, J., den Hamer, B., van IJcken, W., den Bakker, M., Riegman, P., et al. (2010). Gene Expression-Based Classification of Non-Small Cell Lung Carcinomas and Survival Prediction. *Plos One* 5 (4), e10312. doi:10.1371/journal.pone.0010312

Jones, J., Otu, H., Spentzos, D., Kolia, S., Inan, M., Beecken, W. D., et al. (2005). Gene Signatures of Progression and Metastasis in Renal Cell Cancer. *Clin. Cancer Res.* 11 (16), 5730–5739. doi:10.1158/1078-0432.ccr-04-2225

Kasahara, M., and Hinkle, P. C. (1977). Reconstitution and Purification of the D-Glucose Transporter from Human Erythrocytes. *J. Biol. Chem.* 252 (20), 7384–7390. doi:10.1016/s0021-9258(19)66976-0

Kato, H., Takita, J., Miyazaki, T., Nakajima, M., Fukai, Y., Masuda, N., et al. (2002). Glut-1 Glucose Transporter Expression in Esophageal Squamous Cell Carcinoma Is Associated with Tumor Aggressiveness. *Anticancer Res.* 22 (5), 2635–2639.

Ki, D. H., Jeung, H.-C., Park, C. H., Kang, S. H., Lee, G. Y., Lee, W. S., et al. (2007). Whole Genome Analysis for Liver Metastasis Gene Signatures in Colorectal Cancer. *Int. J. Cancer* 121 (9), 2005–2012. doi:10.1002/ijc.22975

Kim, S. M., Park, Y.-Y., Park, E. S., Cho, J. Y., Izzo, J. G., Zhang, D., et al. (2010). Prognostic Biomarkers for Esophageal Adenocarcinoma Identified by Analysis of Tumor Transcriptome. *Plos One* 5 (11), e15074. doi:10.1371/journal.pone.0015074

Landi, M. T., Dracheva, T., Rotunno, M., Figueroa, J. D., Liu, H., Dasgupta, A., et al. (2008). Gene Expression Signature of Cigarette Smoking and its Role in Lung Adenocarcinoma Development and Survival. *Plos One* 3 (2), e1651. doi:10.1371/journal.pone.0001651

Li, J.-H., Liu, S., Zhou, H., Qu, L.-H., and Yang, J.-H. (2014). starBase v2.0: Decoding miRNA-ceRNA, miRNA-ncRNA and Protein-RNA Interaction Networks from Large-Scale CLIP-Seq Data. *Nucl. Acids Res.* 42 (Database issue), D92–D97. doi:10.1093/nar/gkt1248

Li, C., Liu, X., Liu, Y., Liu, X., Wang, R., Liao, J., et al. (2018). Keratin 80 Promotes Migration and Invasion of Colorectal Carcinoma by Interacting with PRKDC via Activating the AKT Pathway. *Cell Death Dis.* 9 (10), 1009. doi:10.1038/s41419-018-1030-y

Li, Y., Xiao, J., Bai, J., Tian, Y., Qu, Y., Chen, X., et al. (2019). Molecular Characterization and Clinical Relevance of m6A Regulators across 33 Cancer Types. *Mol. Cancer* 18 (1), 137. doi:10.1186/s12943-019-1066-3

Liu, Z., Zhao, Q., Zuo, Z.-X., Yuan, S.-Q., Yu, K., Zhang, Q., et al. (2020). Systematic Analysis of the Aberrances and Functional Implications of Ferroptosis in Cancer. *iScience* 23 (7), 101302. doi:10.1016/j.isci.2020.101302

Liu, X.-S., Gao, Y., Wu, L.-B., Wan, H.-B., Yan, P., Jin, Y., et al. (2021). Comprehensive Analysis of GLUT1 Immune Infiltrates and ceRNA Network in Human Esophageal Carcinoma. *Front. Oncol.* 11, 665388. doi:10.3389/fonc.2021.665388

Liu, X.-S., Zhou, L.-M., Yuan, L.-L., Gao, Y., Kui, X.-Y., Liu, X.-Y., et al. (2021). NPM1 Is a Prognostic Biomarker Involved in Immune Infiltration of Lung Adenocarcinoma and Associated with m6A Modification and Glycolysis. *Front. Immunol.* 12, 724741. doi:10.3389/fimmu.2021.724741

Ma, H., Wu, Z., Peng, J., Li, Y., Huang, H., Liao, Y., et al. (2018). Inhibition of SLC1A5 Sensitizes Colorectal Cancer to Cetuximab. *Int. J. Cancer* 142 (12), 2578–2588. doi:10.1002/ijc.31274

Martini, G., Cardone, C., Vitiello, P. P., Belli, V., Napolitano, S., Troiani, T., et al. (2019). EPHA2 Is a Predictive Biomarker of Resistance and a Potential Therapeutic Target for Improving Antiepidermal Growth Factor Receptor Therapy in Colorectal Cancer. *Mol. Cancer Ther.* 18 (4), 845–855. doi:10.1158/1535-7163.MCT-18-0539

Nersisyan, S., Galatenko, A., Chekova, M., and Tonevitsky, A. (2021). Hypoxia-Induced miR-148a Downregulation Contributes to Poor Survival in Colorectal Cancer. *Front. Genet.* 12, 662468. doi:10.3389/fgene.2021.662468

Ning, C., Li, Y.-Y., Wang, Y., Han, G.-C., Wang, R.-X., Xiao, H., et al. (2015). Complement Activation Promotes Colitis-Associated Carcinogenesis through Activating Intestinal IL-1β/IL-17A axis. *Mucosal Immunol.* 8 (6), 1275–1284. doi:10.1038/mi.2015.18

Okayama, H., Kohno, T., Ishii, Y., Shimada, Y., Shiraishi, K., Iwakawa, R., et al. (2012). Identification of Genes Upregulated in ALK-Positive and EGFR/KRAS/ALK-Negative Lung Adenocarcinomas. *Cancer Res.* 72 (1), 100–111. doi:10.1158/0008-5472.CAN-11-1403

Paraskevopoulou, M. D., Georgakilas, G., Kostoulas, N., Vlachos, I. S., Vergoulis, T., Reczko, M., et al. (2013). DIANA-microT Web Server v5.0: Service Integration into miRNA Functional Analysis Workflows. *Nucleic Acids Res.* 41 (W1), W169–W173. doi:10.1093/nar/gkt393

Pei, H., Li, L., Fridley, B. L., Jenkins, G. D., Kalari, K. R., Lingle, W., et al. (2009). FKBP51 Affects Cancer Cell Response to Chemotherapy by Negatively Regulating Akt. *Cancer Cell* 16 (3), 259–266. doi:10.1016/j.ccr.2009.07.016

Peng, K., Zhuo, M., Li, M., Chen, Q., Mo, P., and Yu, C. (2020). Histone Demethylase JMJD2D Activates HIF1 Signaling Pathway via Multiple Mechanisms to Promote Colorectal Cancer Glycolysis and Progression. *Oncogene* 39 (47), 7076–7091. doi:10.1038/s41388-020-01483-w

Pereira, K. M. A., Chaves, F. N., Viana, T. S. A., Carvalho, F. S. R., Costa, F. W. G., Alves, A. P. N. N., et al. (2013). Oxygen Metabolism in Oral Cancer: HIF and GLUTs (Review). *Oncol. Lett.* 6 (2), 311–316. doi:10.3892/ol.2013.1371

Rhodes, D. R., Yu, J., Shanker, K., Deshpande, N., Varambally, R., Ghosh, D., et al. (2004). ONCOMINE: A Cancer Microarray Database and Integrated Data-Mining Platform. *Neoplasia* 6 (1), 1–6. doi:10.1016/S1476-5586(04)80047-2

Rhodes, D. R., Kalyana-Sundaram, S., Mahavisno, V., Varambally, R., Yu, J., Briggs, B. B., et al. (2007). Oncomine 3.0: Genes, Pathways, and Networks in a Collection of 18,000 Cancer Gene Expression Profiles. *Neoplasia* 9 (2), 166–180. doi:10.1593/neo.07112

Rudlowski, C., Moser, M., Becker, A. J., Rath, W., Buttner, R., Schroder, W., et al. (2004). GLUT1 mRNA and Protein Expression in Ovarian Borderline Tumors and Cancer. *Oncology* 66 (5), 404–410. doi:10.1159/000079489

Salmena, L., Poliseno, L., Tay, Y., Kats, L., and Pandolfi, P. P. (2011). A ceRNA Hypothesis: The Rosetta Stone of a Hidden RNA Language? *Cell* 146 (3), 353–358. doi:10.1016/j.cell.2011.07.014

Sanchez-Carbayo, M., Socci, N. D., Lozano, J., Saint, F., and Cordon-Cardo, C. (2006). Defining Molecular Profiles of Poor Outcome in Patients with Invasive Bladder Cancer Using Oligonucleotide Microarrays. *J. Clin. Oncol.* 24 (5), 778–789. doi:10.1200/jco.2005.03.2375

Selamat, S. A., Chung, B. S., Girard, L., Zhang, W., Zhang, Y., Campan, M., et al. (2012). Genome-scale Analysis of DNA Methylation in Lung Adenocarcinoma and Integration with mRNA Expression. *Genome Res.* 22 (7), 1197–1211. doi:10.1101/gr.132662.111

Shen, C., Xuan, B., Yan, T., Ma, Y., Xu, P., Tian, X., et al. (2020). m6A-dependent Glycolysis Enhances Colorectal Cancer Progression. *Mol. Cancer* 19 (1), 72. doi:10.1186/s12943-020-01190-w

Shen, X., Ye, Z., Wu, W., Zhao, K., Cheng, G., Xu, L., et al. (2021). lncRNA NEAT1 Facilitates the Progression of Colorectal Cancer via the KDM5A/Cul4A and Wnt Signaling Pathway. *Int. J. Oncol.* 59 (1), 51. doi:10.3892/ijo.2021.5231

Skrzypczak, M., Goryca, K., Rubel, T., Paziewska, A., Mikula, M., Jarosz, D., et al. (2010). Modeling Oncogenic Signaling in Colon Tumors by Multidirectional Analyses of Microarray Data Directed for Maximization of Analytical Reliability. *Plos One* 5 (10), e13091. doi:10.1371/journal.pone.0013091

Su, L.-J., Chang, C.-W., Wu, Y.-C., Chen, K.-C., Lin, C.-J., Liang, S.-C., et al. (2007). Selection of DDX5 as a Novel Internal Control for Q-RT-PCR from Microarray Data Using a Block Bootstrap Re-sampling Scheme. *Bmc Genomics* 8 (1), 140. doi:10.1186/1471-2164-8-140

Su, H., Hu, N., Yang, H. H., Wang, C., Takikita, M., Wang, Q.-H., et al. (2011). Global Gene Expression Profiling and Validation in Esophageal Squamous Cell Carcinoma and its Association with Clinical Phenotypes. *Clin. Cancer Res.* 17 (9), 2955–2966. doi:10.1158/1078-0432.CCR-10-2724

Subramanian, A., Tamayo, P., Mootha, V. K., Mukherjee, S., Ebert, B. L., Gillette, M. A., et al. (2005). Gene Set Enrichment Analysis: A Knowledge-Based

Approach for Interpreting Genome-wide Expression Profiles. *Proc. Natl. Acad. Sci.* 102 (43), 15545–15550. doi:10.1073/pnas.0506580102

Sung, H., Ferlay, J., Siegel, R. L., Laversanne, M., Soerjomataram, I., Jemal, A., et al. (2021). Global Cancer Statistics 2020: GLOBOCAN Estimates of Incidence and Mortality Worldwide for 36 Cancers in 185 Countries. *CA Cancer J. Clin.* 71 (3), 209–249. doi:10.3322/caac.21660

Tokar, T., Pastrello, C., Rossos, A. E. M., Abovsky, M., Hauschild, A.-C., Tsay, M., et al. (2018). mirDIP 4.1-integrative Database of Human microRNA Target Predictions. *Nucleic Acids Res.* 46 (D1), D360–D370. doi:10.1093/nar/gkx1144

Tomczak, K., Czerwińska, P., and Wiznerowicz, M. (2015). Review the Cancer Genome Atlas (TCGA): an Immeasurable Source of Knowledge. *Contemp. Oncol. (Pozn)* 19 (1A), A68–A77. doi:10.5114/wo.2014.47136

Uldry, M., and Thorens, B. (2004). The SLC2 Family of Facilitated Hexose and Polyol Transporters. *Pflugers Archiv Eur. J. Physiol.* 447 (5), 480–489. doi:10.1007/s00424-003-1085-0

van Laarhoven, H. W. M., Kaanders, J. H. A. M., Lok, J., Peeters, W. J. M., Rijken, P. F. J. W., Wiering, B., et al. (2006). Hypoxia in Relation to Vasculature and Proliferation in Liver Metastases in Patients with Colorectal Cancer. *Int. J. Radiat. Oncol. Biol. Phys.* 64 (2), 473–482. doi:10.1016/j.ijrobp.2005.07.982

Wang, Y., Wang, K., Han, G.-C., Wang, R.-X., Xiao, H., Hou, C.-M., et al. (2014). Neutrophil Infiltration Favors Colitis-Associated Tumorigenesis by Activating the Interleukin-1 (IL-1)/IL-6 axis. *Mucosal Immunol.* 7 (5), 1106–1115. doi:10.1038/mi.2013.126

Wang, Q., Chen, C., Ding, Q., Zhao, Y., Wang, Z., Chen, J., et al. (2020). METTL3-mediated m6A Modification of HDGF mRNA Promotes Gastric Cancer Progression and Has Prognostic Significance. *Gut* 69 (7), 1193–1205. doi:10.1136/gutjnl-2019-319639

Wang, D.-S., Yang, H., Liu, X.-Y., Chen, Z.-G., Wang, Y., Fong, W. P., et al. (2021). Dynamic Monitoring of Circulating Tumor DNA to Predict Prognosis and Efficacy of Adjuvant Chemotherapy after Resection of Colorectal Liver Metastases. *Theranostics* 11 (14), 7018–7028. doi:10.7150/thno.59644

Yang, Z., Wang, T., Wu, D., Min, Z., Tan, J., and Yu, B. (2020). RNA N6-Methyladenosine Reader IGF2BP3 Regulates Cell Cycle and Angiogenesis in colon Cancer. *J. Exp. Clin. Cancer Res.* 39 (1), 203. doi:10.1186/s13046-020-01714-8

Yang, C., Zhang, Y., Lin, S., Liu, Y., and Li, W. (2021). Suppressing the KIF20A/NUAK1/Nrf2/GPX4 Signaling Pathway Induces Ferroptosis and Enhances the Sensitivity of Colorectal Cancer to Oxaliplatin. *Aging* 13 (10), 13515–13534. doi:10.18632/aging.202774

Yoshihara, K., Tajima, A., Komata, D., Yamamoto, T., Kodama, S., Fujiwara, H., et al. (2009). Gene Expression Profiling of Advanced-Stage Serous Ovarian Cancers Distinguishes Novel Subclasses and implicatesZEB2in Tumor Progression and Prognosis. *Cancer Sci.* 100 (8), 1421–1428. doi:10.1111/j.1349-7006.2009.01204.x

Yu, G., Wang, L.-G., Han, Y., and He, Q.-Y. (2012). clusterProfiler: an R Package for Comparing Biological Themes Among Gene Clusters. *OMICS: A J. Integr. Biol.* 16 (5), 284–287. doi:10.1089/omi.2011.0118

Zhang, Y., Huang, W., Yuan, Y., Li, J., Wu, J., Yu, J., et al. (2020). Long Non-coding RNA H19 Promotes Colorectal Cancer Metastasis via Binding to hnRNPA2B1. *J. Exp. Clin. Cancer Res.* 39 (1), 141. doi:10.1186/s13046-020-01619-6

Zhao, H., Langerød, A., Ji, Y., Nowels, K. W., Nesland, J. M., Tibshirani, R., et al. (2004). Different Gene Expression Patterns in Invasive Lobular and Ductal Carcinomas of the Breast. *MBoC* 15 (6), 2523–2536. doi:10.1091/mbc.e03-11-0786

Zhao, S., Guan, B., Mi, Y., Shi, D., Wei, P., Gu, Y., et al. (2021). LncRNA MIR17HG Promotes Colorectal Cancer Liver Metastasis by Mediating a Glycolysis-Associated Positive Feedback Circuit. *Oncogene* 40 (28), 4709–4724. doi:10.1038/s41388-021-01859-6

Conflict of Interest: The authors declare that the research was conducted in the absence of any commercial or financial relationships that could be construed as a potential conflict of interest.

Publisher's Note: All claims expressed in this article are solely those of the authors and do not necessarily represent those of their affiliated organizations or those of the publisher, the editors, and the reviewers. Any product that may be evaluated in this article, or claim that may be made by its manufacturer, is not guaranteed or endorsed by the publisher.

frontiers | Frontiers in Cell and Developmental Biology

ORIGINAL RESEARCH
published: 13 May 2022
doi: 10.3389/fcell.2022.833579

Characterization of a Novel LUCAT1/miR-4316/VEGF-A Axis in Metastasis and Glycolysis of Lung Adenocarcinoma

Lishui Wang[1], Yan Xie[2], Jing Wang[2], Ying Zhang[2], Shibiao Liu[2], Yao Zhan[2], Yinghui Zhao[2], Juan Li[2], Peilong Li[2] and Chuanxin Wang[2,3,4,5]**

[1]Department of Clinical Laboratory, Qilu Hospital, Cheeloo College of Medicine, Shandong University, Jinan, China, [2]Department of Clinical Laboratory, The Second Hospital, Cheeloo College of Medicine, Shandong University, Jinan, China, [3]Shandong Engineering & Technology Research Center for Tumor Marker Detection, Jinan, China, [4]Shandong Provincial Clinical Medicine Research Center for Clinical Laboratory, Jinan, China, [5]Shandong Technology Innovation Center for Big Data and Precision Medicine of Cancer, Jinan, China

OPEN ACCESS

Edited by:
Yuanyuan Lu,
Fourth Military Medical University, China

Reviewed by:
Yuanyuan Wang,
First Affiliated Hospital of Zhengzhou University, China
Yang Luo,
Chongqing University, China
Jian Dong,
Fudan University, China

***Correspondence:**
Peilong Li
lipeilong@whu.edu.cn
Chuanxin Wang
cxwang@sdu.edu.cn

Specialty section:
This article was submitted to Epigenomics and Epigenetics, a section of the journal Frontiers in Cell and Developmental Biology

Received: 11 December 2021
Accepted: 25 April 2022
Published: 13 May 2022

Citation:
Wang L, Xie Y, Wang J, Zhang Y, Liu S, Zhan Y, Zhao Y, Li J, Li P and Wang C (2022) Characterization of a Novel LUCAT1/miR-4316/VEGF-A Axis in Metastasis and Glycolysis of Lung Adenocarcinoma. Front. Cell Dev. Biol. 10:833579. doi: 10.3389/fcell.2022.833579

Objective: Accumulating literatures suggested that long non-coding RNAs (lncRNAs) were involved in tumorigenesis and cancer progression in lung adenocarcinoma (LUAD). However, the precise regulatory mechanism of lncRNA Lung cancer-associated transcript 1 (LUCAT1) in LUAD is not well defined. In this study, we aimed to investigate the biological function and mechanism of lncRNA LUCAT1 in regulating tumor migration and glycolysis of LUAD.

Methods: High throughput sequencing was performed to identify differentially expressed lncRNAs between LUAD patients and healthy controls. The expression levels of LUCAT1 in LUAD clinical specimens or cell lines were evaluated by *In situ* hybridization (ISH) and quantitative Real-Time Polymerase Chain Reaction (qRT-PCR). Functional experiments, including wound-healing, transwell invasion assays, glucose absorption, lactate metabolism and tumor xenograft experiments were conducted to identify the biological functions of LUCAT1 in LUAD. Silencing of LUCAT1, over-expression of LUCAT1 and miR-4316 were generated in LUAD cell lines to verify the regulatory mode of LUCAT1-mir-4316-VEGFA axis.

Results: Our findings revealed that lncRNA LUCAT1 was significantly up-regulated in LUAD serum exosomes, tumor tissues, and LUAD cells in comparison with corresponding controls. Receiver operating characteristic curve (ROC) analysis indicated that the area under the curve (AUC) value of serum exosomal LUCAT1 reached 0.852 in distinguishing LUAD patients from healthy individuals. High expression of LUCAT1 in LUAD patient tissues was associated with enhanced Lymph Node Metastasis (LNM), advanced Tumor Node Metastasis (TNM) stage and poorer clinical outcome in LUAD patients. Knockdown of LUCAT1 inhibited LUAD cell metastasis and glycolysis *in vitro* as well as tumor metastasis *in vivo*, while overexpression of LUCAT1 induced a promoted LUAD metastasis and glycolysis. Furthermore, mechanistic investigations revealed that LUCAT1 elevated LUAD cell metastasis and glycolysis by sponging miR-4316, which

further led to the upregulation of VEGFA. Finally, the regulatory axis LUCAT1-miR-4316-VEGFA was verified in LUAD.

Conclusion: Our present research suggested that LUCAT1 facilitate LUAD cell metastasis and glycolysis *via* serving as a competing endogenous RNA to regulate miR-4316/VEGFA axis, which provided a novel diagnostic marker and therapeutic target for LUAD patients.

Keywords: lung adenocarcinoma, exosomes, lncRNA LUCAT1, mir-4316, metastasis, glycolysis

INTRODUCTION

Lung cancer was the most common cause of cancer-related death in the world and the 5-year survival rate was about 15% (Torre et al., 2015; Jia et al., 2019). Non-small cell lung carcinoma (NSCLC) accounts for 85% of all lung cancer cases, approximately half of NSCLC cases are lung adenocarcinoma (LUAD), which arises from type II alveolar cells in the small airway epithelial (Travis et al., 2015; Denisenko et al., 2018). Metastasis and relapse were two main causes of death of patients with LUAD (Li et al., 2016). Although there have been some significant advances in chemotherapy, radiotherapy and immunotherapy, the 5-year survival rate was still unsatisfactory (Hirsch et al., 2017). Hence, there was an urgent need to illustrate the underlying mechanisms of occurrence and development of LUAD and explore potential diagnostic and prognostic biomarkers for LUAD.

Long noncoding RNAs (lncRNAs) were a class of special RNA molecular that are more than 200 nucleotides in length and have extremely limited capacity of protein-coding (Mercer et al., 2009; Ponting et al., 2009). As one of typical modes of epigenetic regulation, lncRNAs were involved in various diseases, including cancer. Several studies have demonstrated that lncRNAs played pivotal roles in a variety of biological processes, such as cellular growth, proliferation, differentiation, migration, and invasion of cancer cells (Kretz et al., 2013; Zhang S. et al., 2019; Wang et al., 2019). The underlying regulatory mechanisms of lncRNAs were diverse, they may participate in the regulation of protein-DNA and protein-protein interactions, or directly bind to mircoRNAs and proteins as decoys, and thus modulate gene expression at transcriptional or post-transcriptional level (Tian et al., 2020). As competitive endogenous RNAs (ceRNAs), lncRNAs played vital roles in the lncRNA-microRNA-mRNA regulatory network of gene expression (Salmena et al., 2011). In addition, previous studies have shown that some aberrantly expressed lncRNAs were associated with occurrence and development of malignant tumors *via* regulation of glycolysis, including colorectal cancer, liver cancer, pancreatic cancer, etc. For example, LncRNA HULC directly binds to two glycolytic enzymes, LDHA, and PKM2, leading to elevated phosphorylation of these two enzymes and consequently speeding up glycolysis in liver cancer (Wang et al., 2020). In pancreatic cancer, LINC00261 promotes c-myc-mediated aerobic glycolysis by activating miR-222-3p/HIPK2/ERK axis and sequestering IGF2BP1, suggesting an essential role of lncRNAs in cell glycolysis (Zhai et al., 2021). Unlike normal cells, cancer cells have a special phonotype of glucose metabolism. Although there was plenty of oxygen, cancer cells tended to produce energy by glycolysis in the cytosol with production of lactic acid, which termed as "aerobic glycolysis" (Helmlinger et al., 2002; Elf and Chen, 2014). Aerobic glycolysis can rapidly provide energy for cancer cells to proliferate and survive. However, there are still a lot of gaps need to explore about lncRNAs which mediated aerobic glycolysis involved in the occurrence and development of LUAD.

Lung cancer-associated transcript 1 (LUCAT1), also identified as smoke and cancer associated lncRNA1 (SCAL1), was a novel lncRNA which first discovered in smoking-related lung cancer (Zhang L. et al., 2019; Liu et al., 2020). Compared with normal tissues, LUCAT1 was highly upregulated in NSCLC tissues. Usually, USCLC patients with higher LUCAT1 level tend to have poorer prognosis (Zheng A. et al., 2019). Evidence has shown that LUCAT1 could participate in proliferation, migration and invasion of esophageal squamous cell carcinoma (Yoon et al., 2018), ovarian cancer (Yu et al., 2018), prostate cancer (Liu et al., 2020), et al. Nevertheless, whether LUCAT1 influences metastasis and glycolysis in LUAD, and if yes, what is the regulatory mechanism, remains to be further explored. VEGF-A was the most potent pro-angiogenic factor that directly induced endothelial cell proliferation, migration and promotes tumor growth (Claesson-Welsh and Welsh, 2013). It has been reported that miR-4316 inhibits gastric cancer proliferation and migration *via* directly targeting VEGF-A. However, it is unclear whether miR-4316 regulate the metastasis of LUAD through VEGF-A (Krawczyk et al., 2017).

In this study, we verified that LUCAT1 was significantly upregulated in LUAD, and enhanced LUCAT1 promoted migration and invasion both *in vitro and in vivo*. In addition, LUCAT1 accelerated aerobic glycolysis. Mechanistically, LUCAT1 acted as miRNA sponge to absorb miR-4316, and thus releasing VEGFA. Therefore, the uncovering of LUCAT1/miR-4316/VEGFA axis in LUAD may provide theoretical support for finding novel diagnostic biomarkers and therapeutic targets of LUAD patients.

RESULTS

Lung Cancer-Associated Transcript 1 Was Upregulated in Lung Adenocarcinoma Serum Exosomal Samples and May Serve as a Biomarker

Exosomal samples isolated from LUAD patients and healthy controls were validated by performing Transmission electron

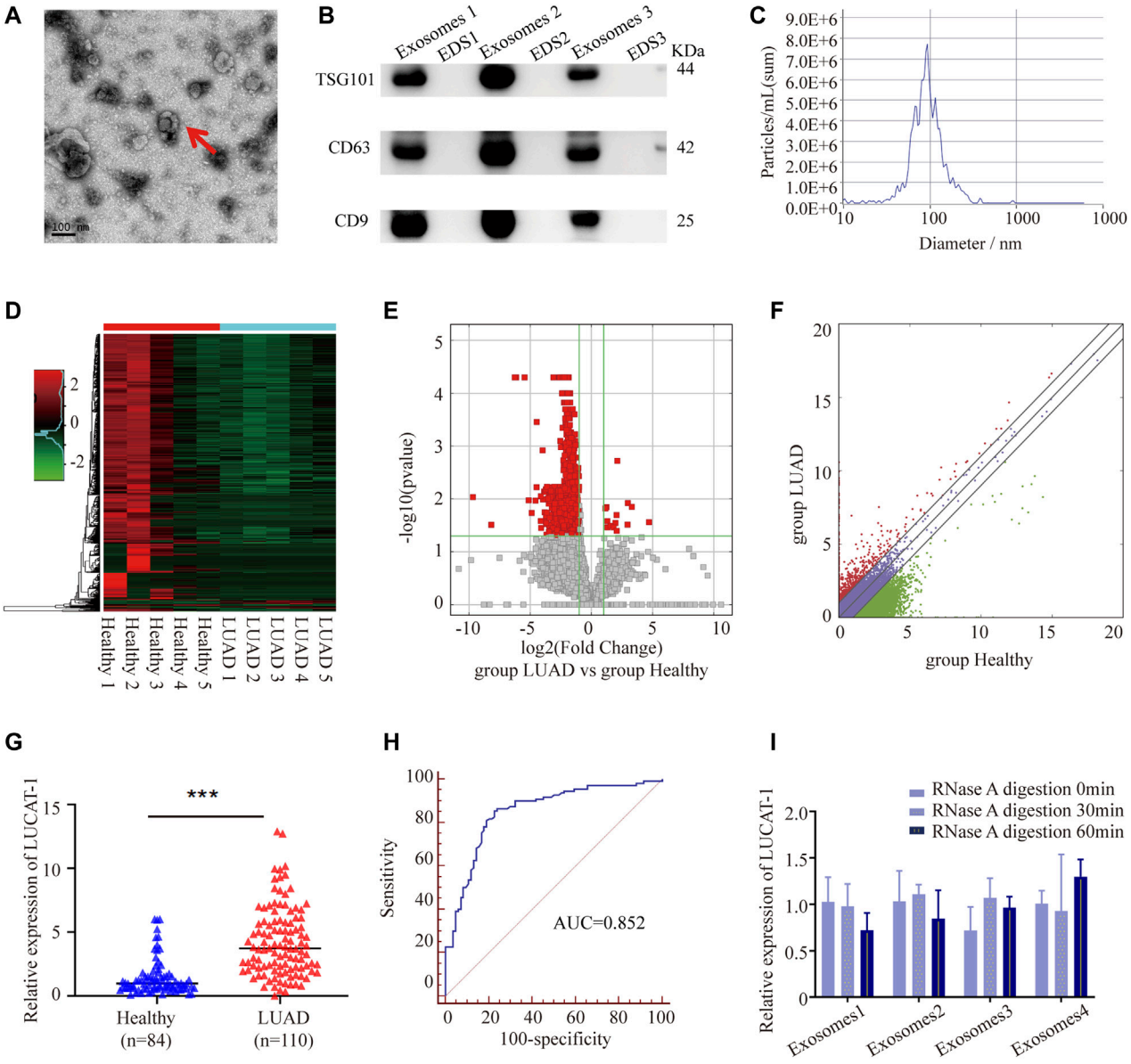

FIGURE 1 | Tumor-originated exosomal LUCAT1 as a circulating biomarker for LUAD. **(A)** Transmission electron microscopy images of exosomes. Scale bar: 100 nm. **(B)** Western blot images of exosomal markers (TSG101, CD63, CD9). **(C)** Size distribution and concentration of serum exosomes. Heatmap **(D)**, volcano plot **(E)** and scatter plot **(F)** showed the differentially expressed serum exosomal lncRNAs from the high-throughput sequencing analysis. **(G)** Comparison of serum exosomal LUCAT1 expression between LUAD patients and healthy controls detected by qRT-PCR. **(H)** ROC curves for the determination of the diagnostic performance of serum exosomal LUCAT1. **(I)** Comparison of the expression level of LUCAT1 before and after RNase A treatment. *p* values were calculated using two-sided paired t-test (*$p < 0.05$; **$p < 0.01$; ***$p < 0.001$).

microscopy (TEM), western blotting (WB) and nanoparticle tracking analysis (NTA). As shown, these vesicles showed typical oval-shaped extracellular vesicles with diameters of 50–150 nm by TEM (**Figure 1A**). WB demonstrated that the concentrations of the exosome surface protein markers, TSG101, CD63, and CD9, were enriched in serum exosomes but not in exosome-depleted supernatants (EDS) (**Figure 1B**). NTA showed that the diameters of most serum exosomes were mainly 91.6 nm (**Figure 1C**). All these results suggested that we successfully purified exosomes from the serum, which laid a foundation for further analysis.

High throughput sequencing was performed using 50 LUAD serum exosomal samples and 50 healthy controls (the 50 LUAD and 50 healthy samples were grouped and mixed into 5 repeats, respectively). The results showed that a total of 722 differentially expressed lncRNAs between the two groups were identified according to our screening disciplines, including 14 up-regulated and 708 down-regulated lncRNAs. Cluster analysis

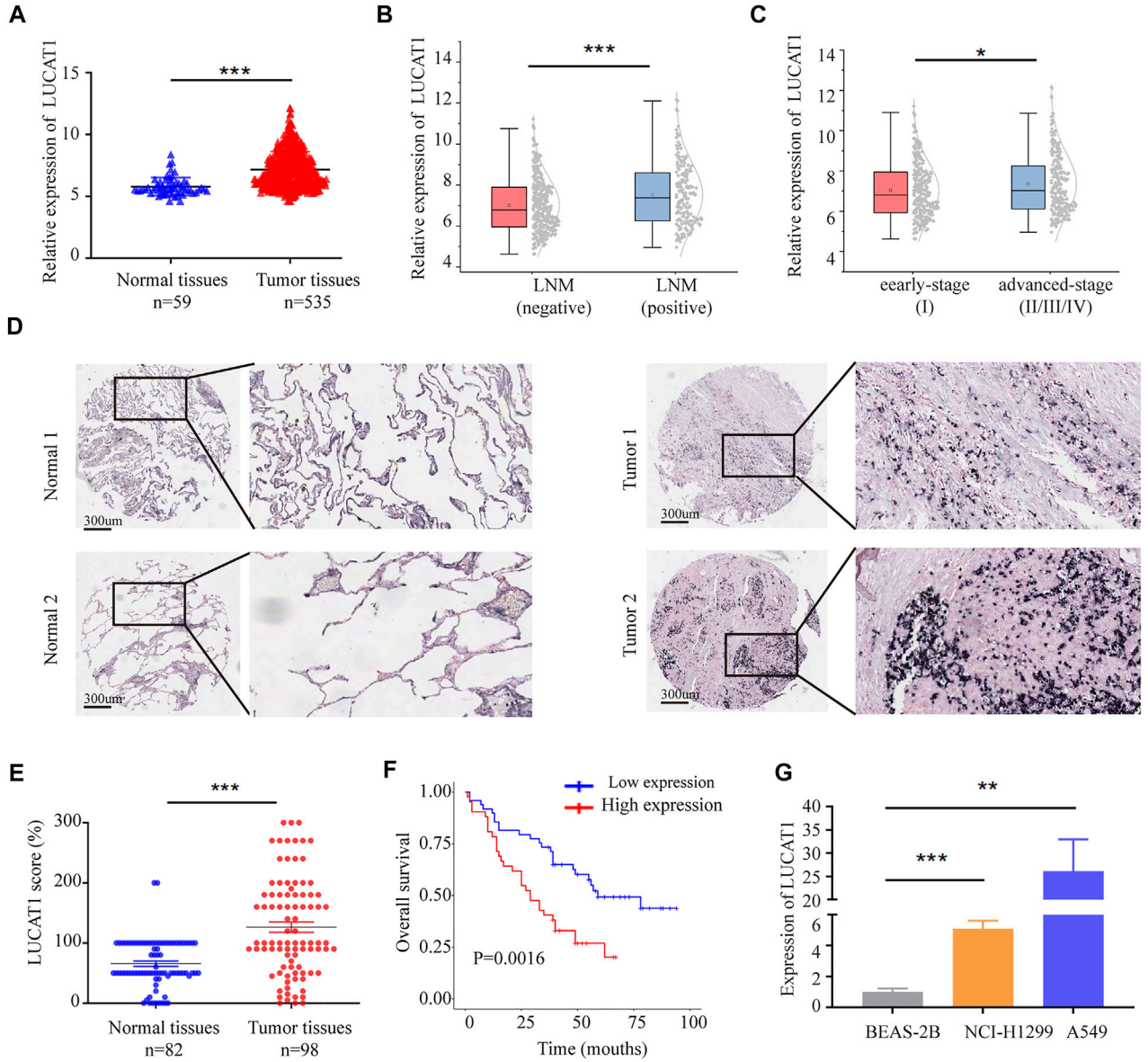

FIGURE 2 | LUCAT1 was upregulated in LUAD tissues, and its overexpression correlates with poor outcome of LUAD. **(A)** Relative expression of LUCAT1 in LUAD compared with normal tissues was analysed by using TCGA datasets. **(B)** Relative expression level of LUCAT1 in LUAD with lymph node metastasis and non-lymph node metastasis. **(C)** Expression level of LUCAT1 in early-stage LUAD patients (stage I) with advanced-stage LUAD patients (stage II/III/IV). **(D,E)** ISH analysis of LUCAT1 expression in LUAD tissues ($n = 98$) and normal tissues ($n = 82$), Scale bar: 300 μm. **(F)** Kaplan-Meier analysis for overall survival of LUAD patients with low and high LUCAT1 expression ($p = 0.0016$). **(G)** qRT-PCR was performed to detect the expression of LUCAT1 in normal lung epithelial cells and LUAD cells. A two-tailed student's t-test was used to analyse the comparison between the two groups (*$p < 0.05$; **$p < 0.01$; ***$p < 0.001$).

heat map, scatter plot, and volcano plot were shown to present the distinguishable lncRNAs expression profiles (**Figures 1D–F**).

Since up-regulated lncRNAs have greater potential to be used as early diagnostic markers or therapeutic targets, we focused on 7 most upregulated lncRNAs, including ENST00000417930, ENST00000578785, TCONS_l2_00006336, uc010jub.1, ENST00000569809, ENST00000430694, and ENST00000513626, among which, only ENST00000417930, uc010jub.1 and ENST00000513626 were successfully designed with specific primers. To confirm the High throughput sequencing results, expression levels of three serum exosomal lncRNAs were measured in 84 LUAD patients and 110 healthy controls through qRT-PCR, the results showed that only ENST00000513626 (LUCAT1) was significantly up-regulated in LUAD patients (**Figure 1G**), while the other two genes were not detectable due to low expression concentrations. The potential diagnostic value of serum exosomal LUCAT1 was evaluated through Receiver operating characteristic curve (ROC) analysis. As expected, the area under the ROC curve (AUC) of serum exosomal LUCAT1 for LUAD diagnosis was

0.852 (95% CI = 0.794–0.898), with a diagnostic sensitivity and specificity reaching 85.45 and 77.38%, respectively (**Figure 1H**). These data suggested that LUCAT1 was a promising biomarker for the diagnosis of LUAD and may play an important role in LUAD progression.

VEGF-A was the most potent pro-angiogenic factor that directly induced endothelial cell proliferation, migration and promotes tumor growth. It has been reported that miR-4316 inhibits gastric cancer proliferation and migration *via* directly targeting VEGF-A. However, it is unclear whether miR-4316 regulate the metastasis of LUAD through VEGF-A.

The instability of majority of the lncRNAs in serum remains a significant limitation for clinical application. Serum exosomes samples were incubated with RNase A for 0, 30, and 60 min, and then exosomal LUCAT1 expression was measured. Interestingly, the expression levels of exosomal LUCAT1 remained unchanged upon RNase A treatment (**Figure 1I**), which fully proved its sufficient suitability as tumor markers for LUAD diagnosis.

Lung Cancer-Associated Transcript 1 Was Significantly Up-Regulated in Lung Adenocarcinoma Tissues and Cell Lines

We also analyzed the expression data of LUCAT1 in 535 LUAD tissues and 59 normal tissues from The Cancer Genome Atlas (TCGA) database. LUCAT1 was significantly up-regulated in LUAD tumors than in non-tumor tissues (**Figure 2A**). Analyzing of clinical data revealed that LUCAT1 expression level was positively correlated with higher rates of Lymph Node Metastasis (LNM) (**Figure 2B**) and advanced Tumor Node Metastasis (TNM) stage (**Figure 2C**).

To further test whether expression level of LUCAT1 correlated with the outcomes of LUAD patients, the expression level of LUCAT1 was detected in 98 LUAD patients with different clinicopathological features and 82 paired normal tissues using *In situ* Hybridization (ISH). Consistent with TCGA results, LUCAT1 expression level was higher in LUAD tissues compared with normal tissues (**Figures 2D,E**). Kaplan-Meier survival analysis revealed that patients with high LUCAT1 expression had a markedly lower overall survival compared to those with low LUCAT1 expression (**Figure 2F**).

To understand the role of LUCAT1 in LUAD cells, the expression of LUCAT1 was detected in normal lung epithelial cells (BEAS-2B) and LUAD cells (NCI-H1299 and A549) by qRT-PCR analysis. As shown in **Figure 2G**, LUCAT1 expression in NCI-H1299 and A549 cells was much higher than that in BEAS-2B cells. Taken together, all these results indicated that LUCAT1 was significantly overexpressed in LUAD and might be a potential biomarker for predicting prognosis in LUAD patients.

Lung Cancer-Associated Transcript 1 Was Required for Efficient Metastasis of Lung Adenocarcinoma *in vitro*

In order to better investigate the biological functions of LUCAT1 in the tumorigenesis and development of LUAD, loss- and gain-of function experiments were conducted in NCI-H1299 and A549 cells. Specific siRNAs were used to knock down LUCAT1 expression, the knockdown efficiency of LUCAT1 in two LUAD cell lines were verified by qRT-PCR (**Figure 3A**). As shown, LUCAT1 knockdown strikingly attenuated the invasive abilities of NCI-H1299 and A549 cells (**Figure 3B**). Similarly, the migration capability of NCI-H1299 and A549 cells in wound healing assays was significantly decreased after the silence of LUCAT1 (**Figure 3C**). Subsequently, NCI-H1299 and A549 cells were transfected with the overexpression lentiviral vector (pcDNA3.1- LUCAT1) (**Figure 3D**). The adverse results were obtained, that is, overexpressed LUCAT1 strikingly enhanced the invasive abilities of two LUAD cells (**Figure 3E**). Additionally, wound healing assay showed that LUCAT1 overexpression significantly promoted the migratory ability of NCI-H1299 and A549 cells (**Figure 3F**).

Also, WB analysis revealed that LUCAT1 silencing could induce a significant elevation in epithelial maker E-cadherin expression, and a decreased expression of mesenchymal makers, including N-cadherin, β-catenin, and vimentin (**Figure 3G**). Conversely, LUCAT1 overexpression significantly increased mesenchymal makers N-cadherin, β-catenin, and vimentin expression, and decreased the expression of epithelial protein E-cadherin (**Figure 3H**).

Lung Cancer-Associated Transcript 1 Knockdown Repressed Lung Adenocarcinoma Cell Metastasis *in vivo*

To further investigate the biological function of LUCAT1, we established *in vivo* xenograft nude mouse model of LUAD metastasis *via* a tail vin injection method. Short hairpin RNA (shRNA) was utilized to stably silence LUCAT1 expression in NCI-H1299 cell lines (**Figure 4A**). In line with the *in vitro* data, the numbers of metastatic nodules in the lungs were significantly decreased in nude mouse injected with NCI-H1299 sh-LUCAT1 cells compared those injected with NCI-H1299 sh-NC cells (**Figure 4B**). Metastatic nodules were dissected out for haematoxylin and eosin (HE) analysis and further confirmed the metastasis nodules (**Figure 4C**). Immunohistochemistry (IHC) was performed to quantity the expression of biomarkers of metastasis in mouse model. Consistent with our observations *in vitro*, silencing of LUCAT1 significantly enhanced E-cadherin expression and attenuated the expression of N-Cadherin in xenografts, suggesting that silencing of LUCAT1 inhibited lung metastasis (**Figure 4D**). And the expression levels of LUCAT1/miR-4316/VEGF-A axis in metastatic LUAD in mouse model were also investigated *via* qRT-PCR. As expected, metastatic nodes formed from NCI-H1299 sh-LUCAT1 cells exhibited decreased LUCAT1 expression, while the expression of miR-4316 were upregulated along with lung metastasis. Similarly, a significant difference was also observed in the expression of VEGFA between NCI-H1299 sh-LUCAT1 and sh-NC groups in metastatic

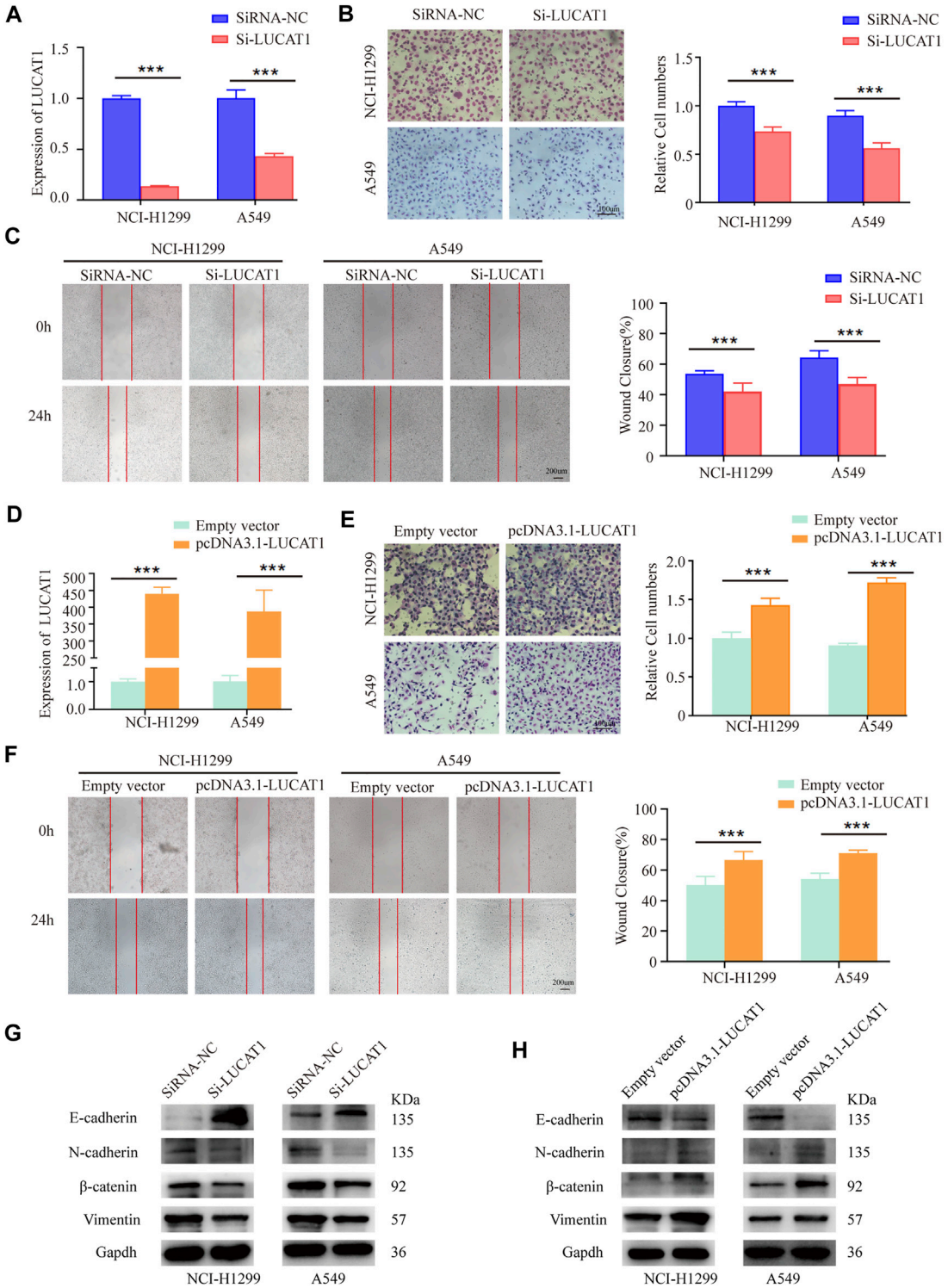

FIGURE 3 | LUCAT1 promotes migration and invasion of LUAD cells *in vitro*. **(A)** LUCAT1 silencing efficiency of NCI-H1299 and A549 cells were verified by qRT-PCR analysis. **(B)** Transwell assay for investigating invasion change in NCI-H1299 and A549 cells after LUCAT1 knockdown, Scale bar: 100 μm. **(C)** The migration of LUCAT1-silenced LUAD cells were detected by wound healing assay. Scale bar: 200 μm. **(D)** The relative mRNA levels of LUCAT1 in LUAD cells transfected with pcDNA3.1- LUCAT1, or control. **(E)** Transwell assay were performed to determine the invasion change in NCI-H1299 and A549 cells upon LUCAT1 was overexpressed. Scale bar: 100 μm. **(F)** The migration of LUCAT1-overexpression LUAD cells were detected by wound healing assay. Scale bar: 200 μm. **(G,H)** The relative expression levels of E-cadherin and vimentin were determined by western blot in NCI-H1299 and A549 cells with LUCAT1 knockdown. Comparisons between two groups were analysed using two-sided paired t-test (*$p < 0.05$; **$p < 0.01$; ***$p < 0.001$).

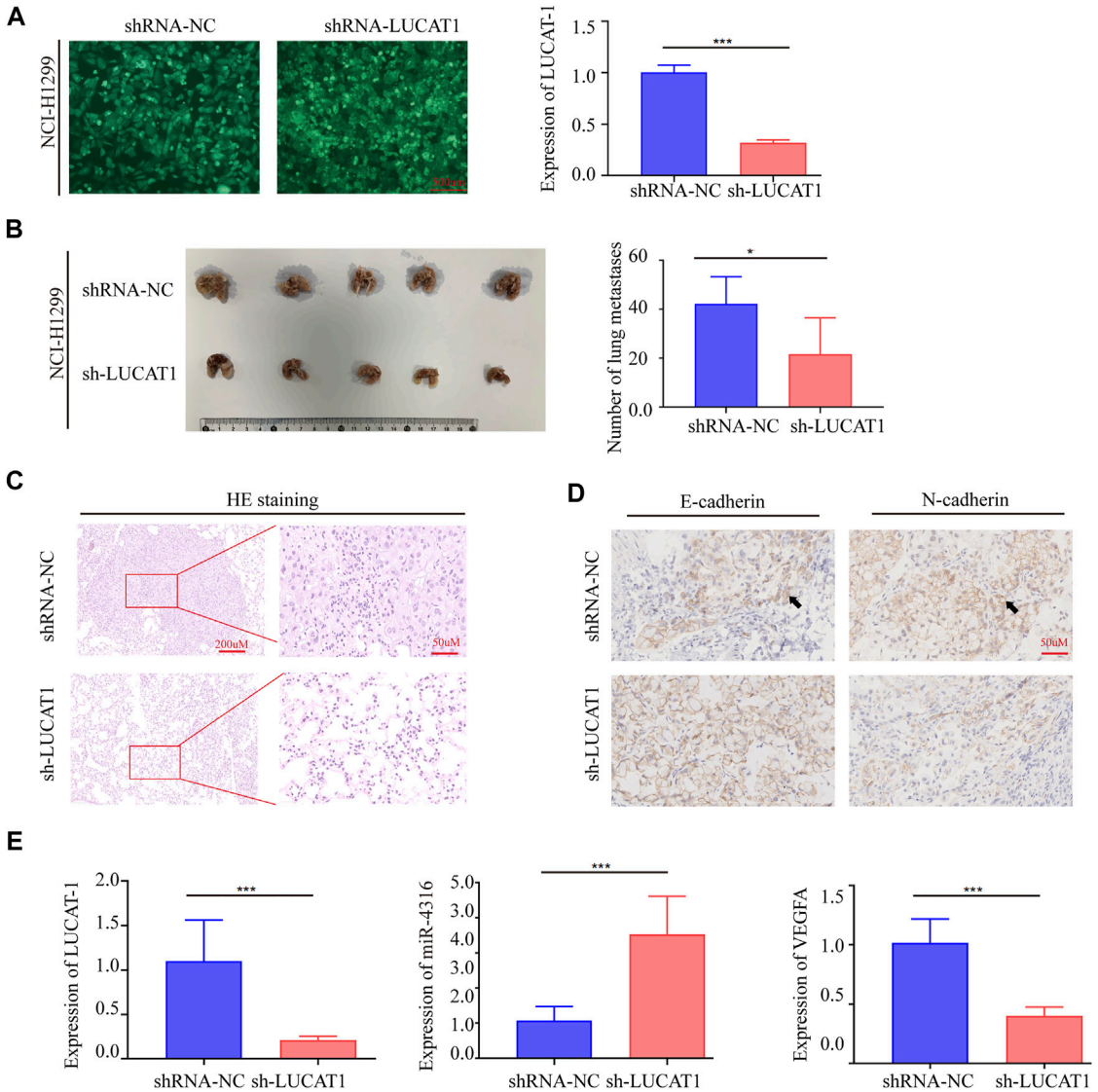

FIGURE 4 | Silencing LUCAT1 inhibits tumor metastasis *in vivo*. **(A)** qRT-PCR results for knockdown efficiency of LUCAT1 in A549 cells by shRNAs. Scale bar: 200 μm. **(B)** Number of metastatic nodules in the lung tissues. **(C)** The microscopic images of lung tissue sections stained by HE. **(D)** IHC were performed to quantity the expression of E-Cadherin and N-Cadherin in metastatic nodes of mouse model. **(E)** qRT-PCR was performed to detect the expression of LUCAT1, miR-4316 and VEGFA of metastatic nodes formed from sh-LUCAT stable cells. *p*-values were determined by two-tailed student's t-test (*$p < 0.05$; **$p < 0.01$; ***$p < 0.001$).

nodules (**Figure 4E**). These data showed that LUCAT1 silencing inhibited tumor metastasis *in vivo*.

Lung Cancer-Associated Transcript 1 Bound Directly to miR-4316 and Negatively Regulated the Expression of miR-4316

To explore whether LUCAT1 promotes LUAD metastasis *via* the competing endogenous RNAs (ceRNAs) mechanism. RNA fluorescence *in situ* hybridization (FISH) assay was performed using an LUCAT1 special probe, and the results revealed that LUCAT1 was mainly localized in the cytoplasm of NCI-H1299 and A549 cells (**Figure 5A**).

The putative candidate miRNAs binding to LUCAT1 were predicted using the bioinformatics tool miRDB (http://mirdb.org/), and miR-4316 was predicted to interact with LUCAT1. Then, we constructed a reporter vector in which the putative miR-4316-3p-binding site in the LUCAT1 sequence was mutated by base mutations, followed by co-transfection with control miRNA and miR-4316 mimics into HEK293T cells (**Figure 5B**). As expected, dual-luciferase reporter assay revealed that miR-4316 mimic reduced luciferase activities with the LUCAT1-WT expression vector, but not the LUCAT1-MUT, which suggested that miR-4316 could directly bind to LUCAT1 (**Figure 5C**). Besides, the regulation of miR-4316 by LUCAT1 in NCI-

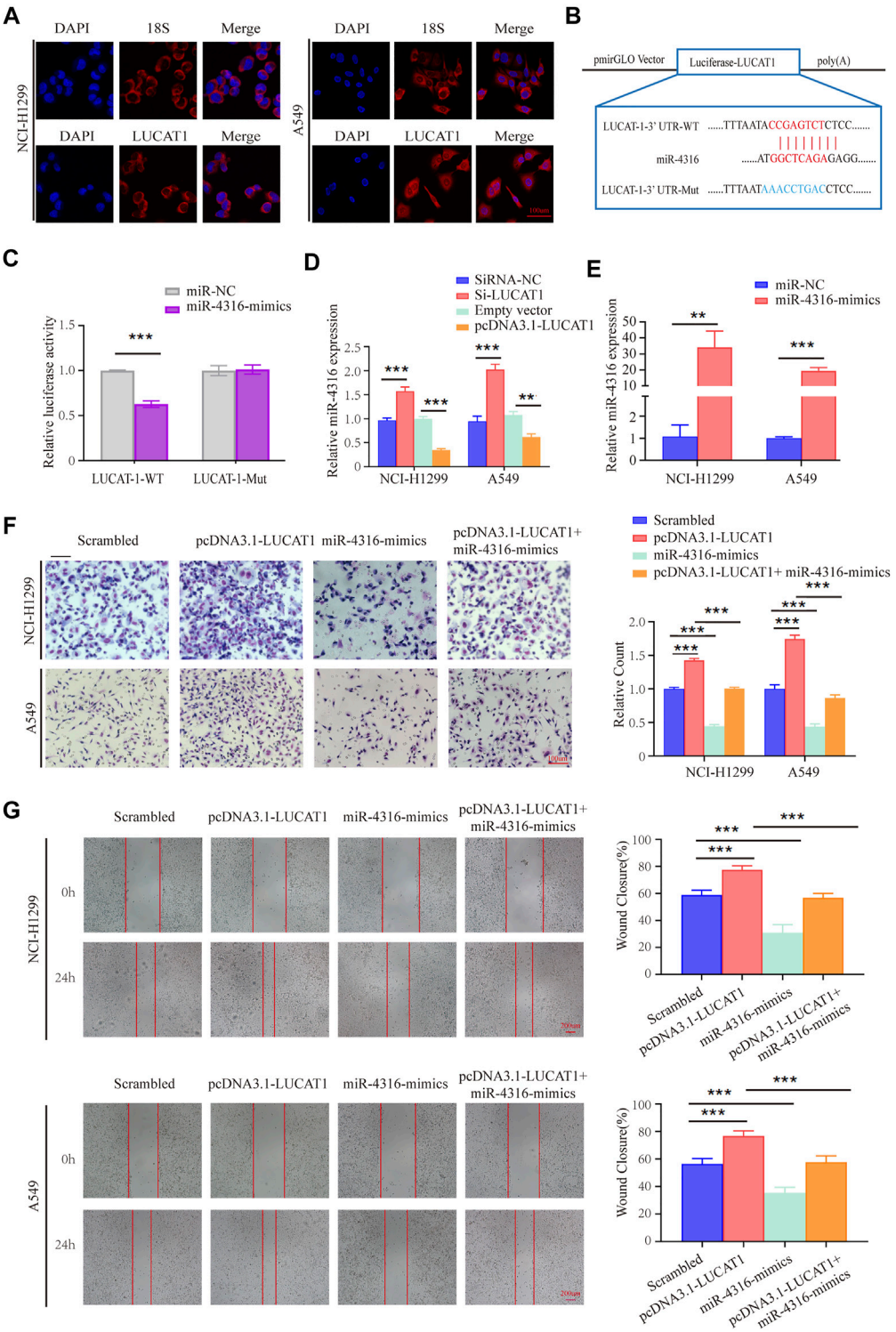

FIGURE 5 | LUCAT1 binds directly to miR-4316 and negatively regulates the expression of miR-4316. **(A)** Subcellular localization of LUCAT1 by RNA FISH. Red fluorescent probe: LUCAT1 and 18s (Cy3 labelled probes); blue fluorescent probe: DAPI. 18s served as a positive control. Scale bar: 100 μm. **(B)** Schematic diagram of the potential binding sites between LUCAT1 and miR-4316. **(C)** The luciferase activity was tested after co-transfection with wild type (WT)/mutant 3′UTR of LUCAT1 and miR-4316 mimics for 48 h. **(D)** Relative expression of miR-4316 in LUAD cells transfected with si-LUCAT, pcDNA3.1- LUCAT1 or control. **(E)** qRT-PCR was performed to detect the expression of miR-4316 in LUAD cells after transfection of miR-4316 mimics, or control. **(F,G)** Migration and invasion ability of LUAD cells co-transfected with negative control mimics, miR-4316 mimics, or/and overexpression plasmid (pcDNA3.1- LUCAT1) were determined by transwell and wound healing assays. *p*-values were calculated using two-tailed student's t-test (*$p < 0.05$; **$p < 0.01$; ***$p < 0.001$).

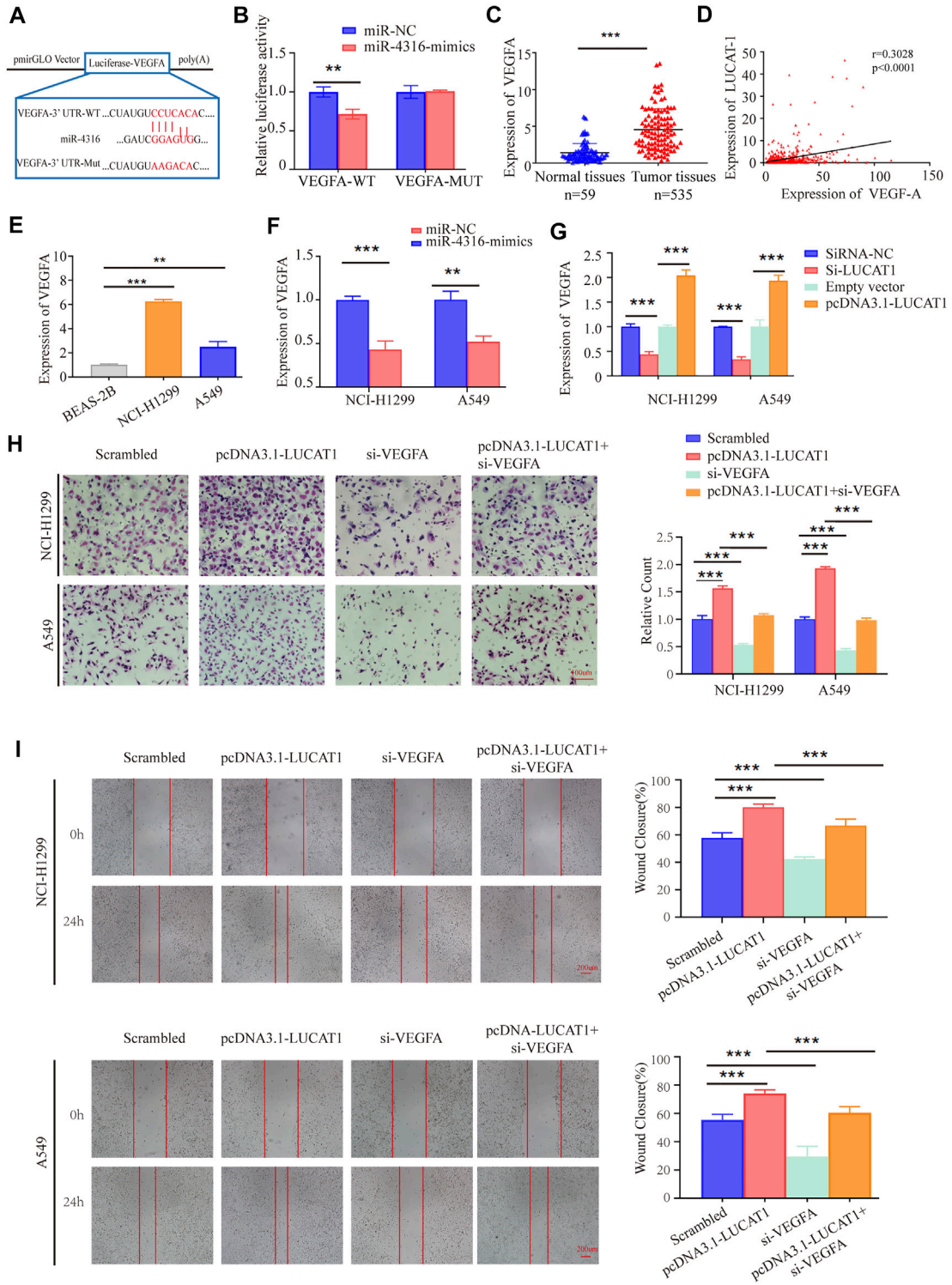

FIGURE 6 | LUCAT1 promotes migration and invasion of LUAD cells *via* LUCAT1/miR-4316/VEGFA axis. **(A)** Schematic representation of WT- and Mut-VEGFA sequences. Red fonts represented the mutant bases. **(B)** The luciferase reporter plasmid containing WT- and Mut-VEGFA was co-transfected into HEK293T cells with miR-4316 or corresponding control. **(C)** VEGFA expression level in LUAD tissues (n = 535) and normal tissues (n = 59) analysed using the TCGA database. **(D)** Relationship between LUCAT1 and VEGFA was measured using the TCGA database. **(E)** VEGFA expression was measured in normal lung epithelial cell line (BEAS-2B) and established LUAD cell lines (NCI-H1299 and A549) using qRT-PCR. **(F)** qRT-PCR was performed to detect the expression of VEGFA in LUAD cells after transfection of miR-4316 mimics, or control. **(G)** Relative expression of VEGFA in LUAD cells transfected with si-LUCAT, pcDNA3.1- LUCAT1 or control. **(H,I)** Migration and invasion ability of LUAD cells after co-transfection with negative control siRNA, si-VEGFA, or/and overexpression plasmid (pcDNA3.1- LUCAT1) were determined by transwell and wound healing assays. p-values were determined by two-tailed student's t-test or one-way ANOVA (*p < 0.05; **p < 0.01; ***p < 0.001).

H1299 and A549 cells were analyzed, and the results showed that knockdown of LUCAT1 significantly promoted the expression of miR-4316. In contrast, the levels of miR-4316 were significantly reduced by LUCAT1 overexpression (**Figure 5D**). These findings indicated that LUCAT1 targeted directly miR-4316 and negatively regulated its expression.

In vitro rescue assays were performed to identify the biological function of LUCAT1/miR-4316 regulatory axis. NCI-H1299 and A549 cells were co-transfected with pcDNA3.1-LUCAT1 and miR-4316 mimics, the transfection efficiency of miR-4316 mimics were determined by qRT-PCR analysis (**Figure 5E**). The results of the transwell invasion assays showed that overexpression of miR-4316 significantly inhibited cell invasion, and rescued the increased cell invasive capability caused by LUCAT1 overexpression in NCI-H1299 and A549 cells (**Figure 5F**). Meanwhile, wound healing assays showed the consistent results (**Figure 5G**), indicating that LUCAT1 attenuating LUAD cells invasion and migration by serving as miR-4316 sponge.

VEGFA Was a Direct Target of miR-4316 and Regulated by Lung Cancer-Associated Transcript 1

MiRNAs have been reported to exert their multiple biological functions mainly through degrading their downstream mRNA. By searching with the online prediction software Target Scan (http://www.targetscan.org/vert_72/), we identified that VEGFA was a potential target of miR-4316. Also, dual-luciferase reporter assay was performed by generating wild-type or WT sequence of VEGFA (**Figure 6A**). The results showed a significant reduction in luciferase activities after co-transfection of miR-4316 mimic and VEGFA-WT, which provided evidence that miR-4316 could directly bind to VEGFA (**Figure 6B**).

VEGFA has been proved to promote the metastasis of various types of solid cancers, including LUAD. We then analyzed the TCGA data, and found that VEGFA was upregulated in LUAD tissues compared with normal tissues (**Figure 6C**). Besides, the expression level of LUCAT1 was positively correlated with the expression level of VEGFA in 535 LUAD samples and 59 normal tissues (**Figure 6D**). Similarly, a higher expression of VEGFA was also observed in our LUAD cell lines (NCI-H1299 and A549) compared with the immortalized lung epithelial cell line BEAS-2B (**Figure 6E**).

To determine whether VEGFA was regulated by miR-4316 in LUAD cells, mRNA of VEGFA were measured when miR-4316 was overexpressed in NCI-H1299 and A549 cells. The results indicated that VEGFA were significantly decreased by miR-4316 mimics (**Figure 6F**). Then, expression levels of VEGFA were also measured when LUCAT1 was overexpressed or knocked down to identify the ceRNA network between LUCAT1 and VEGFA. Results showed that transfection of si-LUCAT1 into NCI-H1299 and A549 cells decreased the mRNA levels of VEGFA *via* releasing miR-4316, and the opposite results were observed when LUCAT1 was upregulated (**Figure 6G**).

Lung Cancer-Associated Transcript 1/ miR-4316/VEGF-A Axis Was Involved in Lung Adenocarcinoma Progression

To identify the effect of LUCAT1/miR-4316/VEGF-A axis on the biological function in LUAD cells, rescue assays were performed. We examined cells co-transfected with pcDNA3.1- LUCAT1 and si-VEGFA, and found that the enhanced invasion capabilities induced by LUCAT1 overexpression were partially reversed by co-transfection with si-VEGFA in NCI-H1299 and A549 cells (**Figure 6H**). Wound healing assays showed that si-VEGFA also partially reversed the enhanced migration capability induced by LUCAT1 overexpression (**Figure 6I**). These results suggested that LUCAT1 upregulated VEGFA expression by acting as miR-4316 sponge, thereby attenuating invasion and migration of LUAD cells.

Lung Cancer-Associated Transcript 1 Regulated Lung Adenocarcinoma Cell Glycolysis *via* miR-4316/VEGF-A Axis

Cancer cells frequently alter their metabolic pathways to adapt to environmental challenges or facilitate tumor proliferation, metastasis (Feng et al., 2020; Yang et al., 2020). Recently, growing evidence have provided for cancer cells' dependent on glycolysis for energy production (Vander Heiden et al., 2009). It was reported that LUCAT1 was upregulated under high-glucose conditions, and knockdown of LUCAT1 inhibited the EMT in HG-treated HK-2 cells (Zhang et al., 2020), however, whether LUCAT1 participate in glycolysis of LUAD cells needs to be confirmed.

We first set out to evaluate the potential influence of high glucose on invasion and migration in LUAD cells. Capabilities of cell's invasion and migration were determined under normal culture conditions or with high concentration of glucose (Normal glucose: 5.5 mM glucose, High glucose: 33 mM glucose). Our data clearly showed that high glucose culture significantly promoted invasion and migration of A549 cells, in comparison with the normal culture medium (**Figures 7A,B**). However, when treating with 2-deoxyglucose (2-DG, 0.5 mM), an inhibitor of glucose metabolism and inhibits glycolysis by acting on hexokinase, we found that the high glucose-induced invasion and migration could be effectively reversed (**Figures 7A,B**).

We also detected metabolic activities and found that silencing LUCAT1 expression in LUAD cells significantly suppressed the expression of metabolic enzymes and transporters, including LDH, GLUT1, GLUT3 (**Figure 7C**). Conversely, LUCAT1 overexpression promoted their expressions in A549 cells (**Figure 7D**). To further determine whether LUCAT1 was associated with the glucose metabolic changes in A549 cells, glucose consumption and metabolites were analyzed. As shown in **Figures 7E,F**, knockdown of LUCAT1 led to a significant decrease in glucose consumptions and lactate productions in A549 cells. In contrast, overexpression of LUCAT1 produced the opposite effects on them in A549 cells. In addition, LUCAT1 overexpression could promote the glucose consumption and lactate productions of A549 cells, while

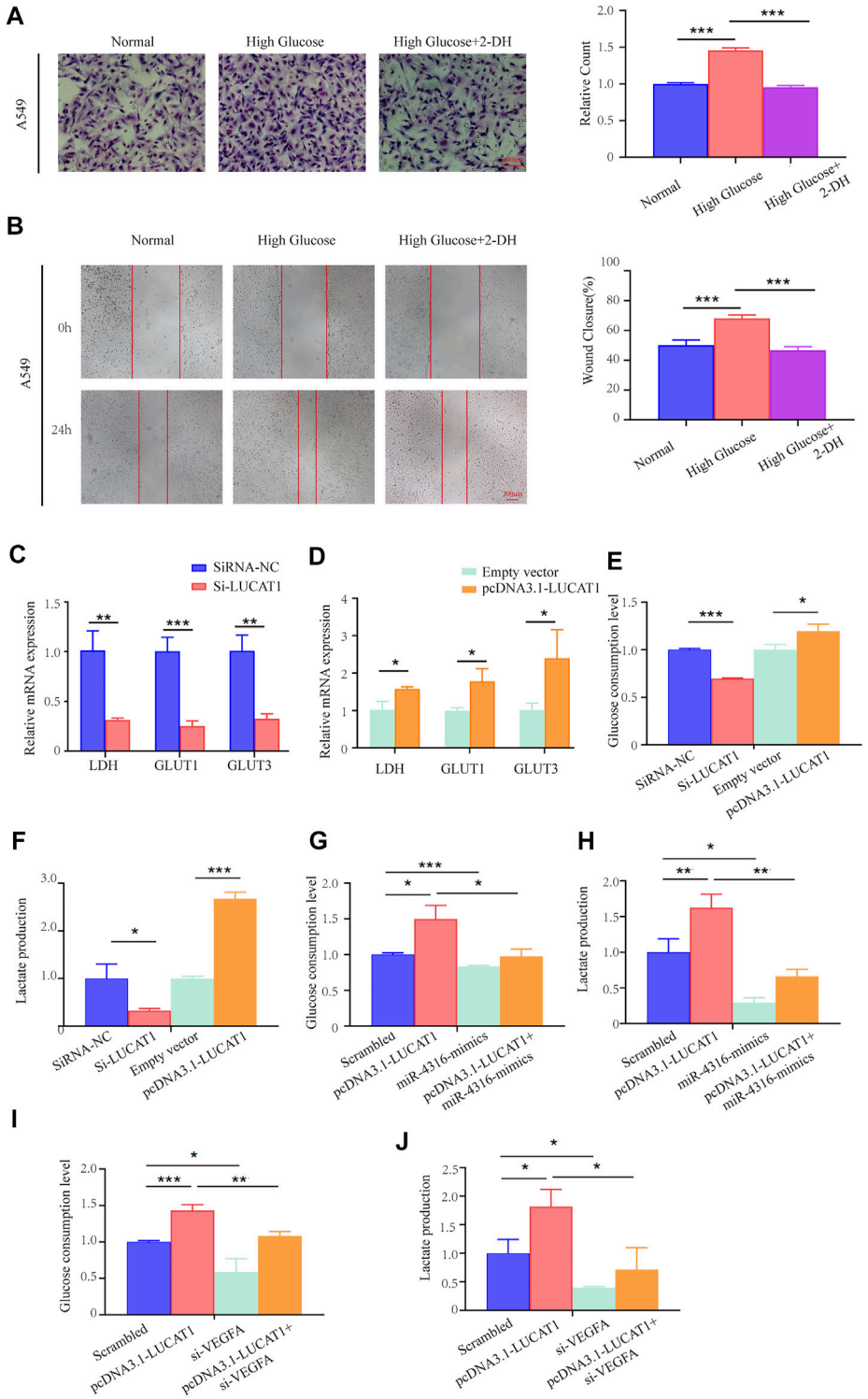

FIGURE 7 | LUCAT1 promotes glycolysis in LUAD cells through the LUCAT1/miR-4316/VEGFA axis. **(A,B)** Migration and invasion ability of LUAD cells were analyzed under normal culture conditions with high concentration of glucose; glycolysis inhibitor 2-DG abolished the ability of the migration and invasion ability of LUAD cells. **(C,D)** qRT-PCR was performed to detect the expression of Glycolysis-related enzyme markers in A549 cells after transfected with si-LUCAT1, pcDNA3.1-LUCAT1 or corresponding negative control. **(E,F)** Lactate production and glucose consumption level were measured after transfected with si-LUCAT1, pcDNA3.1-LUCAT1 or corresponding negative control. **(G,H)** Lactate production and glucose consumption level were measured after co-transfection with negative control mimics, miR-4316 mimics, or/and overexpression plasmid (pcDNA3.1- LUCAT1), using reagent kit according to the instruction of the manufacturers, respectively. **(I,J)** Lactate production and glucose consumption level were measured after co-transfection with negative control siRNA, si-LUCAT1, or/and overexpression plasmid (pcDNA3.1-LUCAT1), using reagent kit according to the instruction of the manufacturers, respectively. *p*-values were calculated by two-tailed student's t-test or one-way ANOVA (*$p < 0.05$; **$p < 0.01$; ***$p < 0.001$).

treatment with miR-4316 mimics partially reversed the phenotypes caused by LUCAT1 overexpression (**Figures 7G,I**). It was consistent with our suspect that knockdown of VEGFA partially reversed the increased glucose consumption and lactate productions induced by LUCAT1 overexpression in A549 cells (**Figures 7H,J**). These results suggested that LUCAT1 promoted glycolysis of LUAD cells *via* the upregulation of VEGFA by acting as miR-4316 sponge.

DISCUSSION

Multiple factors were involved in tumorigenesis, and extensive efforts have been devoted to investigating the molecular and cellular mechanisms of LUAD progression, but potential molecular targets for effective antimetastatic therapies remain to be elucidated. Accumulating evidence suggested that lncRNAs were recognized as important regulators of gene expression involved in malignant processes, or directly participated in cancer initiation and progression. LUCAT1 was first known to render lung cancer and associated with poor survival outcomes of patients with smoking-related non-small cell lung cancer (Sun et al., 2017). Further evidence confirmed that LUCAT1 participated in the regulation of multiple processes of tumor occurrence and development (Shen et al., 2020; Wu et al., 2020; Xing et al., 2021), while the detailed role of LUCAT1 in LUAD metastasis and glycolysis was not well known. Our study clarified the specific mechanism of the promotion of LUAD metastasis and glycolysis by lncRNA LUCAT1 through positively regulating VEGFA and sponging miR-4316, which help provide a better understanding of lncRNA-regulated glycolysis, metastasis and LUAD progression.

With the characteristics of noninvasiveness and stable in various body fluids, such as plasma and serum, lncRNA could be utilized as a promising and sensitive biomarker for cancer diagnosis and prognosis (Huarte, 2015; Huang et al., 2020). Evidence has revealed that exosomes provided a relatively stable environment for its contents, and exosomal lncRNAs had advantages of becoming non-invasive biomarkers to distinguish tumor patients and healthy individuals (Mohankumar and Patel, 2016; Liu et al., 2021). In our study, we demonstrated that serum exosomal LUCAT1 was highly expressed in LUAD patients compared with healthy controls based on our high-throughput sequencing and series of validation. ROC analysis further confirmed that serum exosomal LUCAT1 had prominent value in LUCAT1 diagnosis as a blood-based biomarker.

To address the significance of LUCAT1 in pathogenesis of LUAD, we demonstrated that the levels of LUCAT1 were significantly elevated in the tissues of LUAD patients in contrast to adjacent normal tissues. High expression of LUCAT1 was positively correlated with TNM stage, lymph node metastasis and unfavorable prognosis in patients with LUAD. Since whether LUCAT1 was associated with the metastasis and glycolysis of LUAD cells remains unknown, we mainly explored the functions of LUCAT1 in these two aspects in the following research. In our study, LUCAT1 knockdown can hinder the invasion and migration activity of LUAD cells *in vitro* and inhibit tumor metastasis *in vivo*. All these findings elucidated the oncogenic function of LUCAT1 in LUAD.

Previous studies indicated that lncRNAs located in cytoplasm could function as ceRNA *via* competitively binding to miRNAs, thereby positively regulating the downstream target mRNAs (Hirata et al., 2015; Zhu et al., 2020). You and colleagues reported that oncogenic Linc00284 markedly attenuated the expression level of c-Met by binding miR-27a, thereby promoting colorectal cancer cell proliferation and invasion (You et al., 2021). Zheng et al. found that LncRNA FAM225A affected the expression of ITGB3 by disrupting the binding sites for miR-590-3p/miR-1275, thereby contributing to the tumorigenesis and progression of *nocardia* gastric cancer (Zheng Z.-Q. et al., 2019). After having validated the subcellular location of LUCAT1, we verified miR-4316 as potential target of LUCAT1. Meanwhile, luciferase reporter also verified the endogenous interaction between LUCAT1 and miR-4316. Previous studies have shown that miR-4316 might serve as a tumor suppressor and was downregulated in a variety of cancers, including gastric cancer, hepatocellular carcinoma, and bladder cancer (Wang et al., 2018; Changyong et al., 2019). However, the role of miR-4316 in LUAD still unclear. Here, a negative correlation between the expression of LUCAT1 and miR-4316 was observed in LUAD cells. LUCAT1 acting as a miR-4316 sponge to promote LUAD cells proliferation and invasion. The classic mechanism for miRNA was modulate target genes by binding on its complementary binding sites of mRNA 3′-UTR, inhibiting target mRNA translating or promoting mRNA degradation. In this study, we confirmed that VEGFA may serve as a functional target of miR-4316, which has been proved to have inhibitory effects on proliferation and migration (Mousa et al., 2020). Therefore, we suspected that VEGFA is one of the miR-4316 target genes in LUAD cells.

It is shown that VEGFA, as an oncogene, was upregulated in a variety of cancers, including LUAD, and promotes the initiation, development, and poor prognosis of cancer (Liu et al., 2017; Liang et al., 2019; Zhao et al., 2019; Zou et al., 2020). Consistent with these findings, our study demonstrated that VEGFA was increased in LUAD tissues and cell lines, and the interaction between miR-4316 and the 3′UTR of VEGFA mRNA was then validated. Meanwhile, Pearson analysis showed that there was a negative correlation between the expression of miR-4316 and LUCAT1 in LUAD tissue samples. In addition, VEGFA was suppressed by miR-4316 and increased upon LUCAT1 overexpression. Importantly, the co-transfection experiments proved that changes in the levels of LUCAT1, miR-4316 and VEGFA are related to the migration and invasion of LUAD cells, implying that LUCAT1/miR-4316/VEGFA axis participated in LUAD progression. Based on these findings, we concluded that a comprehensive analysis of expression levels of LUCAT1, miR-4316 and VEGFA may help us identify patients at high risk of poor prognosis, and providing useful information of clinical management for them. However, given the complexity of tumor microenvironment, there exist other mechanisms involved in progress of LUAD, which required further investigation.

Even though growing evidence have shown that glycolysis plays an important role in the growth and metastasis of multiple solid cancers (Hu et al., 2019; Yang et al., 2020), the complex regulatory mechanisms of LUAD glycolysis remain elusive. This study proved that high glucose conditions could enhance the ability of migration and invasion in LUAC cells. Lin and colleagues found that LUCAT1 was upregulated under high-glucose conditions, and knockdown of LUCAT1 inhibited the EMT in HG-treated HK-2 cells (Zhang et al., 2020). Therefore, we assumed that LUCAT1 might regulate migration and invasion of LUAD cells by participating in the process of glucose metabolism. Interestingly, we provided evidence that overexpression of LUCAT promoted the glucose consumption and lactate production, and rescue experiments indicated that the enhanced glucose consumption and lactate productions could be reversed by miR-4316 mimics or si-VEGFA. Taken together, our results suggested that LUCAT1 may promote glycolysis of LUAD cells by acting as a ceRNA to sponge miR-4316 and upregulate VEGFA.

Although we have demonstrated that VEGFA silencing could attenuate migration, invasion, glucose consumption and lactate production of cancer cells, a study limitation should be taken into consideration. Since the role of VEGFA in lung cancer was complicated, more independent experimental evidence was needed to support the hypothesizes about how VEGFA regulates metastasis and glucose metabolism. Therefore, more comprehensive studies about the molecular mechanism of VEGFA activating downstream pathway by direct or indirect ways will remain to be conducted in the future.

In summary, our study demonstrated that LUCAT1 was dysregulated in human LUAD serum exosomes and may serve as a potential biomarker in the diagnosis of LUAD. We also identified a novel regulatory mechanism that LUCAT1 could directly interact with miR-4316 in LUAD cells, resulting in increasing VEGFA to promote LUAD cells metastasis and glucose metabolism. These observations complemented the known mechanisms of LUCAT1 in LUAD and indicated a potential target for development of effective therapeutic strategies in LUAD patients.

MATERIALS AND METHODS

Patients and Specimens

A total of 160 LUAD serum samples and 134 healthy serum samples were collected from The Second Hospital of Shandong University between February 2018 and October 2020. All enrolled patients met the following inclusion criteria: primary LUAD was confirmed by histopathology and showed no evidence of other neoplastic diseases in other organs, serum samples were collected before any antitumor therapies, such as surgery, chemotherapy or radiotherapy. The serum samples of controls were prepared from age-matched healthy volunteers. Clinical features of LUAD patients and healthy controls were described in **Supplementary Table S1**. The tumor stage and grade complied with the 8th Union of International Control of Cancer (UICC) classification.

Fifty LUAD serum samples were randomly selected, mix them thoroughly and divide them into five parts, each of which was regarded as an independent sequencing sample, serum samples of healthy people were also processed in the same way. The remaining samples (including 110 LUAD patients and 84 healthy controls) were selected to verify the expression of LUCAT1 in serum exosomes.

All experiments involved in this study were performed in accordance with relative regulations and manners. All participants have written informed consent and this study was approved by the Clinical Research Ethics Committee of The Second Hospital, Cheeloo College of Medicine, Shandong University [Approval number: KYLL-2019(LW)042].

Exosome Purification and Identification

Serum isolated from coagulation promoting vacuum tubes within 2 h was immediately transferred to a 1.5 ml Eppendorf tube and immediately centrifuged at 1500 g for 5 min and then 13800 g for 5 min at 4°C to eliminate cell sediments. ExoQuick™ solution (EXOQ5A-1; SBI System Biosciences, United States) was mixed evenly with supernatant according to the manufacturer's instructions. Subsequently, incubate at 4°C for 30 min, followed by centrifuged twice at 4°C (1500 g, 30 min and 1500 g, 5 min), supernatants were discarded, and the exosome pellets were resuspended in 250 μL PBS and stored at −80°C for further analysis.

The morphology of isolated exosomes was imaged using the transmission electron microscopy (TEM; G2 spititi FEI; Tecnai). And the size distribution and concentration of exosomes were quantified by ZETASIZER Nano series-Nano-ZS instrument (Malvern, United Kingdom). Total exosome protein was extracted with RIPA extraction reagent (Thermo Fisher, United States) according to manufacturer's instructions. Western blotting analysis (WB) were performed to detect the exosomal surface markers: CD9, CD63, and TSG101.

WB

Proteins from cell lysates were extracted with RIPA buffer (Sigma-Aldrich) according to manufacturer's instructions, separated by SDS-polyacrylamide gel electrophoresis (SDS-PAGE) and then transferred to Immobilon-P PVDF membrane (Millipore, United States). After being blocked with 5% non-fat milk in TBS-Tween, membranes were incubated with primary specific antibodies and horseradish peroxidase-conjugated secondary antibodies sequentially. Immunoreactive bands were detected using the Clarity Western ECL kit (Bio-Rad) and quantified using Image Lab (Bio-Rad, Hercules, CA, United States). All antibodies used in this study were shown in **Supplementary Table S2**.

High Throughput Sequencing

High throughput sequencing service was provided by CloudSeq Biotech (Shanghai, China) and original datasheets could be obtained through access to GEO repository (GSE191209). Briefly, rRNAs were removed from total RNA using Ribo-Zero rRNA Removal Kits (Illumina, United States) according to the manufacturer's instructions. Subsequently, rRNA-depleted RNAs were used to constructed RNA libraries with TruSeq Stranded Total RNA Library Prep Kit (Illumina, United States).

BioAnalyzer 2100 system (Agilent Technologies, United States) was performed to control the quality and quantified. Libraries mentioned above were denatured as single-stranded DNA molecules, after captured on Illumina flow cells, amplified as clusters, and finally sequenced on Illumina HiSeq Sequencer for 150 cycles. The differentially expressed RNAs were selected with $\log_2$ (fold change) > 1 or $\log_2$ (fold change) <−1 and with statistical significance (p value <0.05) by R package–Deseq2.

RNA Extraction and Quantitative Real-Time Polymerase Chain Reaction Analysis

Total exosomal RNA was extracted from miRNeasyMicro Kit (Qiagen) according to the manufacturer's instructions. Concentration and integrity of exosomal RNA were measured by NanoDrop spectrophotometer (Thermo Fisher Scientific). Purified RNA was reversely transcribed into cDNA using the PrimeScript™ RT reagent kit (Takara, Dalian, Liaoning, China) according to manufacturer's instructions.

The expression of lncRNA/mRNA was detected by CFX96™ Real-Time System (Bio-Rad Laboratories, Hercules, CA, United States) using Power SYBR Green (Takara, Dalian, China) and GAPDH was selected as the housekeeping gene. The expression of miRNA was measured using primer of miR-4316 and U6 was used as an internal control. All the primer sequences were available in **Supplementary Table S3**. The relative expressions of lncRNA/mRNA/miRNA were calculated using the $2^{-\Delta\Delta ct}$ method.

in situ Hybridization

The expression level of LUCAT1 in tissues was detected by ISH using a specific digoxigenin-labeled LUCAT1 probe on TMAs, which contained 98 LUAD samples and 82 paired adjacent normal samples. All detailed clinical information (including age, gender, tumor–node–metastasis stage) of these LUAD patients were obtained from Qutdo Biotech (Shanghai, China), and shown in **Supplementary Table S4**. Further, the quantitative scanning approach was taken to analyse the staining and expression of LUCAT1 using a Nikon microscope. The results of ISH were calculated by multiplying the value of positive staining intensity by the proportion of positively stained cells. In our study, ISH score of <1.0 was regarded as LUCAT1 low-expression group, while ≥1.0 indicated LUCAT1 high-expression. All these experiments were approved by the ethics committee of Shanghai Outdo Biotech Company.

Cell Lines

Immortalized lung epithelial cell line BEAS-2B and LUAD cell lines (A549, NCI-H1299) were obtained from the Chinese Academy of Sciences Cell Bank (Shanghai, China). Cell lines were cultured with 1640 (Gibco) supplemented with 10% fetal bovine serum (FBS, Australia Origin, Gibco). All cell lines were cultured in a humidified chamber with 5% CO_2 and 95% air at 37°C.

Cell Transfections

Si-LUCAT1, miR-4316 mimic, si-VEGFA, si-NC, and mimics-NC were obtained from GenePharma (Shanghai, China). LUCAT1 overexpression plasmids pcDNA3.1-LUCAT1, NC plasmids pcDNA3.1-NC were synthesized by Biosune (Shanghai, China). Lipofectamine™ 2000 was employed to accomplish the cell transfections, following guidelines from the manufacturer. **Supplementary Table S5** depicts the sequences of si-RNA and mimics utilized in this study.

Generation of Stable Cell Lines

To establish stable LUCATI knockdown cells, a lentivirus vector encoding specific sh-LUCAT1 or sh-NC sequences was constructed by Vigenebio (Jinan, China), which could express the green fluorescent protein (GFP) and puromycin resistance gene. After incubated lentivirus vector with the LUAD cells for at least 48 h, fluorescence microscope and RT-qPCR were performed to verify the knockdown efficiency.

Transwell Assays and Wound Healing Test

Cell migration ability was measured by the transwell chambers (8 μm pore size; Costar), and the ability of cell invasion was evaluated by the transwell chambers with Matrigel (BD Biosciences, San Jose, CA, United States) in the upper chamber. After incubation at 37°C, 5% CO_2 for 24 h, the lower chambers were fixed in methanol, stained with 0.1% crystal violet, and imaged by Inversion Microscope (Zeiss, Germany). Cell numbers for cell invasion in three random fields were counted.

For wound healing assays, cells were seeded into 6-well plates, and a 200 μL pipette tip was used to create an artificial scratch when incubated to 100% confluence. Subsequently, the cells were cultured in serum-free medium, wound closure images were captured in the same field at 0 and 24 h. The fraction of cell coverage across the line were used to calculate the cell healing rates.

Animal Experiments

For the *in vivo* tumor metastasis experiments, BALB/c nude mice were divided into two groups (n = 5) to establish the lung metastasis model. 1×10^6 NCI-H1299 cells stably transfected with sh-LUCAT1 or shRNA-NC in 0.1 ml PBS were subcutaneously injected into the tail vein of the mice above. Six weeks after injection, the mice were euthanatized and dissected. Lungs of the mice in two groups were removed and photographed, metastatic nodules in lungs were counted by naked eye and investigators were blinded to the group allocation. The criteria used to identify metastatic nodules were as follows: whitish and uniformly colored, round, more than 1 mm in diameter, and the appearance quality was different from the surrounding normal tissue. After tissue were fixed in paraformaldehyde, embedded in paraffin, hematoxylin and eosin (HE) staining were performed to confirm the metastatic nodes. The animal studies were carried out in accordance with NIH Guidelines for the Care and Use of Laboratory Animals and approved by the Animal Care Committee of The Second Hospital, Cheeloo College of Medicine, Shandong University. The ethics approval number of Animal experiments was KYLL-2019(LW)043.

RNA Fluorescence *in situ* Hybridization

Cy3-labeled LUCAT1 and U6 sense probe were obtained from GenePharma (Shanghai, China). Fluorescence processed RNA FISH assay *in Situ* Hybridization Kit (GenePharma, Shanghai, China) were performed according to the manufacturer's instructions. Briefly, NCI-H1299 and A549 cells were washed,

fixed and treated by 0.1% Triton X-100. After incubated with labelled FISH probe pre-mixed solution overnight in the dark, 4,6-diamidino-2-phenylindole (DAPI) (Solarbio, Beijing, China) was used to stain the cell nucleus for 10 min. Finally, fluorescence images were produced by a confocal microscope (Carl Zeiss Microscopy, LLC, United States). All the probe sequences used in this study were available in **Supplementary Table S6**.

Luciferase Reporter Assay

For luciferase reporter assays, we constructed wild-type (WT) LUCAT1/VEGFA reporter plasmid in which the putative miR-4316-binding site in the LUCAT1sequence, and mutated-type (MUT) LUCAT1/VEGFA reporter plasmid in which the putative miR-4316-binding site in the LUCAT1sequence was mutated by base mutations with pmirGLO promoter vector. Luciferase reporter vectors were stably co-transfected with miRNA-4316 mimic or mimic-NC by Lipofectamine™ 2000 Transfection Reagent (Invitrogen, United States) according to the manufacturer's guidelines. Luciferase intensity was measured using a dual-luciferase reagent (Promega) according to the manufacturer's instructions. Renilla luciferase intensity was used as the control. Sequence of luciferase reporter associated with this article were listed in **Supplementary Table S7**.

Glucose Consumption and Lactate Production Assays

A549 cells were seeded into six-well plates at a density of 1×10^6 cells/well and cultured overnight. Glucose assay kits (Solarbio) and lactate assay kits (Solarbio) were used to detect the glucose consumption and lactate production in A549 cells, according to the manufacturer's instructions, respectively. All data were normalized by the cell numbers.

Glucose Conditions

A549 cells were cultured in RPMI-1640 medium (Gibco, Shanghai, China) supplemented with 10% fatal bovine serum (FBS) (Sagecreation, Beijing, China). After reaching 70–80% confluence, A549 cells were washed and then growth arrested in serum-free RPMI-1640 medium for 24 h to synchronize the cell growth. Then, d-glucose (Solarbio, Beijing, China) at a final concentration of 33mM, or 2-Deoxy-D-glucose (2-DG) (Solarbio) at a concentration of 0.5 mmol/L were added to the culture medium for an additional 48 h until further use.

Statistical Analysis

The experimental data were statistically analysed using Graph Pad Prism 6.0 and SPSS 13.0 software. The mean values of two groups were assessed by Student's t test or the Mann-Whitney U test as appropriate. Kaplan–Meier plots and log-rank tests were used for the survival analysis. The diagnostic performance of LUCAT1 was performed on MEDCALC 15.2.2 (Med-Calc, Belgium). Statistical significance was achieved when p values were less than 0.5. All results were expressed as the means ± standard deviation (SD) of three independent experiments.

DATA AVAILABILITY STATEMENT

The original contributions presented in the study are publicly available. This data can be found here: https://www.ncbi.nlm.nih.gov/, GSE191209.

ETHICS STATEMENT

The studies involving human participants were reviewed and approved by Clinical Research Ethics Committee of The Second Hospital, Cheeloo College of Medicine, Shandong University. The patients/participants provided their written informed consent to participate in this study. The animal study was reviewed and approved by Animal Care Committee of The Second Hospital of Shandong University.

AUTHOR CONTRIBUTIONS

LW, YX, and JW contributed substantially to the study design, data analysis, and interpretation, performed experiments, and drafted the manuscript. PL and CW revised the manuscript. LW, YX, YiZ, and SL prepared the figures and performed experiments. YaZ, YHZ, and JL provided clinical information and collected serum samples. PL and CW initiated, organized and supervised the study. All authors contributed to the article and approved the submitted version.

FUNDING

This work was supported by grants from the National Natural Science Foundation of China (81972007, 82002228, 82130067, 82122041), the Key Research and Development Program of Shandong Province (2019GHZ003, 2020CXGC011304, and 2019GSF108091), Shandong Provincial Natural Science Foundation (ZR2020QH280), Taishan Scholars Climbing Program of Shandong Province (NO.tspd20210323), Young Taishan Scholars Program of Shandong Province (NO.tsqn201909176), Qilu Young Scholars Program of Shandong University, Shandong Collaborative Innovation Center for R&D and Transformation of New Tumor Biomarkers Foundation (CXZX2019006), and Innovation Team Foundation of Jinan City (2019GXRC004, 2021GXRC020).

ACKNOWLEDGMENTS

Our work benefited from the database of TCGA. We are grateful to all the staff for their efforts to expand and improve the databases.

SUPPLEMENTARY MATERIAL

The Supplementary Material for this article can be found online at: https://www.frontiersin.org/articles/10.3389/fcell.2022.833579/full#supplementary-material

REFERENCES

Changyong, E., Yang, J., Li, H., and Li, C. (2019). LncRNA LOC105372579 Promotes Proliferation and Epithelial-Mesenchymal Transition in Hepatocellular Carcinoma via Activating miR-4316/FOXP4 Signaling. *Cancer Manag. Res.* 11, 2871–2879. doi:10.2147/CMAR.S197979

Claesson-Welsh, L., and Welsh, M. (2013). VEGFA and Tumour Angiogenesis. *J. Intern Med.* 273 (2), 114–127. doi:10.1111/joim.12019

Denisenko, T. V., Budkevich, I. N., and Zhivotovsky, B. (2018). Cell Death-Based Treatment of Lung Adenocarcinoma. *Cell Death Dis.* 9 (2), 117. doi:10.1038/s41419-017-0063-y

Elf, S. E., and Chen, J. (2014). Targeting Glucose Metabolism in Patients with Cancer. *Cancer* 120 (6), 774–780. doi:10.1002/cncr.28501

Feng, J., Li, J., Wu, L., Yu, Q., Ji, J., Wu, J., et al. (2020). Emerging Roles and the Regulation of Aerobic Glycolysis in Hepatocellular Carcinoma. *J. Exp. Clin. Cancer Res.* 39 (1), 126. doi:10.1186/s13046-020-01629-4

Helmlinger, G., Sckell, A., Dellian, M., Forbes, N. S., and Jain, R. K. (2002). Acid Production in Glycolysis-Impaired Tumors Provides New Insights into Tumor Metabolism. *Clin. Cancer Res.* 8 (4), 1284–1291.

Hirata, H., Hinoda, Y., Shahryari, V., Deng, G., Nakajima, K., Tabatabai, Z. L., et al. (2015). Long Noncoding RNA MALAT1 Promotes Aggressive Renal Cell Carcinoma through Ezh2 and Interacts with miR-205. *Cancer Res.* 75 (7), 1322–1331. doi:10.1158/0008-5472.CAN-14-2931

Hirsch, F. R., Scagliotti, G. V., Mulshine, J. L., Kwon, R., Curran, W. J., Jr., Wu, Y.-L., et al. (2017). Lung Cancer: Current Therapies and New Targeted Treatments. *Lancet* 389 (10066), 299–311. doi:10.1016/S0140-6736(16)30958-8

Hu, Q., Qin, Y., Ji, S., Xu, W., Liu, W., Sun, Q., et al. (2019). UHRF1 Promotes Aerobic Glycolysis and Proliferation via Suppression of SIRT4 in Pancreatic Cancer. *Cancer Lett.* 452, 226–236. doi:10.1016/j.canlet.2019.03.024

Huang, Z., Zhou, J.-K., Peng, Y., He, W., and Huang, C. (2020). The Role of Long Noncoding RNAs in Hepatocellular Carcinoma. *Mol. Cancer* 19 (1), 77. doi:10.1186/s12943-020-01188-4

Huarte, M. (2015). The Emerging Role of lncRNAs in Cancer. *Nat. Med.* 21 (11), 1253–1261. doi:10.1038/nm.3981

Jia, Y., Duan, Y., Liu, T., Wang, X., Lv, W., Wang, M., et al. (2019). LncRNA TTN-AS1 Promotes Migration, Invasion, and Epithelial Mesenchymal Transition of Lung Adenocarcinoma via Sponging miR-142-5p to Regulate CDK5. *Cell Death Dis.* 10 (8), 573. doi:10.1038/s41419-019-1811-y

Krawczyk, P., Powrózek, T., Olesiński, T., Dmitruk, A., Dziwota, J., Kowalski, D., et al. (2017). Evaluation of miR-506 and miR-4316 Expression in Early and Non-invasive Diagnosis of Colorectal Cancer. *Int. J. Colorectal Dis.* 32 (7), 1057–1060. doi:10.1007/s00384-017-2814-8

Kretz, M., Siprashvili, Z., Chu, C., Webster, D. E., Zehnder, A., Qu, K., et al. (2013). Control of Somatic Tissue Differentiation by the Long Non-coding RNA TINCR. *Nature* 493 (7431), 231–235. doi:10.1038/nature11661

Li, Y., Shi, X., Yang, W., Lu, Z., Wang, P., Chen, Z., et al. (2016). Transcriptome Profiling of lncRNA and Co-expression Networks in Esophageal Squamous Cell Carcinoma by RNA Sequencing. *Tumor Biol.* 37 (10), 13091–13100. doi:10.1007/s13277-016-5227-3

Liang, L., Hui, K., Hu, C., Wen, Y., Yang, S., Zhu, P., et al. (2019). Autophagy Inhibition Potentiates the Anti-angiogenic Property of Multikinase Inhibitor Anlotinib through JAK2/STAT3/VEGFA Signaling in Non-small Cell Lung Cancer Cells. *J. Exp. Clin. Cancer Res.* 38 (1), 71. doi:10.1186/s13046-019-1093-3

Liu, L., Bi, N., Wu, L., Ding, X., Men, Y., Zhou, W., et al. (2017). MicroRNA-29c Functions as a Tumor Suppressor by Targeting VEGFA in Lung Adenocarcinoma. *Mol. Cancer* 16 (1), 50. doi:10.1186/s12943-017-0620-0

Liu, C., Wang, L., Li, Y. W., Cui, Y. S., Wang, Y. Q., and Liu, S. (2020). Long Noncoding RNA LUCAT1 Promotes Migration and Invasion of Prostate Cancer Cells by Inhibiting KISS1 Expression. *Eur. Rev. Med. Pharmacol. Sci.* 24 (13), 7213. doi:10.26355/eurrev_202007_21864

Liu, J., Ren, L., Li, S., Li, W., Zheng, X., Yang, Y., et al. (2021). The Biology, Function, and Applications of Exosomes in Cancer. *Acta Pharm. Sin. B* 11 (9), 2783–2797. doi:10.1016/j.apsb.2021.01.001

Mercer, T. R., Dinger, M. E., and Mattick, J. S. (2009). Long Non-coding RNAs: Insights into Functions. *Nat. Rev. Genet.* 10 (3), 155–159. doi:10.1038/nrg2521

Mohankumar, S., and Patel, T. (2016). Extracellular Vesicle Long Noncoding RNA as Potential Biomarkers of Liver Cancer. *Briefings Funct. Genomics* 15 (3), 249–256. doi:10.1093/bfgp/elv058

Mousa, H., Yuan, M., Zhang, X., Li, X., Shopit, A., Almoiliqy, M., et al. (2020). MicroRNA-4316 Inhibits Gastric Cancer Proliferation and Migration via Directly Targeting VEGF-A. *Cancer Cell Int.* 20, 62. doi:10.1186/s12935-020-1132-3

Ponting, C. P., Oliver, P. L., and Reik, W. (2009). Evolution and Functions of Long Noncoding RNAs. *Cell* 136 (4), 629–641. doi:10.1016/j.cell.2009.02.006

Salmena, L., Poliseno, L., Tay, Y., Kats, L., and Pandolfi, P. P. (2011). A ceRNA Hypothesis: the Rosetta Stone of a Hidden RNA Language? *Cell* 146 (3), 353–358. doi:10.1016/j.cell.2011.07.014

Shen, Q., Xu, Z., and Xu, S. (2020). Long Non-coding RNA LUCAT1 Contributes to Cisplatin Resistance by Regulating the miR-514a-3p/ULK1 axis in Human Non-small Cell Lung Cancer. *Int. J. Oncol.* 57 (4), 967–979. doi:10.3892/ijo.2020.5106

Sun, Y., Jin, S.-D., Zhu, Q., Han, L., Feng, J., Lu, X.-Y., et al. (2017). Long Non-coding RNA LUCAT1 is Associated with Poor Prognosis in Human Non-small Cell Lung Cancer and Regulates Cell Proliferation via Epigenetically Repressing P21 and P57 Expression. *Oncotarget* 8 (17), 28297–28311. doi:10.18632/oncotarget.16044

Tian, H., Lian, R., Li, Y., Liu, C., Liang, S., Li, W., et al. (2020). AKT-induced lncRNA VAL Promotes EMT-independent Metastasis through Diminishing Trim16-dependent Vimentin Degradation. *Nat. Commun.* 11 (1), 5127. doi:10.1038/s41467-020-18929-0

Torre, L. A., Bray, F., Siegel, R. L., Ferlay, J., Lortet-Tieulent, J., and Jemal, A. (2015). Global Cancer Statistics, 2012. *CA Cancer J. Clin.* 65 (2), 87–108. doi:10.3322/caac.21262

Travis, W. D., Brambilla, E., Nicholson, A. G., Yatabe, Y., Austin, J. H. M., Beasley, M. B., et al. (2015). The 2015 World Health Organization Classification of Lung Tumors: Impact of Genetic, Clinical and Radiologic Advances since the 2004 Classification. *J. Thorac. Oncol.* 10 (9), 1243–1260. doi:10.1097/JTO.0000000000000630

Vander Heiden, M. G., Cantley, L. C., and Thompson, C. B. (2009). Understanding the Warburg Effect: the Metabolic Requirements of Cell Proliferation. *Science* 324 (5930), 1029–1033. doi:10.1126/science.1160809

Wang, F., Zu, Y., Huang, W., Chen, H., Xie, H., and Yang, Y. (2018). LncRNA CALML3-AS1 Promotes Tumorigenesis of Bladder Cancer via Regulating ZBTB2 by Suppression of microRNA-4316. *Biochem. Biophys. Res. Commun.* 504 (1), 171–176. doi:10.1016/j.bbrc.2018.08.150

Wang, M., Mao, C., Ouyang, L., Liu, Y., Lai, W., Liu, N., et al. (2019). Long Noncoding RNA LINC00336 Inhibits Ferroptosis in Lung Cancer by Functioning as a Competing Endogenous RNA. *Cell Death Differ.* 26 (11), 2329–2343. doi:10.1038/s41418-019-0304-y

Wang, C., Li, Y., Yan, S., Wang, H., Shao, X., Xiao, M., et al. (2020). Interactome Analysis Reveals that lncRNA HULC Promotes Aerobic Glycolysis through LDHA and PKM2. *Nat. Commun.* 11 (1), 3162. doi:10.1038/s41467-020-16966-3

Wu, R., Li, L., Bai, Y., Yu, B., Xie, C., Wu, H., et al. (2020). The Long Noncoding RNA LUCAT1 Promotes Colorectal Cancer Cell Proliferation by Antagonizing Nucleolin to Regulate MYC Expression. *Cell Death Dis.* 11 (10), 908. doi:10.1038/s41419-020-03095-4

Xing, C., Sun, S.-g., Yue, Z.-Q., and Bai, F. (2021). Role of lncRNA LUCAT1 in Cancer. *Biomed. Pharmacother.* 134, 111158. doi:10.1016/j.biopha.2020.111158

Yang, J., Ren, B., Yang, G., Wang, H., Chen, G., You, L., et al. (2020). The Enhancement of Glycolysis Regulates Pancreatic Cancer Metastasis. *Cell. Mol. Life Sci.* 77 (2), 305–321. doi:10.1007/s00018-019-03278-z

Yoon, J.-H., You, B.-H., Park, C. H., Kim, Y. J., Nam, J.-W., and Lee, S. K. (2018). The Long Noncoding RNA LUCAT1 Promotes Tumorigenesis by Controlling Ubiquitination and Stability of DNA Methyltransferase 1 in Esophageal Squamous Cell Carcinoma. *Cancer Lett.* 417, 47–57. doi:10.1016/j.canlet.2017.12.016

You, J., Li, J., Ke, C., Xiao, Y., Lu, C., Huang, F., et al. (2021). Oncogenic Long Intervening Noncoding RNA Linc00284 Promotes C-Met Expression by Sponging miR-27a in Colorectal Cancer. *Oncogene* 40 (24), 4151–4166. doi:10.1038/s41388-021-01839-w

Yu, H., Xu, Y., Zhang, D., and Liu, G. (2018). Long Noncoding RNA LUCAT1 Promotes Malignancy of Ovarian Cancer through Regulation of miR-612/

HOXA13 Pathway. *Biochem. Biophys. Res. Commun.* 503 (3), 2095–2100. doi:10.1016/j.bbrc.2018.07.165

Zhai, S., Xu, Z., Xie, J., Zhang, J., Wang, X., Peng, C., et al. (2021). Epigenetic Silencing of LncRNA LINC00261 Promotes C-Myc-Mediated Aerobic Glycolysis by Regulating miR-222-3p/HIPK2/ERK axis and Sequestering IGF2BP1. *Oncogene* 40 (2), 277–291. doi:10.1038/s41388-020-01525-3

Zhang, L., Liu, S.-K., Song, L., and Yao, H.-R. (2019a). SP1-induced Up-Regulation of lncRNA LUCAT1 Promotes Proliferation, Migration and Invasion of Cervical Cancer by Sponging miR-181a. *Artif. Cell Nanomedicine Biotechnol.* 47 (1), 555–563. doi:10.1080/21691401.2019.1575840

Zhang, S., Zhang, X., Sun, Q., Zhuang, C., Li, G., Sun, L., et al. (2019b). LncRNA NR2F2-AS1 Promotes Tumourigenesis through Modulating BMI1 Expression by Targeting miR-320b in Non-small Cell Lung Cancer. *J. Cell Mol. Med.* 23 (3), 2001–2011. doi:10.1111/jcmm.14102

Zhang, L.-C., Wei, Z.-B., and Tang, S.-F. (2020). Knockdown of the Long Noncoding RNA LUCAT1 Inhibits High-Glucose-Induced Epithelial-Mesenchymal Transition through the miR-199a-5p-ZEB1 Axis in Human Renal Tubular Epithelial Cells. *BioMed Res. Int.* 2020, 1–8. doi:10.1155/2020/8895003

Zhao, W., Cao, L., Ying, H., Zhang, W., Li, D., Zhu, X., et al. (2019). Endothelial CDS2 Deficiency Causes VEGFA-Mediated Vascular Regression and Tumor Inhibition. *Cell Res.* 29 (11), 895–910. doi:10.1038/s41422-019-0229-5

Zheng, A., Song, X., Zhang, L., Zhao, L., Mao, X., Wei, M., et al. (2019a). Long Non-coding RNA LUCAT1/miR-5582-3p/TCF7L2 axis Regulates Breast Cancer Stemness via Wnt/β-Catenin Pathway. *J. Exp. Clin. Cancer Res.* 38 (1), 305. doi:10.1186/s13046-019-1315-8

Zheng, Z.-Q., Li, Z.-X., Zhou, G.-Q., Lin, L., Zhang, L.-L., Lv, J.-W., et al. (2019b). Long Noncoding RNA FAM225A Promotes Nasopharyngeal Carcinoma Tumorigenesis and Metastasis by Acting as ceRNA to Sponge miR-590-3p/miR-1275 and Upregulate ITGB3. *Cancer Res.* 79 (18), 4612–4626. doi:10.1158/0008-5472.CAN-19-0799

Zhu, Y., Gu, L., Lin, X., Cui, K., Liu, C., Lu, B., et al. (2020). LINC00265 Promotes Colorectal Tumorigenesis via ZMIZ2 and USP7-Mediated Stabilization of β-catenin. *Cell Death Differ.* 27 (4), 1316–1327. doi:10.1038/s41418-019-0417-3

Zou, G., Zhang, X., Wang, L., Li, X., Xie, T., Zhao, J., et al. (2020). Herb-sourced Emodin Inhibits Angiogenesis of Breast Cancer by Targeting VEGFA Transcription. *Theranostics* 10 (15), 6839–6853. doi:10.7150/thno.43622

Conflict of Interest: The authors declare that the research was conducted in the absence of any commercial or financial relationships that could be construed as a potential conflict of interest.

Publisher's Note: All claims expressed in this article are solely those of the authors and do not necessarily represent those of their affiliated organizations, or those of the publisher, the editors and the reviewers. Any product that may be evaluated in this article, or claim that may be made by its manufacturer, is not guaranteed or endorsed by the publisher.

frontiers | Frontiers in Cell and Developmental Biology

ORIGINAL RESEARCH
published: 27 May 2022
doi: 10.3389/fcell.2022.893888

HIF-1/2α-Activated RNF146 Enhances the Proliferation and Glycolysis of Hepatocellular Carcinoma Cells via the PTEN/AKT/mTOR Pathway

Guoliang Shen[1,2†], Hao Wang[3†], Ning Zhu[4], Qiliang Lu[4], Junwei Liu[2], Qiuran Xu[4] and Dongsheng Huang[4*]*

[1]Department of Clinical Medicine, Medical College of Soochow University, Suzhou, China, [2]Department of General Surgery, Zhejiang Provincial People's Hospital, Affiliated People's Hospital, Hangzhou Medical College, Hangzhou, China, [3]Department of Hepatobiliary Surgery, The First Affiliated Hospital of Xi'an Jiaotong University, Xi'an, China, [4]The Key Laboratory of Tumor Molecular Diagnosis and Individualized Medicine of Zhejiang Province, Zhejiang Provincial People's Hospital, Affiliated People's Hospital, Hangzhou Medical College, Hangzhou, China

Hypoxia microenvironment, a critical feature of hepatocellular carcinoma, contributes to hepatocarcinogenesis, tumor progression and therapeutic resistance. Hypoxia-inducible factors (HIFs)-activated target genes are the main effectors in hypoxia-induced HCC progression. In this study, we identified ubiquitin E3 ligase ring finger protein 146 (RNF146) as a novel HIFs target gene. Either HIF-1α or HIF-2α knockdown significantly repressed hypoxia-induced RNF146 upregulation in Hep3B and Huh7 cells. TCGA data and our immunohistochemistry analysis consistently revealed the overexpression of RNF146 in HCC tissues. The upregulated expression of RNF146 was also detected in HCC cell lines. The high RNF146 level was correlated with poor clinical features and predicted a shorter overall survival of patients with HCC. RNF146 knockdown suppressed the proliferation, colony formation and glycolysis of HCC cells, but suppressed but RNF146 overexpression promoted these malignant behaviors. Moreover, RNF146 silencing weakened HCC growth in mice. RNF146 inversely regulated phosphatase and tensin homolog (PTEN) protein level, thereby activating the AKT/mechanistic target of rapamycin kinase (mTOR) pathway in HCC cells. MG132 reversed RNF146 overexpression-induced PTEN reduction. RNF146 knockdown decreased the ubiquitination and degradation of PTEN in HCC cells. Therefore, we clarified that PTEN knockdown notably abolished the effects of RNF146 silencing on the AKT/mTOR pathway and Hep3B cells' proliferation, colony formation and glycolysis. To conclude, our data confirmed that RNF146 was transcriptionally regulated by HIF-1/2α and activated the AKT/mTOR pathway by promoting the ubiquitin proteolysis of PTEN, thereby contributing to HCC progression. RNF146 may be a potential new drug target for anti-HCC.

Keywords: hepatocellular carcinoma, hypoxia microenvironment, RNF146, pten, akt/mtor pathway

OPEN ACCESS

Edited by:
Yuanyuan Lu,
Fourth Military Medical University, China

Reviewed by:
Qiongzhu Dong,
Fudan University, China
Chao Sun,
Tianjin Medical University General Hospital, China

****Correspondence:***
Qiuran Xu
windway626@sina.com
Dongsheng Huang
dshuang@hmc.edu.cn

†These authors have contributed equally to this work

Specialty section:
This article was submitted to Epigenomics and Epigenetics, a section of the journal Frontiers in Cell and Developmental Biology

Received: *11 March 2022*
Accepted: *09 May 2022*
Published: *27 May 2022*

Citation:
Shen G, Wang H, Zhu N, Lu Q, Liu J, Xu Q and Huang D (2022) HIF-1/2α-Activated RNF146 Enhances the Proliferation and Glycolysis of Hepatocellular Carcinoma Cells via the PTEN/AKT/mTOR Pathway. Front. Cell Dev. Biol. 10:893888. doi: 10.3389/fcell.2022.893888

1 INTRODUCTION

Hepatocellular carcinoma (HCC) accounts for 75–85% of all primary liver cancer cases and is the third leading cause of cancer-related death worldwide (Sung et al., 2021). In 2020, there are 910,000 new cases of liver cancer worldwide, of which 45% are from China (Sung et al., 2021). Surgical resection is still the best choice for HCC treatment, but most patients are diagnosed with advanced stage and lose the opportunity for surgery (Llovet et al., 2021a). The application of targeted therapy and immunotherapy has brought light to some patients with advanced HCC, but the overall prognosis has not improved significantly (Llovet et al., 2021a). Therefore, it is of great significance to further reveal the precise molecular mechanism of the occurrence and development of HCC and carry out new target discovery and intervention research of anti-cancer drugs to improve the curative effect and prognosis of patients.

Extracellular matrix deposition results in decreased blood flow to the liver, and rapid tumor growth, intense metabolic activity, and poor angiogenesis lead to the formation of a hypoxic microenvironment in HCC (Gilkes et al., 2014; Singleton et al., 2021). Multiple target genes transcriptionally regulated by hypoxia-inducible factors (HIFs) promote HSCs activation as well as the growth, metabolic reprogramming, stem cell-like properties, angiogenesis, invasion and metastasis of HCC (Liu et al., 2019; Cramer and Vaupel 2022). Hypoxia-induced ubiquitin-specific peptidase 13 (USP13) deubiquitinated and stabilized toll-like receptor 4 (TLR4) to activate the myeloid differentiation primary response gene 88/nuclear factor-κB (MyD88/NF-κB) pathway, thereby contributing to HCC progression (Gao et al., 2020). Peptidylarginine deiminase 4 (PADI4) is identified as a novel HIFs target gene and promotes the transcription activity of HIFs by inducing histone citrullination to enhance the growth and angiogenesis of HCC *in vivo* (Wang Y. et al., 2021). In addition to protein-coding genes, hypoxia affects microRNAs (miRNAs) and long non-coding RNAs (lncRNAs) to facilitate HCC progression. Hypoxia-induced miR-671–5p downregulation increases tuftelin1 (TUFT1) expression, promoting HCC growth and metastasis by activating the Ca^{2+}/PI3K/AKT pathway (Dou et al., 2019). TM4SF1-AS1 is transcriptionally activated by HIF-1α and increases the migration, invasion and proliferation of HCC cells by upregulating the TM4SF1 level (Zeng et al., 2021). Therefore, further exploration of new hypoxia target genes is beneficial for revealing the new mechanism of hypoxia-induced HCC progression.

Ring finger protein 146 (RNF146), ubiquitin E3 ligase, belongs to the RING-type E3 ubiquitin ligase family (Darosa et al., 2015). RNF146 positively regulated the Wnt signaling pathway by affecting the protein degradation of AXIN1 (Zhang et al., 2011; Darosa et al., 2015; Matsumoto et al., 2017). RNF146 regulates the liver kinase B1 (LKB1)-AMP-activated protein kinase (AMPK) pathway by mediating LKB1 ubiquitination (Li et al., 2019). Phosphatase and tensin homolog (PTEN) is recognized as a protein substrate of

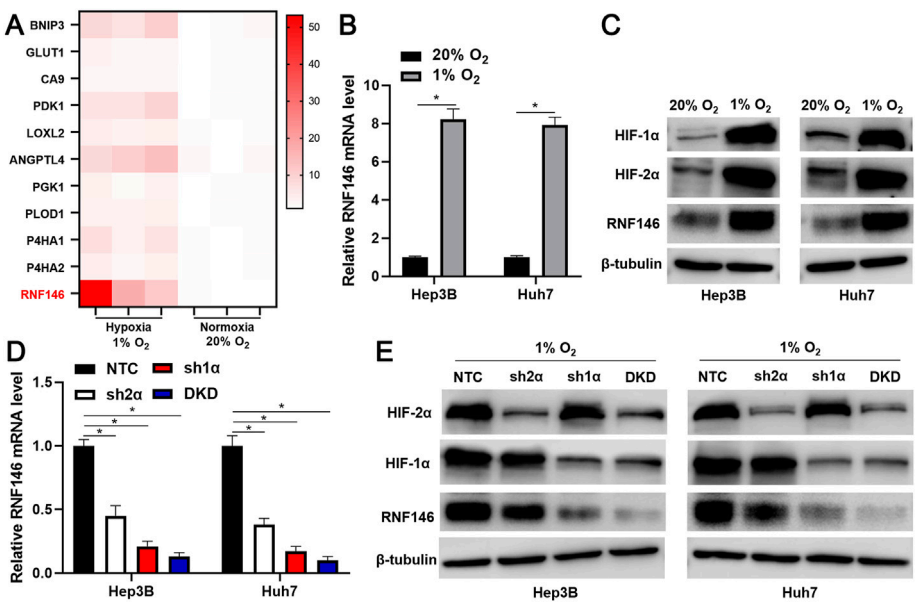

FIGURE 1 | RNF146 is a hypoxia-responsive gene. **(A)** Heatmap of ten known hypoxia target genes and RNF146 expression in Hep3B cells under normoxia (20% O_2) and hypoxia (1% O_2) conditions. **(B)** The expression of RNF146 mRNA in HCC cells under normoxia and hypoxia conditions was measured by RT-qPCR. **(C)** HIF-1α, HIF-2α and RNF146 protein levels were determined by WB in HCC cells under normoxia and hypoxia conditions. **(D)** The lentivirus-mediated shRNAs against HIF-2α (sh2α), HIF-1α (sh1α), HIF-1α/2α (DKD) and non-targeting shRNA (NTC) were transduced into HCC cells. After incubation under hypoxia conditions, RNF146 mRNA level in HCC cells was measured by RT-qPCR. **(E)** HIF-1α, HIF-2α and RNF146 protein levels were determined by WB in transfected HCC cells under hypoxia conditions. *$p < 0.05$.

RNF146. RNF146 results in the ubiquitination and degradation of PTEN to activate the AKT pathway and promotes tumor cell proliferation and glycolysis (Li et al., 2015). In HCC, RNF146 is the regulator of poly (ADP-ribose) polymerase 1 (PARP1) ubiquitination and protein degradation (Zhou et al., 2020). However, the link between hypoxia and RNF146 in HCC remains unclear yet.

In this study, we explore candidate HIFs target genes by analyzing microarray data. The regulatory effects of HIF-1/2α on RNF146 expression were confirmed. The role of RNF146 in HCC cell proliferation and glycolysis, as well as underlying mechanisms, were investigated. We found that hypoxia enhanced RNF146 expression via HIF-1/2α. RNF146 contributed to the proliferation, colony formation and glycolysis of HCC cells by regulating the PTEN/AKT/mechanistic target of rapamycin kinase (mTOR) pathway.

2 MATERIALS AND METHODS

2.1 Tissue Samples

This study collected human HCC tissue samples and paired adjacent tissue samples from 80 patients with HCC in the First Affiliated Hospital of Xi'an Jiaotong University. The included patients had precise pathological diagnoses and had not been treated before surgery. All the collected tissue samples were well were formalin-fixed and paraffin-embedded. Written informed consent was obtained from all patients, and the Ethics Committee of the 1st Affiliated Hospital of Xi'an Jiaotong University approved this study. During 3 years of follow-up, the time between primary surgery and death was the overall survival time.

2.2 Cell Culture

Hep3B, HepG2, HCCLM3 and Huh7 cells were provided by Stem Cell Bank, Chinese Academy of Sciences (Shanghai, China). Human liver cell line MIHA was purchased from bnbio (Beijing, China). Cell lines were cultured in DMEM (Gibco, Thermo Fisher Scientific, Waltham, MA, United States) added with 10% fetal bovine serum (Gibco), penicillin (100 U/ml, Gibco) and streptomycin (100 mg/ml, Gibco). The culture condition in the incubator was a moist environment with 5% CO_2 at 37°C.

2.3 Lentivirus and Plasmid Construction

LKO.1-puro lentiviral vectors encoding small hairpin RNA (shRNA) against HIF-1α (sh1α), HIF-2α (sh2α), RNF146 (shRNF#1 and shRNF#2), PTEN (shPTEN) and non-targeting shRNA (NTC) were provided by GeneChem (Shanghai, China). All lentiviral shuttle vectors were transfected into HEK293T cells for packaging as previously described (Zeng et al., 2021). RNF146 cDNA was sub-cloned into pcDNA3.1 (Invitrogen, Carlsbad, CA, United States) to produce pcDNA3.1/RNF146 (RNF-OE). Lipofectamine 3000 (Thermo Fisher Scientific) was applied for plasmid transfection in HCC cells.

2.4 Real-Time Quantitative PCR

HCC cells were subjected to RNA isolation following the instruction of the Trizol reagent (Invitrogen) and total

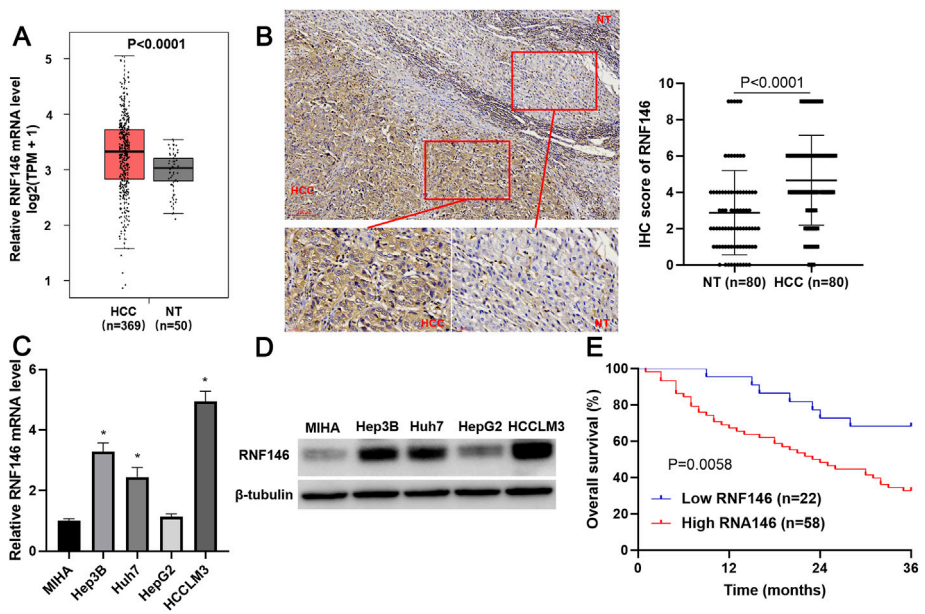

FIGURE 2 | RNF146 expression is increased in HCC. **(A)** TCGA data analysis using the GEPIA platform showed the expression difference of RNF146 mRNA between HCC and normal liver tissues. **(B)** IHC analysis indicated that RNF146 was highly expressed in HCC compared to adjacent nontumor tissues. **(C)** The RNF146 mRNA levels were detected in MIHA, Hep3B, Huh7, HepG2 and HCCLM3 cells by RT-qPCR. **(D)** The RNF146 protein levels were detected in MIHA, Hep3B, Huh7, HepG2 and HCCLM3 cells by WB. **(E)** The comparison of 3-years overall survival of patients with high or low RNF146 expression.

TABLE 1 | Relationship between RNF146 expression and clinicopathologic parameters of patients with hepatocellular carcinoma.

Clinicopathologic Parameters		*n* = 80	RNF146		*p*
			Low Expression (n = 22)	High Expression (*n* = 58)	
Age (years)	<50	33	10	23	0.638
	≥50	47	12	35	
Sex	Male	67	18	49	0.773
	Female	13	4	9	
HBV infection	No	13	5	8	0.333
	Yes	67	17	50	
Serum AFP level (ng/ml)	<20	14	6	8	0.157
	≥20	66	16	50	
Tumor size (cm)	<5	29	12	17	0.036[a]
	≥5	51	10	41	
No. of tumor nodules	1	65	20	45	0.173
	≥2	15	2	13	
Cirrhosis	No	12	5	7	0.233
	Yes	68	17	51	
Venous infiltration	No	44	17	27	0.014[a]
	Yes	36	5	31	
Tumor differentiation	I + II	53	16	37	0.451
	III + IV	27	6	21	
TNM stage	I	32	12	20	0.102
	II + III	48	10	38	
BCLC stage	0 + A	59	19	40	0.114
	B + C	21	3	18	

HBV, hepatitis B virus; AFP, alpha-fetoprotein; TNM, tumor-node-metastasis; BCLC, Barcelona Clinic Liver Cancer.
[a]*Statistically significant.*

RNA was reversely transcribed into cDNA using PrimeScript™ RT Master Mix (Takara, Shiga, Japan). The PCR amplification was performed on ABI HT9600 (Applied Biosystems, Foster City, CA, United States) in accordance with the instruction of SYBR Green PCR Master Mix (Takara). The RNF146 mRNA level was normalized to GAPDH using the $2^{-\Delta\Delta CT}$ method. RNF146 forward primer: 5′-TGT AAG CAC GTT TTC TGC TAT CT-3′; reverse: 5′-AAT CCT CGG GAA TTT CTT GTC G-3′. GAPDH forward primer: 5′-CTG GGC TAC ACT GAG CAC C-3′; reverse: 5′-AAG TGG TCG TTG AGG GCA ATG-3′.

2.5 Western Blotting

Total proteins were obtained from HCC cells using RIPA buffer (Beyotime, Shanghai, China) and quantified by Enhanced BCA Protein Assay Kit (Beyotime). Then, 20 μg proteins were undergoing SDS-PAGE and transferred to the PVDF membrane (Millipore, Billerica, MA, United States). After blocking, the membrane was incubated overnight with primary antibodies at 4°C. The next day, secondary antibody incubation was performed at room temperature for 1–2 h. Enhanced chemiluminescence (ECL) reagent (Millipore) was used for luminous reaction and western blot was photographed by Amersham Imager 680 (GE Healthcare Life Sciences, Pittsburgh, PA, United States). The used primary antibodies: HIF-1α (ab1, Abcam, Cambridge, MA, United States), HIF-2α (ab199, Abcam), RNF146 (ab201212, Abcam), β-tubulin (10094-1-AP, Proteintech, Wuhan, China), PTEN (ab267787, Abcam). p-AKT (Ser473, 66444-1-Ig, Proteintech), AKT (60203-2-Ig, Proteintech), p-mTOR (Ser2448, 67778-1-Ig, Proteintech), mTOR (66888-1-Ig, Proteintech), Ubiquitin (ab7254, Abcam).

2.6 Immunohistochemistry

The embedded-paraffin tissues were sectioned with a thickness of approximately 4–5 μm. Next, paraffin sections were deparaffinized in xylene and rehydrated with ethanol, and used 0.3% hydrogen peroxide to block endogenous peroxidase activity. Finally, the sections were incubated with RNF146 antibody (ab201212, Abcam) and a specific secondary antibody. The intensity score and positive rate score were previously described (Shen et al., 2018). The IHC score (intensity score × positive rate score) ≥4 was defined as high expression.

2.7 Immunoprecipitation and Ubiquitination Assays

The immunoprecipitation and ubiquitination assays were performed as previously described (Shi et al., 2021). In brief, the cells were incubated with 10 μM MG132 (HY-13259, MedChemExpress, Shanghai, China) for 8 h. HCC cells were treated with IP lysis buffer. The total cell lysates were collected and subjected to immunoprecipitation with 2 μg PTEN (ab267787, Abcam) or IgG antibody and 30 μL slurry of Protein G Sepharose (GE Healthcare Life Sciences, Pittsburgh, PA, United States) at 4°C overnight. Western blot analysis was performed with an Anti-Ubiquitin antibody (ab7254, Abcam) to detect the corresponding protein ubiquitination.

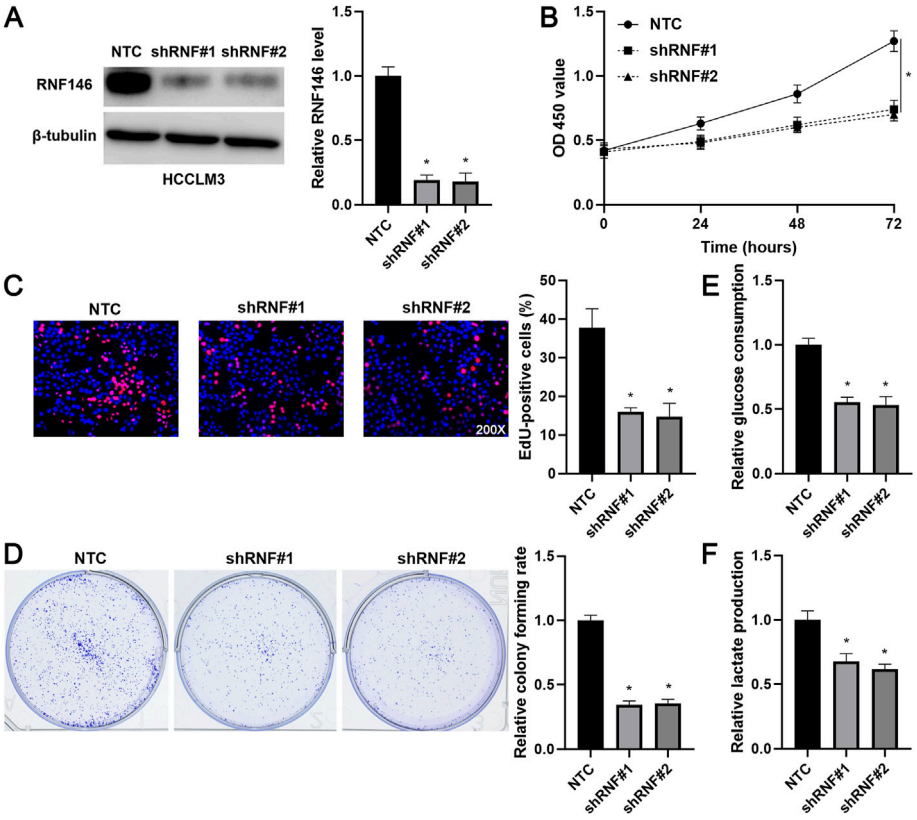

FIGURE 3 | RNF146 knockdown suppresses the proliferation and glycolysis of HCCLM3 cells. **(A)** The lentivirus-mediated shRNAs targeting RNF146 (shRNF#1 and shRNF#2) and non-targeting shRNA (NTC) were transduced into HCCLM3 cells. WB was performed to determine the RNF146 protein level. **(B)** RNF146 knockdown reduced the viability of HCCLM3 cells. **(C)** RNF146 silencing inhibited the proliferation of HCCLM3 cells. **(D)** The inhibitory effects of RNF146 knockdown on HCCLM3 cell colony formation were confirmed. **(E)** RNF146 silencing reduced the glucose consumption of HCCLM3 cells. **(F)** HCCLM3 cells' lactate production was decreased by RNF146 knockdown. *$p < 0.05$.

2.8 Cell Proliferation and Colony Formation Assays

The cell counting kit-8 (CCK-8) kit (Beyotime) and Cell-Light™ EdU Apollo® 488 *In Vitro* Imaging Kit (RIBOBIO, Guangzhou, China) were used for HCC cell proliferation determination as previously described (Shi et al., 2021). For colony formation assay, the logarithmic growth cells (1×10^3) were seeded into 6-well plates and were grown for a period of 2 weeks. Cell colonies were stabilized with 4% paraformaldehyde, stained with 0.1% crystal violet solution and manually counted.

2.9 Glucose Consumption and Lactate Production Assays

Glucose consumption and lactate production of HCC cells were detected using the lactate assay kit (ab65331, Abcam) and glucose assay kit (ab136955, Abcam), respectively, according to the manufacturer's protocols.

2.10 *In vivo* Studies

The animal studies were approved by the Institutional Animal Care and Use Committee of Xi'an Jiaotong University. Male BALB/c nude mice (4 weeks old) were obtained from the Vital River Laboratory Animal Technology Co. (Beijing, China). 5×10^6 HCCLM3 cells stably transfected with RNF146 shRNA or the negative control were respectively injected into the right armpits of five mice, and subcutaneous tumor size was assessed every week. The mice were sacrificed 4 weeks after injection and the xenograft tumors were removed for IHC with Ki-67 antibody (27309-1-AP, Proteintech) or WB with RNF146 antibody (ab201212, Abcam).

2.11 Statistical Analysis

All data in this study were processed by GraphPad Prism 8 (San Diego, CA, United States). Measurement data were shown as mean ± S.D. The Mann–Whitney test and analysis of variance (ANOVA) were applied for the significant test. Survival data were analyzed through the Kaplan-Meier method and log-rank test. *p*-value less than 0.05 denoted statistically significant.

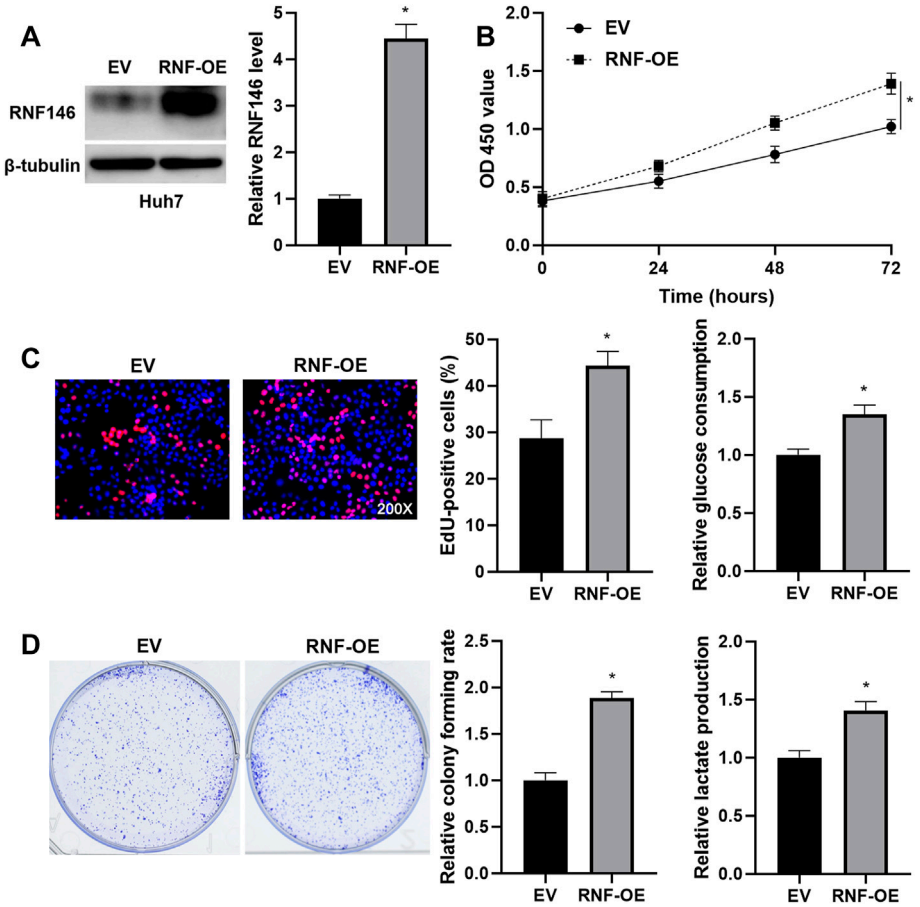

FIGURE 4 | RNF146 overexpression promotes the proliferation and glycolysis of Huh7 cells. **(A)** The pcDNA3.1/RNF146 (RNF-OE) and empty vector (EV) were transduced into Huh7 cells. WB was performed to determine the RNF146 protein level. **(B)** CCK-8, **(C)** EdU, **(D)** colony formation, E glucose consumption and F lactate production assays were performed to detect the proliferation, colony formation and glycolysis of Huh7 cells with or without RNF146 overexpression. *$p < 0.05$.

3 RESULTS

3.1 Hypoxia-Inducible Factor-1/2α Regulates RNF146 Expression in Hepatocellular Carcinoma Cells Under Hypoxic Conditions

We analyzed our previous microarray data (GSE155505) of hypoxia-related mRNAs in Hep3B cells. A significant upregulation of RNF146 in Hep3B cells under hypoxic conditions caught our attention (**Figure 1A**). RT-qPCR and WB analyses consistently confirmed that hypoxia upregulated RNF146 expression in Huh7 and Hep3B cells ($p < 0.05$, **Figures 1B,C**). Then, shRNAs were used to downregulate HIF-1α or HIF-2α or HIF1/2α in HCC cells (**Figure 1E**). The silencing of HIF-1α or HIF-2α or both [double knockdown (DKD)] prominently reduced hypoxia-induced RNF146 expression in HCC cells ($p < 0.05$, **Figures 1D,E**). Furthermore, TCGA data analysis using the GEPIA website (http://gepia.cancer-pku.cn/) (Tang et al., 2019) found positive correlations between RNF146 and HIF1/2α in HCC tissues ($p < 0.05$, **Supplementary Figure S1**). Our data suggest that hypoxia induces RNF146 expression via HIF-1/2α in HCC cells.

3.2 RNF146 is Highly Expressed in Hepatocellular Carcinoma

TCGA data analysis using the GEPIA website (http://gepia.cancer-pku.cn/) (Tang et al., 2019) found that RNF146 mRNA expression in HCC was prominently higher than in normal liver tissues ($p < 0.0001$, **Figure 2A**). IHC data confirmed the upregulated level of RNF146 protein in HCC tissues compared to adjacent nontumor tissues ($p < 0.0001$, **Figures 2B,C**). Moreover, the upregulated levels of RNF146 were also detected in Hep3p, Huh7 and HCCLM3 cells ($p < 0.05$, **Figure 2D**). **Table 1** showed that HCC patients with large tumors and venous infiltration expressed higher levels of RNF146 ($p < 0.05$). Survival analysis indicated a close correlation between high RNF146 expression and poor 3-years overall survival of patients with HCC ($p = 0.0058$, **Figure 2E**). Thus, these results indicate that RNF146 may be a promising prognostic biomarker for HCC.

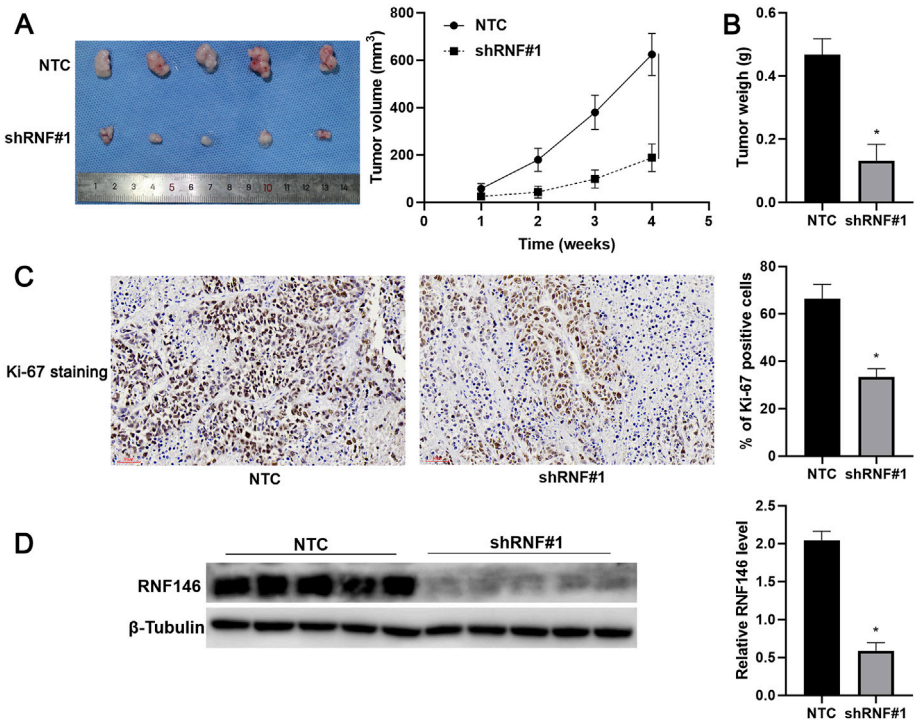

FIGURE 5 | RNF146 knockdown reduces HCC growth *in vivo*. HCCLM3 cells with or without RNF146 knockdown were subcutaneously injected into nude mice. **(A)** Tumor volume and **(B)** weight were consistently reduced by RNF146 knockdown. **(C)** Tumor tissues from the RNF146 knockdown group showed fewer Ki-67 staining cells compared to the control group. **(D)** Tumor tissues from the RNF146 knockdown group showed lower RNF146 protein levels than the control group. *$p < 0.05$.

3.3 RNF146 Promotes Hepatocellular Carcinoma Cell Proliferation and Glycolysis

Lentivirus-mediated shRNAs markedly downregulated RNF146 in HCCLM3 cells ($p < 0.05$, **Figure 3A**). RNF146 knockdown remarkably reduced the viability of HCCLM3 cells ($p < 0.05$, **Figure 3B**). The silencing of RNF146 significantly weakened the proliferation of HCCLM3 cells ($p < 0.05$, **Figure 3C**). The HCCLM3 cell colonies were obviously decreased by RNF146 silencing ($p < 0.05$, **Figure 3D**). Otherwise, RNF146 depletion remarkably decreased the glucose consumption and lactate production of HCCLM3 cells ($p < 0.05$, **Figures 3E,F**). RNF146 overexpression prominently enhanced the proliferation and glycolysis of Huh7 cells ($p < 0.05$, **Figure 4**). Next, *in vivo* experiments confirmed that RNF146 knockdown reduced the volume and weight of subcutaneous tumors formed by HCCLM3 cells ($p < 0.05$, **Figures 5A,B**). IHC staining of Ki-67 in tumor tissues indicated that the percentage of positive cells in the RNF146 knockdown group was obviously lower than in the control group ($p < 0.05$, **Figure 5C**). WB analysis confirmed the downregulated expression of RNF146 in the RNF146 knockdown group compared to the control group ($p < 0.05$, **Figure 5D**). Collectively, we consider RNF146 as an oncogene in HCC.

3.4 RNF146 Regulates the AKT/mTOR Pathway by Reducing Phosphatase and Tensin Homolog

KEGG enrichment pathways analysis suggested that RNF146 might regulate the mTOR signaling pathway in HCC based on TCGA data (**Figure 6A** and **Supplementary Table S1**). RNF146 knockdown decreased while RNF146 overexpression increased p-AKT and p-mTOR levels in HCC cells (**Figures 6B,C**). A previous study has identified RNF146 as a negative regulator of PTEN and activates the PI3K/AKT/mTOR pathway (Li et al., 2015). Interestingly, we found that RNF146 inversely regulated PTEN protein levels in HCC cells (**Figures 6B,C**). A proteasome inhibitor, MG132, blocked RNF146-induced PTEN downregulation in Huh7 cells (**Figure 6D**). Moreover, RNF146 silencing obviously reduced the ubiquitination and degradation of PTEN in HCC cells (**Figures 6E,F**). Therefore, RNF146 promotes PTEN ubiquitination and degradation and activates the AKT/mTOR pathway in HCC.

3.5 The Role of RNF146 Silencing is Reversed by Phosphatase and Tensin Homolog Knockdown in Hepatocellular Carcinoma Cells

We intended to verify the involvement of PTEN in RNF146-induced HCC progression. A specific shRNA downregulated

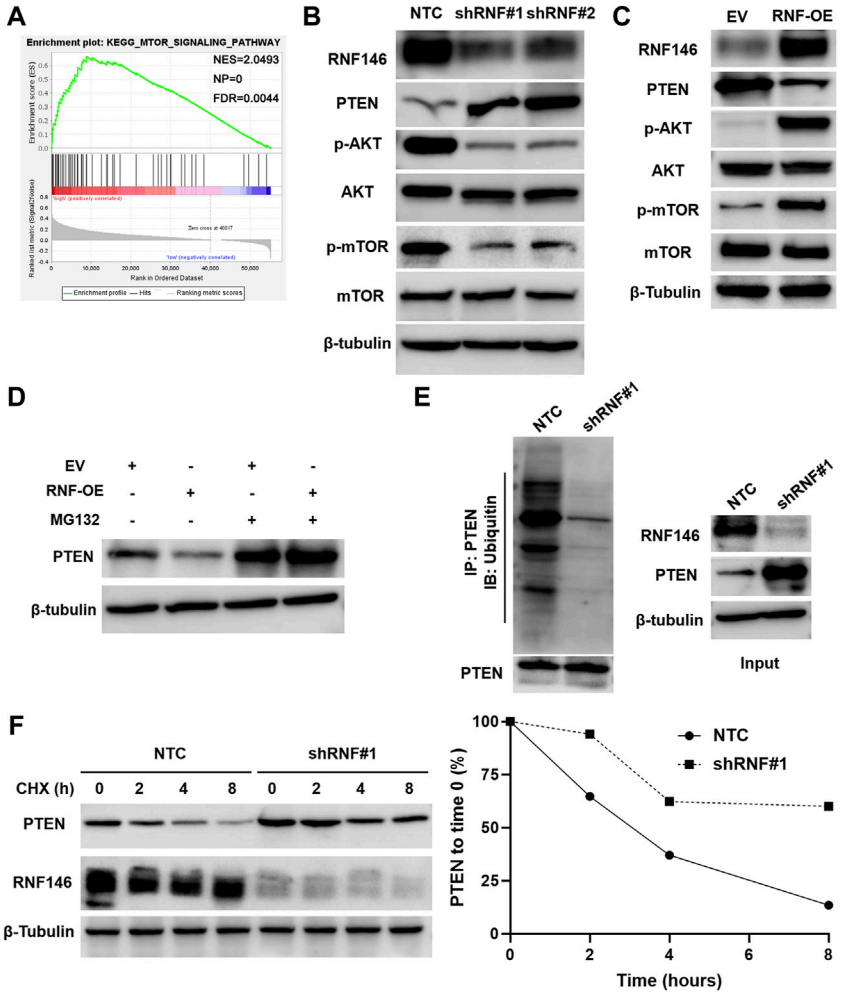

FIGURE 6 | RNF146 regulates the PTEN/AKT/mTOR pathway in HCC cells. **(A)** KEGG pathway enrichment analysis indicated a close correlation between RNF146 and the mTOR signaling pathway in HCC. **(B)** RNF146 knockdown increased PTEN expression but reduced p-AKT (Ser473) and p-mTOR (Ser2448) levels in HCCLM3 cells. **(C)** RNF146 overexpression decreased PTEN expression while increased p-AKT (Ser473) and p-mTOR (Ser2448) levels in Huh7 cells. **(D)** RNF146 overexpression-induced PTEN downregulation was blocked by a proteasome inhibitor MG132 in Huh7 cells. **(E)** The ubiquitination of PTEN was reduced by RNF146 silencing in HCCLM3 cells. **(F)** The degradation of PTEN was reduced by RNF146 silencing in HCCLM3 cells.

PTEN expression in HCCLM3 cells with RNF146 knockdown (**Figure 7A**). PTEN knockdown recovered RNF146 silencing-induced p-AKT and p-mTOR downregulation in HCCLM3 cells (**Figure 7A**). We confirmed that PTEN silencing significantly abolished RNF146 knockdown-induced proliferation inhibition of HCCLM3 cells ($p < 0.05$, **Figures 7B,C**). Moreover, the effects of RNF146 silencing on HCCLM3 cell colony formation, glucose consumption and lactate production were markedly reversed by PTEN knockdown ($p < 0.05$, **Figures 7D–F**). Therefore, PTEN mediates the pro-HCC function of RNF146.

4 DISCUSSION

Hypoxia is one of the core features of the HCC microenvironment and a key factor leading to tumor malignant progression and treatment resistance (Jing et al., 2019). Monoclonal antibodies (bevacizumab and ramucirumab) and small-molecule inhibitors (sorafenib and lenvatinib) targeting the hypoxia-responsive gene VEGF and its receptors have become first-line treatments for advanced HCC (Llovet et al., 2021b). In this study, we aimed to investigate novel hypoxia-responsive genes in HCC. According to microarray data analysis, we selected a hypoxia-upregulated gene, RNF146, for further study. The expression of RNF146 was prominently upregulated in HCC cells under hypoxia conditions. The knockdown of HIF-1α or HIF-2α or DKD significantly blocked hypoxia-induced RNF146 upregulation in HCC cells. These results suggest that RNF146 is a new HIF-1/2α target gene.

RNF146 overexpression is frequently detected in colorectal cancer (CRC) and is an independent biomarker for predicting the poor prognosis (Shen et al., 2018). RNF146 expression is upregulated in non-small cell lung cancer (NSCLC) and is associated with malignant clinical features and poor clinical

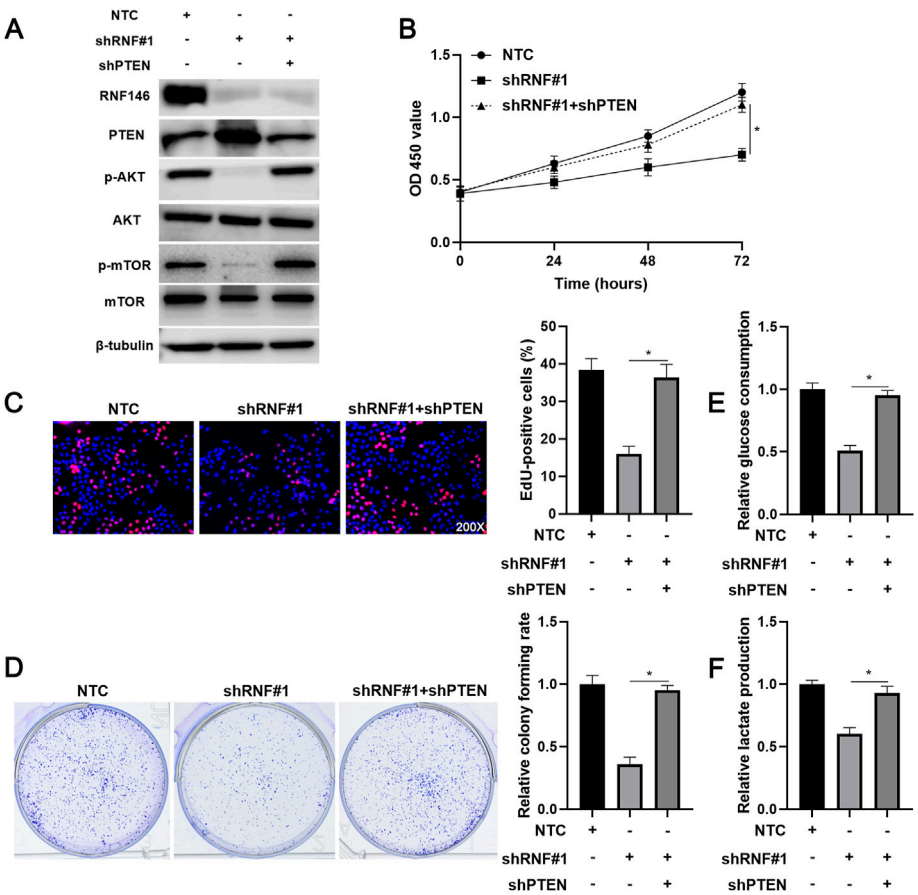

FIGURE 7 | Reducing PTEN expression abolishes the effects of RNF146 knockdown in HCCLM3 cells. **(A)** HCCLM3 cells that were transfected with NTC, shRNF#1 or shRNF#1 + shPTEN were detected by WB for the RNF146, PTEN, p-AKT (Ser473), AKT, p-mTOR (Ser2448) and mTOR levels. **(B)** CCK-8, **(C)** EdU, **(D)** colony formation, **(E)** glucose consumption and **(F)** lactate production assays were performed to detect the proliferation, colony formation and glycolysis of HCCLM3 cells with or without RNF146 overexpression. *$p < 0.05$.

outcomes (Gao et al., 2014). Here, we also verified that RNF146 was highly expressed in HCC based on TCGA data and our IHC data. The upregulated levels of RNF146 were consistently determined in HCC cell lines. Moreover, we found that high RNF146 expression was correlated with large tumors and venous infiltration and predicted a shorter 3-years overall survival of patients with HCC. Our data verify the potential clinical value of RNF146 in the judgment of poor prognosis in HCC.

RNF146 knockdown repressed the proliferation, colony formation and glycolysis of HCC cells, while RNF146 overexpression facilitated these malignant behaviors. RNF146 silencing reduced HCC growth in nude mice. These data recognize RNF146 as an oncogene in HCC. Therefore, we further explored the possible molecular mechanism of RNF146 promoting HCC. Previous studies have demonstrated that RNF146 activates the Wnt/β-catenin pathway by mediating ubiquitination and degradation of AXIN1 (Zhang et al., 2011; Gao et al., 2014; Shen et al., 2018). RNF146 modulates the LKB1-AMPK pathway by promoting LKB1 ubiquitination (Li et al., 2019). RNF146 mediates the ubiquitination and degradation of PTEN to activate the AKT pathway and promotes tumor cell proliferation and glycolysis (Li et al., 2015). RNF146 is a regulator of PARP1 ubiquitination and protein degradation in HCC (Zhou et al., 2020). Here, KEGG pathway analysis based on TCGA data showed that the mTOR pathway is one of the most relevant signaling pathways for RNF146. Next, we confirmed that RNF146 promoted the AKT/mTOR pathway in HCC cells. RNF146 overexpression-induced PTEN downregulation was reversed by MG132 treatment. RNF146 silencing increased the ubiquitination and degradation of PTEN in HCC cells. Thus, we consider that RNF146 regulates the AKT/mTOR pathway by ubiquitinating and degrading PTEN in HCC. The PTEN/AKT/mTOR pathway is one of the critical oncogenic pathways in HCC and participates in the regulation of cell proliferation, glycolysis, stemness and invasion (Liu et al., 2018; Dou et al., 2019; Dou et al., 2020; Wang L. et al., 2021). PTEN knockdown recovered RNF146 silencing-induced the AKT/mTOR pathway inactivation in HCCLM3 cells. Significantly, reducing PTEN expression prominently abolished the effects of RNF146 knockdown in HCC cells.

Thus, RNF146 contributes to HCC progression by regulating the PTEN/AKT/mTOR pathway.

Our findings identified RNF146 as a novel HIF-1/2α target gene in HCC. HIF-1/2α-activated RNF146 facilitated HCC progression by enhancing PTEN ubiquitination and degradation and promoting the AKT/mTOR pathway activation. This study provides a new idea for developing new targets for anti-HCC drugs.

DATA AVAILABILITY STATEMENT

The datasets presented in this study can be found in online repositories. The names of the repository/repositories and accession number(s) can be found below: https://www.ncbi.nlm.nih.gov/geo/, GSE155505;https://portal.gdc.cancer.gov/, TCGA-LIHC.

ETHICS STATEMENT

The studies involving human participants were reviewed and approved by the 1st Affiliated Hospital of Xi'an Jiaotong University. The patients/participants provided their written informed consent to participate in this study. The animal study was reviewed and approved by the Institutional Animal Care and Use Committee of Xi'an Jiaotong University.

AUTHOR CONTRIBUTIONS

QX and DH conceived and designed the experiments; GS, HW, NZ, QL and JL performed the experiments and analyzed the data; GS and DH wrote the paper. All authors read and approved the final manuscript.

FUNDING

This work was supported by the Zhejiang Provincial Department of Education Project (Y202146096).

SUPPLEMENTARY MATERIAL

The Supplementary Material for this article can be found online at: https://www.frontiersin.org/articles/10.3389/fcell.2022.893888/full#supplementary-material

REFERENCES

Cramer, T., and Vaupel, P. (2022). Severe Hypoxia Is a Typical Characteristic of Human Hepatocellular Carcinoma: Scientific Fact or Fallacy? *J. Hepatol.* 76 (4), 975–980. doi:10.1016/j.jhep.2021.12.028

Darosa, P. A., Wang, Z., Jiang, X., Pruneda, J. N., Cong, F., Klevit, R. E., et al. (2015). Allosteric Activation of the RNF146 Ubiquitin Ligase by a poly(ADP-Ribosyl)ation Signal. *Nature* 517, 223–226. doi:10.1038/nature13826

Dou, C., Sun, L., Wang, L., Cheng, J., Wu, W., Zhang, C., et al. (2020). Bromodomain-containing Protein 9 Promotes the Growth and Metastasis of Human Hepatocellular Carcinoma by Activating the TUFT1/AKT Pathway. *Cell Death Dis.* 11, 730. doi:10.1038/s41419-020-02943-7

Dou, C., Zhou, Z., Xu, Q., Liu, Z., Zeng, Y., Wang, Y., et al. (2019). Hypoxia-induced TUFT1 Promotes the Growth and Metastasis of Hepatocellular Carcinoma by Activating the Ca2+/PI3K/AKT Pathway. *Oncogene* 38, 1239–1255. doi:10.1038/s41388-018-0505-8

Gao, S., Chen, T., Li, L., Liu, X., Liu, Y., Zhao, J., et al. (2020). Hypoxia-Inducible Ubiquitin Specific Peptidase 13 Contributes to Tumor Growth and Metastasis via Enhancing the Toll-like Receptor 4/Myeloid Differentiation Primary Response Gene 88/Nuclear Factor-Kb Pathway in Hepatocellular Carcinoma. *Front. Cell Dev. Biol.* 8, 587389. doi:10.3389/fcell.2020.587389

Gao, Y., Song, C., Hui, L., Li, C.-y., Wang, J., Tian, Y., et al. (2014). Overexpression of RNF146 in Non-small Cell Lung Cancer Enhances Proliferation and Invasion of Tumors through the Wnt/β-Catenin Signaling Pathway. *PLoS One* 9, e85377. doi:10.1371/journal.pone.0085377

Gilkes, D. M., Semenza, G. L., and Wirtz, D. (2014). Hypoxia and the Extracellular Matrix: Drivers of Tumour Metastasis. *Nat. Rev. Cancer* 14, 430–439. doi:10.1038/nrc3726

Jing, X., Yang, F., Shao, C., Wei, K., Xie, M., Shen, H., et al. (2019). Role of Hypoxia in Cancer Therapy by Regulating the Tumor Microenvironment. *Mol. Cancer* 18, 157. doi:10.1186/s12943-019-1089-9

Li, N., Wang, Y., Neri, S., Zhen, Y., Fong, L. W. R., Qiao, Y., et al. (2019). Tankyrase Disrupts Metabolic Homeostasis and Promotes Tumorigenesis by Inhibiting LKB1-AMPK Signalling. *Nat. Commun.* 10, 4363. doi:10.1038/s41467-019-12377-1

Li, N., Zhang, Y., Han, X., Liang, K., Wang, J., Feng, L., et al. (2015). Poly-ADP Ribosylation of PTEN by Tankyrases Promotes PTEN Degradation and Tumor Growth. *Genes Dev.* 29, 157–170. doi:10.1101/gad.251785.114

Liu, Y., Lu, T., Zhang, C., Xu, J., Xue, Z., Busuttil, R. W., et al. (2019). Activation of YAP Attenuates Hepatic Damage and Fibrosis in Liver Ischemia-Reperfusion Injury. *J. Hepatology* 71, 719–730. doi:10.1016/j.jhep.2019.05.029

Liu, Z., Wang, Y., Dou, C., Xu, M., Sun, L., Wang, L., et al. (2018). Hypoxia-induced Up-Regulation of VASP Promotes Invasiveness and Metastasis of Hepatocellular Carcinoma. *Theranostics* 8, 4649–4663. doi:10.7150/thno.26789

Llovet, J. M., De Baere, T., Kulik, L., Haber, P. K., Greten, T. F., Meyer, T., et al. (2021a). Locoregional Therapies in the Era of Molecular and Immune Treatments for Hepatocellular Carcinoma. *Nat. Rev. Gastroenterol. Hepatol.* 18, 293–313. doi:10.1038/s41575-020-00395-0

Llovet, J. M., Kelley, R. K., Villanueva, A., Singal, A. G., Pikarsky, E., Roayaie, S., et al. (2021b). Hepatocellular Carcinoma. *Nat. Rev. Dis. Prim.* 7, 6. doi:10.1038/s41572-020-00240-3

Matsumoto, Y., La Rose, J., Lim, M., Adissu, H. A., Law, N., Mao, X., et al. (2017). Ubiquitin Ligase RNF146 Coordinates Bone Dynamics and Energy Metabolism. *J. Clin. Invest.* 127, 2612–2625. doi:10.1172/jci92233

Shen, J., Yu, Z., and Li, N. (2018). The E3 Ubiquitin Ligase RNF146 Promotes Colorectal Cancer by Activating the Wnt/β-Catenin Pathway via Ubiquitination of Axin1. *Biochem. Biophysical Res. Commun.* 503, 991–997. doi:10.1016/j.bbrc.2018.06.107

Shi, Z., Liu, R., Lu, Q., Zeng, Z., Liu, Y., Zhao, J., et al. (2021). UBE2O Promotes Hepatocellular Carcinoma Cell Proliferation and Invasion by Regulating the AMPKα2/mTOR Pathway. *Int. J. Med. Sci.* 18, 3749–3758. doi:10.7150/ijms.63220

Singleton, D. C., Macann, A., and Wilson, W. R. (2021). Therapeutic Targeting of the Hypoxic Tumour Microenvironment. *Nat. Rev. Clin. Oncol.* 18 (12), 751–772. doi:10.1038/s41571-021-00539-4

Sung, H., Ferlay, J., Siegel, R. L., Laversanne, M., Soerjomataram, I., Jemal, A., et al. (2021). Global Cancer Statistics 2020: GLOBOCAN Estimates of Incidence and Mortality Worldwide for 36 Cancers in 185 Countries. *CA A Cancer J. Clin.* 71, 209–249. doi:10.3322/caac.21660

Tang, Z., Kang, B., Li, C., Chen, T., and Zhang, Z. (2019). GEPIA2: an Enhanced Web Server for Large-Scale Expression Profiling and Interactive Analysis. *Nucleic Acids Res.* 47, W556–W560. doi:10.1093/nar/gkz430

Wang, L., Sun, L., Liu, R., Mo, H., Niu, Y., Chen, T., et al. (2021). Long Non-coding RNA MAPKAPK5-AS1/PLAGL2/HIF-1α Signaling Loop Promotes Hepatocellular Carcinoma Progression. *J. Exp. Clin. Cancer Res.* 40, 72. doi:10.1186/s13046-021-01868-z

Wang, Y., Lyu, Y., Tu, K., Xu, Q., Yang, Y., Salman, S., et al. (2021). Histone Citrullination by PADI4 Is Required for HIF-dependent Transcriptional Responses to Hypoxia and Tumor Vascularization. *Sci. Adv.* 7, eabe3771. doi:10.1126/sciadv.abe3771

Zeng, Z., Shi, Z., Liu, Y., Zhao, J., Lu, Q., Guo, J., et al. (2021). HIF-1α-activated TM4SF1-AS1 Promotes the Proliferation, Migration, and Invasion of Hepatocellular Carcinoma Cells by Enhancing TM4SF1 Expression. *Biochem. Biophysical Res. Commun.* 566, 80–86. doi:10.1016/j.bbrc.2021.06.011

Zhang, Y., Liu, S., Mickanin, C., Feng, Y., Charlat, O., Michaud, G. A., et al. (2011). RNF146 Is a poly(ADP-Ribose)-Directed E3 Ligase that Regulates Axin Degradation and Wnt Signalling. *Nat. Cell Biol.* 13, 623–629. doi:10.1038/ncb2222

Zhou, B., Yan, J., Guo, L., Zhang, B., Liu, S., Yu, M., et al. (2020). Hepatoma Cell-Intrinsic TLR9 Activation Induces Immune Escape through PD-L1 Upregulation in Hepatocellular Carcinoma. *Theranostics* 10, 6530–6543. doi:10.7150/thno.44417

Conflict of Interest: The authors declare that the research was conducted in the absence of any commercial or financial relationships that could be construed as a potential conflict of interest.

Publisher's Note: All claims expressed in this article are solely those of the authors and do not necessarily represent those of their affiliated organizations, or those of the publisher, the editors and the reviewers. Any product that may be evaluated in this article, or claim that may be made by its manufacturer, is not guaranteed or endorsed by the publisher.

GLOSSARY

AMPK, AMP-activated protein kinase

CRC, colorectal cancer

HCC: hepatocellular carcinoma

HIFs, hypoxia-inducible factors

LKB1, liver kinase B1

lncRNAs, long non-coding RNAs

miRNAs, microRNAs

mTOR, mechanistic target of rapamycin kinase

MyD88, myeloid differentiation primary response gene 88

NF-κB, nuclear factor-κB

NSCLC, non-small cell lung cancer.

PADI4, peptidylarginine deiminase 4

PARP1, poly (ADP-ribose) polymerase 1

PTEN, phosphatase and tensin homolog

RNF146, ring finger protein 146

TLR4, toll-like receptor 4

TUFT1, tuftelin1

USP13, ubiquitin specific peptidase 13

frontiers in Cell and Developmental Biology

ORIGINAL RESEARCH
published: 01 December 2021
doi: 10.3389/fcell.2021.771824

Negatively Regulated by miR-29c-3p, MTFR1 Promotes the Progression and Glycolysis in Lung Adenocarcinoma *via* the AMPK/mTOR Signalling Pathway

*Yongmeng Li[1], Yanfei Liu[2], Kai Jin[1], Rui Dong[1], Cun Gao[1], Libo Si[1], Zitong Feng[1], Huiying Zhang[1] and Hui Tian[1]**

[1]Department of Thoracic Surgery, Qilu Hospital, Cheeloo College of Medicine, Shandong University, Jinan, China, [2]Department of Anesthesiology, Qilu Children's Hospital of Shandong University, Jinan, China

OPEN ACCESS

Edited by:
Jiayi Wang,
Shanghai Jiaotong University, China

Reviewed by:
Li Zhang,
Huazhong University of Science and Technology, China
Lifang Ma,
Shanghai Jiaotong University, China
Behzad Mansoori,
Wistar Institute, United States

***Correspondence:**
Hui Tian
tianhuiql@126.com

Specialty section:
This article was submitted to Epigenomics and Epigenetics, a section of the journal Frontiers in Cell and Developmental Biology

Received: *07 September 2021*
Accepted: *18 November 2021*
Published: *01 December 2021*

Citation:
Li Y, Liu Y, Jin K, Dong R, Gao C, Si L, Feng Z, Zhang H and Tian H (2021) Negatively Regulated by miR-29c-3p, MTFR1 Promotes the Progression and Glycolysis in Lung Adenocarcinoma via the AMPK/mTOR Signalling Pathway. Front. Cell Dev. Biol. 9:771824. doi: 10.3389/fcell.2021.771824

Background: Lung adenocarcinoma (LUAD) is the major form of lung cancer that presents a major peril to public health. Owing to the high rates of morbidity, mortality and chemoresistance, it is necessary to develop more effective therapeutic targets of LUAD. Mitochondrial fission regulator 1 (MTFR1) affects the occurrence and development of some diseases by regulating mitochondrial dynamics and is dysregulated in LUAD. However, the functions and molecular mechanisms of MTFR1 in LUAD have not been investigated.

Methods: Immunohistochemical (IHC) analysis, real-time quantitative polymerase chain reaction (RT-qPCR), bioinformatic analysis and western blot (WB) were performed to assess the expression of MTFR1 at both protein and mRNA levels. The biological functions of MTFR1 in LUAD cells were assessed based on various *in vivo* and *in vitro* experiments. The dual-luciferase reporter assay and some rescue experiments were performed to evaluate the underlying mechanism of MTFR1 in LUAD.

Results: MTFR1 was upregulated in LUAD cells and tissues and correlated with dismal clinicopathologic features and a worse prognosis of patients with LUAD. Functionally, MTFR1 overexpression stimulated the proliferation, invasion, migration and glycolytic capacity and impeded the apoptosis of LUAD cells; however, opposite results were obtained when MTFR1 expression was knocked down. MTFR1, which was directly targeted by miR-29c-3p, may exert its biological functions through the AMPK/mTOR signalling pathway.

Conclusion: MTFR1 promotes the progression of LUAD. Therefore, targeting MTFR1 can offer an effective therapeutic strategy for LUAD treatment.

Keywords: lung cancer, microRNA, mitochondrial fission regulator 1, Warburg effect, proliferation, invasion, migration

INTRODUCTION

Lung cancer is a major contributor to cancer-associated mortality worldwide, and non-small cell lung cancer (NSCLC) is the major subtype constituting approximately 85% of all lung cancer cases (Chen et al., 2016; Sung et al., 2021). LUAD has been recognised as the most common NSCLC subtype which has high morbidity and fatality rates (Herbst et al., 2018). Although patients with LUAD have benefited significantly from the development of targeted therapy and immunotherapy in recent years, their clinical prognosis remains unsatisfactory. Therefore, it is necessary to discover novel therapeutic targets and biomarkers for LUAD.

Studies have revealed that abnormal metabolism is a typical characteristic of cancer cells and a key contributor to cancer progression (Feng and Levine, 2010; Hanahan and Weinberg, 2011). Mitochondria are the main energy-generating organelles, which are responsible for cellular metabolism in eukaryotic cells (McBride et al., 2006). Mitochondria are in constant dynamic equilibrium between fission and fusion to adapt to functional changes (Chan, 2006; Knott et al., 2008; Chan, 2012). The disruption of this balance may contribute to the occurrence of different diseases, including different types of cancers (Lin and Beal, 2006; Guo et al., 2020). Recent studies have indicated that dysfunctional mitochondrial fission is involved in the progression of some malignancies, including glioblastoma, liver cancer and gastric cancer (Hernandez-Alvarez and Zorzano, 2021; Lenzi et al., 2021; Zhu et al., 2021). Furthermore, some studies have indicated that mitochondrial dynamics have an imperative function in the chemoresistance of cancer cells (Kong et al., 2015; Cai et al., 2016; Huang et al., 2018). Mitochondrial fission regulator 1 (MTFR1), previously called CHPPR or FAM54A2, is a mitochondrial protein with a polyproline-rich region (Tonachini et al., 2004). Some studies have indicated that MTFR1 can promote mitochondrial fission and regulate cellular respiration (Tonachini et al., 2004; Monticone et al., 2010). In addition, MTFR1 has a vital function in oral squamous cell carcinoma, acute myocardial infarction (AMI) and head and neck squamous cell carcinoma (HNSCC) (Wang et al., 2015; Reddy et al., 2019; Huang et al., 2020). Moreover, bioinformatic analyses in a study have indicated that MTFR1 is dysregulated in LUAD (Sanada et al., 2019). However, the function and mechanism of action of MTFR1 in LUAD remain investigated.

MicroRNAs (miRNAs), which are small non-coding RNAs spanning approximately 21 nucleotides, usually impede gene expression by binding to the 3′ untranslated region (3′-UTR) of their target mRNAs (Bartel, 2004). A study has indicated that miRNAs are involved in the regulation of most mammalian mRNAs (Friedman et al., 2009). Therefore, it does not come as a surprise that the dysregulation of miRNA expression may cause a multitude of diseases including cancers (Jiang et al., 2009; Li et al., 2021). miR-29c-3p suppresses the progression of various cancer types, including intrahepatic cholangiocarcinoma, cervical cancer, ovarian cancer and oesophageal cancer (Wang H. et al., 2020; Feng et al., 2020; Hozaka et al., 2021; Zou et al., 2021). However, to date, the expression level and function of miR-29c-3p in LUAD have yet to be investigated.

In this study, we aimed to assess the expression level, biological role and underlying molecular mechanism of MTFR1 in LUAD. We reported for the first time that MTFR1 is overexpressed in LUAD cells and tissues. Furthermore, MTFR1 stimulated the progression of LUAD both *in vivo* and *in vitro*. We propose that MTFR1 is a direct target of miR-29c-3p and may exert its biological effects *via* the AMPK/mTOR signalling pathway. Therefore, this study offers novel insights into the role of MTFR1 as an effective therapeutic target for LUAD treatment.

METHODS

Data Processing

Gene expression data were downloaded from The Cancer Genome Atlas (TCGA, https://tcga-data.nci.nih.gov/tcga/), Genome–Tissue Expression (GTEx, https://www.ncbi.nlm.nih.gov/geo/) and Gene Expression Omnibus (GEO, https://www.ncbi.nlm.nih.gov/geo/) databases. The target miRNAs were predicted using the following bioinformatics software: miRbase (www.mirbase.org), starBase (http://starbase.sysu.edu.cn), miRWalk (www.umm.heidelberg.de/apps/zmf/mirwalk) and miRDB (http://mirdb.org/miRDB).

Collection of Clinical Tissue Specimens

A total of 85 LUAD tissues and matched paracancerous normal tissues of the lung were obtained from our tissue bank to establish the tissue microarray. All tissue samples were extracted through surgical resection at the Department of Thoracic Surgery, Qilu Hospital of Shandong University from 2004 to 2014. In addition, 20 paired fresh LUAD tissues and corresponding paracancerous tissues were obtained immediately after surgical resection in patients with LUAD admitted to our department. This study was reviewed and approved by the Medical Ethics Committee of Qilu Hospital of Shandong University (Approval No. KYLL-2016-097). The patients included in this study or their family members were requested to sign an informed consent document.

Cell Culture and Treatment

A total of five LUAD cell lines (H1299, PC9, A549, H1975, and H157), human embryonic kidney 293 (HEK293) cells and human bronchial epithelial (HBE) cells were provided by the Shanghai Academy of Science (Shanghai, China). The cell lines were cultured in RPMI-1640 medium supplemented with 10% foetal bovine serum (FBS; Gibco, NY, United States). The cells were incubated in a moistened environment with 5% CO_2 at 37°C. The sh-NC, sh-MTFR1, oe-NC and oe-MTFR1 lentiviruses (Jikai Co., Shanghai, China) were transduced into the corresponding cells. The sh-RNA sequences are listed in **Supplementary Table S1**. The cells that were stably transduced were selected using puromycin (2 μg/ml) for 7 days after transduction. Mimics-miR-29c-3p, inhibitor-miR-29c-3p and their corresponding negative controls (NCs) were obtained from GenePharma Co., Ltd. (Shanghai, China). The oligonucleotide sequences were as follows: mimics-miR-29c-3p (5′-UAGCACCAUUUGAAAUCG GUUA-3′), mimics-NC (5′-UUCUCCGAACGUGUCACG UTT-3′), inhibitor-miR-29c-3p (5′-UAACCGAUUUCAAAU

GGUGCUA-3′) and inhibitor-NC (5′-CAGUACUUUUGU GUAGUACAA-3′). The cells were transfected with miRNAs using the jetPRIME transfection reagent (Polyplus-transfection, Illkirch, France) according to the manufacturer's protocol.

Western Blot

Proteins extracted using the radioimmunoprecipitation assay (RIPA) reagent were quantified using a BCA kit (Biyuntian, China). Subsequently, the protein lysates were separated using 6% or 10% sodium dodecyl sulfate-polyacrylamide gel electrophoresis (SDS-PAGE) gels and transferred onto polyvinylidene difluoride (PVDF) membranes. Furthermore, 5% non-fat milk was used to block the membranes at ambient temperature for 1 h. The membranes were subsequently washed with TBST (thrice for 10 min each) and were incubated overnight with primary antibodies at 4°C, followed by incubation with a secondary antibody at ambient temperature for 1 h. Eventually, bands were visualised using an enhanced chemiluminescence (ECL) system. β-tubulin was used as the internal control. The following antibodies were used in this study: anti-N-cadherin (ab18203, Abcam), anti-MTFR1 (ab198192, Abcam), anti-Vimentin (ab92547, Abcam), anti-p-mTOR (ab109268, Abcam), anti-E-cadherin (ab40772, Abcam), anti-mTOR (ab32028, Abcam), anti-Snail (ab216347, Abcam), anti-p-AMPK (ab133448, Abcam), anti-Slug (ab27568, Abcam), anti-Ki-67 (ab16667, Abcam), anti-AMPK (ab32047, Abcam), anti-PARP (ab32064, Abcam), anti-BAX (32503, Abcam), anti-BCL-2 (ab32124, Abcam) and anti-β-Tubulin (ab18207, Abcam).

RNA Isolation and Real-Time Quantitative Polymerase Chain Reaction

Extraction of Total RNA was extracted using the RNAfast200 kit (Fastagen, Shanghai, China). Complementary DNA (cDNA) was synthesised using a reverse transcription kit (Toyobo, Osaka, Japan) according to the manufacturer's instructions. RT-qPCR was then executed in Bio-Rad IQ 5 system (Bio-Rad) using the SYBR Green Supermix (Toyobo, Osaka, Japan). The primers used include the following: *MTFR1* (F, 5′-TGCAACAGAATGGAG TCCCA-3′ and R, 5′-AAGGGGTGGCCTTGATCTGA-3′); *GAPDH* (F, 5′-GCACCGTCAAGGCTGAGAAC-3′ and R, 5′-TGGTGAAGACGCCAGTGGA-3′); miR-29c-3p (F, 5′-CTC CTCCTTTTAGCACCATTTG-3′ and R, 5′-TATGCTTGTTCT CGTCTCTGTGTC-3′) and *U6* (F, 5′-CAGCACATATACTAA AATTGGAACG-3′ and R, 5′-ACGAATTTGCGTGTCATCC-3′). *U6* and *GAPDH* were used as internal references, and all the aforementioned primers were obtained from GenePharma Co., Ltd. (Shanghai, China). The experiment was repeated thrice, and data were analysed using the $2^{-\triangle\triangle Ct}$ method.

Haematoxylin–Eosin Staining and Immunohistochemical Analysis

First, the formalin-fixed and paraffin-embedded tissues samples were split into smaller sections of 4 μm. For HE staining, each section was dewaxed, rehydrated and stained with HE, and images were captured using an inverted microscope. With regards to IHC, each section was dewaxed, rehydrated and incubated with primary antibodies overnight at 4°C, followed by incubation with a secondary antibody at ambient temperature for 1 h. Subsequently, the sections were viewed, and an inverted microscope was used to capture images. Lastly, histochemical scoring (H-score) was used to assess the results of IHC analysis as previously described (Xie et al., 2014). The following antibodies were used: anti-MTFR1 (ab198192, Abcam) and anti-Ki-67 (ab16667, Abcam).

Cell Counting Kit-8 Cell Proliferation Assay

The transduced cells were seeded into 96-well plates (2,000 cells/well) and cultured for 24, 48, 72, and 96 h, sequentially. Subsequently, 10 μL of CCK-8 solution (5 mg/ml; Solarbio, China) was added to each well. After incubating the cells for 2 h in dark, absorbance was recorded at 450 nm using a microplate reader. The experiment was performed in triplicates.

EdU Staining

The transduced cells were seeded into 96-well plates (5×10^3/well) and incubated with complete RPMI-1640 medium containing 5-ethynyl-2-′deoxyuridine (EdU; 1000:1) for 2 h. EdU staining was performed using an EdU kit (RiboBio, Guangzhou, China) according to the manufacturer's protocol. Lastly, the stained cells were photographed using a fluorescence microscope. The experiment was performed in triplicates.

Colony Formation Assay

The transduced cells were seeded in 6-well plates (1,000 cells/well) and incubated for 15 days. Then the cells were fixed with 4% paraformaldehyde for 30 min and stained with 0.1% crystal violet for 15 min. Subsequently, the cells were washed thrice with phosphate-buffered saline (PBS). Lastly, a digital camera was used to capture images. The experiment was performed in triplicates.

Analysis of Cell Cycle and Apoptosis

The cell cycle and apoptosis were assessed using a flow cytometer (BD Biosciences, United States). A propidium iodide (PI) staining kit (Yeasen, Shanghai, China) was used to analyse the cell cycle, whereas the Annexin V-APC Apoptosis Detection Kit (eBioscience, Thermo Fisher) was used to assess cell apoptosis according to the manufacturer's protocol. The experiments were performed in triplicates.

Wound-Healing Assay

The transduced cells were seeded in 6-well plates until they attained confluency. Subsequently, a graze in the monolayer was created using the tip of a 200-μL pipette. After three PBS washes, the medium was replaced with serum-free media (SFM). Subsequently, the width of the wound was visualised and assessed under a microscope at 0 and 24 h. The experiment was performed in triplicates.

Transwell Assay

Cell suspensions (5×10^4 cells/200 uL of SFM) were added to the upper Transwell chamber with or without Matrigel, whereas

600 uL of a medium supplemented with 20% FBS was added to the lower Transwell chamber. After 24 h, the cells in the upper chamber were removed, and those that entered or moved to the lower chamber were fixed using 75% ice-cold alcohol for 30 min. Subsequently, the cells were stained with 0.1% crystal violet for 20 min, and an inverted microscope was used to capture images. The experiment was performed in triplicates.

Measurement of Glucose, Lactate and Extracellular Acidification Rate

The transduced cells were seeded in 6-well plates (1×10^5 cells/well) and incubated for 48 h. Subsequently, the culture medium was harvested, and the levels of glucose and lactate were measured using the CheKine™ Glucose Assay Kit (Abbkine, Wuhan, Hubei, China) and CheKine™ Lactate Assay Kit (Abbkine, Wuhan, Hubei, China), respectively, according to the manufacturer's protocol. For ECAR measurement, cells were seeded into a Seahorse XF 96 cell culture micro-plate and incubated overnight (1×10^4/well; Agilent Technologies). The next day, a Seahorse XFe96 Analyzer (Agilent Technologies) was used to measure the ECAR with a Seahorse XF Glycolysis Stress Test Kit (Agilent Technologies) following the manufacturer's protocols. Data were analysed by the Seahorse XF 96 Wave software. The above experiments were performed in triplicates.

Dual-Luciferase Reporter Assay

HEK-293T cells were seeded into 24-well plates (5×10^4 cells/well). After incubating the cells for 24 h, they were transiently co-transfected with mimics-NC or mimics-miR-29c-3p together with the mutated (MUT) 3′-UTR or wild-type (WT) *MTFR1* mRNA. After 48 h, the luciferase activity was assessed using a dual-luciferase assay kit (Promega). The experiment was replicated in triplicates.

In Vivo Experiments

We procured 4-week-old BALB/c nude mice from GemPharmatech Co., Ltd. (Nanjing, China). To establish a xenograft tumour model, 20 nude mice were categorised randomly into four cohorts. Subsequently, 5×10^6 transduced A549 cells (LV-sh-MTFR1 and LV-sh-NC) or PC9 cells (LV-oe-MTFR1 and LV-oe-NC) were hypodermically implanted into the right armpit area of each mouse. The tumour size was measured every 4 days. The tumour volumes were computed using the following formula: $V = (\text{length} \times \text{width}^2)/2$. The nude mice were sacrificed on the 28th day, and all tumours were collected and weighed. To construct an experimental model for lung metastasis, 20 nude mice were randomly divided into four cohorts, and 2×10^6 transduced cells were introduced into the mice *via* an injection in the tail vein. The mice were euthanised after 2 months, and their lungs were obtained. All specimens were further stained with IHC or HE. The animal experiments were approved by the Shandong University Animal Research Ethics Committee under a project license (SCXK Lu 20090001).

Statistical Analysis

Data were expressed as the mean ± standard deviation (SD). Data were analysed using the GraphPad Prism (GraphPad version 8) and R (version 4.0.3) software. The Student's *t*-test (two-sided), chi-square test, Pearson's correlation analysis and Kaplan–Meier (KM) survival analysis were performed as indicated. Multiple groups were compared for identifying statistically significant differences using one-way analysis of variance (ANOVA). The observed differences were considered statistically significant at $p < 0.05$.

RESULTS

MTFR1 was Overexpressed in LUAD Cells and Tissues and Associated With a Poor Prognosis

First, we compared *MTFR1* gene expression between normal lung tissues and LUAD tissues using high-throughput data from the GEO, TCGA and GTEx databases. *MTFR1* was considerably overexpressed in LUAD tissues as compared with normal lung tissues ($p < 0.0001$, **Figures 1A,B**). The KM analysis revealed that elevated MTFR1 expression was associated with a poor prognosis in patients with LUAD in the TCGA cohort ($p = 0.0088$, **Figure 1C**). Furthermore, the mRNA and protein expression of MTFR1 was evaluated in 20 pairs of clinical samples. As demonstrated in **Figures 1D,E**, compared with those in the adjacent normal lung tissues, the protein and mRNA levels of MTFR1 were considerably elevated in LUAD tumour tissues. A total of 85 pairs of LUAD tissues and their corresponding adjoining normal lung tissues were subjected to IHC analysis with MTFR1 antibody, and the representative pictures are shown in **Figure 1F**. Furthermore, the expression of MTFR1 was quantified in each tissue sample. The result of IHC scoring revealed that the expression of MTFR1 was considerably elevated in LUAD tissues as compared with that in adjoining normal lung tissues. ($p < 0.001$, **Figure 1G**). The correlation between MTFR1 expression and clinical features of patients with LUAD was further examined. High MTFR1 expression was significantly related to the clinical stage ($p = 0.007$), lymph node metastasis ($p = 0.016$) and tumour size ($p = 0.023$) (**Table 1**). In addition, survival analysis revealed that patients with an elevated MTFR1 expression level exhibited worse clinical outcomes ($p = 0.002$, **Figure 1H**). Lastly, MTFR1 expression was examined in various cell lines. At both protein and mRNA levels, the expression of MTFR1 in LUAD cell lines was considerably higher than that in HBE cells (**Figures 1I,IJ**). Altogether, the results indicated that MTFR1 was upregulated in LUAD cells and tissues and associated with a poor prognosis in patients with LUAD.

MTFR1 Promoted the Proliferation and Inhibited the Apoptosis of LUAD Cells

sh-RNA 2 had the best knockdown efficiency among these three sh-RNAs (**Supplementary Table S1**; **Supplementary Figure**

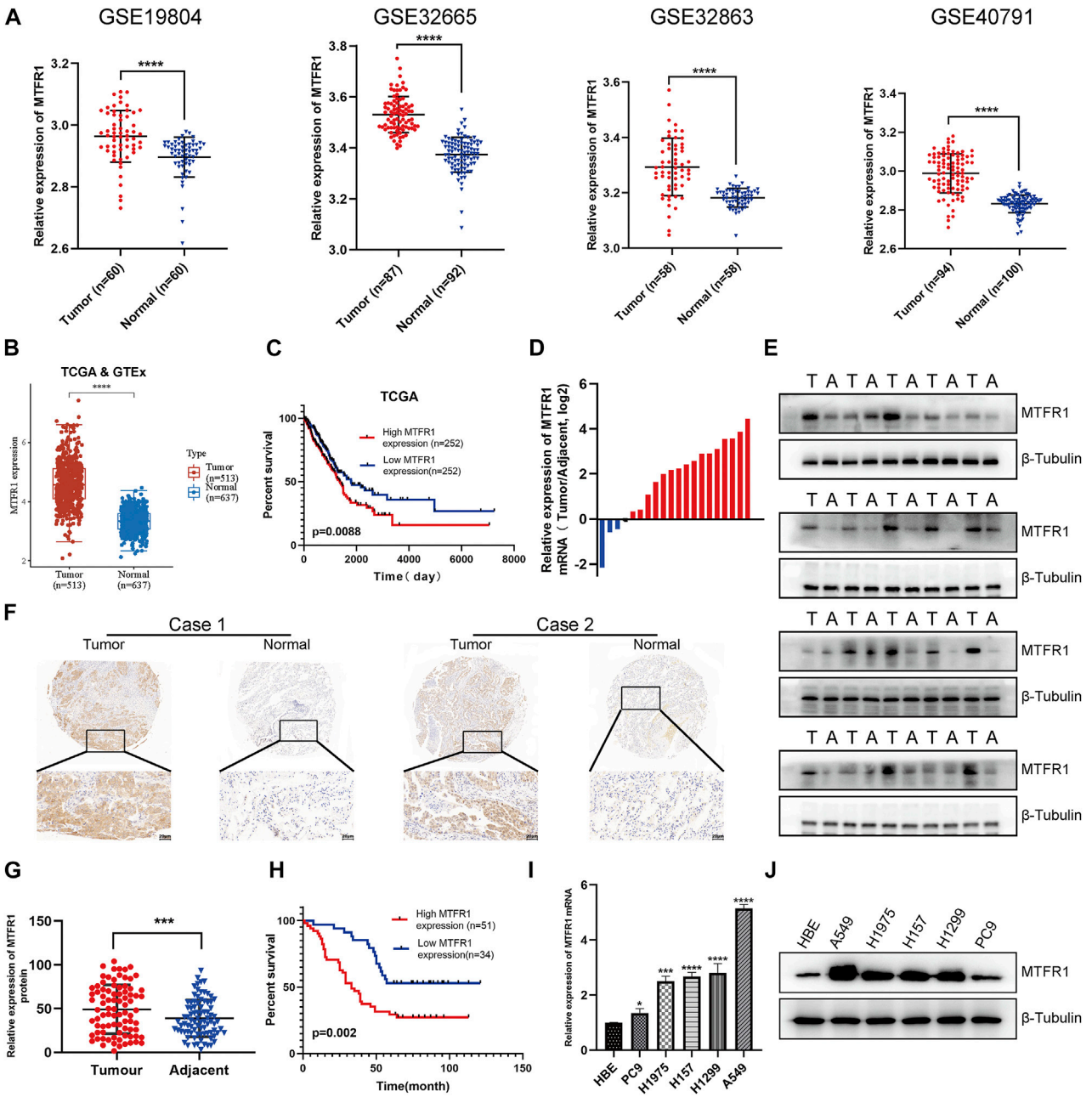

FIGURE 1 | Mitochondrial fission regulator 1 (MTFR1) was overexpressed in lung adenocarcinoma (LUAD) cell lines and tissues. **(A)** The expression levels of MTFR1 in four Gene Expression Omnibus (GEO) datasets. **(B)** MTFR1 expression levels in The Cancer Genome Atlas (TCGA) and Genome–Tissue Expression (GTEx) databases. **(C)** Kaplan–Meier (KM) analysis for TCGA-LUAD samples. **(D, E)** The relative mRNA and protein expression of MTFR1 in 20 pairs of LUAD tumour (T) tissues and their matching adjoining (A) normal tissues. **(F)** Representative immunohistochemical images of LUAD and adjacent nonmalignant specimens stained for analysing MTFR1 expression. **(G)** The immunohistochemical score of 85 pairs of LUAD tissues and adjoining paracancerous tissues ($p < 0.001$). **(H)** Kaplan–Meier survival analyses of 85 patients with LUAD. **(I, J)** The relative protein and mRNA expression of MTFR1 in different cell lines. Data were articulated as the mean ± standard deviation (SD; $^{*}p < 0.05$, $^{***}p < 0.001$, $^{****}p < 0.0001$).

S1A), so that it was selected for the subsequent experiments. Because MTFR1 was expressed at high levels in A549 and H1299 cells but at low levels in PC9 cells (**Figures 1I,J**). Therefore, we downregulated the expression of MTFR1 in A549 and H1299 cells and upregulated its expression in PC9 cells using lentiviral transduction. After transduction, MTFR1 expression was considerably downregulated in A549 and H1299 cells and upregulated in PC9 cells (**Figures 2A,B**). The proliferative ability of the stably transduced A549, H1299, and PC9 cells were then detected using EdU, colony formation and CCK-8

TABLE 1 | Correlation between MTFR1 expression and clinicopathological features in LUAD.

Clinicopathological factors	Sample	MTFR1 expression		*p* value
		High (H-score>40)	Low (H-score ≤40)	
Gender				
Male	50	29	21	0.822
Female	35	22	13	
Age(y)				
≥60	45	25	20	0.506
<60	40	26	14	
Smoking history				
Smoker	52	28	24	0.177
Nonsmoker	33	23	10	
Tumor size (cm)				
<3	21	8	13	***0.023**
≥3	64	43	21	
Lymph node metastasis				
With	44	32	12	***0.016**
Without	41	19	22	
Clinical stage				
I ~ II	49	23	26	****0.007**
III ~ IV	36	28	8	

*LUAD, lung adenocarcinoma; *p < 0.05, **p < 0.01, $\chi 2$ test. High MTFR1 expression was significantly related to the clinical stage, lymphnode metastasis and tumour size.*

assays. The results of these assays revealed that the proliferative ability of sh-MTFR1 A549 and H1299 cells was significantly reduced as compared with that of the cells in the sh-NC groups. However, the proliferative ability of oe-MTFR1 PC9 cells was higher than that of PC9 cells in the oe-NC group (**Figures 2C**, **3A**,**B**). Furthermore, flow cytometry was employed to identify the effects of MTFR1 on the cell cycle progression and apoptosis of LUAD cells. The results revealed that MTFR1 knockdown could promote cell apoptosis in A549 and H1299 cells, whereas MTFR1 upregulation could reduce apoptosis in PC9 cells (**Figure 3C**). In addition, we observed that MTFR1 had no apparent effect on cell cycle progression (figure not shown). Lastly, cell proliferation and apoptosis-related proteins were identified in transduced A549, H1299 and PC9 cells. The expression of Ki-67 and Bcl-2 proteins was decreased, whereas that of PARP and BAX proteins was increased after the knockdown of MTFR1 in H1299 and A549 cells. However, we observed opposite results after upregulating MTFR1 expression in PC9 cells (**Figure 3D**). These results indicated that MTFR1 promoted the proliferation and inhibited the apoptosis of LUAD cells.

MTFR1 Promoted the Migration and Invasion of LUAD Cells

To assess the impact of MTFR1 on the migratory and invasive abilities of LUAD cancer cells, we performed Transwell and wound-healing assays. The results of the Transwell assay revealed that the numbers of invaded and migrated cells were considerably decreased after MTFR1 knockdown in H1299 and A549 cells (**Figures 4A,B**). Consistently, the numbers of invaded and migrated cells were considerably higher in the oe-MTFR1 cohort than in the oe-NC cohort (**Figure 4C**; $p < 0.01$). The results of the wound-healing assay revealed that MTFR1 downregulation in H1299 and A549 cells was associated with a considerably smaller wound closure area in the sh-MTFR1 cohort than in the NC cohort (**Figures 4D,E**; $p < 0.001$). However, when MTFR1 was upregulated in PC9 cells, the wound closure area was considerably larger in the oe-MTFR1 cohort than in the oe-NC cohort (**Figure 4F**; $p < 0.01$). Because epithelial–mesenchymal transition (EMT) is vital for tumour invasion and metastasis, we assessed the expression of EMT-related proteins in the transduced cells. The results revealed that MTFR1 knockdown decreased the expression of vimentin, N-cadherin, snail, and slug proteins but increased the expression of E-cadherin in H1299 and A549 cells. However, contradictory results were obtained when MTFR1 was upregulated in PC9 cells (**Figure 4G**). Altogether, these results suggested that MTFR1 stimulated the migration and invasion of LUAD cells.

MTFR1 Regulated Glycolysis and the AMPK/mTOR Signalling Pathway in LUAD Cells

To investigate whether MTFR1 affected glycolysis in LUAD cells, we measured the ECAR, the glucose consumption and lactate production rates in the transduced LUAD cells. The rates were increased in PC9 cells after MTFR1 overexpression whereas decreased in H1299 and A549 cells after MTFR1 downregulation (**Figures 5A–C**). These findings indicated that MTFR1 promoted aerobic glycolysis in LUAD cells.

Many studies have reported that the AMPK/mTOR signalling pathway is involved in the regulation of tumour metabolism. Therefore, we detected the expression of the major molecules that participate in the AMPK/mTOR pathway (mTOR, p-mTOR, AMPK, and p-AMPK). The results indicated that the expression of p-MTOR was reduced whereas that of p-AMPK was elevated when MTFR1 expression was downregulated in H1299 and A549 cells. However, contrasting effects were obtained when MTFR1 expression was upregulated in PC9

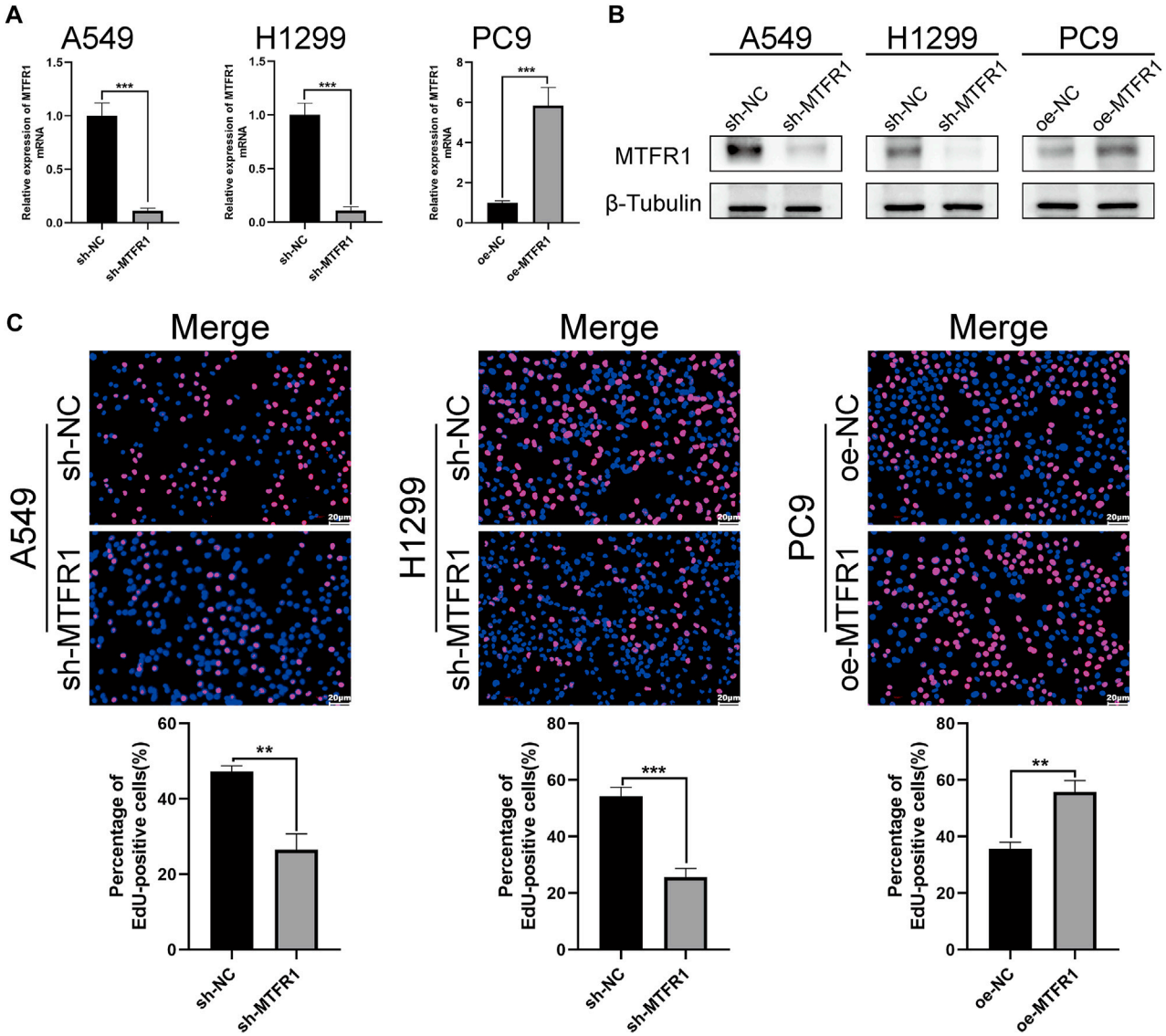

FIGURE 2 | MTFR1 stimulated the proliferation of LUAD cells. **(A, B)** Evaluation of the effectiveness of lentiviral transduction by real-time quantitative polymerase chain reaction (RT-qPCR) and western blotting (WB). **(C)** EdU staining of the transduced cells. Data were articulated as the mean ± standard deviation (SD; $^{**}p < 0.01$, $^{***}p < 0.001$).

cells (**Figure 5D**). In conclusion, MTFR1 may exert its pro-oncogenic functions by targeting the AMPK/mTOR signalling pathway in LUAD cells.

MTFR1 was Directly Targeted by miR-29c-3p

First, we predicted the upstream miRNAs of MTFR1 based on bioinformatic analysis and chose three of them for primary study (**Supplementary Tables S2, S3**). After transfecting the inhibitors and mimics of these three miRNAs into the corresponding cells, we observed that miR-29c-3p had the most obvious effects on MTFR1 expression (**Supplementary Figure S1B–D**). Thus, we eventually selected miR-29c-3p for further study. At the cellular level, miR-29c-3p expression was noticeably higher in HBE cells than in the four LUAD cell lines (**Figure 6A**). At the tissue level, miR-29c-3p expression was higher in paracancerous tissues than that in the LUAD tissues (**Figure 6B**). Moreover, KM survival analysis demonstrated that elevated expression of miR-29c-3p was associated with a good prognosis in patients with LUAD in the TCGA cohort ($p = 0.018$; **Figure 6C**). Furthermore, we searched the starBase database to assess the relationship between MTFR1 and miR-29c-3p expression in patients with LUAD. We found miR-29c-3p expression exhibited an inverse relationship with MTFR1 expression (**Figure 6D**; $r = -0.283$, $p < 0.0001$). Subsequently, we performed the dual-luciferase reporter assay to further assess whether a direct regulatory correlation existed between MTFR1 and miR-29c-3p. Fluorescence intensity

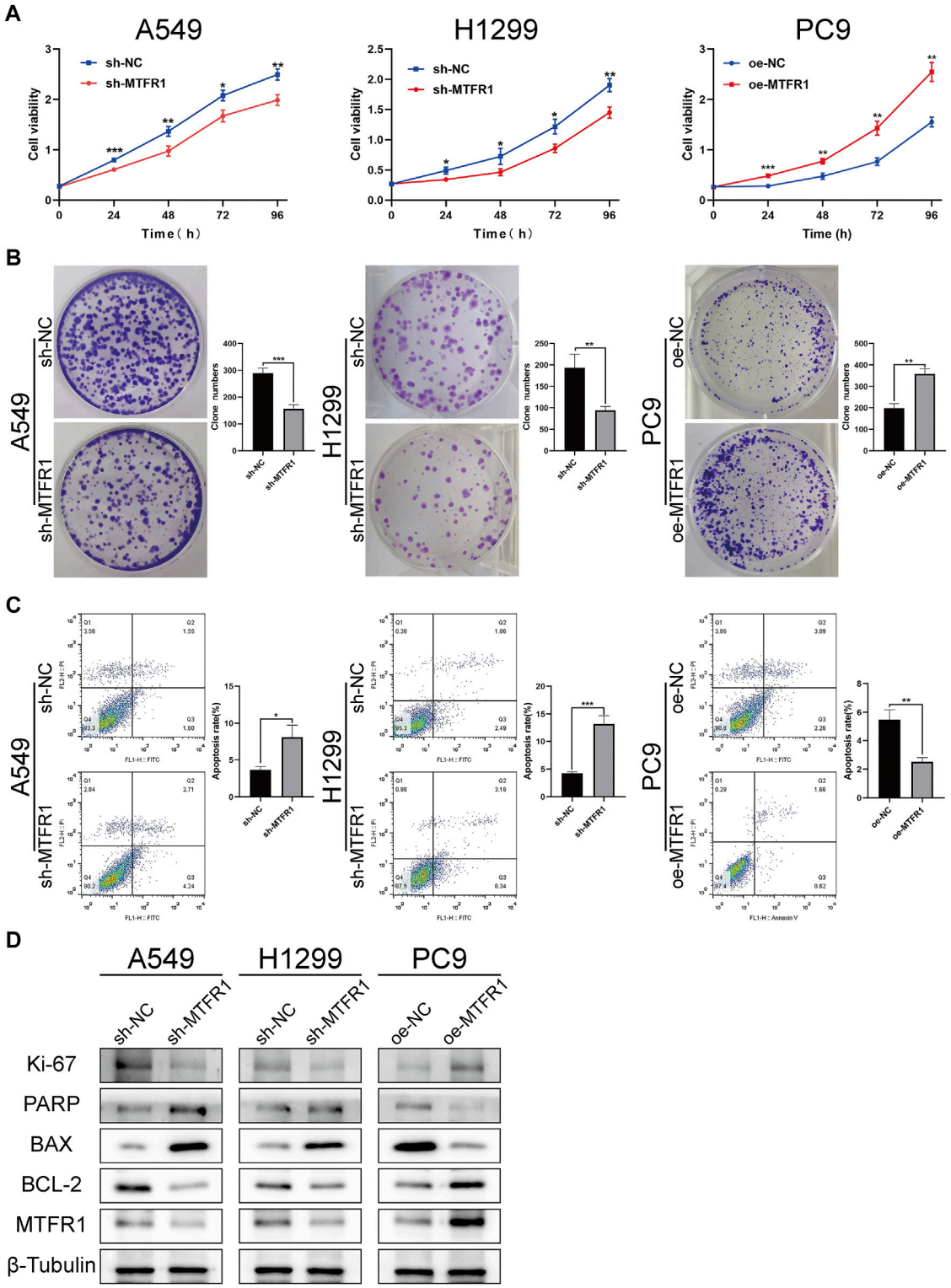

FIGURE 3 | MTFR1 stimulated proliferation and suppressed apoptosis of LUAD cells. **(A)** Cell Counting Kit-8 (CCK-8) assay of the transduced cells. **(B)** Colony formation assay of the transduced cells. **(C)** Evaluation of apoptosis by flow cytometry. **(D)** Evaluation of the expression of cell proliferation and apoptosis-related protein by WB. Data were articulated as the mean ± standard deviation (SD; $*p < 0.05$, $**p < 0.01$ $***p < 0.001$).

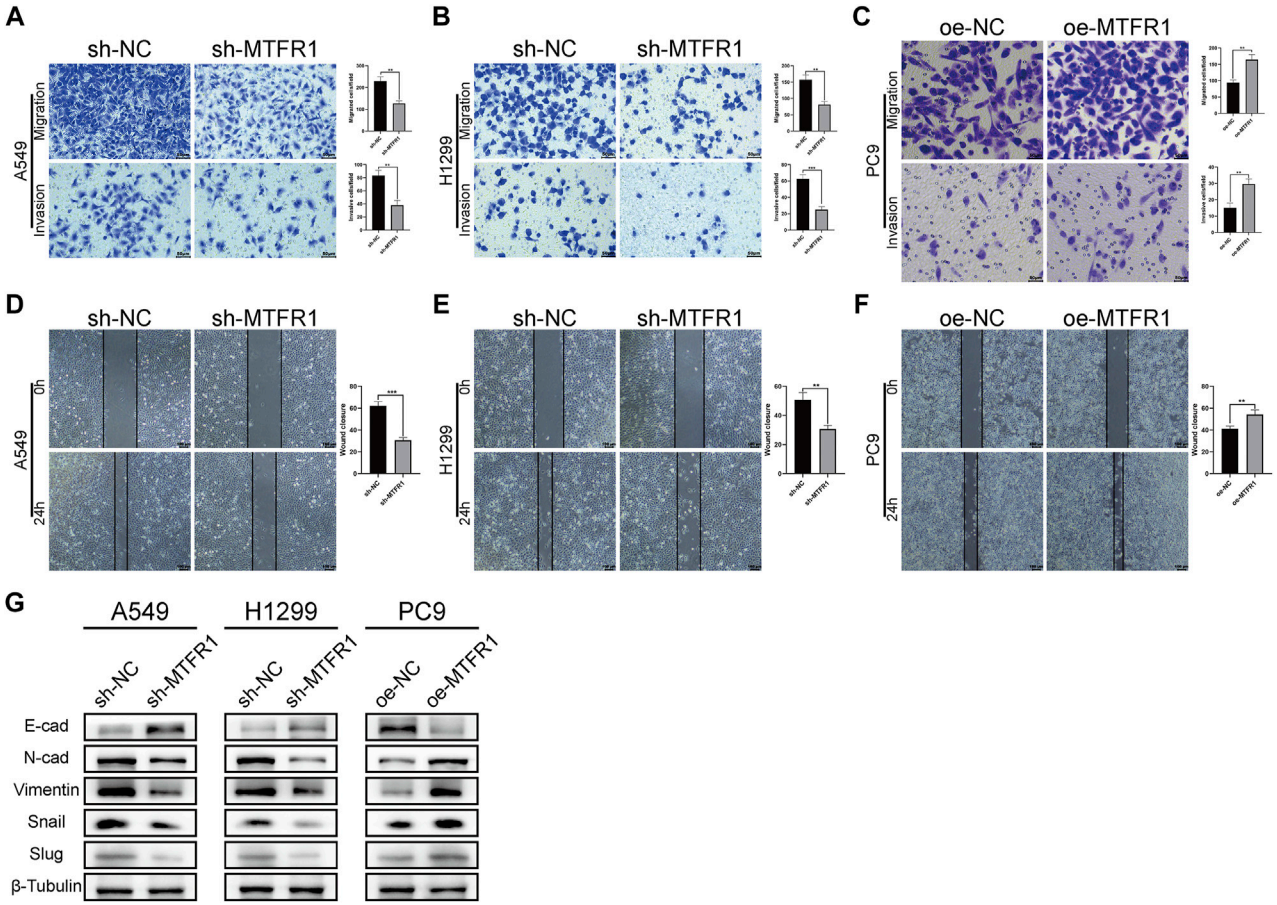

FIGURE 4 | (A–F) Evaluation of the invasion and migration abilities of transduced cells by Transwell and wound-healing assays. **(G)** Evaluation of the levels of epithelial–mesenchymal transition (EMT)-related proteins by WB. Data were articulated as the mean ± standard deviation (SD; $^{**}p < 0.01$ $^{***}p < 0.001$).

in the mimics-miR-29c-3p + MTFR1 WT cohort was lower than that in the other cohorts ($p < 0.0001$) as demonstrated in **Figure 6E**. These results indicated that miR-29c-3p could directly bind to the 3′-UTR of MTFR1 mRNA. **Figure 6F** demonstrates the predicted binding sites between *MTFR1* mRNA and miR-29c-3p. Lastly, we transfected A549 and H1299 cells with inhibitor-miR-29c-3p and PC9 cells with mimics-miR-29c-3p to evaluate the expression of miR-29c-3p and MTFR1. We observed that when miR-29c-3p expression was upregulated in H1299 and A549 cells, MTFR1 was downregulated at both protein and mRNA levels; however, when miR-29c-3p expression was downregulated in PC9 cells, MTFRI was upregulated at both protein and mRNA levels (**Figures 6G–I**). In conclusion, these results revealed that MTFR1 was directly targeted by miR-29c-3p.

miR-29c-3p Could Partly Rescue the Phenotypic Changes Caused by MTFR1

We performed rescue experiments to assess whether MTFR1 was functionally regulated by miR-29c-3p. First, we transfected sh-MTFR1 A549 and H1299 cells with inhibitor-miR-29c-3p and oe-MTFR1 PC9 cells with mimics-miR-29c-3p and evaluated the transfection efficiency at both protein and mRNA levels (**Figures 7A,B**). Furthermore, the results of CCK-8 and Transwell assays revealed that miR-29c-3p could reverse the phenotypic changes on the proliferation, migration and invasion of LUAD cells caused by MTFR1 (**Figures 7C,D**). Moreover, the evaluation of ECAR, glucose and lactate levels indicated that miR-29c-3p could rescue the changes in glycolytic capacity induced by MTFR1 (**Figures 8A–C**). Moreover, the expression of proteins associated with cell proliferation, apoptosis, EMT and AMPK/mTOR pathway changed accordingly (**Figures 8D–F**). Altogether, the results indicated that phenotype changes induced by MTFR1 could be reversed by miR-29c-3p.

MTFR1 Promoted Tumour Growth and Metastasis *in Vivo*

A tumour xenograft-harbouring nude mouse model and a tail-vein injection-induced metastasis model were constructed to assess the *in vivo* impacts of MTFR1 on tumour growth and metastasis. Tumours in the sh-NC cohort exhibited a faster growth rate than that of the sh-MTFR1 cohort. Moreover, the

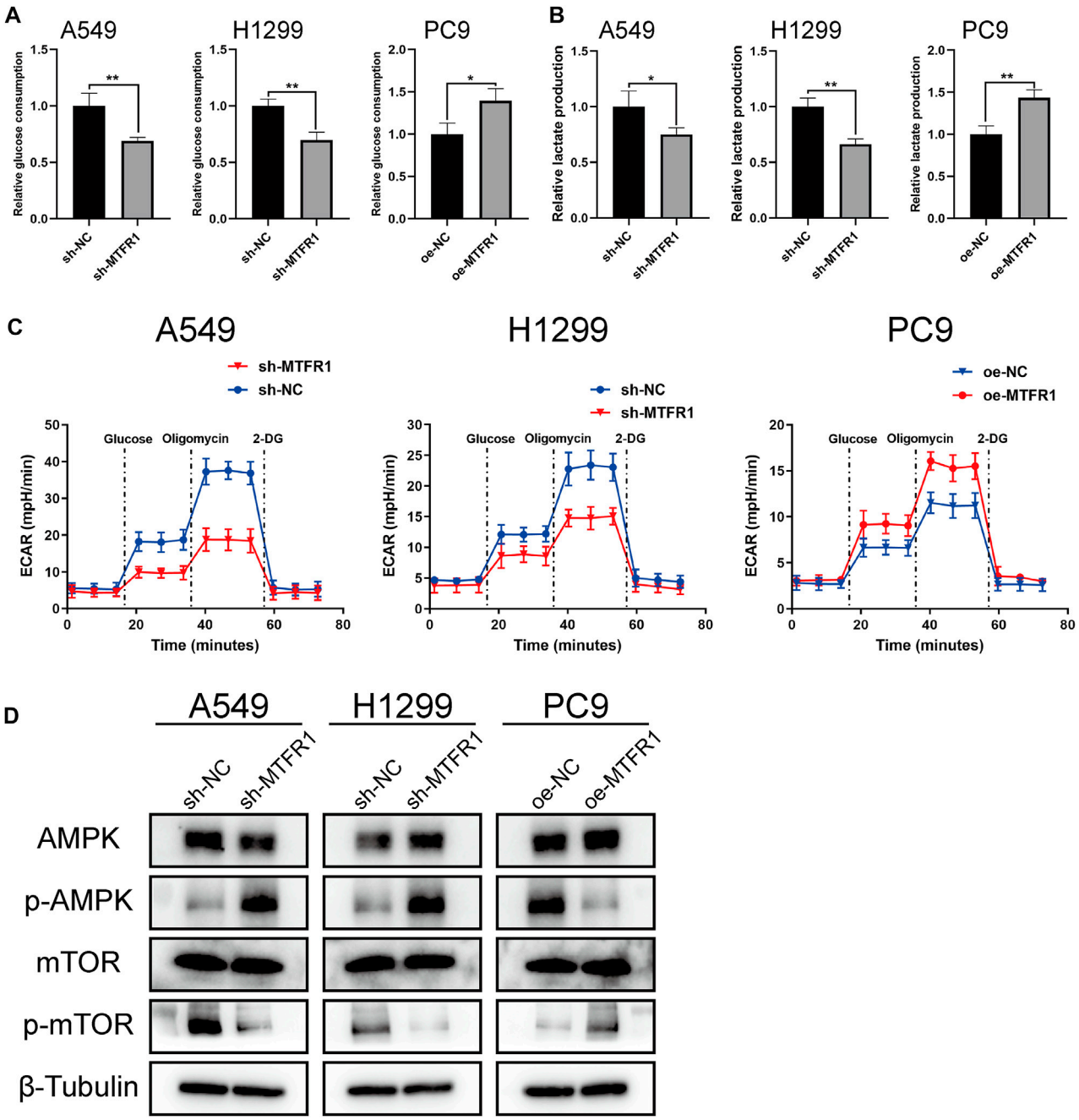

FIGURE 5 | MTFR1 regulated glycolysis and AMPK/mTOR signalling pathway in LUAD cells. **(A)** Relative glucose consumption of the transduced cells. **(B)** Relative lactate production of the transduced cells. **(C)** Relative extracellular acidification rate (ECAR) of the transduced cells. **(D)** Evaluation of the expression of AMPK, p-AMPK, mTOR, and p-mTOR in the transduced cells by WB. Data were articulated as the mean ± standard deviation (SD; $^{*}p < 0.05$, $^{**}p < 0.01$).

average tumour weight and volume in the sh-NC cohort were significantly higher than those in the sh-MTFR1 cohort (**Figure 9A**). Simultaneously, tumours in the oe-MTFR1 cohort exhibited a faster growth rate and a significantly higher average weight and volume than those in the oe-NC group (**Figure 9B**). Furthermore, HE staining and IHC analysis were performed on tumour xenografts to analyse Ki-67 and MTFR1 expressions. Groups with high MTFR1 expression exhibited higher Ki-67 expression than that exhibited by groups with low MTFR1 expression (**Figure 9C**). The results of the lung metastasis model assay revealed that MTFR1 overexpression increased and MTFR1 knockdown decreased the number of lung metastatic nodules (**Figure 9D**). Altogether, the results indicated that MTFR1 promoted LUAD tumour growth and metastasis *in vivo*.

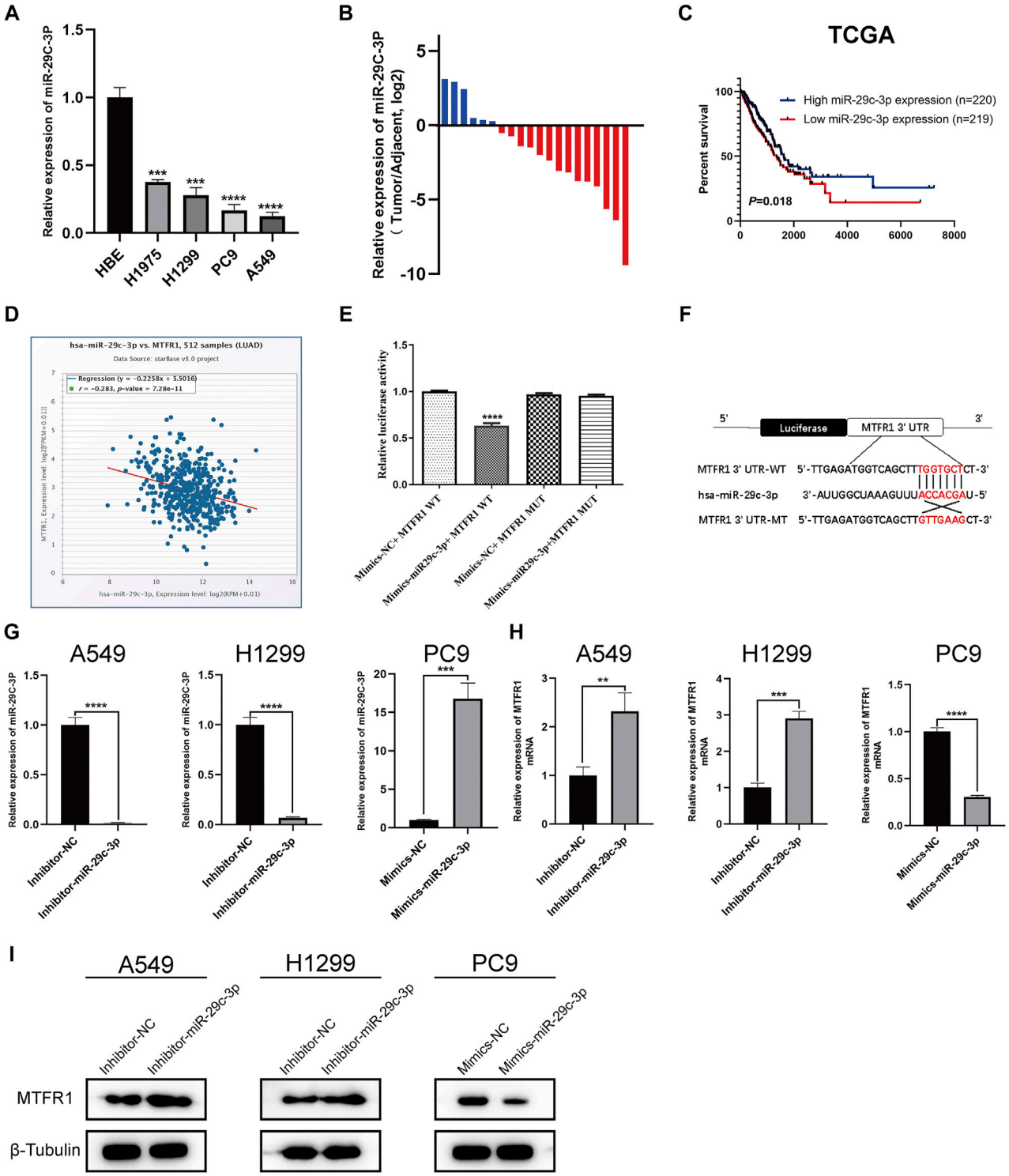

FIGURE 6 | MTFR1 is directly targeted by miR-29c-3p. **(A)** miR-29c-3p expression in different cell lines. **(B)** The relative expression of miR-29c-3p in 20 pairs of LUAD tissues and their corresponding adjoining paracancerous tissues. **(C)** Kaplan–Meier analysis of TCGA LUAD samples based on miR-29c-3p expression. **(D)** Pearson's correlation analysis for assessing the relationship between miR-29c-3p and MTFR1 expression. **(E, F)** Results of the dual-luciferase reporter assay and the predicted binding site between miR-29c-3p and MTFR1 3′-UTR. **(G–I)** The expression of miR-29c-3p and MTFR1 in cells transfected with inhibitor-miR-29c-3p or mimic-miR-29c-3p. Data were articulated as the mean ± standard deviation (SD; $^{**}p < 0.01$, $^{***}p < 0.001$, $^{****}p < 0.0001$).

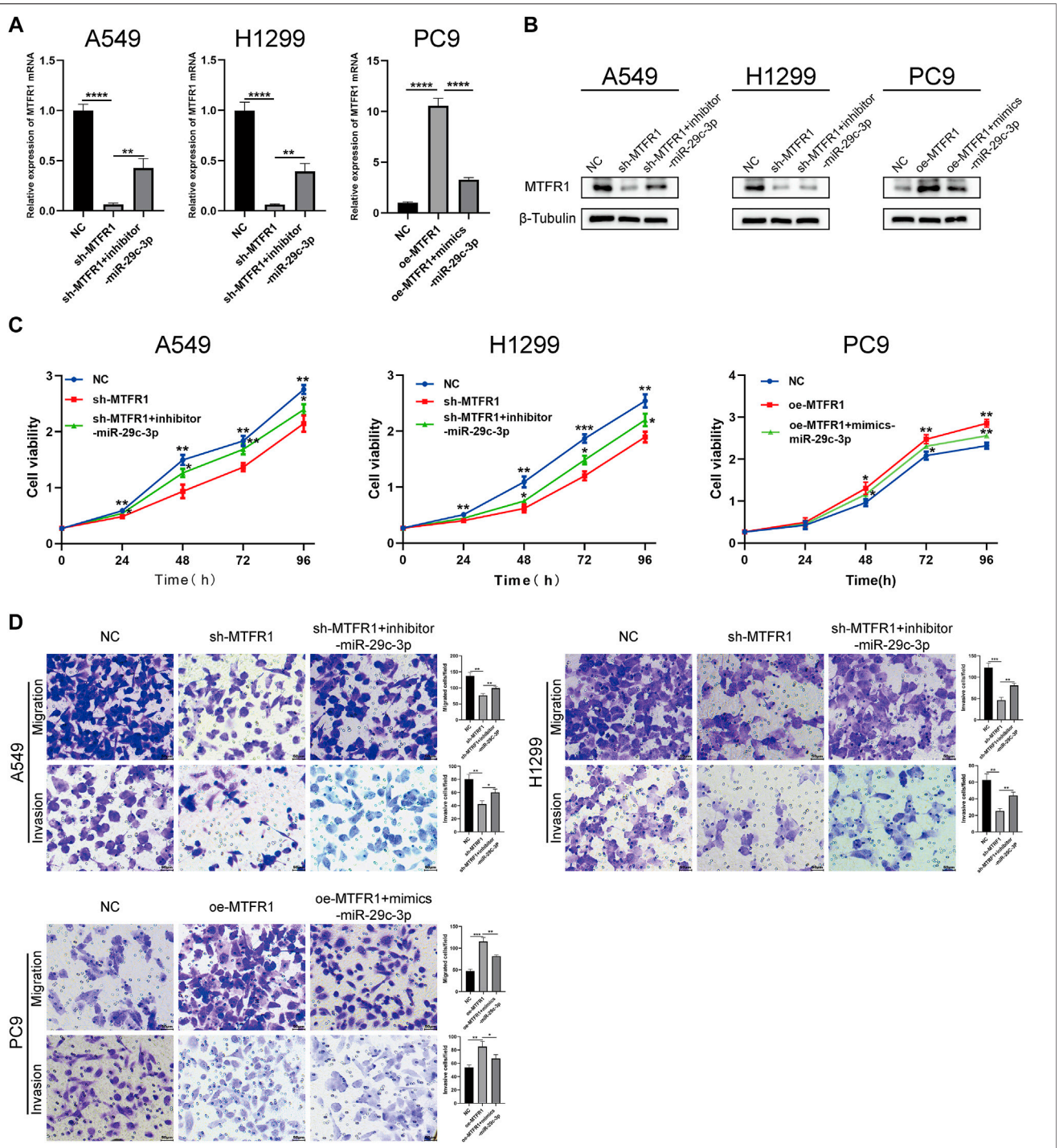

FIGURE 7 | miR-29c-3p could partly rescue the phenotypic changes caused by MTFR1. **(A, B)** Transfection efficacy validated using real-time quantitative polymerase chain reaction (RT-qPCR) and WB. **(C)** miR-29c-3p could rescue the effect of MTFR1 on the proliferation of LUAD cells. **(D)** miR-29c-3p could rescue the effect of MTFR1 on the invasion and migration of LUAD cells. Data were articulated as the mean ± standard deviation (SD; *$p < 0.05$, **$p < 0.01$, ***$p < 0.001$, ****$p < 0.0001$).

DISCUSSION

This study reported for the first time that MTFR1 was markedly overexpressed in LUAD cell lines and tissue samples. Moreover, high expression of MTFR1 was associated with adverse clinicopathological features and poor overall survival of LUAD patients. Findings from both *in vivo* and *in vitro* experiments demonstrated that

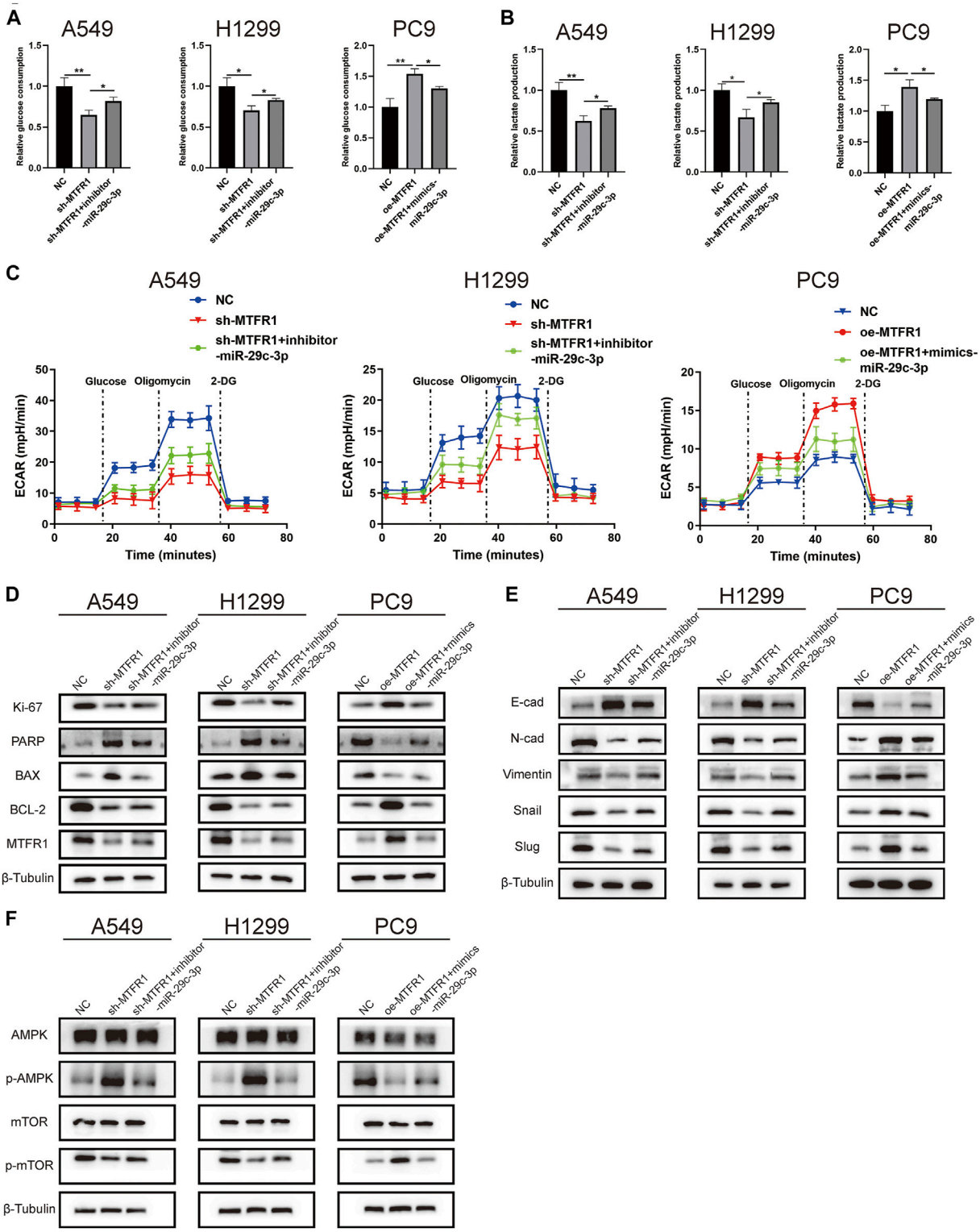

FIGURE 8 | miR-29c-3p could partly rescue the changes of glycolytic capacity and the expression of the phenotype-associated proteins caused by MTFR1 in LUAD cells. **(A–C)** miR-29c-3p could rescue the effect of MTFR1 on the glycolytic capacity of LUAD cells. **(D–F)** miR-29c-3p could reverse MTFR1-induced alterations in the expression of proteins associated with cell proliferation, apoptosis, EMT and the AMPK/mTOR signalling pathway in LUAD cells. Data were articulated as the mean ± standard deviation (SD; $^{*}p < 0.05$, $^{**}p < 0.01$).

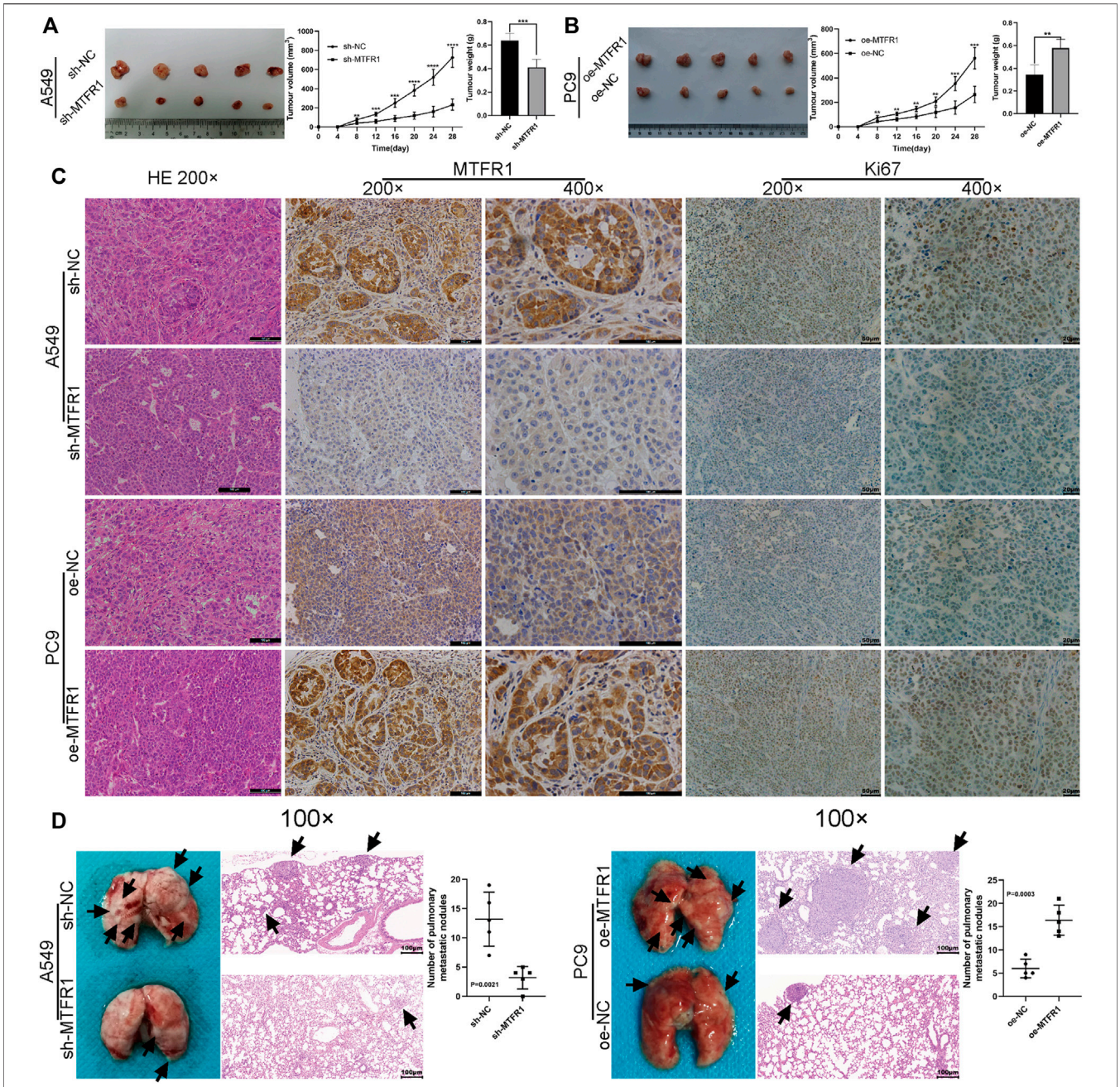

FIGURE 9 | MTFR1 promoted the progression of LUAD cells *in vivo*. **(A,B)** Tumour images, tumour growth curves and tumour weights of each group. **(C)** Haematoxylin–eosin (HE) staining and immunohistochemical analysis of the Ki-67 and MTFR1 proteins of tumours in each group. **(D)** Photographs (left) and HE-stained images (right) of the lungs in each group; the black arrowheads denote lung metastasis nodules (**$p < 0.01$, ***$p < 0.001$, ****$p < 0.0001$).

overexpressed MTFR1 stimulated the proliferation, invasion, migration and glycolytic capacity and repressed the apoptosis of LUAD cells, whereas MTFR1 knockdown exerted contradictory effects. In addition, we discovered that miR-29c-3p was a direct upstream target of MTFR1 and could inhibit the cancer-promoting functions of MTFR1. Furthermore, we also discovered that MTFR1 exerts its biological functions by regulating the AMPK/mTOR signalling pathway. All these results indicate that MTFR1 suppression may serve as a new therapeutic strategy for treating patients with LUAD.

In recent years, the essential role of mitochondrial dynamics (fusion/fission) in the development of cancers has gained increasing recognition. Rehman et al. reported

that mitochondrial fission promotes the progression of lung cancer (Rehman et al., 2012). In addition, Zhao et al. suggested that mitochondrial fission also promotes the progression of breast cancer. MTFR1, a mitochondrial protein, facilitates mitochondrial fission. In addition, MTFR2, which belongs to the same family as MTFR1, promotes the progression of breast cancer and oral squamous carcinoma when its expression is dysregulated (Lu et al., 2019; Wang W. et al., 2020). However, to date, only a few studies have used bioinformatic analyses to assess whether MTFR1 is involved in the development of cancers (Wang et al., 2015; Reddy et al., 2019; Sanada et al., 2019). In our study, we demonstrated that MTFR1 was abnormally upregulated in patients with LUAD and might act as a prognostic marker. Moreover, MTFR1 promoted the progression of LUAD. Therefore, our study provided an ideal biomarker for the diagnosis, therapeutic intervention and prognosis of LUAD.

Metabolic reprogramming has been recognised as one of the most remarkable hallmarks of cancer cells. Metabolic reprogramming in cancer cells can be best explained by the Warburg effect, in which cancer cells preferentially use glycolysis for energy generation regardless of the presence of oxygen (Vander Heiden et al., 2009). As mentioned previously, cancer cells can regulate mitochondrial dynamics to meet their metabolic requirements. Therefore, we hypothesised that MTFR1 could regulate the Warburg effect by altering mitochondrial dynamics in LUAD cells. To verify our hypothesis, we analysed the ECAR, the glucose consumption and lactate production rates of the transduced cells. We found that when MTFR1 expression was upregulated, the ECAR and the rates of glucose consumption and lactate production in LUAD cells were concomitantly elevated. However, the opposite result was observed when MTFR1 expression was downregulated. These findings indicate that MTFR1 stimulates the Warburg effect of LUAD cells. Our findings offer a new understanding of the treatment of LUAD by targeting cancer metabolism.

The occurrence and development of LUAD are accompanied by the alteration of multiple signalling pathways. Among these pathways, the AMPK/mTOR pathway is closely associated with tumour metabolism (Han et al., 2013). AMPK is considered an energy status sensor that contributes to maintaining cellular energy homeostasis. In addition, AMPK performs other functions such as regulation of cell growth and proliferation, autophagy, mitochondrial biogenesis and recycling and maintenance of cell polarity (Hardie, 2011). mTOR, which is negatively regulated by AMPK, is a central integrator of both growth factors and nutrient signals. It regulates numerous cellular processes including cell growth, cell cycle and angiogenesis (Chapuis et al., 2010). Previous studies have indicated that targeting AMPK/mTOR may be an efficient strategy for treating NSCLC (Han et al., 2013). Based on these studies and our finding that MTFR1 could promote aerobic glycolysis in LUAD, we hypothesised that MTFR1 could perform its biological function by regulating the AMPK/mTOR signalling pathway. Therefore, we identified the expression levels of several critical proteins of the AMPK/mTOR signalling pathway. As expected, MTFR1 overexpression elevated p-AMPK expression and reduced p-mTOR expression. Opposing findings were observed when MTFR1 expression was downregulated. These results confirmed our hypothesis that MTFR1 expression changes could change the expression of AMPK/mTOR signalling pathway and it may perform its biological through this pathway.

miRNAs are a class of non-coding RNAs that have been extensively studied, and aberrant miRNA expression is associated with many human diseases, including various cancers (Jiang et al., 2009). In our study, we predicted and validated miR-29c-3p as a direct upstream miRNA of MTFR1. miR-29c-3p expression was not only downregulated in LUAD cells but also inversely correlated with MTFR1. Furthermore, we performed rescue experiments to confirm that miR-29c-3p might partly rescue the malignant phenotypes induced by MTFR1. These findings indicate that the miR-29c-3p/MTFR1/AMPK/mTOR axis plays an important role in LUAD. However, because MTFR1 exerts robust cancer-promoting effects on LUAD, further investigation is required to identify proteins that interact with MTFR1 to exercise such effects.

In conclusion, MTFR1 serves as a strong tumour-promoting factor in LUAD, and targeting MTFR1 may provide a better disease outcome for patients with LUAD.

DATA AVAILABILITY STATEMENT

The original contributions presented in the study are included in the article/**Supplementary Material**, further inquiries can be directed to the corresponding author.

ETHICS STATEMENT

The studies involving human participants were reviewed and approved by Medical Ethics Committee of Qilu Hospital of Shandong University. The patients/participants provided their written informed consent to participate in this study. The animal study was reviewed and approved by Shandong University Animal Research Ethics Committee.

AUTHOR CONTRIBUTIONS

YL, LS, and HT designed this study. KJ, RD, and ZF collected samples and information of LUAD patients. YL performed the experiments and wrote the manuscript. YLI analyzed the data. CG and HZ revised the manuscript. All authors contributed to the article and approved the submitted version.

FUNDING

This research was funded by the Youth Fund of Qilu Hospital of Shandong University (No. 2019QLQN50), the Natural Science Foundation of Shandong Province (No. ZR2020QH213), and the Taishan Scholar Program of Shandong Province (No. ts201712087).

ACKNOWLEDGMENTS

We thank Professor Qingjie Wang for the guidance of the written manuscript.

SUPPLEMENTARY MATERIAL

The Supplementary Material for this article can be found online at: https://www.frontiersin.org/articles/10.3389/fcell.2021.771824/full#supplementary-material

REFERENCES

Bartel, D. (2004). MicroRNAs: Genomics, Biogenesis, Mechanism, and Function. *Cell* 116, 281–297. doi:10.1016/s0092-8674(04)00045-5

Cai, J., Wang, J., Huang, Y., Wu, H., Xia, T., Xiao, J., et al. (2016). ERK/Drp1-dependent Mitochondrial Fission Is Involved in the MSC-Induced Drug Resistance of T-Cell Acute Lymphoblastic Leukemia Cells. *Cell Death Dis* 7 (11), e2459. doi:10.1038/cddis.2016.370

Chan, D. C. (2012). Fusion and Fission: Interlinked Processes Critical for Mitochondrial Health. *Annu. Rev. Genet.* 46, 265–287. doi:10.1146/annurev-genet-110410-132529

Chan, D. C. (2006). Mitochondria: Dynamic Organelles in Disease, Aging, and Development. *Cell* 125 (7), 1241–1252. doi:10.1016/j.cell.2006.06.010

Chapuis, N., Tamburini, J., Green, A. S., Willems, L., Bardet, V., Park, S., et al. (2010). Perspectives on Inhibiting mTOR as a Future Treatment Strategy for Hematological Malignancies. *Leukemia* 24 (10), 1686–1699. doi:10.1038/leu.2010.170

Chen, W., Zheng, R., Baade, P. D., Zhang, S., Zeng, H., Bray, F., et al. (2016). Cancer Statistics in China, 2015. *CA: A Cancer J. Clinicians* 66 (2), 115–132. doi:10.3322/caac.21338

Feng, S., Luo, S., Ji, C., and Shi, J. (2020). miR-29c-3p Regulates Proliferation and Migration in Ovarian Cancer by Targeting KIF4A. *World J. Surg. Onc* 18 (1), 315. doi:10.1186/s12957-020-02088-z

Feng, Z., and Levine, A. J. (2010). The Regulation of Energy Metabolism and the IGF-1/mTOR Pathways by the P53 Protein. *Trends Cel Biol.* 20 (7), 427–434. doi:10.1016/j.tcb.2010.03.004

Friedman, R. C., Farh, K. K.-H., Burge, C. B., and Bartel, D. P. (2009). Most Mammalian mRNAs Are Conserved Targets of microRNAs. *Genome Res.* 19 (1), 92–105. doi:10.1101/gr.082701.108

Guo, L., Cui, C., Wang, J., Yuan, J., Yang, Q., Zhang, P., et al. (2020). PINCH-1 Regulates Mitochondrial Dynamics to Promote Proline Synthesis and Tumor Growth. *Nat. Commun.* 11 (1), 4913. doi:10.1038/s41467-020-18753-6

Han, D., Li, S.-J., Zhu, Y.-T., Liu, L., and Li, M.-X. (2013). LKB1/AMPK/mTOR Signaling Pathway in Non-small-cell Lung Cancer. *Asian Pac. J. Cancer Prev.* 14 (7), 4033–4039. doi:10.7314/apjcp.2013.14.7.4033

Hanahan, D., and Weinberg, R. A. (2011). Hallmarks of Cancer: the Next Generation. *Cell* 144 (5), 646–674. doi:10.1016/j.cell.2011.02.013

Hardie, D. G. (2011). AMP-activated Protein Kinase-An Energy Sensor that Regulates All Aspects of Cell Function. *Genes Dev.* 25 (18), 1895–1908. doi:10.1101/gad.17420111

Herbst, R. S., Morgensztern, D., and Boshoff, C. (2018). The Biology and Management of Non-small Cell Lung Cancer. *Nature* 553 (7689), 446–454. doi:10.1038/nature25183

Hernández-Alvarez, M. I., and Zorzano, A. (2021). Mitochondrial Dynamics and Liver Cancer. *Cancers* 13 (11), 2571. doi:10.3390/cancers13112571

Hozaka, Y., Seki, N., Tanaka, T., Asai, S., Moriya, S., Idichi, T., et al. (2021). Molecular Pathogenesis and Regulation of the miR-29-3p-Family: Involvement of ITGA6 and ITGB1 in Intra-hepatic Cholangiocarcinoma. *Cancers* 13 (11), 2804. doi:10.3390/cancers13112804

Huang, L., Guo, B., Liu, S., Miao, C., and Li, Y. (2020). Inhibition of the LncRNA Gpr19 Attenuates Ischemia-reperfusion Injury after Acute Myocardial Infarction by Inhibiting Apoptosis and Oxidative Stress *via* the miR-324-5p/Mtfr1 axis. *IUBMB Life* 72 (3), 373–383. doi:10.1002/iub.2187

Huang, L., Luan, T., Chen, Y., Bao, X., Huang, Y., Fu, S., et al. (2018). LASS2 Regulates Invasion and Chemoresistance *via* ERK/Drp1 Modulated Mitochondrial Dynamics in Bladder Cancer Cells. *J. Cancer* 9 (6), 1017–1024. doi:10.7150/jca.23087

Jiang, Q., Wang, Y., Hao, Y., Juan, L., Teng, M., Zhang, X., et al. (2009). miR2Disease: a Manually Curated Database for microRNA Deregulation in Human Disease. *Nucleic Acids Res.* 37 (Database issue), D98–D104. doi:10.1093/nar/gkn714

Knott, A. B., Perkins, G., Schwarzenbacher, R., and Bossy-Wetzel, E. (2008). Mitochondrial Fragmentation in Neurodegeneration. *Nat. Rev. Neurosci.* 9 (7), 505–518. doi:10.1038/nrn2417

Kong, B., Tsuyoshi, H., Orisaka, M., Shieh, D.-B., Yoshida, Y., and Tsang, B. K. (2015). Mitochondrial Dynamics Regulating Chemoresistance in Gynecological Cancers. *Ann. N.Y. Acad. Sci.* 1350, 1–16. doi:10.1111/nyas.12883

Lenzi, P., Ferese, R., Biagioni, F., Fulceri, F., Busceti, C. L., Falleni, A., et al. (2021). Rapamycin Ameliorates Defects in Mitochondrial Fission and Mitophagy in Glioblastoma Cells. *Int. J. Mol. Sci.* 22 (10), 5379. doi:10.3390/ijms22105379

Li, Y., Dong, R., Lu, M., Cheng, C., Feng, Z., Zhao, R., et al. (2021). Let-7b-3p Inhibits Tumor Growth and Metastasis by Targeting the BRF2-Mediated MAPK/ERK Pathway in Human Lung Adenocarcinoma. *Transl Lung Cancer Res.* 10 (4), 1841–1856. doi:10.21037/tlcr-21-299

Lin, M. T., and Beal, M. F. (2006). Mitochondrial Dysfunction and Oxidative Stress in Neurodegenerative Diseases. *Nature* 443 (7113), 787–795. doi:10.1038/nature05292

Lu, G., Lai, Y., Wang, T., Lin, W., Lu, J., Ma, Y., et al. (2019). Mitochondrial Fission Regulator 2 (MTFR2) Promotes Growth, Migration, Invasion and Tumour Progression in Breast Cancer Cells. *Aging (Albany NY)* 11 (22), 10203–10219. doi:10.18632/aging.102442

McBride, H. M., Neuspiel, M., and Wasiak, S. (2006). Mitochondria: More Than Just a Powerhouse. *Curr. Biol.* 16 (14), R551–R560. doi:10.1016/j.cub.2006.06.054

Monticone, M., Panfoli, I., Ravera, S., Puglisi, R., Jiang, M.-M., Morello, R., et al. (2010). The Nuclear Genes Mtfr1 and Dufd1 Regulate Mitochondrial Dynamic and Cellular Respiration. *J. Cel. Physiol.* 225 (3), 767–776. doi:10.1002/jcp.22279

Reddy, R. B., Khora, S. S., and Suresh, A. (2019). Molecular Prognosticators in Clinically and Pathologically Distinct Cohorts of Head and Neck Squamous Cell Carcinoma-A Meta-Analysis Approach. *PLoS One* 14 (7), e0218989. doi:10.1371/journal.pone.0218989

Rehman, J., Zhang, H. J., Toth, P. T., Zhang, Y., Marsboom, G., Hong, Z., et al. (2012). Inhibition of Mitochondrial Fission Prevents Cell Cycle Progression in Lung Cancer. *FASEB j.* 26 (5), 2175–2186. doi:10.1096/fj.11-196543

Sanada, H., Seki, N., Mizuno, K., Misono, S., Uchida, A., Yamada, Y., et al. (2019). Involvement of Dual Strands of miR-143 (miR-143-5p and miR-143-3p) and

Their Target Oncogenes in the Molecular Pathogenesis of Lung Adenocarcinoma. *Int. J. Mol. Sci.* 20 (18), 4482. doi:10.3390/ijms20184482

Sung, H., Ferlay, J., Siegel, R. L., Laversanne, M., Soerjomataram, I., Jemal, A., et al. (2021). Global Cancer Statistics 2020: GLOBOCAN Estimates of Incidence and Mortality Worldwide for 36 Cancers in 185 Countries. *CA A. Cancer J. Clin.* 71 (3), 209–249. doi:10.3322/caac.21660

Tonachini, L., Monticone, M., Puri, C., Tacchetti, C., Pinton, P., Rizzuto, R., et al. (2004). Chondrocyte Protein with a Poly-Proline Region (CHPPR) Is a Novel Mitochondrial Protein and Promotes Mitochondrial Fission. *J. Cel. Physiol.* 201 (3), 470–482. doi:10.1002/jcp.20126

Vander Heiden, M. G., Cantley, L. C., and Thompson, C. B. (2009). Understanding the Warburg Effect: the Metabolic Requirements of Cell Proliferation. *Science* 324 (5930), 1029–1033. doi:10.1126/science.1160809

Wang, H., Fu, L., Wei, D., Wang, B., Zhang, C., Zhu, T., et al. (2020a). MiR-29c-3p Suppresses the Migration, Invasion and Cell Cycle in Esophageal Carcinoma *via* CCNA2/p53 Axis. *Front. Bioeng. Biotechnol.* 8, 75. doi:10.3389/fbioe.2020.00075

Wang, W., Xiong, M., Jiang, L., Chen, Z., and Shao, Y. (2020b). MTFR2 Promotes the Proliferation, Migration, and Invasion of Oral Squamous Carcinoma by Switching OXPHOS to Glycolysis. *Front. Oncol.* 10, 858. doi:10.3389/fonc.2020.00858

Wang, W., Lim, W. K., Leong, H. S., Chong, F. T., Lim, T. K. H., Tan, D. S. W., et al. (2015). An Eleven Gene Molecular Signature for Extra-capsular Spread in Oral Squamous Cell Carcinoma Serves as a Prognosticator of Outcome in Patients without Nodal Metastases. *Oral Oncol.* 51 (4), 355–362. doi:10.1016/j.oraloncology.2014.12.012

Xie, P., Zhang, M., He, S., Lu, K., Chen, Y., Xing, G., et al. (2014). The Covalent Modifier Nedd8 Is Critical for the Activation of Smurf1 Ubiquitin Ligase in Tumorigenesis. *Nat. Commun.* 5, 3733. doi:10.1038/ncomms4733

Zhu, H., Wang, G., Zhu, H., and Xu, A. (2021). MTFR2, A Potential Biomarker for Prognosis and Immune Infiltrates, Promotes Progression of Gastric Cancer Based on Bioinformatics Analysis and Experiments. *J. Cancer* 12 (12), 3611–3625. doi:10.7150/jca.58158

Zou, T., Gao, Y., and Qie, M. (2021). MiR-29c-3p Inhibits Epithelial-Mesenchymal Transition to Inhibit the Proliferation, Invasion and Metastasis of Cervical Cancer Cells by Targeting SPARC. *Ann. Transl Med.* 9 (2), 125. doi:10.21037/atm-20-7272

Conflict of Interest: The authors declare that the research was conducted in the absence of any commercial or financial relationships that could be construed as a potential conflict of interest.

Publisher's Note: All claims expressed in this article are solely those of the authors and do not necessarily represent those of their affiliated organizations, or those of the publisher, the editors and the reviewers. Any product that may be evaluated in this article, or claim that may be made by its manufacturer, is not guaranteed or endorsed by the publisher.

frontiers | Frontiers in Cell and Developmental Biology

TYPE Correction
PUBLISHED 31 August 2022
DOI 10.3389/fcell.2022.870313

OPEN ACCESS

EDITED AND REVIEWED BY
Jiayi Wang,
Shanghai Jiao Tong University, China

*CORRESPONDENCE
Hui Tian,
tianhuiql@126.com

SPECIALTY SECTION
This article was submitted to Epigenomics and Epigenetics, a section of the journal Frontiers in Cell and Developmental Biology

RECEIVED 06 February 2022
ACCEPTED 09 August 2022
PUBLISHED 31 August 2022

CITATION
Li Y, Liu Y, Jin K, Dong R, Gao C, Si L, Feng Z, Zhang H and Tian H (2022), Corrigendum: Negatively regulated by miR-29c-3p, MTFR1 promotes the progression and glycolysis in lung adenocarcinoma via the AMPK/mTOR signalling pathway.
Front. Cell Dev. Biol. 10:870313.
doi: 10.3389/fcell.2022.870313

Corrigendum: Negatively regulated by miR-29c-3p, MTFR1 promotes the progression and glycolysis in lung adenocarcinoma via the AMPK/mTOR signalling pathway

Yongmeng Li[1], Yanfei Liu[2], Kai Jin[1], Rui Dong[1], Cun Gao[1], Libo Si[1], Zitong Feng[1], Huiying Zhang[1] and Hui Tian[1]*

[1]Department of Thoracic Surgery, Qilu Hospital, Cheeloo College of Medicine, Shandong University, Jinan, China, [2]Department of Anesthesiology, Qilu Children's Hospital of Shandong University, Jinan, China

KEYWORDS

lung cancer, microRNA, mitochondrial fission regulator 1, warburg effect, proliferation, invasion, migration

A Corrigendum on
Negatively regulated by miR-29c-3p, MTFR1 promotes the progression and glycolysis in lung adenocarcinoma *via* the AMPK/mTOR signalling pathway

by Li Y, Liu Y, Jin K, Dong R, Gao C, Si L, Feng Z, Zhang H and Tian H (2021). Front. Cell Dev. Biol. 9:771824. doi: 10.3389/fcell.2021.771824

In the original article, there was a mistake in Figure 9D as published. When we were arranging the panel, we misused the HE staining pictures by using the wrong folder. The corrected Figure 9D appears below.

The authors apologize for this error and state that this does not change the scientific conclusions of the article in any way. The original article has been updated.

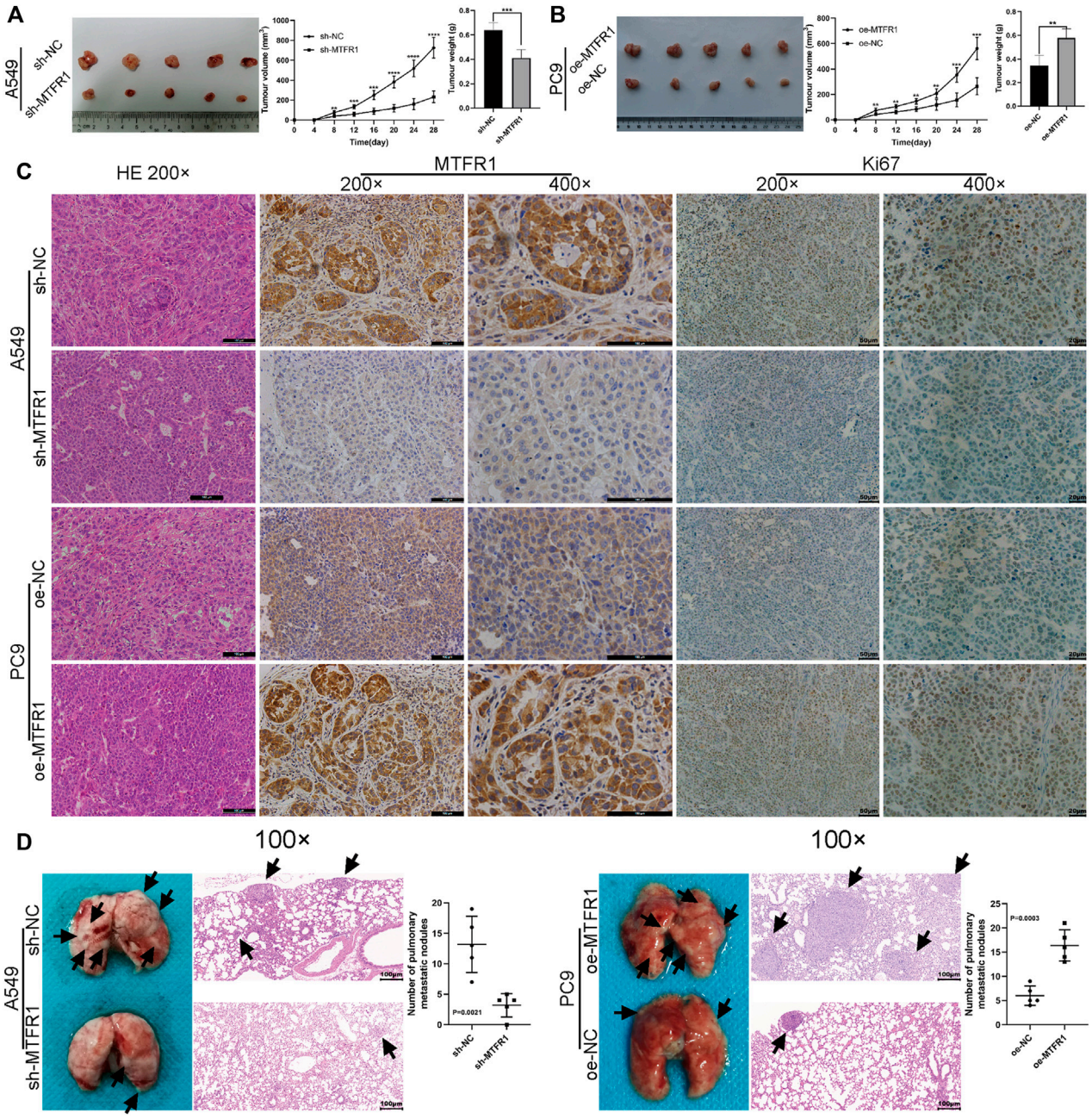

FIGURE 9
MTFR1 promoted the progression of LUAD cells *in vivo*. **(A,B)** Tumour images, tumour growth curves and tumour weights of each group. **(C)** Haematoxylin–eosin (HE) staining and immunohistochemical analysis of the Ki-67 and MTFR1 proteins of tumours in each group. **(D)** Photographs (left) and HE-stained images (right) of the lungs in each group; the black arrowheads denote lung metastasis nodules (**$p < 0.01$, ***$p < 0.001$, ****$p < 0.0001$).

Publisher's note

Advantages of publishing in Frontiers

OPEN ACCESS
Articles are free to read for greatest visibility and readership

FAST PUBLICATION
Around 90 days from submission to decision

HIGH QUALITY PEER-REVIEW
Rigorous, collaborative, and constructive peer-review

TRANSPARENT PEER-REVIEW
Editors and reviewers acknowledged by name on published articles

Frontiers
Avenue du Tribunal-Fédéral 34
1005 Lausanne | Switzerland

Visit us: www.frontiersin.org
Contact us: frontiersin.org/about/contact

REPRODUCIBILITY OF RESEARCH
Support open data and methods to enhance research reproducibility

DIGITAL PUBLISHING
Articles designed for optimal readership across devices

FOLLOW US
@frontiersin

IMPACT METRICS
Advanced article metrics track visibility across digital media

EXTENSIVE PROMOTION
Marketing and promotion of impactful research

LOOP RESEARCH NETWORK
Our network increases your article's readership